

THE UNDRAINED BEHAVIOR OF SATURATED, DILATANT SILTS

by

Andrew Thomas Rose

Dissertation submitted to the Faculty of the
Virginia Polytechnic Institute and State University
in partial fulfillment of the requirements for the degree of

DOCTOR OF PHILOSOPHY

in

Civil Engineering

APPROVED:

Thomas Brandon

T. L. Brandon, Chairman

J. M. Duncan

J. M. Duncan

J. R. Martin

J. R. Martin

George Fitz

G. M. Fitz

Ronald Kriz

R. D. Kriz

January, 1995

Blacksburg, Virginia

C.2

LD

5655

V850

1994

R673

v. 1

C.2

THE UNDRAINED BEHAVIOR OF SATURATED, DILATANT SILTS

by

Andrew T. Rose

Committee Chairman: T. L. Brandon

Civil Engineering

(ABSTRACT)

An extensive literature review and experimental study were performed to investigate whether cavitation and dissolved gases exiting solution from soil pore water are the cause of the erratic undrained behavior often observed in triaxial tests on saturated, dilatant silts.

The literature indicates that ground water contains various amounts of dissolved gases and that gases dissolved in soil pore water will have sufficient time to exit solution to some extent, due to the pore pressure reductions which occur during sampling and unconsolidated-undrained triaxial tests. The exit of dissolved gases from solution would increase the soil volume and affect its undrained behavior.

Experiments were performed on saturated silts to measure the pore pressure reductions which occur during sampling and unconsolidated-undrained triaxial tests. The amount of dissolved air that could come out of solution and the desaturation that a saturated soil sample could experience were also estimated.

Gas bubble formation and growth within the pores of a saturated silt could affect intergranular forces and influence the stress-strain behavior of the soil in undrained tests. Variations in the amount of dissolved gas exiting solution and forming bubbles from one specimen to another could be the cause of the erratic undrained behavior

often observed for saturated silts. Bubble growth within the soil pores is believed to have lead to abrupt strain-softening in a number of the undrained tests performed in this research.

Variations in specimen disturbance may also contribute to the erratic behavior observed in undrained tests on silts. Disturbance levels and their influence on soil behavior are difficult to quantify.

Due to the unusual properties of water under negative pressure, the initial value of pore water pressure within the soil appears to have a direct influence on the undrained strength of the soil. As a result, laboratory pore water pressures should be similar to in-situ pore water pressures, in order to give reasonable undrained strength measurements. The findings of this research are believed to be worthy of further study.

ACKNOWLEDGEMENTS

I would to thank my advisor, Professor Tom Brandon for his support, guidance, and friendship during my research and academic studies. His contributions and direction of the research project, combined with his allowing me the independence to work and think on my own, significantly enhanced my development as researcher and helped to make my work at Virginia Tech an enjoyable and rewarding experience.

I also wish to thank Professor J. M. Duncan for his numerous contributions to this research. His suggestions and ideas related to the performance of this research, as well as his concern that the research address the practical aspects of the problem being studied, are gratefully acknowledged.

My gratitude also goes to Professors J. R. Martin II, G. M. Filz, and R. D. Kriz for their willingness to be involved with my research and academic studies. Their contributions are appreciated.

I also wish to thank my friends and classmates at Virginia Tech, for sharing thier ideas, comments, and suggestions, as well as their friendship.

The funding for this research and my academic studies was provided by the U.S. Army Corps of Engineers, the Via Fellowship program, the Charles E. Via Department of Civil Enginnering, and Pratt Fellowship funds of the Virginia Tech College of Engineering. This support was greatly appreciated.

TABLE OF CONTENTS

Abstract	ii
Acknowledgements	iv
Table of Contents	v
List of Tables	xi
List of Figures	xviii
Chapter 1	Introduction.....1
1.1	Research Objectives.....2
1.2	Organization of Dissertation.....3
Chapter 2	Undrained Behavior of Saturated Soils.....5
2.1	Introduction.....5
2.2	Expected vs. Observed Behavior of Saturated Soils in Q Tests.....6
2.3	Summary and Conclusions.....39
Chapter 3	Cavitation and Related Phenomena.....52
3.1	Introduction.....52
3.2	Types of Pressure Reductions in Liquids.....53
3.3	Types of Cavitation.....56
3.3.1	Gaseous Cavitation56
3.3.2	Vaporous Cavitation57
3.4	Tensile Strength of Water.....60
3.5	Cavitation Nuclei.....62
3.5.1	Organic Skin Theory63
3.5.2	Crack and Crevice Theory65
3.5.3	Removal of Cavitation Nuclei70
3.5.4	Theoretical and Experimental Studies of Cavitation Nuclei75

3.6	Tribonucleation.....	86
3.7	Effect of the Dissolved Gas Content of the Liquid on Cavitation.....	88
3.7.1	Theoretical Consideration of the Effect of Dissolved Air Content on Cavitation	91
3.7.2	Experimental Studies of the Effect of Dissolved Air Content on Cavitation	92
3.8	Effect of Temperature on Cavitation.....	93
3.9	Consideration of Cavitation in Soil Mechanics and Laboratory Testing.....	95
3.10	Summary and Conclusions.....	100
Chapter 4	Solubility of Air in Water, Air-Water Relationships in Soils, and Rate at which Air Goes Into and Comes Out of Solution in Water.....	103
4.1	Application of Henry's and Boyle's Laws to Air-Water Systems.....	103
4.2	Dissolved Gas Content of Soil Pore Water.....	111
4.2.1	Dissolved Gas Content of Soil Pore Water in Remolded Specimens	111
4.2.2	Dissolved Gas Content of Soil Pore Water in the Ground	113
4.2.3	Measurement of Dissolved Air Content of Water	134
4.3	Pressure Reduction in the Pore Water of Saturated Silts.....	140
4.3.1	Pore Pressure Reduction Due to Sampling	141
4.3.2	Pore Pressure Reduction Due to Dilation	143
4.4	Effect of Temperature Variations on the Solubility of Dissolved Gases in Soil Pore Water.....	146
4.5	Amount of Air that Could Potentially Come Out of Solution from Soil Pore Water.....	148
4.5.1	Amount of Air that Could Come Out of Solution Due to Temperature Variations	148

4.5.2	Amount of Air that Could Come Out of Solution due both an Increase in Temperature and a Decrease in Pore Water Pressure	150
4.6	Relationship between Pore Air and Pore Water Pressures in Partially Saturated Soils.....	158
4.7	Studies of Gas Going Into and Coming Out of Solution from the Pore Water of Soils.....	165
4.7.1	Increasing the Degree of Saturation of Partially Saturated Test Specimens	178
4.7.2	Studies on the Rate of Diffusion of Air Through Soil Pore Water and the Time Required to Back Pressure Saturate Triaxial Specimens	187
4.7.3	Studies of Gas Coming Out of Solution from the Pore Water of Marine Soils	199
4.8	Rate at Which Air Goes Into and Comes Out of Solution from Water.....	213
4.8.1	Transmission of Gases Into and Out of Water by Diffusion	214
4.8.2	Transmission of Gases Into Water by Streaming	230
4.8.3	Application of Streaming Equations to Gases Exiting from Water	239
4.8.4	Effect of Disturbance on the Rate at which Air Comes Out of Solution from Water	243
4.9	Summary and Conclusions.....	246
Chapter 5	Experimental Study.....	257
5.1	Properties of the Soil Used in this Study....	257
5.2	Laboratory Tests Performed in this Study....	262
5.3	Midheight Pore Pressure Monitoring of Triaxial Specimens.....	262
5.3.1	Review of Midheight Pore Pressure Monitoring Techniques	265
5.3.2	Midheight Pore Pressure Monitoring System Used in this Study	276

5.4	Q Tests with Midheight Pore Pressure Measurements.....	280
5.4.1	Comparison of Q Tests Performed at the Same Cell Pressure	282
5.4.1.1	Q Tests Performed as Unconfined Compression Tests	282
5.4.1.2	Q Tests Performed at 10 psi Cell Pressure	286
5.4.1.3	Q Tests Performed at 20 psi Cell Pressure	292
5.4.2	Comparison of Q Tests Performed on Specimens Trimmed from the same Batch Sample	300
5.4.3	Comparison of Q Tests Performed on Specimens with Similar Void Ratios ...	311
5.4.4	Adjustment of Pore Pressures in Tests with Erratic Pore Pressure Measurements	329
5.5	Consolidated-Undrained Unloading Tests.....	343
5.5.1	CU Tests	354
5.5.2	Q Tests from Unloading Test Specimens	363
5.6	Q Tests Performed in Prepressurization Study.....	374
5.7	Q Tests with Pore Air and Pore Water Pressure Measurements.....	408
5.8	Q Tests at Different Strain Rates.....	426
5.9	Conventional Q Tests.....	445
5.9.1	Old LMVD Silt	447
5.9.2	New LMVD Silt	490
5.10	CU Tests with Different Back Pressures.....	505
5.11	Q Tests on Back Pressure Saturated Specimens.....	528
5.12	Summary and Conclusions.....	567
Chapter 6	Analysis and Discussion of Experimental Results.....	580
6.1	Analysis of Q Tests with Midheight Pore Pressure Measurements.....	581

6.1.1	Discussion of Measured Pore Pressures	581
6.1.2	Estimation of Final Degree of Saturation of Q Test Specimens	609
6.1.3	Estimation of the Rate at which Air Comes Out of Solution from Soil Pore Water	629
6.2	Effect of Sampling on Pore Pressure Changes.....	640
6.3	Discussion of Q Tests Performed on Specimens Trimmed from Quarters of 4-inch Diameter Unloading Test Specimens.....	648
6.4	Perfect Sampling of LMVD Silt.....	654
6.5	Discussion of Effective Stress Strength Parameters of LMVD Silt.....	661
6.6	Discussion of the Prepressurization Study....	663
6.7	Discussion of Q Tests with Pore Air and Pore Water Pressure Measurements.....	667
6.8	Discussion of Q Tests Performed at Different Strain Rates.....	669
6.9	Discussion of Results of CU Tests with Different Back Pressures.....	671
6.10	Discussion of Undrained Strength of LMVD Silt.....	673
6.11	Discussion of Back Pressure Saturated Q Tests.....	707
6.12	Consideration of Observed Stress-Strain Behavior.....	712
6.12.1	Strain-hardening of Saturated, Dilatant Materials	714
6.12.2	Strain-softening in Saturated, Dilatant Materials	717
6.12.3	Experimental Studies and Model Predictions of the Behavior of Materials Containing Voids	721
6.12.4	Consideration of Undrained Behavior of Saturated, Dilatant Silts	732
6.13	Summary and Conclusions.....	767
Chapter 7	Summary, Conclusions and Recommendations.....	777

7.1	Summary of the Work Accomplished.....	778
7.2	Conclusions.....	779
7.3	Recommendations for Further Study.....	785
References	787
Appendicies	801
Appendix A	Notation.....	802
Appendix B	Conversion Factors.....	811
Vita	812

LIST OF TABLES

Table 4.1:	Solubility of air in water at various temperatures (CRC Handbook of Chemistry and Physics, 1988).....	105
Table 4.2:	Molecular weights and assumed fractional-volume composition of sea-level dry air (CRC Handbook of Chemistry and Physics, 1993).....	115
Table 4.3:	Solubility of oxygen in water exposed to water-saturated air at standard atmospheric pressure at various temperatures (Standard Methods, 1992).....	120
Table 4.4:	Dissolved oxygen (D.O.) content of soil pore water from Olmstead Lock and Dam Tube No. AS-900, Sample # 1.....	137
Table 4.5:	Dissolved oxygen (D.O.) content of various waters measured in the laboratory.....	138
Table 4.6:	Volume of free air that could potentially come out of solution from 100 cm ³ of pore water and expand in a saturated soil sampled from various depths. Pore water temperature assumed to change from 11°C in-situ to 20°C in the laboratory.....	157
Table 4.7:	Approximate analysis of conditions for an air bubble to grow into a void in a clay, sand, and silt soil, following Terzaghi (1943) (T=20°C, T _S =0.0004154 lbf/in).....	175

Table 4.8:	Increase in cell pressure, pore water pressure, and back pressure required to achieve full saturation of soil specimens under undrained conditions, using Eqs. 4-38, 4-39 and 4-40 ($P_i=14.7$ psia, $H=0.02$).....185
Table 4.9:	Time required to back pressure saturate ($S_f = 100\%$) a specimen with an initial degree of saturation, S_i , of 98%, based on Eq. 4-42.....196
Table 4.10:	Approximate times for complete solution of air bubbles in water with various degrees of undersaturation with dissolved air and different initial bubble sizes.....223
Table 4.11:	Time for air bubbles to dissolve in water as measured by Lee and Black (1972), t_d , and calculated using the equations of Epstein and Plesset (1950), t_A and t_S225
Table 4.12:	Approximate time for an air bubble to grow from an initial radius R_0 to $10R_0$ in water with various degrees of oversaturation with dissolved air.....227
Table 5.1:	Components of LMVD silt, based on grain size.....260
Table 5.2:	Moisture contents of undisturbed samples of new LMVD silt.....260
Table 5.3:	Summary of tests performed on LMVD silt in this study.....263
Table 5.4:	Initial properties of Q test triaxial specimens in which pore water pressures were measured at the midheight of the specimens.....281

Table 5.5:	Maximum deviator stress, maximum change in pore pressure, minimum pore water pressure, and the axial strain at which each of these occurred, for the Q tests performed with midheight pore pressure monitoring.....	300
Table 5.6:	Stress-strain data based on 10% axial strain failure criterion.....	336
Table 5.7:	Initial properties of the 1.4-inch diameter specimens used in the CU unloading tests.....	344
Table 5.8:	Approximate initial properties of the 4-inch diameter specimens of remolded LMVD silt used in the CU unloading tests.....	344
Table 5.9:	\bar{A}_u values measured for undrained unloading tests conducted on LMVD silt.....	353
Table 5.10:	Initial properties of the remolded old LMVD silt CU test specimen trimmed from the 4-inch diameter unloading test specimen ($\sigma'_{3con} = 10.5$ psi).....	360
Table 5.11:	Initial properties of the remolded LMVD silt Q test specimens obtained from the quarters of the 4-inch diameter unloading test specimens.....	363
Table 5.12:	Maximum change in pore pressure and minimum absolute pore pressure measured or calculated in the three Q tests on remolded LMVD silt.....	369
Table 5.13:	Initial void ratio for various initial degrees of saturation.....	380
Table 5.14:	Initial properties of the remolded LMVD silt unconfined compression test specimens used in the prepressurization study (Based on specimen dimensions measured prior to prepressurization).....	386

Table 5.15:	Initial properties of the remolded LMVD silt Q test specimens tested at a cell pressure of 10 psi in the prepressurization study (Based on specimen dimensions measured prior to prepressurization).....	388
Table 5.16:	Initial properties of the remolded LMVD silt Q test specimens tested at a cell pressure of 20 psi in the prepressurization study (Based on specimen dimensions measured prior to prepressurization).....	394
Table 5.17:	Values of pore water pressure estimated by Eq. 5-1 for total stresses measured at 10% axial strain in the Q tests performed in the prepressurization study ($\phi'=37^\circ$)	403
Table 5.18:	Values of pore water pressure estimated by Eq. 5-1 for total stresses measured at maximum deviator stress in the Q tests performed in the prepressurization study($\phi'=37^\circ$)	405
Table 5.19:	Initial properties of Q test specimens of compacted new LMVD silt in which pore air and pore water pressures were measured during shear.....	412
Table 5.20:	Initial degree of saturation and void ratio of compacted Q test specimens of new LMVD silt prior to application of 10 psi cell pressure; and pore air and pore water pressures measured after application of 10 psi cell pressure.....	425
Table 5.21:	Specimen data for Q tests performed at different strain rates.....	429
Table 5.22:	Initial properties of triaxial specimens tested in conventional Q tests.....	447

Table 5.23: Initial specimen data for CU test specimens with different values of back pressure.....506

Table 5.24: Initial specimen data prior to consolidation for CD test specimens of remolded old LMVD silt.....522

Table 5.25: Initial specimen data for back pressure saturated Q test specimens of new LMVD silt ($\sigma'_{3con} = 2$ psi).....530

Table 6.1: Initial air and pore water pressure prior to cell pressure application, along with calculated air-water interface radius, r , for the Q test specimens in which erratic pore pressure measurements were not observed....600

Table 6.2: Initial air and pore water pressure and air-water interface radius, r , after application of cell pressure for the Q test specimens in which erratic pore pressure measurements were not observed....604

Table 6.3: Initial pore air pressure, initial and final pore water pressures, and maximum change in pore water pressure measured in Q tests in which erratic pore pressure measurements were not observed ($P_a=13.7$ psi at Virginia Tech).....610

Table 6.4: Final degree of saturation of Q test specimens in which erratic pore pressure measurements were not observed, estimated using Eq. 4-41 ($S_i=100\%$, $H=0.02$ @ 20°C)614

Table 6.5: Approximate times for an existing air bubble with a radius of $R_o = 0.000513$ in = 0.01303 cm, to grow to a size of $10R_o$ and $100R_o$, using the equations of Epstein and Plesset (1950) (t_A = time required neglecting surface tension effects, t_S = time required including surface tension effects).....637

Table 6.6:	Change in pore water pressure associated with sampling calculated using the values of determined in the undrained unloading tests, for the conditions shown in Figure 6.12.....	642
Table 6.7:	Possible final degree of saturation of soil sampled from various depths below the ground water surface estimated using Eq. 4-41, for the pore pressure reductions presented in Table 6.6 (H=0.02, P _f =14.7 psi).....	643
Table 6.8:	Final pore air and pore water pressures and air-water interface radii, r, for saturated soil sampled from various depths.....	646
Table 6.9:	Perfect sampling effective stress for batch consolidometer specimens of old LMVD silt calculated using the values of \bar{A}_u from the undrained unloading tests ($\sigma'_{v0} = 56$ psi, $K_0 = 0.4$).....	656
Table 6.10:	Initial air and pore water pressure prior to cell pressure application for the three Q test specimens obtained from the 4-inch diameter unloading test specimen of old LMVD silt.....	657
Table 6.11:	Ratio of σ'_r to σ'_{ps} for Q tests with midheight pore pressure monitoring.....	658
Table 6.12:	Ratio of σ'_r to σ'_{ps} for Q tests with midheight pore pressure monitoring obtained from the 4-inch diameter unloading test specimen.....	659
Table 6.13:	Undrained strength parameters determined from Q tests on remolded old LMVD silt, based on a failure criterion of 9 or 10% axial strain.....	676

Table 6.14: Undrained strength parameters determined from Q tests on remolded old LMVD silt, based on a failure criterion of less than 9% axial strain at failure....681

Table 6.15: Undrained strength parameters determined from Q tests on remolded old LMVD silt, based on peak deviator stress failure criterion (linear envelopes).....685

Table 6.16: Undrained strength parameters determined from Q tests on remolded old LMVD silt, based on peak deviator stress failure criterion (bilinear envelopes).....688

Table 6.17: Undrained strength parameters determined from Q tests on remolded new LMVD silt, based on a limiting axial strain failure criterion.....692

Table 6.18: Undrained strength parameters determined from Q tests on remolded new LMVD silt, based on peak deviator stress failure criterion.....697

LIST OF FIGURES

Figure 2.1.	Total stress Mohr-Coulomb failure envelope for Q tests conducted on saturated clay (after Golder and Skempton, 1948).....8
Figure 2.2.	Total stress Mohr-Coulomb failure envelope for Q tests conducted on saturated silt (after Golder and Skempton, 1948).....8
Figure 2.3.	Pore pressure-strain relationship for a soil with a tendency for dilation (after Bishop and Eldin, 1950).....11
Figure 2.4.	Total stress Mohr's circles for undrained tests (after Penman, 1953).....19
Figure 3.1.	Cavitation nucleus stabilized in a crack on the surface of a hydrophobic solid (after Hayward, 1970).....68
Figure 3.2.	Formation of a bubble from a nucleus due to a reduction in the pressure of the liquid (after Young, 1989).....68
Figure 3.3.	Removal of a cavitation nucleus by prepressurizing the liquid to dissolve the trapped gas.....73
Figure 4.1.	Conditions under which a gas bubble in water will expand into a gas-filled void (after Terzaghi, 1943).....169
Figure 4.2.	Variation of pore air (u_a) and pore water (u_w) pressure with cell pressure for two specimens with different initial degrees of saturation under undrained conditions (after Bishop and Henkel, 1962).....181

Figure 4.3.	Relationship between void ratio and minor principal effective stress for dilatant soil specimen during undrained shear (after Esrig and Kirby, 1977).....	205
Figure 5.1	Schematic diagram of batch consolidometer used in forming remolded specimens.....	259
Figure 5.2.	Gradation curves for old and new LMVD silt.....	261
Figure 5.3.	Pore pressure monitoring system used by Crawford (1963).....	268
Figure 5.4.	Pore pressure monitoring methods used by Blight (1965).....	271
Figure 5.5.	Pore pressure monitoring methods presented by Yong and Warkentin (1966).....	272
Figure 5.6.	Pore pressure monitoring system used by Hight (1982) and Baldi, Hight and Thomas (1988).....	274
Figure 5.7.	Pore pressure monitoring system used by Dupas et al. (1988).....	275
Figure 5.8.	Schematic drawing of midheight pore pressure monitoring system used in this study.....	278
Figure 5.9.	Deviator stress-strain and change in pore pressure-strain relationships measured in UU tests 1 and 4 on remolded LMVD silt.....	283
Figure 5.10.	Deviator stress-strain and change in pore pressure-strain relationships measured in UU tests 10, 11, 12, and 13 on remolded LMVD silt.....	284

Figure 5.11.	Deviator stress-strain and change in pore pressure-strain relationships measured in UU tests 2, 5, and 8 on remolded LMVD silt.....	287
Figure 5.12.	Deviator stress-strain and change in pore pressure-strain relationships measured in UU tests 14, 15, and 16 on remolded LMVD silt.....	288
Figure 5.13.	Deviator stress-strain and change in pore pressure-strain relationships measured in UU tests 3, 6, and 7 on remolded LMVD silt.....	293
Figure 5.14.	Deviator stress-strain and change in pore pressure-strain relationships measured in UU tests 18 and 19 on remolded LMVD silt.....	294
Figure 5.15.	Deviator stress-strain and change in pore pressure-strain relationship measured in UU test 9 on undisturbed new LMVD silt.....	299
Figure 5.16.	Deviator stress-strain and change in pore pressure-strain relationships measured in UU tests 1, 2, 3, and 4 performed on specimens from the same batch sample of remolded LMVD silt.....	302
Figure 5.17.	Total stress Mohr's circles at 8.5% axial strain for UU tests 1, 2, and 3 on remolded LMVD silt.....	304
Figure 5.18.	Deviator stress-strain and change in pore pressure-strain relationships measured in UU tests 5 and 6 performed on specimens trimmed from the same batch sample of remolded LMVD silt.....	306
Figure 5.19.	Deviator stress-strain and change in pore pressure-strain relationships measured in UU tests 7 and 8 performed on specimens trimmed from the same batch sample of remolded LMVD silt.....	310

Figure 5.20.	Deviator stress-strain and change in pore pressure-strain relationships measured in UU tests 3, 8, 10, and 14 on remolded LMVD silt.....	312
Figure 5.21.	Total stress Mohr's circles at 8% axial strain for UU tests 8 and 10 on remolded LMVD silt.....	314
Figure 5.22.	Total stress Mohr's circles at 8% axial strain for UU tests 3, 8, 10, and 14 on remolded LMVD silt.....	315
Figure 5.23.	Deviator stress-strain and change in pore pressure-strain relationships measured in UU tests 10, 13, 14, and 18 on remolded LMVD silt.....	316
Figure 5.24.	Total stress Mohr's circles at 10% axial strain for UU tests 13 and 14 on remolded LMVD silt.....	319
Figure 5.25.	Total stress Mohr's circles at 10% axial strain for UU tests 10, 13, 14, and 18.....	320
Figure 5.26.	Deviator stress-strain and change in pore pressure-strain relationships measured in UU tests 6, 11, 15, and 16 on remolded LMVD silt.....	321
Figure 5.27.	Total stress Mohr's circles at 10% axial strain for UU tests 6, 11, 15, and 16 on remolded LMVD silt.....	323
Figure 5.28.	Deviator stress-strain and change in pore pressure-strain relationships measured in UU tests 4, 5, 7, and 12 on remolded LMVD silt.....	324
Figure 5.29.	Total stress Mohr's circles at 9% axial strain for UU tests 4, 5, 7, and 12 on remolded LMVD silt.....	327

Figure 5.30.	Deviator stress-strain and change in pore pressure-strain relationships measured in UU tests 3, 13, and 14 on remolded LMVD silt.....	328
Figure 5.31.	Total stress Mohr's circles at 10% axial strain for UU tests 3, 13, and 14 on remolded LMVD silt.....	330
Figure 5.32.	Calculated and measured change in pore pressure-strain relationships for UU test 4 on remolded LMVD silt.....	332
Figure 5.33.	Calculated and measured change in pore pressure-strain relationships for UU test 7 on remolded LMVD silt.....	334
Figure 5.34.	Calculated and measured change in pore pressure-strain relationships for UU test 2 on remolded LMVD silt.....	335
Figure 5.35.	Total stress Mohr's circles for UU tests 2, 4, and 7 on remolded LMVD silt....	337
Figure 5.36.	Effective stress Mohr's circles for UU tests 2, 4, and 7 on remolded LMVD silt....	338
Figure 5.37.	Effective stress path measured in UU test 4 on remolded LMVD silt.....	339
Figure 5.38.	Effective stress path measured in UU test 2 on remolded LMVD silt.....	340
Figure 5.39.	Effective stress path measured in UU test 7 on remolded LMVD silt.....	341
Figure 5.40.	Stress paths measured for the consolidated-undrained unloading tests conducted on the 1.4-inch diameter specimen of remolded old LMVD silt.....	348
Figure 5.41.	Stress paths measured for the consolidated-undrained unloading tests conducted on the 1.4-inch diameter specimen of undisturbed new LMVD silt.....	350

Figure 5.42.	Stress path measured for the consolidated undrained unloading test conducted on the 4-inch diameter specimen of remolded old LMVD silt.....	351
Figure 5.43.	Stress path measured for the consolidated undrained unloading test conducted on the 4-inch diameter specimen of remolded new LMVD silt.....	352
Figure 5.44.	Deviator stress-strain behavior and minor principal effective stress-strain behavior for the consolidated undrained test conducted on remolded LMVD silt.....	355
Figure 5.45.	Principal stress ratio-strain relationship and effective stress path measured in the CU test on the unloading test sample of remolded old LMVD silt.....	356
Figure 5.46.	Deviator stress-strain behavior and minor principal effective stress-strain behavior for the consolidated undrained test conducted on undisturbed LMVD silt....	357
Figure 5.47.	Principal stress ratio-strain relationship and effective stress path measured in the CU test on the sample of undisturbed new LMVD silt tested in an unloading test.....	359
Figure 5.48.	Deviator stress-strain and effective stress-strain relationships measured in the CU test on the sample of remolded old LMVD silt obtained from the 4-inch diameter unloading test specimen.....	361
Figure 5.49.	Principal stress ratio-strain relationship and effective stress path measured in the CU test on the sample of remolded old LMVD silt obtained from the 4-inch diameter unloading test specimen.....	362

Figure 5.50. Deviator stress-strain and change in pore pressure-strain relationships measured in UU tests 22, 23, and 24 performed on samples trimmed from the quarters of the 4-inch diameter undrained unloading test specimen of remolded old LMVD silt.....365

Figure 5.51. Total stress Mohr's circles for the three Q tests performed on samples of remolded old LMVD silt obtained from the 4-inch diameter unloading test specimen.....367

Figure 5.52. Calculated and measured change in pore pressure-strain relationships for UU tests 23 and 24 performed on samples trimmed from quarters of the 4-inch diameter undrained unloading test specimen of remolded LMVD silt.....370

Figure 5.53. Deviator stress-strain relationships measured in UU tests 25, 26, and 27 performed on samples trimmed from quarters of the 4-inch diameter undrained unloading test specimen of remolded new LMVD silt.....373

Figure 5.54. Total stress Mohr's circles for the three Q tests performed on samples of remolded new LMVD silt obtained from the 4-inch diameter unloading test specimen.....375

Figure 5.55. Deviator stress-strain relationships measured in the four unconfined compression tests performed on samples of remolded LMVD silt as part of the prepressurization study.....387

Figure 5.56. Deviator stress-strain relationships measured in the four Q tests performed at 10 psi cell pressure on samples of remolded LMVD silt as part of the prepressurization study.....389

Figure 5.57. Deviator stress-strain relationships measured in the four Q tests performed at 10 psi cell pressure on samples of remolded LMVD silt as part of the prepressurization study.....390

Figure 5.58. Deviator stress-strain relationships measured in the four Q tests performed at 10 psi cell pressure on samples of remolded LMVD silt as part of the prepressurization study.....391

Figure 5.59. Deviator stress-strain relationships measured in the Q tests performed at 10 psi cell pressure on samples of remolded LMVD silt as part of the prepressurization study.....393

Figure 5.60. Deviator stress-strain relationships measured in the four Q tests performed at 20 psi cell pressure on samples of remolded LMVD silt as part of the prepressurization study.....395

Figure 5.61. Deviator stress-strain relationships measured in the Q tests performed at 0, 10 and 20 psi cell pressure on samples of remolded LMVD silt as part of the prepressurization study.....398

Figure 5.62. Total stress Mohr's circles at 10% axial strain for the six Q tests performed on non-prepressurized samples of remolded LMVD silt.....400

Figure 5.63. Total stress Mohr's circles at 10% axial strain for the six Q tests performed on prepressurized samples of remolded LMVD silt.....401

Figure 5.64. Pore water pressure at failure estimated by Eq. 5-1 for the Q tests performed at cell pressures of 0, 10, and 20 psi in the prepressurization study, based on 10% axial strain at failure.....404

Figure 5.65. Pore water pressure at failure estimated by Eq. 5-1 for the Q tests performed at cell pressures of 0, 10 and 20 psi in the prepressurization study, based on maximum deviator stress at failure.....406

Figure 5.66. Deviator stress-strain and pore air and pore water pressure-strain relationships measured in test Q4 performed on compacted new LMVD silt.....414

Figure 5.67. Deviator stress-strain and pore air and pore water pressure-strain relationships measured in test Q5 performed on compacted new LMVD silt.....415

Figure 5.68. Deviator stress-strain and pore air and pore water pressure-strain relationships measured in test Q9 performed on compacted new LMVD silt.....416

Figure 5.69. Deviator stress-strain and pore air and pore water pressure-strain relationships measured in test Q2 performed on compacted new LMVD silt.....418

Figure 5.70. Deviator stress-strain and pore air and pore water pressure-strain relationships measured in test Q3 performed on compacted new LMVD silt.....419

Figure 5.71. Deviator stress-strain and pore air and pore water pressure-strain relationships measured in test Q1 performed on compacted new LMVD silt.....421

Figure 5.72. Deviator stress-strain and pore air and pore water pressure-strain relationships measured in test Q7 performed on compacted new LMVD silt.....422

Figure 5.73. Deviator stress-strain and pore air and pore water pressure-strain relationships measured in test Q8 performed on compacted new LMVD silt.....423

Figure 5.74.	Deviator stress vs. axial strain behavior measured in Q tests performed at different strain rates on remolded old LMVD silt.....	430
Figure 5.75.	Deviator stress vs. axial strain behavior measured in Q tests performed at different strain rates on remolded old LMVD silt.....	431
Figure 5.76.	Deviator stress vs. axial strain behavior measured in Q tests performed at different strain rates on remolded old LMVD silt.....	432
Figure 5.77.	Deviator stress vs. axial strain behavior measured in Q tests performed at different strain rates on remolded old LMVD silt.....	433
Figure 5.78.	Deviator stress vs. axial strain behavior measured in Q tests performed at a strain rate of 0.01%/min on remolded old LMVD silt.....	438
Figure 5.79.	Deviator stress vs. axial strain behavior measured in Q tests performed at strain rates ranging from 0.1%/min to 0.2%/min on remolded old LMVD silt.....	440
Figure 5.80.	Deviator stress vs. axial strain behavior measured in Q tests performed at a strain rate ranging from 0.9 to 1.2%/min on remolded old LMVD silt.....	441
Figure 5.81.	Deviator stress vs. axial strain behavior measured in Q tests performed at a strain rate ranging from 5 to 10%/min on remolded old LMVD silt.....	443
Figure 5.82.	Deviator stress-strain relationship measured in Q test B4-4 on remolded old LMVD silt.....	448

Figure 5.83. Deviator stress-strain relationships measured in Q tests B7-1 and B7-2 on remolded old LMVD silt.....450

Figure 5.84. Deviator stress-strain relationships measured in Q tests B8-1, B8-2, B8-3, and B8-4 on remolded old LMVD silt.....451

Figure 5.85. Total stress Mohr's circles at 8.5% axial strain for Q tests B8-1, B8-2, B8-3, and B8-4 on remolded old LMVD silt.....453

Figure 5.86. Total stress Mohr's circles at peak deviator stress for Q tests B8-1, B8-2, B8-3, and B8-4 on remolded old LMVD silt.....454

Figure 5.87. Deviator stress-strain relationships measured in Q tests B9-1, B9-2, and B9-4 on remolded old LMVD silt.....456

Figure 5.88. Total stress Mohr's circles at 10% axial strain for Q tests B9-1, B9-2, and B9-4 on remolded old LMVD silt.....458

Figure 5.89. Total stress Mohr's circles at peak deviator stress for Q tests B9-1, B9-2, and B9-4 on remolded old LMVD silt.....459

Figure 5.90. Deviator stress-strain relationships measured in Q tests B11-1, B11-2, B11-3, and B11-4 on remolded old LMVD silt.....460

Figure 5.91. Total stress Mohr's circles at 9% axial strain for Q tests B11-1, B11-2, B11-3, and B11-4 on remolded old LMVD silt.....462

Figure 5.92. Total stress Mohr's circles at peak deviator stress for Q tests B11-1, B11-2, B11-3, and B11-4 on remolded old LMVD silt.....463

Figure 5.93. Deviator stress-strain relationships measured in Q tests B12-1 and B12-3 on remolded old LMVD silt.....464

Figure 5.94. Total stress Mohr's circles at 7.7% axial strain for Q tests B12-1 and B12-3 on remolded old LMVD silt.....466

Figure 5.95. Total stress Mohr's circles at peak deviator stress for Q tests B12-1 and B12-3 on remolded old LMVD silt.....467

Figure 5.96. Deviator stress-strain relationships measured in Q tests B13-1 and B13-2 on remolded old LMVD silt.....468

Figure 5.97. Total stress Mohr's circles at 7% axial strain for Q tests B13-1 and B13-2 on remolded old LMVD silt.....470

Figure 5.98. Total stress Mohr's circles at peak deviator stress for Q tests B13-1 and B13-2 on remolded old LMVD silt.....471

Figure 5.99. Deviator stress-strain relationships measured in Q tests B4-4, B9-1, B9-2, and B9-4 on remolded old LMVD silt.....472

Figure 5.100. Total stress Mohr's circles at 10% axial strain for Q tests B4-4, B9-1, B9-2, and B9-4 on remolded old LMVD silt.....474

Figure 5.101. Total stress Mohr's circles at peak deviator stress for Q tests B4-4, B9-1, B9-2, and B9-4 on remolded old LMVD silt.....475

Figure 5.102. Deviator stress-strain relationships measured in Q tests B8-1, B8-2, B8-4, B7-1, and B7-2 on remolded old LMVD silt.....476

Figure 5.103. Total stress Mohr's circles at 9% axial strain for Q tests B8-1, B8-2, B8-4, B7-1, and B7-2 on remolded old LMVD silt.....478

Figure 5.104. Total stress Mohr's circles at peak deviator stress for Q tests B8-1, B8-2, B8-4, B7-1, and B7-2 on remolded old LMVD silt.....479

Figure 5.105. Deviator stress-strain relationships measured in Q tests B9-1, B9-2, B9-4, and B10-1 on remolded old LMVD silt.....481

Figure 5.106. Total stress Mohr's circles at 10% axial strain for Q tests B9-1, B9-2, B9-4, and B10-1 on remolded old LMVD silt.....482

Figure 5.107. Total stress Mohr's circles at peak deviator stress for Q tests B9-1, B9-2, B9-4, and B10-1 on remolded old LMVD silt.....483

Figure 5.108. Deviator stress-strain relationships measured in Q tests B8-1, B8-2, B8-4, B11-1, B11-2 and B11-3 on remolded old LMVD silt.....485

Figure 5.109. Total stress Mohr's circles at peak deviator stress for Q tests B8-1, B8-2, B8-4, B11-1, B11-2, and B11-3 on remolded old LMVD silt.....486

Figure 5.110. Deviator stress-strain relationships measured in Q tests B11-1, B11-2, B11-3, B9-1, B9-2, and B9-4 on remolded old LMVD silt.....487

Figure 5.111. Total stress Mohr's circles at 9% axial strain for Q tests B11-1, B11-2, B11-3, B9-1, B9-2, and B9-4 on remolded old LMVD silt.....489

Figure 5.112. Total stress Mohr's circles at peak deviator stress for Q tests B11-1, B11-2, B11-3, B9-1, B9-2, and B9-4 on remolded old LMVD silt.....491

Figure 5.113. Deviator stress-strain relationships measured in Q tests B17-1, B17-2, B17-3, and B17-4 on remolded new LMVD silt.....492

Figure 5.114. Total stress Mohr's circles at 4.5% axial strain for Q tests B17-1, B17-2, B17-3, and B17-4 on remolded new LMVD silt.....494

Figure 5.115. Total stress Mohr's circles at peak deviator stress for Q tests B17-1, B17-2, B17-3, and B17-4 on remolded new LMVD silt.....495

Figure 5.116. Deviator stress-strain relationships measured in Q tests B18-1, B18-2, B18-3, and B18-4 on remolded new LMVD silt.....497

Figure 5.117. Total stress Mohr's circles at 10% axial strain for Q tests B18-1, B18-2, B18-3, and B18-4 on remolded new LMVD silt.....498

Figure 5.118. Total stress Mohr's circles at peak deviator stress for Q tests B18-1, B18-2, B18-3, and B18-4 on remolded new LMVD silt.....499

Figure 5.119. Deviator stress-strain relationships measured in Q tests B17-1, B17-2, B17-3, B17-4, B18-1, B18-2, B18-3, and B18-4 on remolded new LMVD silt.....501

Figure 5.120. Total stress Mohr's circles at peak deviator stress for Q tests B17-1, B17-2, B17-3, B17-4, B18-1, B18-2, B18-3, and B18-4 on remolded new LMVD silt.....504

Figure 5.121. Deviator stress vs. axial strain and pore pressure vs. axial strain relationships measured in CU tests on remolded old LMVD silt.....507

Figure 5.122. Deviator stress vs. axial strain and pore pressure vs. axial strain relationships measured in CU test B5-1 on remolded old LMVD silt.....509

Figure 5.123. Deviator stress vs. axial strain and pore pressure vs. axial strain relationships measured in CU test B5-2 on remolded old LMVD silt.....510

Figure 5.124. Deviator stress vs. axial strain and pore pressure vs. axial strain relationships measured in CU test B5-4 on remolded old LMVD silt.....512

Figure 5.125. Deviator stress vs. axial strain and pore pressure vs. axial strain relationships measured in CU test B5-3 on remolded old LMVD silt.....514

Figure 5.126. Effective stress paths measured in CU tests on remolded old LMVD silt.....516

Figure 5.127. Minor principal effective stress vs. axial strain and vs. axial strain for CU test B5-1 on remolded old LMVD silt.....518

Figure 5.128. Minor principal effective stress vs. axial strain and vs. axial strain for CU test B5-2 on remolded old LMVD silt.....519

Figure 5.129. Minor principal effective stress vs. axial strain and vs. axial strain for CU test B5-4 on remolded old LMVD silt.....520

Figure 5.130. Minor principal effective stress vs. axial strain and vs. axial strain for CU test B5-3 on remolded old LMVD silt.....521

Figure 5.131. Deviator stress vs. axial strain and volumetric strain vs. axial strain relationships measured in CD tests on old LMVD silt.....523

Figure 5.132. Effective stress Mohr's circles for CD tests on remolded old LMVD silt, based on maximum deviator stress failure criterion.....525

Figure 5.133. Deviator stress vs. axial strain behavior measured in Q tests B19-1, B19-2, B19-3, and B19-4 on back pressure saturated specimens of remolded new LMVD silt.....531

Figure 5.134. Total stress Mohr's circles at 5% axial strain for Q tests B19-1, B19-2, B19-3, and B19-4 on back pressure saturated specimens of remolded new LMVD silt.....534

Figure 5.135. Total stress Mohr's circles at peak deviator stress for Q tests B19-1, B19-2, B19-3, and B19-4 on back pressure saturated specimens of remolded new LMVD silt.....535

Figure 5.136. Deviator stress vs. axial strain behavior measured in Q tests B20-1, B20-2, B20-3, and B20-4 on back pressure saturated specimens of remolded new LMVD silt.....536

Figure 5.137. Total stress Mohr's circles at 10% axial strain for Q tests B20-1, B20-2, B20-3, and B20-4 on back pressure saturated specimens of remolded new LMVD silt.....539

Figure 5.138. Total stress Mohr's circles at peak deviator stress for Q tests B20-1, B20-2, B20-3, and B20-4 on back pressure saturated specimens of remolded new LMVD silt.....540

Figure 5.139. Deviator stress vs. axial strain behavior measured in Q tests on back pressure saturated specimens of remolded new LMVD silt.....541

Figure 5.140. Deviator stress vs. axial strain behavior measured in Q tests B17-1, B19-1, and B20-1 on specimens of remolded new LMVD silt.....543

Figure 5.141. Deviator stress vs. axial strain behavior measured in Q tests B17-2, B19-2, and B20-2 on specimens of remolded new LMVD silt.....546

Figure 5.142. Deviator stress vs. axial strain behavior measured in Q tests B17-3, B18-1, B19-3, and B20-3 on specimens of remolded new LMVD silt.....548

Figure 5.143. Deviator stress vs. axial strain behavior measured in Q tests B17-4, B19-4, and B20-4 on specimens of remolded new LMVD silt.....551

Figure 5.144. Deviator stress vs. axial strain behavior measured in Q tests B17-2 and B19-1 on specimens of remolded new LMVD silt.....553

Figure 5.145. Deviator stress vs. axial strain behavior measured in Q tests B17-3, B18-1, B19-2, and B20-1 on specimens of remolded new LMVD silt.....556

Figure 5.146. Deviator stress vs. axial strain behavior measured in Q tests B17-4, B19-3, and B20-2 on specimens of remolded new LMVD silt.....559

Figure 5.147. Deviator stress vs. axial strain behavior measured in Q tests B18-2, B19-4, and B20-3 on specimens of remolded new LMVD silt.....562

Figure 5.148. Total stress Mohr's circles at 5% axial strain for Q tests B19-1, B19-2, and B19-3 on back pressure saturated specimens of remolded new LMVD silt.....565

Figure 5.149. Total stress Mohr's circles at peak deviator stress for Q tests B19-1, B19-2, and B19-3 on back pressure saturated specimens of remolded new LMVD silt.....566

Figure 6.1.	Deviator stress vs. axial strain relationships measured in Q tests in which erratic pore pressure measurements were not observed.....	584
Figure 6.2.	Change in pore pressure vs. axial strain relationships measured in Q tests in which erratic pore pressure measurements were not observed.....	585
Figure 6.3.	Total stress Mohr's circles for remolded old LMVD silt at 10% axial strain for Q tests in which erratic pore pressure measurements were not observed.....	586
Figure 6.4.	Total stress Mohr's circles at 10% axial strain for Q tests UU-12, UU-15, and UU-18 performed on remolded old LMVD silt.....	588
Figure 6.5.	Total stress Mohr's circles at 10% axial strain for Q tests UU-3, UU-10, and UU-14 performed on remolded old LMVD silt.....	589
Figure 6.6.	Change in pore pressure vs. axial strain relationships measured in Q tests performed as unconfined compression tests on specimens of remolded old LMVD silt.....	593
Figure 6.7.	Change in pore pressure vs. axial strain relationships measured in Q tests performed at a cell pressure of 10 psi on specimens of remolded old LMVD silt.....	595
Figure 6.8.	Change in pore pressure vs. axial strain relationships measured in Q tests performed at a cell pressure of 20 psi on specimens of remolded old LMVD silt.....	597

Figure 6.9. Variation of $P_a - P_w$ or suction with specimen void ratio measured prior to application of cell pressure in Q test specimens with midheight pore pressure monitoring.....601

Figure 6.10. Deviator stress vs. axial strain and change in pore pressure vs. axial strain relationships measured in Q test UU-10 performed as an unconfined compression test, on remolded old LMVD silt.....626

Figure 6.11. Void ratio vs. minor principal effective stress for Q test specimen UU-10 (Note: location of critical state line is assumed and is presented for illustrative purposes only. The actual location of the critical state line was not determined for the old LMVD silt in this research.).....627

Figure 6.12. Soil conditions considered in sampling analysis of saturated silts.....641

Figure 6.13. Undrained strength envelopes for remolded old LMVD silt, based on 9% to 10% axial strain at failure.....677

Figure 6.14. Undrained strength envelopes for remolded old LMVD silt, based on a failure criterion of less than 9% axial strain at failure.....683

Figure 6.15. Undrained strength envelopes for remolded old LMVD silt, based on the peak deviator stress failure criterion.....687

Figure 6.16. Bilinear undrained strength envelopes for remolded old LMVD silt, based on the peak deviator stress failure criterion.....689

Figure 6.17. Undrained strength envelopes for remolded new LMVD silt, based on 4.5% and 5.5% axial strain at failure.....694

Figure 6.18. Undrained strength envelope for remolded new LMVD silt, based on 10% axial strain at failure.....695

Figure 6.19. Undrained strength envelopes for remolded new LMVD silt, based on the peak deviator stress failure criterion.....699

Figure 6.20. Total stress Mohr's circles for Q tests B8-1, B8-2, and B8-4, based on 6% axial strain as the failure criterion.....700

Figure 6.21. Total stress Mohr's circles for Q tests B8-1, B8-2, and B8-4, based on 15% axial strain as the failure criterion.....701

Figure 6.22. Total stress Mohr's circles for Q tests B9-1, B9-2, and B9-4, based on 15% axial strain as the failure criterion.....703

Figure 6.23. Total stress Mohr's circles for Q tests B11-1, B11-2, B11-3, and B11-4, based on 15% axial strain as the failure criterion.....704

Figure 6.24. Schematic diagram of grain boundary sliding model proposed by Vaandrager and Pharr (1989) showing cavity formation in the liquid phase.....726

Figure 6.25. Schematic diagram of material microstructures considered by Evans and Rana (1980) for cavity formation and growth within a material.....728

Figure 6.26. Stress-strain curves for unconfined compression tests performed with midheight pore pressure monitoring on remolded old LMVD silt.....734

Figure 6.27. Schematic diagram showing a cross-section through a saturated silt along with a potential shear plane.....735

Figure 6.28. Schematic diagram showing how negative pore water pressure acts essentially equally all around the silt particle, resulting in no change in the intergranular forces between the silt particles.....737

Figure 6.29. Schematic diagram showing a cross-section through a saturated silt in which, as a result of the pore water pressure reduction which occurred during undrained shear, a gas-filled bubble has formed within the pore water along the potential shea.....738

Figure 6.30. Schematic diagram showing that once a gas-filled bubble has formed in the pore water adjacent to the silt particle, the negative pore water pressure tends to pull the silt particle away from the bubble, thereby reducing the intergranular forc.....740

Figure 6.31. Deviator stress-strain and change in pore pressure-strain relationships measured in two Q tests on remolded old LMVD silt, in which failure of the pore pressure monitoring system occurred.....746

Figure 6.32. Stress-strain curves for Q tests performed on Batch 11 of remolded old LMVD silt.....750

Figure 6.33. Stress-strain curves for Q tests performed on Batch 8 of remolded old LMVD silt.....751

Figure 6.34. Deviator stress-strain curves for Q tests on reconstituted specimens of Alaskan Silt tested by Fleming and Duncan (1990) (after dela Pena, 1991).....756

Figure 6.35. Deviator stress-strain curves for Q tests on undisturbed specimens of Yazoo silt (from Brandon, Duncan, and Huffman, 1990).....757

Figure 6.36. Deviator stress-strain curves for Q tests on remolded specimens of Yazoo silt (from Brandon, Duncan, and Huffman, 1990).....759

Figure 6.37. Deviator stress-strain curves for Q tests on remolded specimens of LMVD silt (from Brandon, Duncan, and Huffman, 1990).....760

Figure 6.38. Deviator stress-strain curves for Q tests on undisturbed samples of Gray silt, West Williamson L.P.P. Pump Station (Sample UD-101-S2-A), tested by Duncan and Sehn (1987) (after dela Pena, 1991).....762

Figure 6.39. Deviator stress-strain curves for Q tests on undisturbed samples of Brown silt, West Williamson L.P.P. Pump Station (Sample UD-85-4-9), tested by Duncan and Sehn (1987) (after dela Pena, 1991).....763

Figure 6.40. Deviator stress-strain curves for Q tests on undisturbed samples of Brown silt, West Williamson L.P.P. Pump Station (Sample UD-85-4-11B), tested by Duncan and Sehn (1987) (after dela Pena, 1991).....764

Chapter 1

INTRODUCTION

The undrained shear strength of saturated, fine-grained soils is often used in performing geotechnical engineering analyses. Saturated silts of low plasticity are fine-grained soils that are often encountered on geotechnical engineering projects. Their engineering properties and undrained behavior, however, are not very well understood. Because of this, the presence of silts often causes difficulty for practicing geotechnical engineers. Recent studies (Torrey, 1982; Fleming and Duncan, 1990; Brandon, Duncan, and Huffman, 1990) have provided an improved understanding of silt behavior, but important questions concerning the fundamental behavioral characteristics still remain unanswered.

Undrained strength tests performed on saturated silts often show considerable scatter, making the selection and interpretation of the results a difficult task for engineers. A study of the shear strength of silt sponsored by the Corps of Engineers (Brandon, Duncan, and Huffman, 1990) suggested that the scatter often observed in the measured undrained strengths of silt specimens determined by

Q(*) tests may be due to cavitation, or the formation of bubbles of water vapor and air within the pores of the soil. The formation and growth of bubbles could be the result of the decrease in pore pressure which occurs during undrained shear. This is believed to be a problem unique to silts. Although cavitation may occur in sands, conventional Q tests are not performed on sands, and undrained strengths are not often used in analyses. Cavitation does not appear to be an issue for clays due to the small pore size.

1.1 Research Objectives

The objectives of this research were to investigate more fully the phenomenon of cavitation and its possible influence on the erratic behavior of saturated silts often observed in Q tests.

Based on the work of Brandon, Duncan, and Huffman (1990), the research performed was directed at exploring the following questions:

- 1.) What is the magnitude of the pore water pressure reduction which occurs during Q tests on saturated silts?

(*) For convenience, symbols and abbreviations are listed in the Notation (Appendix A).

- 2.) What is the rate at which air comes out of solution from the pore water of a soil specimen?
- 3.) Is cavitation or air coming out of solution from pore water a feasible explanation for the observed behavior of saturated silts in Q tests?
- 4.) If cavitation of pore water is found to be an influence on the erratic behavior of saturated silt Q test specimens, what is the best way to perform and interpret the results of such tests for use in engineering analysis and design?

1.2 Organization of Dissertation

The following chapters of this dissertation discuss the various findings of this research regarding cavitation and its possible influence on the engineering behavior of silts.

Chapter 2 discusses the behavior expected for undrained tests on saturated soils and how the behavior which is often observed for saturated silts deviates from this expected behavior.

Chapter 3 presents a review of the cavitation literature and its applications to soil behavior.

Chapter 4 reviews the geotechnical literature on pore air - pore water systems. Additional information from the

literature on the solubility of air in water, the dissolved gas content of ground water, and the rate at which air goes into or comes out of solution in water is also presented.

Chapter 5 presents the results of laboratory tests performed on silts in this study.

Chapter 6 analyzes and discusses the results of the laboratory tests and applies the information presented in Chapter 4 to the tests performed on silts in this research. Also discussed are the limitations of the information presented in Chapter 4, relative to the laboratory test results. The influence of the formation and growth of bubbles within the soil pores on the observed stress-strain behavior of the soil is also considered.

Chapter 7 presents the summary and conclusions from this research, and recommendations for further study.

Chapter 2

UNDRAINED BEHAVIOR OF SATURATED SOILS

2.1 Introduction

The behavior of saturated soils tested in undrained tests has been studied to a considerable extent and generally yields a well-understood and expected behavior. During undrained shear, changes in pore water pressure occur within saturated soil specimens. These changes in pore pressure are developed as a result of the volume change characteristics of the soil during shear. The pore pressures which develop can be positive or negative, relative to the initial pore water pressure, depending on whether the soil is loose with a tendency to contract or dense with a tendency to expand during undrained shear. The increase or decrease in pore pressure which occurs will influence the effective confining pressure acting on the specimen, which in turn, will affect the measured shear strength of the soil. If a group of specimens have the same void ratio initially, the change in pore pressure developed during undrained shear should be the same for all of the specimens in the group, regardless of the cell pressure used in the test. As a result of this, the measured shear

strength of the soil should be the same for all of the specimens in the group (Bishop and Eldin, 1950).

Theoretically, this should be true for all soils, whether or not they experience an increase or decrease in pore water pressure during undrained shear. The erratic behavior often observed in undrained tests on saturated silts, however, may very well be a result of the dilatant behavior and decrease in pore water pressure which occurs during the tests. Loose soils attempt to contract during undrained shear and therefore experience an increase in pore water pressure. Dense silts attempt to dilate or expand during undrained shear. This results in a decrease in pore water pressure. One of the main factors which must be considered is that water subjected to negative pressure or tension exhibits different behavior than water which experiences an increase in pressure or is placed in compression.

2.2 Expected vs. Observed Behavior of Saturated Soils in Q Tests

For a saturated soil tested in an unconsolidated-undrained (UU or Q) triaxial test, an angle of shearing resistance or undrained friction angle, ϕ_u , equal to zero should be obtained. According to Bishop and Eldin (1950), this is the result of three principles:

- (1) The strength of soil is governed completely by the intergranular forces,
- (2) The contact area between soil grains is very small, so that the pore water pressure acts on virtually the entire surfaces of the soil grains, and therefore, positive or negative changes in the pore water pressure do not influence the intergranular forces, and
- (3) As a result of water being incompressible compared to the soil structure, changes in cell pressure are carried wholly by the pore water. If no drainage is allowed, the stresses in the soil structure do not change due to the different cell pressures used in the tests.

Under these conditions, a series of Q tests performed on a group of saturated soil specimens at the same void ratio should result in a strength independent of confining pressure. The Mohr-Coulomb failure envelope obtained for the soil should be characterized by a $\phi_u = 0$, $S_u = c$ condition, as shown in Figure 2.1. For the tests on silt shown in Figure 2.2, however, the undrained friction angle, ϕ_u , is considerably greater than zero.

Golder and Skempton (1948) studied the shear strength of saturated cohesive soils in unconsolidated-undrained (Q) triaxial tests. For both soft and stiff fully saturated

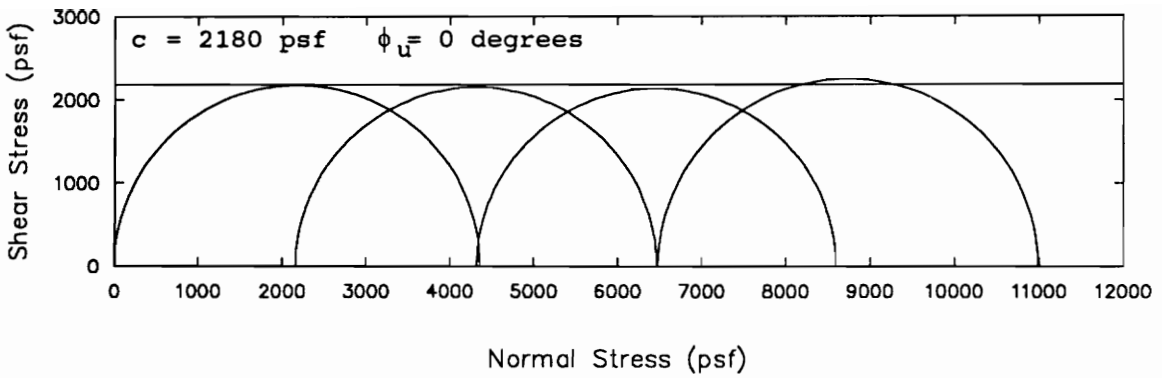


Figure 2.1. Total stress Mohr-Coulomb failure envelope for Q tests conducted on saturated clay (after Golder and Skempton, 1948)

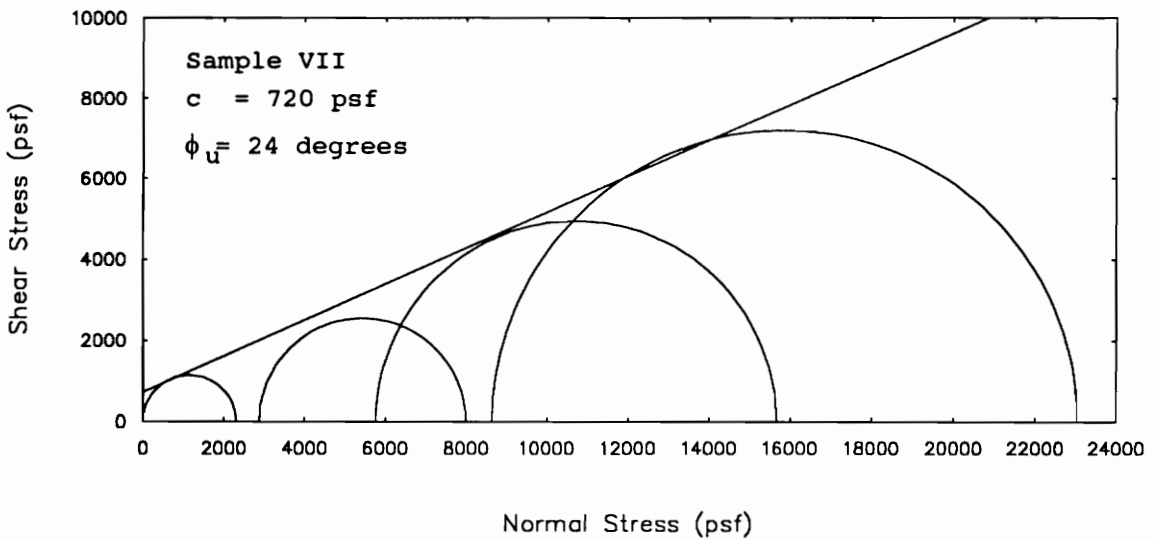


Figure 2.2. Total stress Mohr-Coulomb failure envelope for Q tests conducted on saturated silt (after Golder and Skempton, 1948)

clays, they found that the angle of shearing resistance of the soil was equal to zero for all practical purposes.

For some saturated silts, however, the angle of shearing resistance of the soil in Q tests was found to be significantly greater than zero. Golder and Skempton (1948) attributed this to the dilatant behavior of silts. They proposed that the tendency for dilation under undrained conditions lead to a decrease in pore water pressure within the specimens. This resulted in a corresponding increase in effective stress within the specimens and the measured strength of the soil increased with increasing cell pressure. They did not state what criterion was used to define failure nor did they present stress-strain curves for the tests. They noted that all of the silts tested had liquid limits below 35. Further review of their results shows that the silts studied had plasticity indices between 4 and 23. The liquidity indices of the silt specimens tested in the Q tests ranged between 0.1 and 0.5, indicating that the water contents of the silt specimens were generally closer to their plastic limits than their liquid limits.

Bishop and Eldin (1950) studied the shear strength of soils as determined from undrained triaxial tests on saturated samples. From their study, they concluded that, in general, the undrained friction angle of a saturated soil

determined from a series of unconsolidated-undrained tests should be too small to measure and should therefore be essentially zero for all soils, including those with dilatant tendencies. They recognized, however, that for certain soils which appeared to be fully saturated, appreciable undrained friction angles could be measured under certain conditions.

According to Bishop and Eldin (1950), one such condition would arise if the soil contained amounts of air too small to be detected. This situation might result from formation of air bubbles or voids in the pore water of the specimen as the in-situ stresses were released during sampling. As the pore pressure decreased during sampling, air might come out of solution in the pore water, in accordance with Henry's law. If Q tests were performed on these samples at low cell pressures, the presence of the air bubbles could result in undrained friction angles greater than zero.

A second condition noted by Bishop and Eldin (1950), would occur if the soil sample had a tendency to dilate during shear, thereby leading to a reduction in pore water pressure within the specimen. The decrease in pore water pressure during shear could also lead to air coming out of solution from the pore water, in accordance with Henry's

law. Even if the pore water contained no dissolved gases, if a large enough decrease in pore pressure occurred, cavitation of the pore water could take place. The formation of vapor filled cavities within the pores of the soil would result in the sample being less than fully saturated, and undrained friction angles greater than zero. This behavior is characterized by the pore pressure-strain relationship shown in Figure 2.3.

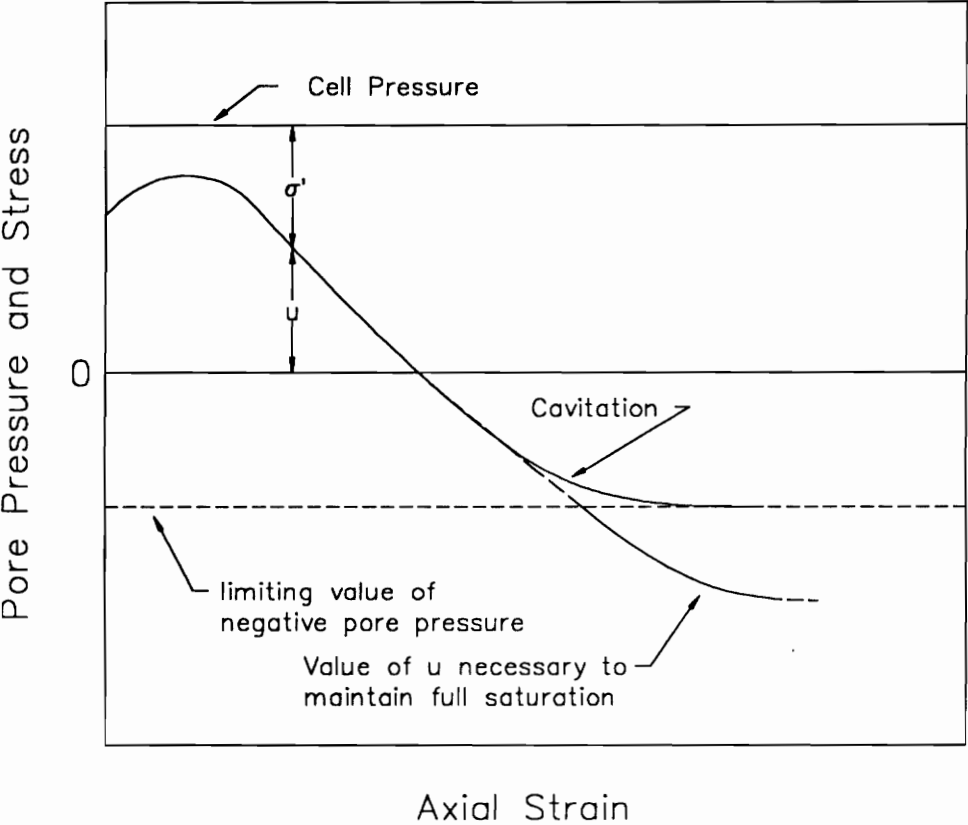


Figure 2.3. Pore pressure-strain relationship for a soil with a tendency for dilation (after Bishop and Eldin, 1950)

Odenstad (1948) stated that for dilatant soils tested in undrained shear, as a triaxial specimen experiences increasing axial strain, a decrease in pore water pressure occurs and the deviator stress increases or strain-hardening occurs. He noted that this strengthening would continue until either:

- (1) The strength of the solid grains had been reached and particle breakage occurred, or
- (2) The decrease in pore water pressure reached its limiting value and cavitation of the pore water took place.

Bishop and Eldin (1953) found that in specimens which had a strong tendency to dilate, an undrained friction angle, ϕ_u , of zero could be obtained for a series of tests on sand samples with similar initial void ratios tested at different cell pressures as long as:

- (1) The samples were initially fully saturated, and
- (2) The negative pore water pressures which developed during shear were not large enough for cavitation to occur.

They found that in order to avoid the large negative pore pressures which developed during undrained shear, after consolidating the specimens to the desired consolidation pressure, it was necessary to increase the cell pressure to

a value large enough to prevent cavitation from occurring. The increase in cell pressure increased the pore water pressure within the saturated specimens by an equal amount. The increased pore water pressure counteracted the decrease in pore water pressure which occurred during undrained shear, such that the pore water did not cavitate. Above a certain limiting cell pressure, a series of tests on fully saturated specimens yielded a $\phi_u = 0$, $S_u = c$ failure envelope. Below this limiting cell pressure, cavitation of the pore water took place and a series of undrained tests on the soil did not yield a $\phi_u = 0$ failure envelope. As long as the cell pressure was above the limiting value, the magnitude of the cell pressure used in the test had no influence on the effective stresses in the sample or the measured undrained shear strength.

In undrained triaxial tests on a fine, saturated sand, Nash (1953) noted that if even a small amount of air was present in the triaxial specimen or pore pressure monitoring system, it could have a considerable effect on the test results. In order to avoid this situation, he boiled the saturated sand in order to remove dissolved air from the soil pore water. He also formed his specimens by placing the soil slurry into the rubber membrane in a split mold within the triaxial cell. This procedure reduced the possibility of trapping air at the specimen-membrane

interface. Once the specimens were formed, he consolidated them to the same consolidation pressure. An increase in cell pressure was then applied undrained and the specimens were sheared.

Nash (1953) observed that the dense sand specimens tested showed a slight increase in pore water pressure initially, followed by a decrease in pore water pressure with further strain. He considered the tests to be complete when the pore water pressure had become constant. He noted that in a dilatant soil, when the pore water pressure stops decreasing, the maximum deviator stress will be reached for the soil. He added, however, that if the pore water pressure decreases to about -14.7 psi or zero absolute pressure, the pore water "boils" or cavitation occurs. Once cavitation of the pore water takes place, no further increase in strength is possible.

Similar to Bishop and Eldin (1953), Nash (1953) noted that for dense specimens of saturated, fine sand tested in undrained tests, after consolidation was complete, a large increase in cell pressure had to be applied to the specimen undrained. This high cell pressure was necessary so that the sample could reach its peak strength without cavitation of the soil pore water taking place. His test results indicated that when lower cell pressures were used, the pore

water in dense specimens tended to experience cavitation, resulting in lower peak strengths being measured for the soil.

Nash (1953) concluded that for dense sands which may have the tendency for considerable dilation during undrained shear, high cell pressures are necessary in undrained tests if triaxial specimens are to mobilize their full strength without cavitation of the pore water occurring.

The undrained tests performed by Nash (1953) indicated that when cavitation of the pore water did not occur, a peak in the deviator stress-strain curve was reached but not until very high strains. In addition, for undrained shear, the peak strength determined by the maximum principal stress ratio at failure occurred at a lower axial strain than the strength obtained by the maximum deviator stress. For one dense specimen tested in which cavitation did not occur, the peak deviator stress occurred at an axial strain of about 35%, whereas the maximum principal stress ratio occurred at only about 10% axial strain.

Penman (1953) performed undrained triaxial tests on a saturated silt. The tests were performed at a strain rate of about 1% per minute and pore water pressures were measured during the tests. The saturated silt specimens were prepared in the laboratory by placing a silt slurry

into a triaxial membrane within a split-mold while applying a vacuum to the base of the specimen. Prior to placing the silt into the mold, the slurry was subjected to a vacuum to remove dissolved air from the pore water. Forming the specimens from a deaired slurry within the triaxial membrane reduced the possibility of trapping air pockets within the pore water as well as at the specimen-membrane interface, which, as will be discussed in Chapter 6, may have an effect on the behavior observed in tests on trimmed specimens.

Penman (1953) was able to vary the density of the specimens by using different magnitudes of suction and rodding the silt slurry to different extents during specimen formation. He found that the dilatancy of silt specimens increased as the void ratio of the specimens decreased.

The undrained test specimens were isotropically consolidated to 5 psi. After consolidation was complete, the cell pressure was increased under undrained conditions to the particular value for that test. The increase in cell pressure under undrained conditions lead to a corresponding increase in the pore water pressure, which was used as an indication of full saturation. Samples which appeared to be less than fully saturated were rejected.

For undrained tests on dilatant silts, Penman (1953) observed that in tests performed at low cell pressures, if

the pore pressure decreased to about -14 psi, "gas [was] drawn out of the pore water." He noted that this would have resulted in the expansion of the specimen so that its volume would no longer be constant and the soil would therefore fail at a lower strength than expected for its initial void ratio.

Similar to Bishop and Eldin (1953), Penman (1953) observed that in a series of undrained tests on samples with the same void ratio but performed at different cell pressures, a critical cell pressure existed above which the soil behaved as a $\phi_u = 0$, $S_u = c$ material. Below the critical cell pressure, the attempted dilation of the silt during shear resulted in the pore water pressure decreasing to -14 psi at which point cavitation occurred. This resulted in the silt behaving as a $\phi_u > 0$ material.

Penman (1953) stated that as long as the cell pressure used in the test was large enough to prevent cavitation of the pore water, the magnitude of the cell pressure had no influence on the magnitude of the pore pressure reduction which occurred in the test. The cell pressure, therefore, had no influence on the minor principal effective stress which governs the strength of the silt. Under these conditions, the silt was observed to behave as a frictionless material and a $\phi_u = 0$, $S_u = c$ Mohr-Coulomb

failure envelope was obtained. The maximum deviator stress used in obtaining the failure envelope for tests in which cavitation did not occur, however, was not reached until the specimens had undergone axial strains on the order of 28%.

Penman (1953) found that when the cell pressure was too low to prevent cavitation of the pore water from taking place, the effective stress was directly proportional to the total stress. In this case, the silt behaved as a frictional material with respect to total stresses. The test results therefore yielded a $\phi_u > 0$ Mohr-Coulomb failure envelope.

This behavior is shown in Figure 2.4 for the Braehead silt tested by Penman (1953). As can be seen from Figure 2.4, for the given soil at the given void ratio, when the cell pressure used in the tests was above 65 psi, the strength of the soil remained constant and a $\phi_u = 0$ failure envelope resulted. For tests performed at cell pressures below 65 psi, the strength of the soil varied with cell pressure, as characterized by the $\phi_u > 0$ failure envelope obtained.

For a different initial void ratio, the critical cell pressure would have been different than 65 psi. A denser specimen with a lower void ratio would have likely required a higher critical cell pressure in order to prevent

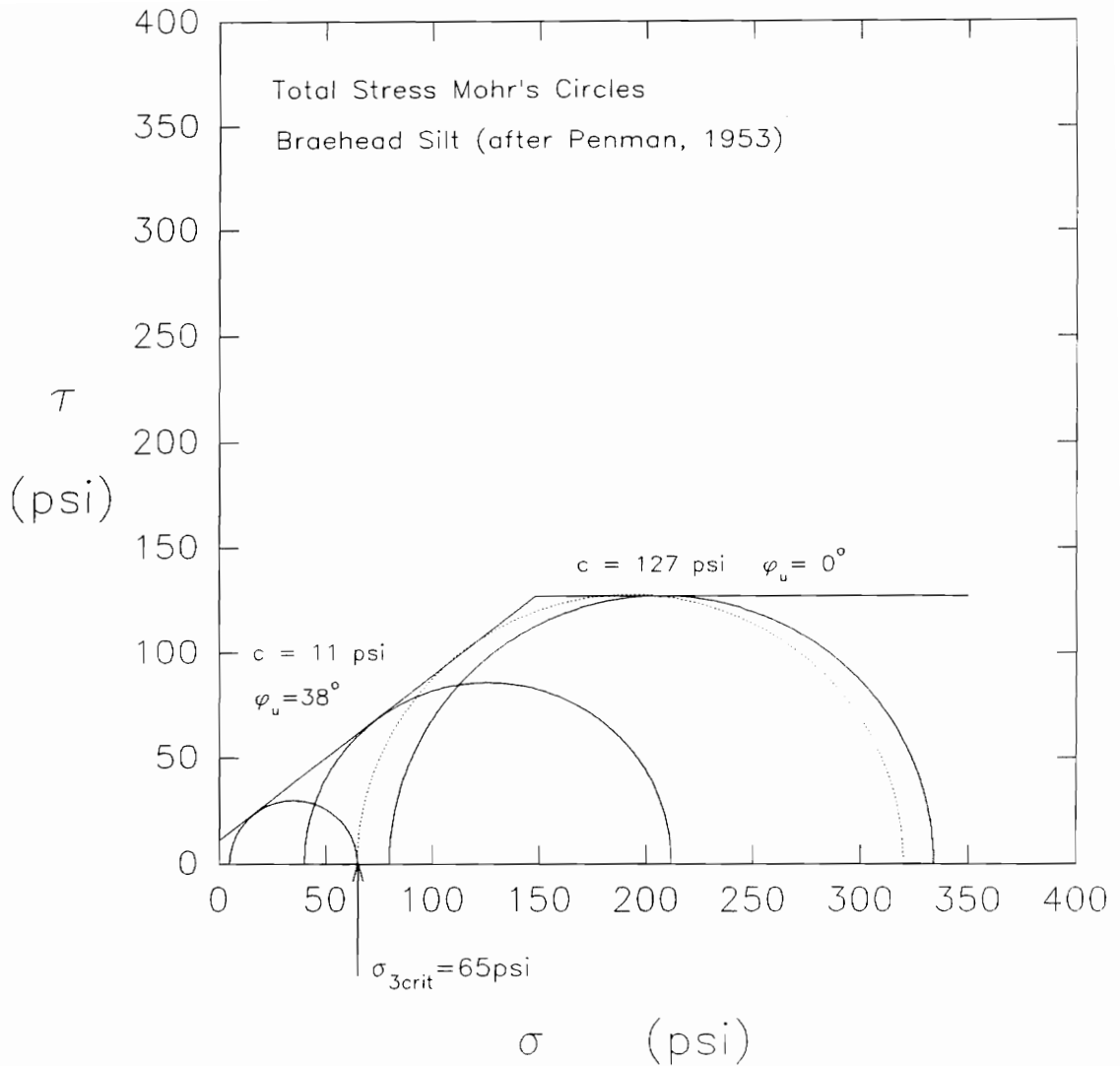


Figure 2.4. Total stress Mohr's circles for undrained tests (after Penman, 1953)

cavitation from occurring, due to the increased dilatant tendency of the denser specimen. On the other hand, a looser specimen with a higher void ratio would have had a smaller tendency to dilate. It would therefore develop a smaller decrease in pore water pressure during shear and would have required a lower critical cell pressure to prevent cavitation.

Schultze and Horn (1965) compared the behavior of saturated silts in drained and undrained tests. They found that in drained tests where the change in pore water pressure was zero throughout the tests, failure of the soil occurred when the volumetric strain, $\Delta V/V$, the deviator stress, $(\sigma_1 - \sigma_3)$, and the principal stress ratio, σ'_1/σ'_3 , were all at their maximum values, so that the failure point could be considered unique.

In the undrained tests, sample failure was observed when the deviator stress, $(\sigma_1 - \sigma_3)$, reached its maximum value. This generally occurred at large strains, usually greater than 30%. In the undrained tests, when $(\sigma_1 - \sigma_3)$ was at its maximum value, the pore water pressure in the specimen was not zero. In addition, the maximum principal stress ratio, σ'_1/σ'_3 , was observed at a lower axial strain than the maximum deviator stress, $(\sigma_1 - \sigma_3)_{\max}$.

Seed and Lee (1967) considered the undrained strength characteristics of saturated soils. They studied the undrained behavior of cohesionless soils using the critical void ratio and critical confining pressure concepts. According to Seed and Lee (1967), the critical confining pressure is the confining pressure for which a sample of granular soil will exhibit no volume change at failure during shear. It tends to be higher for soils which are strongly dilatant (silts) than for soils which are not. They stated that the soils which are most strongly dilatant are dense cohesionless materials and soils with very sound, rounded grains.

According to Seed and Lee (1967), for a saturated sand tested in an undrained test at a confining pressure below the critical confining pressure, the sample would tend to dilate during loading and this would result in a decrease in pore water pressure and a corresponding increase in the effective confining pressure. The pore water pressure in the specimen would continue to decrease until one of two limiting conditions occurred:

- (1) The effective confining pressure reached the critical confining pressure of the soil at which point no further change in pore pressure would occur and the sample would fail with the effective confining pressure equal to the critical confining pressure, or

(2) Prior to the effective confining pressure reaching the critical confining pressure, the pore water pressure would decrease to a value of about -1 atmosphere, at which point cavitation of the pore water would occur.

Similar to other researchers who have studied the behavior of silts, Börgesson (1981) noted that failure of a silt defined by maximum deviator stress usually occurs only after large deformations have taken place.

Because of the difficulties involved in determining the undrained shear strength of dilatant silts, the Corps of Engineers (Torrey, 1982) has examined the selection of certain undrained shear strength parameters for these soils. The study performed by Torrey (1982) addressed the total stress interpretation of \bar{R} tests and did not consider the interpretation of Q test results on saturated silts.

For \bar{R} or CU tests on dilatant silts, Torrey (1982) recommended that failure be taken as the point during the test when the change in pore water pressure is equal to zero. Initially in a CU test on a saturated dilatant silt, the pore water pressure will increase slightly. With further strain, however, the specimen will attempt to dilate and a decrease in pore water pressure will occur. When the pore water pressure has increased and then decreased back to its initial value at the start of the test, the change in

pore water pressure will be zero, and the deviator stress corresponding to this condition should be used in determining the undrained strength of the soil.

According to Torrey (1982), the reasoning behind this recommendation is that in the field, the additional decrease in pore water pressure which develops with further strain will eventually dissipate over time so that zero change in pore water pressure will ultimately occur. The strength the soil gains from the negative change in pore pressure will be lost once the negative pore water pressures dissipate. Thus, using the point at which the change in pore water pressure is zero as a failure criterion, is a conservative approach to interpreting the undrained strength of a dilatant soil.

Torrey (1982) indicated that for saturated clays, where drainage occurs more slowly than in silts, it seems realistic to consider short-term stability in terms of undrained strengths. For saturated silts, however, drainage can possibly occur at a rate rapid enough so that using the drained strength for both short- and long-term stability, may be a realistic and reasonable approach. This failure criterion, however, can not be readily applied to Q tests because pore water pressures are not measured in Q tests.

Torrey (1982) stated that the pore water pressure in a laboratory sample of a dilatant soil will continue to decrease as long as the sample has sufficient back pressure. He added that a peak deviator stress does not occur unless the decrease in pore water pressure leads to desaturation of the specimen. If the decrease in pore water pressure which occurs during shear eliminates the back pressure initially in the specimen, air will come out of solution from the pore water. He noted that another possibility that could occur is if the pore water pressure reaches a gage pressure of -1 atmosphere or zero absolute, cavitation of the pore water will take place.

Torrey (1982) noted that if air comes out of solution from the pore water or cavitation occurs, a peak in the deviator stress-strain curve will result. He emphasized, however, that it would be incorrect to use this peak deviator stress as the strength of the soil. This tends to imply that Torrey (1982) does not consider cavitation of soil pore water to be a possibility in the field, but rather only a problem encountered in laboratory tests.

Torrey (1982) noted that for \bar{R} test specimens consolidated to different consolidation pressures, defining failure by some limiting strain such as 10 or 15%, would yield different magnitudes of the change in pore water

pressure at failure for each specimen. He stated that these "unrelated" total stress Mohr's circles from \bar{R} tests can not be used to define the failure envelope for the soil. Such a failure envelope would not represent the behavior of the soil in an accurate and consistent way.

Torrey's (1982) recommendations seem to be a reasonable approach to use for saturated dilatant silts subjected to loading conditions for which \bar{R} tests are applicable (i.e., soils consolidated prior to undrained loading). For conditions where the loading is applied at a rapid enough rate that saturated silts can not consolidate to the new effective stresses imposed, \bar{R} tests are not applicable and Q tests must be used. In Q tests, however, pore pressures are not usually measured and Torrey's (1982) recommendations can not be applied. Another method is necessary for interpreting the strengths obtained from Q tests on saturated dilatant silts.

Ladd et al. (1985) stated that the attempted dilation of saturated silts tested in undrained tests results in a decrease in pore water pressure and a corresponding increase in effective stress. The increase in effective stress gives the soil increased shear strength with increasing strain. They noted that the strengthening of the soil with

increasing strain makes it difficult to select an appropriate value of undrained shear strength for the soil.

Axelsson et al. (1989) stated that in many consolidated-undrained tests on saturated silts, no peak deviator stress occurs even at strains of up to 15%. This results from the strain-hardening caused by the development of negative pore water pressures within the specimens.

Fleming and Duncan (1990) performed an extensive series of undrained triaxial tests on reconstituted samples of Alaskan silts. They stated that the strength-deformation characteristics of silts are quite different from those of clays. Unlike normally consolidated clays, normally consolidated silts tend to dilate upon shearing. For both IC-U and AC-U tests the pore pressures increased to a peak value and then gradually decreased with increasing strain. Because of the decreasing pore water pressure, the specimen becomes stronger so that the deviator stress increases continually with increasing strain. As a result, no unique value of undrained shear strength is obtained for a dilatant silt.

In their study, Fleming and Duncan used the deviator stress of the silt at 15% axial strain to determine the undrained shear strength of the soil. They chose 15% as the

strain at failure because it represented a reasonable performance limit for many engineering purposes.

Fleming and Duncan (1990) stated that their test results indicated that sample disturbance and stress release can have a very appreciable effect on the undrained strength of silt specimens measured in the laboratory. They stated that UU test results may give strengths that are lower than the actual in-situ strength. Whereas, CU tests, in which samples are reconsolidated in the laboratory and then tested, give undrained strength values that are higher than the in-situ strength. Even undisturbed samples reconsolidated in the lab to in-situ stresses give strengths greater than in-situ strengths. They concluded that sample disturbance should be minimized in order to obtain reliable estimates of the shear strength of saturated silts. They also found that there was considerable scatter in the strengths measured in UU tests on undisturbed specimens.

In addition, they noted that the densities of silts, unlike those of clay, are not uniquely controlled by their consolidation pressures and consolidation stress histories. The densities of many silts can be influenced by vibrations. Over time the effects of individual vibration events can accumulate to alter the density of the soil considerably.

Fleming and Duncan (1990) noted several characteristics of silt behavior as follows:

- (1) Silt samples are much more easily disturbed than clays,
- (2) The undrained strengths of silts are likely to be more seriously affected by disturbance than are those of clays,
- (3) Efforts to minimize disturbance are important in testing silts,
- (4) For the silts tested, strength anisotropy was observed to be significant, and
- (5) Strength loss due to creep was found to be very small for silts as compared to clays.

Based on their investigation, Fleming and Duncan (1990) concluded that silts generally fall into two categories:

- (1) Silts located at the coarse end of the silt spectrum can be expected to behave like a fine sand. They will be more likely to densify due to vibrations, and will be difficult or impossible to characterize using normalized strength concepts.
- (2) Silts located at the fine end of the silt spectrum will likely behave similar to a clay. They will probably not be influenced by short-term vibrations, and can possibly be characterized using normalized strength concepts. The normalized strength values, however, can show considerable variation from one silt to another.

As a result, individual analysis of the normalized strength would have to be performed for each different silt deposit.

Brandon, Duncan and Huffman (1990) performed an additional study of the undrained behavior of saturated silts. Their study involved laboratory testing of both undisturbed and remolded specimens of saturated silt. They stated that problems are often encountered in evaluating the undrained shear strength of silts. Saturated silts tested in Q tests often give erratic and unreliable results. The dilatant tendencies of low plasticity silts make it difficult to define failure in undrained tests. They added that dilatant silts may experience desaturation in \bar{R} tests during shear.

Their study reemphasized several important aspects regarding the testing of silts in the laboratory:

- (1) Silt specimens can be disturbed very easily during sampling and normal laboratory handling procedures,
- (2) During sampling, the negative pore water pressures which develop within silt specimens are generally less than those which develop in clays, making silt specimens more difficult to trim and test in the lab,
- (3) Silts tend to experience greater compression under static pressure than sands, and

(4) Silts are much more likely to densify due to vibrations than are clays.

Brandon, Duncan and Huffman (1990) discussed the effect of disturbance on silt behavior. They stated that sample disturbance tends to increase the pore water pressure in the soil. This increase in pore water pressure results in a decrease in the initial effective stress in the specimen. They added that the effective stress in the specimen after sampling will always be less than the perfect sampling effective stress (Ladd and Lambe, 1963), due to disturbance.

Brandon, Duncan and Huffman (1990) noted that in unconfined compression tests and Q tests at low cell pressures on saturated silts, cavitation of soil pore water can occur prior to a peak deviator stress being reached in the tests. Neglecting the effect of disturbance, if cavitation occurs, the undrained shear strength of the soil will be less than if cavitation did not occur.

When disturbance effects are considered, Brandon, Duncan and Huffman (1990) noted that it may have two possible influences on the behavior of the soil:

- (1) Disturbance will lead to an increase in the initial pore water pressure in the specimen which could result in cavitation occurring at a higher strain, and

- (2) Disturbance will cause densification of the specimen which gives the sample a greater tendency to dilate during shear, suggesting that cavitation will occur at a lower strain.

They postulated that the increased pore water pressure and increased density which result from disturbance may have counteracting influences on the possible occurrence of cavitation of the soil pore water.

Brandon, Duncan and Huffman (1990) compared the strength of saturated dilatant silts obtained using various failure criteria. They noted that the maximum deviator stress, which is a very common failure criterion, often does not occur within a reasonable range of strains for dilatant soils. In undrained tests on many dilatant soils, a maximum deviator stress does not occur until axial strains of 30% or greater have been reached. They stated that within the range of strains considered reasonable for most geotechnical applications, the sample never really "fails." This continuously dilatant behavior makes the selection of a consistent and reliable failure criterion difficult for engineers working with dilatant silts.

They added that dilatant soils often do not reach a peak deviator stress until high axial strains due to the strain-hardening behavior resulting from the dilatant

tendencies of the soil. As the sample attempts to dilate under undrained conditions, the pore water pressure decreases, the effective confining pressure increases and the sample becomes stronger. This hardening effect results in a peak deviator stress not being reached until very high axial strains (Brandon, Duncan and Huffman, 1990).

Brandon, Duncan and Huffman (1990) noted that at strains greater than 15%, triaxial specimens tend to be very deformed. Area corrections applied to such specimens can have a significant effect on the subsequent stress computations. In most engineering applications, large strains are not tolerable. They added, however, that it is difficult to correlate field displacements to axial strains measured in laboratory tests.

Another failure criterion considered by Brandon, Duncan and Huffman (1990) is the maximum principal stress ratio. This failure criterion is based on effective stresses, however, so it is not applicable to Q tests in which pore pressures are not measured. They noted that in \bar{R} tests on saturated dilatant silts, the maximum principal stress ratio often occurs at axial strains of less than 8%. They added that this may be a reasonable failure criterion in situations where pore water pressures and effective stresses

are known. It tends to lead to conservative values of shear strength for the soil.

Brandon, Duncan and Huffman (1990) also considered the $\bar{A} = 0$ or change in pore pressure equal to zero, failure criterion proposed by Torrey (1982). They stated that this failure criterion is only applicable to \bar{R} tests. In S or consolidated-drained triaxial tests, the change in pore water pressure is zero throughout the test. In Q tests, pore pressures are not measured. They noted that the advantage of this failure criterion is that the strength of the soil is not dependent on the hardening effect resulting from the development of negative pore water pressures. A disadvantage that they identified is that for some soils in certain field applications, \bar{A} may not reach zero until the soil has reached high strains.

For \bar{R} tests, Brandon, Duncan and Huffman (1990) stated that the point at which the stress path reaches the K_f -line is often applied as a failure criterion. In dilatant soils, the stress path measured in \bar{R} tests clearly defines the K_f -line.

The use of a limiting strain may also be used as a failure criterion for dilatant soils. Brandon, Duncan and Huffman (1990) noted that this criterion can be applied to Q, \bar{R} , and S tests. They added that it is usually applied

to Q tests when a peak deviator stress does not occur within a reasonable amount of strain. They stated that the values of the limiting strain at failure used for dilatant silts vary from 5 to 15% in the literature. A problem with using a limiting strain as a failure criterion is that it is difficult to estimate the appropriate magnitude of strain at failure for a given loading condition in the field. Because of this, Brandon, Duncan and Huffman (1990) concluded that this is "a rather subjective failure criterion."

Brandon, Duncan and Huffman (1990) discussed the possible loss of saturation that dilatant, low-plasticity silts can experience during undrained shear. Soil specimens tested in \bar{R} tests are usually back pressure saturated. Back pressure is used in the tests to improve the accuracy of the pore pressure measurements in the tests, as well as to prevent cavitation of the pore water. The application of back pressure to a soil specimen leads to saturation of the specimen by compressing the air present and forcing this air into solution in the pore water.

Brandon, Duncan and Huffman (1990) stated that when the change in pore water pressure developed in an undrained triaxial test returns to zero ($\bar{A}=0$), the pore water pressure in the specimen will be equal to the back pressure used in the saturation process. As the pore pressure

continues to decrease with increasing strain, the benefits gained by using the back pressure to saturate the specimen, begin to diminish. As this occurs, air forced into solution during the back pressure saturation process, can begin to come back out of solution. In this situation, the volume of the specimen increases, and the accuracy of the pore water pressure measurements decreases. They noted that a solution to this problem is to use a back pressure higher than that needed to saturate the specimen.

Brandon, Duncan and Huffman (1990) stated that in \bar{R} tests on saturated dilatant silts, high back pressures are often used to prevent cavitation from occurring. They noted that in field conditions where the hydrostatic pore pressure is low, cavitation of soil pore water may occur under undrained loading conditions. If cavitation of soil pore water can occur in the field, an undisturbed sample of soil tested in the laboratory with a back pressure higher than its in-situ hydrostatic pressure, will yield an undrained strength that is higher than the actual field strength. This is because the pore water in the laboratory sample does not cavitate due to the high back pressure while the pore water in-situ has the potential to cavitate.

Brandon, Duncan and Huffman (1990) noted that in the \bar{R} tests they performed on saturated dilatant silts, the

specimens experienced large decreases in pore water pressure. They added that cavitation of the pore water would have occurred in the tests if they had not used large enough back pressures.

In the Q tests they performed, Brandon, Duncan and Huffman (1990) observed that the maximum deviator stress always occurred at axial strains of 13% or greater. Because of this, using a failure criterion of 10% axial strain resulted in an undrained shear strength, S_u , of the soil which was conservative, relative to the maximum deviator stress failure criterion.

They noted that the deviator stress-strain curves for the silts tested were very different for the Q tests, as compared to those for the \bar{R} tests. They suspected that the differences in the observed stress-strain behavior were due to differences in the pore water pressures developed during the tests. They concluded that the undrained behavior of saturated dilatant silts in Q tests is different than their behavior in \bar{R} tests. They stated that "if Q test specimens behaved like the \bar{R} specimens, the undrained shear strengths measured [in the Q tests] would have been much greater." They suggested that the differences in the observed behaviors may possibly be due to gas coming out of solution from the pore water at pressures above -14.7 psi in the Q

tests. The high back pressures used in the \bar{R} tests would have prevented this. Another possibility which they identified as a possible cause of the differences in behavior is disturbance. Samples with different levels of disturbance will likely exhibit different stress-strain behaviors.

Brandon, Duncan and Huffman (1990) stated that the effective stress friction angle, ϕ' , of dilatant silts is relatively insensitive to the failure criterion used. The undrained shear strength, S_u , however, is very dependent on the particular failure criterion used. The undrained shear strength varies with strain and increases with increasing strain. They noted that the dependence of S_u on strain is secondary. The undrained shear strength, S_u , is really dependent on the pore water pressures generated during shear. This means that S_u is dependent on the pore pressure parameter \bar{A} of a given test specimen.

They noted that when S_u is determined from \bar{R} tests using $\bar{A}=0$ as a failure criterion, there is generally less scatter in the values of S_u . They stated that the lower the value of \bar{A} , the less influence the choice of failure criterion has on the value obtained for S_u . They added that the use of the pore pressure parameter \bar{A} as a failure criterion could be useful in determining the undrained shear

strength, S_u , for dilatant, low-plasticity silts. This is only useful, however, where the pore pressure parameter, \bar{A} , is known, as in undrained tests where pore pressures are measured. It can not be directly applied to conventional Q tests.

Although cavitation or air coming out of solution from soil pore water has been observed in undrained tests on saturated dilatant sands and silts, heavily overconsolidated clays, which also exhibit dilatant tendencies, have not been known to exhibit similar behavior (Golder and Skempton, 1948; Bishop and Eldin, 1950). Studies performed by Chace (1975, 1985), Lee and Black (1972), and Barden and Sides (1967) indicated that as the size of the soil pores decreases, the rate at which air goes into solution or comes out of solution from the pore water decreases. Thus, even though the pore water in a dilatant overconsolidated clay experiences a reduction in pressure during undrained shear, sufficient time may not be available for air dissolved in the pore water to come out of solution due to the pressure reduction. This may partially explain why the erratic behavior observed in Q tests on saturated silts is not observed in similar tests on saturated clays. In addition, the extremely small pore size in clays allows suctions or negative pore water pressures considerably less than -14.7 psi to develop before air bubbles will grow into voids

within the pores of the soil (Terzaghi, 1943). This indicates that even though the pore water pressure is below the vapor pressure of water, the water does not cavitate when it is within the extremely small pores of a clay soil.

Another possibility is that in clays, where the particles are colloidal and have electrostatic charges on their surfaces, the bond between the water molecules and the solid clay particle surface is likely to be stronger than the bond between the water molecules and an inert silt particle. With a stronger bond between the water and the soil particles, the pore water of clay specimens can be expected to more fully wet the clay particle surfaces and to be less likely to cavitate than would the pore water in a silt specimen. This may very well be a result of the water adsorbed on the surfaces of the clay particles having different properties than pure water (Terzaghi and Peck, 1967; Mitchell, 1993).

2.3 Summary and Conclusions

Dense soils experience decreases in pore water pressure during undrained triaxial tests as a result of the attempted dilation of the soil. Silts have been observed to exhibit considerable dilatant tendencies during undrained shear. The resulting pore pressure reductions lead to increases in the effective confining pressure acting on the specimens.

This in turn, increases the strength of the soil specimens so that a strain-hardening effect occurs. This continuous increase in strength with increasing strain makes it difficult to select an appropriate undrained shear strength for the soil (Ladd et al., 1985; Axelsson et al., 1989; Fleming and Duncan, 1990; Brandon, Duncan and Huffman, 1990). In fact, it is often observed that undrained tests on dilatant silts reach peak deviator stresses only after experiencing very high axial strains (Nash, 1953; Penman, 1953; Schultze and Horn, 1965; Börgesson, 1981; Axelsson et al., 1989; Fleming and Duncan, 1990; Brandon, Duncan and Huffman, 1990).

Bishop and Eldin (1950) showed that if a group of soil specimens all with the same void ratio were initially fully saturated, the change in pore water pressure developed during undrained shear should be the same for all of the specimens in the group, regardless of the cell pressure used in the tests. As a result of this, the measured shear strength of the soil should be the same for all of the specimens in the group.

This is consistently observed for soils which have a tendency to contract during shear. Loose soil specimens tend to contract and experience increases in pore water pressure with increasing strain. An increase in pore

pressure results in a decrease in the effective confining pressure acting on the soil. The looser a given specimen is, the more contractive it will be during shear. It will therefore develop larger increases in pore water pressure and give a smaller measured strength than a specimen which is not as loose and develops smaller increases in pore water pressure during shear.

If a group of contractive soil specimens are all at the same void ratio initially and are tested undrained at different cell pressures, their initial pore water pressures will be different due to the different cell pressures used in the tests. Because the specimens are initially fully saturated, the application of an increase in cell pressure under undrained conditions will cause an equal increase in pore water pressure, so that the effective stress in the sample will not change. With the specimens at the same void ratio and having the same effective stress initially, during undrained shear they should develop the same increase in pore water pressure. If the specimens develop the same positive changes in pore water pressure during shear, they should yield the same strength for the soil, independent of the cell pressure used in the particular test.

Soil specimens which are dense tend to dilate or expand during shear. The attempted dilation during undrained shear

leads to a decrease in the pore water pressure in the specimens. A decrease or negative change in pore water pressure increases the effective confining pressure acting on the specimen. The effective confining pressure, in turn, influences the measured strength of the soil. The denser a given specimen is, the greater its tendency for dilation. This results in a larger decrease in pore water pressure in the soil, giving the soil a higher measured strength. Similar to specimens with a tendency to contract during shear, if a group of dilatant specimens are at the same void ratio initially, they should develop the same decrease in pore water pressure during undrained shear. A series of Q tests performed on these samples should therefore all yield a strength for the soil which is independent of the cell pressure used in the test.

This is not always the case for dilatant soils, however. This results from the fact that the properties of water are somewhat different when negative pressure (tension) is applied than when positive pressure (compression) is applied. The development of positive pore water pressure places the water in compression. Water is essentially incompressible. The water appears to have no limiting value of positive pressure which can be applied to it as the soil shears. The undrained strength of a group of contractive soil specimens will be the same for all

specimens, because all specimens will be able to develop the same increase in pore water pressure during shear, regardless of the cell pressure and initial pore water pressure in each test.

During undrained shear, soil specimens with a tendency to dilate experience a decrease in pore water pressure. Water is unable, however, to withstand an infinite decrease in pore water pressure. Two different possibilities exist which may limit the strength of the soil. As the pore water pressure decreases, the shear strength of the soil will increase. The strength of the soil will continue to increase until either the strength of the solid soil grains has been reached and the grains break during shear or the decrease in pore water pressure reaches some sort of limiting value (Odenstad, 1948).

For the cases where the strength of the soil grains is reached and the shearing causes particle breakage, the test will yield a peak in the deviator stress-axial strain curve. This peak, however, usually does not occur until very high axial strains have been reached. These high axial strains, often on the order of 30%, are considerably larger than are considered reasonable for geotechnical engineering applications.

For the situation where the decrease in pore water pressure reaches some limiting value, two different things can occur. One possibility is that as the pore water pressure decreases, gases dissolved in the pore water will come out of solution, in accordance with Henry's law (Bishop and Eldin, 1950). The exit of gases from solution in the water would lead to an increase in the overall volume of the soil specimen, thereby changing the void ratio of the specimen, and affecting the measured strength of the soil.

Another possibility that could take place would be if the pore water pressure decreases to the vapor pressure of water (about -14.7 psi at sea level and 20°C). When water reaches its vapor pressure it will cavitate and bubbles of water vapor will form within the soil pores (Bishop and Eldin, 1950). This also would lead to an increase in the overall volume of the specimen. The resulting increase in void ratio would yield a decrease in the measured strength of the soil.

A group of dilatant soil specimens, all at the same void ratio initially, sheared undrained at different cell pressures could experience different decreases in pore water pressure during shear. The cell pressure used in a particular test will influence the initial value of pore water pressure in the specimen prior to shear. For

saturated specimens tested in Q tests, the initial pore water pressure should be essentially equal to the applied cell pressure. The higher the cell pressure used in a given test, the higher the initial value of pore water pressure within the specimen. In the specimens tested at higher cell pressures, a larger decrease in pore water pressure could take place before gas would come out of solution or cavitation of the pore water would occur, than for specimens tested at a lower cell pressure. Because the strength of the soil increases as the pore water pressure decreases, the specimens which can develop larger decreases in pore water pressure will yield higher strengths than those which reach a limiting decrease in pore water pressure more rapidly. At low cell pressures, this results in an undrained shear strength of the soil which appears to increase with increasing cell pressure.

It is important to consider whether the decrease in pore water pressure results in gas dissolved in the pore water coming out of solution or vaporous cavitation of the pore water. Some studies (Bishop and Eldin, 1950, 1953; Nash, 1953; Penman, 1953) used soil pore water which had the dissolved air removed prior to performing the tests. Other researchers did not state whether any similar procedures were taken in their studies (Golder and Skempton, 1948;

Schultze and Horn, 1965; Seed and Lee, 1967; Börgesson, 1981).

The results of several of the studies (Nash, 1953; Penman, 1953; Bishop and Eldin, 1950; Seed and Lee, 1967) indicated that during undrained shear, the pore water pressure decreased to about -14.7 psi at which point cavitation occurred. If air had been allowed to remain dissolved in the pore water rather than being removed prior to testing, dissolved air may have come out of solution at pore water pressures above -14.7 psi.

Several studies (Seed and Lee, 1967; Torrey, 1982; Brandon, Duncan and Huffman, 1990) noted that in CU tests where back pressure is often used to achieve fully saturated specimens, as the pore water pressure decreases below the initial value of back pressure, air forced into solution during the back pressure saturation process, can begin to come back out of solution and desaturate the specimens. These studies also noted that back pressures considerably higher than those necessary to saturate the specimens can be used to prevent or delay the desaturation of CU test specimens with dilatant tendencies.

Similarly, several researchers (Bishop and Eldin, 1953; Nash, 1953; Penman, 1953) noted that in unconsolidated-undrained tests, the use of high cell pressures was

necessary to prevent cavitation from occurring during the tests. Bishop and Eldin (1953) and Penman (1953) both identified a limiting cell pressure for a given soil at a given void ratio which must be applied to the specimen in order to prevent cavitation during undrained shear. At cell pressures above the limiting cell pressure, the pore water pressure in the specimen prior to shear was large enough so that the decrease in pore water pressure which occurred during shear did not result in cavitation occurring in the specimens. The strength of the soil was therefore independent of the cell pressure used in the test and a $\phi_u = 0$, $S_u = c$ failure envelope was obtained.

When the cell pressure was below the limiting cell pressure, the initial pore water pressure in the specimen was not at a high enough value. As a result, the decrease in pore water pressure which occurred during shear lead to cavitation or air coming out of solution from the pore water. This yielded an undrained strength which varied with cell pressure and resulted in a $\phi_u > 0$ failure envelope for the soil.

The value of limiting cell pressure will be different for different soils and will vary with void ratio or density. For a given soil, a denser specimen would have a greater tendency to dilate and would therefore require a

higher limiting cell pressure to prevent cavitation. A specimen which was not as dense would experience a smaller decrease in pore water pressure and therefore would require a lower cell pressure to prevent cavitation.

A major question which must be considered is whether or not cavitation or air coming out of solution from soil pore water is a possibility in the field. Torrey (1982) implied that he does not consider this a possibility. Brandon, Duncan and Huffman (1990), however, noted that it may be a factor in the behavior of saturated silts in-situ.

If cavitation of soil pore water is a possibility in field loading conditions, the initial pore water pressure in triaxial test specimens should be representative of the initial hydrostatic pressure in the field. The use of high back pressures in \bar{R} tests and high cell pressures in Q tests in order to prevent or delay cavitation, may not be reasonable if the soil experiences a hydrostatic pressure in the field which is lower than the initial pore water pressure in the laboratory test specimen. When the hydrostatic pressure of the soil pore water in the field is low enough, cavitation of the pore water in-situ may possibly occur during undrained loading.

Several variables must be considered in assessing whether or not cavitation of soil pore water will occur in

the field. The dissolved gas content of soil pore water, the rate at which pore pressures will dissipate in the soil along with the rate at which the loading is applied may influence cavitation of soil pore water in-situ.

In general, undrained strengths are used when the loading is applied rapidly enough, relative to the permeability of the soil, so that the soil will not have sufficient time to drain due to the applied load. Coarse soils and even the fine sand tested by Nash (1953), will likely be able to drain rapidly enough under most loading conditions so that the negative pore water pressures which develop will dissipate somewhat and will not experience a decrease large enough to cause cavitation. Thus, the use of high back pressures and cell pressures to prevent cavitation in the laboratory seems reasonable for these soils, based on their expected field behavior. For a finer soil, such as a silt, drainage or dissipation of negative pore water pressures in the field will be slower. This slower dissipation of negative pore water pressures may allow for the decrease in pore water pressure to be great enough that cavitation will occur in the field. Laboratory conditions should therefore use pore water pressures which are similar to those the soil will be subjected to in the field.

Recent studies by Fleming and Duncan (1990) and Brandon, Duncan and Huffman (1990) have provided an improved understanding of silt behavior. They noted that silts are considerably more subject to disturbance than clays. The increased levels of disturbance are more likely to affect the undrained strengths of silts than clays. They added that care must be taken when handling silts and preparing specimens for testing, in order to minimize disturbance. This is necessary because silts are more likely to densify due to vibrations than are clays.

The combination of the ease of disturbance of silt specimens along with their dilatant behavior has caused difficulties in the interpretation of undrained tests on saturated silts. Undrained shear strengths are often difficult to evaluate and often give erratic and scattered results. The study performed by Brandon, Duncan and Huffman (1990) suggested that the scatter often observed in the measured undrained strengths of silt specimens may be due to cavitation, or the formation of bubbles of water vapor and air within the pores of the soil, as a result of the decrease in pore water pressure which occurs during undrained tests. This research was undertaken to more fully investigate the phenomenon of cavitation, the rate at which air goes into and comes out of solution in water, and their relationship to the pore pressure reductions which occur

during Q tests on saturated silts, as well as the observed behavior of silts in such tests.

Chapter 3

CAVITATION AND RELATED PHENOMENA

3.1 Introduction

Because cavitation has been identified as a possible reason for the erratic behavior often observed in Q tests on saturated silts (Bishop and Eldin, 1950; Brandon, Duncan, and Huffman, 1990), an extensive review of the cavitation literature was conducted as part of this study in order to better understand cavitation and its causes.

The phenomenon of cavitation is a very extensively studied, yet not fully understood aspect of liquid behavior. Cavitation occurs in many different types of fluids and is important in many different fields of study. It has therefore been investigated from a number of different points of view. It has detrimental and beneficial aspects associated with it in fields as diverse as medicine; mechanical, civil, chemical, and marine engineering; botany; physics; acoustics and ultrasonics.

The literature review performed in this study has resulted in a better understanding of cavitation and has provided considerable insight into the possible occurrence of cavitation in Q tests on saturated silts. In this

chapter, the important aspects of cavitation will be summarized. Special emphasis will be placed on the aspects of cavitation phenomena which are felt to be related to soil mechanics in general, and laboratory testing in particular.

Several general references (Johnson, 1963; Knapp, Daily, and Hammitt, 1970; Trevena, 1975; Temperley and Trevena, 1978; Trevena, 1987; Young, 1989) present overviews of cavitation and related phenomena. They all contain very good descriptions of the state of knowledge regarding cavitation, at the time of their publication. These references were consulted originally in this study and were used to locate more specific original references regarding the different aspects of cavitation. The information presented in this chapter was obtained from the original sources whenever possible. The contributions of the general references on cavitation, however, are acknowledged, because they enabled the location of much additional supporting information and provided an introductory explanation and understanding of cavitation and related phenomena.

3.2 Types of Pressure Reductions in Liquids

When a liquid is subjected to a negative pressure or tension of sufficient magnitude, the liquid may cavitate and form vapor or air filled bubbles within the liquid. Cavitation itself will be discussed in more detail in

Section 3.3. In this section a brief overview will be presented on the ways in which a liquid can be subjected to negative pressures.

A reduction in pressure which causes cavitation to occur in a liquid can be applied basically in three different ways. The major difference between the different methods is the rate at which negative pressure is applied to the liquid. Trevena (1967, 1975, 1984, 1987) gives several reviews of cavitation and the various methods which can be used to subject liquids to negative pressures.

One method which can be used to cause cavitation of a liquid is by the static application of negative pressure to the liquid. Subjecting a liquid to a vacuum until cavitation occurs is an example of the static application of negative pressure to a liquid. In this case, the pressure reduction takes place relatively slowly and cavitation occurs when a limiting negative pressure has been reached.

Dynamic application of negative pressure to a liquid, is another method which can be used to cause cavitation in a liquid. In this case, the pressure is reduced more rapidly, usually in a single pulse. Because of this, cavitation occurs more rapidly than it does for static methods. An example of a dynamic reduction in pressure would be the pressure decrease that occurs as water flowing in a tunnel

passes through a constriction. If the resulting pressure reduction is large enough, cavitation may occur. Here the cavitation bubbles which form in the low pressure region would rapidly collapse as they move with the flowing water into high pressure regions.

A third method which can be used to reduce the pressure of a liquid and cause cavitation is by the use of ultrasonic or acoustic methods. This procedure utilizes the pressures associated with sound waves to stress a liquid extremely rapidly, often on the order of milliseconds. In this case, the liquid is subjected to a series of compressive and tensile stresses during the positive and negative half periods of the pressure cycle (Trevena, 1975).

During the negative half cycle, when a sufficient negative pressure has been reached, cavitation bubbles will form and grow in the liquid. In the positive half cycle where the pressure increases, these bubbles rapidly collapse. One of the main advantages of this method is that it can be used to force cavitation to initiate within the body of the liquid, rather than at the liquid-container boundary, as is often the case with statically and dynamically induced cavitation.

Based on these descriptions, the pressure reduction which takes place in saturated silts during sampling and Q

tests occurs relatively slowly and can be considered a static application of pressure reduction to the liquid. For this reason, the cavitation that may possibly occur in saturated silts can be considered to have the potential to occur gradually over a longer time period, relative to many of the other occurrences of cavitation discussed in the literature.

3.3 Types of Cavitation

There are two different types of cavitation which have been identified experimentally. The first type results in a gas-filled bubble, while the second forms a vapor-filled bubble. They have come to be called *gaseous cavitation* and *vaporous cavitation*, respectively (Trevena, 1975).

3.3.1 Gaseous Cavitation

During gaseous cavitation, the cavitation bubble forms by gas or air which was previously dissolved in the liquid, coming out of solution and diffusing into the bubble due to a pressure reduction, in accordance with Henry's law. These gas-filled bubbles form relatively quietly and slowly by what is described as "rectified diffusion" (Blake, 1949). This type of cavitation is not truly cavitation, but rather, simply a degassing of the liquid (Eisenberg, 1961). It has however, come to be called cavitation by many of the

researchers who are concerned with the cavitation behavior of real liquids. The extent to which gaseous cavitation will occur is dependent on the magnitude of the pressure reduction, its rate of application and the amount of dissolved gas present in the liquid.

Gaseous cavitation will be discussed in a number of sections throughout Chapter 3, as it was encountered throughout the cavitation literature. The effect of the dissolved air content of a liquid on the occurrence of cavitation has been given considerable importance in cavitation studies. Information from the chemistry, physics, and geotechnical engineering literature dealing with Henry's law, the solubility of air in water, and the rate at which air goes into or comes out of solution in water will be discussed in detail in Chapter 4.

3.3.2 Vaporous Cavitation

In addition to gas coming out of solution due to a reduction in pressure, a liquid subjected to sufficient negative pressures can produce vapor-filled cavities (Blake, 1949). The rapid, almost explosive formation of vapor-filled cavities is considered to be true cavitation. These bubbles contain liquid vapor with very little gas present. This is because the time for bubble formation, growth and

collapse often occurs so rapidly that gas cannot diffuse into the cavity quickly enough (Eisenberg, 1961).

According to Johnson (1963), a vapor-filled cavity which forms in a liquid subjected to tension will rapidly collapse if the tension is removed or if the cavity moves from a low pressure zone into a high pressure region of the liquid. A cavity formed in a low pressure region, when subjected to a high pressure, will collapse inward. High pressures, reportedly up to 200,000 psi (Eisenberg, 1961), will be developed as the bubble collapses. These high pressures will result from the extreme change in momentum which occurs when the fluid moving inward toward the center of the collapsing bubble is finally brought to zero velocity (Johnson, 1963). This will cause a shock wave to be radiated into the liquid which can result in very high pressures which are capable of denting and damaging adjacent materials. The pressures developed depend on the rate of collapse of the cavity, which is related to the pressure in the liquid and that inside the cavity itself (Trevena, 1984).

Vaporous cavitation is analogous to boiling of a liquid. From a purely physical-chemical point of view, there is no distinction between boiling and cavitation (Eisenberg, 1961). During cavitation, cavities form and

grow by decreasing the pressure outside of the cavity. During boiling, cavities form and grow by increasing the pressure inside the cavity (Johnson, 1963). When a liquid is subjected to its vapor pressure at a given temperature, vapor-filled bubbles will begin to form in the liquid. For water at room temperature, the vapor pressure is about -1 atmosphere (zero absolute pressure). For water at 100°C , the vapor pressure is equal to normal atmospheric pressure (1 atmosphere above zero absolute pressure). In other words, at normal atmospheric pressure, water boils at 100°C . At reduced pressures, as is the case at high altitudes, the temperature at which boiling occurs is less than 100°C .

The occurrence of vaporous cavitation is also dependent on the magnitude of the pressure reduction and its rate of application. The dissolved gas content, however, has no effect on vaporous cavitation. In order for vaporous cavitation to occur, the pressure in the liquid must go below the vapor pressure of the liquid. As will be explained subsequently, it should not be assumed that cavitation will always occur at the vapor pressure or that the vapor pressure represents the true limiting pressure to which a liquid can be subjected before cavitating. Gaseous cavitation however, can occur at pressures above or below the vapor pressure, as long as the dissolved gas content of the liquid exceeds the equilibrium gas content of the liquid

at that pressure (Eisenberg, 1961) and provided sufficient time is allowed for the gas to come out of solution.

As it is almost impossible to totally deair water, usually both types of cavitation can be expected to occur to different degrees, depending on the dissolved gas content of the liquid and the magnitude and duration of the pressure reduction. In some cases, the typical cavitation bubble will contain a mixture of both liquid vapor and gas, with one usually being more prevalent and controlling the bubble's behavior (Trevena, 1987).

3.4 Tensile Strength of Water

When a liquid cavitates, a tear forms in the liquid due to an applied tension. Studies in which tension is applied to water so that cavitation occurs have been used to estimate the tensile strength of water. In addition, theoretical approaches have also been used to estimate the tensile strength of water. Considerable discrepancies exist however, between the tensions water has resisted experimentally and those expected theoretically. Because the measured values are so much lower than the strengths expected theoretically, the study of cavitation and the failure of liquids in tension has received considerable interest for quite some time, in hopes that an explanation for the discrepancies could be found.

Theoretically, the tensile strength of water should be very high and cavitation or the failure of the liquid in tension should not occur until the ultimate tensile strength of the liquid has been reached. Real liquids however, tend to cavitate as soon as the pressure reaches the vapor pressure of the liquid, implying that liquids have essentially no tensile strength. Commercially distilled water has even been observed to cavitate at very low tensions. Because the tensile strength of water is so much lower than predicted by theory, it is believed that there are weak spots present in the liquid at which point the liquid is able to tear and form a cavity (Knapp, 1958).

The forces tending to hold a liquid together are the external pressure and intermolecular cohesive forces. Due to the intermolecular forces, a liquid should be able to withstand tension (Knapp, Daily, and Hammitt, 1970). Estimates of the theoretical tensile strength of water have been made using van der Waal's equation. Even though water does not obey this theory very well, an estimate of the magnitude of the tensile strength can be obtained. The tensile strengths estimated range from 100s to 10,000s of atmospheres. The tensile strength of "ideal" water at room temperature is believed however, to be on the order of 500 atmospheres (Temperley and Trevena, 1978). This value is much higher than any value measured experimentally. The

highest value of tensile strength measured for water was about 280 atmospheres, which was determined by Briggs in 1950 (Trevena, 1967; Briggs, 1950).

Experiments to determine the tensile strength of water show that appreciable tensions can be resisted. There are however, a wide range of measured values among the different researchers and even among the same researcher. The large variation in measured tensile strengths is again believed to be due to the presence of weak spots in the liquid. The variation in size and number of weak spots is felt to allow cavitation to occur at tensions which are below those predicted theoretically and which vary from one experiment to another (Knapp, Daily, and Hammitt, 1970).

3.5 Cavitation Nuclei

The generally accepted theory as to why liquids such as water break or cavitate at tensions much lower than those expected theoretically is that there are weak spots in the liquid at which the rupture initiates. These weak spots serve as nuclei for the formation of cavitation bubbles when a liquid is subjected to negative pressures. If these nuclei were not present in the liquid, cavitation would not occur until much higher tensions had been reached.

According to Trevena (1987), there are two types of cavitation nuclei which have been proposed and appear to be feasible. The first theory, which is generally less accepted based on experimental evidence, is that a liquid may contain a large number of minute spherical gas bubbles which are stabilized against gaseous diffusion by an immiscible skin of organic impurity. The second and generally more accepted theory is based on the idea that pockets of gas can be trapped and remain stable in tiny cracks and crevices on the walls of the container holding the liquid and on microscopic suspended solids present in the liquid. When a liquid containing these gas-filled nuclei is subjected to a sufficient tension, the nuclei can grow into visible bubbles which are characteristic of cavitation.

3.5.1 Organic Skin Theory

The organic skin theory was originally proposed by Fox and Herzfeld (1954). They hypothesized that cavitation nuclei were very small bubbles present in the liquid, which were completely surrounded by an impermeable organic skin. The organic skin stabilizes the nuclei by mechanically preventing the loss of gas from the bubble by diffusion into solution. As the pressure in the liquid is decreased, the organic skin of the bubble is stretched until at some point,

the organic skin is torn, allowing gas dissolved in the liquid to come out of solution and enter the bubble, thereby enlarging it to visible size.

The type of organic skin proposed by Fox and Herzfeld could exist in water; however, it would dissolve in organic substances such as alcohol, which should therefore not contain nuclei and accordingly not cavitate. These substances do cavitate, so another explanation is necessary. Protein skins, as suggested by Moore (1953), provide a more reasonable explanation according to Fox and Herzfeld, because they would not dissolve in organic liquids. Their presence in numerous liquids however, can not be fully explained.

Yount (1979, 1982) found that bubble formation in gelatin appeared to be due to the presence of cavitation nuclei stabilized by organic skins of variable permeability, rather than the impermeable organic skins proposed by Fox and Herzfeld. He implied that this type of organic skin could be extended to liquids such as water, as well.

Although the organic skin theory of cavitation nuclei has not been conclusively disproven, it is not as widely accepted as the theory that cavitation nuclei are stabilized in cracks and crevices on solid surfaces, as will be described subsequently. In fact, Yount (1979) noted that

even Herzfeld himself abandoned his organic skin theory around 1957. Although Strasberg (1959) was unable to differentiate between the two different types of nuclei in his cavitation experiments, several experimental and theoretical studies (Willard, 1953; Knapp, 1958; Hayward, 1970; Apfel, 1970; Crum, 1979) add support to the crack and crevice theory and tend to discredit the organic skin theory. The study performed by Hayward (1970) was especially significant because it provided considerable support for the crack and crevice theory while tending to refute the organic skin theory, as will be discussed in Section 3.5.4.

3.5.2 Crack and Crevice Theory

A more generally accepted and physically likely theory for cavitation nuclei is that tiny pockets of undissolved gas, trapped in cracks and crevices on the surfaces of container walls and suspended solids in a liquid, serve as nuclei for cavitation bubble formation when a liquid is subjected to a reduction in pressure.

Tomlinson (1869) observed the effect of different solid materials on the behavior of liquids during boiling. He found that most solid material placed in water, caused increased bubbling during boiling until the solid had become "chemically clean," after which it had little effect on the

boiling. He concluded that the solids served as nuclei for the liberation of liquid vapor during boiling. He found that as the degree of cleanliness of the solid increased, the ability of the liquid to wet the surface of the solid increased and the effect the solid had on bubbling during boiling decreased. Certain solids had a greater effect on boiling and required different periods of time before becoming chemically clean. Porous solids such as coke and charcoal did not appear to ever become chemically clean. They were observed to continuously cause vigorous bubbling of the liquid during boiling.

Harvey et al. (1944a, 1944b, 1945, 1947) hypothesized that the nuclei that lead to cavitation were small pockets of undissolved gas which were trapped and stabilized in cracks and crevices on the surfaces of container walls and tiny suspended solids present in all liquids. They reasoned that as the pressure in a liquid is reduced, gas dissolved in solution in the liquid will diffuse into the gas pocket, causing it to increase in size so that it becomes a visible bubble.

According to Harvey et al. (1944a), a free spherical gas bubble in a liquid is usually unstable. Above a certain critical size, it would float to the surface due to the surrounding pressure in the liquid. Below a certain

critical size, surface tension forces in the liquid would cause it to dissolve in the liquid. A gas mass present on an irregular surface, however, would not be spherical and presents a very complicated situation. In this case, the configuration of the gas-liquid-solid interface becomes very important. They noted that in order for a gas nucleus to exist in a crack or crevice on a solid surface in a liquid, the characteristics of the surface are very important. Gas bubbles tend to adhere to hydrophobic surfaces, particularly those that are rough and irregular. This will also influence the contact angle at the gas-liquid-solid interface.

With the right combination of crevice geometry, gas pressure, liquid pressure, and surface tension in the liquid, the gas-liquid boundary can be concave toward the liquid. In this situation, the surface tension would tend to prevent the gas pocket from dissolving in the liquid. This would lead to an equilibrium condition such that the nucleus would remain in the liquid indefinitely (Pease and Blinks, 1947).

Figure 3.1 shows a gas pocket stabilized in an idealized crack on a solid surface. In this case the interface between the liquid and gas is concave toward the liquid. As the pressure in the liquid is reduced, the

interface between the liquid and gas will be pulled outward toward the liquid and can become convex toward the liquid. If the magnitude and duration of the pressure reduction are sufficient, the gas pocket will continue to enlarge and eventually form a bubble in the liquid, as shown in Figure 3.2.

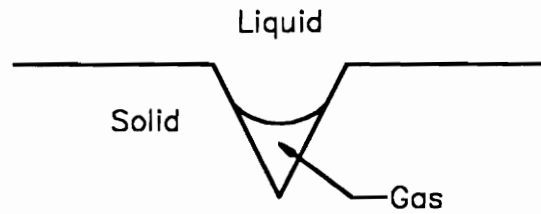


Figure 3.1. Cavitation nucleus stabilized in a crack on the surface of a hydrophobic solid (after Hayward, 1970)

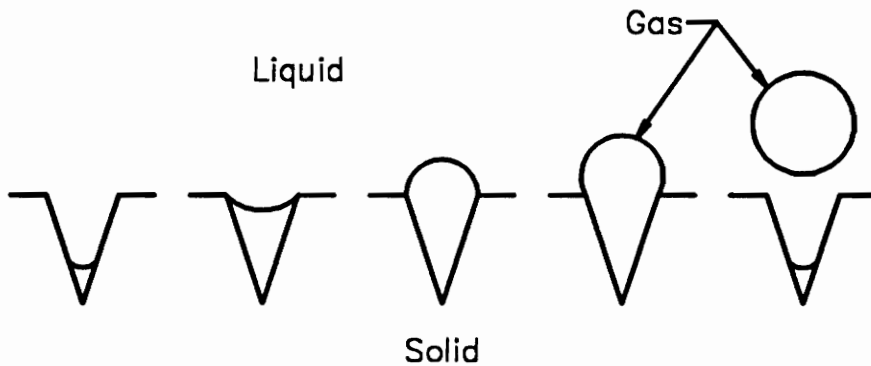


Figure 3.2. Formation of a bubble from a nucleus due to a reduction in the pressure of the liquid (after Young, 1989)

Because of variations in the geometry of the minute cracks and crevices on solid surfaces, cavitation nuclei of many different shapes and dimensions can exist in a liquid at the same time. For each successive decrease in pressure, different groups of nuclei may become unstable. For example, if a sample of water saturated with air at 1 atmosphere, has its pressure successively reduced to 1/2, 1/4, and 1/8 atmosphere, a new set of bubbles should form for each successive decrease in pressure (Harvey et al., 1944a). After a sufficient time at each pressure, no more bubbles should form until the next pressure decrease occurs.

Several other observations concerning cavitation can also be addressed through the crack and crevice theory of cavitation nuclei. When water is brought to boiling in a pot on a stove, the bubbles initiate on the walls and bottom of the pot (Knapp, Daily, and Hammitt, 1970). They remain there visibly stable until enough gas or water vapor enters them so that they are large enough to be brought to the surface by buoyancy. Fewer bubbles are usually observed on the surface of a glass pot than on a metal pot because glass tends to be less hydrophobic than metal. The most bubbles would probably be observed on the surface of a pot which has a nonstick surface. These surfaces usually have a rough texture when compared to a pot without such a surface. In fact, the basic principle of a nonstick cookware surface may

be related to the idea of enhanced nucleation to increase cavitation and weaken the bond between the food being cooked and the cooking surface.

3.5.3 Removal of Cavitation Nuclei

The major justification for the existence of cavitation nuclei has been the ability of a number of researchers to perform procedures which in effect, remove the nuclei from the liquid. With the nuclei removed, the liquids have been found to be less likely to cavitate than similar liquids which had not been subjected to such procedures.

Harvey et al. (1944b, 1945), in their study of the effects of high altitude flight and reduced pressures on organisms, presented techniques for the removal of gas cavitation nuclei from liquids. For their cavitation experiments, they wanted the liquid to be essentially free of all nuclei. They felt that if they removed all dust particles and thoroughly wetted all surfaces in contact with the liquid, no nuclei would be present. They found that the liquid could be made partially free of nuclei by thoroughly cleaning the test container surfaces and by strongly centrifuging the liquid under investigation. They also attempted to filter the liquid to remove dust particles but found it to be less effective than centrifuging.

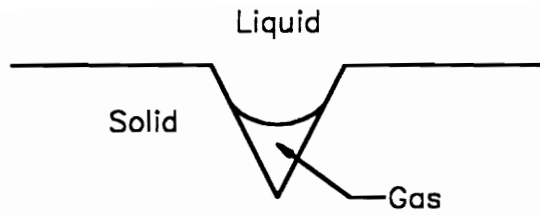
According to Harvey et al. (1945), the centrifuge treatment removed all gas nuclei which would grow to visible bubbles at the vapor pressure of water at 22°C. These nuclei they called "gas macronuclei." They found however, that when the container was tapped lightly or placed in a high frequency sound field, gas bubbles appeared due to what they called "gas micronuclei" which had not been removed by the centrifuging.

Harvey et al. (1944b) pointed out two more effective means of removing gas cavitation nuclei from liquids. The first is prolonged boiling of the liquid or evacuation under vacuum. In this procedure, a cavitation nucleus is removed by forcing it to form a bubble and rise to the surface and leave the liquid. It has the disadvantage however, that any dissolved gas present in the liquid will also be removed by the process. This procedure was not useful to Harvey et al. because they were interested in the effect of the dissolved gas content on bubble formation. Because of this limitation, they developed a second procedure to remove gas cavitation nuclei from a liquid, without altering its dissolved gas content.

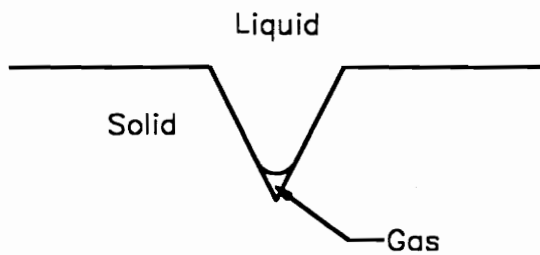
They found that by applying a high hydrostatic pressure to the liquid, the gas nuclei stabilized in cracks and crevices on the surfaces of container walls and suspended

solids could be made inactive. The high pressure forced the interface between the liquid and gas present in the nuclei up into the apex of the crack or crevice, thereby forcing the gas in the nuclei into solution in the liquid and causing the surface of the crack or crevice to be wetted by the liquid. The prepressurization of the liquid essentially eliminated all of the liquid-gas interfaces present in the liquid. When the prepressurization pressure was removed, there were no liquid-gas interfaces remaining, so that the recently dissolved gas from the nuclei stayed in solution and could not reform into gas-filled nuclei.

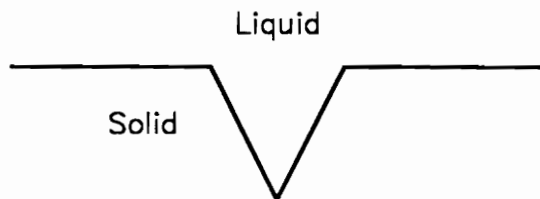
A liquid treated with prepressurization could then withstand tensions considerably larger than a sample of the same liquid which had not been treated with high hydrostatic pressure because no nuclei or liquid-gas interfaces were present to initiate the bubble formation. One of the main benefits of this method for Harvey et al. in their experiments, was that the liquid became denucleated without removing the dissolved gas from solution. Figure 3.3 shows how cavitation nuclei can be removed from a liquid by subjecting the liquid to high pressures which force the gas present in the nuclei into solution.



(a) Gas pocket in equilibrium with liquid



(b) Pressure applied to liquid forces liquid toward apex of crack



(c) Gas pocket completely dissolved in liquid due to applied pressure

Figure 3.3. Removal of a cavitation nucleus by prepressurizing the liquid to dissolve the trapped gas

In their experiments, Harvey et al. (1944b, 1945) exposed water and its container to a pressure of 16,000 psi for 15 to 30 minutes. They found that the resulting liquid could be heated to over 200°C without bubbling, although a significant amount of evaporation did take place from the liquid surface. When they lowered the pressure of the liquid to its vapor pressure at a temperature of 20°C, no bubbles formed in the liquid unless the vessel holding the liquid was struck by a very severe blow, which caused significant tensions to develop in the liquid. They estimated that by subjecting the water to a pressure of 16,000 psi, all nuclei with radii greater than 13.5 angstroms were dissolved into solution in the water.

Harvey et al. (1945) concluded that unless special procedures have been used to denucleate a liquid, gas cavitation nuclei must be present in every container and liquid in which cavitation occurs at tensions below those expected theoretically. They stated that treating liquids and their containers with high pressures to remove cavitation nuclei should be significant in future studies of the tensile strength of liquids and investigations into cavitation phenomena in liquids such as water.

It should be noted that the prepressurization process that Harvey et al. used to remove cavitation nuclei could

work as well for nuclei stabilized by organic skins. In this case, the high prepressurization pressure would crush the organic skin surrounding the minute gas nuclei bubble, thereby forcing the gas in the nuclei to dissolve into the liquid. Upon removal of the high pressure, the organic impurity would remain, but no gas would be present within the skin to serve as a nuclei, and accordingly, higher tensions would be required to initiate cavitation. As some of the experimental studies presented in Section 3.5.4 will show however, the crack and crevice theory appears to be much more justified and is currently almost universally accepted as the cause of cavitation in liquids.

3.5.4 Theoretical and Experimental Studies of Cavitation Nuclei

A number of researchers have investigated the theory that nuclei present in liquids are the cause of cavitation in liquids under tension (Pease and Blinks, 1947; Plesset, 1949; Willard, 1953; Knapp, 1958; Strasberg, 1959; Hayward, 1970; Winterton, 1977; Crum, 1979). A number of experimental studies have been performed to investigate and study the effects of high hydrostatic prepressurization on deactivation of nuclei. Other studies have looked into the nature of the nuclei themselves and have provided support for the nuclei theory proposed by Harvey et al.

Pease and Blinks (1947) applied high pressures on the order of 12,000 psi for 5 minutes to remove gas cavitation nuclei from water. They found that once gas nuclei were removed from water by the application of high pressure, the liquid would not cavitate unless subjected to large tensile forces. In liquids where gas nuclei are absent, cavitation occurs when the liquid is literally torn away from the solid surface, with the tear beginning at the weak point in the liquid-solid system.

According to Pease and Blinks (1947), when a nucleus-free liquid is subjected to a large tensile force, the liquid wants to tear away from the solid surface. The liquid molecules are able to move away from the solid surface due to the applied tension, but the solid molecules which want to follow can not, and the tear forms at the liquid-solid boundary. The bond between adjacent liquid molecules is stronger than the bond between the liquid and solid molecules, so the failure or cavity forms at the liquid-solid boundary.

Plesset (1949) performed cavitation experiments in a water tunnel and found that when water saturated with air was subjected to high hydrostatic pressures on the order of 10,000 psi for several minutes, the nuclei were forced into solution. When the pressure in the liquid was brought back

to atmospheric pressure, the water was found not to cavitate at tensions which had previously caused cavitation in unpressurized samples.

Willard (1953) believes that the cavitation nuclei present in the water used in his tests had a wide range of strengths and sizes. The weaker (larger) nuclei were felt to be less plentiful than the stronger (smaller) nuclei. The nuclei were stable and resulted from solid particles in the liquid. These solid particles were either not wetted by the liquid or contained cracks or pores in which gas was trapped. In both cases, gas molecules could have separated the solid and liquid phases and served as the initiation point for a cavitation bubble.

Willard's experiments using ultrasonically induced cavitation, produced cavitation sporadically in water subjected to relatively constant negative pressures. In addition, the tensile strengths measured experimentally were well below the theoretical range of tensile strengths reported. These facts indicated to Willard that each cavitation event was triggered by the chance circulation of a cavitation nuclei or weak spot in the liquid, into the high intensity zone of the ultrasonic field, helping to justify the feasibility of the nucleus theory.

Willard also considered denucleation and enhanced nucleation of liquids. Denucleation of the liquid by applying increased hydrostatic pressures to the liquid tends to force the air nuclei into solution. He noted that the main difficulty involved with this procedure in practical applications would be the prepressurizing of large quantities of a liquid to several thousand psi of pressure. Willard also foresaw some of the important possible future applications of enhanced nucleation. He reasoned that if nuclei could be added to a liquid so that cavitation were to occur more readily with small sonic power requirements, then ultrasonic cleaning, degreasing, dispersion of pigments, emulsification and other processes would become much more practical.

According to Knapp (1958), the tensile strength of the interface between an undissolved solid and liquid is dependent on the wettability of the solid's surface by the liquid. He stated that if the degree of wetting is high, the adhesive force between the liquid and solid is very high. Even for a low degree of wetting, the adhesion is stronger than most of the tensile strengths observed for ordinary liquids. This reduced the types of impurities which can cause weak spots in liquids to undissolved gases and unwetted hydrophobic solids. The presence of free undissolved gas bubbles in liquids is unlikely however,

because they would be expected to either float to the surface or go into solution in the liquid. Pockets of undissolved gas trapped on the surfaces of solids could however, be expected to exist stably in a liquid.

Knapp (1958) studied the effect of prepressurization on cavitation. He varied the range of pressure and its duration of application, and then compared the physical characteristics of unpressurized water with those of similar samples which had been subjected to high pressures. He found that the effective tensile strength of water increased due to prepressurization. The amount of the increase was found to vary with the level of prepressurization until an upper limit of prepressurization of 2000 to 3000 psi had been reached. He found that prepressurization pressures of 300 to 400 psi produced definite increases in the effective tensile strength and even lower pressures showed some noticeable effect. The duration of the prepressurization appeared to have little effect on the increase in tensile strength. He varied the treatment time from 1 minute (the minimum duration possible with his equipment) to several days. He suggested however, that very short treatment times (less than 1 minute) may have some effect.

Knapp found the effects of the prepressurization process to last for at least 19 days if the liquid was

adequately shielded from contamination by foreign nuclei during the period between prepressurization and testing. The initial degree of purity of the water did not appear to have a significant effect on the effective tensile strength after prepressurization. In fact, there was no noticeable difference between doubly distilled water and ordinary tap water. In using both static and dynamic experiments, he observed no relationship between the duration of the applied tension and the tensile strength of the liquid.

Knapp (1958) concluded that his results tend to support the idea that cavitation nuclei are tiny pockets of undissolved gas trapped in cracks and crevices on the hydrophobic surfaces of solid impurities present in the liquid. The effect of these nuclei however, can be reduced or eliminated by prepressurizing the liquid with sufficiently high pressures. The level of prepressurization necessary depends on the sharpness of the cracks involved and the relative resistance of the solid surface to wetting by the liquid. He further felt that his study indicated that the concentration of cavitation nuclei which are highly resistant to prepressurization, is relatively low in typical water samples.

Strasberg (1959) studied the conditions influencing the onset of ultrasonically induced cavitation in tap water. He

was especially interested in the effect of air-filled cavitation nuclei on cavitation inception. In his experiments, he measured the sound pressure necessary for cavitation inception and the corresponding air content of the water. He used water which had been treated in three different ways in his tests: 1) water which had been allowed to stand undisturbed for some time after drawing it from the tap, 2) water which had been partially deaired, and 3) water which had been prepressurized prior to testing. His experiments were designed to evaluate the possible existence of three different types of nuclei: 1) free air bubbles in the liquid, 2) air trapped in cracks and crevices on the surfaces of suspended solid particles and container walls, and 3) air bubbles surrounded by skins of organic impurities.

Strasberg observed an aging effect with regard to the cavitation threshold pressure of tap water. Samples which were left standing for several days required a higher negative pressure to cause cavitation than freshly drawn tap water. He felt that this aging effect could possibly be the result of nuclei in the form of free air bubbles, slowly rising to the surface over a period of time. He also found that prepressurizing the liquid caused an increase in the cavitation threshold pressure, and the threshold pressure increased with increasing prepressurization pressure. He

further noted that even prepressurization pressures of one-third atmosphere showed some measurable increase in the cavitation threshold pressure in his experiments.

He concluded that his results supported the possible existence of two types of cavitation nuclei: air trapped in cracks and crevices on the surfaces of container walls and minute suspended solids, and air bubbles surrounded by skins of organic impurities. Through his experiments however, he was unable to distinguish between the two different types of nuclei.

Hayward (1970) performed a very interesting study in which he sought to obtain further experimental evidence of the nature of cavitation nuclei and their role in cavitation inception. He used a static tension manometer in his experiments and defined a prepressurization threshold by which the stability of nuclei in a liquid could be quantified. He utilized the idea that a liquid can be freed of cavitation nuclei by subjecting it to a sufficient positive pressure for a period of time. He defined the prepressurization threshold (PPT) of a liquid as the minimum positive pressure to which a liquid must be subjected for a period of 30 minutes, to enable the liquid to withstand a negative pressure of 0.15 bar in a tension manometer test apparatus without cavitating (1 bar = 14.504 psi). The

prepressurization was applied to the liquid while it was in the test apparatus.

Hayward (1970) stated that once a liquid had been subjected to its PPT, it could withstand a negative pressure of 0.15 bar indefinitely, even if the liquid had a high dissolved air content. If the prepressurization had left small nuclei, gas in solution would have been expected to diffuse into the nuclei under negative pressure and the nuclei would have grown into visible bubbles. This was not observed to happen, however, so the prepressurization process was felt to effectively remove the gas nuclei which had the potential to become unstable at a negative pressure of 0.15 bar.

Based on his experiments, the PPT appears to have a critical value for a given liquid. For liquids subjected to prepressurizations just below the PPT, the liquid could not withstand negative pressures of 0.15 bar without cavitating. On the other hand, for liquids subjected to prepressurizations just above the PPT, hydrostatic tensions of 0.15 bar could be maintained without cavitation of the liquid taking place.

In his study, Hayward (1970) determined the PPT for distilled water, tap water, heavily polluted river water, nine organic substances, and distilled water with one of

five different contaminants added. Both the distilled water and tap water were found to have a PPT of 3 bars absolute (abs). The sample of heavily polluted river water had a PPT of 4 bars abs. All of the organic substances tested had a PPT of 1 bar abs, indicating that no prepressurization was necessary for these liquids in order for them to resist 0.15 bar tension.

Hayward performed five tests with different contaminants added to distilled water in order to investigate the nature and effectiveness of different nuclei in the liquid. He evaluated four different organic contaminants to investigate the organic skin nuclei theory. The addition of 0.1% of the different contaminants tested in distilled water yielded liquids with PPT's of 3, 4, or 5 bars abs, the same as or slightly higher than those for distilled water without the contaminants. The fifth contaminant used was hydrophobic dust to investigate the crack and crevice nuclei theory. The addition of 0.1% hydrophobic dust to distilled water caused the PPT to increase to 140 bars abs.

From his experiments, Hayward (1970) concluded that water appeared to be the only liquid that contains stabilized gas cavitation nuclei. He felt that the presence of these nuclei was not related to the cleanliness of the

water as they were detected in distilled water as well as river water which was heavily polluted with suspended soil and organic matter. He observed that the addition of organic contaminants to distilled water did not appreciably effect the PPT of the liquid, tending to make the organic skin theory of cavitation nuclei less feasible. The addition of a very fine powder coated with water repellent to make it hydrophobic, yielded a significant increase in the PPT of the liquid. As a result of Hayward's (1970) experiments, the crack and crevice theory of cavitation nuclei appears to be a quite reasonable explanation for the occurrence of cavitation in liquids.

Winterton (1977) used a theoretical and experimental approach to consider stabilized cavitation nuclei. From his theoretical and experimental studies, he estimated the radius of a stable gas nucleus to be $6.7\mu\text{m}$. He also considered the effect of prepressurization on deactivating the nuclei. He found that in most cases, the cavitation threshold pressure increased as the prepressurization pressure increased, but not always. This led Winterton to conclude that prepressurization of a liquid prior to testing may make the liquid more resistant to bubble formation or it may have no effect at all.

Crum (1979) assumed that the body of a liquid contains numerous nonpolar solid impurities that have cracks and crevices on their surfaces. Within these cracks and crevices, pockets of undissolved gas can be stabilized against dissolution in the liquid. He used a filter with a pore size of $0.45\mu\text{m}$ to filter out solid impurities from distilled water. Scanning electron micrographs of a solid impurity filtered from the water, showed that the surface of the impurity was extremely irregular with numerous possible sites in which gas nuclei could have been stabilized.

3.6 Tribonucleation

Another theory regarding the origin of cavitation bubbles is called tribonucleation. The theory behind tribonucleation is that when two solid surfaces are rubbed against each other within a liquid subjected to tension, a bubble will form due to the rubbing of the two surfaces (Trevena, 1987). Harvey et al. (1944b, 1947) made reference to the idea that a solid surface, such as a glass rod, when rubbed over the inner surface of a glass container holding water at its vapor pressure, will lead to bubble formation at the point of contact.

Hayward (1967) was the first to call this process of bubble formation by rubbing, *tribonucleation*. (Tribo comes from the Greek meaning to rub or create friction). He

encountered this phenomenon accidentally in his experiments. His apparatus consisted of a test chamber filled with deaired water subjected to negative pressure. A magnetic stirrer was located inside the chamber on its base. The chamber was then placed on top of a magnetic stirrer platform. When the magnetic stirrer inside the chamber was moved the smallest possible distance (less than 1 mm), a bubble was formed in the liquid at the location of the magnetic stirrer.

Other experiments followed from which Hayward (1967) developed several conclusions about tribonucleation. Tribonucleation of bubbles can occur in liquids under negative pressure by the extremely gentle rubbing of solid surfaces against each other. The occurrence of tribonucleation did not appear to be dependent on the dissolved air content of the liquid. It occurred just as readily in deaired liquids as in liquids saturated with dissolved air at one atmosphere. Every liquid-solid combination tested resulted in tribonucleation of a bubble due to very gentle rubbing. He also found that the elimination of gas cavitation nuclei from a liquid by prepressurization did not prevent cavitation bubbles from forming by tribonucleation. When denucleated liquids were subjected to sufficiently low pressures, bubbles were still

observed to form when moving parts rubbed against each other within the liquid.

Although the identification of tribonucleation as an initiator of cavitation in liquids seems quite significant, particularly with regard to cavitation of pore water in saturated silt Q test specimens, no additional studies on this phenomenon have been found in the literature.

3.7 Effect of the Dissolved Gas Content of the Liquid on Cavitation

Because the water present in the pores of Q test silt specimens may very likely contain dissolved gas or air, it was of special interest to note theoretical or experimental studies where the effect of the dissolved air content of a liquid on cavitation had been investigated.

Although a detailed discussion of the solubility of air in water and the rate at which air goes into and comes out of solution in water will be presented in Chapter 4, a brief discussion of the concepts will be given here so that cavitation studies involving the dissolved air content of water can be addressed.

Under normal equilibrium conditions, the amount of air which can be dissolved in solution in water can be determined in accordance with Henry's law. According to

Henry's law (Henry, 1803), for a given temperature, the mass of gas which can be dissolved in a volume of liquid, is directly proportional to the partial pressure of the gas in contact with the liquid. For a temperature of 20°C and normal atmospheric pressure, the volume of gas that can be dissolved in fresh water is equal to 0.02 times the volume of the water (CRC Handbook of Chemistry and Physics, 1988).

As the pressure of a liquid decreases, air dissolved in the liquid will tend to come out of solution in order to maintain equilibrium in accordance with Henry's law. The amount of air that will come out of solution due to a given decrease in pressure is dependent on the magnitude and duration of the pressure reduction and the initial air content of the liquid. The air present in solution requires sufficient time to come out of solution and if the pressure is reduced over a very short time period and then increases again, little or no gas can be expected to come out of solution, as is the case in ultrasonic and most dynamic cavitation experiments. On the other hand, if the pressure is reduced slowly over a sufficient time period, gas will have time to come out of solution and form gas-filled bubbles.

In order for the gas to diffuse out of solution however, a gas-liquid interface must be available for the

gas to diffuse across. For this reason, in order for bubbles to form due to a pressure reduction in a liquid with no free gas surface, nuclei must be present to provide a gas-liquid interface. If there are no nuclei present in the liquid or if the liquid has been denucleated by applying high pressure to the liquid, the formation of gas-filled bubbles will not occur or will be delayed until larger tensions have been reached, causing a vapor-filled bubble to be formed. Once a vapor bubble forms, a vapor-liquid interface will be available across which gas diffusion can occur.

Some researchers, especially those trying to measure the ultimate tensile strength of a liquid, do not consider the formation of gas-filled bubbles resulting from a pressure reduction as true cavitation. They view this simply as degassing of the liquid. Their interest is more in the formation of vaporous cavitation bubbles. They often use deaired water in order to eliminate the possibility of gas bubble formation during their tests.

Most researchers are interested in the behavior of real liquids which often can contain impurities as well as dissolved gases. They consider the formation of gas-filled bubbles as gaseous cavitation, while the formation of vapor-filled bubbles is considered vaporous cavitation. In real

liquids encountered in nature, the dissolved air content of the liquid may make the liquid undersaturated, saturated or supersaturated with air at a given temperature and pressure. As this is the condition in which the liquid may be present in a particular problem or application, the experimental studies often attempt to determine the effect of the dissolved air content on the cavitation behavior of the liquid.

3.7.1 Theoretical Consideration of the Effect of Dissolved Air Content on Cavitation

Theoretically, the tensile strength of water should be reduced by less than one-half of one percent for water saturated with air at 1 atmosphere (Kupper and Trevena, 1952). Because of this, the presence of dissolved gas in water is not felt to be the reason there are differences between theoretical and measured tensile strengths. The difference between theoretical and measured tensile strengths of water is therefore not the result of dissolved gas being present in the liquid but rather a consequence of the presence of gas nuclei trapped in cracks and crevices on the surfaces of container walls and suspended solids.

3.7.2 Experimental Studies of the Effect of Dissolved Air Content on Cavitation

A number of researchers have found that as the degree of saturation of a liquid with gas decreases, the negative pressure or tension required for gaseous cavitation to occur increases (Willard, 1953; Connolly and Fox, 1954; Galloway, 1954; Iyengar and Richardson, 1958; Strasberg, 1959; Trevena, 1967; Sedgewick and Trevena, 1976).

Willard (1953) found that vaporous cavitation occurred in both deaired and nondeaired water at about the same negative pressure, indicating that the dissolved air content had relatively little effect on the threshold pressure for vaporous cavitation. He observed, however, that the gas content of water did have an effect on the pressure at which gaseous cavitation or degassing of the liquid began.

Trevena (1967) found that deaired liquids required larger peak negative pressures to cavitate than liquids containing dissolved air. For liquids containing dissolved air, he found that cavitation initiated when the peak negative pressure reached atmospheric pressure, at which point degassing of the liquid began.

Similarly, Galloway (1954) found that for water saturated with air at 1 atmosphere, as the hydrostatic pressure was reduced below 1 atmosphere, air began to come

out of solution. He observed that for water at 22°C, the dissolved air content of the liquid appeared to be the dominant factor limiting the maximum negative pressure or tension that the liquid could resist prior to gaseous cavitation occurring. This was true as long as the dissolved air content of the water was greater than 5% of the dissolved air content of water saturated with air at one atmosphere. At lower air contents, the threshold pressure appeared to be essentially independent of dissolved air content and vaporous rather than gaseous cavitation was dominant.

In his observations on tribonucleation, Hayward (1967) found that cavitation bubbles still formed due to surfaces rubbing against each other, even though the liquid was essentially deaired. He found that when two solid surfaces were rubbed against each other within a liquid subjected to negative pressure, bubbles formed as easily in deaired water as in water saturated with air at 1 atmosphere.

3.8 Effect of Temperature on Cavitation

Several studies have investigated the effect of liquid temperature on the tension required to cause cavitation (Briggs, 1950; Connolly and Fox, 1954; Galloway, 1954; Sedgewick and Trevena, 1976). All have found that the

tensile strength or negative pressure at which cavitation occurs varies with temperature.

Briggs (1950) measured a maximum tension for water at a negative pressure of 277 atmospheres at 10°C. At temperatures above 10°C, the tensile strength gradually decreased. In the 0°C to 5°C range, the tensile strength underwent enormous change, dropping to less than 10% of its maximum value.

Connolly and Fox (1954) found that the pressure necessary to induce cavitation varied nonlinearly with temperature for temperatures between 0° and 30°C. Their results showed that the cavitation threshold pressure decreased with increasing temperature and increased with increasing liquid viscosity.

Sedgewick and Trevena (1976) studied the breaking tension of ordinary tap water as a function of temperature from 2°C to 70°C. They found that the maximum breaking tension was obtained when the temperature was around that corresponding to the maximum density of water. The maximum tensile strength was measured at about 5°C while the maximum density of water occurs at 4°C. They reasoned that this made sense physically because at the maximum density, the water molecules would be in their most closely packed state, and the tension necessary to pull them apart should also be

greatest at this temperature. As temperature increased, the molecules began to move more freely and it became easier to pull them apart and form a cavity. As the temperature decreased toward 0°C and solidification was approached, the tensile strength was found to decrease rapidly. This was felt to be consistent with other anomalies for water in this temperature range.

Galloway (1954) found that for a constant air content, the cavitation threshold pressure for water decreased linearly with increasing temperature. This temperature dependence was similar to that of the solubility coefficient of a gas in a liquid. This is as expected by correlating the threshold pressure for gaseous cavitation with the air content of the water, because the solubility of gas in water also decreases as temperature increases.

3.9 Consideration of Cavitation in Soil Mechanics and Laboratory Testing

The review of the literature regarding cavitation phenomena has revealed several interesting aspects of cavitation which seem to be applicable to soil mechanics and Q tests on silt specimens. These aspects will now be addressed in the context of soil mechanics and laboratory testing.

The theory that cavitation occurs due to the presence of nuclei in the water, and that these nuclei are believed to consist of pockets of undissolved gas trapped in cracks and crevices on tiny solids present in the water, can be seen to have considerable applicability to Q tests on silt specimens. The specimens contain an abundance of solid soil particles which can provide numerous cracks and crevices in which cavitation nuclei could be stabilized. Most of the large cracks and crevices on a silt particle would be expected to be wetted by the water, but the minute cracks and crevices and the apexes of some of the larger cracks could provide stable locations for gas pockets. Even the organic skin theory of cavitation nuclei could have some possible justification in silt specimens. The silt being tested in this study was found to contain trace roots and small shells and was deposited in an alluvial environment where organic substances could very likely have been present in the transport and depositional water.

The idea that cavitation of soil pore water can initiate from nuclei within the pore water has been identified by others, as well. Bishop and Eldin (1950) stated that the limiting negative pressure which the pore water of fine-grained soils can sustain can be dependent on the soil grain size, as well as on the amount of dissolved

gas in the water and the presence of minute bubbles to act as nuclei for gas to come out of solution.

Chace (1975) noted that pockets of undissolved gas trapped in cracks and crevices on the surfaces of solid particles can serve as nuclei for air coming out of solution from the pore water of soil. He believes that sand particles could be expected to have an abundant number of cracks and crevices in which bubble nuclei could remain stable.

The cavitation literature indicates that gas coming out of solution and forming bubbles, due to a reduction in pressure, is considered to be cavitation. Gaseous cavitation, as many researchers refer to this, is encountered in many real liquids where dissolved gas is present in the liquid. This is the type of cavitation that is expected in Q tests on saturated silts because the pore water of saturated soil will likely contain dissolved gases. The dilatant tendencies of these soils will result in pore pressure reductions in the specimens during undrained shear. As a result of these reductions in pore pressure, air dissolved in the pore water could potentially come out of solution, in accordance with Henry's law. Even if the reduction in pore pressure does not reach the vapor pressure of water where vaporous cavitation would be expected to

occur, gas would still be able to come out of solution and affect the observed behavior of the soil.

The effect of the dissolved air content of the pore water on cavitation or air coming out of solution is an important consideration in cavitation studies as well as in soil mechanics problems. In general, studies have shown that as the dissolved air content of water increases, the tension or negative pressure which the liquid can resist without cavitating decreases. In addition, it has been indicated that for liquid in contact with large particles, which silt particles would be in terms of sources of cavitation nuclei, the dissolved gas content of the liquid may have a greater effect on the occurrence of cavitation (Apfel, 1970). The solubility of air in water and the rate at which air goes into and comes out of solution in water, along with the dissolved gas content of groundwater, will be discussed in more detail in Chapter 4.

The mineralogy of the soil particles and the cleanliness of their surfaces may have some effect on cavitation as different minerals have different degrees of wettability. Mitchell (1993) indicates that soil particles are very easily wetted by water and that the water molecules are bonded quite strongly to the soil particle surfaces. If impurities are present on the surfaces of the soil

particles, the ability of water to wet the particle surface may be reduced. The presence of impurities or contamination on the surfaces of soil particles may lead to weaker bonds between the water molecules and the soil particles (Bloomsburg and Corey, 1964). Saturated silts may show some difference in their Q test behavior if the silt particles have different mineralogy or if the soil particles have foreign contaminants on their surfaces. Slight variations of these variables may affect the bond between the water and the soil particles which may then influence the pressure at which cavitation will occur in the pore water.

Another potential cause of cavitation in Q tests on silt specimens is tribonucleation. Tribonucleation of cavitation bubbles or the idea that cavitation bubbles can be formed by solid particles rubbing against each other in a liquid under negative pressure, could have great significance in Q tests on silt specimens. During Q tests, numerous shear planes can develop along which particles will rub against each other. For tests at low confining pressures where pore pressures often become negative as the specimen attempts to dilate during shear, the rubbing of soil particles against each other along a shear plane may possibly result in the nucleation of cavitation bubbles.

The effect of temperature on the occurrence of cavitation or gas coming out of solution from pore water is also an important consideration in the sampling of saturated silts. As temperature increases, the solubility of air in water decreases. The significance of this will be discussed in detail in Chapter 4.

3.10 Summary and Conclusions

The review of the cavitation literature has provided a better understanding of the phenomenon of cavitation and its potential occurrence in saturated silts during sampling and Q tests. A number of the major concepts obtained from the cavitation literature which can be applied to the potential occurrence of cavitation in soil mechanics and laboratory testing of soils are as follows:

- (1) Gas coming out of solution from water is considered *gaseous cavitation* and can occur if the dissolved gas content of the liquid exceeds the equilibrium dissolved gas content at some reduced pressure. Unlike *vaporous cavitation*, gaseous cavitation can occur at pressures above the vapor pressure of water.
- (2) The dissolved gas content of a liquid will influence the pressure at which gaseous cavitation will occur. In addition to the magnitude of the pressure reduction,

the rate at which the reduction in pressure takes place will also affect the amount of gas that can potentially come out of solution.

- (3) Cavitation bubbles are believed to initiate from nuclei in the form of pockets of air trapped in cracks and crevices present on solid surfaces in contact with the liquid. Soil grains could potentially contain a number of such nuclei on their surfaces.
- (4) The reduction in pore water pressure which occurs in Q tests on dilatant silts takes place gradually and can be considered as a static application of tension to a liquid. This gradual reduction in pressure makes the possibility that dissolved gases will come out of solution from the pore water appear reasonable.
- (5) Tribonucleation or the formation of cavitation bubbles as a result of soil grains rubbing against each other within a liquid under negative pressure may be a potential cause of cavitation in saturated dilatant soils.
- (6) Temperature tends to influence the cavitation of water in a relationship that is similar to the variation of gas solubility with temperature. This may be

significant where notable changes in temperature occur between soil pore water in-situ and in the laboratory.

- (7) Cavitation of soil pore water, in the form of gases dissolved in the pore water coming out of solution during sampling and undrained shear tests, appears to be a distinct possibility for saturated dilatant soils such as silts, when tested in undrained triaxial tests.

Chapter 4

SOLUBILITY OF AIR IN WATER, AIR-WATER RELATIONSHIPS IN SOILS, AND RATE AT WHICH AIR GOES INTO AND COMES OUT OF SOLUTION IN WATER

As discussed in Chapter 3, air or gas coming out of solution from water due to a reduction in pressure is considered gaseous cavitation in the cavitation literature. In addition to being considered by those studying the cavitation behavior of liquids, gaseous cavitation is also studied by chemistry and physics researchers who are concerned with the solubility of gases in liquids, as well as the rate at which air or gas goes into and comes out of solution in water.

In this chapter, a review of the literature on the solubility of air in water and its rate of solution and dissolution will be presented. Additional studies found in the literature involving air-water systems in soil mechanics problems will also be discussed.

4.1 Application of Henry's and Boyle's Laws to Air-Water Systems

The relationship between the air in contact with a water surface and the air dissolved in the water is based on Henry's Law of Solubility and Boyle's law. Henry's law

states that at low to moderate pressures, the solubility of a slightly soluble gas in a liquid is directly proportional to the pressure of the gas above the liquid (Henry, 1803; Masterton, Slowinski, and Stanitski, 1981).

Henry's law can be somewhat confusing. It can be clarified by emphasizing that it is the mass rather than the volume of gas that can be dissolved in a given mass of liquid at a given temperature, which is proportional to the pressure of the gas above the liquid (Hawley's Condensed Chemical Dictionary, 1987). As will be shown subsequently, by applying Boyle's law to the gas as well, the volume of gas which can be dissolved in a given volume of liquid is found to be independent of pressure and varies only with temperature. The relationship for the volume of gas which can be dissolved in a liquid is given as follows (Henry, 1803; Rau and Chaney, 1988):

$$V_{dg} = H V_w \quad (4-1)$$

where V_{dg} = the volume of gas dissolved in the liquid at equilibrium conditions,

H = the coefficient of solubility of the gas in the liquid for a given temperature, and

V_w = the volume of the liquid.

The coefficient of solubility, H , is often referred to as Henry's coefficient of solubility in the geotechnical literature (Bishop and Eldin, 1950; Rau and Chaney, 1988).

In the chemistry and physics literature the same coefficient of solubility is given as L, and is referred to as the Ostwald coefficient (Fogg and Gerrard, 1991; CRC Handbook of Chemistry and Physics, 1988). In this research, the letter H will be used to refer to the coefficient of solubility of air in water.

At room temperature (about 20°C), the coefficient of solubility of air in water, H, is approximately equal to 0.02 (Bishop and Eldin, 1950; Rau and Chaney, 1988). This means that for equilibrium conditions at 20°C, the volume of air which can be dissolved in a unit volume of water is 2 percent of the water volume. Table 4.1 gives values of the coefficient of solubility of air in water at various temperatures.

Table 4.1: Solubility of air in water at various temperatures (CRC Handbook of Chemistry and Physics, 1988)

Temperature (°C)	Coefficient of Solubility of Air in Water, H (volume/volume)
5	0.02587
10	0.02352
15	0.02151
20	0.01999
25	0.01880
30	0.01778

Although the molecular structure of liquid water is felt to be variable and is not fully understood, according to Fredlund (1976), water molecules tend to form a lattice structure in which there are holes or voids present within the structure. Molecules of the gases which make up atmospheric air are able to diffuse into these voids and exist within the water structure as dissolved gas. The water molecules basically form a cage around the gas molecules (Rodehush and Buswell, 1958). The size of the holes or voids is dependent on temperature, and at 20°C the holes make up approximately 2 percent of the water volume (Fredlund, 1976).

Boyle's law states that the volume of a gas sample at constant temperature is inversely proportional to its pressure (Masterton, Slowinski, and Stanitski, 1981). Because the air which dissolves in the water remains in the form of a gas and does not form a liquid itself or chemically react with the water to any great extent, the Ideal Gas Law and Boyle's law can be applied to the air in solution as well as the free air. The Ideal Gas Law can be written as (Masterton, Slowinski, and Stanitski, 1981):

$$PV = nRT \quad (4-2)$$

where P = the absolute pressure of the gas,
V = the volume occupied by the gas,
n = the number of moles of gas present,

R = the universal gas constant, and

T = the absolute temperature of the gas.

When the amount or number of moles of gas present, n , is kept constant and a constant temperature is maintained, the above equation reduces to Boyle's law:

$$PV = \text{Constant} \quad (4-3)$$

or

$$V = \frac{\text{Constant}}{P} \quad (4-4)$$

In a closed system, such as a Q test specimen where no drainage is allowed, the masses of air and water are constant throughout the test and the temperature can be assumed to be constant as well. In this case, Henry's law and Boyle's law can be combined and applied to the air-water mixture.

Fredlund (1976) applied Henry's and Boyle's laws to a constant volume, constant temperature system. He stated that, by Boyle's law, the volume of a gas decreases with increasing pressure just as rapidly as the weight of dissolved gas increases by Henry's law; therefore, the volume of gas dissolved in a liquid is independent of pressure. He proved this by applying Boyle's and Henry's laws to an air-water system.

Using subscripts *i* and *f* to denote initial and final conditions, the Ideal Gas Law can be applied to the air dissolved in the water and can be written as (Fredlund, 1976):

$$P_{ai}V_{di} = w_{di}R_aT \quad (4-5)$$

$$P_{af}V_{df} = w_{df}R_aT \quad (4-6)$$

where P_{ai} = the initial pressure of the dissolved air,
 P_{af} = the final pressure of the dissolved air,
 V_{di} = the initial volume of dissolved air,
 V_{df} = the final volume of dissolved air,
 w_{di} = the initial mass of dissolved air,
 w_{df} = the final mass of dissolved air,
 R_a = the specific gas constant for air (converted from the universal gas constant in terms of moles of gas to specific gas constant for air in terms of average molecular weight of air), and
 T = the absolute temperature (K) which is assumed to be constant.

Because the weight of dissolved air is proportional to the pressure of the air, using similar notation, Henry's law can be written as:

$$\frac{w_{di}}{w_{df}} = \frac{P_{ai}}{P_{af}} \quad (4-7)$$

This equation can be rearranged to give:

$$w_{df} = w_{di} \frac{P_{af}}{P_{ai}} \quad (4-8)$$

Equations 4-5 and 4-6 can be rearranged to give:

$$V_{di} = \frac{w_{di} R_a T}{P_{ai}} \quad (4-9)$$

$$V_{df} = \frac{w_{df} R_a T}{P_{af}} \quad (4-10)$$

Substituting the relationship for w_{df} from Eq. 4-8 into Eq. 4-10 gives:

$$V_{df} = \frac{w_{df} R_a T}{P_{af}} = w_{di} \frac{P_{af}}{P_{ai}} \frac{R_a T}{P_{af}} \quad (4-11)$$

which reduces to:

$$V_{df} = \frac{w_{di} R_a T}{P_{ai}} \quad (4-12)$$

Because the right-hand side of Eq. 4-12 is equal to the right-hand side of Eq. 4-9, the left-hand sides of Eqs. 4-12 and 4-9 must be equal as well, so that $V_{di} = V_{df}$. Thus, the volume of dissolved air present in the liquid is the same at any pressure, as long as the temperature remains constant.

According to Fredlund (1976), because the volume of dissolved air remains constant, the volumes of free and dissolved air can be combined and Boyle's law applied to the entire volume of air. Thus, for a closed system of free air in contact with water containing dissolved air, Boyle's law can be written as:

$$P_g (V_g + V_{dg}) = \text{Constant} \quad (4-13)$$

where P_g = the absolute pressure of the air above the liquid,

V_g = the volume of free air present, and

V_{dg} = the volume of dissolved air present in the liquid.

Special note should be made of the assumption that the temperature remains constant throughout the process considered in the above derivation. According to Masterton, Slowinski, and Stanitski (1981), when a gas goes into solution in a liquid, heat is usually given off from the system and the liquid cools. Alternatively, heat is required during the process of gas coming out of solution. This means that as gas comes out of solution from water, the temperature of the liquid increases, or in other words, as the temperature of the water increases, the amount of gas which can be dissolved in the liquid decreases. In this research, however, a constant temperature was assumed as a justified simplification when analyzing Q tests, because the

value of the coefficient of solubility for air in water over the range of temperatures expected in the laboratory working environment does not vary considerably, as shown in Table 4.1 (CRC Handbook of Chemistry and Physics, 1988).

Temperature variations between in-situ and laboratory conditions, however, may have a significant effect on the solubility of gases in soil pore water during and after sampling. This will be discussed in more detail in Sections 4.4 and 4.5.

4.2 Dissolved Gas Content of Soil Pore Water

When a saturated silt experiences a reduction in pore water pressure, gas dissolved in the pore water will have a tendency to come out of solution, in accordance with Henry's law. This will be true if the reduction in pressure results in the dissolved gas content of the liquid exceeding the equilibrium value at the reduced pressure. One of the variables which must therefore be considered is how much dissolved gas is present in the pore water of saturated silts.

4.2.1 Dissolved Gas Content of Soil Pore Water in Remolded Specimens

For the saturated silt specimens remolded from a slurry in the laboratory and used in the majority of the tests described in Chapter 5, the mixing of the silt with

distilled water at atmospheric pressure very likely resulted in the soil pore water being saturated with dissolved gas at atmospheric pressure. For the laboratory environment and the silt used in this study, the gases likely to be dissolved in the pore water would be those present in atmospheric air.

For these remolded, fully saturated soil specimens, Q tests performed at confining pressures greater than atmospheric pressure would have likely yielded soil pore water which was undersaturated with dissolved air at the cell pressure used in the test. Thus, as the pore pressure decreased during the test, air would not have tended to come out of solution until the decrease in pore pressure had negated the increase in pore pressure resulting from the applied cell pressure. Once the pore pressure was reduced below atmospheric pressure, the equilibrium dissolved gas content of the liquid would have been exceeded and air would have had the potential to come out of solution.

On the other hand, if the specimen was not fully saturated but had small pockets of undissolved air present in the specimen initially, the applied cell pressure would have possibly forced this free air into solution to give a fully saturated sample. With this additional air in solution, as the pore pressure of the specimen decreased

during undrained shear, this air could have come back out of solution as the equilibrium dissolved gas content of the water at a given pressure was exceeded.

4.2.2 Dissolved Gas Content of Soil Pore Water in the Ground

For saturated silts present below the ground water table, the dissolved gas content of the pore water is more difficult to assess. A review of the literature indicates that the dissolved gas content of ground water is a complex function of a number of factors and may vary considerably.

According to Henry's law, under equilibrium conditions at a given temperature, the dissolved gas content of water is dependent on the pressure of the gas in contact with the water. For a volume of water in equilibrium with the gas above it, the dissolved gas content at any depth in the liquid should be dependent only on the pressure of the gas above the liquid and the temperature of the gas-water system. Thus, for equilibrium conditions, the dissolved gas content of the liquid should be the same throughout the depth of the liquid, and be independent of the variation of hydrostatic pressure within the liquid. For this reason, the pore water in a silt sampled from a considerable depth below the ground water table should not have a higher dissolved gas content than a sample taken from a shallower

depth below the ground water table, because the hydrostatic pressure of the ground water should not be a factor. This should be true as long as there is equilibrium by Henry's law between the pore water system and the soil-gas system above the saturated zone.

Water at the earth's surface is in contact with atmospheric air and should be saturated with dissolved air under equilibrium conditions. Atmospheric air is composed of several different gases which are present in certain proportions. The composition of air and the proportion of each gas present varies slightly between urban and rural areas and with altitude within the earth's atmosphere (Matthess and Harvey, 1982). The U.S. Standard Atmosphere (CRC Handbook of Chemistry and Physics, 1993) gives the standard composition of the earth's atmosphere and is presented in Table 4.2.

Pure water in contact with air should contain dissolved gases in the same proportions as are present in atmospheric air, as long as equilibrium conditions are maintained. In bodies of surface water where the water is not necessarily pure, some of the dissolved gases present in the water may react with other substances present in the liquid, thus reducing the amount of dissolved gas in the liquid.

Table 4.2: Molecular weights and assumed fractional-volume composition of sea-level dry air (CRC Handbook of Chemistry and Physics, 1993)

Gas	Molecular Weight (g/mol)	Fractional Volume	Percent of Atmospheric Air by Volume (%)
N ₂	28.0134	0.78084	78.08
O ₂	31.9988	0.209476	20.95
Ar	39.948	0.00934	0.93
CO ₂	44.00995	0.000314	0.03
Other Gases	-	0.000027	< 0.01

Dissolved oxygen present in the water may be utilized by biologic organisms or foreign chemicals present in the water. Organisms such as microscopic bacteria, fish and plants will use dissolved oxygen from the water. Foreign chemicals present in the water also may use dissolved oxygen in oxidation processes. If the dissolved oxygen is used faster than it can be replenished from the atmosphere at the water surface, depletion of the dissolved oxygen will eventually result. It has been observed that in open bodies of water such as lakes, the concentration of dissolved oxygen often decreases to zero at some depth within the body of the water. This is a result of biological and chemical depletion of the dissolved oxygen in the lake (Vesilind and Peirce, 1982).

Dissolved gases should be present in ground water as well as in surface water. Rain drops descending through the

atmosphere are typically saturated with dissolved air (Davis and DeWiest, 1966; Rose and Long, 1988). A certain percentage of this rain will infiltrate the soil and recharge the ground water system. Davis and DeWiest (1966) stated that because this recharge water should be saturated with dissolved air, it might be expected that the resulting ground water would be saturated with dissolved air as well. They added, however, that ground water may contain variable amounts of dissolved atmospheric gases, as well as some gases not commonly found in abundance in the atmosphere.

Davis and DeWiest (1966) noted that the dissolved gas content of water when it first enters the soil can be considerably different than the dissolved gas content of the ground water at some point below the surface. Water saturated with dissolved atmospheric gases is estimated to contain between 20 and 40 ppm of dissolved gas, depending on temperature. Davis and DeWiest (1966) stated that ground water may contain dissolved gases in concentrations between 1 and 100 ppm. They added that once the infiltrated water reaches the fully saturated zone of an aquifer, the dissolved gas content of the ground water should remain relatively constant. Long term reactions, such as oxidation of minerals, however, may result in slight variations in dissolved gas content of ground water. As of the mid-1960s, however, analyses of the dissolved gas content of ground

water were not typically performed (Davis and DeWiest, 1966).

According to Freeze and Cherry (1979), the dissolved gas content of ground water located at some depth below the ground surface can often be different from that of water simply exposed to atmospheric gases prior to infiltration. This is a result of two processes:

- (1) Exposure of water to soil gases in the unsaturated zone during infiltration may alter the dissolved gas content of the water because the composition of soil gas in contact with the soil water can be somewhat different than atmospheric air, and
- (2) Additional gases produced in the saturated zone through chemical or biochemical reactions involving the ground water, minerals, organic matter, and bacterial activity, can become dissolved in the ground water.

According to Freeze and Cherry (1979), the gases which are most often dissolved in ground water are N_2 , O_2 , CO_2 , CH_4 , H_2S , and N_2O . The first three of these gases (N_2 , O_2 , CO_2) are the major gases which make up the atmosphere, as shown in Table 4.2, so their presence in ground water is not unusual. The other three gases (CH_4 , H_2S , and N_2O) are also often found in ground water in significant concentrations.

They stated that these three gases are produced below the ground surface by *biogeochemical* processes.

Freeze and Cherry (1979) stated that two of the most important gases which can be dissolved in ground water are oxygen and carbon dioxide. They noted that the oxidation of organic soil matter utilizes oxygen gas from the unsaturated zone of the soil. This gives the soil gas a lower oxygen content than atmospheric air. Dissolved oxygen from the infiltrating water can also be used by organic matter in the upper layers of the soil. The use of dissolved oxygen (D.O.) from the infiltrating water, as well as the low oxygen content of the soil gas in contact with the ground water, often leads to a lower dissolved oxygen content in ground water than in surface water exposed to atmospheric gases.

The biologic processes which utilize oxygen gas and dissolved oxygen result in the production of carbon dioxide in both the partially saturated and saturated zones of the soil. This, in turn, increases the carbon dioxide content of soil gas above that of atmospheric air. The increased carbon dioxide content of soil gas results in a higher partial pressure of carbon dioxide in the soil gas, relative to atmospheric air. Under this condition, more carbon dioxide can be dissolved in ground water than in surface

water (Freeze and Cherry, 1979). Trainer and Heath (1976) stated that it is not unusual for soil gas to contain several hundred times more CO₂ gas than atmospheric air.

Freeze and Cherry (1979) stated that water infiltrating through the highly organic layers of a soil usually loses much of its D.O. to the oxidation of the organic matter. They added that the removal of D.O. in the organic soil layers is affected by several factors. The soil structure, porosity, permeability, the nature and distribution of organic matter, the frequency of infiltration events, the depth to the water table, and temperature all can affect the amount of D.O. which could be removed from the infiltrating water.

Freeze and Cherry (1979) made the following generalizations on the removal of D.O. from soil water:

- (1) For recharge areas with high permeability soils, such as sandy or gravelly soils or in cavernous limestone, shallow ground water typically contains dissolved oxygen at detectable levels.
- (2) For recharge areas with soils of low permeability, such as silts and clays, shallow ground water typically does not contain dissolved oxygen at detectable levels.

- (3) For areas where little or no organic soil is present, detectable levels of dissolved oxygen are often present within the aquifer to considerable depths.

The dissolved oxygen content of water is often measured in surface waters as an indication of water quality. Its measurement in ground water has also been performed in limited studies as an indication of ground water quality. For water at sea level ($P_{atm} = 14.7$ psi abs), the amount of oxygen which can be dissolved in water at various temperatures is given in Table 4.3. The solubilities for oxygen given in Table 4.3 assume that the water has no dissolved salts present. As the dissolved salt content of water increases, the solubility of oxygen and other gases decreases (Freeze and Cherry, 1979).

Table 4.3: Solubility of oxygen in water exposed to water-saturated air at standard atmospheric pressure at various temperatures (Standard Methods, 1992)

Temperature (°C)	Oxygen Solubility (ppm by weight) or (mg/L)
0	14.62
5	12.77
10	11.29
15	10.08
20	9.09
25	8.26
30	7.56

Brubaker (1993) noted that high quality shallow ground water typically contains 4 to 6 ppm dissolved oxygen. He

added, however, that if the ground water becomes contaminated by a biodegradable material, the D.O. content of the ground water can fall to less than 0.5 ppm.

Research has shown that the distribution of dissolved oxygen in ground water aquifers tends to be random or erratic (Barker and Patrick, 1985). Other studies have shown more systematic variations of D.O. (Pionke and Urban, 1987; Rose and Long, 1988). Still another study (Ronen et al., 1987) indicated a relatively uniform dissolved oxygen content throughout a ground water aquifer.

In more temperate climates where organic soil layers are more highly developed, studies have shown an erratic and larger variation in the dissolved oxygen content of ground water (Barker and Patrick, 1985; Pionke and Urban, 1987). Ground water in arid regions tends to show less variation of dissolved oxygen content (Winograd and Robertson, 1982; Ronen et al., 1987; Rose and Long, 1982). The dissolved oxygen content of ground water was found to decrease where sewage effluent was used for irrigation (Ronen et al., 1987) and where organic hydrocarbons were injected into the ground water (Barker and Patrick, 1985). Heaton and Vogel (1980) noted that certain soil environments may be more favorable than others for rapid removal of dissolved oxygen from ground water.

Rose and Long (1988) noted that supersaturation of ground water with dissolved oxygen was not observed anywhere within the aquifer they studied. They added that it would be unlikely for ground water to be supersaturated with dissolved oxygen.

Although it has been suggested that the D.O. content of ground water decreases as the age of the ground water increases (Lloyd and Heathcote, 1985), field studies still observed significant D.O. concentrations in ground water ranging in age from several thousand years to tens of thousands of years old (Rose and Long, 1988; Winograd and Robertson, 1982). In another instance, the D.O. content was observed to decrease with increasing age within an aquifer (Pionke and Urban, 1987). These differences may possibly be attributed to the different soil mineralogy and organic matter present in the aquifers studied.

Davis and DeWiest (1966) also stated that certain types of bacteria will utilize nitrogen gas dissolved in ground water and may lead to the depletion of dissolved nitrogen, as well.

While the dissolved oxygen content of ground water is often reduced or depleted by oxidation of organics or minerals within the soil, other gases may be produced and contribute to the dissolved gas content of ground water.

Carbon dioxide (CO_2) gas is produced by biologic processes, and its production is related to the use of dissolved oxygen. In general, as the D.O. content of ground water decreases, the amount of dissolved carbon dioxide present in the ground water increases (Matthess and Harvey, 1982).

According to Freeze and Cherry (1979), some of the CO_2 gas produced in the soil and ground water likely escapes into the atmosphere and partially saturated zone above the ground water table. Much of it, however, can become dissolved in the ground water. Once in the ground water, some of it (about 1%) reacts chemically with the water to form carbonic acid (H_2CO_3) (Matthess and Harvey, 1982). The presence of carbonic acid in ground water is responsible for the dissolution of carbonate rocks such as limestone.

Trainer and Heath (1976) noted that vegetative cover and soil properties can play an important role in whether CO_2 is able to escape to the atmosphere or remains trapped in the soil. The carbon dioxide content of soil gas tends to be higher beneath grasslands than beneath cultivated fields. They added that it may be more difficult for CO_2 gas to escape from silty or fine-grained soils than from coarser soils. Freeze and Cherry (1979) noted that CO_2 pressures in soil gas vary from one location to another as well as seasonally.

Carbon dioxide gas dissolved in ground water may come out of solution when water is sampled or where a spring occurs and water exits the ground water system. During sampling of ground water, CO₂ gas coming out of solution will alter the acidity of the water and its pH (Matthess and Harvey, 1982). For this reason, pH measurements of ground water should be made in-situ or in the field as soon after sampling as possible.

For the condition where ground water containing dissolved gas exits the ground at a spring, not only can gas come out of solution due to the temperature increase but also due to the partial pressures of the gases present being reduced to the partial pressures for atmospheric gases. In this situation, dissolved gases will likely be released from solution and if the water contains dissolved carbonates, limestone deposits will precipitate (Matthess and Harvey, 1982). The existence of so-called naturally carbonated spring waters is possibly a result of this process. The ground water exiting the ground at the spring is supersaturated with dissolved CO₂, relative to atmospheric pressure, so that CO₂ bubbles form within the spring water.

Davis and DeWiest (1966) noted that temperature fluctuations in the ground water flow system may lead to dissolved gases coming out of solution. The mixing of warm

and cool ground water plumes in an aquifer may result in dissolved gases being released from the cooler ground water plume. Similarly, hot water springs would be able to contain less dissolved gas than cold water springs. At some hot water springs, ammonia gas can also be released.

Davis and DeWiest (1966) also noted that gas coming out of solution and forming bubbles within the ground water system can hamper ground water flow. This can be especially true near wells where pressure reductions occur due to pumping and gas bubbles can clog well screens and be drawn up into wells.

Another gas which can sometimes be found dissolved in ground water is methane gas (CH_4) which is produced as a result of organic decomposition within the soil. According to Davis and DeWiest (1966), methane gas can come out of solution from ground water and accumulate in buildings, pumps and wells in explosive concentrations.

According to Freeze and Cherry (1979), hydrogen sulfide gas (H_2S) is another gas which is sometimes dissolved in ground water. It is produced by the chemical reduction of certain sulfur containing minerals present in the soil. Even the smallest amount of hydrogen sulfide coming out of solution can lead to an undesirable odor which makes the water unfit for consumption.

Freeze and Cherry (1979) also discussed the entrapment of gas within the soil zone during significant recharge events. They stated that during periods of very intense rainfall, a zone of saturation can form in the soil near the ground surface. Between this saturated zone near the ground surface and the ground water table below, soil gas can become trapped. As the saturated plume advances downward toward the ground water table, pressure in the gas trapped between the two saturated zones becomes greater than atmospheric pressure. They stated that eventually this soil gas under increased pressure will escape laterally from between the water saturated zones. It is possible, however, that the increased pressure developed in the trapped gas will temporarily force some of these gases into solution in the ground water.

Smith and Browning (1942) discussed the trapping of soil gases in soils during saturation. They observed that silty soils were often more difficult to saturate than clays or sandy soils. They stated that this resulted from the entrapment of air bubbles within the intermediate sized pores of the silt.

Smith and Browning (1942) performed experiments in which samples of clay, silt and sand were first allowed to absorb water by capillarity from an adjacent supply of

water. Water was then allowed to flow through the specimens under an applied head. They found that the clay reached almost full saturation primarily as a result of capillarity. The sand, on the other hand, did not take in much water by capillarity but under a head of flowing water, it became essentially fully saturated. The silty soils, however, tended to remain somewhat less than fully saturated even after allowing the soil to absorb water by capillarity followed by flowing water through the soil under an applied head. Even when the head of water was applied to the silt for a longer period of time, the silt continued to remain less than fully saturated. The clay and sand samples reached essentially a degree of saturation of 100 percent. The silt samples, however, only reached an average degree of saturation of about 91 percent.

Smith and Browning (1942) stated that in the clay, the pore size and the strong surface adsorption characteristics of the clay particles lead to strong capillary tension forces. Either these strong capillary or surface tension forces compressed the air and forced it into solution relatively quickly or the swelling of the clay forced the air out of the soil. In the sand, the larger pores would still contain a considerable amount of air after capillary suction of water was complete. Because of the larger pores and coarse structure of the soil, flowing water through

the soil under sufficient head, tended to force this air out of the soil so that essentially complete saturation was reached.

According to Smith and Browning (1942), the intermediate pore sizes in the silt resulted in the trapping of air pockets or bubbles within the soil structure. Capillary suction caused a considerable amount of water to be drawn into the soil. Some of this water was able to fill in the pores of the soil but much of the water was likely retained at the contact points between the soil grains as a result of capillary tension. Air bubbles therefore became trapped in soil pores by water menisci in the grain-to-grain contacts surrounding the pores. Water flowing through the soil under an applied head was unable to force these trapped air bubbles out of the pores of the soil and the air in the bubbles was therefore forced to diffuse into solution. This process resulted in a longer period of time being necessary before full saturation could be reached in the silt. Eventually, surface tension forces would force the air in the bubbles into solution in the pore water, supersaturating the pore water with dissolved air. Over time, diffusion of the dissolved air through the pore water would take place in order to reestablish equilibrium between the dissolved gas content of the water and the pressure of the soil gas.

Chahal (1964) considered the desorption process in soils composed of *inert* particles, such as sand and silt. He stated that because the solubility of air in water is dependent on temperature and pressure, air dissolved in the soil pore water may come out of solution as pressure decreases and as temperature increases. He also mentioned the possible nucleation of air bubbles in soil pore water. As water drains from a soil, the tension in the pore water increases and air bubbles can form by several possible mechanisms. Air may become trapped in pores previously drained as particles shift and redistribution of pore water occurs in the soil. Air bubbles also may nucleate or form within the soil pore water as dissolved air comes out of solution.

Chahal and Yong (1965) noted that air bubbles can become trapped in soil pore water during the saturation and desaturation processes. They added that the bubbles may form within soil pore water at reduced pressures as a result of nuclei present in the soil from which bubbles can grow. As pressure is reduced, air dissolved in the pore water may come out of solution and form bubbles which would grow in size as the pressure continued to decrease.

Elrick (1963) noted that the inflow and outflow of water to soil pores occurs relatively slowly in soils with a

high degree of saturation. At high moisture contents, full saturation of a soil is achieved very slowly. This is believed to be due to the presence of trapped air within the soil pores. These pockets or bubbles of trapped air can not escape to the atmosphere and must therefore diffuse through the pore water to the atmosphere. The time to reach full saturation in this case is dependent on the distribution of pore sizes in the soil, as well as the distance between the trapped air and the external atmosphere.

Hillel (1980) noted that it is very difficult to completely saturate a soil without trapping some air. Entrapped air pockets tend to block pore passages. As water flows through the soil it is unable to force all of these air pockets out of the soil. In order for full saturation to be reached, the air trapped in these bubbles must dissolve into the pore water. Hillel (1980) added that temperature changes will influence whether gases come out of or go into solution in the soil pore water. If a change in temperature occurs in the soil pore fluid, the gas phase of the pore fluid will experience a change in volume.

Considering the above discussion, it is expected that the dissolved gas content of the pore water of a recently saturated silt deposit could be higher than the equilibrium dissolved gas content. Thus, sampling and undrained testing

of a recently saturated silt may have a greater chance of releasing dissolved gas from solution than a silt which has been continuously saturated for a long period of time and has reached equilibrium between the dissolved gas content and gas pressure. The times involved in considering whether a silt has been recently saturated or saturated for a long time are uncertain, relative to the dissolved gas content of the pore water.

Air bubbles may also become trapped in the pores of a soil during its deposition in an alluvial environment. Depending on the hydraulic conditions and the use of dissolved gases by biological and chemical demands in the river, the pore water of soil deposited in an alluvial environment may be undersaturated, saturated, or possibly supersaturated with dissolved gases at atmospheric pressure. Gas bubbles present in the soil-water mixture during deposition, could possibly remain as bubbles if they are trapped within the voids of the soil. Gas bubbles near the surface of the alluvial deposit may be able to work their way to the surface and leave the pore water of the soil.

Gas bubbles somewhat deeper in the alluvial deposit may however, be trapped within the soil pores and not be able to leave the pore water at the soil surface. It would be expected that fine-grained soils would have a better chance

of trapping undissolved gas bubbles within the soil matrix than would coarse-grained soils, due to the differences in pore size. With these trapped bubbles present in the soil pores, the addition of new layers of alluvial soil deposits would increase the pressure on the underlying soil layers and thereby force the undissolved bubbles into solution in the pore water. In this case, the dissolved gas content of the pore water would be greater than that under purely atmospheric pressure conditions. Over time, diffusion of dissolved gas from the supersaturated pore water to the soil gas zone would take place. Eventually, equilibrium conditions would be reached between the pressure of gases in the partially saturated soil zone and the dissolved gas content of the pore water. Prior to equilibrium conditions being reached, if such a soil was sampled and brought to the ground surface, dissolved gases could come out of solution from the supersaturated pore water.

If, however, when the soil was deposited, the soil pore water was only saturated with dissolved air at atmospheric pressure and no free air bubbles were trapped in the soil pores, when the soil was sampled and brought to the surface, the reduction of the air pressure to atmospheric pressure should not lead to dissolved air coming out of solution from the pore water. If the soil deposit was allowed to dry out and then became resaturated by flooding or a rise in the

ground water level, the soil pore water may only be saturated with dissolved gas at atmospheric pressure. As indicated by Smith and Browning (1942) however, gas bubbles may become trapped in certain soils during saturation. These trapped bubbles will eventually be forced into solution by surface tension forces, so that the pore water would be supersaturated with dissolved gases until equilibrium conditions had been reached over time.

Based on the above discussions, the dissolved gas content of soil pore water can be seen to have the potential to show considerable variation. It may be undersaturated with certain gases, relative to atmospheric conditions. It also may be supersaturated with other dissolved gases. A gas which the ground water was supersaturated with, such as CO_2 , would tend to come out of solution when the soil and pore water are exposed to atmospheric conditions. A gas which the ground water was undersaturated with, such as oxygen, would tend to go into solution when the soil and pore water are exposed to atmospheric conditions.

It does not appear to be realistic to assume that ground water is saturated with a mass of dissolved gas corresponding to the hydrostatic pressure of the water at some depth below the ground water level. An assumption such as this would provide an extreme upper bound on the mass of

dissolved gas present in the soil pore water. It would also yield an unrealistically high amount of gas that could possibly come out of solution from the pore water when the pore gas and pore water pressures are reduced during sampling.

It does appear, however, that variations in the dissolved gas content of ground water can be reasonably expected and that ground water may be supersaturated with some dissolved gases relative to atmospheric conditions. This may be especially true for silts which tend to trap more air bubbles during saturation than clays or sands (Smith and Browning, 1942). Variable dissolved gas contents of the pore water of saturated silts may result in different amounts of the various dissolved gases present coming out of solution during sampling and undrained triaxial tests. A group of specimens obtained from approximately the same depth in a saturated silt deposit, however, would be expected to have pore water with relatively the same dissolved gas content for all of the specimens in the group.

4.2.3 Measurement of Dissolved Air Content of Water

Several methods can be used to determine the amount of air dissolved in water. These include: the Winkler test to determine the amount of dissolved oxygen present in water; a dissolved oxygen probe; a Van-Slyke apparatus or other

device in which gases are extracted from a liquid under a vacuum while measuring pressure; and equilibrium methods where Henry's law is applied (Eisenberg, 1961).

According to Vesilind and Peirce (1982), the Winkler test involves the addition of chemicals to water which react with the dissolved oxygen to form a precipitate from which the dissolved oxygen content of the liquid can be determined. A dissolved oxygen probe uses electrodes to measure an electric current in the liquid which can be related to the dissolved oxygen content of the water. With both of these methods, the amount of dissolved air in the water would be inferred from the dissolved oxygen content, based on the proportion of oxygen in air. This may be a reasonable approach in pure water exposed to atmospheric gases. If, however, the water contains impurities which utilize dissolved oxygen, using the measured D.O. content of the water to infer the amount of other atmospheric gases present would likely underestimate the amount of these other gases dissolved in the water.

In a Van-Slyke gas apparatus, the air content of a liquid is measured by placing a 10 cm³ sample of liquid into the apparatus. The liquid sample is then agitated under a vacuum until all of the air is removed. The removed air is then compressed to a volume of 2 cm³ and its pressure is

measured. The volume of the air at normal temperature and pressure can then be calculated using the Ideal Gas law (Strasberg, 1959).

In assessing the amount of dissolved gas present in the pore water of soils, a dissolved oxygen meter was used as part of this research to measure the dissolved oxygen content of pore water samples obtained from a saturated, undisturbed soil specimen. The meter used was a YSI Model 54 Oxygen Meter, on loan from the Virginia Tech Environmental Engineering Division of the Civil Engineering Department. The meter measured the dissolved oxygen content of water in parts per million (ppm) which is equivalent to milligrams of dissolved oxygen per liter of water.

Undisturbed samples of silt were provided by the U.S. Army Corps of Engineers for this research. These samples were only about 50 percent saturated so no attempt was made to extract water from these samples in this analysis.

Undisturbed samples of a saturated silty clay from the Olmstead Lock and Dam project were available, however, and were used in this analysis. A specimen approximately 5 in. long and 5 in. in diameter was removed from a Shelby tube taken from a depth of approximately 20 ft. The sample was trimmed to about 4 inches in diameter and was placed in a triaxial cell. A consolidation pressure of about 250 psi

was then applied to squeeze water out of the soil and into a collection tube. Water was then drained from the tube into a small beaker and the D.O. content of the water was measured. The time required to squeeze a sufficient amount of water out of the soil to make the measurements was about 30 minutes.

Three samples of soil pore water were obtained from this specimen and the D.O. content of each sample was measured. The measured D.O. contents of these three pore water samples are presented in Table 4.4.

Table 4.4: Dissolved oxygen (D.O.) content of soil pore water from Olmstead Lock and Dam Tube No. AS-900, Sample # 1

Pore Water Sample Number	Temperature (°C)	Saturation D.O. Content* (ppm)	Measured D.O. Content of Soil Pore Water (ppm)
1	22	8.2	1.2
2	23	8.1	1.9
3	21.5	8.3	1.8

* Corrected for Blacksburg, VA (EL 2080 ft.)

As can be seen from these measured values of D.O., the soil pore water had dissolved oxygen concentrations which were less than the saturation values for water at the given temperatures. The soil from which the pore water was obtained was a silty clay. It had a dark color as well as an organic odor and appeared to contain organic material such as roots. This may explain the low D.O. content of

these soil pore water samples. Measurement of the CO₂ content of the pore water was not performed but may have shown more dissolved CO₂ in the pore water than its saturation value for atmospheric conditions at the given temperatures.

It is felt that because of the organic characteristics of the soil from which the pore water was obtained, the measured D.O. values can not be extrapolated to determine the amount of other atmospheric gases dissolved in the pore water. The use of these low D.O. values would probably underestimate the amount of other atmospheric gases present in the soil pore water.

Other samples of water from the Virginia Tech Geotechnical Engineering Laboratory, including tap, distilled and deaired water, were tested for their D.O. contents. The results of these measurements are given in Table 4.5.

Table 4.5: Dissolved oxygen (D.O.) content of various waters measured in the laboratory

Water Type	Temp. (°C)	Saturation D.O. Content* (ppm)	Measured D.O. Content (ppm)
Tap Water	23	8.1	7.7
Distilled Water	24	7.9	6.9
Deaired Water No. 1	22	8.2	1.7
Deaired Water No. 2	20	8.6	2.3

* Corrected for Blacksburg, VA (EL 2080 ft.)

Both the sample of tap water and distilled water showed D.O. contents which were close to but less than the saturation values at the given temperatures. This indicates that the water was somewhat undersaturated with dissolved oxygen, and probably, other atmospheric gases as well.

As expected, the two samples of deaired water showed considerably less dissolved oxygen present in the water than their saturation values for atmospheric conditions. Both samples still showed the presence of measurable D.O. This indicates that in the 1.5 to 3 minutes between releasing the vacuum in the deaerator chamber and measuring a constant value of D.O. in the water sample, either some dissolved gas had gone back into solution in the water or not all of the dissolved gas had been removed by the deaerator. The samples of deaired water consisted of about 40 ml of water in a 100 ml beaker. One of these samples was monitored over time and it was observed that within about four hours the D.O. content had risen to its saturation value.

In another test, distilled water was placed in a triaxial cell chamber and exposed to air at a pressure of 60 psig for 10 days. After ten days a sample of the water was extracted and the variation of the D.O. content of the water was observed over time. Assuming that equilibrium had been reached between the pressurized air and the dissolved gas

content of the water, in accordance with Henry's law, after ten days the water would have been saturated with D.O. at a pressure of 60 psig. A water sample was extracted from the triaxial chamber under somewhat agitated conditions and the D.O. content was measured over time. These measurements indicated that a majority (about 90 percent) of the dissolved oxygen came out of solution during the first minute after the reduction to atmospheric pressure conditions. Over time, the D.O. content of the water sample continued to decrease. After four hours the D.O. content of the pore water was still greater than its saturation value at the given temperature. The saturation value for atmospheric conditions was not reached until after about 17 hours had elapsed.

4.3 Pressure Reduction in the Pore Water of Saturated Silts

Air or gas dissolved in soil pore water may come out of solution from the pore water of a saturated silt specimen when a reduction in the pore water pressure takes place. The amount of gas which will come out of solution is dependent on the initial dissolved gas content of the liquid and the magnitude of the pressure reduction.

In addition to these two factors, another important variable to consider is the rate at which gas can come out of solution from the pore water due to the reduction in pore

pressure. According to Henry's law, as pressure decreases, the mass of gas which can be dissolved in the water also decreases. For a given pressure reduction, a certain amount of time will be required for the dissolved gas content of the liquid to decrease to reach its equilibrium condition at the lower pressure. It is the magnitude of this time, and the associated rate at which gas comes out of solution from water, that are important considerations in this research.

The pore water present in the voids of a saturated silt can be subjected to a pressure reduction in two different ways. First, when a saturated silt is sampled, the reduction in total stress causes the pore pressure to decrease in an attempt to maintain the effective stress within the sample (Ladd and Lambe, 1963). Second, a reduction in pore pressure may occur in a Q test performed on a saturated silt if the sample has a tendency for dilation during shear.

4.3.1 Pore Pressure Reduction Due to Sampling

A reduction in pore pressure occurs during the sampling of saturated silts. A saturated silt present at some depth below the ground surface will be subject to a certain state of total stress conditions. When the silt is sampled and brought to the surface, the total stress acting on the soil will be reduced. In an attempt to maintain the effective

stress in the sample, a decrease in the pore water pressure will occur in the soil (Ladd and Lambe, 1963).

Taylor (1948) stated that soils at a considerable depth below the ground water table will experience a significant pressure decrease during sampling. These soils may swell as air comes out of solution and expands within the specimen. Taylor (1948) added that the volume change which occurs as air or gas bubbles form and grow in the soil not only decreases the degree of saturation of the soil, "but also changes all soil properties which vary with the void ratio."

One of the main factors to be considered in this case is whether or not the reduction in pore pressure due to sampling results in the dissolved gas content of the liquid exceeding the equilibrium value at the reduced pressure. This in turn, will be dependent on the dissolved gas content of the soil pore water in the ground, which can be somewhat variable, as discussed in Section 4.2.2.

Another important consideration in assessing the possibility of air or gas coming out of solution from the pore water is whether sufficient time is available for the air or gas to come out of solution due to the pore pressure reduction associated with sampling. The time between sampling and testing soil in the laboratory ranges from several hours at the very least to tens or hundreds of days

in many cases. If gas or air has been released from the pore water of the silt and remains in the voids of the soil, the silt will no longer be fully saturated and its behavior in a Q test can be expected to be different from that of a fully saturated specimen.

4.3.2 Pore Pressure Reduction Due to Dilation

During Q tests on saturated silt specimens, a reduction in pore water pressure can occur due to the dilatant behavior of silts. Seed and Lee (1967) stated that the types of soils which usually exhibit strongly dilatant behavior are dense cohesionless soils with very sound, rounded grains. They added that soils composed of subangular or angular particles tend to be less dilatant due to particle crushing which may occur in these soils during shear.

When a silt specimen is tested in a triaxial test, shear stress develops within the specimen leading to the formation of a shear plane. As the shear stress in the specimen increases, the silt grains subjected to the shear stress can either break and crush to form a shear plane or they can rise up over each other as shearing proceeds (Odenstad, 1949).

For Q tests performed at low confining pressures, the rising of the silt grains over each other during shear attempts to expand the volume of the sample. Because the specimen is fully saturated and no drainage is allowed during a Q test, the potential volume expansion resulting from the rising of the silt grains over each other can not occur and instead a reduction in the pore water pressure takes place within the specimen (Nash, 1953). This reduction in pore pressure may lead to cavitation of the pore water at the vapor pressure of the liquid (Bishop and Henkel, 1962) or it may possibly result in the release of air or gas from solution, in accordance with Henry's law (Brandon, Duncan and Huffman, 1990).

If cavitation occurs or gas comes out of solution from the pore water during shear, vapor- or gas-filled bubbles would form in the pores of the soil and the specimen would no longer be fully saturated. Because the Q test specimen would now be less than fully saturated, the behavior of the silt in the test could be considerably different than for a sample in which no water vapor or gas were released from solution and the specimen remained fully saturated throughout the test.

Again, one of the major considerations here is the amount of dissolved gas present in the soil pore water. If

the pore pressure reduction resulting from dilation leads to a condition where the dissolved gas content of the liquid exceeds the equilibrium value at the lower pressure, gas will tend to come out of solution.

Another question which again arises is whether or not gas or air dissolved in the pore water of a saturated silt specimen has sufficient time to come out of solution during the duration of a Q test. During a typical Q test the strain rate at which the specimen is sheared is 1 percent per minute. For a specimen tested to an axial strain of 20 percent, the test would take 20 minutes to complete. It is uncertain to what extent air or gas dissolved in the pore water of a saturated silt specimen could be expected to come out of solution during this time for the magnitude of the pore pressure reduction which occurs during a Q test.

As will be discussed in Section 5.3, the magnitude of the pore pressure reduction which occurs during Q tests on saturated silts can be measured using midheight pore pressure monitoring techniques. Pore pressure measurements of this type were performed in this study and will be discussed in more detail in Section 5.4. The reductions in pore pressure measured in these Q tests were then used in Chapter 6, to evaluate the amount of air which may possibly

have come out of solution from the pore water during these tests.

4.4 Effect of Temperature Variations on the Solubility of Dissolved Gases in Soil Pore Water

As mentioned previously, another factor which must be considered in evaluating whether dissolved gas comes out of solution during sampling, is the effect of the temperature variations to which a soil sample may be subjected. The pore water of a saturated silt will have a certain temperature in the ground. When it is sampled and brought to the ground surface and into the laboratory, the temperature will likely increase. As shown by the values given in Table 4.1, as temperature increases, the solubility of air in water decreases. This means that as the temperature of the soil pore water increases after sampling, less gas is able to be dissolved in the pore water, and gas will tend to come out of solution in order to reestablish equilibrium.

Taylor (1948) noted that at a given temperature, a certain amount of gas can be dissolved in soil pore water. He added that if the pore water undergoes a temperature increase, gases dissolved within the pore water can come out of solution. The formation and growth of air or gas bubbles will increase the volume of the specimen while decreasing

its degree of saturation. This volume increase will also affect soil properties and behavior which depend on the void ratio of the soil.

According to the U. S. Environmental Protection Agency (EPA) (1990), the temperature of shallow ground water is related to the air temperature and thus will vary from one climatic region to another, as well as from season to season in temperate areas. The temperature of shallow ground water ranges from 3°C in colder northern climates to as high as 25°C in southern Florida. The EPA noted, however, that in central Iowa, ground water located at some depth maintains a temperature of about 11°C throughout the year.

When a saturated silt with a pore water temperature of 11°C is sampled and brought to the ground surface and later extruded in the laboratory, the soil specimen could have experienced fluctuations in temperature which may have allowed gas dissolved in the pore water to come out of solution and form bubbles within the voids of the soil. This can be expected in the laboratory environment where the temperature would likely be higher than 11°C and gas could come out of solution from the soil pore water, in order to maintain equilibrium. In addition, the time between sampling and testing is often quite long and may very well be sufficient for dissolved gases to come out of solution

from the pore water, as a result of the increase in temperature.

4.5 Amount of Air that Could Potentially Come Out of Solution from Soil Pore Water

Before considering the rate at which air or gas comes out of solution from water due to a temperature increase or pressure reduction, it is useful to consider the amount of air or gas which could theoretically come out of solution from the pore water of a saturated soil due to an increase in temperature as well as a reduction in pore pressure.

4.5.1 Amount of Air that Could Come Out of Solution Due to Temperature Variations

As shown in Table 4.1, the solubility of air in water decreases with increasing temperature. This means that the volume of air that can be dissolved in a given volume of water will be less at a higher temperature than at a lower one. As an example, consider a saturated soil sampled from the ground and extruded in the laboratory. If the pore water was initially saturated with dissolved air at 11°C in the ground, when its temperature stabilized at 20°C in the laboratory, the solubility of air in the pore water would have decreased from 0.02312 to 0.01999. For a pore water volume of 100 cm³, the volume of air which could have been dissolved in the water initially at 11°C would have been

2.312 cm³ while at 20°C only 1.999 cm³ could have been dissolved in the pore water. The volume of air, V_{air} , which could potentially come out of solution due to such a temperature change is equal to:

$$V_{air} = (0.02312 - 0.01999) 100 \text{ cm}^3 = 0.31 \text{ cm}^3 \quad (4-14)$$

This would correspond to a decrease in the degree of saturation of the soil from 100 percent to 99.7 percent.

This small decrease in the degree of saturation of the soil may initially seem to be insignificant. In fact it would very likely be undetected by the normal sample measurements used to determine the degree of saturation (Bishop and Eldin, 1950). The formation and presence of small air bubbles within the soil, however, may have a significant effect on the undrained behavior of a soil with dilatant tendencies during shear. This small amount of air could affect the undrained behavior directly or these small bubbles could serve as initiation points for more air to come out of solution as the pore pressure decreases during undrained shear. If these small bubbles of air grow as shearing proceeds, they may very well influence the undrained strength of the soil.

4.5.2 Amount of Air that Could Come Out of Solution due both an Increase in Temperature and a Decrease in Pore Water Pressure

The gases dissolved in soil pore water which could potentially come out of solution due to the temperature increase associated with sampling, would experience an increase in volume as well, due to the decrease in pressure which occurs as the soil is sampled. This volume increase would take place in accordance with Boyle's law.

Bishop and Eldin (1950) and Rau and Chaney (1988) present similar approaches to determine the amount of gas which could potentially come out of solution from the pore water of a saturated soil specimen due to a reduction in pressure. These analyses are similar to the work of Hamilton (1939) who considered the change in pore pressure resulting from the decrease in specimen volume associated with compression of the free gas present in the pores of a partially saturated soil.

Both Bishop and Eldin (1950) and Rau and Chaney (1988) assumed the temperature to be constant throughout the process of air coming out of solution from soil pore water. This may be a realistic assumption for a triaxial test performed in the controlled temperature environment of a geotechnical laboratory. If, however, the temperature change of the pore water which occurs during sampling is

considered as well, a slight modification of their analyses results.

Using Eq. 4-13 for Boyle's law, Rau and Chaney (1988) considered a constant temperature situation where at some point in time after a reduction in pressure, a certain volume of the gas is in the form of free gas (V_g) and a portion remains as dissolved gas (V_{dg}).

$$P_g(V_g + V_{dg}) = \text{Constant} \quad (4-13)$$

If temperature, T , can vary, Boyle's law can not be used, however, and the Ideal Gas Law must be applied to the free and dissolved gases in the pore water:

$$PV = nRT \quad (4-2)$$

For a system in which the total mass of the gas remains constant, this equation can be rearranged to give:

$$\frac{PV}{T} = nR = \text{Constant} \quad (4-14)$$

Following the assumption of Rau and Chaney (1988) that a portion of the gas is in the form of free gas and some is present as dissolved gas, Eq. 4-14 can be modified to give:

$$\frac{P_g}{T}(V_g + V_{dg}) = \text{Constant} \quad (4-15)$$

The volume of dissolved gas, V_{dg} , was given in terms of the coefficient of solubility, H , and the volume of water, V_w , in Eq. 4-1 as:

$$V_{dg} = H V_w \quad (4-1)$$

Following the work of Rau and Chaney (1988), but using Eq. 4-15 in place of Eq. 4-13, and assuming that only gas comes out of solution and no water vapor is produced, V_w is a constant and Eq. 4-1 can be substituted into Eq. 4-15 to give:

$$\frac{P_g}{T} (V_g + H V_w) = \text{Constant} \quad (4-16)$$

or

$$\frac{P_g}{T} \left(\frac{V_g}{V_w} + H \right) = \text{Constant} \quad (4-17)$$

Considering an initial state denoted by the subscript i and a final state denoted by the subscript f , the initial and final conditions of equilibrium can be equated to each other and simplified as follows:

$$\frac{P_{gi}}{T_i} \left(\frac{V_{gi}}{V_w} + H_i \right) = \frac{P_{gf}}{T_f} \left(\frac{V_{gf}}{V_w} + H_f \right) \quad (4-18)$$

$$\frac{T_f P_{gi}}{T_i P_{gf}} \left(\frac{V_{gi}}{V_w} + H_i \right) = \frac{V_{gf}}{V_w} + H_f \quad (4-19)$$

$$\frac{V_{gf}}{V_w} = \frac{T_f P_{gi}}{T_i P_{gf}} \left(\frac{V_{gi}}{V_w} + H_i \right) - H_f \quad (4-20)$$

Rau and Chaney (1988) assumed that there was initially no free gas present in the soil pores so that $\frac{V_{gi}}{V_w} = 0$. The resulting equation can then be written as:

$$\frac{V_{gf}}{V_w} = \frac{T_f P_{gi}}{T_i P_{gf}} H_i - H_f \quad (4-21)$$

Knowing that the porosity of the saturated soil is $n = \frac{V_w}{V_T}$, where V_T is the total volume of the soil specimen, combined with the relationship between the porosity and void ratio of the soil, $n = \frac{e}{(1+e)}$, Eq. 4-21 can be rewritten as:

$$\frac{V_{gf}}{V_T} = \left(\frac{e}{1+e} \right) \left[\frac{T_f P_{gi}}{T_i P_{gf}} H_i - H_f \right] \quad (4-22)$$

The volume of gas which could potentially come out of solution from the pore water of an initially fully saturated soil specimen due to an increase in temperature from T_i to T_f and a reduction in pore air pressure from P_{gi} to P_{gf} is therefore:

$$V_{gf} = \left(\frac{e}{1+e} \right) V_T \left[\frac{T_f P_{gi}}{T_i P_{gf}} H_i - H_f \right] \quad (4-23)$$

Equation 4-23, modified from the work of Rau and Chaney (1988), indicates that the amount of gas that could potentially come out of solution from the pore water of a saturated soil specimen is a function of: (1) the total volume of the soil specimen, V_T ; (2) the void ratio of the specimen, e ; (3) the coefficients of solubility, H , for a given gas in water at the initial and final temperatures; (4) the ratio of the initial and final pressures of the gas, P_{gi}/P_{gf} ; and (5) the ratio of the final and initial temperatures, T_f/T_i .

If a soil specimen is not initially fully saturated, there will be some free gas present and $\frac{V_{gi}}{V_w} \neq 0$. In this case, Eq. 4-20 must be used and can be rewritten as:

$$V_{gf} = V_w \left[\frac{T_f P_{gi}}{T_i P_{gf}} \left(\frac{V_{gi}}{V_w} + H_i \right) - H_f \right] \quad (4-24)$$

which simplifies to:

$$V_{gf} = \frac{T_f P_{gi}}{T_i P_{gf}} \left(V_{gi} + H_i V_w \right) - H_f V_w \quad (4-25)$$

If the degree of saturation, S , the void ratio, e , and the total sample volume, V_T , are known, the volume of water, V_w , in the soil can be calculated as follows:

$$V_w = \frac{S\%}{100\%} \left(\frac{e}{1+e} \right) V_T \quad (4-26)$$

From Eqs. 4-25 and 4-26, the volume of gas which could potentially come out of solution ($\Delta V_g = V_{gf} - V_{gi}$) from the pore water of a specimen which is not fully saturated, can be determined. If the temperature remains constant throughout the process being analyzed, the ratio T_f/T_i reduces to 1.0 and H_i and H_f are equal.

The difficulty in using Eqs. 4-23 and 4-25 comes in determining the initial and final pore air pressures, P_{gi} and P_{gf} , in the soil, along with whether or not the pore water is actually saturated with dissolved air at the initial pressure. It is also difficult to determine the initial volume of free air present, which is needed in Eq. 4-25. In addition, the gases dissolved in soil pore water may be different than those present in atmospheric air. If this is the case, the values of coefficient of solubility for air in water given in Table 4.1, can not be used. Solubility coefficients would have to be determined for the specific gases present in the ground water.

The temperature increase which may occur during sampling discussed in Sections 4.4 and 4.5.1, can now be considered along with the pressure decrease which occurs during sampling. Similar to the problem considered in Section 4.5.1, if the initial temperature, T_i , of the soil pore water as well as the dissolved air is taken as 11°C,

the initial solubility of air in water, H_i , is 0.02312. At a final temperature of 20°C in the laboratory, the final solubility of air in water, H_f , is equal to 0.01999. Assuming a soil sample with a volume of pore water, V_w , of 100 cm³ and no free air initially present in the pores of the soil, Eq. 4-25 can be used to estimate the volume of free air present in the soil after the temperature increase and pressure decrease which occur during sampling.

For a soil sample initially at a depth of 30 feet below the ground water table, the initial absolute pore air and pore water pressure, P_{gi} , would be 27.7 psia. When the soil was sampled and brought to the ground surface, the final pore air pressure, P_{gf} , would be reduced to atmospheric pressure or 14.7 psia. From Eq. 4-25, the final volume of free air in the pores of the soil can be calculated as:

$$V_{gf} = \frac{T_f P_{gi}}{T_i P_{gf}} \left(V_{gi} + H_i V_w \right) - H_f V_w \quad (4-25)$$

$$V_{gf} = \left[\left(\frac{20+273K}{11+273K} \right) \frac{27.7\text{psia}}{14.7\text{psia}} (0 + 0.02312(100\text{cm}^3)) - 0.01999(100\text{cm}^3) \right] \\ = 2.496 \text{ cm}^3 \quad (4-27)$$

The final degree of saturation of the soil specimen would therefore be:

$$S = \frac{V_w}{V_v} \times 100\% = \frac{100\text{cm}^3}{100\text{cm}^3 + 2.496\text{cm}^3} \times 100\% = 97.6\% \quad (4-28)$$

Similar calculations have been made for samples taken from different depths below the ground water table (different values of P_{gi}). The results of these calculations are presented in Table 4.6.

Table 4.6: Volume of free air that could potentially come out of solution from 100 cm³ of pore water and expand in a saturated soil sampled from various depths. Pore water temperature assumed to change from 11°C in-situ to 20°C in the laboratory

Sample Depth Below Ground Water Table (ft)	P_{gi} (psia)	P_{gf} (psia)	Calculated Volume of Free Air in Soil After Sampling V_{gf} , (cm ³)	Final Degree of Saturation, S_f (%)
10	19.03	14.7	1.09	98.9
20	23.37	14.7	1.79	98.2
30	27.70	14.7	2.49	97.6
40	32.03	14.7	3.20	96.9
50	36.37	14.7	3.90	96.2
60	40.70	14.7	4.61	95.6
70	45.03	14.7	5.31	94.7
80	49.37	14.7	6.01	94.3
90	53.70	14.7	6.72	93.7
100	58.03	14.7	7.42	93.1

As can be seen from this table, the final degrees of saturation for soil samples taken from depths between 10 and 100 feet below the ground water table, vary from 98.9 percent to 93.1 percent. As expected, the final degree of saturation of soil specimens after sampling decreases with increasing sampling depth, due to the larger pressure reduction which occurs.

The decrease in the degree of saturation that the soil can experience during sampling may very likely be significant enough to affect the behavior of the soil in Q tests. It may influence the undrained behavior of the soil directly, or it may allow additional dissolved gases to come out of solution and expand within the soil more readily, as pore pressures decrease during undrained shear.

As noted previously, it can be expected that for many cases, the time between sampling (pressure decrease and temperature increase) and actual triaxial testing in the laboratory will be long enough for gases dissolved in the pore water to come out of solution, possibly to the extent indicated in Table 4.6.

4.6 Relationship between Pore Air and Pore Water Pressures in Partially Saturated Soils

In applying Eqs. 4-23 and 4-25 to the system of pore air and pore water in Q test silt specimens, the relationship between the pore air pressure and the pore water pressure must be considered. If a soil specimen is initially fully saturated, the initial pore air pressure is equal to the initial pore water pressure (Sowers, 1979).

Bishop and Eldin (1950) however, stated that even if a triaxial specimen is determined to be initially fully saturated, immeasurable deviations from full saturation may

exist within the specimen. They noted that the estimation of the quantity of air present in soil specimens is only accurate to about 1 percent using normal density measurements. Because of this, many test specimens which are believed to be 100 percent saturated may actually contain 1 percent or more of air in the voids of the soil.

Similarly, Hamilton (1939) noted that it is almost impossible to have absolutely no air present in a soil specimen. Based on his experiences, he stated that even undisturbed samples taken from below the ground water surface can contain some small amount of free air.

Terzaghi (1943) also noted that soils which are thought to be completely saturated can contain some amount of free gas. This gas can exist as bubbles completely surrounded by water or as gas particles contained in a void. For the case of a void, the boundaries are made up of the surfaces of the soil particles and air-water menisci between particles.

Taylor (1948) noted that soil specimens tested in the laboratory usually contain some amount of gas, unless special preventive measures have been taken during sampling, transport and trimming. He added that specimens considered to be saturated will very likely contain small amounts of air or other gases in the voids of the soil. He attributed the presence of this gas to several possible causes:

- (1) Air bubbles that became trapped in the soil during capillary rise or water table rise,
- (2) Air or gas bubbles attached to soil particles during soil deposition in water, and
- (3) Gas bubbles produced within saturated soils containing organic material.

Ladd and Lambe (1963) also noted that air may come out of solution from the pore water of a saturated soil during sampling. They added that for samples where air has come out of solution, the measured value of the pore pressure parameter B will be less than one. In this case, it is preferable to perform Q tests at confining pressures high enough to give a B value equal to one, rather than to perform unconfined compression tests on samples that are less than fully saturated.

If a soil sample is not fully saturated initially and as air comes out of solution due to a decrease in pore water pressure, the air pressure will be different from the pore water pressure due to the surface tension in the water. The equation relating the pore air pressure to the pore water pressure and the surface tension in the water can be given as (Williams, 1967):

$$P_a - P_w = \frac{2 T_s}{r} \cos\theta \quad (4-29)$$

where P_a = the pore air pressure,
 P_w = the pore water pressure,
 T_s = the surface tension of the water,
 r = the radius of curvature of the air-water interface, and
 θ = the angle of intersection between the water surface and the soil grains.

The contact angle, θ , is dependent on the properties of the surface in contact with the water. When water is in contact with clean glass, the contact angle, θ , is essentially zero (Taylor, 1948). For water in the pores of a soil, if a thin film of adsorbed water is assumed to completely surround the surface of the soil grains, then the contact angle, θ , between the free water in the soil pores and the adsorbed water film can be assumed to be zero as well (Gibbs et al., 1960).

By rearranging Eq. 4-29, the pore water pressure is given as:

$$P_w = P_a - \frac{2T_s}{r} \cos\theta \quad (4-30)$$

As can be seen from Eq. 4-30, the pore water pressure is less than the pore air pressure by an amount equal to $\frac{2 T_s}{r}$, when θ is assumed to be equal to zero. At 20°C, the surface tension of water, T_s , is equal to 72.75 dyne/cm or

0.0004154 lbf/in for air at ordinary pressures. At 11°C, the surface tension of water is 74.07 dyne/cm or 0.0004228 lbf/in (National Research Council, 1933).

Richards (1928) stated that for equal weights of a fine-grained and coarse-grained soil, the finer soil would have more surface area than the coarse soil, as well as more points of contact between the individual soil particles. If the soils were partially saturated and had the same moisture content, in the finer soil there would be more contact points so that less water would be available for each contact point. This would result in a larger difference between the pore air and pore water pressures or a higher suction in the fine-grained soil than in the coarse-grained soil.

Richards (1928) also noted that the density of partially saturated soils affects the difference between the pore air and pore water pressures in the soil. For a given moisture content, a more densely packed soil would have smaller pore spaces, so that the radii of curvature of the air-water interfaces would be smaller. This would result in an increase in the difference between the pore air and pore water pressures as the density of a given soil increases.

As the degree of saturation of a soil sample increases, the difference between the pore air and pore water pressure decreases (Bishop and Henkel, 1962).

Gibbs et al. (1960) stated that because the pores in a soil mass are interconnected, at equilibrium, all of the menisci will have the same radius of curvature, r , and all of the water will have the same negative pressure, provided that the mass of soil is small enough for gravity to be neglected.

Sowers (1979) stated that although the pores of a soil are irregular in geometry, they are continuous and do form capillary tubes. He added that for a cohesionless soil, the soil pores form a capillary tube with an effective diameter of approximately $\frac{1}{5} D_{10}$, where D_{10} is the particle size of the soil in millimeters, for which 10% of the soil by weight, is smaller in size.

Sowers (1979) noted that in a completely saturated soil where no air-water interfaces are present, the capillary tension is zero. He stated that capillary tension develops in the pore water of a soil when a saturated soil is exposed to air and evaporation occurs from the water surface creating menisci at the air-water interface. He added that the capillary potential or tension developed in the pore water of a soil will vary within a soil depending on the

degree of saturation and the diameter of the soil pores. If the degree of saturation is high enough, however, the pore water in a soil will be continuous throughout the sample so that the capillary tension developed at the air-water interfaces will be felt by all of the pore water in the soil (Sowers, 1979).

Lambe and Whitman (1969) similarly noted that capillary tensions develop during the undisturbed sampling of saturated clays. They stated that these tensions develop when the soil is sampled and brought to the ground surface as a result of menisci forming around the perimeter of the sample.

Bishop and Henkel (1962) and Head (1986) noted the possibility of trapping air between triaxial specimens and the membrane when the membrane is placed around the specimen for a triaxial test. They stated that the volume of air trapped is seldom less than 0.2 percent of the total sample volume. They considered this to be a type of "bedding" error which would tend to disappear at increased cell pressures.

For unconfined compression tests and Q tests at low cell pressures, any free air or gas bubbles present in a dilatant soil specimen may possibly serve as initiation points for more gas to come out of solution during undrained

shear. Even when higher cell pressures are used to force this trapped air into solution, as pore pressures decrease during undrained shear, this recently dissolved air may easily come back out of solution and affect the undrained behavior of the soil.

4.7 Studies of Gas Going Into and Coming Out of Solution from the Pore Water of Soils

Several studies considering air going into or coming out of solution in water have been found in the geotechnical literature. Some of these studies have dealt with gases dissolved in the pore water of marine soils coming out of solution during sampling while others have considered the time required for air to go into solution in pore water during back pressure saturation. One study actually measured the time required for air to come out of solution from the pore water of soil during a pressure reduction.

Bruggeman, Zangar, and Brahtz (1939) analyzed the compressibility of a partially saturated soil in which no air or water was allowed to escape from the soil pores during consolidation. Their analysis related the change in volume that the specimen experienced during undrained loading, to the pressures developed within the pore fluid of the soil. During consolidation, the application of load caused a decrease in the volume of a partially saturated

soil under undrained conditions. Because no drainage was allowed and the water and soil grains were essentially incompressible, the volume decrease resulted from the change in volume of the free air.

As the volume of the free air decreased, by Boyle's law, the pore pressure in the specimen increased. The increase in pressure also forced some of the free air into solution in the pore water, in accordance with Henry's law. By combining Henry's and Boyle's laws; Bruggeman, Zangar, and Brahtz (1939) developed an equation relating the pore pressure after an application of load, to the initial pore pressure, the initial and final volumes of free air, the volume of dissolved air and the volume change the soil experienced due to the applied load.

Hamilton (1939) performed a similar analysis for the increase in pore pressure a partially saturated soil would experience due to a decrease in pore air volume resulting from an application of undrained loading. He similarly used Boyle's and Henry's laws to consider how the change in volume of the free air in the soil pores affected the pore pressure within the soil. Although some discrepancy was observed, he generally found in his experiments that the measured pore pressures were close to the theoretical predictions. He noted that his assumption that the initial

pressure of the entrapped air was atmospheric, may have been incorrect. The actual initial pore air pressure may have been greater than atmospheric pressure, thereby explaining the slight differences between measured and predicted pore pressures.

Hamilton (1939) also noted that the observed differences between measured and predicted pore pressures may have been due to not enough time being allowed for the air to dissolve in the water prior to pore pressure measurement. He concluded that the ability of and rate at which the water can dissolve air are important considerations in determining the pore water pressure during undrained loading of partially saturated soils.

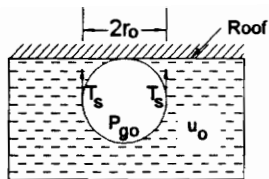
Terzaghi (1943) also considered the existence and stability of gas bubbles in soils. He stated that many soils which are felt to be completely saturated can contain bubbles of undissolved gas within the pore water. He considered two possibilities in which free gas can exist in a close to fully saturated soil. In one case, gas may be present in bubbles located between soil grains. These bubbles would be spherical and completely surrounded by water. The other possibility is that gas can be present in voids within the soil. The boundaries of the gas voids would be made up of the surfaces of the soil grains

surrounding the void and the water menisci between the grains.

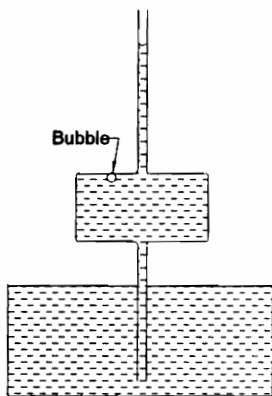
Terzaghi (1943) stated that these gas bubbles or voids may have been trapped within the soil as water entered the soil during saturation. They also may contain gases which were previously dissolved in the pore water or which were produced within the soil by chemical processes. He indicated that the possible size of a gas filled bubble or void is dependent on the tension in the surrounding liquid and the gas pressure in the bubble or void.

Terzaghi (1943) noted that as the pressure decreases in the soil pore water, the largest gas bubbles will expand and completely fill voids. The smaller bubbles will also expand. According to Terzaghi (1943), the tension required to start this expansion process depends on the initial state of stress in the water and the size of the gas bubbles initially present in the water.

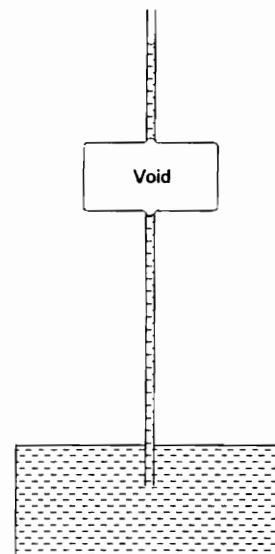
Terzaghi (1943) presented an approximate analysis for the conditions under which a gas bubble of a given size would grow into a void within a soil. He presented Figure 4.1 to depict the conditions under which a gas bubble will expand into a gas-filled void. In Figure 4.1a, a gas-filled bubble is present in a vessel of water under negative pressure. The bubble is located at the wall of the vessel.



b) Gas-filled bubble stabilized on roof of container holding water under negative pressure



a) Gas bubble in water under negative pressure



c) Gas bubble expands into gas-filled void as water pressure becomes more negative

Figure 4.1. Conditions under which a gas bubble in water will expand into a gas-filled void (after Terzaghi, 1943)

This is similar to a gas bubble being adjacent to a soil particle surface within the pores of a soil. Figure 4.1b shows the forces acting on the bubble. Negative pressure in the water is attempting to expand the bubble while surface tension forces are tending to collapse the bubble. Under the right combination of water pressure and bubble size, the bubble can remain stable in the liquid. As the water pressure decreases by raising the capillary tube and vessel, the bubble will tend to expand. With a large enough decrease in water pressure, the bubble may expand to fill the entire vessel with gas, as shown in Figure 4.1c. This is similar to a gas bubble in a soil pore expanding into a gas-filled void within the soil.

Terzaghi (1943) considered surface tension effects and used Boyle's law to consider the initial and final conditions of a gas bubble in the soil pore water. As a result of surface tension effects, the absolute pressure in a gas bubble can be given as (Terzaghi, 1943):

$$P_{g0} = u_o + \frac{2T_s}{r_o} \quad (4-31)$$

where P_{g0} = the initial absolute gas pressure,
 u_o = the initial absolute pressure of the water (the hydrostatic pressure of the water plus atmospheric pressure),
 T_s = the surface tension in the water, and
 r_o = the initial radius of the gas bubble.

Terzaghi (1943) then applied Boyle's law to the initial and final conditions of the air bubble. In his analysis, he neglected the solubility of the gas in the water, or Henry's law. He assumed that the mass of gas in the bubble remained constant, when in fact, some of the gas would have come out of solution from the pore water as a result of a decrease in pressure. From this approximate analysis, he developed the following equation for the absolute pore water pressure after the bubble expanded:

$$u = \frac{r_o^3}{r^3} \left(u_o + \frac{2T_s}{r_o} \right) - \frac{2T_s}{r} \quad (4-32)$$

where u = the final absolute pore water pressure, and
 r = the final radius of the bubble.

From Eq. 4-32, Terzaghi (1943) developed an equation for the rate at which the bubble radius, r , expands with decreasing pore water pressure, u , as:

$$\frac{dr}{du} = \frac{r^2}{\frac{3r_o^3}{r^2} u_o + 2T_s \left(\frac{3r_o^2}{r^2} - 1 \right)} \quad (4-33)$$

He noted that when the denominator in Eq. 4-33 is equal to zero, the bubble radius will increase at an infinite rate and form a void within the soil. According to Terzaghi (1943), this will occur when the radius, r , is equal to r_1 :

$$r = r_1 = r_o \sqrt{3 \sqrt{\frac{r_o u_o}{2T_s} + 1}} \quad (4-34)$$

where r_1 = the bubble radius, r , for which the denominator in Eq. 4-33 will be equal to zero.

For this value of bubble radius, the absolute pore water pressure will be u_1 . The value of u_1 can be determined by combining Eqs. 4-32 and 4-34 to get:

$$u_1 = -\frac{4T_s}{3r_1} \quad (4-35)$$

The hydrostatic pressure in the water, u_{w1} , can then be determined as:

$$u_{w1} = u_1 - P_{atm} = -\left(\frac{4T_s}{3r_1} + P_{atm}\right) \quad (4-36)$$

where u_{w1} = the hydrostatic (gage) pressure of the pore water, and

P_{atm} = atmospheric pressure.

Similar to Eq. 4-31, the final absolute gas pressure in the bubble is:

$$P_{g1} = u_1 + \frac{2T_s}{r_1} = \frac{2T_s}{3r_1} \quad (4-37)$$

When the radius of a gas bubble has expanded to the value of r_1 given by Eq. 4-34 and the hydrostatic pore water

pressure becomes equal to u_{w1} , the bubble will expand at a infinite rate into a void within the soil. Once the bubble expands into a void, the walls of the void will be made up of the soil grains and the menisci between the soil grains. The gas pressure in the void will therefore be a function of the volume of the void and the radii of the menisci between the soil grains.

Using the above equations, Terzaghi (1943) presented an example comparing the growth of a bubble in a clay to that in a sand. Following the examples presented by Terzaghi, the initial pore air pressure, P_a , has been assumed to be atmospheric, 14.7 psi (1033 g/cm²). The initial water pressure, u_{w0} , was taken as zero, so that the absolute pore water pressure, u_0 , is equal to atmospheric pressure as well, 14.7 psia (1033 g/cm²). For a constant temperature of 20°C, the surface tension of water, T_s , is 0.0004154 lbf/in.

For the clay, Terzaghi (1943) assumed that the initial bubble radius, r_0 , was equal to 1.97×10^{-5} in. (5×10^{-5} cm), or the size of a medium-sized clay particle. Using Eq. 4-34, r_1 is calculated to be 3.96×10^{-5} in. (10×10^{-5} cm), or twice the initial bubble radius. The absolute pore water pressure, u_1 , is calculated by Eq. 4-35 to be -13.99 psia. The hydrostatic water pressure, u_{w1} , at which the bubble will grow into a void is therefore equal to -28.69 psi.

For the sand, Terzaghi (1943) assumed that the initial bubble radius, r_0 , was 0.020 in. (0.05 cm), or the size of a particle of fine sand. Using Eq. 4-34, r_1 is calculated to be 0.637 in. (1.62 cm). The absolute value of the pore water pressure, u_1 , is calculated by Eq. 4-35 to be -0.001 psia. The hydrostatic water pressure at which the bubble will grow and expand into a void, u_{w1} , is therefore -14.701 psi.

An additional example has been analyzed in this research for a silt. An initial bubble radius, r_0 , of 0.00039 in. (0.001 cm), or the size of a medium-sized silt particle, can be used in an analysis similar to that performed by Terzaghi (1943) for a clay and sand. Using Eq. 4-34, r_1 is calculated to be 0.00192 in. (0.0049 cm). The absolute value of the pore water pressure, u_1 , is calculated by Eq. 4-35 to be -0.289 psia. The hydrostatic water pressure at which the bubble will grow and expand into a void, u_{w1} , is therefore -14.99 psi. The results from this analysis are summarized in Table 4.7.

Table 4.7: Approximate analysis of conditions for an air bubble to grow into a void in a clay, sand, and silt soil, following Terzaghi (1943) ($T=20^{\circ}\text{C}$, $T_s=0.0004154$ lbf/in)

Soil	r_0 (in)	r_1 (in)	u_1 (psia)	u_{w1} (psi)
Clay	1.97×10^{-5}	3.96×10^{-5}	-13.99	-28.69
Sand	0.020	0.637	-0.001	-14.701
Silt	0.00039	0.00192	-0.209	-14.99

The results presented in Table 4.7 indicate that a bubble in a sand or silt will grow into a void at a water pressure that is less negative than would be required for a bubble in a clay soil to grow into a void. The clay soil would require a larger decrease in pore water pressure during undrained shear before air bubbles would grow into voids within the pores of the soil.

As can be seen from the values given in the table, for a silt, the negative pore water pressure at which point a bubble would grow into a void is much closer to the value for a sand than the value calculated for a clay. For both the sand and silt, a bubble would grow into a void at a negative pore water pressure only slightly less than an absolute pressure of 0 psi. A clay soil would require a negative pore water pressure considerably less than 0 psi absolute, before a bubble would grow into a void. This is in agreement with Bishop and Eldin (1950), who noted that the negative pore water pressure at which cavitation will

occur in a soil specimen is partially dependent on the grain size of the soil.

Terzaghi (1943) reemphasized that this example and the above analysis are only approximate because they are based on the assumption that the mass of gas in the bubble remains constant. He noted that this is incorrect because a decrease in pressure would result in gas coming out of solution from the pore water. It appears reasonable that if dissolved gases coming out of solution are considered as well, bubble growth would probably occur more readily with smaller decreases in pore water pressure than calculated by Terzaghi's (1943) analysis. The behavior indicated by Terzaghi's approximate procedure implies, however, that a gas bubble in a clay soil is less likely to expand into a void than is a bubble in a silt or sand, due to a given pressure reduction. This may very well explain why saturated overconsolidated clays tested in Q tests do not appear to cavitate ($\phi_u = 0$, $S_u = c$), even though they experience a decrease in pore water pressure as they attempt to dilate during undrained shear. In order for the pore water in a heavily overconsolidated clay to cavitate and form voids within the soil pores during undrained shear, a much larger decrease in pore water pressure would be necessary.

Roscoe, Schofield and Wroth (1958) noted that during many undrained triaxial tests on cohesionless soils, pore water pressures increase initially but then decrease and become negative. They added that when the pore pressure goes below atmospheric pressure, air may be able to come out of solution making the constant volume condition assumed for the test incorrect. Even if deaired water is used as the soil pore water to prevent air from coming out of solution, water vapor may form within the pores of the soil if the pore water pressure reaches the vapor pressure of water.

According to Roscoe, Schofield and Wroth (1958), if air or water vapor bubbles form within the pores of the soil and the volume of the specimen increases, the test may result in the correct stress measurements, but the void ratio associated with these measured stresses will be incorrect. They noted that this will be true unless the volume increase resulting from the formation of air or water vapor bubbles is measured and included in the analysis of the test results. They suggested the use of a triaxial cell in which changes in cell fluid volume can be measured during the triaxial test, as a possible way of measuring the volume increase of the triaxial specimen.

4.7.1 Increasing the Degree of Saturation of Partially Saturated Test Specimens

It is possible to increase the degree of saturation of partially saturated soil specimens under undrained conditions by increasing the cell pressure on the specimen. In this process, the increase in cell pressure compresses the air present in the voids of the soil and forces it into solution in the pore water. The compressibility of the air also results in the compression of the soil structure and a decrease in specimen void ratio. For specimens with high initial degrees of saturation, full saturation is possible if the increase in cell pressure is sufficient and the soil has adequate compressibility. This procedure appears to have originated in the work of Bruggeman, Zangar and Brahtz (1939) and Hamilton (1939).

Bishop and Eldin (1950) presented an equation for the approximate minimum increase in cell pressure needed to dissolve all of the free air in a partially saturated specimen of soil under undrained conditions as:

$$\sigma_s = \left(\frac{\chi}{1 - \chi} \right) \frac{P_o}{H} + \chi \frac{n}{C_s} \quad (4-38)$$

where σ_s = the saturation pressure or the minimum cell pressure, above atmospheric, needed to completely dissolve all free air,

- χ = the fraction of voids filled with free air at the initial pressure of an unconfined specimen, $\chi = V_{\text{free air}}/V_v$, ($\chi = 1 - S_i$, where S_i = the initial degree of saturation of the specimen),
- P_o = the initial pressure of the air in the voids when the sample is unconfined (absolute),
- H = the coefficient of solubility of air in water at a given temperature,
- n = the initial porosity of the specimen, and
- C_s = the volumetric compressibility of the soil structure.

As an example, Bishop and Eldin (1950) stated that for a silt specimen which is initially 99 percent saturated ($\chi = 0.01$), the saturation pressure, σ_s , required to achieve full saturation is 9 psi. Bishop and Eldin (1950) used the following information in their analysis: $P_o = 14.7$ psia, $H = 0.02$, $n = 0.35$, and $C_s = 2 \times 10^{-3}$ in²/lb. These values can similarly be used to calculate σ_s for other values of χ .

In their analyses, Bishop and Eldin (1950) noted that the relationship given in Eq. 4-38 is only approximate because it neglects the effects of the vapor pressure and surface tension of the water. They added that the effect of the vapor pressure is small at room temperature and that the surface tension becomes more important as the air bubbles approach the size of clay particles.

Bishop and Henkel (1962) noted that an increase in cell pressure in an undrained test on a soil specimen which is

not fully saturated results in changes in the pore air and pore water pressures. The changes in the pore air and pore water pressures will not be equal however, due to the surface tension of the water. As the cell pressure increases and the degree of saturation of the soil specimen increases, the difference between the pore air and pore water pressure decreases.

Bishop and Henkel (1962) presented a plot of pore air and pore water pressure vs. cell pressure for two soil specimens with initial degrees of saturation of 67 and 86 percent. This plot, which is reproduced in Figure 4.2, indicates that, for a given cell pressure, the difference between the pore air and pore water pressures is less for the specimen with an initial degree of saturation of 86 percent than for the specimen with an initial degree of saturation of 67 percent. The plot also shows that as the cell pressure on the specimen increases, the difference between the pore air and pore water pressure decreases. For the specimen with an initial degree of saturation of 86 percent, when the cell pressure was greater than about 60 psi, the pore air and pore water pressures in the specimen were almost the same.

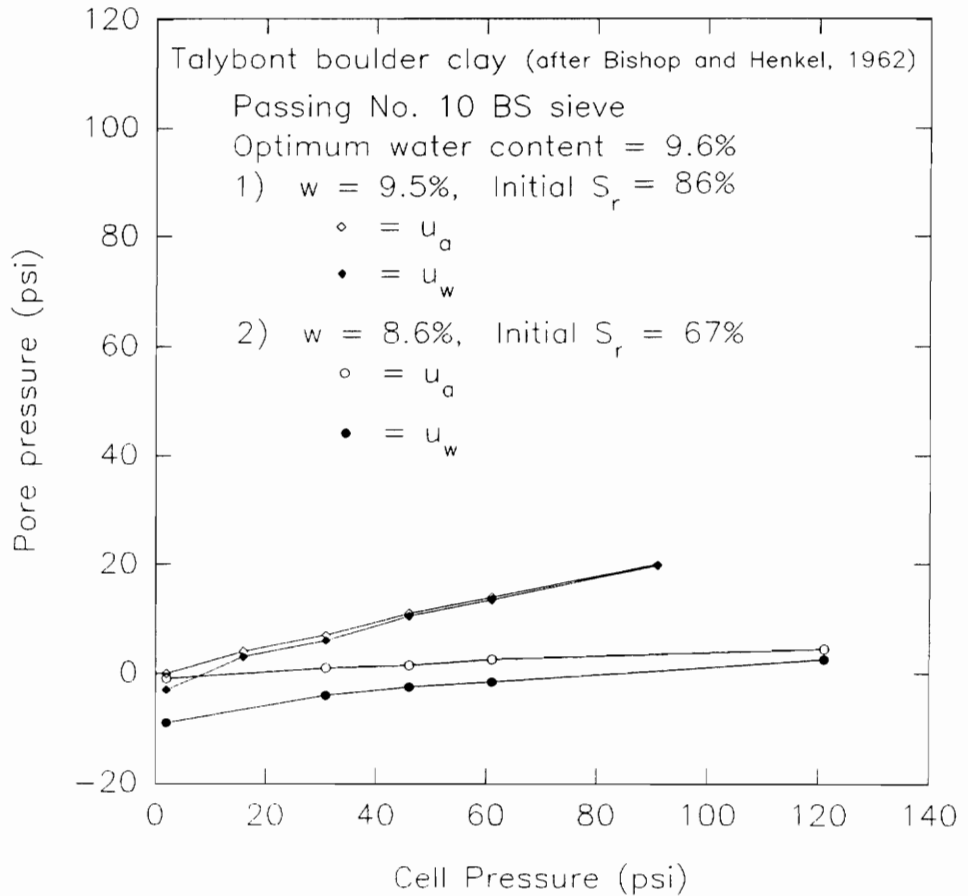


Figure 4.2. Variation of pore air pressure (u_a) and pore water (u_w) pressure with cell pressure for two specimens with different initial degrees of saturation under undrained conditions (after Bishop and Henkel, 1962)

Lowe and Johnson (1960) discussed the procedures for back pressure saturation of triaxial specimens. They noted the work of Bishop and Eldin (1950) on the increase in pressure required to fully saturate a partially saturated specimen. According to Lowe and Johnson (1960), if a partially saturated undrained test specimen is subjected to a pore pressure increase while the water content and total air content are kept constant, as assumed by Bishop and Eldin (1950), the required increase in pore water pressure, Δu_w , to obtain 100 percent saturation can be given as:

$$\Delta u_w = \frac{P_i(1-S_i)}{S_i H} \quad (4-39)$$

where Δu_w = the increase in pore water pressure required to obtain 100 percent saturation while maintaining a constant water content in the specimen,

P_i = the initial pressure of the free air in the voids of the soil (assumed to be absolute),

S_i = the initial degree of saturation of the specimen, and

H = the coefficient of solubility of air in water.

In Eq. 4-39, Δu_w is the increase in pore water pressure necessary to go from an initial degree of saturation, S_i , at an initial pore air pressure of P_i , to a final degree of saturation equal to 100 percent. Because this equation assumes that the water content remains

constant, the volume of the specimen must decrease as the free air goes into solution.

The increase in cell pressure required to reach full saturation calculated using Eq. 4-38 includes a term to account for the compressibility of the soil skeleton. The increase in cell pressure calculated using Eq. 4-38 will vary with soil type and the compressibility of the soil skeleton. The increase in pore water pressure necessary to reach full saturation calculated by Eq. 4-39 is based only on the first term of Eq. 4-38. It will give the same value of increase in pore water pressure for any type of soil. The increase in pore water pressure in the specimen, as calculated by Eq. 4-39, will be smaller than the cell pressure applied to the specimen, as calculated by Eq. 4-38, due to the compressibility of the soil skeleton.

Lowe and Johnson (1960) noted that in the procedure presented by Bishop and Eldin (1950), in order to increase the degree of saturation to 100 percent, the soil structure would be compressed and the void ratio of the specimen would be less than it was initially. Because this change in specimen void ratio was undesirable, Lowe and Johnson (1960) developed a procedure for back pressure saturating triaxial specimens. In the back pressure saturation process, increases in cell pressure are combined with equal but

independent increases in the pore water pressure within the specimen, so that the void ratio of the specimen would not be considerably altered while trying to achieve full saturation. This back pressure saturation procedure does not apply to this research because it allowed water to flow into the specimen thereby changing the water content of the specimen. In this case, the volume of the specimen would not change as air was forced into solution. Instead, the water content of the sample would increase as water was forced into the soil by the back pressure, taking up the space formerly containing the free air.

According to Lowe and Johnson (1960), the increase in pore water pressure necessary to go from an initial degree of saturation, S_i , to a final degree of saturation, S_f , if no decrease in sample volume occurs but the water content increases, is governed by the equation:

$$\Delta u_v = P_i \left[\frac{1 - S_i(1-H)}{1 - S_f(1-H)} - 1 \right] \quad (4-40)$$

where Δu_v = the increase in back pressure required to go from an initial degree of saturation, S_i , to a final degree of saturation, S_f , for a constant volume, increasing water content condition,

P_i = the initial pressure of the free air in the soil (assumed to be absolute),

S_i = the initial degree of saturation of the specimen,

S_f = the final degree of saturation of the specimen, and

H = the coefficient of solubility of air in water.

Equation 4-40, developed by Lowe and Johnson (1960) assumes that the water flowing into the specimen during the back pressure saturation process contains no dissolved air initially. It is the same equation presented in the U.S. Army Corps of Engineers (1980) manual on Laboratory Soils Testing (Figure 15, page X-31).

Using Eqs. 4-38, 4-39 and 4-40 and assuming several different initial degrees of saturation, the increases in cell pressure, pore water pressure, and back pressure required to achieve full saturation of soil specimens have been calculated and are presented in Table 4.8.

Table 4.8: Increase in cell pressure, pore water pressure, and back pressure required to achieve full saturation of soil specimens under undrained conditions, using Eqs. 4-38, 4-39 and 4-40 ($P_i=14.7$ psia, $H=0.02$)

Initial Degree of Saturation, S_i (%)	σ_s (psi) Eq. 4-38	Δu_w (psi) Eq. 4-39	Δu_y (psi) Eq. 4-40
80	215	184	144
85	153	130	108
90	97	82	72
95	47	39	36
96	37	31	29
97	28	23	22
98	18	15	14.4
99	9	7.4	7.2

It can be seen from the values given in Table 4.8 that there is a slight difference between the values of increase in cell pressure calculated by Eq. 4-38 and the increase in pore water pressure calculated by Eq. 4-39, required to achieve full saturation of partially saturated soil specimens under constant water content conditions. The increases in pore water pressure calculated by Eq. 4-39 is always less than the increase in cell pressure calculated by Eq. 4-38, due to the compressibility of the soil structure. A more noticeable difference exists between the increase in back pressure calculated by Eq. 4-40 and the values calculated by Eqs. 4-38 and 4-39. This is likely because Eq. 4-40, given by Lowe and Johnson (1960) to calculate Δu_v , assumes that the water flowing into the specimen during the back pressure saturation process contains little to no dissolved air. The process of back pressure saturation proposed by Lowe and Johnson increases the degree of saturation of the soil while maintaining a constant volume for the specimen. Because deaired water has a greater ability to dissolve air, a smaller increase in back pressure is required by Eq. 4-40 to reach full saturation.

By rearranging Eq. 4-39 and adjusting the variable subscripts, the final degree of saturation, S_f , can be estimated for a specimen assumed to be initially fully saturated, and subject to a decrease in pore water pressure,

Δu_w , so that air comes out of solution and the final pore air pressure is P_f (absolute).

$$S_f = \frac{P_f}{H \Delta u_w + P_f} \quad (4-41)$$

where S_f = the final degree of saturation of the soil,

P_f = the final absolute pore air pressure,

H = the coefficient of solubility of air in water, and

Δu_w = the decrease in pore water pressure.

If the change in pore water pressure is measured during Q tests, as will be discussed in Section 5.4, the final degree of saturation of the specimen can be estimated by Eq. 4-41, assuming that the pore water was saturated with air at the initial pressure and that the air had sufficient time to come out of solution due to the decrease in pore water pressure. The application of Eq. 4-41 to the saturated silt Q test specimens tested in this study will be discussed in more detail in Chapter 6.

4.7.2 Studies on the Rate of Diffusion of Air Through Soil Pore Water and the Time Required to Back Pressure Saturate Triaxial Specimens

Bloomsburg and Corey (1964) considered the diffusion of entrapped air through porous media. They stated that air can become trapped in pockets within the soil during infiltration. Air can also come out of solution from soil

pore water and form bubbles. They added that well-graded soils tend to trap more air than uniform soils.

Bloomsburg and Corey (1964) noted that at high degrees of saturation, undissolved gas present in the soil will tend to be discontinuous and will exist as bubbles surrounded by water. They added that this gas can leave the soil in two ways. One possibility is that the gas bubbles will move through the soil with flowing water. The other possibility is that the gas present in the bubbles will diffuse into solution in the pore water. Variations in the concentration of dissolved gas in the pore water will then exist, resulting in the diffusion of the dissolved gas through the pore water until it can exit solution at an exposed free water surface.

Bloomsburg and Corey (1964) stated that entrapped air bubbles tend to dissolve faster in fine-grained soils than in coarse-grained soils. In fine-grained soils, trapped air will be present in very small bubbles, whereas in coarse soils, the bubble size can be larger. The smaller the radius of the air bubbles, the more important surface tension effects become. Surface tension will tend to cause smaller bubbles to dissolve more rapidly than larger bubbles.

Bloomsburg and Corey (1964) noted that contamination in soil pore water may provide nuclei for air to come out of solution. In experiments with glass beads, they observed that in some instances, the water did not fully wet the surfaces of the beads. They felt that this may have been due to surface contaminants. They stated that even the slightest amount of contamination on a glass surface will affect the wettability characteristics of the surface.

Bloomsburg and Corey (1964) added that the amount of entrapped air present in soil pores may be dependent on the condition of the soil particle surfaces. Because surface contamination can affect the wettability of the particle surfaces, the amount of entrapped air in the soil can be influenced by the amount of surface contamination (Bloomsburg and Corey, 1964). They also stated that soils with relatively uniform pores and particles with smooth surfaces tend to contain less entrapped air.

Barden and Sides (1967) studied the diffusion of air through the pore water of saturated and partially saturated compacted clays. They found that the average coefficient of diffusion of air through pore water of clays was much lower than the diffusion coefficient of air through free or open water. On the other hand, the diffusion coefficient of air in the pore water of a saturated coarse porous stone was

very close to that for free water. They also found that the average coefficient of diffusion decreased as the water content of the soil decreased. This suggested that as the surface of the clay particles was approached, the diffusion coefficient decreased and the viscosity of the adsorbed water increased.

Based on their study, Barden and Sides (1967) concluded that the reduced coefficient of diffusion for air in the pore water of soil, as compared to that for free water, results in a large increase in the time required for the air-water mixture in a partially saturated soil to reach equilibrium. In considering the lower rate of diffusion of air into the pore water of partially saturated soils, Barden and Sides (1967) expressed some doubt as to the exact applicability of Henry's law. They thought that the solubility of air in water may have been influenced by the highly curved air-water interfaces resulting from capillary tension. They also considered that the tortuous path the air must follow when diffusing through the pore water of a soil specimen might be the cause of the much slower rates of diffusion observed.

Barden and Sides (1967) reached the conclusion however, that in cohesive soils where water is present on the surface of clay particles as adsorbed water, the increased viscosity

of the adsorbed water results in the observed decrease in the coefficient of diffusion for air going into solution in soil pore water. This appeared to be a more reasonable explanation than questioning the applicability of Henry's law or the tortuous path which the air must diffuse across within the soil pores.

In tests on kaolin, Barden and Sides (1967) found that for samples consolidated to pressures of 5 psi and 70 psi, the diffusion coefficient decreased as the void ratio and pore size of the soil decreased. They also observed that the diffusion coefficient for air through soil pore water was smaller for partially saturated soils than for fully saturated soils.

Barden and Sides (1967) noted that many calculations of the rate at which air dissolves in the pore water of partially saturated soils assume that the rate of diffusion is the same for soil pore water as for free water. These calculations often indicate that equilibrium conditions between pore air and pore water can be reached rapidly. From their results they concluded that for partially saturated clays, equilibrium between pore air and pore water, in accordance with Henry's law, may require a more considerable period of time than usually considered.

There appears to be some contradiction between the findings of Bloomsburg and Corey (1964) and Barden and Sides (1967). Bloomsburg and Corey (1964) stated that air bubbles will dissolve more rapidly in a fine-grained soil than in one which is coarse-grained. Barden and Sides (1967) however, found that the coefficient of diffusion for air through water was less for pore water in a fine-grained soil than in a coarse-grained soil.

As noted by Bloomsburg and Corey (1964), a fine-grained soil will typically contain smaller air bubbles than a coarse-grained soil. Surface tension forces will result in smaller bubbles dissolving more rapidly than larger bubbles. Once an air bubble of a given size has dissolved in the soil pore water, the dissolved air will diffuse through the pore water toward a free water surface, in order to establish equilibrium with Henry's law.

According to Barden and Sides (1967), the diffusion of the air through the pore water will be slower in the fine-grained soil than it will be in the coarse-grained soil. For air bubbles of the same size present in a fine- and coarse-grained soil, the bubble in the coarse-grained soil would be expected to dissolve more rapidly because the coefficient of diffusion would be greater than in the fine-grained soil, even though the effect of surface tension

would be the same in both cases. For fine- and coarse-grained soils in which the pore water contains similar amounts of excess dissolved gas, a longer time would be required for the fine-grained soil to reach equilibrium in accordance with Henry's law. Based on the above discussion, the findings of Bloomsburg and Corey (1964) and Barden and Sides (1967) are felt to be compatible with each other.

Lee and Black (1972) studied the time required for an air bubble to dissolve in water. They found that air bubbles of the same size were able to dissolve much faster in a large body of water than in a tube. They also found that bubbles of the same size dissolve faster in a large tube than in a small tube. This indicates that the size of the pores in a soil has an effect on the rate of diffusion of air into the pore water of soils, as was observed by Barden and Sides (1967). Because of this, the grain size and void ratio of a soil may also be expected to have an effect on the rate of solution of air in water. It can be expected that the rate at which air comes out of solution will be affected by grain size and void ratio as well. The rate at which air would come out of solution from the pore water of a fine-grained soil would probably be slower than that for a coarse-grained soil.

Black and Lee (1973) studied the time required to back pressure saturate laboratory test specimens. They stated that some soils that are not fully saturated require a period of time of up to several days to achieve complete saturation, even when back pressures higher than those required by theory are used. They felt that the time delay was caused by the rate of diffusion of the air into the water, rather than by the limitations of the permeability of the soil.

Black and Lee (1973) performed experiments from which they developed an equation for the time required to dissolve the free air present in a partially saturated soil specimen by increasing the back pressure in the specimen to reach a final degree of saturation, S_f . The equation developed takes into account the air going into solution due to a pressure increase, according to Henry's law, as well as the flow of water into the pores of the specimen as the air dissolves. The time required to back pressure saturate a soil specimen is given as:

$$t_d = \left(\frac{1}{K} \left(\frac{1-S_i}{1+49R(1-S_i)} - (1 - S_f) \right) \right)^{\frac{1}{x}} \quad (4-42)$$

where t_d = the time in minutes required for the free air to dissolve due to an increase in back pressure so that the soil specimen goes from an initial degree of saturation S_i to a final degree of saturation S_f ,

S_i = the initial degree of saturation of the soil specimen,

S_f = the final degree of saturation of the soil specimen,

$$R = \frac{P_b}{P_{10}}$$

P_b = the applied back pressure,

P_{100} = the minimum increase in back pressure required to achieve 100% saturation,
 $P_{100} = 49P_i(1 - S_i)$

P_i = the initial absolute pressure corresponding to the initial degree of saturation, S_i ,

$$K = 0.0094 - 0.01 S_i; \quad \text{for } S_i < 0.8,$$

$$K = 0.0014; \quad \text{for } S_i > 0.8, \text{ and}$$

$$x = 0.085 + 0.133 S_i; \quad \text{for } 0 < S_i < 1.0$$

For an example of the application of Eq. 4-42, consider a specimen initially 98 percent saturated at atmospheric pressure ($S_i = 0.98$, $P_i = 14.7$ psia) going to a final degree of saturation of 100 percent ($S_f = 1.0$). For this specimen, the change in pore pressure required to achieve 100 percent saturation, P_{100} , is equal to:

$$P_{100} = 49(14.7 \text{ psia})(1-0.98) = 14.41 \text{ psi} \quad (4-43)$$

For this example, the coefficients K and x are equal to:

$$K = 0.0014 \quad (4-44)$$

$$x = 0.085 + 0.133(0.98) = 0.215 \quad (4-45)$$

The times required for the specimen to go from 98 to 100 percent saturated, for different values of $R = P_b/P_{100}$, have been calculated using Eq. 4-42 and are presented in Table 4.9.

Table 4.9: Time required to back pressure saturate ($S_f = 100\%$) a specimen with an initial degree of saturation, S_i , of 98%, based on Eq. 4-42

R	P_b (psi)	t_d (min)
1.0	14.41	9,813
1.5	21.62	3,509
2.0	28.82	1,512
4.0	57.64	142
5.0	72.05	61

As can be seen from this table, the time required to raise the degree of saturation of the specimen from 98 to 100 percent by increasing the back pressure to that required for equilibrium, $R = 1.0$, is over 9,800 minutes, or 6.8 days. The use of a back pressure 5 times the required equilibrium pressure, or 72 psi, still needs to be applied for one hour in order to achieve full saturation.

There appears to be some question regarding the applicability of Eq. 4-42, developed by Black and Lee (1973), to different soil types. Barden and Sides (1967) observed that the rate of diffusion of air through the pore water of soils was less than that for air in free water. As

soil pore size was reduced, the rate of diffusion of air through soil pore water was also observed to decrease. Similarly, the work of Lee and Black (1972) implied that the size of the soil pores should affect the rate of solution of the pore air in the pore water.

The equation presented by Black and Lee (1973) for the time required to back pressure saturate a soil specimen, can be seen, however, to be independent of soil type and pore size. The soil used by Black and Lee (1973) was dense standard Ottawa sand. They noted that this soil was used in their experiments because with the relatively large pore sizes of the soil, the pore water could be expected to behave similarly to normal water. This may indicate that the equation developed by Black and Lee (1973) and given by Eq. 4-42, may not be applicable to fine-grained soils, especially those containing significant amounts of clay. For this reason, the times to back pressure saturate a fine-grained soil with an initial degree of saturation of 98 percent may be considerably different and possibly longer than the values given in Table 4.9.

It is worth commenting on the results presented in Table 4.9 as compared to those presented in Table 4.8. In the problem considered in Table 4.9, $S_i = 98\%$ and $S_f = 100\%$. From the results presented in Table 4.8, for an initial

degree of saturation, S_i , of 98%, σ_s , calculated by Eq. 4-38 is equal to 18 psi, Δu_w calculated by Eq. 4-39 is equal to 15 psi, while Δu_v calculated by Eq. 4-40 is equal to 14.4 psi. From Table 4.9 for $R = 1.0$, the required back pressure, P_b , is 14.41 psi, while for $R = 2.0$, the required back pressure, P_b , is 28.82 psi. These values of back pressure are one to two times σ_s , Δu_w , and Δu_v given in Table 4.8. Even with an initial degree of saturation of 98%, the times required to dissolve the relatively small amount of free air present in the pore water of the soil using back pressures on this order of magnitude, range from 1,500 minutes to over 9,800 minutes or between about 1 and 6.8 days. The magnitude of these times and the similarity in the values of P_b , σ_s , Δu_w , and Δu_v , suggests that even if a freshly trimmed undisturbed specimen of close to fully saturated soil contains a small amount of free air (2%), an increase in cell pressure or pore water pressure to a value in the range of 15 to 30 psi may not yield a fully saturated specimen until a considerable amount of time has elapsed.

If the time required to achieve full saturation of such a specimen due to an increase in cell pressure is on the same order of magnitude as the time calculated to back pressure saturate the specimen, within the limits of testing efficiency, increasing the cell pressure in a Q test to a value such as 20 psi would not yield a fully saturated

specimen by the time the test would probably be performed. The use of a much higher cell pressure would be expected to enable the specimen to reach full saturation in a more reasonable amount of time. The use of a high cell pressure, however, may not be reasonable for the field conditions to which the laboratory test results will be applied.

4.7.3 Studies of Gas Coming Out of Solution from the Pore Water of Marine Soils

The effect of gas coming out of solution from the pore water of soil specimens due to a pressure reduction has been studied in the area of sampling and testing of marine sediments. Lee (1985) presented a review of the methods available to determine the strength of marine soils in the laboratory. He stated that many marine soils, especially those rapidly deposited, can contain significantly high concentrations of gas in the pore water. The majority of this gas is usually biogenic methane.

According to Lee (1985), when the in-situ stresses acting on a soil element are removed during sampling, a corresponding reduction in pore pressure occurs which can result in gas exiting solution and forming bubbles. The formation and growth of gas bubbles within the soil increases the volume of the soil sample prior to testing. Lee (1985) added that gas bubbles expanding within the voids

of the soil could lead to disturbance of the structure of the soil resulting in the measurement of significantly altered shear strengths.

Lee (1985) stated that when no specialized equipment is available, laboratory tests should be performed as soon as possible because it takes some time for the gas to come out of solution and alter the soil structure. However, he gave no indication of the magnitude of the time required for gas to come out of solution. He indicated that it may be possible to resaturate the samples in which gas has come out of solution by applying high back pressures in the laboratory. He added that consolidation stresses should be applied for a long enough period of time before testing to redissolve the gas and thereby redevelop some of the original soil structure.

The procedures given by Lee (1985) however, are not applicable to Q test specimens because Q test specimens are not back pressure saturated or consolidated prior to testing. The best approach currently available for sampling and testing marine soils, according to Lee, is to use pressurized core barrels and pressurized storage containers on ship to reduce the possibility of gas coming out of solution. Lee made no reference to specific techniques available for performing Q tests on marine sediments.

Rau and Chaney (1988) studied the triaxial testing of marine sediments with high gas contents. They stated that the gases present in marine sediments can exist as: (1) gas dissolved in the pore water of the soil; (2) bubbles or pockets of free gas in the voids of the soil; and (3) solid gas hydrates. During the large stress release associated with sampling of marine soils, dissolved gas can come out of solution from the pore water and expand within the sample. When gas comes out of solution in a marine soil, it changes the physical and engineering properties of the soil. The formation and growth of gas bubbles within the voids of the soil causes the volume of the soil sample to increase. The increase in volume results in a decrease in the unit weight and degree of saturation of the soil and leads to irreversible changes in the strength and compressibility of the soil (Rau and Chaney, 1988).

When dissolved gas is present in the pore water, Rau and Chaney (1988) recommended that triaxial tests be performed quickly, so that little gas has a chance to come out of solution. They gave no indication, however, of the time frame within which the tests should be performed.

According to Rau and Chaney (1988), if samples with all gas initially in solution are returned to a shore laboratory for testing, gas will likely have had sufficient time to

come out of solution and will be present as bubbles within the voids of the soil. In this case, they agree with Lee (1985) that it may be possible to resaturate the soil by applying large back pressures. This test procedure is based on the principle that gas goes into solution faster than it can come out of solution. According to Chace (1985), the diffusion gradient is generally larger for a gas going from a bubble into a fluid that is undersaturated with dissolved gas than it is when dissolved gas is moving from a saturated fluid into a bubble. Rau and Chaney (1988) indicated, as did Lee (1985), that consolidation pressures should be applied for a long period of time to redevelop the soil structure prior to testing. They also agreed with Lee (1985) regarding the advantages of sampling the soil with pressurized core barrels and then storing the cores in pressurized containers until ready to test.

Esrig and Kirby (1977) studied the effects of sampling of marine sediments with high gas contents on the undrained behavior of the soil. They stated that marine sediments commonly contain gases at high concentrations. These gases may be dissolved in the pore water or they may be in discrete bubbles. They noted that as a result of the pressure reduction which occurs during the sampling of marine sediments, gas bubbles in the soil will expand in size. Dissolved gases will also tend to come out of

solution. They added that samples of marine sediments taken from considerable depths are often observed to grow out of the sampling tubes once on ship.

Esrig and Kirby (1977) stated that as gas bubbles expand and dissolved gas comes out of solution as a result of sampling stress release, the increase in sample volume which takes place will lead to the soil sample having a lower degree of saturation than it had in-situ. Knowing the final conditions after sampling, they used Henry's and Boyle's laws to estimate what the initial degree of saturation must have been in-situ. In their analysis, they assumed that the temperature remained constant during this process. They noted, however, that temperature changes do occur during sampling a soil from below the ground and bringing it to the surface.

By neglecting the effect of temperature changes on the process, Esrig and Kirby (1977) estimated the in-situ degree of saturation of the soil to be somewhat less than it actually would be. For soils sampled from a depth of 15 meters, if the degree of saturation of the soil on ship was greater than about 80 percent, they estimated the degree of saturation in-situ to be greater than about 90 percent. At a depth of 60 meters, the in-situ degree of saturation would have been greater than 95 percent. They stated that even

though the soil was not fully saturated in-situ, the high degree of saturation indicated that the gas was present in individual bubbles and effective stress concepts used for saturated soils can be used if the slight difference in pressure between the pore water and pore gas is neglected.

Esrig and Kirby (1977) noted that sampling stress relief results in gas expansion within the soil and a corresponding decrease in the degree of saturation of the soil. They added that if the soil possesses a tendency for dilation during undrained shear, an additional increase in gas volume and void ratio may occur.

Figure 4.3 shows this behavior in a form similar to that given by Esrig and Kirby (1977) and discussed by Roscoe, Schofield and Wroth (1958). In this figure, a dilatant soil specimen at some initial void ratio, e , and minor principal effective stress, σ'_3 , (point 1) will experience a decrease in pore water pressure during undrained shear. As shearing proceeds, the specimen will attempt to reach the critical state line at a constant void ratio (point 2) as the pore pressure decreases and the minor principal effective stress increases. If the decrease in

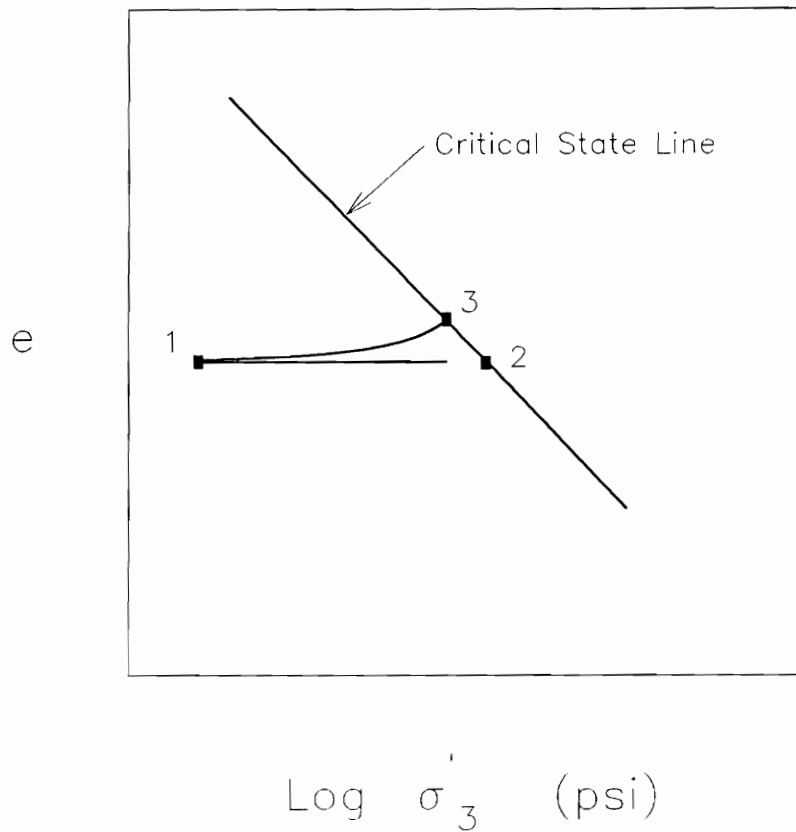


Figure 4.3. Relationship between void ratio and minor principal effective stress for dilatant soil specimen during undrained shear (after Esrig and Kirby, 1977)

pore water pressure results in gas bubbles expanding and dissolved gases exiting solution, the void ratio of the specimen will increase. This could result in the specimen reaching the critical state line at a lower minor principal effective stress and higher void ratio (point 3) than if no dissolved gases exited from solution in the pore water.

Wheeler (1988a) proposed a model for the behavior of gas bearing marine soils with degrees of saturation greater than 90 percent. Wheeler (1988b) also performed a series of triaxial tests on remolded specimens of gassy marine soils to assess the accuracy of the model. In these triaxial tests (Wheeler, 1988b), the volume change of the specimens, and thus the gas bubbles, was determined during undrained shear by measuring changes in the volume of the cell fluid in a specially designed and calibrated triaxial cell. In all of the triaxial tests performed, the volumes of the soil specimens were observed to decrease during undrained shear. This indicated to Wheeler (1988b) that the gas bubbles were compressed during undrained shear, forcing gas into solution in the pore water. The model (Wheeler, 1988a) predicted that if the volume of free gas present in bubbles within the sample decreased during undrained shear, the stress-strain curve of the specimen should exhibit strain-hardening. This behavior was observed in the triaxial tests on remolded

specimens of normally consolidated soil containing bubbles of methane gas (Wheeler, 1988b).

Although none of the specimens tested by Wheeler (1988b) had dilatant tendencies, the model proposed by Wheeler (1988a) predicted that if the gas bubbles expanded during shear, the stress required to cause further deformation would have decreased, resulting in strain-softening behavior. All of Wheeler's (1988b) triaxial tests were on normally consolidated specimens which had compressive tendencies so that bubble shrinkage occurred rather than bubble expansion. If tests had been performed on overconsolidated samples containing bubbles of methane gas, bubble expansion may have resulted, leading to strain-softening during undrained shear.

Chace (1975, 1985) studied the effect of a decrease in pressure on saturated Ottawa sand and kaolinite. He measured changes in the bulk density of the soil with time using a gamma-ray densitometer transmission gage. The gamma-ray densitometer was designed and built to continuously monitor the variation of the linear attenuation coefficient, μD , of soil samples as a function of pressure, soil type, time, gas content, and the initial bulk density of the soil, while the samples were subjected to changes in hydrostatic confining pressure. The linear attenuation

coefficient of the soil is related to the distance that gamma rays will travel through the soil sample before being scattered off path by the Compton effect. Changes in μD will occur as the density of the soil specimen varies. The measured linear attenuation coefficient of the soil could then be related to the time dependent changes in bulk density of the soil which resulted from a decrease in pressure and dissolved gases exiting solution.

The experiments Chace (1975, 1985) performed were designed to investigate the release of gas from solution and the resulting sample expansion which occurs due to the reduction in pressure experienced by a core of soil sampled from the sea floor and brought to the surface. In his experiments, he continuously monitored μD while releasing the confining pressure on soil samples in the laboratory. In this way, he was able to assess the time dependence and magnitude of the disturbance associated with the pressure release.

Although his study was addressed toward the disturbance effects of sampling on marine sediments, Chace (1975, 1985) used Ottawa sand and kaolinite clay in his laboratory experiments, while the liquid used was fresh water and the gas was air.

The experiments performed by Chace (1975, 1985) were based on the principal that for a given reduction in hydrostatic pressure, air dissolved in the pore water of the soil will come out of solution in accordance with Henry's law. As the dissolved air came out of solution, the measured variable, μD , varied until a steady state condition had been reached, indicating that all of the air that should have come out of solution due to that reduction in pressure had done so.

Chace (1975, 1985) found that the bulk density and the closely related linear attenuation coefficient of a soil varied with time due to a change in hydrostatic pressure. He found that the time for air to go into solution due to a pressure increase was shorter than the time required for air to come out of solution due to a pressure decrease of the same magnitude. He proposed that the reason for this was that the diffusion gradient for air going from a bubble into an undersaturated solution was generally greater than that for dissolved air going from a saturated solution into a bubble.

Chace (1975) found that for air going into solution in the pore water of soil, the time to reach equilibrium decreased as the applied pressure increased. He also found that the times required for samples to reach full saturation

due to an increase in applied pressure were of the same order of magnitude as those calculated by the model proposed by Black and Lee (1973).

Chace (1975, 1985) used two different types of holding devices in which to test the soil in his experiments and found that the time required for the sample to reach equilibrium depended on the device used. One device had a porous stone at the base which allowed for air to be bubbled up through the specimen to saturate the pore water with air prior to testing. This device also allowed the base of the specimen to be exposed to an external source of air during the pore pressure reduction in the same way that the base of a sampling tube is exposed during sampling. In this device, sample expansion took an average time of three hours for the Ottawa sand tested under a pressure reduction from 1500 psi to atmospheric pressure. The other device was sealed at the bottom and required an average time of 17 hours to complete expansion of the Ottawa sand under the same pressure reduction. The two different devices were used to simulate different portions of marine core samples which would be subjected to sources of external air to different degrees.

Tests on kaolinite clay had longer average durations of sample expansion than tests on Ottawa sand. One of the tests on kaolinite showed an initially high rate of

expansion which then decreased to a slower rate. After 90 hours, however, when the test was terminated, the sample was still undergoing expansion. When comparing the tests on kaolinite to those on sand, Chace (1975) concluded that grain size has an effect on the rate at which air comes out of solution from the pore water of soil.

Chace (1975, 1985) also studied the effect of a decrease in the hydrostatic pressure for a period of time followed by repressurization to the original hydrostatic pressure. For Ottawa sand samples, if the pressure was reduced to atmospheric pressure for a period of less than four hours and then repressurized to the original confining pressure of 1500 psi, the sand samples returned to approximately the same density. If the duration of the pressure reduction was greater than 5 hours, however, the samples failed to regain their original density when repressurized to their original confining pressure.

In his experiments, Chace (1975) observed gas bubbles which were completely surrounded by water as well as those which were in contact with the surfaces of soil grains. Bubbles trapped in the pore water present in the voids of a soil are usually shaped by the pore spaces unless the bubbles are small enough to be completely surrounded by water within the pores of the soil. He added that as a

bubble grows within the voids of a soil due to air coming out of solution, the bubble may lose some of its surface area as the bubble walls reach the soil grains. This would eliminate some of the surface area across which air could come out of solution. He noted, however, that the magnitude of this effect on the rate at which air comes out of solution is unknown.

Chace (1975) considered the theory of cavitation nuclei in his research. He stated that pockets of undissolved gas trapped in cracks and crevices on the surfaces of solid particles can remain stable in a liquid and serve as nuclei for air coming out of solution. Chace believes that soil particles could be expected to have an abundant number of cracks and crevices in which bubble nuclei could possibly remain stable.

Chace (1975) concluded that dissolved gases are present in all marine sediments and that an adequate number of bubble nuclei are likely present in the soil so that a reduction in applied pressure can be expected to result in a decrease in specimen bulk density, due to gas coming out of solution from the liquid. He added that the magnitude of the change in density which can be expected to occur due to a drop in pressure should be dependent on the amount of dissolved gas present in the pore water.

4.8 Rate at Which Air Goes Into and Comes Out of Solution from Water

Knowing the approximate volume of air that can potentially come out of solution from the pore water of a saturated soil specimen is somewhat useful in assessing the magnitude of volume change possible in a Q test in which a reduction in pore water pressure occurs. As stated previously, however, another important consideration is the rate at which the air will come out of solution or the time required for equilibrium to be reached due to a pressure reduction.

In Section 4.7.2, studies from the geotechnical literature on the rate of diffusion of air through soil pore water and the time required to back pressure saturate triaxial specimens was discussed. In this chapter studies from the physics and chemistry literature on the rate at which air goes into and comes out of solution in water will be presented. In Chapter 6, after the results of the Q tests performed in this research have been presented in Chapter 5, the problem of air coming out of solution from the pore water present in the voids of a silt will be considered.

Much of the information available in the literature on solubility rates concerns the rate at which gases go into solution in water rather than the rate at which they come

out of solution. Two mechanisms have been recognized to explain the process by which air goes into solution and becomes distributed throughout a volume of water. Both are based on the process of diffusion which is governed by Frick's law (Barrow, 1979). The first mechanism is the diffusion process alone. The other mechanism which has been studied, was identified by Adeney (1905) and his co-workers. It includes the process of diffusion along with *streaming* or mixing of the liquid.

4.8.1 Transmission of Gases Into and Out of Water by Diffusion

According to Dorsey (1940), diffusion of a solute into a liquid occurs at constant temperature in accordance with Frick's first law:

$$\left(\frac{dq}{dt}\right)_x = - D \left(\frac{dc}{dx}\right)_t dy dz \quad (4-46)$$

- where
- dq = the amount of the solute which passes in the positive x direction through the area $dy dz$ at a point x during time dt ,
 - dt = the time increment over which diffusion occurs,
 - $\frac{dc}{dx}$ = the rate of change of the concentration of the solute in the liquid at point x occurring over time dt ,
 - D = the coefficient of diffusion or the diffusivity of the solute in the liquid, and

$dy dz =$ the cross sectional area of the interface across which the solute diffuses into the liquid.

The diffusivity, D , of air in open water has been given as $2.0 \times 10^{-5} \text{ cm}^2/\text{s}$ (Fredlund, 1976). In the diffusion process, a gas would enter a liquid at a gas-liquid interface and would then diffuse throughout the body of the liquid due to the concentration gradients existing between different points in the liquid. The diffusion process would cause gas to move from areas with a high concentration of dissolved gas to areas with a low concentration of dissolved gas. In this way, dissolved gas would move systematically from the region of the liquid in contact with the gas, to the portions of the liquid away from the exposed surface.

In a vessel of deaired water with a water surface exposed to the atmosphere and kept at constant temperature, during the diffusion of air into the water, the concentration of dissolved air would be expected to be greatest at the surface exposed to the atmosphere and would decrease with increasing distance from the exposed surface. A concentration gradient would exist in the liquid to some extent until some point in time when the equilibrium conditions associated with Henry's law would have essentially been achieved and the dissolved air content would be the same throughout the entire body of the liquid.

Wyman et al. (1952) performed an experimental study of the rate of solution of air bubbles in sea water. They observed the variation of the rate of solution with pressure, temperature and initial bubble diameter. In their study, they considered the rate of change of the radius of an air bubble with time, based on Frick's law of diffusion, using the following equation:

$$\frac{dr}{dt} = -RT\delta \frac{(P - P_0)}{P} \quad (4-47)$$

where

- r = bubble radius,
- t = time,
- R = gas constant,
- T = absolute temperature,
- P = pressure in the bubble,
- P₀ = partial pressure of the gas in the liquid,
- $\delta = \frac{\Delta\alpha}{d}$,
- Δ = the diffusion coefficient of the gas in the water,
- α = the solubility of the gas in the water, and
- d = the thickness of the shell surrounding the bubble into which the gas diffuses.

They found that $\frac{dr}{dt}$ was approximately constant for a given value of pressure, P, indicating that the radius of the bubble tended to decrease uniformly with time. They also observed that as the pressure, P, increased, the rate

at which the bubble radius changed, $\frac{dr}{dt}$, also increased. They found that $\frac{dr}{dt}$ was essentially independent of temperature because changes in temperature resulted in little variation in the absolute temperature. They also noted that the diffusion coefficient, Δ , increased with increasing temperature, while the solubility of the gas, α , decreased with increasing temperature. These two variables were therefore felt to possibly have offsetting effects. They found that their experimental results agreed with the theoretical predictions.

Wyman et al. (1952) also considered gas bubble growth in sea water. They noted that their experimental procedure and results on bubble growth were felt to be much cruder and should only be considered approximations. In their experiments, they used a syringe with a closed nozzle. Initially, the syringe contained water saturated with dissolved air but with no free air present. The piston was then pulled back and held in position, and air was observed coming out of solution. They used Eq. 4-47 to provide a rough estimate on the amount of air expected to come out of solution in a given amount of time.

They set $P = 0$ atm, and $P_0 = 1$ atm and considered the surface area of the cavity as A . The number of moles of gas

entering the cavity in time t could then be calculated using the following equation:

$$\int_0^t \frac{dn}{dt} dt = A\delta P_0 t \quad (4-48)$$

where n = the number of moles of gas which entered the bubble in time t , and

A = area across which gas was able to diffuse to come out of solution.

If the piston was released after the gas had come out of solution, the volume, V , that the gas molecules would then occupy at a pressure of 1 atmosphere would be:

$$V = RTA\delta P_0 t \quad (4-49)$$

In their experiments, Wyman et al. (1952) observed about twice as much air entering the cavity in time t as calculated using Eq. 4-49. They stated that the value assumed for the area, A , across which air came out of solution may have been incorrect.

Wyman et al. (1952) noted that their equations neglected the surface tension of the water. They added that when the bubble diameter was below 0.1 mm, the increase in gas pressure inside the bubble due to surface tension can become significant and can dominate the behavior of the bubble.

Epstein and Plesset (1950) developed approximate equations for the rate of solution and rate of growth of gas bubbles in liquids. They stated that the growth or shrinking of gas bubbles in a liquid depends on the degree of saturation of the liquid with dissolved gas. Their analysis considered the effect of surface tension on the diffusion process.

Bloomsburg and Corey (1964) reviewed the work of Epstein and Plesset (1950). According to Bloomsburg and Corey (1964), Epstein and Plesset (1950) developed theoretical equations for the rate at which air bubbles go into and come out of solution in water. Epstein and Plesset used a spherical coordinate system and analyzed the process of a bubble of a given size shrinking or growing within a liquid using Frick's first and second laws. Frick's first law calculates the rate of change of the mass of dissolved gas with time as follows:

$$\frac{dm}{dt} = AD \frac{\partial c}{\partial r} \quad (4-50)$$

where

- m = the mass of air going into or out of solution,
- t = time,
- A = the area across which diffusion occurs,
- D = the coefficient of diffusion of air in the liquid,
- c = the concentration of dissolved air in the liquid, and

r = the radial distance from the center of the bubble.

They combined this with Frick's second law which gives the change in the concentration of dissolved gas with time as follows:

$$\frac{\partial c}{\partial t} = D \left[\frac{\partial^2 c}{\partial r^2} + \frac{1}{r} \frac{\partial c}{\partial r} \right] \quad (4-51)$$

Using the above equations, they developed two equations for the rate of change of the bubble radius with time. One equation neglected surface tension effects while the other equation included the effects of surface tension on the rate of bubble growth and shrinkage. For the situation in which surface tension is neglected, the following equation was obtained:

$$\frac{dr}{dt} = \frac{D(c_i - c_s)}{\rho_a} \left[\frac{1}{r} + \frac{1}{(\pi D t)^{0.5}} \right] \quad (4-52)$$

where r = the radius of the air bubble,
 t = time,
 D = the coefficient of diffusion of air in the liquid,
 c_i = the uniform concentration of dissolved air at the bubble boundary,
 c_s = the saturation dissolved air concentration in the liquid at a given temperature and pressure, and
 ρ_a = the density of air at atmospheric pressure and the temperature of the system.

For the case where surface tension forces are considered, the following equation was obtained:

$$\frac{dr}{dt} = \frac{D(c_i - c_s)}{\rho_a + \frac{4MT_s}{3RTr}} \left[\frac{1}{r} + \frac{1}{(\pi Dt)^{0.5}} \right] \quad (4-53)$$

where M = the molecular weight of the gas,
 T_s = the surface tension of the liquid,
 R = the universal gas constant, and
 T = the absolute temperature.

According to Bloomsburg and Corey (1964), by neglecting the term $\frac{1}{(\pi Dt)^{0.5}}$ in the brackets in Eqs. 4-52 and 4-53, Epstein and Plesset (1950) were able to solve these equations in an approximate manner. Bloomsburg and Corey (1964) noted that the second term would not be negligible when the time, t , was close to zero.

In addition to neglecting the second term in brackets in the above equations, Epstein and Plesset (1950) also noted that the movement of the bubble walls during growth or collapse introduced a transport term into the diffusion equation. They added that this additional term made it very difficult to obtain an analytical solution.

As a result of this, Epstein and Plesset (1950) neglected the transport term resulting from the movement of the bubble walls in order to obtain an approximate solution.

They felt that the approximation was still reasonable because the concentration of dissolved gas in the liquid adjacent to the bubble was smaller than the gas density within the bubble. This would make the region around the bubble in which diffusion occurs much larger than the bubble itself. The bubble size therefore would become less significant in this aspect of the diffusion process. They noted, however, that the bubble size would be important with respect to the surface area across which the gas diffuses into or out of solution. They stated that the times calculated by their approximate equations for a bubble to dissolve or expand in water would be slower than the actual times, where the movement of the bubble walls would be included.

For a gas bubble dissolving in a liquid, Epstein and Plesset (1950) presented solutions to both the equation which neglects surface tension effects and the other equation which includes surface tension. Both solutions were approximate to some extent, because they neglected the transport term which resulted from the movement of the bubble walls.

Epstein and Plesset (1950) used these equations to calculate values for the time required for air bubbles of different sizes to dissolve in water with different initial

degrees of undersaturation with dissolved air. In their table, which is reproduced here in Table 4.10, the value f represents the degree of undersaturation of the water with dissolved air, or the ratio between the initial dissolved air content of the water and the saturation dissolved air content; R_0 is the initial radius of the air bubble; t_A represents the approximate time for an air bubble to dissolve, neglecting surface tension effects; and t_S represents the approximate time for an air bubble to dissolve in water, including the effects of surface tension.

Table 4.10: Approximate times for complete solution of air bubbles in water with various degrees of undersaturation with dissolved air and different initial bubble sizes

f	$R_0=10^{-3}$ cm		$R_0=10^{-2}$ cm		$R_0=10^{-1}$ cm	
	t_A (s)	t_S (s)	t_A (s)	t_S (s)	t_A (s)	t_S (s)
0	1.25	1.17	125	124	12,500	12,500
0.25	1.67	1.46	167	164	16,700	16,600
0.50	2.50	1.96	250	241	25,000	24,900
0.75	5.00	2.99	500	460	50,000	49,500
1.00	∞	6.63	∞	5,880	∞	58,000

As can be seen from Table 4.10, the time calculated for a bubble of a given radius to dissolve in water is faster when surface tension effects are considered. This is a result of the fact that surface tension increases the air pressure in the bubble causing the bubble to dissolve faster than if surface tension effects are neglected. It can also

be seen that for a given initial bubble radius, the time required for a bubble to dissolve in water decreases as the initial degree of saturation of the water with dissolved air, f , decreases. In other words, a bubble of a given size will dissolve fastest in water which contains the least amount of dissolved air initially. It can also be seen that the smaller the initial bubble radius, the more rapidly the bubble will dissolve in water with a given degree of undersaturation with dissolved air.

Considering surface tension effects, for water with a dissolved air content of half of its saturation value ($f = 0.5$), the time required to dissolve an air bubble with an initial radius, R_0 , of 10^{-3} cm, is 1.96 seconds, while the time required to dissolve a larger air bubble with an initial radius, R_0 , of 10^{-2} cm, is 241 seconds or 123 times as long. Similarly, for an air bubble with an initial radius, R_0 , of 10^{-1} cm, 24,900 seconds or 6.9 hours are necessary for the bubble to dissolve in water. This is over 12,700 times longer than the time necessary for a bubble with an initial radius, R_0 , of 10^{-3} cm to dissolve.

The experimental data presented by Lee and Black (1972) for the time required for a bubble to go into solution has been analyzed using the approximate equations of Epstein and Plesset (1950). The times for an air bubble with an initial

radius R_0 , to dissolve in water, as measured by Lee and Black (1972), along with the times calculated using the equations of Epstein and Plesset (1950), are given in Table 4.11.

Table 4.11: Time for air bubbles to dissolve in water as measured by Lee and Black (1972), t_d , and calculated using the equations of Epstein and Plesset (1950), t_A and t_S

Test No.	R_0 (cm)	T (°C)	Measured t_d (min)	Calculated t_A (min)	Calculated t_S (min)
B1	0.11303	27	243	413	288
B2	0.11405	24	250	356	284
B3	0.11494	28	197	367	303

Comparing the times calculated using the equations of Epstein and Plesset (1950) to the times actually measured by Lee and Black (1972), it can be seen that the actual times (t_d) for the bubbles to dissolve in water were always faster than the calculated times (t_A and t_S). As noted by Epstein and Plesset (1950) this is a result of the transport term being neglected in obtaining the calculated values. It can also be seen that when surface tension effects were neglected, the calculated times were 42 to 86 percent greater than the measured times. When the effects of surface tension were included, the calculated times for a bubble to dissolve in water were 14 to 54 percent greater than the measured values. For this reason, the equations given by Epstein and Plesset (1950) which include surface

tension effects, should be used to give more reasonable estimates of the time required for bubbles to dissolve in water.

Epstein and Plesset (1950) also solved their equations to estimate the time required for a bubble to grow in water which is oversaturated with dissolved air. The solutions are again approximate because they neglect the transport term associated with the movement of the bubble walls during growth. The solution to one of the equations includes the effects of surface tension on bubble growth while the solution to the other equation neglects these effects.

The values calculated by Epstein and Plesset (1950) and presented in Table 4.12, are the times required for an air bubble to grow from an initial bubble radius, R_0 , to a final bubble radius of $10R_0$, in water with different degrees of oversaturation with dissolved air. In this table, f , is the degree of oversaturation of the water with dissolved air, or the ratio between the original saturation dissolved gas content at time $t=0$ and the dissolved gas content of the water at the reduced pressure condition at time t ; t_A is the approximate time required for an air bubble to grow from an initial radius, R_0 , to $10R_0$, neglecting surface tension effects; and t_S is the approximate time required when surface tension effects are included.

Table 4.12: Approximate time for an air bubble to grow from an initial radius R_0 to $10R_0$ in water with various degrees of oversaturation with dissolved air

f	$R_0=10^{-3}$ cm		$R_0=10^{-2}$ cm	
	t_A (s)	t_S (s)	t_A (s)	t_S (s)
1.25	496	567	49,600	50,100
1.50	248	266	24,800	24,900
1.75	165	174	16,500	16,600
2.00	124	129	12,400	12,400
5.00	30.9	31.7	3,090	3,100

As can be seen from Table 4.12, the approximate times calculated for a bubble to grow when surface tension effects are included are slightly longer than when surface tension effects are neglected. This is because the surface tension forces act against the expansion and a longer time is therefore needed to expand the bubble. From the values given in Table 4.12, it can be speculated that for a soil sample which initially contained an air bubble with a radius of 10^{-3} cm (0.01 mm), or about the size of a medium sized silt particle, if the pore water was initially saturated with dissolved air at the initial pressure, when the pore pressure was reduced by half, ($f = 2.0$), it would have taken approximately 129 seconds or 2.15 minutes for the bubble radius to increase by a factor of 10 to 0.1 mm or 10^{-2} cm. This indicates that during the time over which a saturated silt is sampled or tested in a Q test, a very small pre-existing air bubble could grow quite rapidly if the pore

water was saturated with dissolved air initially and an adequate reduction in pressure occurred.

Another estimate of the relative magnitude of the time necessary for dissolved gases to come out of solution from a liquid due to a pressure decrease, can be found in diving tables and literature on decompression procedures. According to the U.S. Navy Diving Manual (1970), during diving increased amounts of gas become dissolved in a diver's blood and body tissues. This is due to the increase in hydrostatic pressure associated with the depth below the water surface. When a diver at some depth in the water ascends back to the water surface, the gas pressure will return to atmospheric conditions and the gases dissolved in the blood and tissue will tend to come out of solution.

The gases enter and exit solution in the blood through the lungs. The circulation of the blood throughout the body transfers the dissolved gases between the blood and various body tissues. If the diver ascends to the surface too rapidly, the dissolved gases may come out of solution within the blood and tissues faster than the circulating blood and respiration can remove gases from the body. If this occurs, gas bubbles may form within the diver's body and could possibly cause decompression sickness. The formation of gas bubbles within muscle tissue near joints is generally felt

to be the cause of a painful form of decompression sickness known as *the bends*. For this reason, diving tables are available which indicate the safe rate of ascent for divers as well as periodic stops at various depths to allow gases to exit solution from the body through normal respiration.

There are several factors which influence the values of ascent time and required stops given in diving tables. These include: the maximum depth of the diver below the water surface, the composition of the gas that the diver is breathing, the length of time that the diver is at a given depth, and the physiological conditions which control the ability of the body to absorb and release dissolved gases.

According to the U.S. Navy Diving Manual (1970), for a diver breathing air for 300 minutes at a water depth of 40 ft (water pressure of 17.3 psi), the diver should ascend from 40 ft to 10 ft ($\Delta u = 13$ psi) at a rate of 60 ft/min. In this case, the ascent to 10 ft would take 30 seconds. At 10 ft depth, the diver should wait 19 minutes before ascending to the surface. Following this decompression schedule will allow the gases which became dissolved in the diver's blood and tissues during the 300 minutes at 40 ft depth to exit solution gradually through the respiration process. If the diver went to the surface immediately without stopping for 19 minutes at 10 ft depth, dissolved

gases would probably have come out of solution within the diver's blood and tissues and formed bubbles.

Because several complicated factors are involved in decompression from diving, including the removal of dissolved gases from blood and tissues by respiration, direct comparison with the processes which are going on in Q tests on saturated silts are difficult. The fact that slightly over 19 minutes are necessary for a sufficient amount of dissolved gas to exit solution from a diver's blood and tissues due to a pressure reduction of about 17 psi (40 ft of water), however, suggests that in the 20 minutes that it takes to perform a Q test on a saturated silt specimen, dissolved gases could very likely have sufficient time to exit solution from the pore water. Unlike in a diver's body, these gases coming out of solution would not be removed from the system by respiration. The dissolved gases coming out of solution in soil pore water would be trapped within the triaxial specimen as bubbles within the soil pores.

4.8.2 Transmission of Gases Into Water by Streaming

Adeney (1905) studied the mechanisms by which gases go into solution in water and become distributed throughout the body of the liquid. He found that the transmission of gases to depths below the gas-liquid surface appeared to occur

much more rapidly than calculated by the diffusion theory. He felt, therefore, that a mechanism other than diffusion of gas molecules into the depths of the liquid must also be considered. He investigated the theory that downward *streaming* helps to distribute dissolved air throughout the water. In the downward streaming mechanism, as the gas diffuses into the water at the exposed water surface, the upper water layer becomes heavier and sinks downward in the body of water, leaving water undersaturated with gas near the surface into which more gas can diffuse. This mixing process would continue until equilibrium conditions had essentially been achieved in the liquid.

The experiments performed by Adeney (1905) initially indicated that this downward streaming effect was the mechanism by which dissolved gases were able to move throughout the body of a liquid much more rapidly than the diffusion theory suggested. Some of his experiments however, indicated that under similar conditions, the streaming effect was more noticeable in sea water than in distilled water. He further found that if extremely clean filtered air was used, the streaming effect was greatly reduced. He hypothesized that in the tests where the air was not filtered, the streaming may have resulted from minute dust particles or other potential centers of condensation, possibly electrically charged, being passed

from the air into the water along with the dissolving gases. He believed that these tiny particles and dissolved gases then combined in some way to increase the density of the upper layer of the water, resulting in streaming and the transmission of the gases throughout the body of the liquid by gravitational forces.

Adeney (1905) concluded that for large open bodies of sea and fresh water where surface disturbance is considerable, the transmission of dissolved gases through the body of water by diffusion could essentially be neglected when compared to the streaming effect.

Further studies by Adeney and Becker (1918, 1919) considered the rate of solution of air and other gases in water. They found that for water which was kept thoroughly mixed and had a gas-water surface which was unbroken, such as a bubble, the solution of the gas took place in accordance with the equation:

$$\frac{dw}{dt} = a - bw \quad (4-54)$$

where $\frac{dw}{dt}$ = the rate of solution of the gas in the water,

a = the initial rate of solution of the gas in the water,

bw = the rate of escape of the gas from the water, and

b = a constant which is dependent on the gas and temperature.

The procedure used in their experiments consisted of allowing a large bubble of gas, of known volume, to pass repeatedly upward through a narrow tube containing initially deaired water until the water became saturated with the gas. The pressure in the bubble was measured after each two passes up the tube, thereby giving data for calculating the absorption which took place at each step of the process until saturation was reached. The experiments were conducted at various temperatures to account for the effect of temperature on the absorption process. Gas bubbles of five different volumes were used and photographed while moving up through the tube relative to a measuring scale adjacent to the tube. These photographs were then analyzed by microscope to determine the length of each bubble so that the surface area of the bubble could be calculated at various steps of the absorption process for use in the analysis.

Based on their results, the rate of solution of air in water, for any conditions of exposed surface area, depth of the body of the liquid, or degree of saturation can be calculated provided that the water is kept uniformly mixed. The solution of Equation 4-54 can be expressed in the form (Adeney and Becker, 1919):

$$w = (w_o - w_1)(1 - e^{-bt}) \quad (4-55)$$

where w = the weight per unit volume of gas which dissolved in the liquid during time t ,

w_0 = the weight per unit volume of dissolved gas present in the liquid at $t = \infty$,

w_1 = the weight per unit volume of gas dissolved in the liquid initially,

e = exponential function,

t = time in minutes, and

b = a constant.

The constant b given by Adeney and Becker (1919) is defined as follows:

$$b = f \frac{A}{V_w} \quad (4-56)$$

where f = the coefficient of escape of the gas from the liquid per unit area and volume, cm/min,

A = the surface area across which the gas diffuses to go into solution, cm^2 , and

V_w = the volume of the liquid, cm^3 .

For air dissolving in water, $f = 0.0099(T - 239)$, where $T = ^\circ\text{C} + 273$. Using Eq. 4-56 for the constant b , Eq. 4-55 then becomes:

$$w = (w_0 - w_1) \left(1 - e^{-\frac{fA}{V_w}t} \right) \quad (4-57)$$

In their work, Adeney and Becker (1919) found that it was more convenient to work in percentages of saturation in many applications rather than using dissolved air concentrations. As an example of using Eq. 4-57 for air

going into solution in water, consider air dissolving in 1000 cm³ of water with an exposed surface area of 10 cm², a temperature of 20°C and an initial gas content of 40 percent of saturation ($w_1=0.4w_0$). The percentage increase in the dissolved air content of the water which would occur during one hour ($t=60$ minutes) can be calculated as:

$$w = (100\% - 40\%) \left(1 - e^{-0.0099(20+273-239)\frac{10}{1000}(60)}\right) \quad (4-58)$$

$$w = (60\%) (1 - e^{-0.32076}) = 16.5\% \quad (4-59)$$

According to an example presented by Adeney and Becker (1919), in one hour, the dissolved air content of the water would have increased by 16.5 percent from the initial value of 40 percent to a dissolved air content of 56.5 percent of the eventual final dissolved air content of the water. Over time, the dissolved air content of the liquid would continue to increase until 100 percent saturation had been reached.

The equations developed by Adeney and Becker (1918, 1919) assume that thorough mixing of the water takes place throughout the solution process. The equations were developed from experiments in which an air bubble repeatedly traveled upward through a tube of water. The pressure of the air within the bubble increased as the bubble size decreased, in accordance with Boyle's law. As the bubble moved upward through the tube, the bubble was constantly

coming into contact with water which was undersaturated with air relative to the air pressure within the bubble. The solution process therefore occurred much more rapidly than if the bubble was stationary and the mixing of the water had not been forced by the bubble moving continuously through the column of water to come into contact with undersaturated water. Adeney and Becker's (1918, 1919) equations therefore provide an upper bound on the rate of solution of air in water, if agitation of the water is not involved.

In another study by Adeney and Becker (1920), they again considered the rate of solution of air in water. They stated that the solution of air in water may occur in three ways: (1) solution of air in the water at the exposed surface with thorough and rapid mixing of the water to the unexposed portions; (2) solution of air in the water at the exposed surface with no mixing; and (3) solution of air in the water at the exposed surface with slow or imperfect mixing.

They noted that if there was no mixing of the water, the only process by which dissolved air could become distributed throughout the body of the water was by diffusion of the dissolved gas molecules from the exposed water surface into the depths of the liquid. In this situation, the law of diffusion of solutes through liquids,

governed by Frick's first and second laws, would apply. They added that there was no experimental evidence to show that no mixing occurs under natural conditions and they doubted if such conditions could ever be reproduced in the laboratory.

Adeney and Becker (1920) stated that calculations based on the diffusion theory for open bodies of water are of little practical value. They felt that air went into solution at the exposed water surface and was distributed throughout the body of water by slow mixing. The rate of solution of air in water was therefore felt to be dependent on the rate of mixing.

Adeney and Becker (1920) also found that the humidity of the air in contact with the water had an effect on the rate of solution of air in water. When the air above the water was very dry, the rate of solution of atmospheric gases was much more rapid than usual. For air containing a high concentration of water vapor, the rate of solution was significantly slower. They felt that because evaporation is greatest when the air is dry and minimal when the air is moist, the process by which dissolved gases moved downward into the body of a liquid was affected by evaporation from the surface of the liquid. Their explanation was that as evaporation occurred from the exposed water surface, the

surface layer cooled and became more dense and sank downward within the body of the liquid. The sinking layer of water carried dissolved gases with it, thereby increasing the rate of solution of air in the water. If little to no evaporation occurred due to high humidity in the air, less mixing would have resulted and the rate of solution was much slower.

In another study, Adeney, Leonard, and Richardson (1922) concluded that the aeration of quiescent bodies of fresh and salt water, under normal conditions, occurred by the mixing of the exposed water surface with the unexposed portions of the water to depths of at least 10 feet. They found that the mixing process occurred more rapidly in salt water than in fresh water. They also found that the mixing occurred more rapidly at temperatures above 10°C and was less rapid and uniform to depths of 10 feet at temperatures below 8°C. This was especially true in fresh water.

Becker and Pearson (1923) found that during the early stages of air dissolving in water, their experimental data were in agreement with the theoretical predictions based on the equations presented by Adeney and Becker (1918, 1919). This indicated that during the early stages of absorption, the water was kept slowly but steadily mixed. Once the water became 60 to 70 percent saturated with dissolved air,

however, the rate of solution decreased below that predicted by theory. This implied that for water with high degrees of saturation with air, the mixing process was less predominant and the rate of solution of the air in the water was below that suggested by the equations of Adeney and Becker (1918, 1919).

Adeney (1926) also considered the effect of agitation of the water surface on the rate of solution of air in water. He found that disturbance of the air-water interface increased the rate of solution of air in the water. He noted that this disturbance could occur naturally such as wind causing waves on the surface of an open body of water or it could be promoted such as the use of agitation on the surface of sewage treatment plant aerators. He stated that disturbance of the water surface increases the effective area across which air can diffuse into the water and this thereby increases the rate of solution of the air in the water.

4.8.3 Application of Streaming Equations to Gases Exiting from Water

Dorsey (1940) presented a thorough compilation of information on the properties of water. In the area of interest, he summarized the work of Adeney and Becker (1918, 1919) and presented the "Rate of Solution of Gases in Water"

along with tables of the "Entrance Coefficient of Gases into Water" and the "Exit Coefficient of Gases from Water." For gases exiting water, Dorsey (1940) gave the equation:

$$(c - c_0) = (c_\infty - c_0)(1 - e^{-\beta \frac{At}{V_w}}) \quad (4-60)$$

where c = concentration of the gas in water at time t ,
 c_0 = concentration of the gas in water at time $t = 0$ (equilibrium dissolved gas concentration at higher pressure),
 c_∞ = concentration of the gas in water at time $t = \infty$ (equilibrium dissolved gas concentration at lower pressure),
 e = exponential function,
 β = the exit coefficient from water of a given gas at a given temperature,
 A = the surface area across which the gas comes out of solution from the water, cm^2 ,
 V_w = the volume of the water, cm^3 , and
 t = time in minutes.

Dorsey (1940) presented tabulated values of the exit coefficient, β , for air and other gases exiting water at various temperatures. According to Dorsey, the exit coefficient, β , for air exiting water is the same as the coefficient f used by Adeney and Becker (1918, 1919) and is given as:

$$\beta = 0.0099(T - 239) \quad (4-61)$$

where $T = ^\circ\text{C} + 273$, and β is in units of cm/minute .

Considering the same water sample volume, area and temperature conditions analyzed previously, Eqs. 4-60 and 4-61 can be applied to a situation in which the water is going from being 100 percent saturated with air to water containing 40 percent of the initial saturated dissolved air content ($c_{\infty}=0.4c_0$). During one hour ($t=60$ minutes), the amount of air which would come out of solution can be calculated as:

$$c - 100\% = (40\% - 100\%)(1 - e^{-0.32076}) = -16.5\% \quad (4-62)$$

$$\text{or} \quad c = 100\% - 16.5\% = 83.5\% \quad (4-63)$$

In this case, in one hour, the dissolved air content of the water would have decreased by 16.5 percent from an initial dissolved air content of 100 percent to a dissolved air content which was only 83.5 percent of the initial dissolved air content. With time, the dissolved air content of the liquid would continue to decrease until equilibrium conditions had been reached.

This last example of a situation of air exiting from solution was not addressed directly by Adeney and Becker (1918, 1919). It was however, inferred in the information presented by Dorsey (1940) and has been included here as part of this research. It is not certain whether this is a correct application of the work of Adeney and Becker (1918, 1919). In any case, the example presented above would

require the water to be thoroughly mixed throughout the process of the air coming out of solution. According to Adeney and Becker (1918, 1919), the equations they presented were developed for air going into solution in water which was thoroughly mixed.

The coefficient f in Eq. 4-51 and 4-52 given by Adeney and Becker (1918, 1919), is defined as the coefficient of escape of the gas from the liquid per unit area and volume. Dorsey (1940) appears to have interpreted this definition and the experiments of Adeney and Becker (1918, 1919) to be applicable to gases exiting from solution as well as going into solution. The mechanism by which water would be thoroughly mixed while gases are exiting from solution however, is unclear.

If a vessel of water is in equilibrium with the air above an exposed surface and the pressure of the air-water system is reduced, dissolved air will come out of solution in order to reestablish equilibrium. As the dissolved air exits from the water at the exposed water surface, the density of the water layer at the surface would be expected to decrease due to the loss of the weight of the dissolved air. With a lower density than the water below it, which now contains higher concentrations of dissolved air, the upper layer of water would not be expected to sink downward

in the vessel and mixing of the water would likely be hindered. If little to no mixing of the water occurs, the rate of gas evolution should be reduced below that expected if mixing were to take place.

Because of this, it is questionable whether or not the equation presented by Dorsey (1940), for gases exiting from solution, is an accurate interpretation of the work of Adeney and Becker (1918, 1919). It may very well be that the rate at which gas comes out of solution is controlled to a greater extent by the diffusion mechanism rather than the mixing process identified by Adeney (1905). Based on this, air would tend to go into solution faster than it would come out of solution. This in fact, appears to be in agreement with the observations of Chace (1975, 1985).

4.8.4 Effect of Disturbance on the Rate at which Air Comes Out of Solution from Water

Schweitzer and Szebehely (1950) studied the solubility of air in several liquids, including distilled water, and measured the rate at which air went into and came out of solution when equilibrium was disturbed. Their procedure consisted of taking a container of water and allowing it to reach equilibrium with the air pressure above the liquid, in accordance with Henry's law. The air pressure was then changed to a value either above or below the initial

pressure while rapidly shaking the container. Accurate measurements of the pressure of the air above the water were made throughout the process of air going into or coming out of solution. The variation of the air pressure during and after agitation was related to the amount of air which went into or came out of solution and the rate at which it occurred. They considered the solution to be in equilibrium when further shaking no longer caused any change in the air pressure above the liquid.

They found that the rate at which air came out of solution was proportional to the degree of supersaturation of the liquid with air, and that the rate at which air went into solution was proportional to the degree of undersaturation of the liquid with air.

Schweitzer and Szebehely (1950) were concerned mainly with the rate of solution and evolution of air in flowing liquids. For this reason, they performed experiments in which the system was agitated to simulate the conditions in the flowing liquid. They noted that the rates for solution and evolution of air in water not subjected to agitation would be much slower than determined in their experiments. They found that the rate at which air came out of solution under agitated conditions was always thousands of times greater than the rate would have been for non-agitated

conditions. They also observed that air came out of solution from distilled water faster under agitated conditions than it went into solution.

The fact that the rate at which air came out of solution from water under agitated conditions was many times higher than the rate for nonagitated conditions indicates that disturbance may play a very important role in the formation of air filled bubbles in samples of saturated silt during and after sampling. Saturated silts sampled in-situ and subjected to considerable disturbance would be expected to have considerably more air come out of solution, or at least come out of solution sooner, thereby altering the soil structure to a greater extent than would be expected in similar silt samples in which disturbance was minimal.

Even though the temperature increase and pressure decrease associated with sampling may very well eventually result in dissolved gases coming out of solution and increasing the volume of the soil, disturbance or agitation will accelerate this process. Disturbance and agitation of soil sampling tubes should be kept to a minimum to delay the exit of dissolved gases from solution. If triaxial tests can be performed as quickly after sampling as possible while agitation of sampling tubes is kept to a minimum, less

dissolved gas may come out of solution and better test results may be obtained.

4.9 Summary and Conclusions

A number of important concepts have been presented in this chapter regarding the solubility of air in water and the rate at which air or gas goes into and comes out of solution in water. Additional findings on the dissolved gas content of ground water and air-water relationships in soils have also been presented. From the information presented in this chapter, the main points can be summarized and a number of important conclusions made:

- 1.) Henry's law states that the mass of a slightly soluble gas that can be dissolved in a given mass of water is proportional to the partial pressure of the gas in contact with the water (Henry, 1803).
- 2.) For a gas-liquid system, the volume of a gas decreases with increasing pressure by Boyle's law, just as rapidly as the weight of dissolved gas increases by Henry's law. Because of this, the volume of the dissolved gas in a given volume of water is independent of pressure, as long as the temperature remains constant (Fredlund, 1976).

- 3.) The volume of gas which can be dissolved in a given volume of water decreases as the temperature of the gas-water system increases (CRC Handbook of Chemistry and Physics, 1988).
- 4.) The dissolved gas content of ground water can be expected to vary, depending on the chemical, biological and physical conditions in the ground. In addition, the gases commonly dissolved in ground water may be different from the gases present in atmospheric air (Freeze and Cherry, 1979).
- 5.) Ground water may be saturated with certain dissolved gases while being supersaturated or undersaturated with other dissolved gases, relative to atmospheric conditions of gas composition, temperature and pressure. When a saturated soil is sampled and brought to the ground surface, gases which the pore water is supersaturated with will tend to come out of solution, while gases which the water is undersaturated with will tend to go into solution.
- 6.) Saturated silts can experience a decrease in pore water pressure as a result of the attempted dilation during undrained shear as well as during the stress release associated with sampling the soil from some depth in the ground.

- 7.) The amount of time available for dissolved gas to come out of solution from soil pore water is dependent on the time over which the reduction in pore water pressure takes place. The pore pressure reduction which occurs during undrained shear (Q tests) typically takes place over a period of about 20 minutes, during which dissolved gases can come out of solution. The reduction in pore water pressure which occurs during sampling takes place over a relatively short period of time as the soil is sampled. The time between sampling stress release and actual laboratory testing, however, will vary from several hours to hundreds of days in many cases, allowing dissolved gases to come out of solution over a considerable period of time.
- 8.) Temperature fluctuations of soil pore water, especially those which occur as a result of sampling, may lead to dissolved gases being released from solution.
- 9.) Gases released from solution due to a temperature increase during sampling will tend to expand in volume according to Boyle's law as a result of the pressure decrease associated with sampling.
- 10.) The potential volume increase that a soil specimen may experience during sampling as a result of dissolved gases coming out of solution may be quite significant.

The final degree of saturation has been estimated to be as low as 93 percent for a sample taken from a depth of 100 feet below the ground water level at an initial temperature of 11°C and brought into a typical soil mechanics laboratory.

- 11.) At very high degrees of saturation, pore air and pore water pressures are often assumed to be essentially equal when performing effective stress analyses. Triaxial specimens with high initial degrees of saturation often have slight differences between their pore air and pore water pressures. These differences in pressure may have some significance with respect to dissolved air coming out of solution during a decrease in pore water pressure. The difference between the pore air and pore water pressure in a triaxial specimen indicates that somewhere in the specimen, an air-water interface exists across which surface tension forces are acting. These air-water interfaces and small pockets of air within the sample can serve as initiation points for more air to come out of solution and grow into bubbles and voids within the soil pores as pore pressure reductions occur.
- 12.) A number of soil mechanics researchers (Hamilton, 1939; Terzaghi, 1943; Taylor, 1948; Bishop and Eldin, 1950)

indicate that soils thought to be fully saturated can contain small pockets of undissolved air or gas within the pores of the soil which are often undetectable. In addition, air pockets may become trapped between the specimen and the rubber membrane during triaxial tests performed at low cell pressures (Bishop and Henkel, 1962; Head, 1986).

13.) Terzaghi (1943) showed approximately that the pore water in a clay soil needs to be subjected to a significantly larger reduction in pressure than that in a sand, in order for an existing bubble to grow into a void within the pores of the soil. A silt appears to require a negative pore water pressure that is on the same order of magnitude as that for a sand, in order for an existing bubble to grow into a void. This suggests that the pore water of clays is less likely to experience cavitation than the pore water of sands and silts. This may explain why $\phi_u = 0$, $S_u = c$ undrained strength envelopes are often obtained for clays with a tendency for dilation, while dilatant silts which would be expected to cavitate at smaller reductions in pore pressure, often exhibit $\phi_u > 0$ strength envelopes.

14.) Several studies (Bishop and Eldin, 1950; Lowe and Johnson, 1960; Bishop and Henkel, 1962) have considered

the process of increasing the degree of saturation of partially saturated triaxial specimens by increasing the cell pressure. Other studies (Lowe and Johnson, 1960; Black and Lee, 1973) have shown how a back pressure can be utilized to increase the degree of saturation of triaxial specimens. These studies have shown that an increase in cell pressure or back pressure compresses the free air and forces it into solution in the pore water, thereby increasing the degree of saturation of the soil. Conversely, a decrease in pore water pressure during undrained shear would be expected to allow air dissolved in the soil pore water to come out of solution and expand within the voids of the soil. This would result in a decrease in the degree of saturation of the soil as well as an increase in its void ratio.

- 15.) The rate of diffusion of air into water has been observed to be slower for soil pore water than for free water (Barden and Sides, 1967; Lee and Black, 1972). It has also been observed to be slower in fine-grained soils than in coarse soils, due to the smaller pore sizes (Barden and Sides, 1967; Lee and Black, 1972). The rate of diffusion of air in soil pore water can be related to air coming out of solution as well as going into solution. It is thus expected that air may

diffuse out of solution from soil pore water at a slower rate than dissolved air would come out of solution from free water.

- 16.) Air bubbles present in a fine-grained soil would tend to be smaller than those in a coarse-grained soil and would tend to go into solution more rapidly due to surface tension effects (Bloomsburg and Corey, 1964). Surface tension effects would also tend to resist bubble growth in soil pore water. These resisting surface tension forces would be largest in fine-grained soils because bubble sizes are smaller than they are in coarse soils.

- 17.) Chace (1975, 1985) observed that the time for air to come out of solution from soil pore water was longer than the time required for air to go into solution, due to the same change in pressure. He also observed that dissolved air came out of solution more rapidly from the pore water of a coarse-grained soil than a fine-grained soil for the same reduction in pressure. He also found that dissolved air came out of solution more rapidly from soil samples which had exposure to a source of external air than from samples essentially sealed off from an external air source. The volume increase which occurred due to the reduction in

pressure and air coming out of solution could be negated if the pressure on the soil was increased within a certain amount of time after pressure release. Beyond this limiting time, the soil specimen did not return to its original density or volume when the pressure was increased.

- 18.) Even for a soil specimen with a very high initial degree of saturation, a typical increase in cell pressure applied to the specimen in order to force any free air into solution in the pore water, may not yield a fully saturated specimen until a considerable amount of time has elapsed. Within the time frame over which the cell pressure is applied and a Q test performed, a specimen thought to be fully saturated as a result of the increase in cell pressure used in the test, may not be fully saturated and may yield stress-strain behavior more characteristic of a partially saturated specimen.
- 19.) Studies on the sampling and testing of marine soils (Esrig and Kirby, 1977; Lee, 1985; Rau and Chaney, 1988; Chace, 1975, 1985) indicate that gases exiting from solution and expanding within a soil are common and are of major concern. Marine soils in sampling tubes are often observed to grow out of the tubes as dissolved gases are released and expand within the soil

(Esrig and Kirby, 1977). Performing tests as quickly as possible, using pressurized core barrels and storage containers as well as applying sufficient cell pressures and back pressures for an adequate period of time prior to testing, are all suggested procedures to counteract the release of dissolved gases from the pore water of marine soils (Lee, 1985; Rau and Chaney, 1988; Chace, 1975, 1985).

- 20.) Dissolved gases coming out of solution from soil pore water during the pore pressure reduction resulting from sampling or undrained shear will increase the volume and void ratio of the soil (Taylor, 1948; Rau and Chaney, 1988). This will affect the structure of the soil and will influence any properties of the soil which are dependent on the void ratio (Taylor, 1948), including shear strength.
- 21.) Two mechanisms have been identified by which gases can go into and come out of solution in liquids: diffusion and streaming (Dorsey, 1940). The diffusion process appears to be the more likely process by which dissolved gases would come out of solution from water. The equations presented by Epstein and Plesset (1950) and based on the diffusion process indicate that within the times considered for pore pressure reduction during

both sampling and a typical Q test, pre-existing air bubbles may very likely expand and additional dissolved air may be able to come out of solution in quantities significant enough to influence the behavior of the soil.

- 22.) Schweitzer and Szebehely (1950) showed that agitation of water influences the rate at which dissolved gases go into and come out of solution from water. Gases will go into and come out of solution in water more rapidly under agitated conditions than under non-agitated conditions. This indicates that sample handling procedures and disturbance levels may influence the rate at which dissolved gases come out of solution as well as the amount of gas which exits solution from soil pore water prior to testing. Disturbance of soil samples during transport, trimming and preparation should be minimized so that as little gas as possible will come out of solution in the time between sampling and testing. In addition, saturated silts should be tested as soon after sampling as possible, so that a minimum amount of dissolved gas will have been able to come out of solution within the soil pores.

23.) The information presented in this chapter suggests that dissolved gases present in soil pore water are capable of coming out of solution during sampling as well as during Q tests on soils with a tendency to dilate. In addition, small bubbles of free gas will very likely be present in many soil specimens thought to be fully saturated. These gas bubbles will tend to grow in size as reductions in pore pressure occur. If pre-existing gas bubbles within the soil pores grow large enough or if new bubbles form and grow, it is possible that they could influence the behavior of saturated, dilatant silt specimens tested in undrained shear.

Chapter 5

EXPERIMENTAL STUDY

In order to investigate the possible occurrence of cavitation in Q tests on saturated silts, a laboratory testing program was developed to address the questions regarding the influence of cavitation of pore water on silt behavior.

5.1 Properties of the Soil Used in this Study

The soil used in this study was obtained from the Corps' Lower Mississippi Valley Division (LMVD) and is referred to as LMVD silt. Most of the LMVD silt used in this research was available from a previous study (Brandon, Duncan, and Huffman, 1990) and will be referred to as "old LMVD silt." Test specimens of this silt were remolded from a slurry in a batch consolidometer. In the batch consolidometer, a slurry of saturated silt was consolidated under K_0 conditions. This resulted in a 5-inch diameter by 5-inch high sample of saturated silt. From the batch consolidometer sample, four triaxial specimens could be trimmed and tested. These four specimens would be essentially fully saturated and have similar void ratios.

A schematic diagram of the batch consolidometer is shown in Figure 5.1.

Undisturbed specimens of LMVD silt were also provided by the LMVD for this project and will be referred to as "new LMVD silt." Several tests have been performed on these undisturbed specimens. Additional specimens of the new LMVD silt were remolded from a slurry in the batch consolidometer. Since the majority of the tests were performed on specimens of old LMVD silt, only in tests where new LMVD silt was used will this be specifically noted in tables, figures and discussion. Where no mention is made of which silt was used in a particular test, it should be assumed that the test was performed on old LMVD silt.

Four undisturbed tubes of new LMVD silt were received in July, 1991 and were labeled 1, 2, 3, and 4. Soil from these tubes has been used for index and strength tests on the soil.

The LMVD silt used in this research was tan in color and was composed of predominantly silt-sized grains. Hydrometer and sieve analyses of the new LMVD silt were performed on samples taken from tubes No. 3 and 4. The gradation curves for these analyses along with a gradation

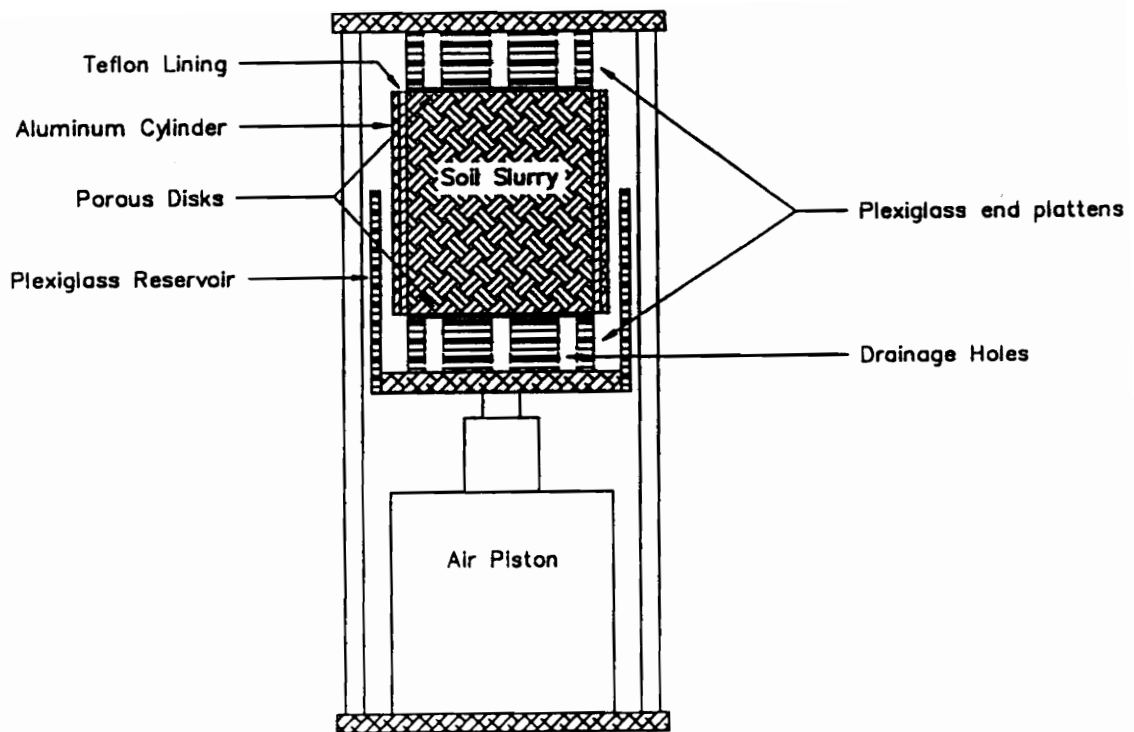


Figure 5.1 Schematic diagram of batch consolidometer used in forming remolded specimens

curve for the old LMVD silt remaining from the previous study are shown in Figure 5.2. The percentages of the different grain size components of the old and new LMVD silt are presented in Table 5.1.

Table 5.1: Components of LMVD silt, based on grain size

Component	Old LMVD Silt	New LMVD Silt
% Sand	11%	2-5%
% Silt	77%	87-90%
% Clay	12%	8%

Atterberg limits for the new LMVD silt were determined. The new LMVD silt was found to have a liquid limit of 28 and a plasticity index of 3. The old LMVD silt was reported to have a liquid limit of 26 and a plasticity index of 4 (Brandon, Duncan, and Huffman, 1990). The specific gravity of the soil solids for the new LMVD silt was determined to be 2.69. In-situ moisture contents of the four undisturbed tubes of new LMVD silt were determined and are summarized in Table 5.2.

Table 5.2: Moisture contents of undisturbed samples of new LMVD silt

Tube No.	w (%)
1	17.5
2	18.1
3	17.2
4	16.8

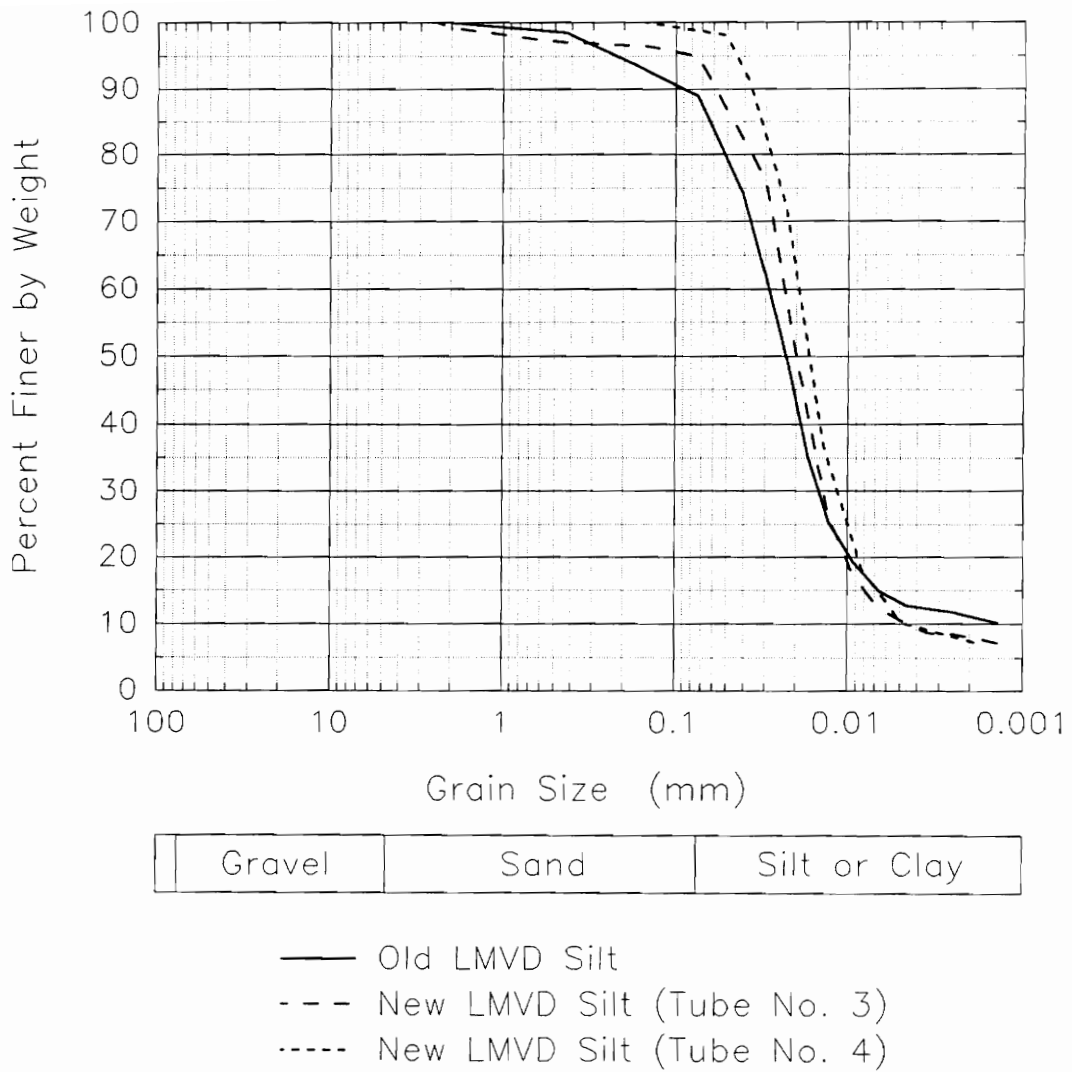


Figure 5.2. Gradation curves for old and new LMVD silt

An analysis of the mineralogy of the new LMVD silt was performed using X-ray defraction techniques. The silt-sized grains were found to be primarily quartz with some feldspar also present. The clay component of the new LMVD silt was found to be composed predominantly of montmorillinite with vermiculite, mica and kaolinite also present in lesser quantities. The clay component of the soil had an average cation exchange capacity of 60 meq/100g and a specific surface of about 650 m²/g. The organic content of the new LMVD silt was found to be about 2 percent by weight.

5.2 Laboratory Tests Performed in this Study

A total of 119 triaxial tests have been performed in this research to study the undrained behavior of saturated, dilatant silts. The test series which were performed in this research are summarized in Table 5.3. The following sections will present the results of these test series.

5.3 Midheight Pore Pressure Monitoring of Triaxial Specimens

One of the areas of interest in this study was the magnitude of the pore pressure change which occurs during Q tests on saturated silts. During a conventional Q test, the pore water pressure in the specimen is not measured. In order to measure the magnitude of the change in pore

Table 5.3: Summary of tests performed on LMVD silt in this study

Type of Test	Number Performed	Section	Comments
Q	18	5.4	<ul style="list-style-type: none"> - with midheight pore pressure measurements - 17 remolded specimens of old LMVD silt - 1 undisturbed specimen of new LMVD silt
Anisotropically Consolidated Undrained Unloading	6	5.5	<ul style="list-style-type: none"> - 4 tests on 1.4-in. dia. specimens 2 tests on remolded specimen of old LMVD silt 2 tests on undisturbed specimen of new LMVD silt - 2 tests on 4-in. dia. specimens 1 test on remolded specimen of old LMVD silt 1 test on remolded specimen of new LMVD silt
\bar{R}	3	5.5	<ul style="list-style-type: none"> - 2 specimens tested after undrained unloading tests 1 remolded specimen of old LMVD silt 1 undisturbed specimen of new LMVD silt - 1 specimen trimmed from 4-in. dia. undrained unloading test specimen of remolded old LMVD silt
Q	6	5.5	<ul style="list-style-type: none"> - specimens trimmed from 4-in. dia. remolded undrained unloading test specimens - 3 tests with midheight pore pressure monitoring on old LMVD silt - 3 tests without midheight pore pressure monitoring on new LMVD silt

Table 5.3 (continued): Summary of tests performed on LMVD silt in this study

Type of Test	Number Performed	Section	Comments
Q	20	5.6	<ul style="list-style-type: none"> - 10 specimens subjected to prepressurization - 10 specimens not subjected to prepressurization - no midheight pore pressure monitoring - all tests on remolded specimens of old LMVD silt
Q	9	5.7	<ul style="list-style-type: none"> - Partially saturated specimens of compacted new LMVD silt - Pore air and pore water pressures measured during shear
Q	19	5.8	<ul style="list-style-type: none"> - 10 specimens of remolded old LMVD silt tested in Q tests at various strain rates - no midheight pore pressure monitoring
Q	18	5.9	<ul style="list-style-type: none"> - Conventional Q tests on 1.4-in. dia. specimens of remolded old LMVD silt - no pore pressure measurements
\bar{R}	4	5.10	<ul style="list-style-type: none"> - 1.4-in. dia. specimens of remolded old LMVD silt - $\sigma'_{3con} = 10$ psi for all four specimens - different values of back pressure used
Q	16	5.11	<ul style="list-style-type: none"> - 8 conventional Q tests on 1.4-in. dia. specimens of remolded new LMVD silt - 8 Q tests on 1.4-in. dia. specimens of remolded new LMVD silt, specimens had 10 or 20 psi back pressure applied prior to increasing cell pressure undrained - no pore pressure measurements in any tests

water pressure, it was proposed to measure the pore water pressure at the midheight of Q test specimens using a hypodermic needle attached to a pressure transducer.

5.3.1 Review of Midheight Pore Pressure Monitoring Techniques

Prior to undertaking this phase of the research, a review of the literature regarding midheight pore pressure measurements was performed. This was intended to allow assessment of the different techniques of midheight pore pressure measurement and their advantages and disadvantages. The three main types of midheight pore pressure measurement devices are needles inserted into the specimen, ceramic probes inserted into the specimen, and transducers mounted on the circumference of the specimen.

Gibbs et al. (1960) discussed the Bureau of Reclamation's experiences with pore pressure measuring techniques. They had experimented with short and long rigid vertical inserts, flexible vertical inserts, rigid horizontal inserts, small vertical central sand cores and small resistance transducers on 3-1/4 inch diameter specimens of a plastic lean clay. All of the procedures had some disadvantages. Difficulty was experienced keeping air out of the inserts or saturating the area around the insert. These problems often lead to readings which were

too low or too high on unsaturated specimens. A similar disadvantage was experienced with the sand cores. Pore pressure readings were often extremely erratic. Some flexible tubes and sand cores were completely cut off by the shear failure movements. In a number of instances, the inserts were found to influence the strength of the specimen and the position of the failure plane.

They found that the inserts with which they had the most success were small, flexible plastic tubes, with fine porous stones at the end of the tubes. These were inserted vertically into the ends of large, 9-inch diameter compacted specimens. Inserting a relatively small foreign object into specimens of this size had no apparent effect on the measured strength. They noted that installation of the insert and ceramic devices was extremely difficult and installation techniques and experience were still in the development stage in 1960. They added that a slightly tipped insert, an insert against a large void, or a poor soil contact against a ceramic plate could lead to inaccurate pore pressure measurements.

Marsal and Resines (1960) used a needle to measure pore pressures within triaxial specimens. When testing clay the needle was inserted near the middle of the sample at an angle of 45 degrees with the horizontal. When

testing sandy soils, it was found to be preferable to fix the needle at the base of the triaxial chamber and extend the porous tip 2 cm into the specimen along its vertical axis.

Bishop, Blight, and Donald (1960) discussed the difference in pore pressures measured at the middle and ends of triaxial samples using porous ceramic elements with high air entry values. They discussed the time required for equalization of pore pressure within triaxial specimens during undrained loading. They gave no sketch or further details of the midheight pore pressure probe used.

Crawford (1963) used medical hypodermic needles (0.12 cm O.D.) in the soil to measure pore pressures within triaxial specimens. The monitoring system was filled with deaired water. Dry ice was used to freeze the water in the needle so that soil particles would not enter the needle during insertion into the specimen.

Two needles were used in each specimen as shown in Figure 5.3. One was inserted along the axis of the specimen through the top cap down to midheight. The other was inserted horizontally to the center of the specimen, at a height 2 cm above the bottom. Liquid latex was used in an attempt to seal the hole through the membrane but the

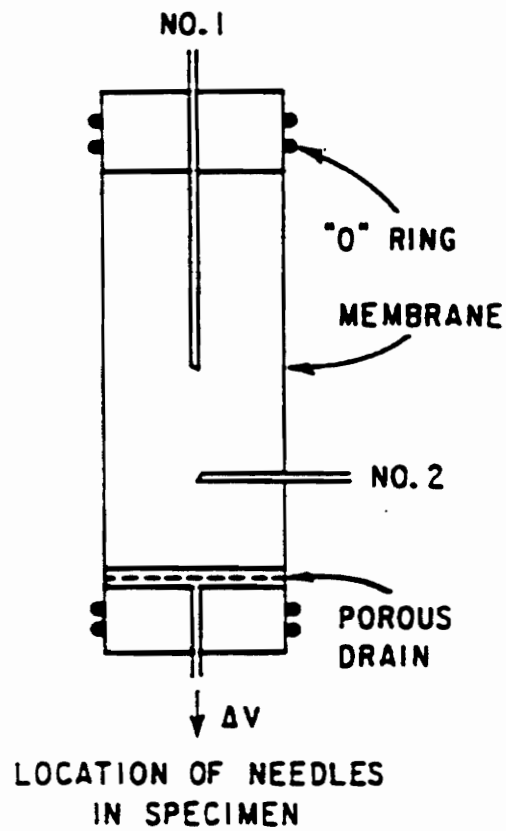


Figure 5.3. Pore pressure monitoring system used by Crawford (1963)

easiest and most reliable seal was obtained using rubber cement.

Crawford (1963) concluded that hypodermic needles "appear to provide satisfactory pore pressure pick-ups provided a small volume pore pressure system with few opportunities for leaks is used."

Olson (1963) reported using needles successfully in measuring pore water pressures in samples of sensitive Leda clay. He noted that the relatively high permeability and sensitive structure of this clay made it ideally suited for such measurements.

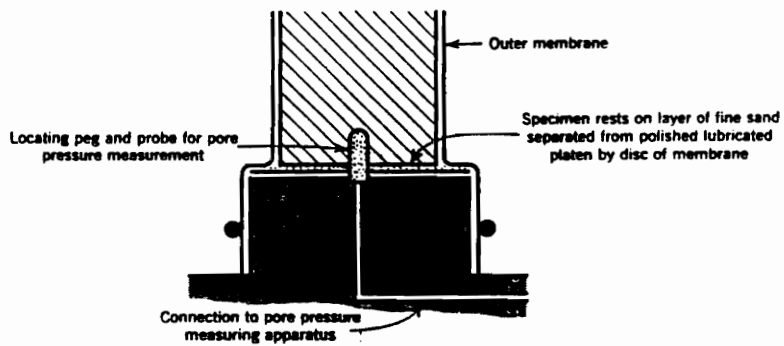
For impervious clays however, the following difficulties were encountered when using needles (Olson, 1963):

- 1) Inserting the needle into the specimens during shear lead to disturbance of the specimens and affected the pore water pressures measured.
- 2) For tests in which failure of the specimen occurred at strains above a few percent, the relative displacement between the tip of the needle and the soil appeared to have a significant effect on the measured pore water pressure.

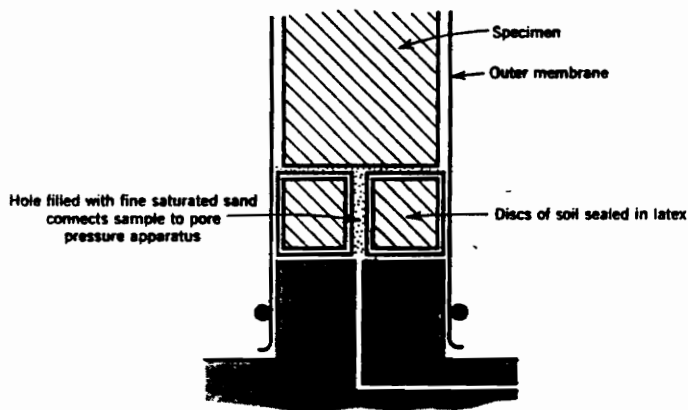
Olson also felt that the small contact area between the needle and the soil may be a serious limitation if temperature changes occur during the test. As the temperature increases, the fluid in the measuring system expands and water would flow into the specimen. For an impervious clay, the resistance of the clay to this flow would result in an increase in the measured pore water pressure.

Blight (1965) discussed the use of a porous ceramic probe imbedded in the specimen at midheight, as shown in Figure 5.4. The pore pressure transducer was external to the probe. The hole through the outer membrane was sealed by a 1/8-inch I.D. O-ring. Disturbance effects of the probe were not discussed.

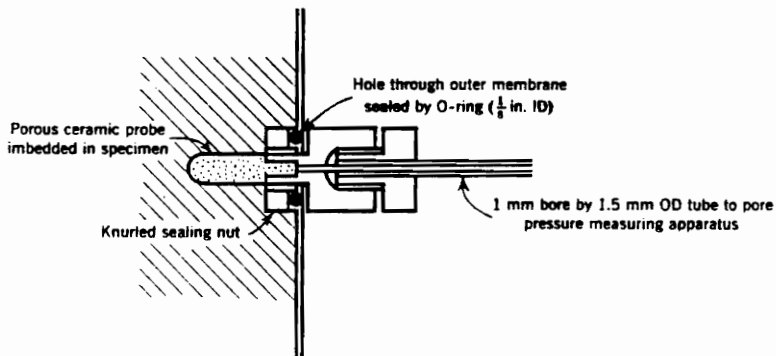
Yong and Warkentin (1966) discussed the use of different types of pore pressure probes to measure the pore pressure within triaxial specimens, as shown in Figure 5.5. The probes and needles described would be inserted into the side of the specimen and connected to an electrical transducer or mechanical null-point system. They stated that the disadvantage of using needles to measure pore pressures in triaxial specimens was that they may influence the shear strength and behavior of the sample.



(a) LUBRICATED LOADING PLATEN



(b) SEGMENTAL SPECIMEN



(c) PROBE FOR MEASUREMENT OF PORE PRESSURE

Figure 5.4. Pore pressure monitoring methods used by Blight (1965)

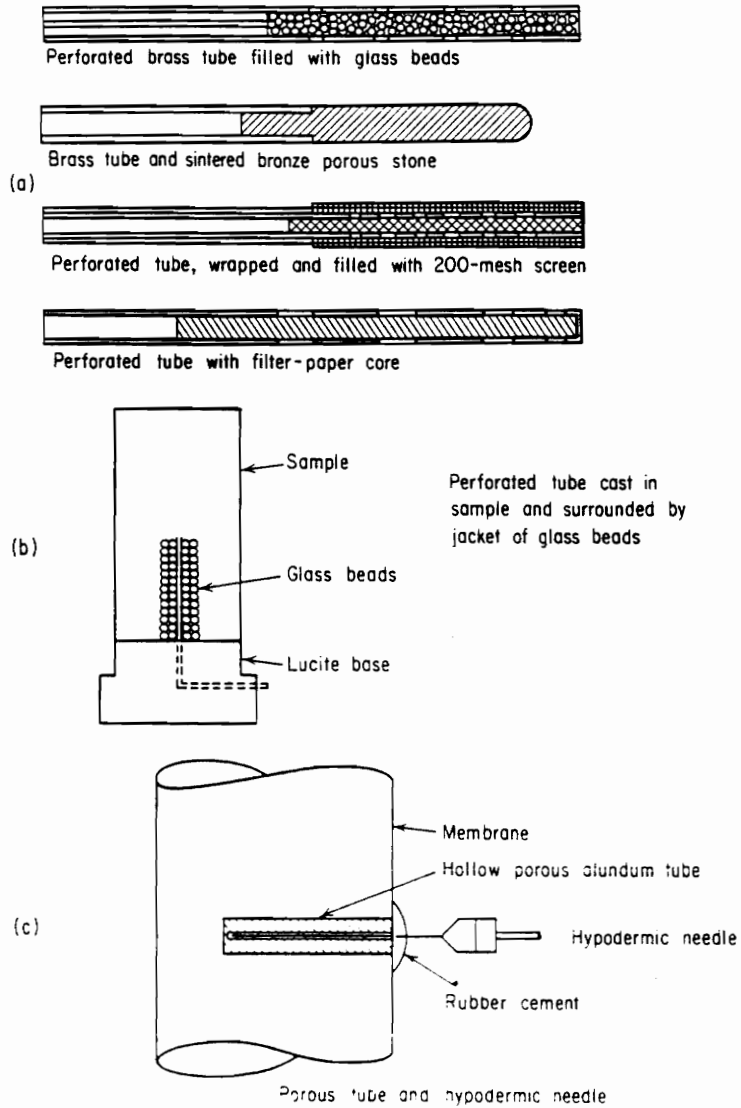


Figure 5.5. Pore pressure monitoring methods presented by Yong and Warkentin (1966)

Hight (1982) discussed the use of a miniature silicon diaphragm pressure transducer mounted on the circumference of a triaxial specimen at its midheight, as shown in Figure 5.6. The connection and sealing details between the transducer and rubber membrane are complicated as shown in the figure. This is the same device described by Head (1986).

In discussing the measurement of pore pressures at the midheight of triaxial specimens, Head (1986) noted that a porous ceramic pore pressure probe can be used to monitor pore water pressures at the midheight of 100-mm diameter samples.

Baldi, Hight, and Thomas (1988) and Fourie and Xiaobi (1991) used a midheight pore pressure transducer of the type described by Hight (1982) and Head (1986). This device was shown in Figure 5.6.

Dupas et al. (1988) used a needle to measure pore pressures in the middle of 300-mm diameter samples, as shown in Figure 5.7. The needle was inserted 11-cm horizontally into the sample at its midheight. The pore pressure transducer appears to have been external to the triaxial cell.

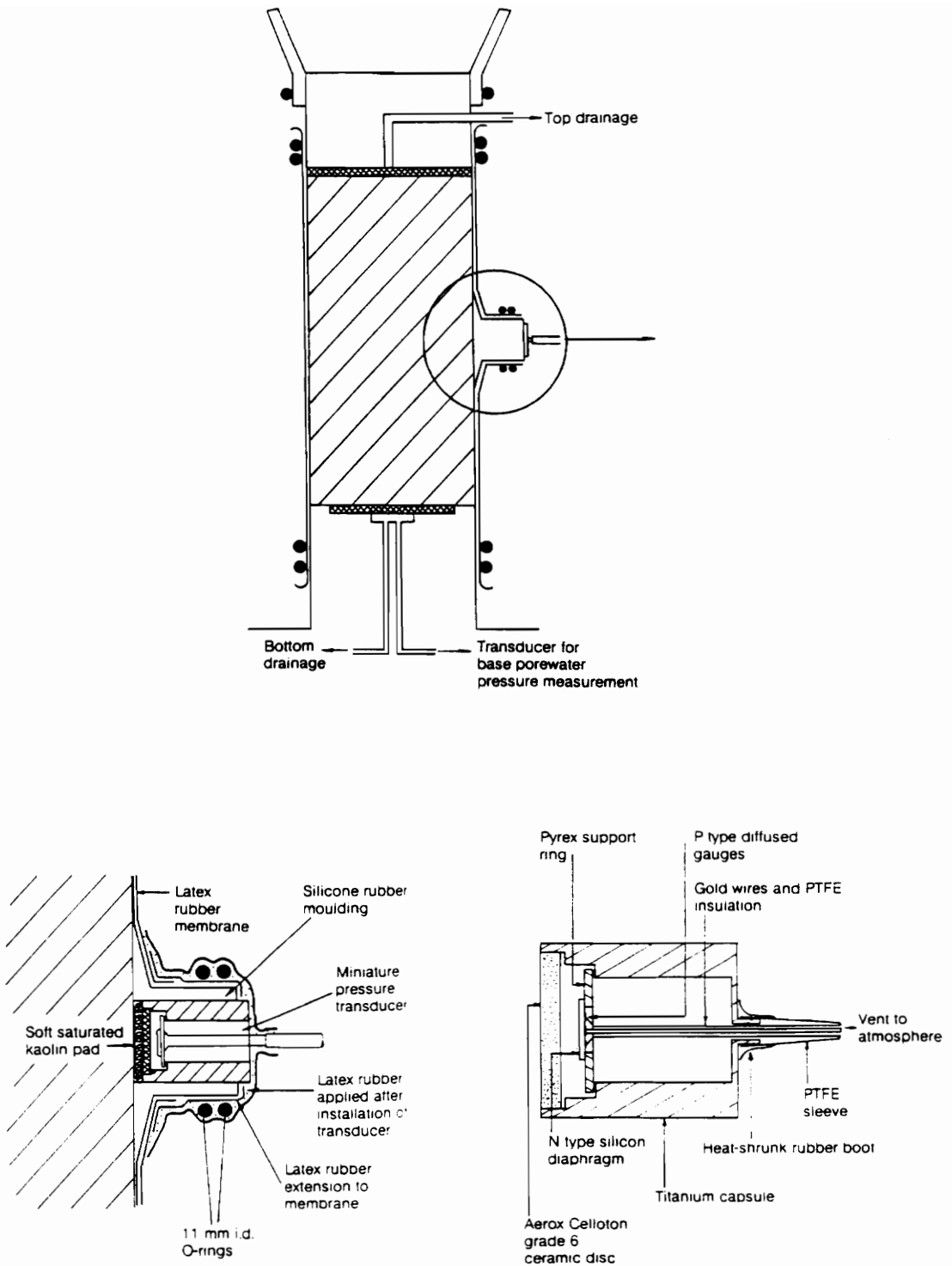


Figure 5.6. Pore pressure monitoring system used by Hight (1982) and Baldi, Hight and Thomas (1988)

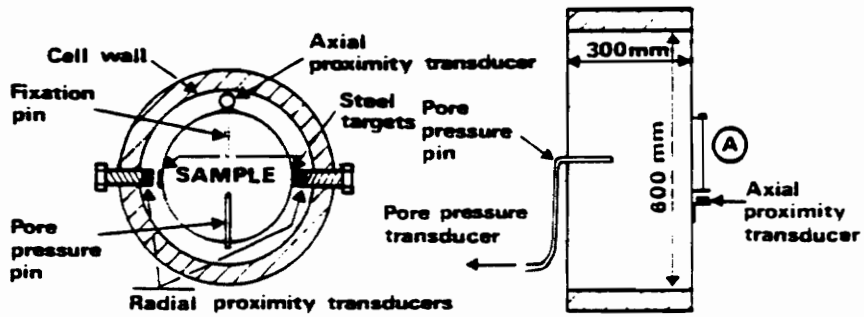


Figure 5.7. Pore pressure monitoring system used by Dupas et al. (1988)

5.3.2 Midheight Pore Pressure Monitoring System Used in this Study

After reviewing the different techniques of measuring pore pressures at the midheight of triaxial specimens, it was felt that the use of a hypodermic needle inserted into the specimen and attached to a pressure transducer, as originally proposed, would be the best method to use since the disturbance to the specimen during installation would be smaller compared to using larger inserts. It also would be easier to install the needle and seal the hole in the membrane surrounding the specimen than the other devices, and its effect on the sample during testing was felt to be less than the larger circumferentially mounted devices used by others.

The needle used was 0.94 inches long with an outside diameter of 0.015 inches and was specially adapted for use with a pressure transducer. The needle was filled with deaired water prior to being attached to the transducer. The transducer used was an Entran Model EPX which was calibrated for use at confining pressures of 0, 10, and 20 psi. The triaxial specimens tested were nominal 1.4-inch diameter by 3-inch high specimens surrounded by two rubber membranes. Prior to inserting the needle into the specimen, transducer pressure readings were taken for the water-filled needle in atmospheric pressure to determine

the zero reading for the transducer. The needle was then inserted through the two membranes into the sample. It was found that vertical support was necessary for the transducer to prevent movement of the needle within the specimen resulting from the weight of the transducer. Figure 5.8 shows a schematic diagram of the midheight pore pressure monitoring system used in this study.

At the location where the needle was inserted, the membrane and needle were coated with rubber cement after the needle was in place, to seal off the specimen from the triaxial cell. Pressure readings were taken after the rubber cement was applied to estimate the initial negative pore water pressure within the specimen. After several layers of rubber cement were applied and allowed to dry, the triaxial cell was assembled and the confining pressure applied. Pressurized air was used as the cell fluid since the pressure transducer was located within the triaxial cell and would likely be damaged by water. After applying the cell pressure, the pore pressure reading was noted periodically and when no further variation in pore pressure was observed due to the increase in cell pressure, the Q test was performed.

Because the pore pressure transducer was located within the triaxial cell, it measured the differential

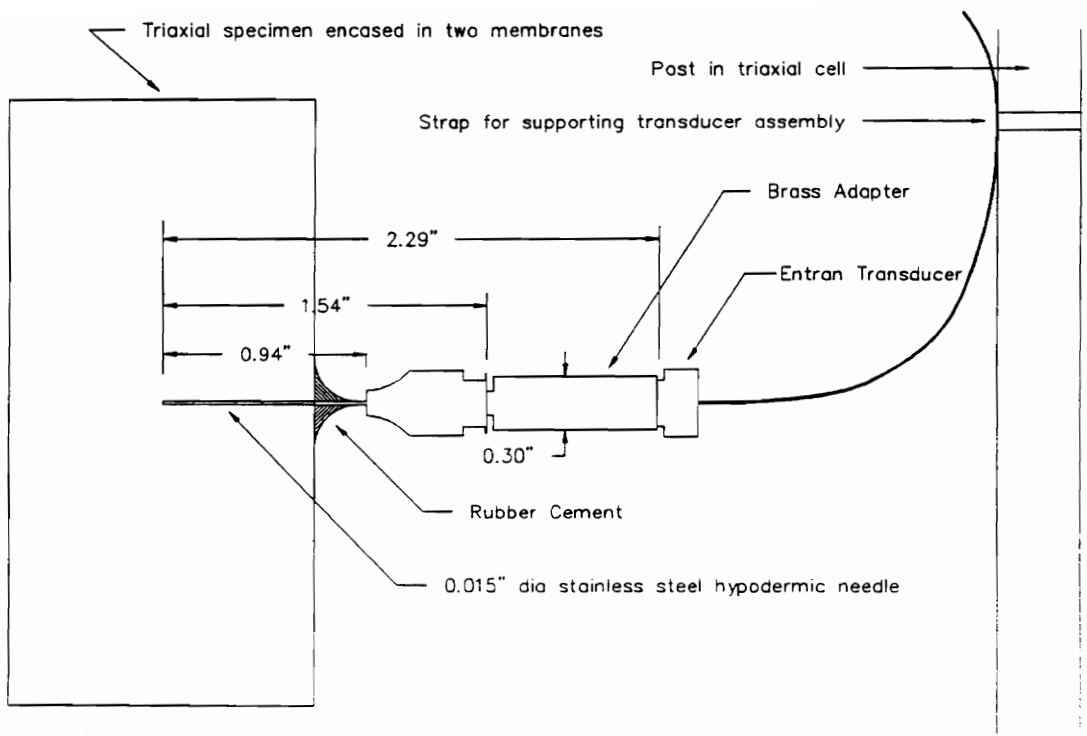


Figure 5.8. Schematic drawing of midheight pore pressure monitoring system used in this study

pressure between the specimen and the cell. When the cell pressure was initially applied, the measured pore pressure changed by an amount approximately equal to the cell pressure. Almost instantaneously, as the pore pressure within the specimen began to increase due to the applied cell pressure, the pressure measured by the transducer returned to approximately the initial pressure reading prior to applying the cell pressure. This was expected for specimens which were 100 percent saturated or close to 100 percent saturated. As the sample was sheared, the pressure measured by the transducer was the differential pressure between the pore pressure within the specimen and the cell pressure. Calibration of the transducer had been performed prior to testing, to relate the differential pressure measured to the actual pressure in the sample at the various confining pressures used.

Although every effort was made to provide an adequate seal at the needle-membrane interface, on several occasions, especially in the early stages of this research, erratic pore pressure measurements occurred. Almost all of these instances were believed to be the result of leaks between the specimen and triaxial cell since the differential pressure reading returned to the initial pressure reading measured prior to applying the cell pressure. It was found that by applying numerous layers of

rubber cement and allowing for vertical movement in the transducer support system within the triaxial cell, the possibility of a leak at the needle-membrane interface could be reduced.

5.4 Q Tests with Midheight Pore Pressure Measurements

A total of 18 Q tests have been performed on silt specimens in which pore water pressures were measured in the specimens at their midheights. Seventeen of these tests were performed on remolded samples of old LMVD silt, and one Q test was performed on an undisturbed sample of new LMVD silt. Confining pressures of 0, 10, and 20 psi were used in the tests. The tests were performed at a strain rate of one percent per minute. This is the strain rate at which conventional Q tests are performed. Table 5.4 gives the initial properties of the triaxial specimens.

Some of these tests tended to show erratic fluctuations in measured pore pressure with increasing strain, whereas others had pore pressure measurements which appeared reasonable. Most of the erratic pore pressure behavior was related to difficulties in the midheight pore pressure monitoring procedure. As the testing progressed, the majority of these difficulties were eliminated. In other instances, what appears to be somewhat erratic pore

pressure behavior may actually be characteristic of the pore pressure behavior of saturated silts during Q tests.

Table 5.4: Initial properties of Q test triaxial specimens in which pore water pressures were measured at the midheight of the specimens

Sample No.	σ_3 (psi)	w (%)	γ_d (pcf)	S (%)	e
1	0	20.4	108.0	99	0.554
2	10	20.5	107.9	95	0.555
3	20	20.8	109.2	100	0.537
4	0	20.8	109.6	100	0.532
5	10	20.2	109.8	100	0.528
6	20	20.3	111.9	100	0.500
7	20	21.3	109.6	100	0.531
8	10	21.3	109.2	100	0.538
9*	20	20.5	81.5	49	1.059
10	0	21.1	109.0	100	0.541
11	0	21.7	110.5	100	0.519
12	0	21.7	109.6	100	0.531
13	0	21.2	108.9	100	0.542
14	10	21.6	109.1	100	0.539
15	10	21.7	111.3	100	0.509
16	10	21.6	111.7	100	0.502
18	20	21.8	108.9	100	0.541
19	20	21.7	110.1	100	0.524

* Undisturbed specimen of new LMVD silt

The results of the Q tests with midheight pore pressure monitoring will be considered in three different ways. First the Q tests will be compared to others performed at the same cell pressure. Then the Q tests performed on specimens trimmed from the same batch consolidometer sample will be compared. Finally, the results from Q tests on specimens with similar void ratios will be compared with each other.

5.4.1 Comparison of Q Tests Performed at the Same Cell Pressure

The stress-strain behavior for the Q tests along with the changes in pore pressure measured during the tests for each of the different confining pressures used will now be presented. A summary of the peak deviator stress and maximum change in pore pressure measured in each of the tests discussed will be presented in tabular form at the end of this discussion.

5.4.1.1 Q Tests Performed as Unconfined Compression Tests

Six Q tests were performed with midheight pore pressure monitoring as unconfined compression tests on remolded specimens of LMVD silt. Figures 5.9 and 5.10 show plots of deviator stress vs. axial strain and change in pore pressure vs. axial strain for these six tests. It can be seen from Figure 5.9a that the deviator stress for test UU-1 rose to a peak of 19 psi at an axial strain of about 8.75 percent and then decreased and reached a steady value. For test UU-4, the deviator stress reached a peak of 30 psi at an axial strain of 12 percent and then underwent a slight decrease with increasing strain.

Figure 5.9b shows that the changes in pore pressure measured during tests UU-1 and UU-4 were somewhat erratic. Test UU-1 showed very little change in measured pore

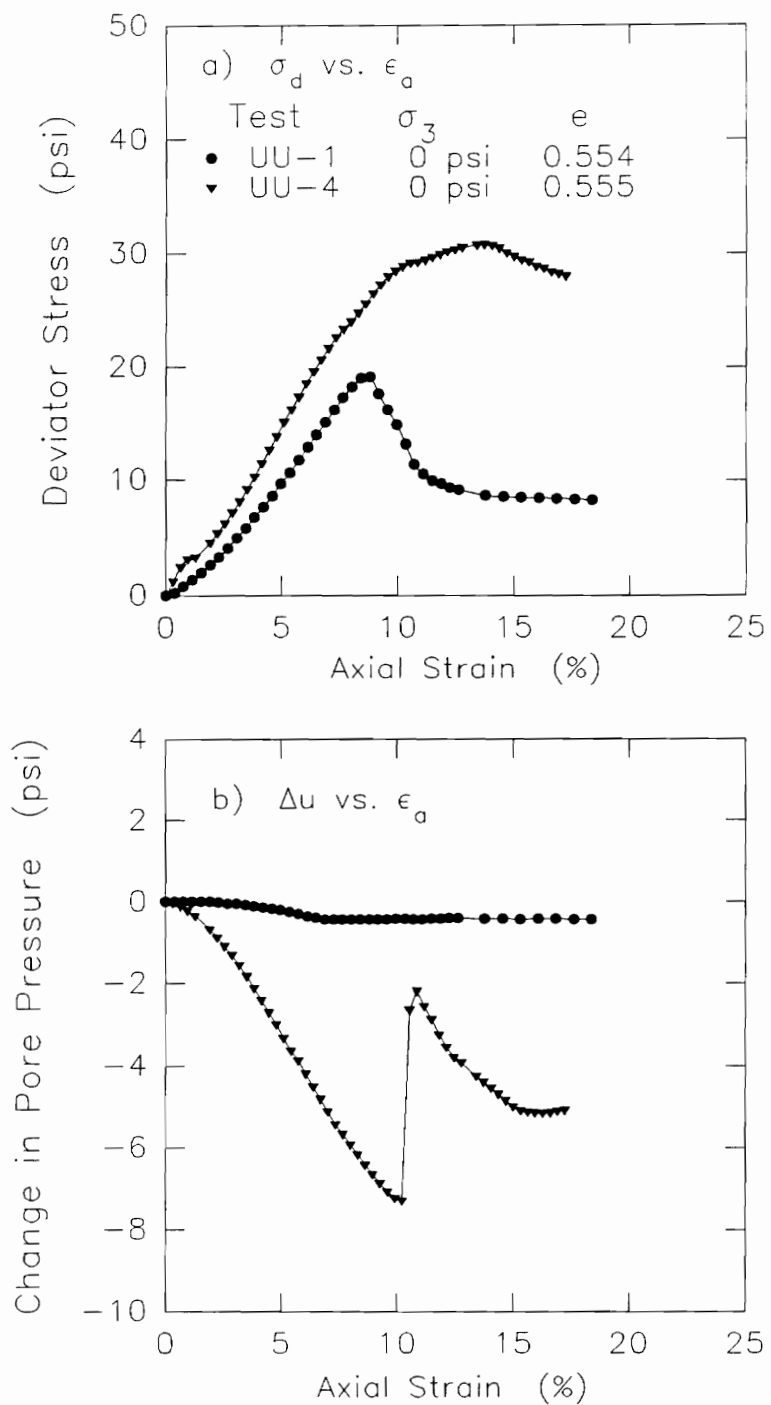


Figure 5.9. Deviator stress-strain and change in pore pressure-strain relationships measured in UU tests 1 and 4 on remolded LMVD silt

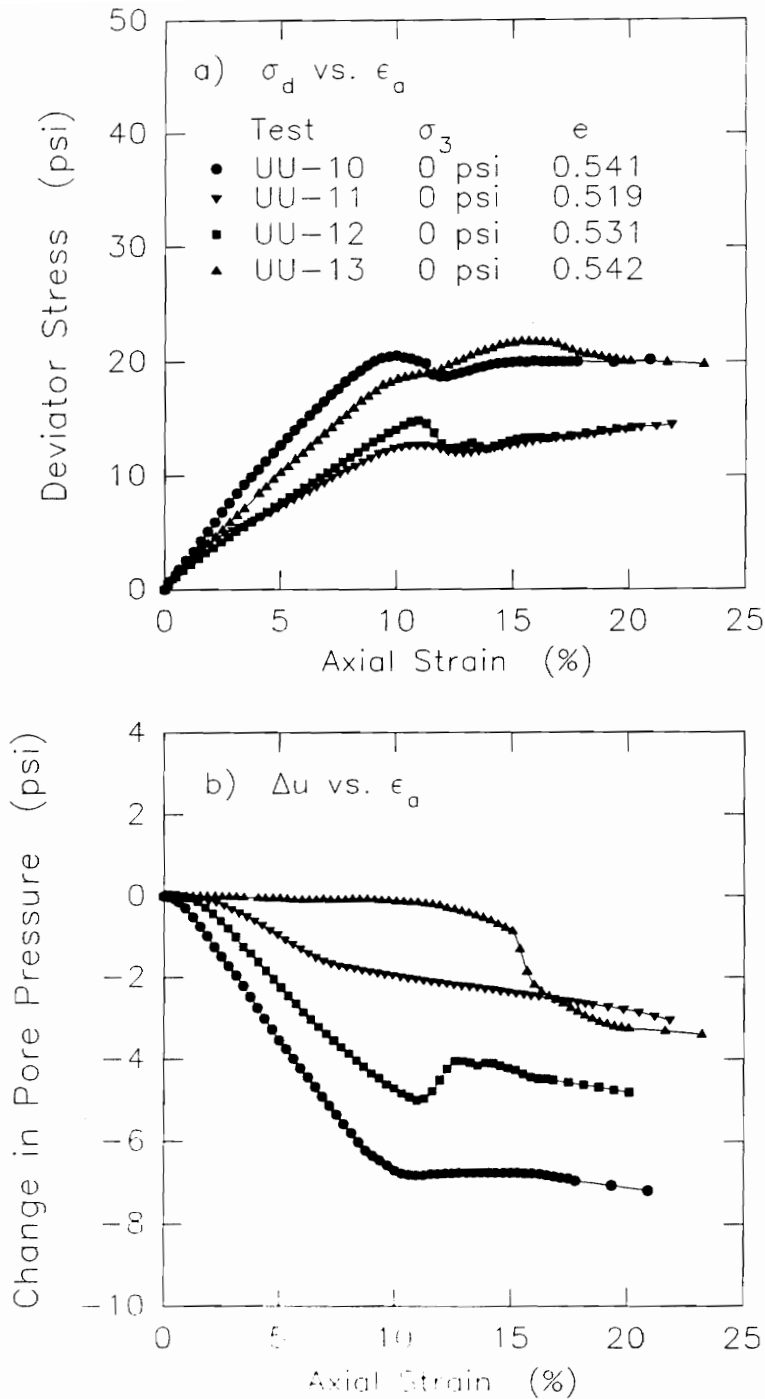


Figure 5.10. Deviator stress-strain and change in pore pressure-strain relationships measured in UU tests 10, 11, 12, and 13 on remolded LMVD silt

pressure during the test. Test UU-4, on the other hand, showed a definite decrease in pore pressure until about 12 percent axial strain at which point the pore pressure increased rapidly and then began decreasing again. The abrupt increase in measured pore pressure in this test is believed to be a result of a problem in the pore pressure monitoring system.

Figure 5.10a shows that for Q tests UU-10 through UU-13, the deviator stress-strain curves reached a peak or showed a change in slope at about 10 percent strain. Above 10 percent strain, tests UU-10, UU-11, and UU-12 showed slight decreases in deviator stress followed by increases in deviator stress with further increase in strain. Test UU-13, after showing a slight change in slope at about 10 percent strain, continued to experience an increase in deviator stress until an axial strain of about 15 percent. With further increase in strain, the deviator stress began to decrease. At an axial strain of 10 percent, the values of peak deviator stress for these four Q tests, ranged from about 12.5 psi to 20.5 psi.

Figure 5.10b, shows that the changes in pore pressure measured in Q tests UU-10 through UU-13 were generally more reasonable than those measured in tests UU-1 and UU-4. A decrease in pore pressure was measured in all four tests.

Test UU-13 showed relatively no change in measured pore pressure until an axial strain of about 12 percent, at which point the pore pressure began to decrease. This may have resulted from a problem with the pore pressure monitoring system.

The other three tests included in Figure 5.10b all showed some variation in the shapes of the measured change in pore pressure vs. axial strain plots. Tests UU-10 and UU-11 showed changes in the slopes of the curves but continued to show a decrease in pore pressure throughout the tests. Test UU-12 reached a minimum pore pressure and then underwent a slight increase, followed by a subsequent decrease in pore pressure.

5.4.1.2 Q Tests Performed at 10 psi Cell Pressure

Six Q tests were performed with midheight pore pressure measurements on samples of remolded LMVD silt at a confining pressure of 10 psi. Three of the tests showed erratic pore pressure measurements whereas the other three did not.

Figures 5.11 and 5.12 show plots of deviator stress vs. axial strain and change in pore water pressure vs. axial strain for these six Q tests. As can be seen by comparing Figures 5.11a and 5.12a, the stress-strain

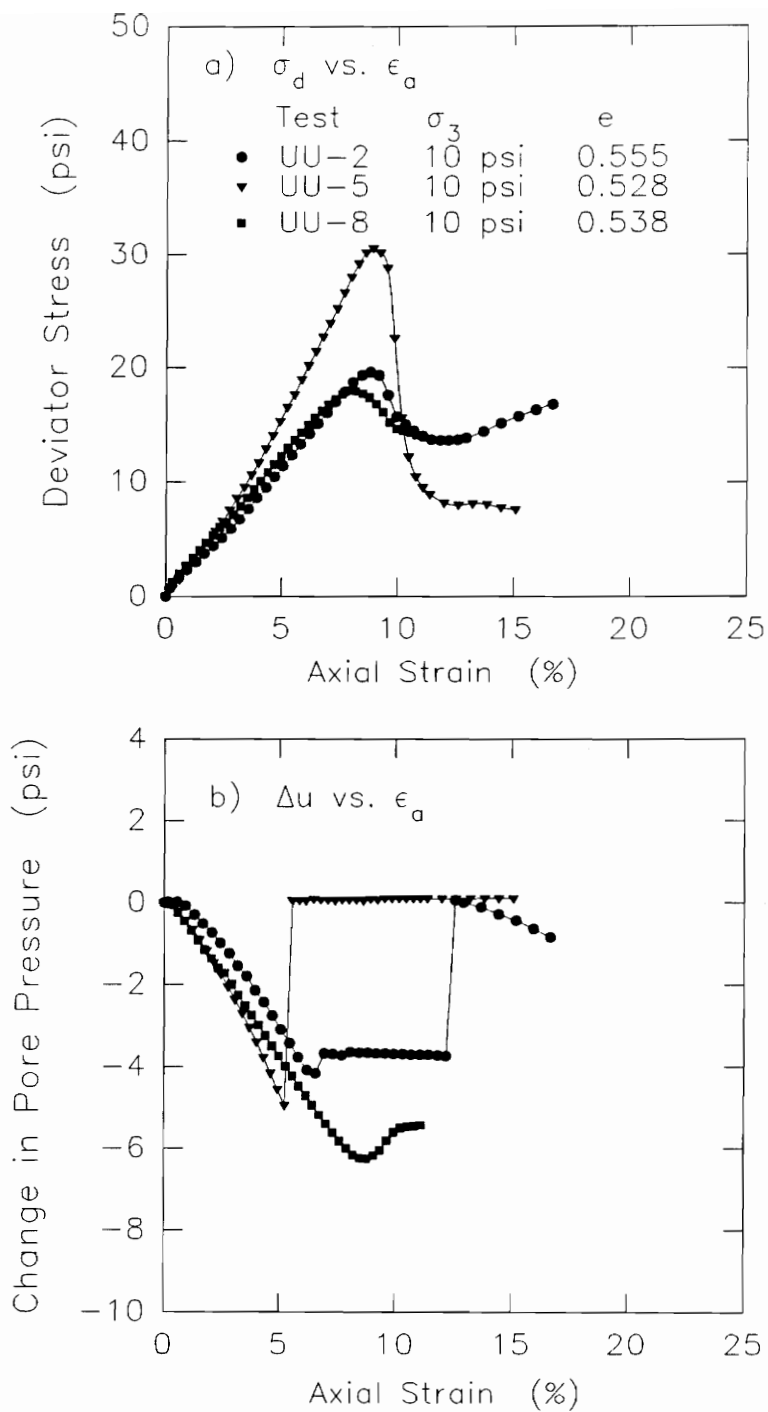


Figure 5.11. Deviator stress-strain and change in pore pressure-strain relationships measured in UU tests 2, 5, and 8 on remolded LMVD silt

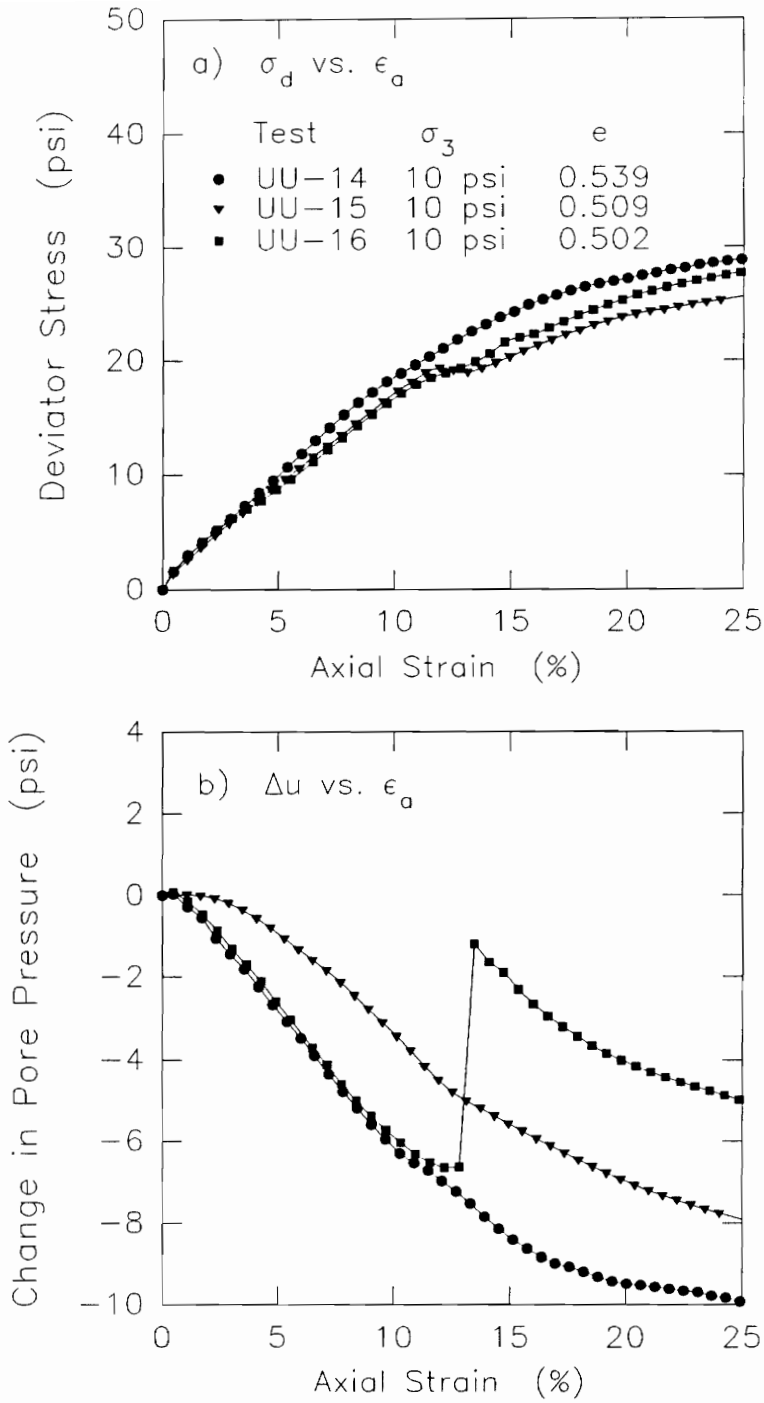


Figure 5.12. Deviator stress-strain and change in pore pressure-strain relationships measured in UU tests 14, 15, and 16 on remolded LMVD silt

behavior of tests UU-2, UU-5, and UU-8 is different from that of tests UU-14, UU-15, and UU-16. Tests UU-2, UU-5, and UU-8 all showed definite peaks in the stress-strain curves at strains on the order of 8 to 9 percent. These peaks were followed by decreases in deviator stress with increasing strain.

On the other hand, Q tests UU-14, UU-15, and UU-16 showed continuous increases in deviator stress with increasing strain. This continued until the tests were terminated at strains above 25 percent. For this second group of three tests, the stress-strain curves were very similar up to strains of about 12 percent. Above 12 percent strain, the three curves showed more variation in magnitude from each other while maintaining similar shapes. Test UU-15 showed a slight decrease in deviator stress at about 12 percent axial strain. It then experienced an increase in magnitude with further increase in strain, reaching values of deviator stress well above the value at the slight peak.

The changes in pore pressure measured in the six Q tests performed at a cell pressure of 10 psi are summarized in Figures 5.11b and 5.12b. Figure 5.11b shows the pore pressure measurements for tests UU-2, UU-5, and UU-8. In test UU-2, the pore pressure decreased until an axial

strain of about 6.5 percent at which point the pore pressure increased slightly and remained constant until a strain of about 12 percent. The measured change in pore pressure then increased rapidly to zero and then began to decrease again with increasing strain. In test UU-5, the measured change in pore pressure decreased until an axial strain of about 5 percent and then increased rapidly back to zero and remained at zero throughout the remainder of the test.

The increases of the measured change in pore pressure from negative values to zero in these two tests are the best examples of what is believed to be the result of failure of the rubber cement seal around the hypodermic needle. The hypodermic needle had been inserted into the specimen and was connected to a pore pressure transducer. This assembly was supported vertically within the triaxial cell so that the weight of the transducer did not pull the needle out of the specimen. As the specimen experienced increasing axial strain, the pore pressure measuring system could have been pulled slightly such that the rubber cement seal surrounding the needle at the membrane surface would have been stretched. If the rubber cement seal failed, pressurized air surrounding the specimen would have been able to enter the specimen and be detected by the pore pressure transducer attached to the needle. The transducer

would then have detected 10 psi pressure within the specimen as well as 10 psi pressure in the triaxial cell, giving a measured differential pressure reading of zero.

Prior to performing Q test UU-8, the needle support system within the triaxial cell was made more flexible and numerous layers of rubber cement were applied at the needle-membrane interface. Figure 5.11b shows that the measured pore pressure decreased during this test, until an axial strain of about 8.75 percent after which it increased slightly and then began to become relatively constant toward the end of the test.

Figure 5.12b shows the measured change in pore pressure vs. axial strain relationships for tests UU-14, UU-15, and UU-16. As can be seen from this figure, tests UU-14 and UU-15 showed a continual decrease in pore pressure with increasing strain throughout the tests. Both tests showed slight changes in the slopes of these curves, but at different axial strains. These changes in slope indicate that the rate at which the pore pressure decreased varied for different ranges of axial strain. The curves for these two tests differ from the curve for test UU-8 shown in Figure 5.11b. In tests UU-14 and UU-15, peak minimum pore pressures were not reached as had been the case in test UU-8.

The plot of measured change in pore pressure vs. axial strain for test UU-16 shows an abrupt increase in pore pressure at about 13 percent axial strain. This was followed by a decrease in measured pore pressure with further increase in strain. The abrupt increase in pore pressure measured in test UU-16 is again believed to be the result of a problem in the pore pressure monitoring system and not characteristic of the true pore pressure response of the silt. Based on the curve for UU-16 before and after the sudden increase in measured pore pressure, it is believed that the actual shape of the pore pressure-strain curve for test UU-16 would have been similar to that of tests UU-14 and UU-15.

5.4.1.3 Q Tests Performed at 20 psi Cell Pressure

A total of six Q tests were performed with midheight pore pressure monitoring on samples at a confining pressure of 20 psi. Five tests were performed on remolded specimens of old LMVD silt and one test was conducted on an undisturbed specimen of new LMVD silt. Of the five tests performed on remolded specimens at this confining pressure, four did not show erratic pore pressure measurements whereas one test did. Figures 5.13 and 5.14 show plots of deviator stress vs. axial strain and change in pore pressure vs. axial strain for these five tests.

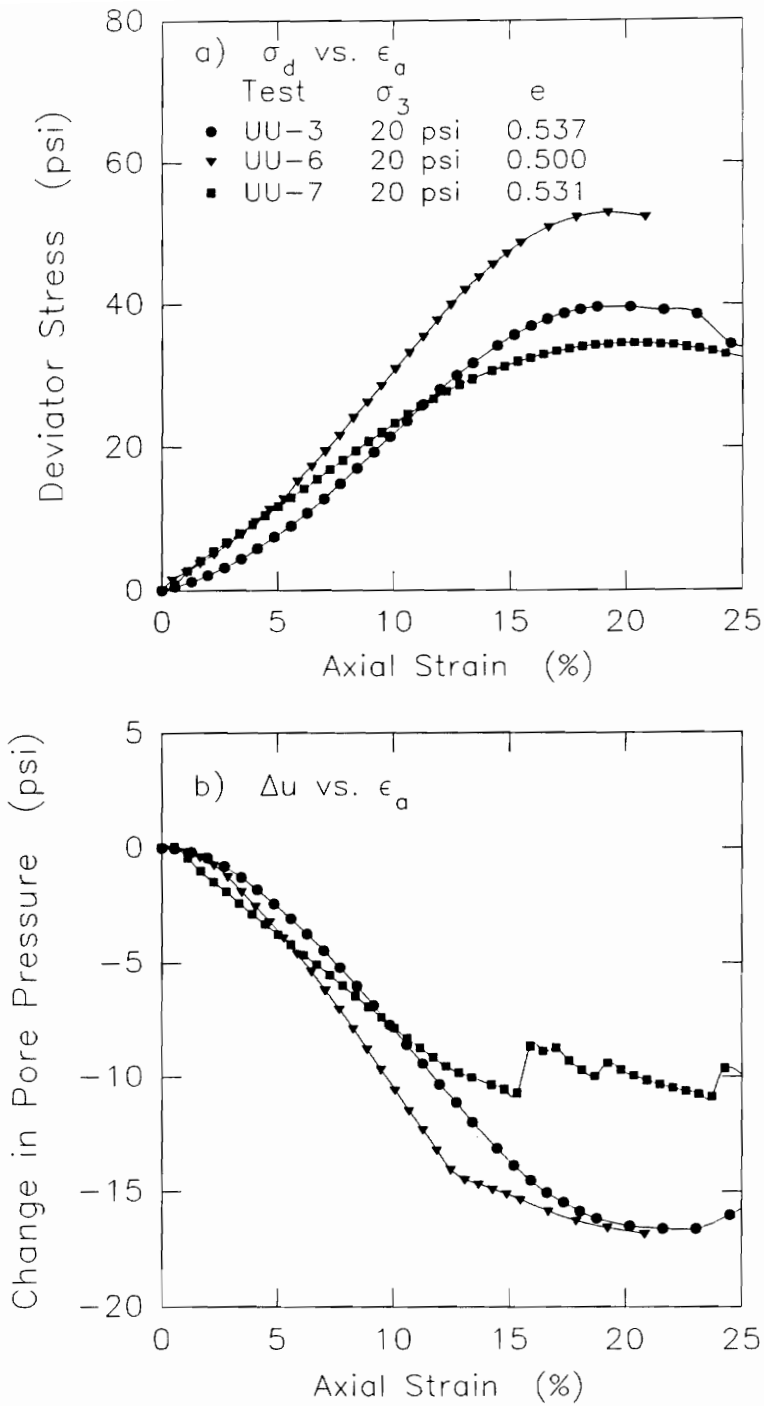


Figure 5.13. Deviator stress-strain and change in pore pressure-strain relationships measured in UU tests 3, 6, and 7 on remolded LMVD silt

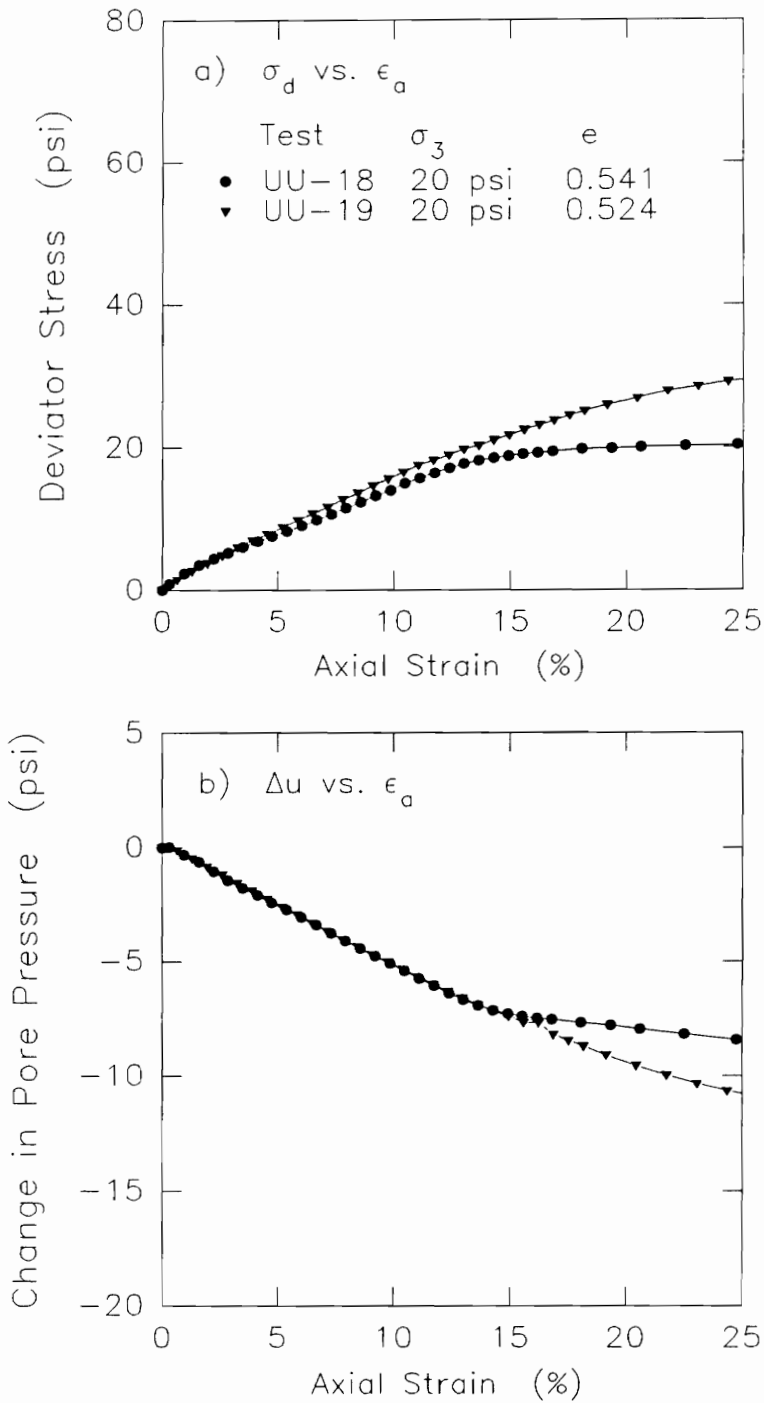


Figure 5.14. Deviator stress-strain and change in pore pressure-strain relationships measured in UU tests 18 and 19 on remolded LMVD silt

For tests UU-3, UU-6, and UU-7, the stress-strain behavior shown in Figure 5.13a indicates that peak deviator stresses between 35 and 53 psi occurred at axial strains ranging from 18 to 20 percent. All three tests showed a slight decrease in deviator stress at strains above 20 percent.

For tests UU-3, UU-6 and UU-7, the change in pore pressure vs. axial strain relationships are shown in Figure 5.13b. Both tests UU-3 and UU-6 experienced decreases in pore pressure to minimum values at about 22 percent axial strain. Test UU-3 then showed a slight increase in pore pressure with further increase in strain. The measured change in pore pressure for test UU-6 showed a noticeable change in the slope of the curve at an axial strain of about 12.5 percent.

For Q test UU-7, the pore pressure decreased with increasing strain until about 15 percent axial strain at which point the pore pressure increased slightly and then began to decrease again. The pore pressure went through a series of decreases followed by slight and abrupt increases until the conclusion of the test, as shown in Figure 5.13b. The erratic pore pressure behavior observed in this test is believed to be related to problems with the pore pressure monitoring system.

After completing the test on this specimen, the sample was observed to have numerous failure planes, as would be expected for a silt specimen subjected to axial strains as great as 25 percent. The repeated slight increases in pore pressure followed by pore pressure decreases could possibly be related to the formation of the multiple failure planes. As the load was applied to the silt, the specimen would attempt to dilate and the pore pressure in the specimen would decrease. As failure along the shear plane took place within the sample, the particles along the shear plane would have reoriented themselves into a more compact state, leading to a slight increase in pore pressure. As the sample continued its attempted dilation under further strain, additional decreases in pore pressure would have occurred until a new failure plane developed and the pore pressure again increased. This cycle could have continued throughout the test.

Similar behavior, however, was not observed for other test specimens in which multiple failure planes developed. Nor was this behavior observed in \bar{R} tests. After considering the erratic pore pressures measured in other tests as well, it is felt that the erratic pore pressure measurements observed in test UU-7 are the result of repeated temporary failures of the rubber cement seal at

the needle-membrane interface, leading to a series of abrupt increases in measured pore pressure.

Figure 5.14a shows the stress-strain curves for tests UU-18 and UU-19. Both specimens had similar stress-strain behavior up to about 14 percent axial strain. At higher strains, the deviator stress for test UU-18 began to level off whereas the deviator stress for test UU-19 increased continuously until the end of the test.

The change in pore pressure vs. axial strain plots for tests UU-18 and UU-19 shown in Figure 5.14b, indicate that both test specimens experienced essentially the same decrease in pore pressure until about 14 percent axial strain. At higher strains, a decrease in pore pressure occurred in both specimens but the pore pressure decreased at a smaller rate with increasing strain in specimen UU-18 than in specimen UU-19.

One Q test was performed on an undisturbed specimen of LMVD silt at a confining pressure of 20 psi. The test was conducted using the same midheight pore pressure monitoring technique as in the other tests. The undisturbed specimen was highly fissured and very difficult to trim. As a result of the soil structure, the sample experienced a brittle failure with an almost vertical failure plane forming from end to end of the specimen. In addition, the

sample had a low dry density and was only about 50 percent saturated, which made accurate measurement of pore pressures extremely difficult if not impossible.

Figure 5.15 shows a plot of deviator stress vs. axial strain and change in pore pressure vs. axial strain for this test. The brittle behavior of this specimen is easily seen in Figure 5.15a by the measurement of a peak deviator stress of 14 psi at an axial strain of less than one percent. It can be seen from Figure 5.15b that very little change in pore pressure was measured in this test. This was largely a result of the partly saturated condition of the specimen. In order for meaningful pore pressure measurements to have been made during this test, the undisturbed specimen should have been saturated.

Table 5.5 summarizes the peak deviator stress, maximum change in pore pressure, the minimum pore water pressure, and the associated axial strains, for the eighteen Q tests performed on LMVD silt with midheight pore pressure monitoring. Tests in which erratic pore pressure measurements occurred are noted in the table.

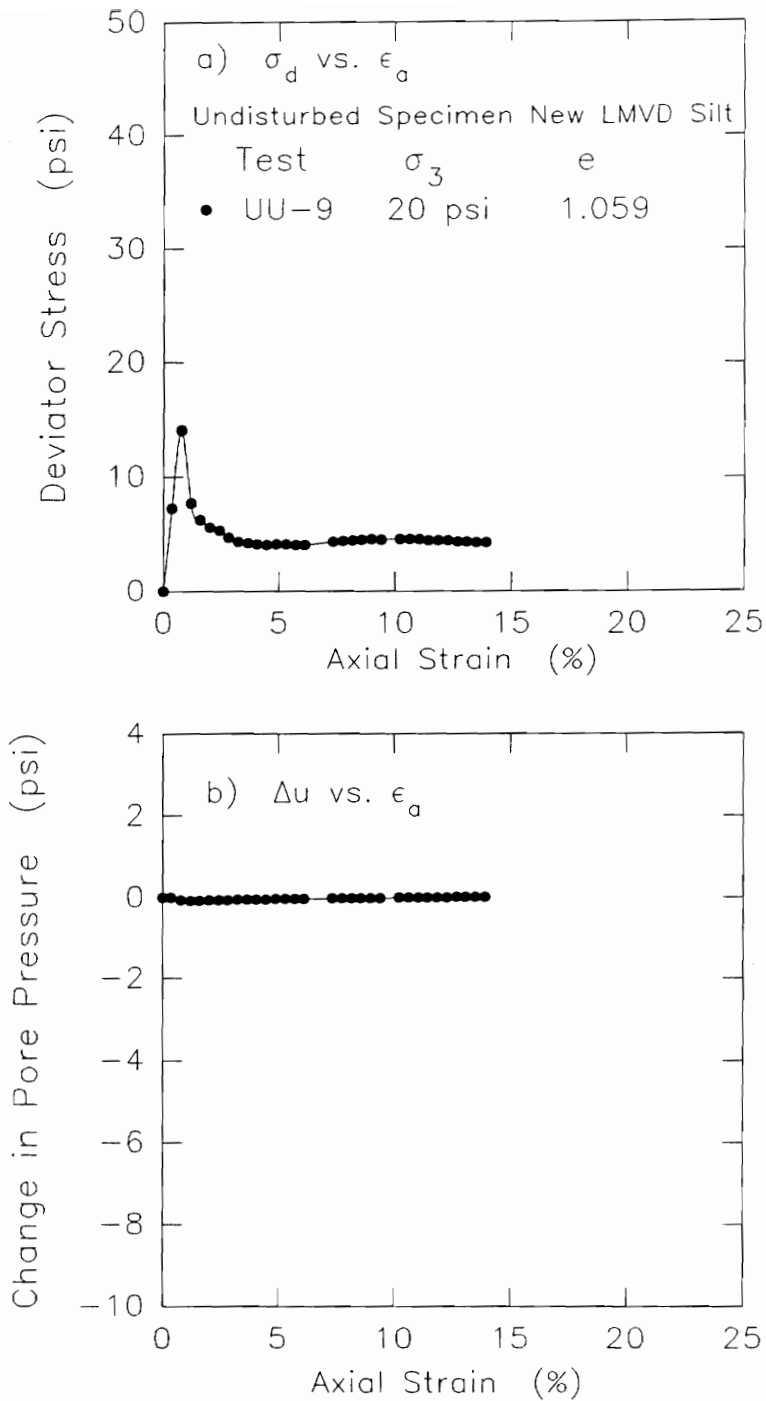


Figure 5.15. Deviator stress-strain and change in pore pressure-strain relationship measured in UU test 9 on undisturbed new LMVD silt

Table 5.5: Maximum deviator stress, maximum change in pore pressure, minimum pore water pressure, and the axial strain at which each of these occurred, for the Q tests performed with midheight pore pressure monitoring

Test No.	σ_{cell} (psig)	σ_{dmax} (psi)	$\epsilon_a \text{ @ } \sigma_{dmax}$ (%)	Measured Δu_{max} (psig)	$\epsilon_a \text{ @ } \Delta u_{max}$ (%)	Measured u_{min} (psig)
1+	0	19.1	8.8	-0.43	8.8	-1.71
2+	10	19.6	8.8	-3.73	12.2	5.07
3	20	39.8	19.5	-16.61	23.1	3.43
4+	0	30.8	13.7	-5.14	10.2	-8.61
5+	10	30.6	8.9	-4.94	5.2	3.46
6	20	53.0	19.3	-16.95	21.5	1.33
7+	20	34.6	20.4	-10.92	24.0	7.78
8	10	18.0	7.9	-6.24	8.8	2.56
9*	20	14.1	0.8	-0.08	1.2	14.08
10	0	20.5	10.0	-7.19	20.9	-8.78
11	0	12.7	10.9	-3.04	21.8	-3.97
12	0	14.8	11.0	-4.99	11.0	-6.07
13+	0	21.8	15.4	-3.39	23.2	-4.34
14	10	29.2	28.3	-10.39	28.3	-1.65
15	10	26.0	27.0	-8.21	27.0	0.84
16+	10	28.1	27.1	-6.64	12.2	2.24
18	20	20.3	24.8	-8.56	26.3	10.10
19	20	30.4	28.3	-11.33	28.3	7.30

+ Tests with erratic pore pressure measurements

* Undisturbed specimen of new LMVD silt

5.4.2 Comparison of Q Tests Performed on Specimens Trimmed from the same Batch Sample

As noted previously, the remolded specimens used in this study were trimmed from 5-inch diameter samples which were remolded from a slurry in a batch consolidometer. Each batch consolidometer sample ideally provided four 1.4-inch diameter specimens for testing. In several cases, specimens were disturbed during trimming or placement in the triaxial cell such that tests were not performed on

them, and only two or three tests were run on specimens from the same batch.

The specimens from the same batch all should have had similar void ratios and water contents, thereby allowing for meaningful comparisons to be made. In some cases, due to the tests being performed over two or three days after removing the soil from the batch consolidometer, slight variations in void ratio and water content were observed for the different samples.

For Q tests UU-10 through UU-19, each batch of samples was tested at the same cell pressure. For these tests, the behavior of the different samples from the same batch, which were tested at the same cell pressure, have already been compared in Section 5.4.1.

Tests UU-1 through UU-4 were all performed on specimens obtained from the same batch consolidometer sample. Table 5.4, however, indicates that the initial void ratios of the specimens varied from 0.532 to 0.555. The four tests were performed at cell pressures of 0, 10, and 20 psi. Figure 5.16 shows the deviator stress-strain curves and the changes in pore pressure measured in these four tests. It appears from Figure 5.16a that tests UU-1 and UU-2 had similar stress-strain behavior. These two specimens also had very similar void ratios. The other two

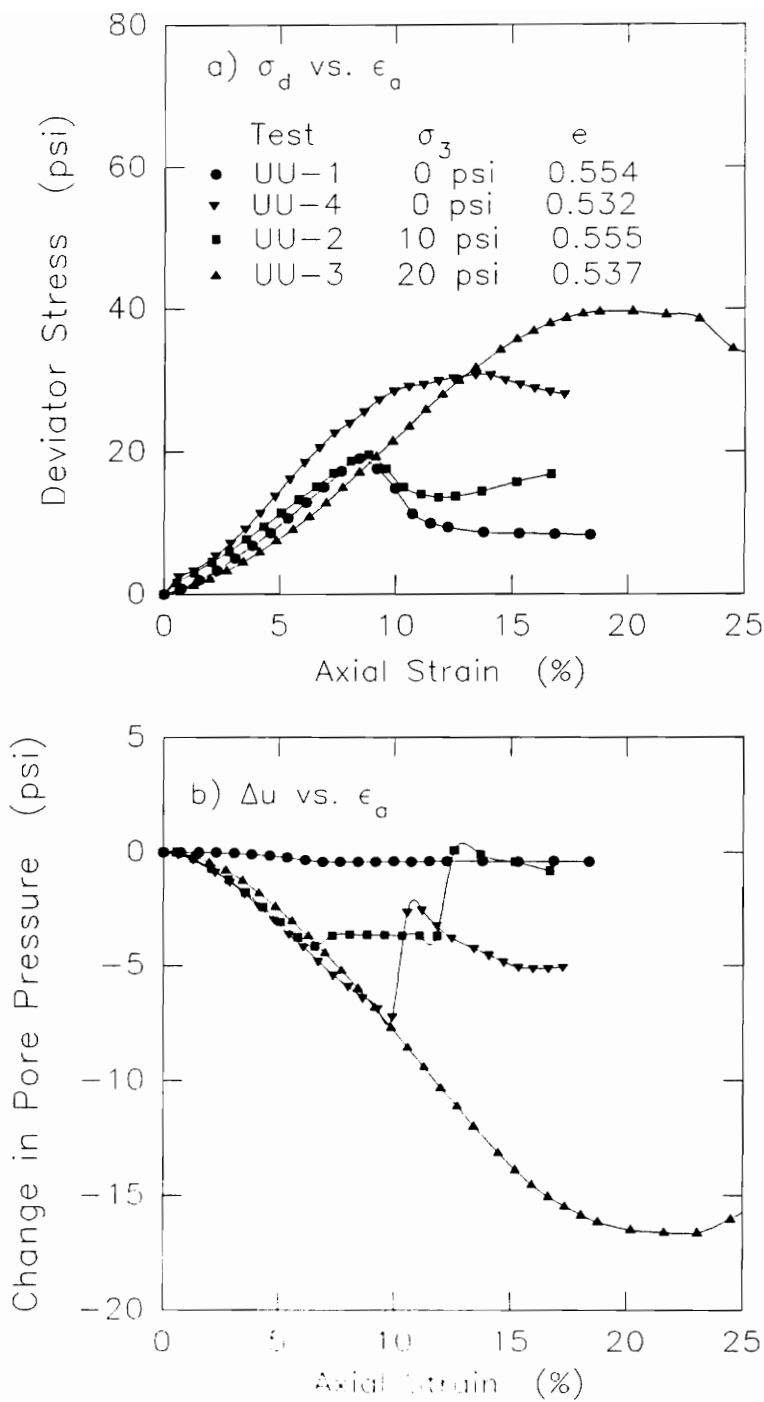


Figure 5.16. Deviator stress-strain and change in pore pressure-strain relationships measured in UU tests 1, 2, 3, and 4 performed on specimens from the same batch sample of remolded LMVD silt

test specimens, UU-3 and UU-4, had lower void ratios and showed somewhat different stress-strain behavior. The void ratio of test specimen UU-3 was closer than that of test specimen UU-4 to the void ratios of specimens UU-1 and UU-2. Similarly, the stress-strain behavior of specimen UU-3 was also closer to that of specimens UU-1 and UU-2, at least until an axial strain of about 9 percent. At higher strains, the behavior of specimen UU-3 was quite different from that of specimens UU-1 and UU-2.

Figure 5.16b shows that three of these four tests showed erratic pore pressure measurements which are believed to be the result of a failure of the monitoring system. Prior to the erratic pore pressure measurements, at small strains, the pore pressure responses measured for tests UU-2, UU-3 and UU-4 were all quite similar. It is believed that the failure of the pore pressure monitoring system in these tests resulted in a condition where drainage of the specimens was allowed, making these tests meaningless as Q tests. Despite this, defining failure as an axial strain of about 8.5 percent, tests UU-1, UU-2, and UU-3 yielded an approximate $\phi_u = 0$, $S_u = c = 9.8$ psi, total stress failure envelope, as shown in Figure 5.17.

Tests UU-5 and UU-6 were performed on samples trimmed from the same batch sample. Test UU-5 was performed at a

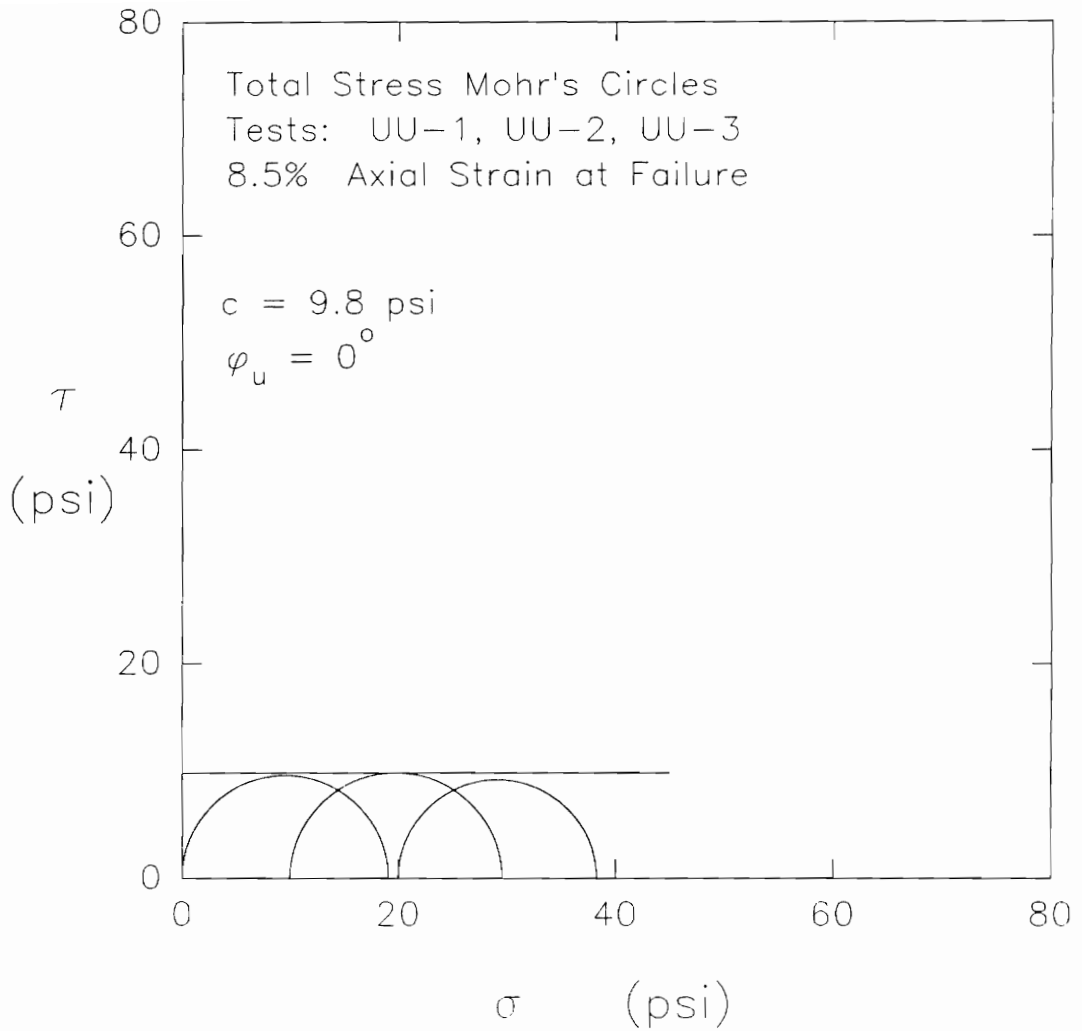


Figure 5.17. Total stress Mohr's circles at 8.5% axial strain for UU tests 1, 2, and 3 on remolded LMVD silt

cell pressure of 10 psi and UU-6 was performed at a cell pressure of 20 psi. The initial void ratio of specimen UU-5 was 0.500 and that of specimen UU-6 was 0.531.

As can be seen in the plot of deviator stress vs. axial strain given in Figure 5.18a, the stress-strain behavior of both test specimens was somewhat similar up to about 9 percent axial strain. Above 9 percent strain, the deviator stress-strain behavior of the two specimens was remarkably different. The deviator stress of test specimen UU-5 decreased rapidly and achieved a relatively constant value at about 12 percent strain, whereas that of specimen UU-6 increased considerably to a peak value at about 19 percent strain.

Plots of the change in pore pressure measured for these two specimens are shown in Figure 5.18b. It can be seen from this figure that a problem with the pore pressure monitoring system was encountered in test UU-5. The measured change in pore pressure for test specimen UU-6 appears to be reasonable.

After reviewing the stress-strain behavior of test specimens UU-1 through UU-6 shown in Figures 5.16a and 5.18a, along with the changes in pore pressure measured for these tests in Figures 5.16b and 5.18b, it appears that the tests in which problems occurred with the pore pressure

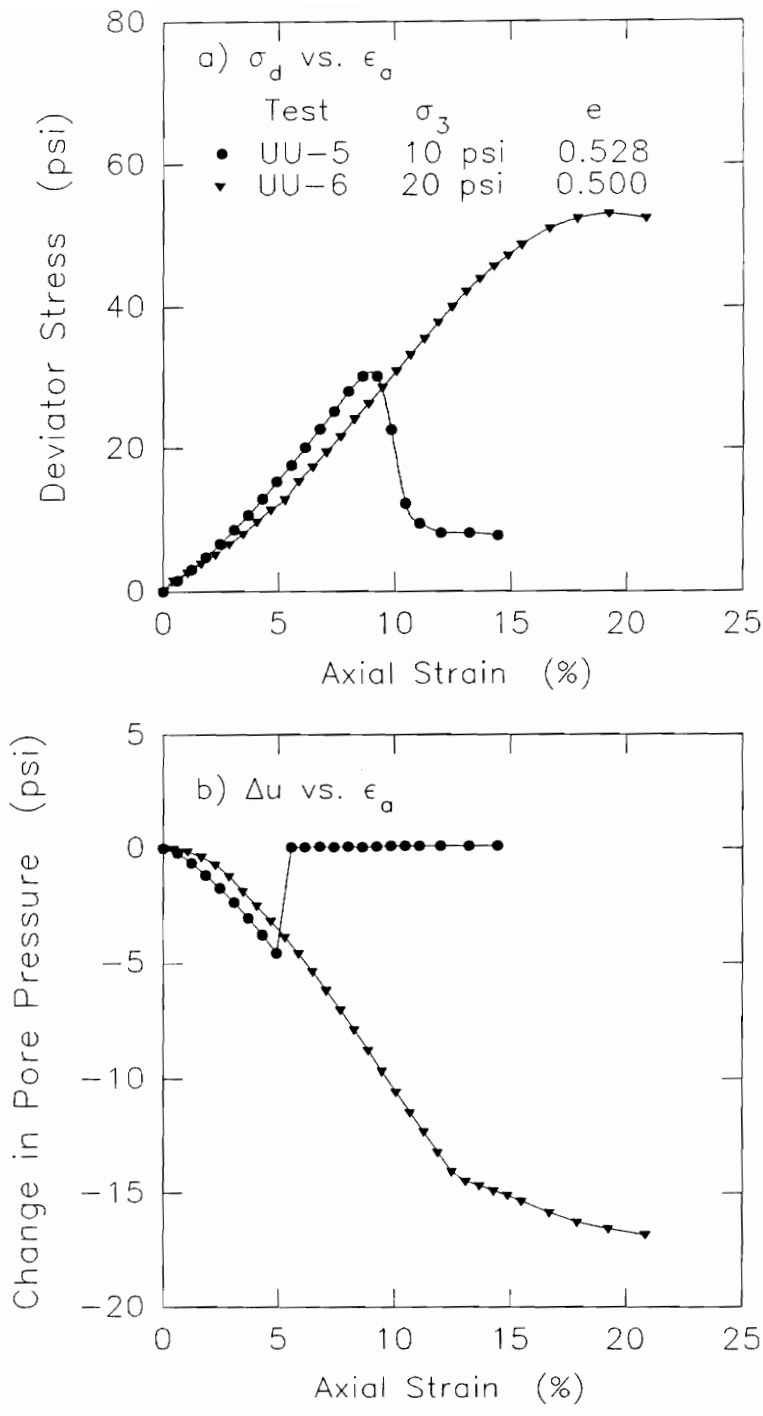


Figure 5.18. Deviator stress-strain and change in pore pressure-strain relationships measured in UU tests 5 and 6 performed on specimens trimmed from the same batch sample of remolded LMVD silt

monitoring system, showed somewhat similar characteristics in their stress-strain behavior as well. For test specimens UU-1, UU-2, and UU-5, the measured change in pore pressure remained at or increased rapidly to zero at some point during the test.

The measurement of zero change in pore pressure in these tests indicates that the pore pressure transducer measured the pore pressure within the specimen as being equal to the cell pressure outside the specimen. This condition would have resulted if the rubber cement seal at the needle-membrane interface had failed and the specimen was no longer truly undrained but had the capability for drainage to the outside of the specimen. Because these specimens had drainage to some extent during the tests, they gave a stress-strain behavior different from that of the specimens which remained undrained and gave reasonable pore pressure measurements. The tests with pore pressure monitoring problems all had stress-strain behavior characterized by a peak deviator stress being reached, followed by a considerable decrease in deviator stress with further strain.

The measurement of reasonable pore pressures in the other tests implies that these specimens remained undrained during the tests. As undrained specimens, these tests

showed stress-strain behavior which was different from the specimens which experienced drainage when the rubber cement seal at the needle-membrane interface failed.

Test specimen UU-4 showed an abrupt increase in measured change in pore pressure but the measured pore pressure did not rise to zero. Instead it began to decrease again. This suggests that a partial failure of the pore pressure measuring system may have occurred. A partial failure of the midheight pore pressure monitoring system would have allowed the specimen to momentarily experience drainage. If this condition occurred, however, it does not appear to have progressed to the point where it strongly affected the stress-strain behavior of the soil. The abrupt increase in measured change in pore pressure in this test took place at an axial strain of just over 10 percent. The stress-strain curve for this test does show a noticeable change in slope at about the same axial strain. This change in slope may have resulted from the partial drainage of the specimen and the erratic pore pressures within the sample.

Test specimens UU-7 and UU-8 were both trimmed from the same batch sample. Test specimen UU-7 had an initial void ratio of 0.531 and was tested at a cell pressure of 20

psi, whereas specimen UU-8 had an initial void ratio of 0.538 and was tested at a cell pressure of 10 psi.

The stress-strain behavior of these two test specimens, presented in Figure 5.19a, shows that the two specimens experienced almost identical stress-strain behavior up to an axial strain of about 8 percent. Above 8 percent axial strain the stress-strain behavior of the two specimens began to differ. The deviator stress of test specimen UU-8 decreased whereas that of specimen UU-7 increased to a peak value at about 20 percent axial strain.

The change in pore pressure measured for these two tests is shown in Figure 5.19b. As can be seen from this figure, both tests showed very similar changes in pore pressure up to about 8 percent axial strain. The pore pressure of specimen UU-8 then increased slightly and appeared to be approaching a constant value when the test was stopped. The pore pressure of specimen UU-7 continued to decrease until just over 15 percent axial strain when a series of increases and decreases in pore pressure occurred.

The erratic pore pressure measurements observed in test UU-7 are felt to be the result of repeated temporary failures of the rubber cement seal at the needle-membrane

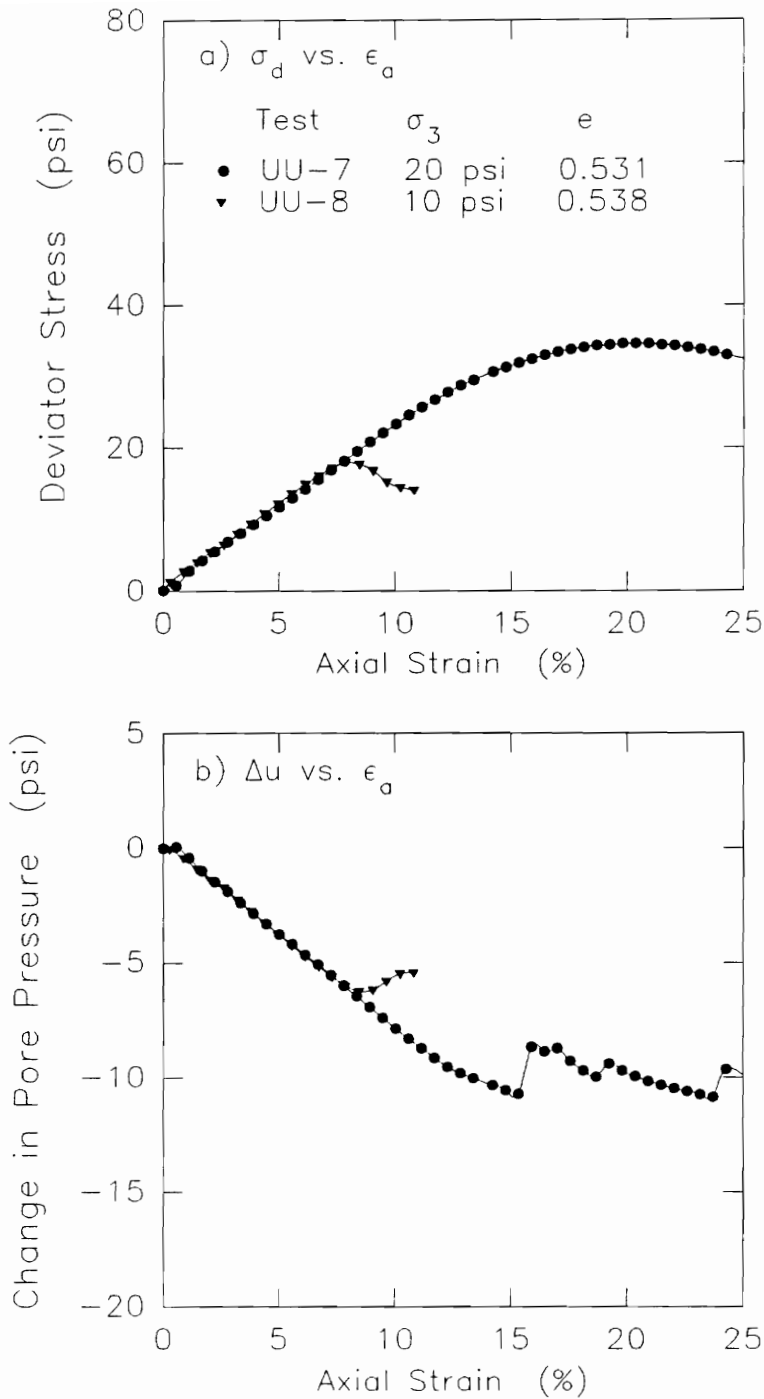


Figure 5.19. Deviator stress-strain and change in pore pressure-strain relationships measured in UU tests 7 and 8 performed on specimens trimmed from the same batch sample of remolded LMVD silt

interface, leading to a series of abrupt increases in measured pore pressure.

5.4.3 Comparison of Q Tests Performed on Specimens with Similar Void Ratios

The next way in which the results of the Q tests can be compared is to look at samples which had similar initial void ratios, but which were obtained from different batches and tested at different cell pressures.

Figure 5.20a shows a plot of deviator stress vs. axial strain for Q tests UU-3, UU-8, UU-10, and UU-14, performed at cell pressures of 20, 10, 0, and 10 psi, respectively. The initial void ratios of these specimens varied from 0.537 to 0.541.

As can be seen from Figure 5.20a, specimens UU-8 and UU-10 had similar stress-strain behavior up to about 8 percent axial strain after which the deviator stress for specimen UU-8 decreased. The deviator stress for specimen UU-10 continued to increase until about 10 percent axial strain after which it also experienced a decrease. Specimens UU-3 and UU-14 had stress-strain behavior which differed from the other two specimens as well as from each other.

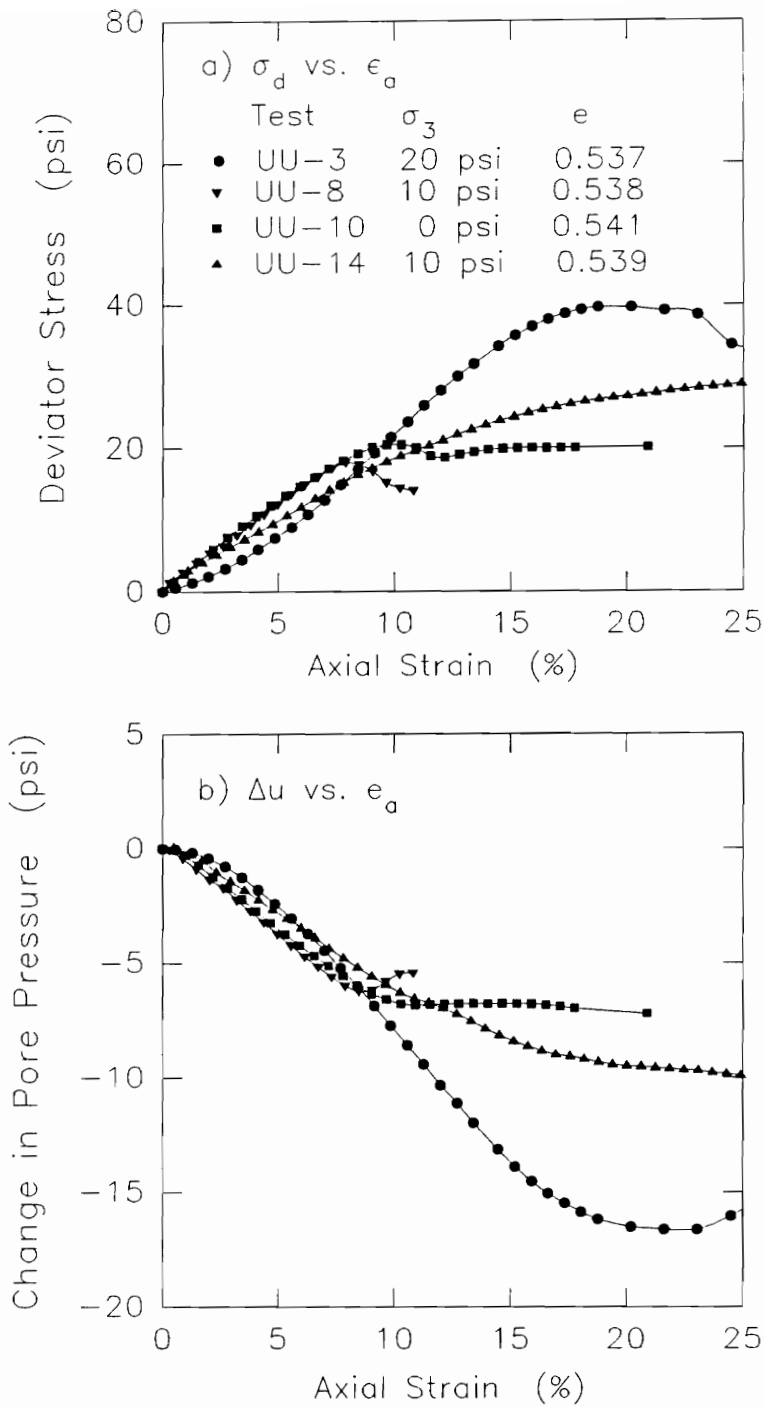


Figure 5.20. Deviator stress-strain and change in pore pressure-strain relationships measured in UU tests 3, 8, 10, and 14 on remolded LMVD silt

The changes in pore pressure measured in these four tests are plotted in Figure 5.20b. It can be seen that up to an axial strain of about 9 percent, similar changes in pore pressure were measured for all four specimens; however, slight differences still exist between the four measured responses. Above 9 percent strain, considerably different changes in pore pressure were measured for the four specimens. The measured changes in pore pressure for all four specimens appear to be reasonable and problems with the pore pressure monitoring system probably did not occur in any of these tests.

Defining failure as the deviator stress at 8% axial strain, specimens UU-8 and UU-10 give an approximate $\phi_u = 0$, $S_u = c = 9.5$ psi, total stress failure envelope, as shown in Figure 5.21. If specimens UU-3 and UU-14 are included, however, more erratic total stress Mohr's circles are obtained at 8 percent strain, as shown in Figure 5.22.

The deviator stress-strain curves for Q tests UU-10, UU-13, UU-14, and UU-18 are plotted together in Figure 5.23a. These four Q tests were performed at cell pressures of 0, 0, 10, and 20 psi, respectively. The initial void ratios of these specimens varied from 0.539 to 0.542.

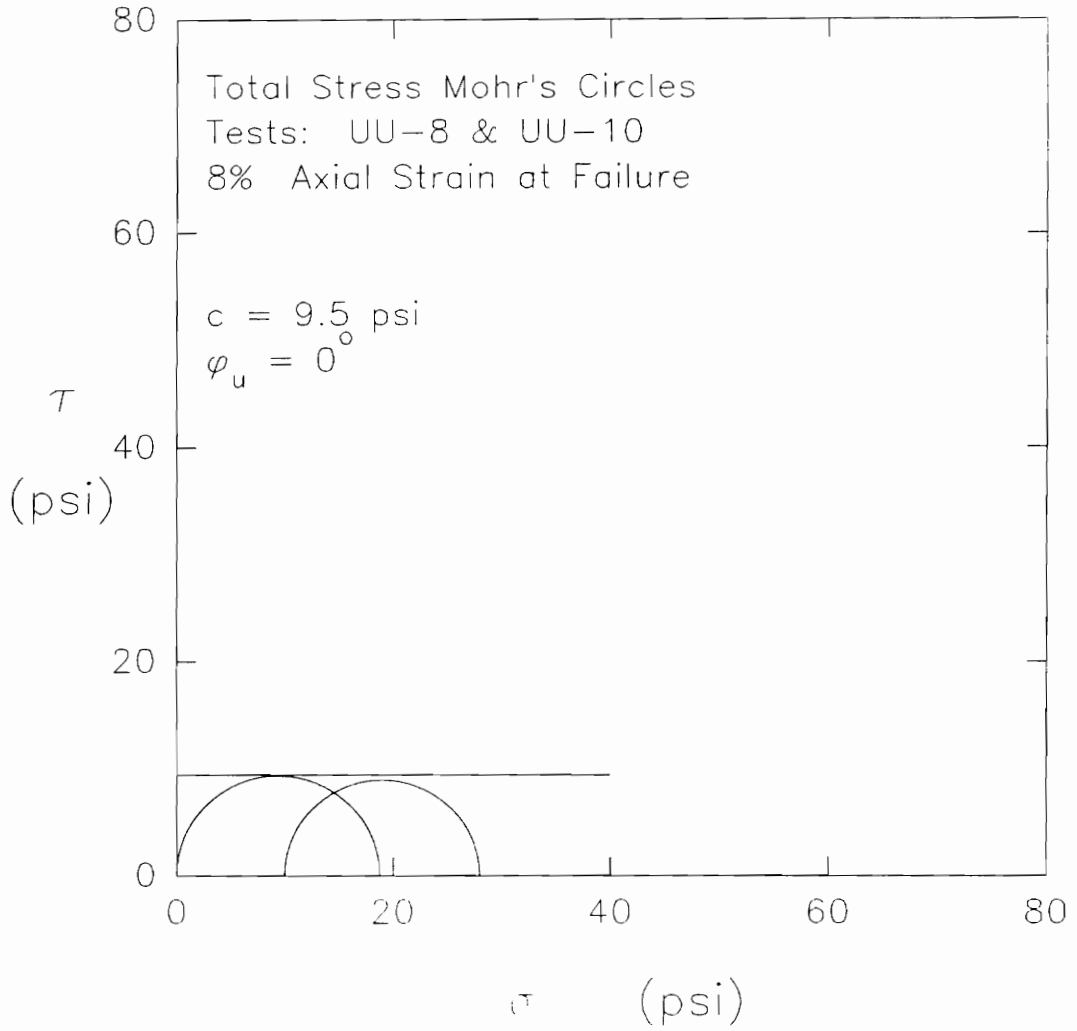


Figure 5.21. Total stress Mohr's circles at 8% axial strain for UU tests 8 and 10 on remolded LMVD silt

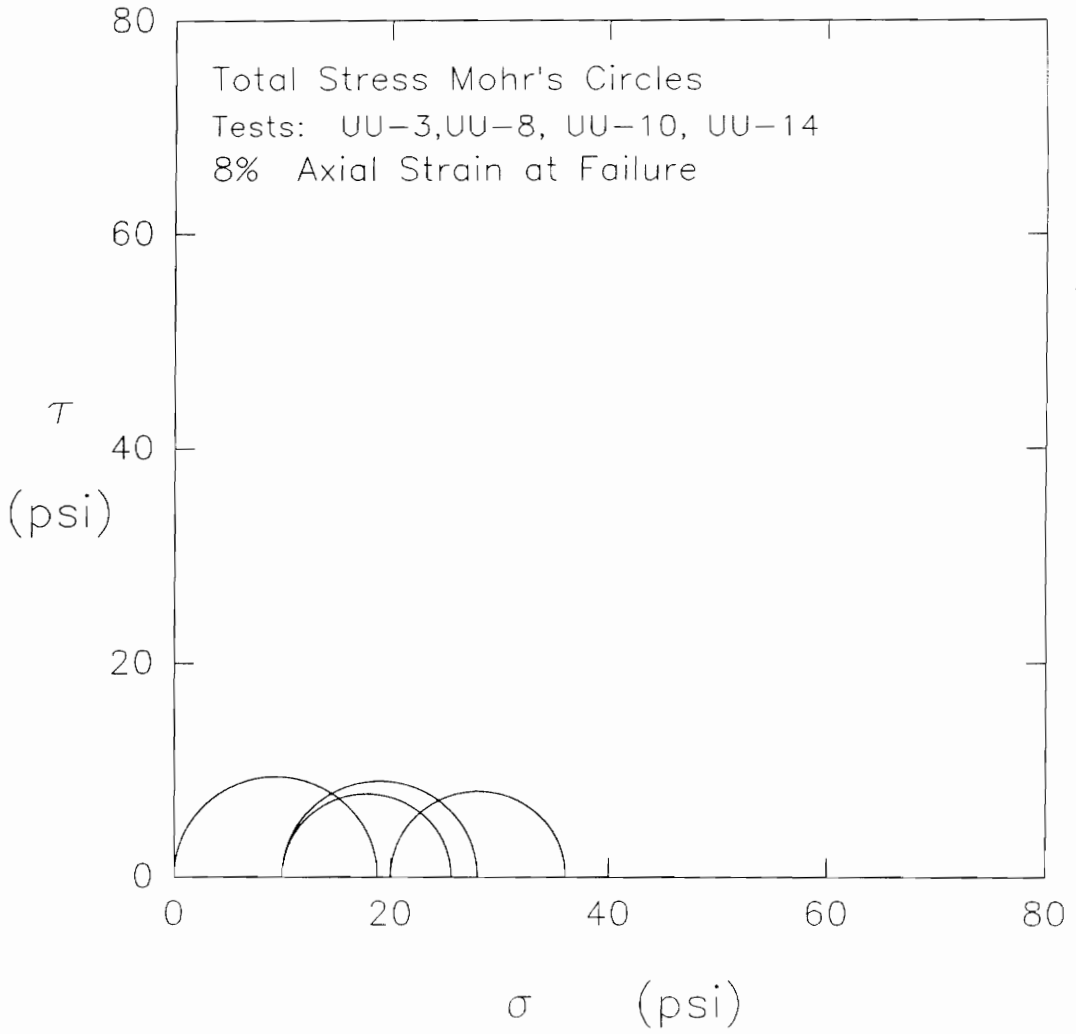


Figure 5.22. Total stress Mohr's circles at 8% axial strain for UU tests 3, 8, 10, and 14 on remolded LMVD silt

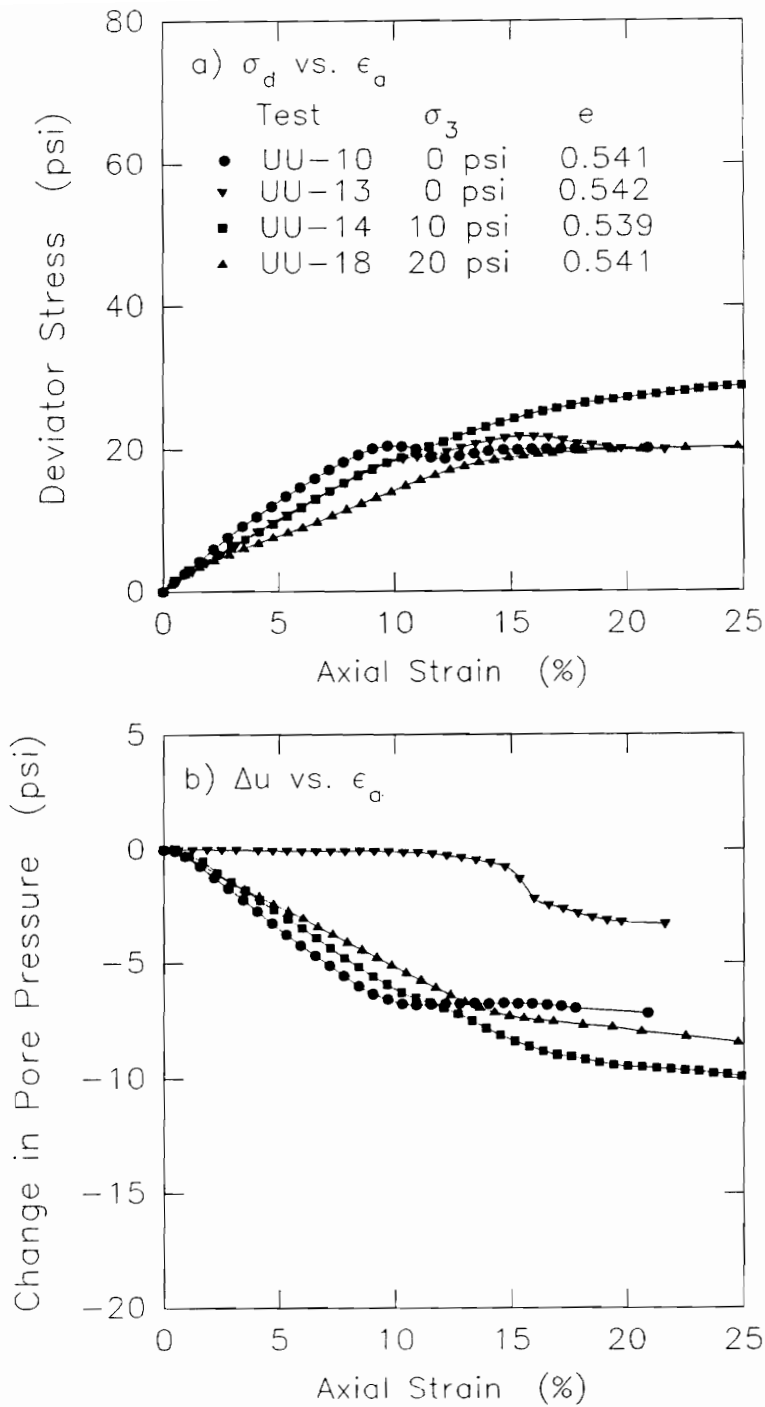


Figure 5.23. Deviator stress-strain and change in pore pressure-strain relationships measured in UU tests 10, 13, 14, and 18 on remolded LMVD silt

From this figure, it can be seen that Q test specimens UU-13 and UU-14 had very similar stress-strain curves up to about 10 percent axial strain, after which variations in the two curves took place. The deviator stress-strain curves of specimens UU-10 and UU-18 are different from the curves for the other two specimens as well as from each other. One interesting thing to note in this figure is that Q test specimens UU-10, UU-13, and UU-18 all reached the same constant value of deviator stress, 20 psi, at about 20 percent axial strain. The three stress-strain curves followed quite different paths leading up to that point.

Figure 5.23b shows the changes in pore pressure measured in these four tests. As can be seen from this figure, for Q tests UU-10, UU-14, and UU-18, similar changes in pore pressure were measured up to axial strains of 9 to 12 percent. All three tests also showed a decrease in the slope of the curves indicating that the rate of pore pressure decrease at higher strains was less than at smaller strains. Test UU-13 showed relatively no change in pore pressure until strains greater than about 12 percent had been reached. This behavior may possibly be the result of a leak in the rubber cement seal at the needle-membrane interface which somehow became sealed as the specimen underwent further axial strain during the test.

For axial strains up to about 10 percent, specimens UU-13 and UU-14 give a $\phi_u = 0$, $S_u = c = 9.2$ psi, total stress failure envelope, as shown in Figure 5.24. When specimens UU-10 and UU-18 are included as well, however, more erratic total stress Mohr's circles are obtained at 10 percent axial strain, as shown in Figure 5.25.

Figure 5.26a shows the deviator stress vs. axial strain relationships for Q tests UU-6, UU-11, UU-15, and UU-16, performed at cell pressures of 20, 0, 10, and 10 psi, respectively. The initial void ratios of these four specimens varied from 0.500 to 0.519.

From this figure it can be seen that for Q test specimens UU-15 and UU-16, both performed at 10 psi cell pressure, very similar stress-strain curves were obtained. For specimens UU-6 and UU-11, quite different deviator stress-strain behaviors were measured. Only at strains less than 3 percent, were the stress-strain curves of the four specimens similar.

The changes in pore water pressure measured during these four Q tests are plotted in Figure 5.26b. For these four tests, the change in pore pressure-strain behavior measured was quite different for each of the tests. The pore pressure responses of test specimens UU-6 and UU-16 showed some brief similarity at strains below about 3

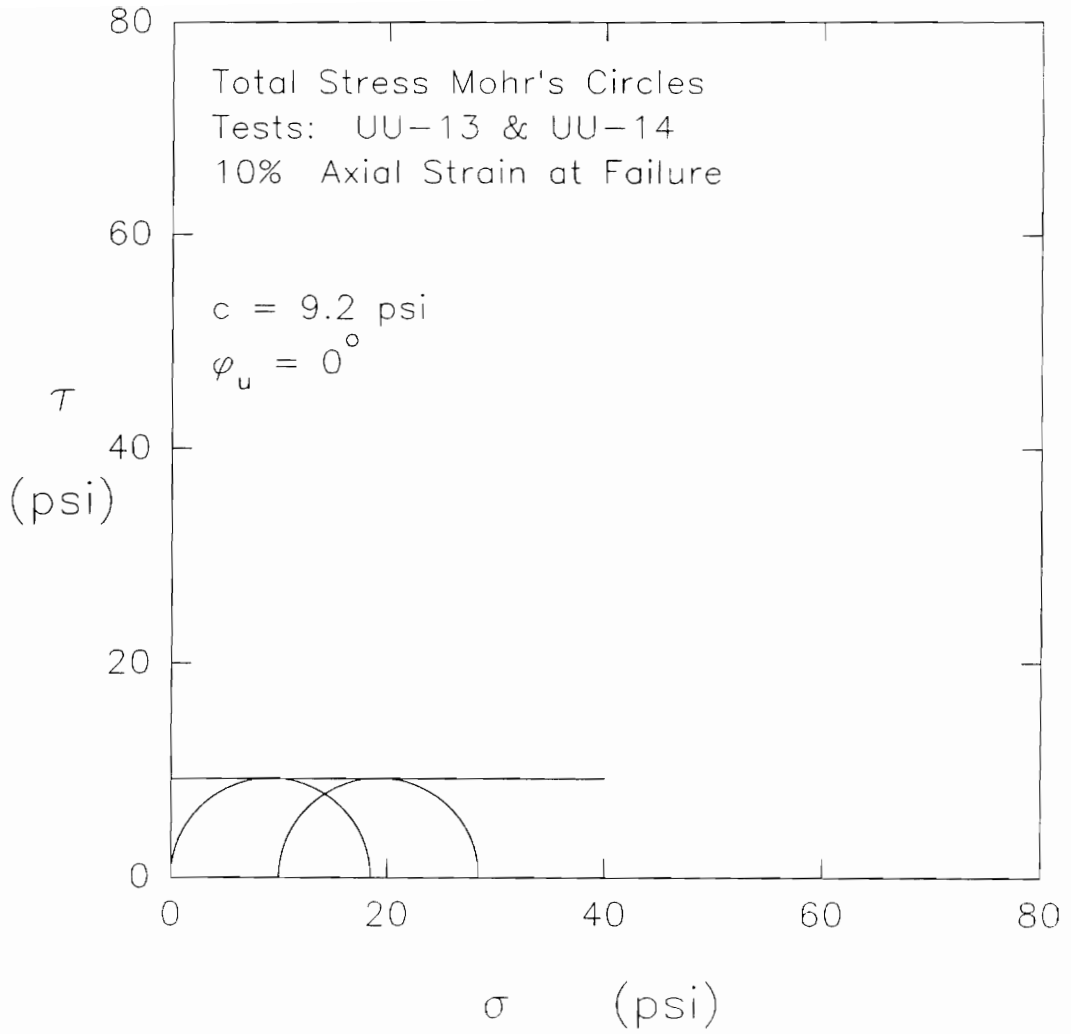


Figure 5.24. Total stress Mohr's circles at 10% axial strain for UU tests 13 and 14 on remolded LMVD silt

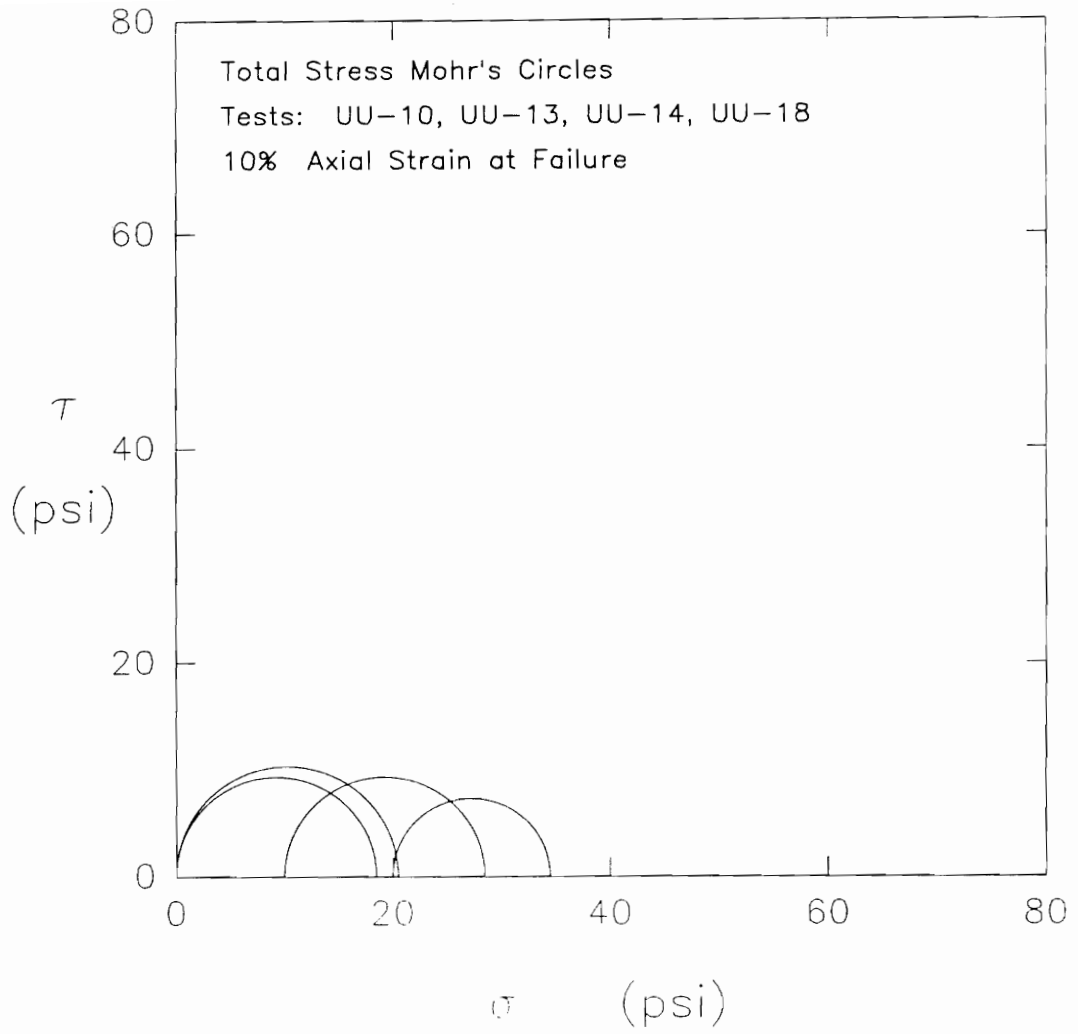


Figure 5.25. Total stress Mohr's circles at 10% axial strain for UU tests 10, 13, 14, and 18

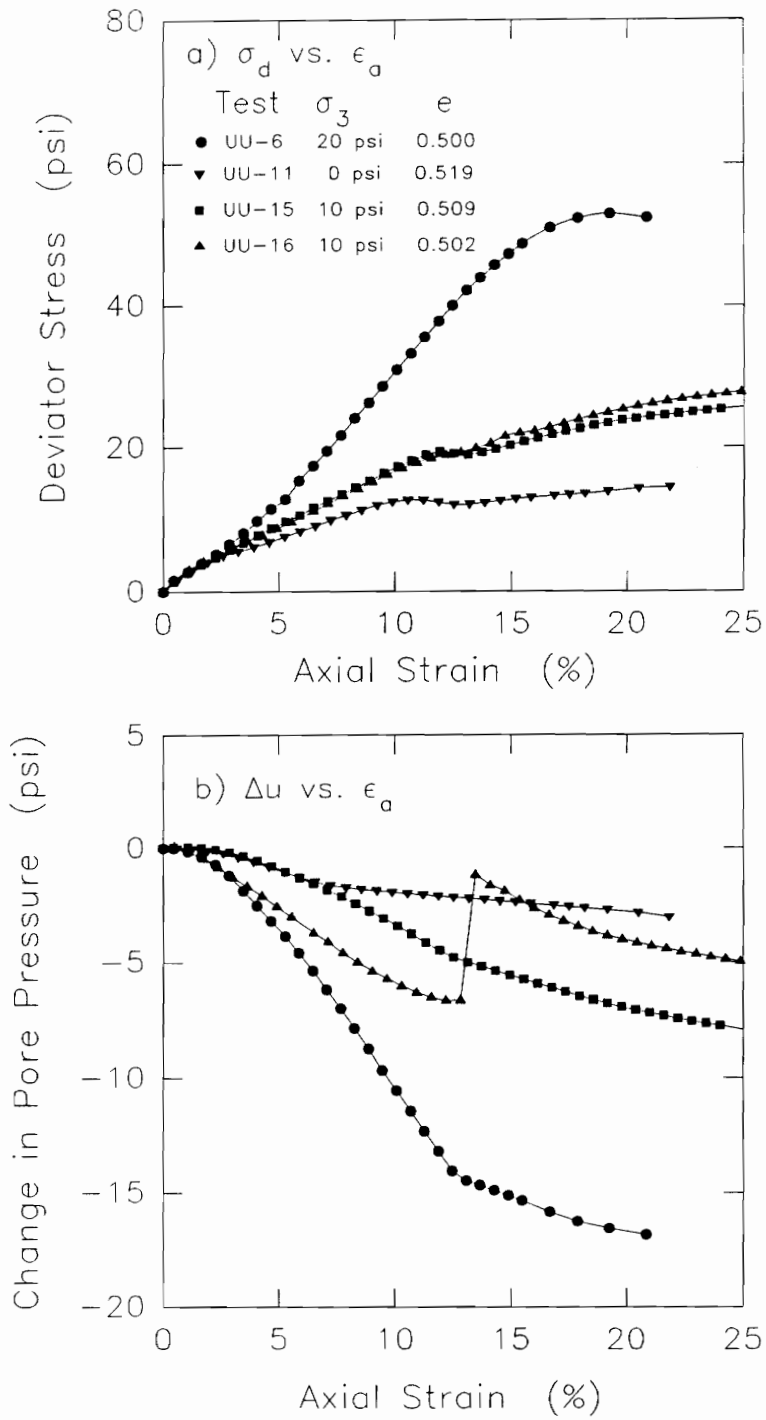


Figure 5.26. Deviator stress-strain and change in pore pressure-strain relationships measured in UU tests 6, 11, 15, and 16 on remolded LMVD silt

percent and then varied considerably with increasing strain. Test UU-16 showed an increase in measured change in pore pressure to 0 psi indicating a failure of the rubber cement seal at the needle-membrane interface. The changes in pore pressure measured in test specimens UU-11 and UU-15 showed some similarity up to an axial strain of about 7 percent. Above 7 percent strain, however, the changes in pore pressure measured for these two tests varied. Of these four tests, specimen UU-6 showed the largest decrease in pore pressure. This test also exhibited a noticeable decrease in the slope of the pore pressure-strain curve at about 12.5 percent strain. The other tests in this group also showed a decrease in the rate at which the pore pressures decreased at higher strains.

For a failure criterion of 10 percent axial strain, these four tests yielded the total stress Mohr's circles shown in Figure 5.27. This plot shows a definite increase in soil strength with increasing cell pressure.

Plots of deviator stress vs. axial strain for Q tests UU-4, UU-5, UU-7, and UU-12 are shown in Figure 5.28a. These tests were performed at cell pressures of 0, 10, 20, and 0 psi, respectively, and had initial void ratios which varied from 0.528 to 0.532.

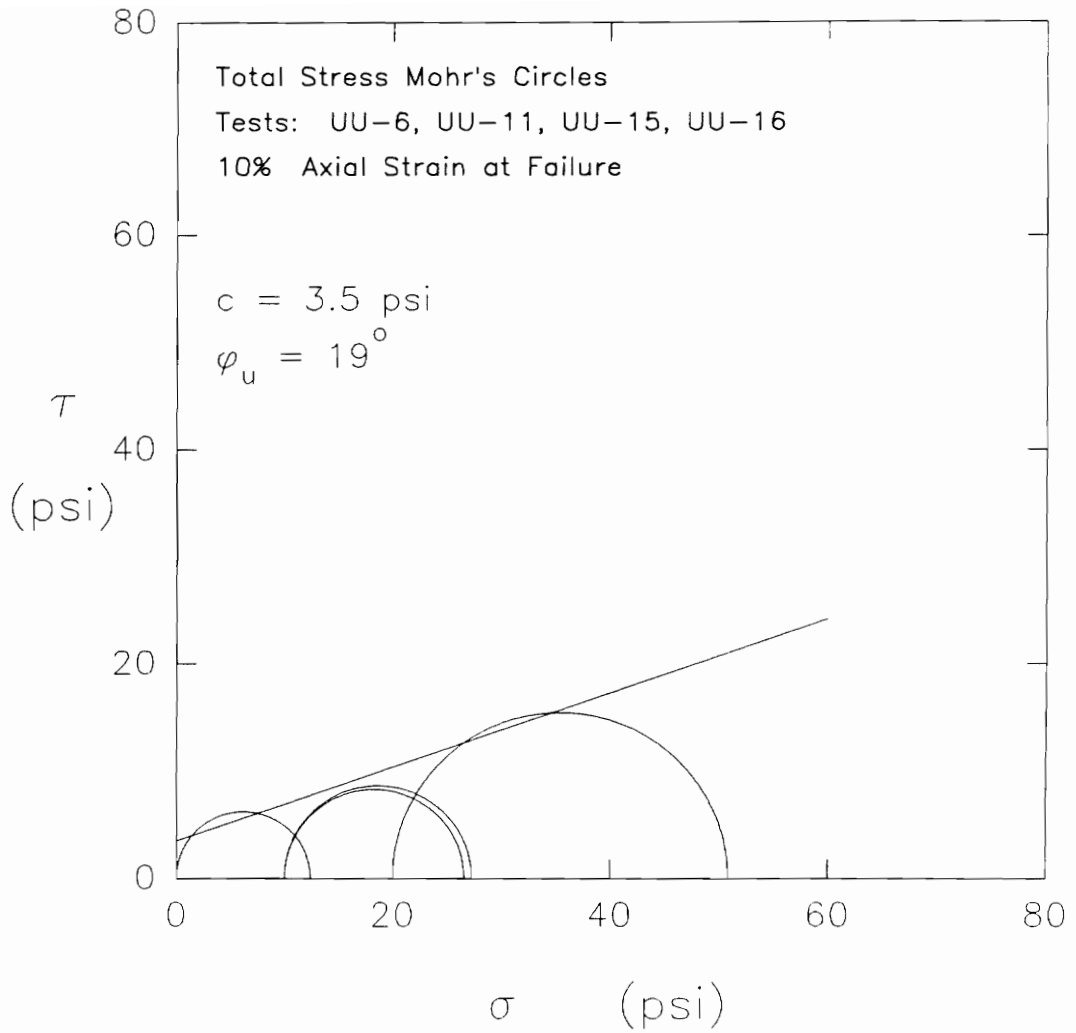


Figure 5.27. Total stress Mohr's circles at 10% axial strain for UU tests 6, 11, 15, and 16 on remolded LMVD silt

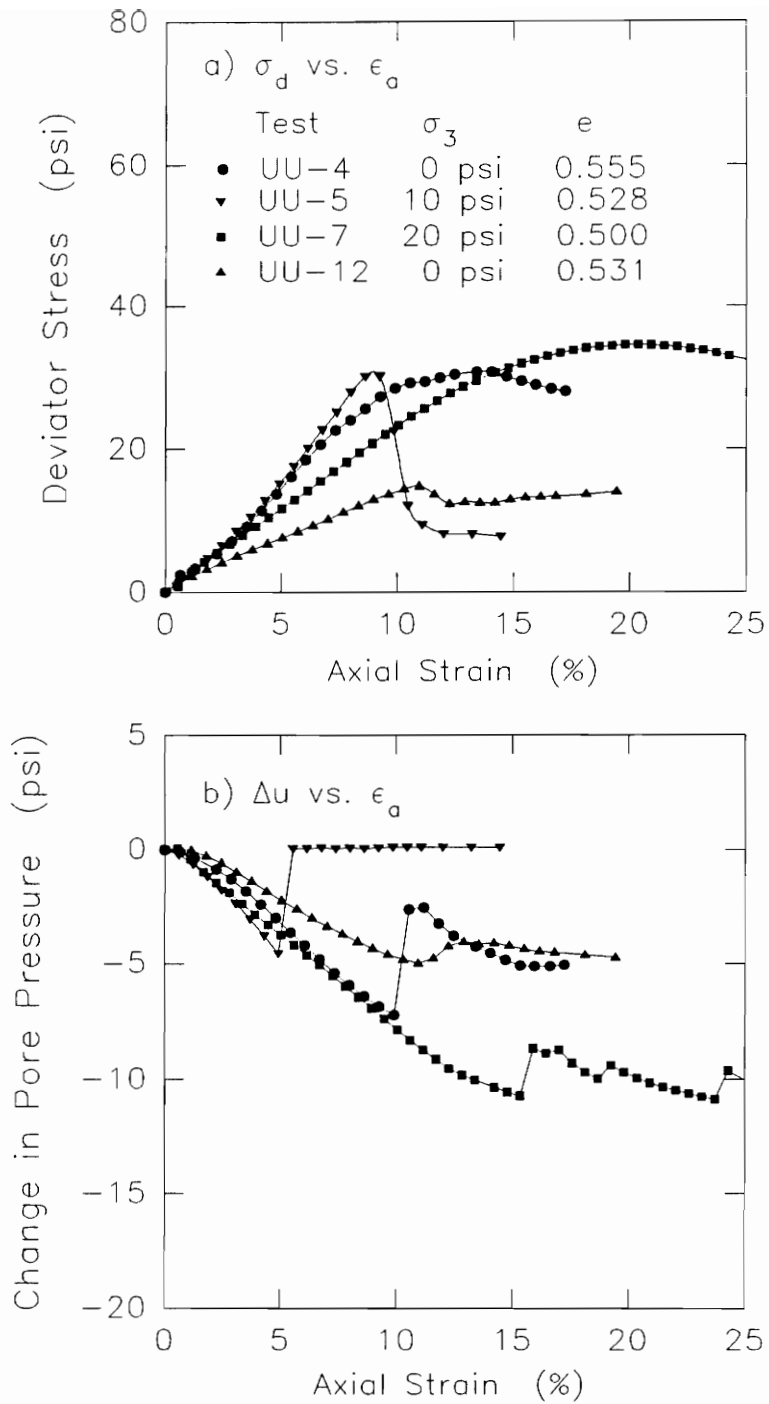


Figure 5.28. Deviator stress-strain and change in pore pressure-strain relationships measured in UU tests 4, 5, 7, and 12 on remolded LMVD silt

As can be seen from this figure, Q test specimens UU-4 and UU-5 had similar stress-strain curves up to about 7 percent axial strain. At higher strains, the stress-strain behavior of these two tests varied considerably. Test specimen UU-4 reached a peak deviator stress at about 14 percent strain and then decreased slightly with increasing strain. Test specimen UU-5 reached a peak deviator stress at about 9 percent strain and then underwent a rapid decrease in deviator stress to less than one-third its peak value. The other two tests in this group, UU-7 and UU-12, both showed stress-strain behavior that was different from the other two tests, as well as from each other.

Figure 5.28b shows the changes in pore pressure that were measured in these four Q tests. As can be seen from this plot, three of the four specimens had erratic pore pressure measurements, indicative of a failure of the rubber cement seal at the needle-membrane interface. Only the change in pore pressure measured for specimen UU-12 showed somewhat reasonable behavior. The other three tests did show somewhat similar changes in pore pressure at small strains.

For a failure criterion of about 9 percent axial strain, these four tests yielded the total stress Mohr's

circles shown in Figure 5.29, indicating very erratic strengths for this group of four specimens.

Figure 5.30a presents plots of deviator stress vs. axial strain for Q test specimens UU-3, UU-13, and UU-14, performed at cell pressures of 20, 0, and 10 psi, respectively. The initial void ratios of these three specimens ranged from 0.537 to 0.542.

From this figure it can be seen that Q test specimens UU-13 and UU-14 have very similar stress-strain behavior up to about 10 percent axial strain. At higher strains, the stress-strain curves of these two tests showed more variation. Specimen UU-13 showed a slight leveling off of the deviator stress followed by an increase to a peak value followed by a decrease in deviator stress with increasing strain. Specimen UU-14 showed a continual increase in deviator stress until the end of the test. The stress-strain behavior of specimen UU-3 was different from that of the other two tests but yielded a similar value of deviator stress at strains on the order of 7 to 8 percent. This test specimen reached a peak deviator stress much higher than the other two test specimens, at an axial strain of about 19.5 percent.

The changes in pore pressure measured in these three Q tests are presented in Figure 5.30b. As can be seen from

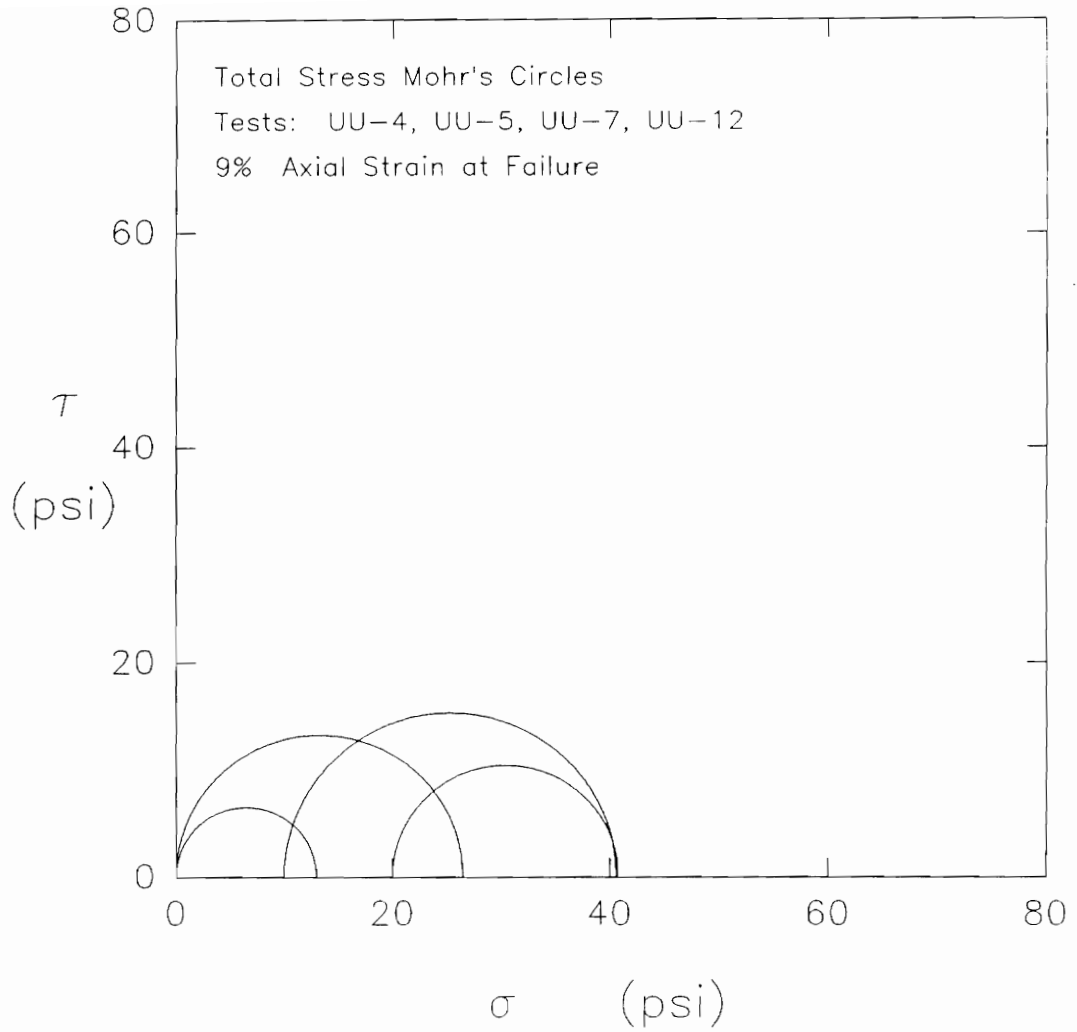


Figure 5.29. Total stress Mohr's circles at 9% axial strain for UU tests 4, 5, 7, and 12 on remolded LMVD silt

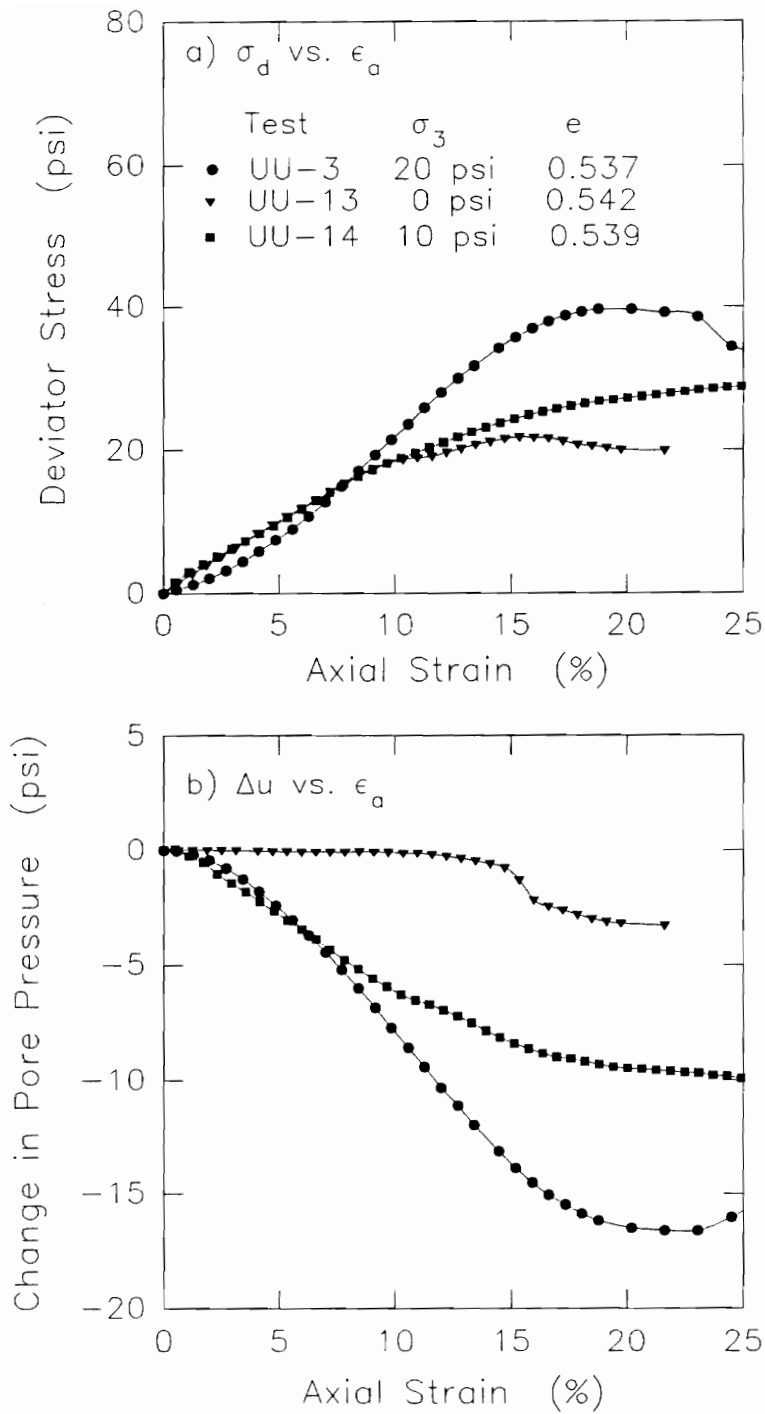


Figure 5.30. Deviator stress-strain and change in pore pressure-strain relationships measured in UU tests 3, 13, and 14 on remolded LMVD silt

this figure, the changes in pore pressure measured for each of these three tests were quite different from each other. Only at strains below about 7 percent, did test specimens UU-3 and UU-14 show any similarities in their measured changes in pore pressure. Test specimen UU-13 again showed no measured change in pore pressure until strains above about 12 percent.

Figure 5.31 shows a plot of the total stress Mohr's circles for these three tests based on an axial strain of about 10 percent at failure. Based on this plot, a failure envelope approximating a $\phi_u = 0$, $S_u = c$ condition is not quite achieved, as the test performed at 20 psi cell pressure had a higher strength than the two tests performed at lower cell pressures. For the failure envelope shown, the undrained strength parameters are $c = 8.1$ psi and $\phi_u = 5.4^\circ$.

5.4.4 Adjustment of Pore Pressures in Tests with Erratic Pore Pressure Measurements

For the Q test specimens where erratic pore pressure measurements occurred, it is possible to estimate the pore pressure at failure that theoretically would occur, based on the maximum total stresses (Brandon, Duncan, and Huffman, 1990). Assuming that the effective stress path

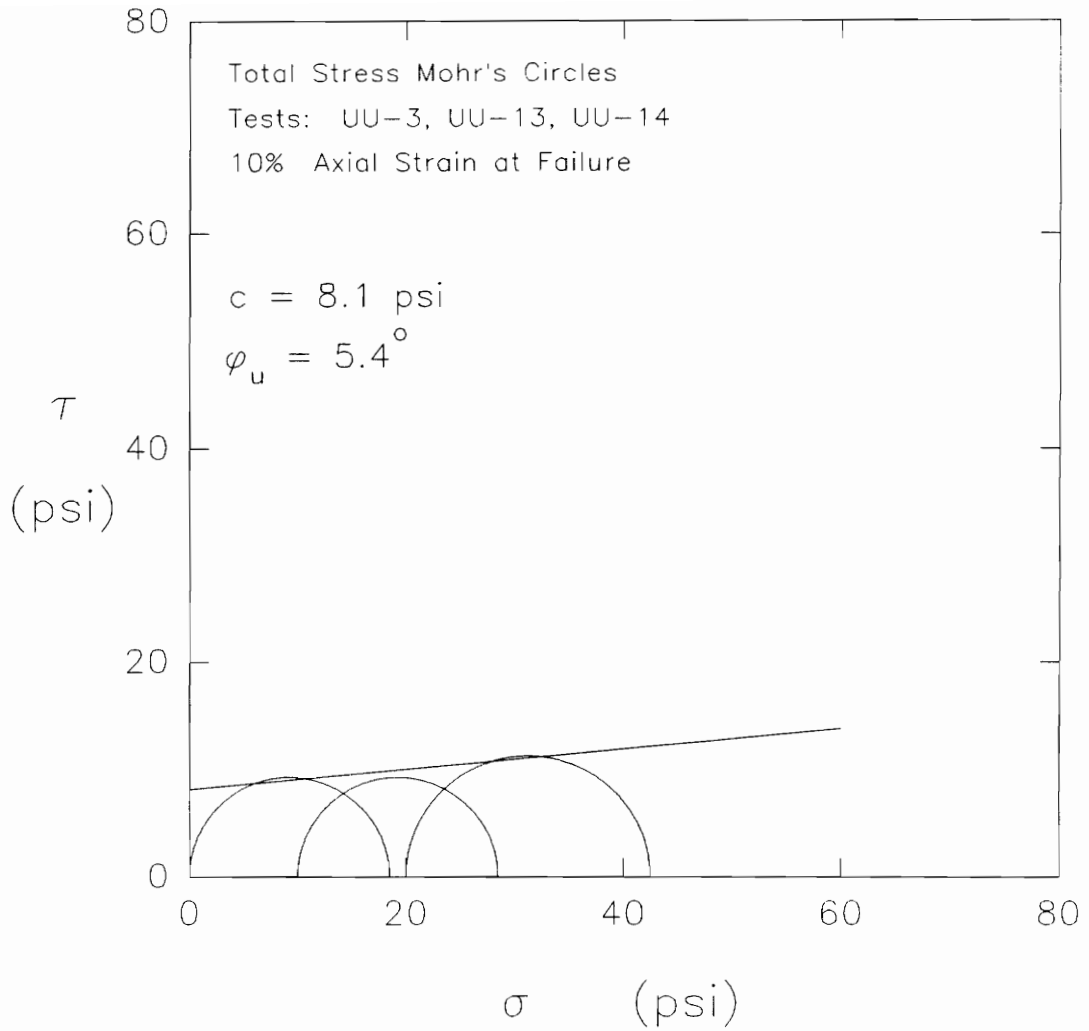


Figure 5.31. Total stress Mohr's circles at 10% axial strain for UU tests 3, 13, and 14 on remolded LMVD silt

follows the K_f line for the soil, the pore pressure at failure, u_f , is given by the equation:

$$u_f = \frac{\sigma_1 - \sigma_3 (\tan^2(45 + \phi'/2))}{1 - \tan^2(45 + \phi'/2)} \quad (5-1)$$

where u_f = pore water pressure at failure,
 σ_1 = major principal total stress at failure,
 σ_3 = minor principal total stresses at failure,
and
 ϕ' = effective stress friction angle of the soil.

With this equation, the pore pressure throughout a given test can be estimated based on an assumed effective stress friction angle at failure, ϕ' . By varying the value of effective stress friction angle, the value of pore pressure calculated by Eq. 5-1 can be adjusted so that the calculated pore pressures would closely correspond to the pore pressures actually measured during the early stages of the test.

In order to match the calculated and measured pore pressures, a failure criterion of 10 percent axial strain was chosen as the value of axial strain at which the estimated and measured pore pressures should correspond (Brandon, Duncan, and Huffman, 1990). Figure 5.32 shows the variation of estimated and measured change in pore

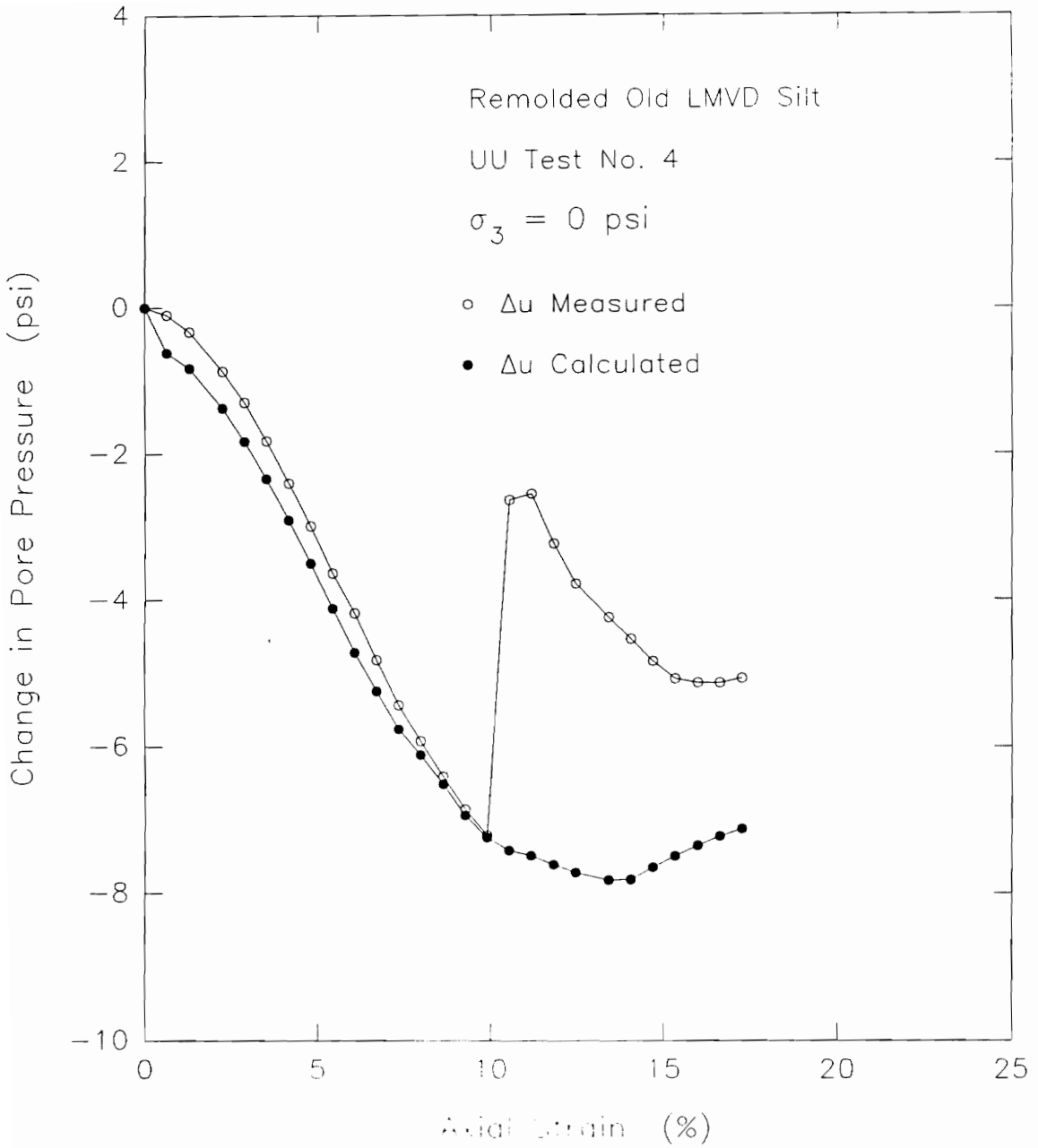


Figure 5.32. Calculated and measured change in pore pressure-strain relationships for UU test 4 on remolded LMVD silt

pressure vs. axial strain for unconfined compression test UU-4. In this case, an effective stress friction angle of 41.5 degrees was necessary so that the estimated pore pressure corresponded with the measured pore pressure at an axial strain of 10 percent.

Figure 5.33 shows a similar plot for Q test UU-7 performed at a confining pressure of 20 psi. In this case, an effective stress friction angle of 36.5 degrees was necessary so that the estimated pore pressure corresponded with the measured pore pressure at an axial strain of 10 percent.

Figure 5.34 shows the estimated and measured change in pore pressure vs. axial strain curves for Q test UU-2 performed at a confining pressure of 10 psi. In this case the erratic pore pressure behavior began at an axial strain of about 6.25 percent, well below the 10 percent axial strain failure criterion assumed. For this test, an effective stress friction angle of 39.5 degrees was used in Eq. 5-1 so that the estimated change in pore pressure corresponded with the measured change in pore pressure at an axial strain of 6.25 percent.

From these plots of estimated change in pore pressure vs. axial strain, the change in pore pressure at which the

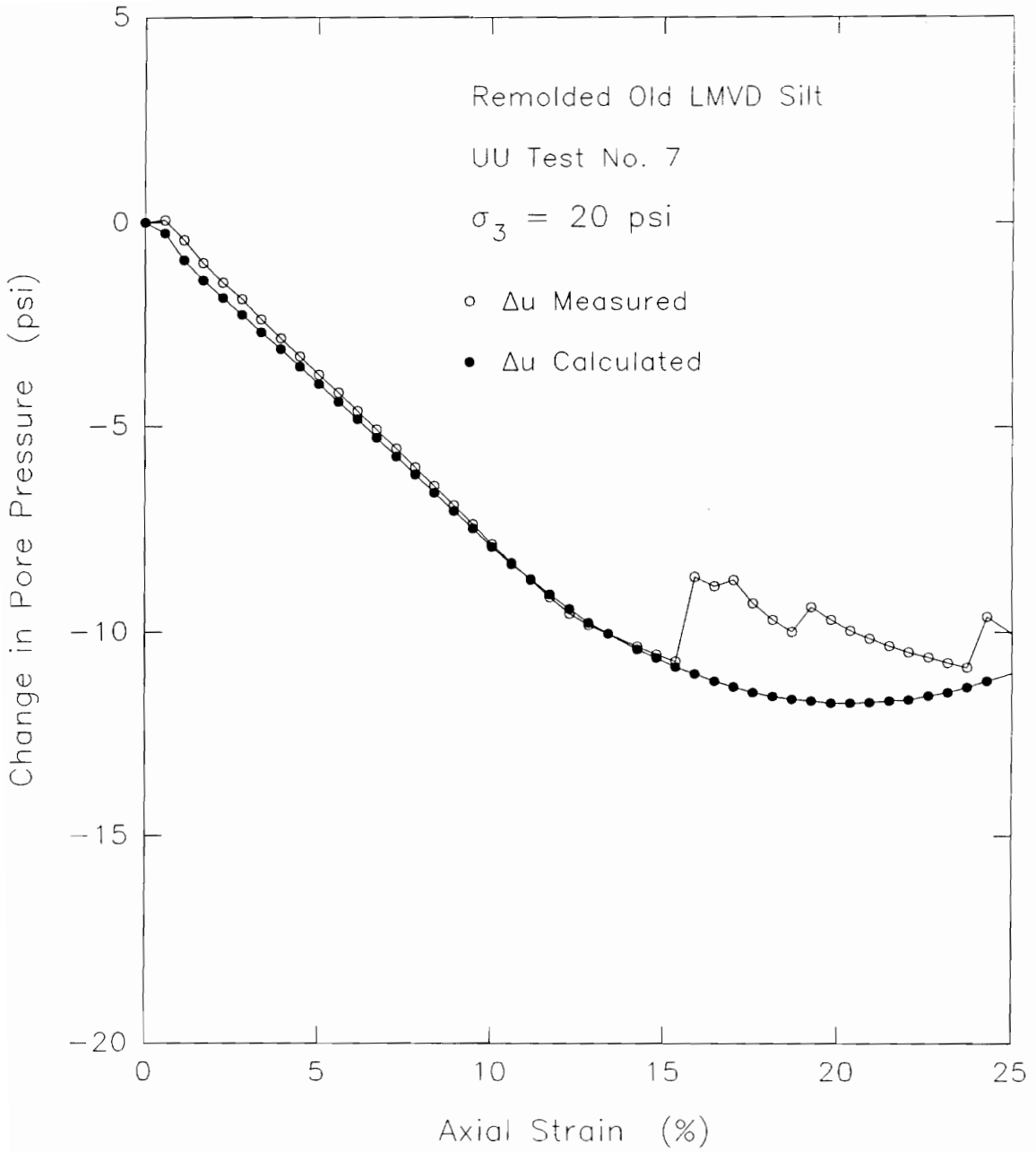


Figure 5.33. Calculated and measured change in pore pressure-strain relationships for UU test 7 on remolded LMVD silt

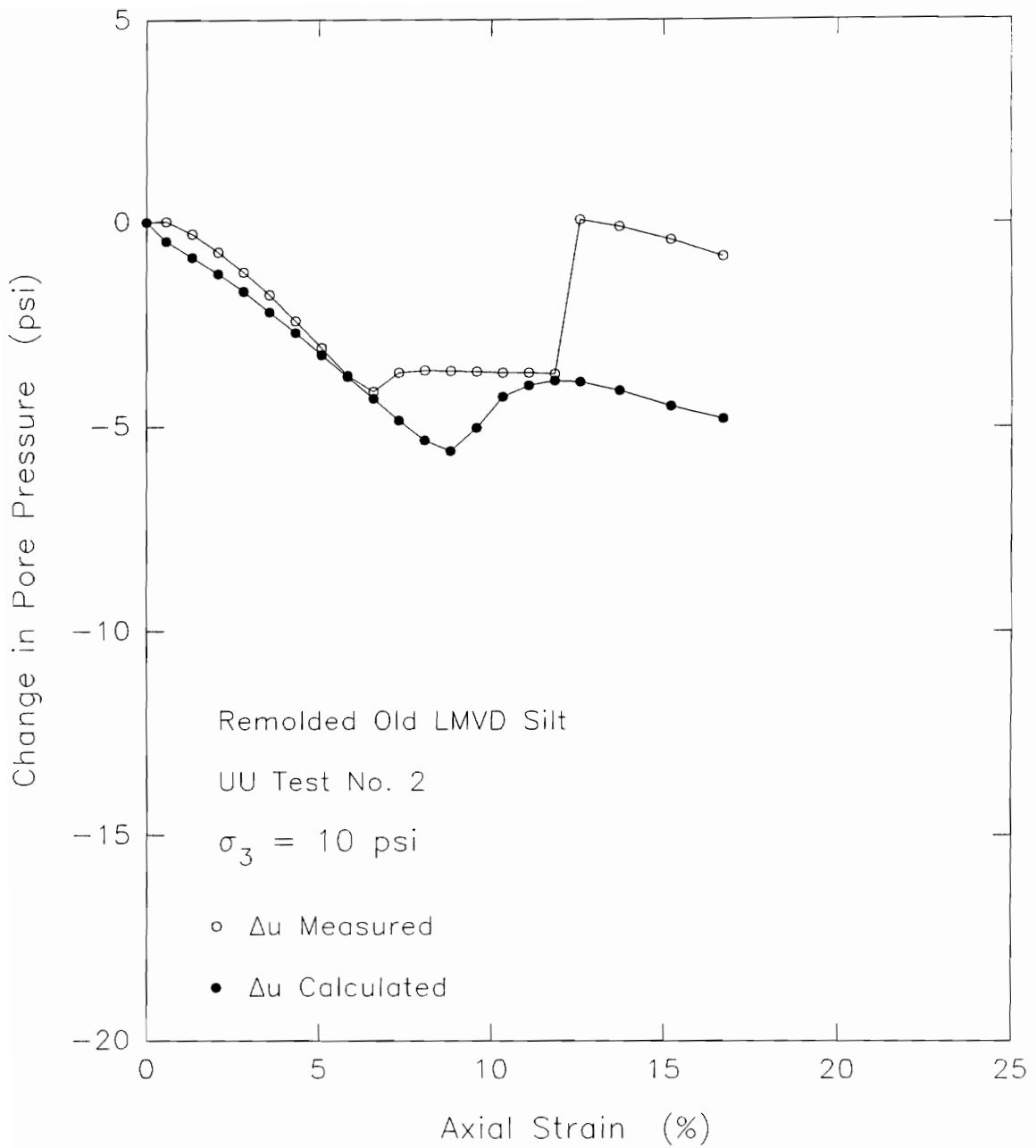


Figure 5.34. Calculated and measured change in pore pressure-strain relationships for UU test 2 on remolded LMVD silt

peak deviator stress occurred can be determined, and used to develop a plot of the effective stress failure envelope. Table 5.6 summarizes the stress-strain data at failure necessary to plot the failure envelope.

Table 5.6: Stress-strain data based on 10% axial strain failure criterion

UU Test No.	σ_3 (psi)	$(\sigma_1 - \sigma_3)_f$ (psi)	u_o (psi)	Δu (psi)	u_f (psig)
4	0	28.9	-1.3	-7.3	-8.6
2	10	15.7	8.8	-4.5	4.3
7	20	23.3	18.7	-7.9	10.8

Figure 5.35 shows the total stress Mohr's circles for the three tests. The effective stress circles are shown in Figure 5.36.

The effective stress paths for these three tests are plotted in Figures 5.37, 5.38, and 5.39. The stress paths shown are based on the actual measured pore pressures. The plots appear to be reasonable up until the point where the erratic pore pressure measurements began. After this point, the stress paths also show erratic behavior.

The effective stress paths for these three tests very clearly define the K_f line for the soil, except where erratic pore water pressure measurements occurred. These three test specimens give values of α of about 31° , which

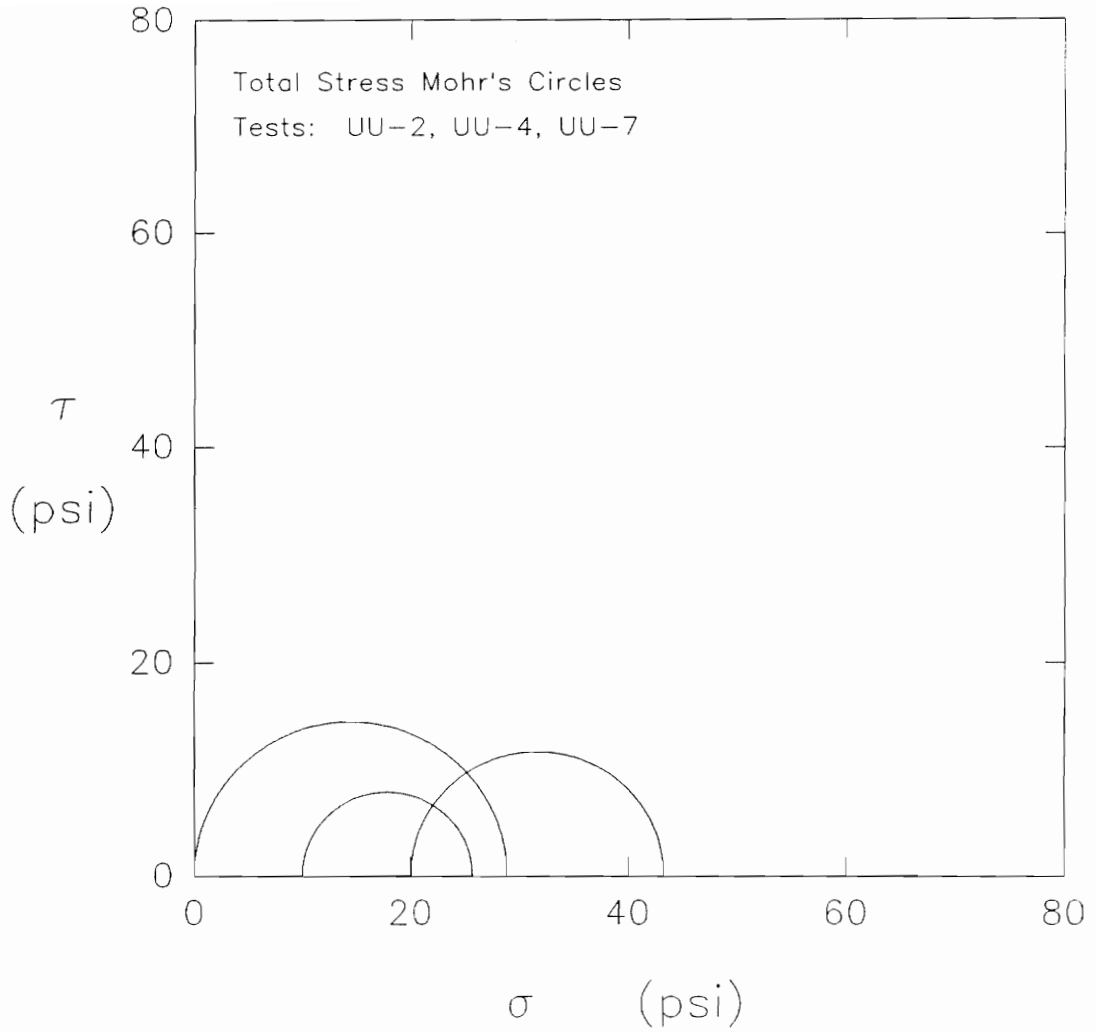


Figure 5.35. Total stress Mohr's circles for UU tests 2, 4, and 7 on remolded LMVD silt

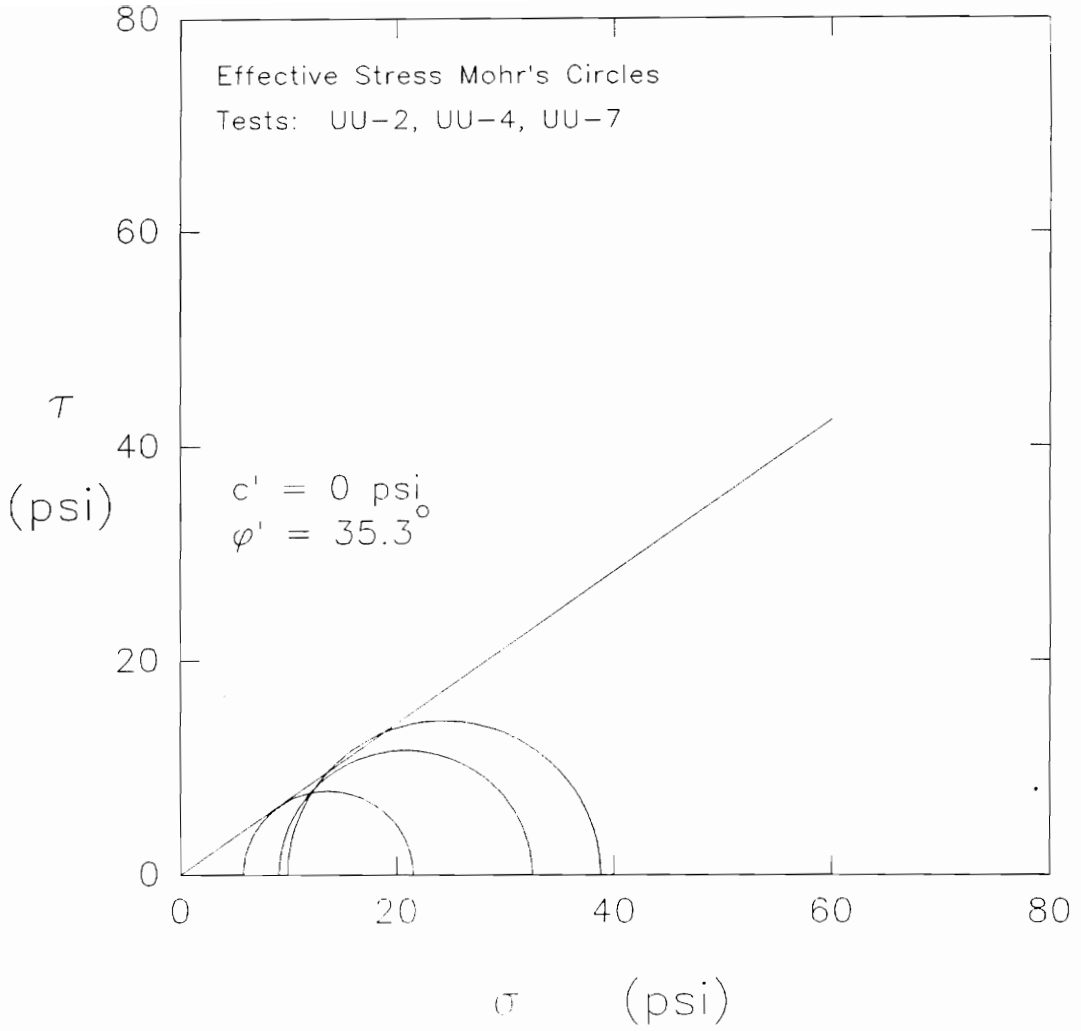


Figure 5.36. Effective stress Mohr's circles for UU tests 2, 4, and 7 on remolded LMVD silt

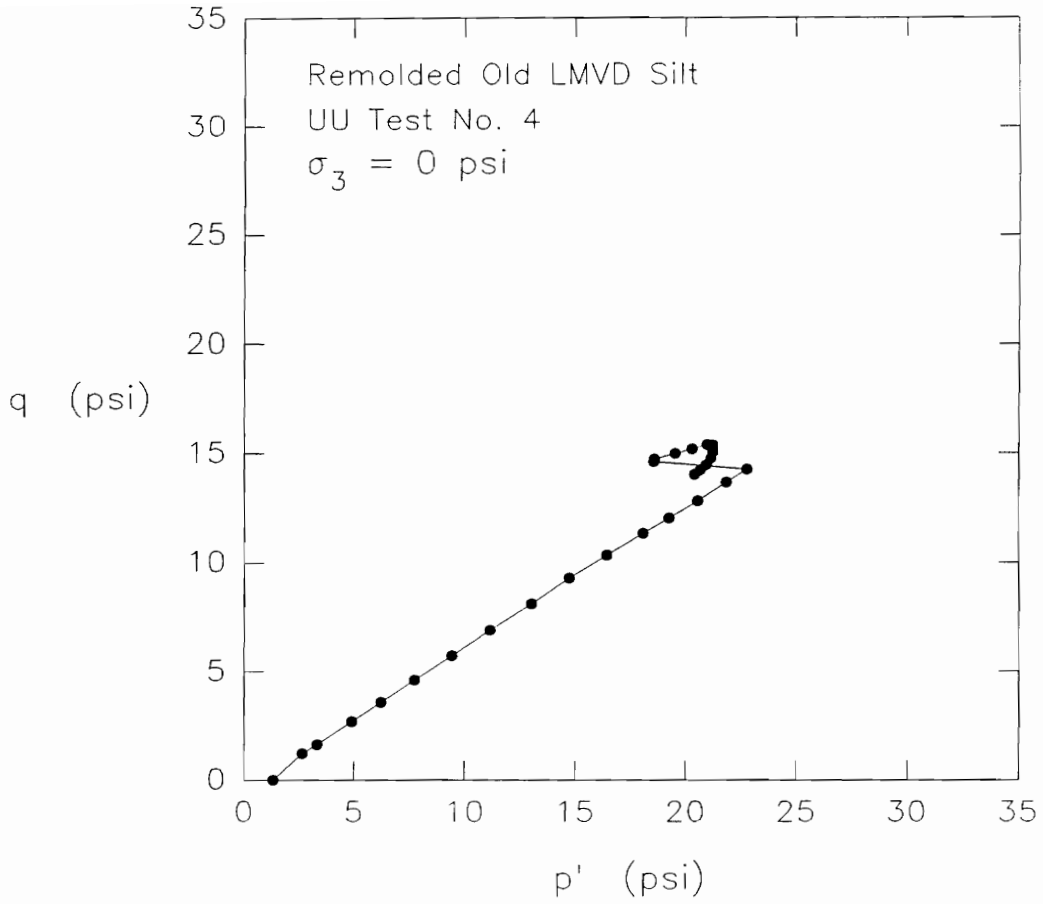


Figure 5.37. Effective stress path measured in UU test 4 on remolded LMVD silt

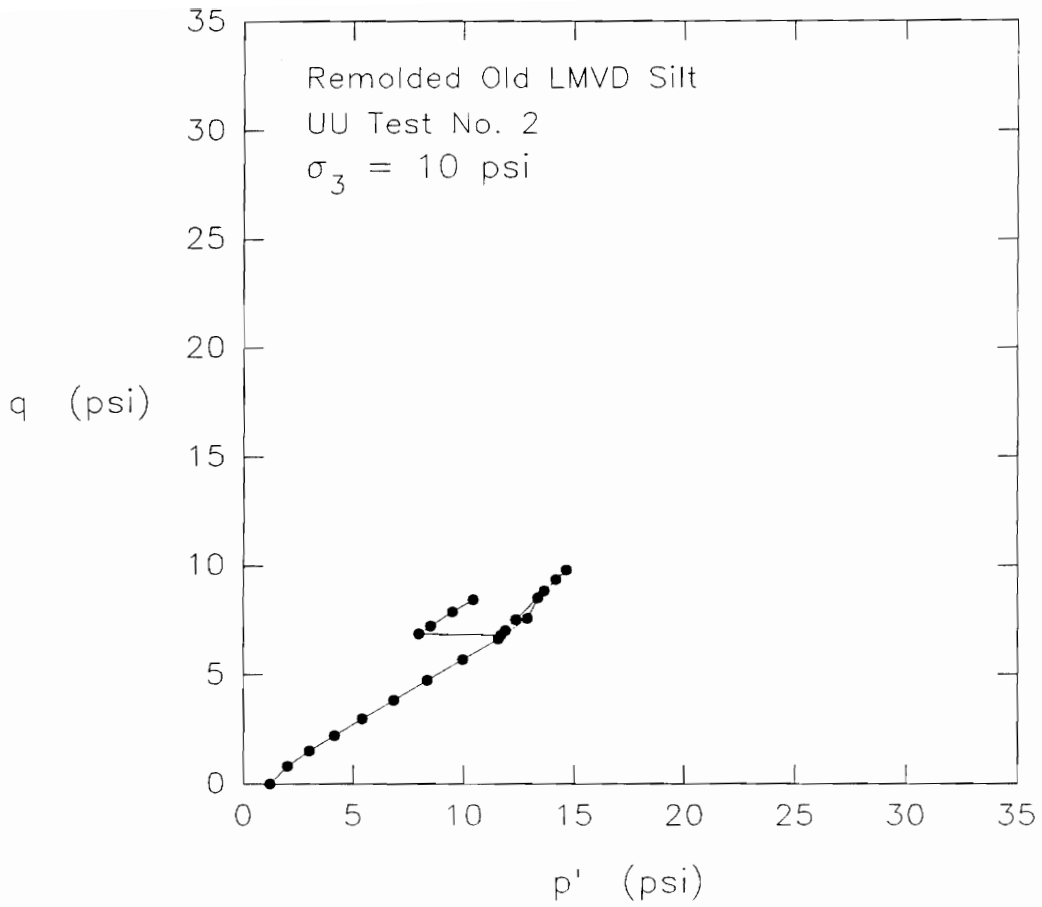


Figure 5.38. Effective stress path measured in UU test 2 on remolded LMVD silt

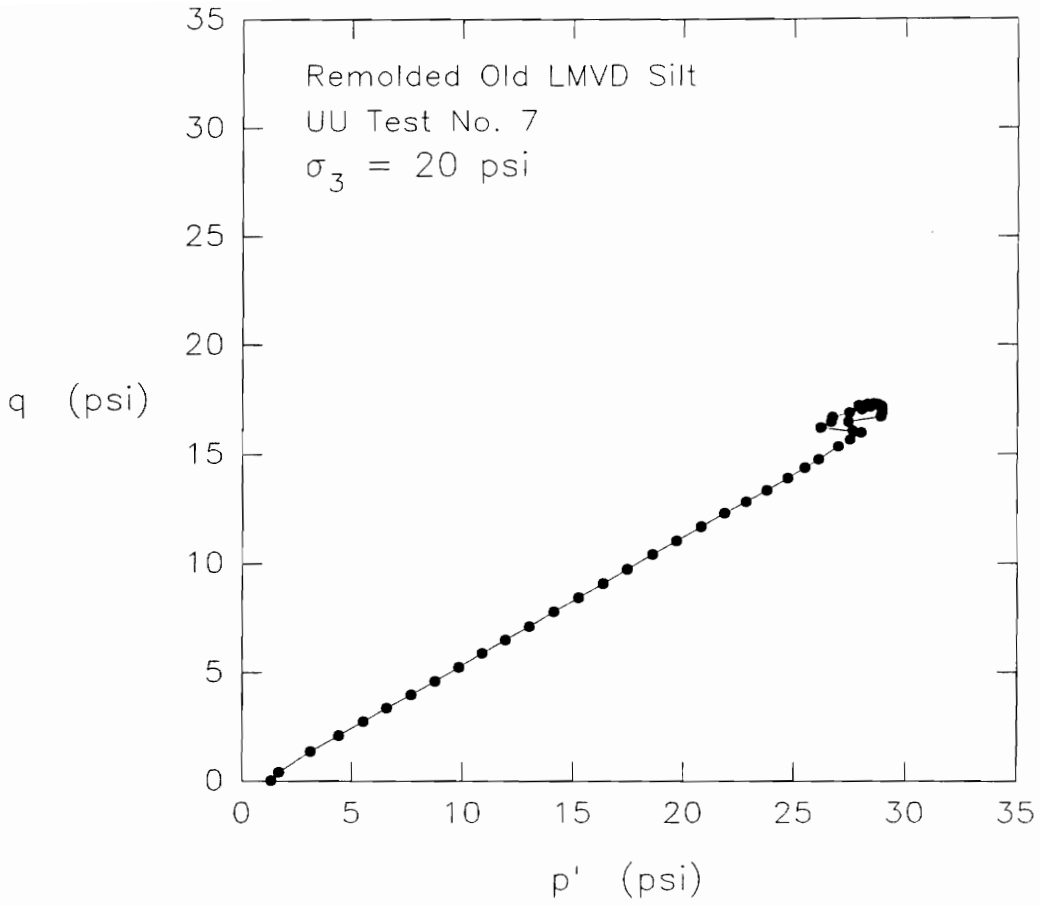


Figure 5.39. Effective stress path measured in UU test 7 on remolded LMVD silt

corresponds to a value of effective stress friction angle, ϕ' , of 37° . This illustrates that the effective stress parameters of dilatant silts are very easily determined from triaxial tests in which pore water pressures are measured. It is the measurement and interpretation of undrained strengths which are most difficult, due to the dilatant tendencies of the soil.

It is debatable if the use of Eq. 5-1 to determine the pore water pressure of the specimens in which erratic pore pressure measurements occurred is reasonable. Equation 5-1 uses the total stresses which were measured in the tests to estimate the pore pressures within the specimens throughout the tests. In these tests with erratic pore pressure measurements, however, it is believed that the erratic pore pressure measurements resulted from the failure of the rubber cement seal at the needle-membrane interface. When this failure of the seal occurred, the specimens would have experienced drainage and the deviator stress-strain behavior of the specimens would have been influenced by this condition. Thus, the stresses used in Eq. 5-1 to estimate the pore pressures within the specimen were for specimens which very likely experienced drainage during shear, rather than the total stresses for truly undrained specimens. This makes the use of Eq. 5-1 in these tests seem questionable.

5.5 Consolidated-Undrained Unloading Tests

A total of six consolidated-undrained unloading triaxial tests were conducted on specimens of LMVD silt. Two 1.4-inch diameter specimens and two 4-inch diameter specimens were used in these tests. The 1.4-inch diameter specimens consisted of one undisturbed specimen and one remolded specimen. Two consolidated-undrained unloading tests were performed on each of these 1.4-inch diameter specimens. This was accomplished by back pressure saturating the specimens, consolidating each specimen to a given anisotropic condition, and then performing an undrained unloading test on the specimen. This was followed by consolidating the same specimen to a higher anisotropic consolidation condition and performing a second undrained unloading test. The 4-inch diameter specimens tested were remolded from a slurry in a 5-inch diameter batch consolidometer and trimmed to a diameter of 4-inches. Both of the 4-inch diameter specimens were tested in a single consolidated-undrained unloading test.

These consolidated-undrained unloading tests were conducted primarily to measure values of the pore pressure parameter \bar{A}_u for unloading, in accordance with the perfect sampling approach of Ladd and Lambe (1963). The specimens were anisotropically consolidated to a K_c value equal to 2.5, where $K_c = \sigma_1'_{con}/\sigma_3'_{con}$. This value of K_c was based

on an assumption that the material had a value of K_0 in-situ equal to $1 - \sin \phi' = 0.4$, where ϕ' was assumed to be equal to 37° . Table 5.7 gives the initial properties of the two 1.4-inch diameter triaxial specimens used in the CU unloading tests.

Table 5.7: Initial properties of the 1.4-inch diameter specimens used in the CU unloading tests

Sample No.	w (%)	γ_d (pcf)	Initial S (%)	e
1	21.5	108.8	96.6	0.542
2*	18.3	79.9	44.8	1.102

* Undisturbed specimen of new LMVD silt

Table 5.8 gives the approximate initial properties of the two 4-inch diameter triaxial specimens used in the CU unloading tests. It should be noted that the initial properties in Table 5.8 are approximate since they are based on the water content of the trimmings rather than that of the specimens themselves. In addition, initial sample dimensions used in the calculations were only measured using approximate methods.

Table 5.8: Approximate initial properties of the 4-inch diameter specimens of remolded LMVD silt used in the CU unloading tests

Sample No.	w (%)	γ_d (pcf)	Initial S (%)	e
3	21.6	100.4	86	0.672
4*	26.3	98.1	100	0.679

* New LMVD silt

The procedure used for the unloading tests on the 1.4-inch diameter samples was as follows:

- 1.) The sample was first back-pressure saturated and consolidated to an isotropic consolidation stress of 10 psi.
- 2.) The sample was then sheared drained at a slow rate of strain until a K_c value of 2.5 was achieved. The deviator stress was maintained until full anisotropic consolidation had occurred.
- 3.) The drainage valve to the triaxial specimen was then closed and the deviator stress was slowly reduced in small increments until isotropic stress conditions were obtained.
- 4.) The sample was then consolidated to an isotropic stress equal to 20 psi. The process of anisotropically consolidating the specimen to a K_c value of 2.5, followed by undrained unloading of the sample was then repeated.
- 5.) At the end of the second unloading under undrained conditions, the sample was once again consolidated isotropically to 20 psi, and then sheared undrained in a conventional manner.

Consolidated-undrained unloading tests were also performed on 4-inch diameter specimens of remolded LMVD silt. In addition to performing these tests to measure the value of the pore pressure parameter \bar{A}_u for unloading, the use of 4-inch diameter specimens also provided samples for Q tests which could be used to evaluate the effects of the sampling process on Q test results. After completing the consolidated-undrained unloading tests, the 4-inch diameter specimens could be split into quarters. These quarters could then be trimmed to provide four 1.4-inch diameter triaxial specimens for testing.

The 4-inch diameter silt specimens used in these unloading tests were initially consolidated from a slurry in a 5-inch diameter batch consolidometer. After removal from the batch consolidometer, the soil was rough-trimmed to a diameter of 4-inches, placed in a triaxial cell and back pressure saturated. The specimens were then anisotropically consolidated to a K_c value equal to 2.5, based on the assumption that the material had a value of K_0 in-situ equal to $1 - \sin 37^\circ = 0.4$.

The procedure for performing these tests followed steps 1 through 3 of the procedure given above for the 1.4-inch diameter specimens, except that the specimens were initially consolidated to an isotropic consolidation stress

of 26 psi rather than 10 psi. After the unloading test was completed and isotropic stress conditions had been reached, the drainage valves were opened, and the cell pressure and back pressure were reduced simultaneously, with the objective of maintaining the effective isotropic consolidation stress at a constant value. After the back pressure was reduced to zero, the cell pressure was also reduced to zero while drainage was allowed. The sample was then removed from the triaxial cell, split into quarters, and the quarters were then trimmed to 1.4-inch diameter specimens for use in other tests.

For one of the 4-inch diameter specimens, 3 of the 4 quarters were trimmed into 1.4-inch diameter specimens and tested in Q tests with midheight pore pressure monitoring. The fourth quarter was trimmed to a 1.4-inch diameter specimen and was tested in a conventional CU test. For the other 4-inch diameter specimen, only 3 of the 4 quarters could be trimmed to give 1.4-inch diameter specimens and these were tested in Q tests without midheight pore pressure monitoring.

Shown in Figure 5.40 are the effective stress paths measured for the undrained unloading tests conducted on the 1.4-inch diameter specimen of remolded LMVD silt. For the 1.4-inch diameter undisturbed specimen, the unloading

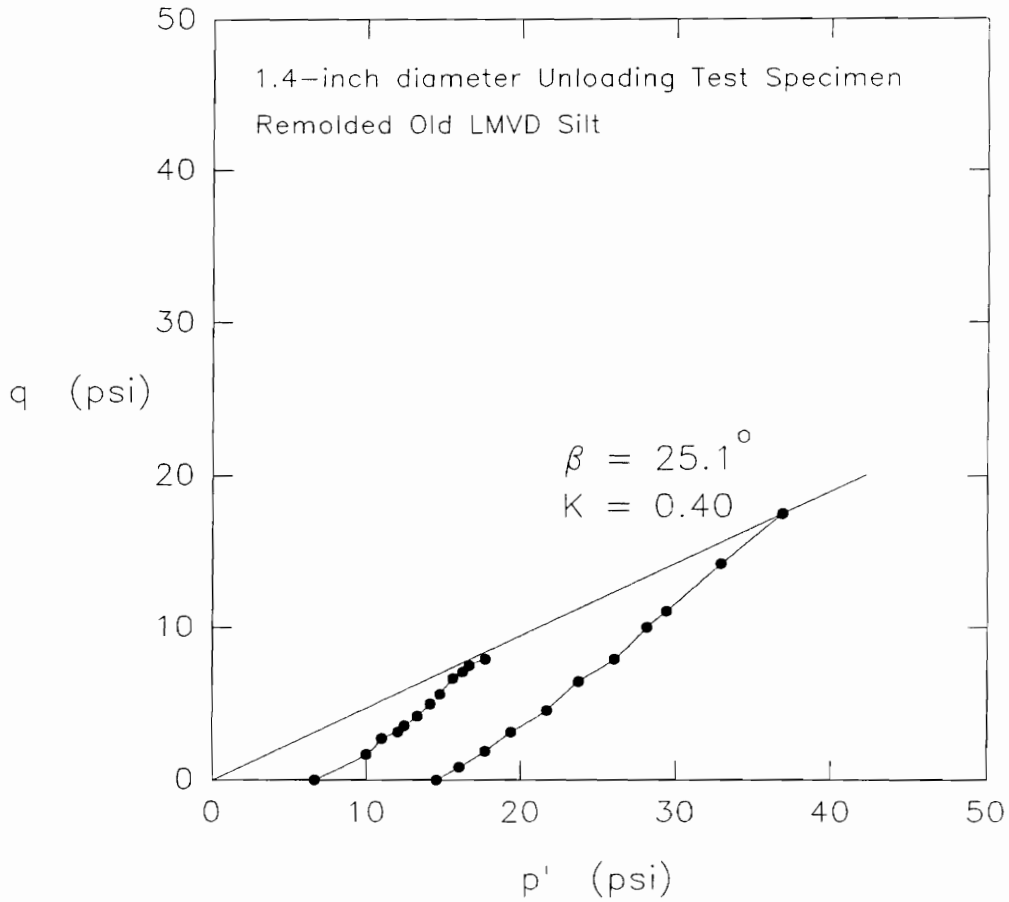


Figure 5.40. Stress paths measured for the consolidated-undrained unloading tests conducted on the 1.4-inch diameter specimen of remolded old LMVD silt

stress paths are shown in Figure 5.41. Figures 5.42 and 5.43 show the stress paths measured for the two undrained unloading tests conducted on 4-inch diameter specimens of remolded LMVD silt.

The values of \bar{A}_u were calculated for each step of the unloading process in accordance with the procedure of Ladd and Lambe (1963), using the equation:

$$\bar{A}_u = \frac{\Delta u_d}{\left(\Delta \sigma_1 - \Delta \sigma_3 \right)} \quad (5-2)$$

where: \bar{A}_u = the pore pressure parameter, \bar{A} , for unloading,

Δu_d = the change in pore water pressure resulting from a change (decrease) in deviator stress acting on the specimen, and

$\Delta \sigma_1 - \Delta \sigma_3$ = the change in deviator stress (total stress) acting on the specimen.

For the unloading portion of the tests, σ_3 was constant so that $\Delta \sigma_3 = 0$. The value of $\Delta \sigma_1$ was equal to the change in vertical stress measured from the start of the unloading test to the end of a given step of the unloading. The value of $\Delta \sigma_1$ was controlled by manually decreasing the vertical load on the specimen in step-like increments. For each increment of decreasing vertical load, the change in minor principal effective stress, $\Delta \sigma_3'$, from the initial value at the start of the test was

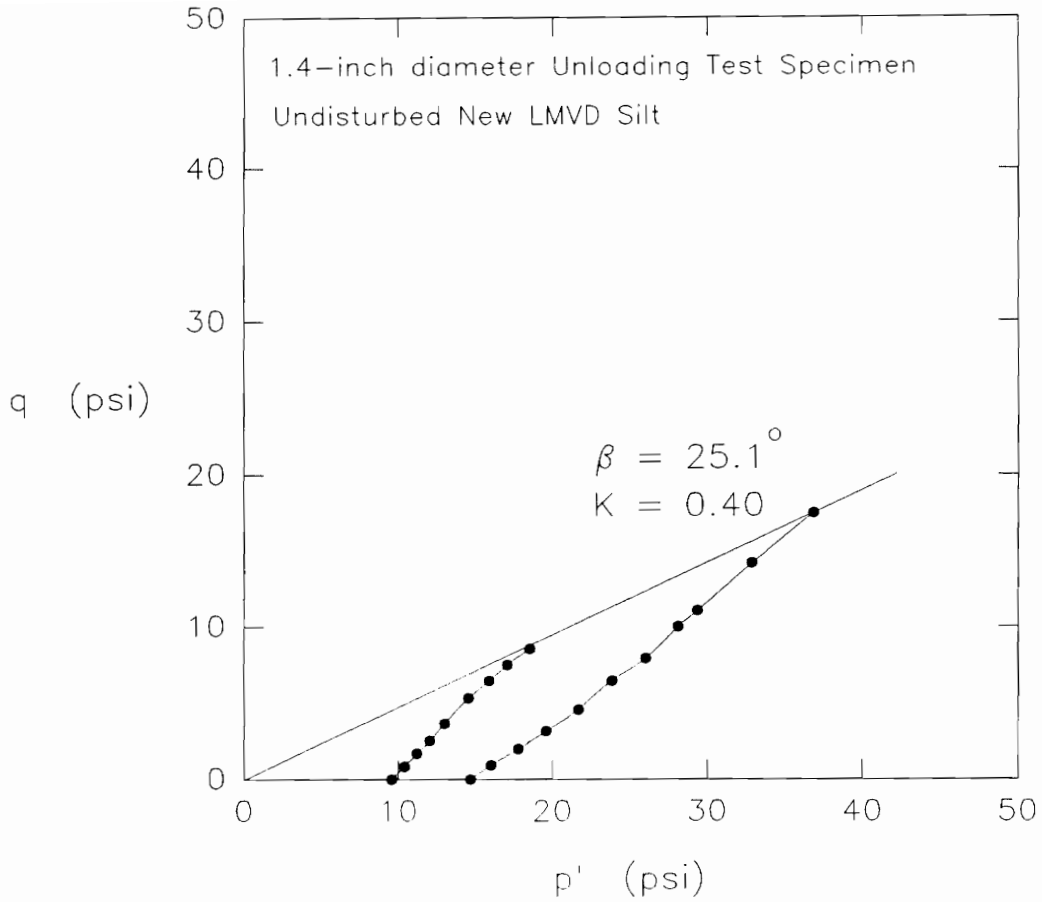


Figure 5.41. Stress paths measured for the consolidated-undrained unloading tests conducted on the 1.4-inch diameter specimen of undisturbed new LMVD silt

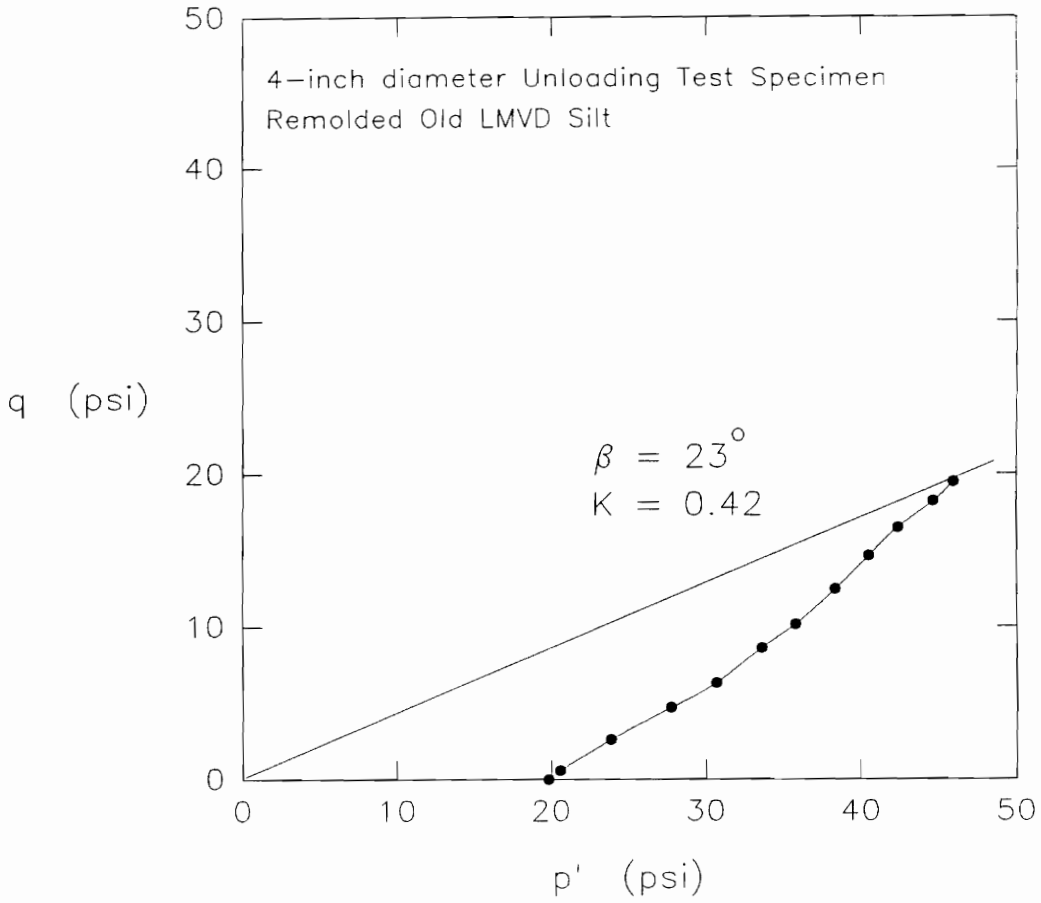


Figure 5.42. Stress path measured for the consolidated-undrained unloading test conducted on the 4-inch diameter specimen of remolded old LMVD silt

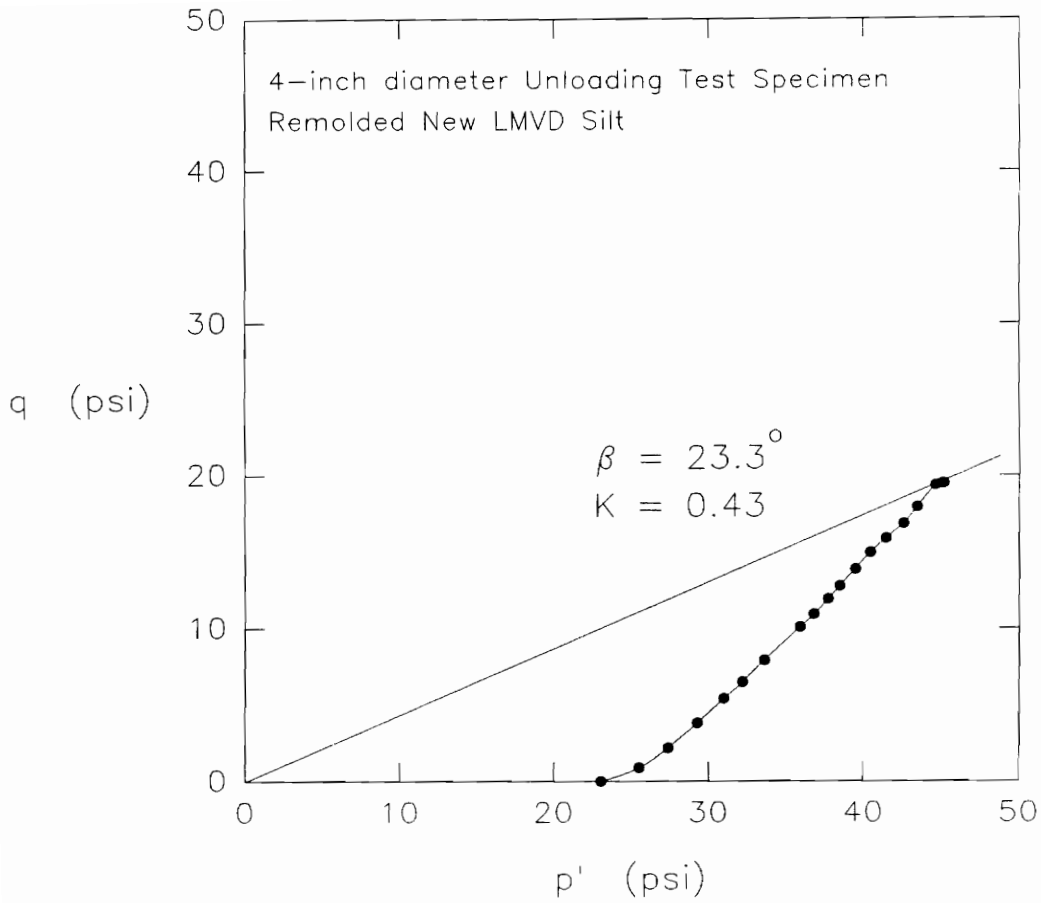


Figure 5.43. Stress path measured for the consolidated-undrained unloading test conducted on the 4-inch diameter specimen of remolded new LMVD silt

measured. The measured value of $\Delta\sigma_3'$ was equal to the change in pore water pressure, Δu_d , resulting from the decrease in deviator stress on the specimen. Using this information, the value of \bar{A}_u was calculated at the end of each step in the unloading process.

The values of \bar{A}_u calculated from the undrained unloading tests are given in Table 5.9. The values of \bar{A}_u were calculated based on the changes in vertical stress $\Delta\sigma_1$, and pore water pressure, Δu_d , which occurred from the start of the unloading tests, where anisotropic stress conditions existed, to the end of the tests when isotropic stress conditions had been reached.

Table 5.9: \bar{A}_u values measured for undrained unloading tests conducted on LMVD silt

Sample	σ_3' con (psi)	σ_1' con (psi)	\bar{A}_u
1.4-in. dia. Undisturbed*	10	25	0.0
1.4-in. dia. Undisturbed*	20	50	-0.1
1.4-in. dia. Remolded	10	25	0.0
1.4-in. dia. Remolded	20	50	-0.1
4-in. dia. Remolded	26	65	-0.2
4-in. dia. Remolded*	26	65	-0.1

* New LMVD silt

As can be seen from Table 5.9, the values of \bar{A}_u measured in the undrained unloading tests range from 0 to -0.2 with an average value of -0.1. These values of \bar{A}_u

are similar to the values ranging from 0 to -0.1, reported for clayey silt by Ladd and Lambe (1963).

5.5.1 CU Tests

After completion of the undrained unloading tests, the two 1.4-inch diameter specimens were sheared in CU tests. Shown in Figure 5.44 are the deviator stress-strain behavior and the minor principal effective stress-strain behavior for the shear portion of the test conducted on the remolded silt specimen. The specimen did not reach a peak deviator stress over the range of strain tested, and exhibited dilative tendencies. The test results are very similar to those reported by Brandon, Duncan, and Huffman (1990) for CU triaxial tests conducted on remolded LMVD Silt.

Plots of principal stress ratio versus axial strain along with the effective stress path for the CU test specimen are given in Figure 5.45. The stress path for the test, shown in Figure 5.45b, defines the K_f line for the silt, and yields an angle α of 31° . This corresponds to an effective stress friction angle, ϕ' , equal to 37° .

Shown in Figure 5.46 are the deviator stress-strain behavior and the minor principal effective stress-strain behavior for the shear portion of the test conducted on the

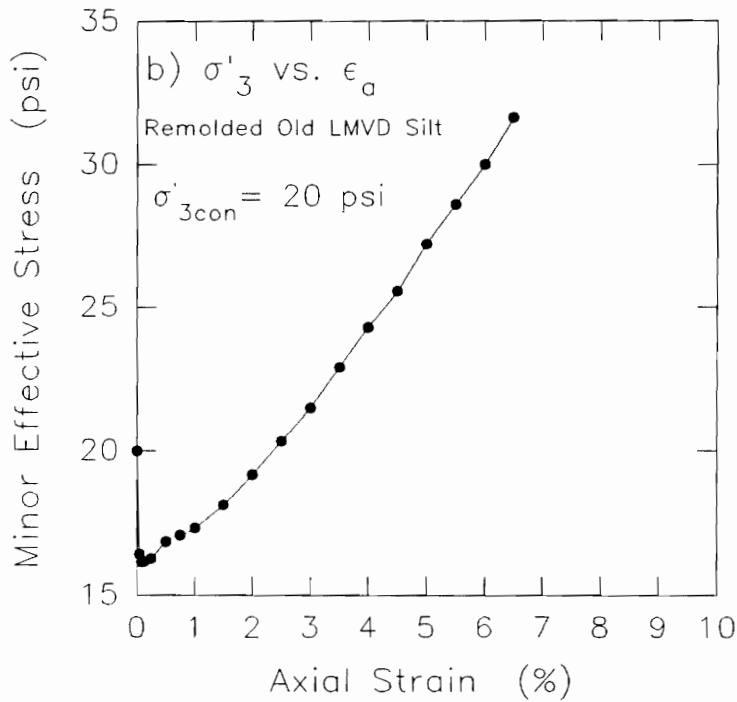
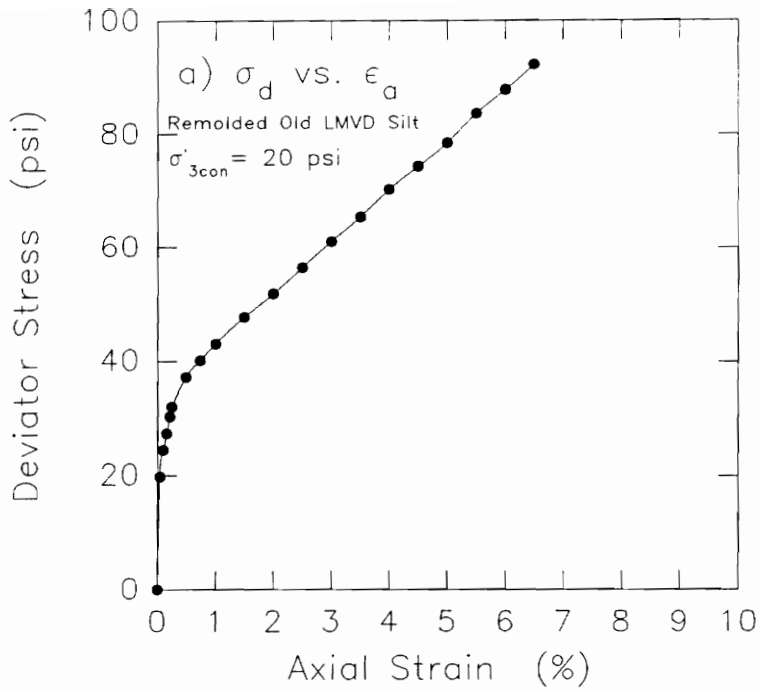


Figure 5.44. Deviator stress-strain behavior and minor principal effective stress-strain behavior for the consolidated-undrained test conducted on remolded LMVD silt

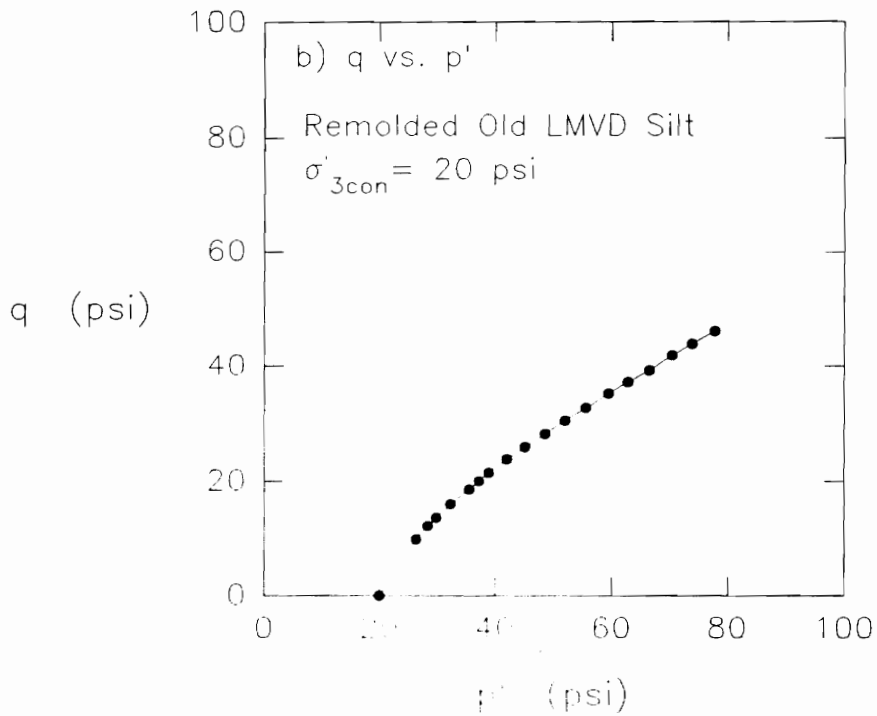
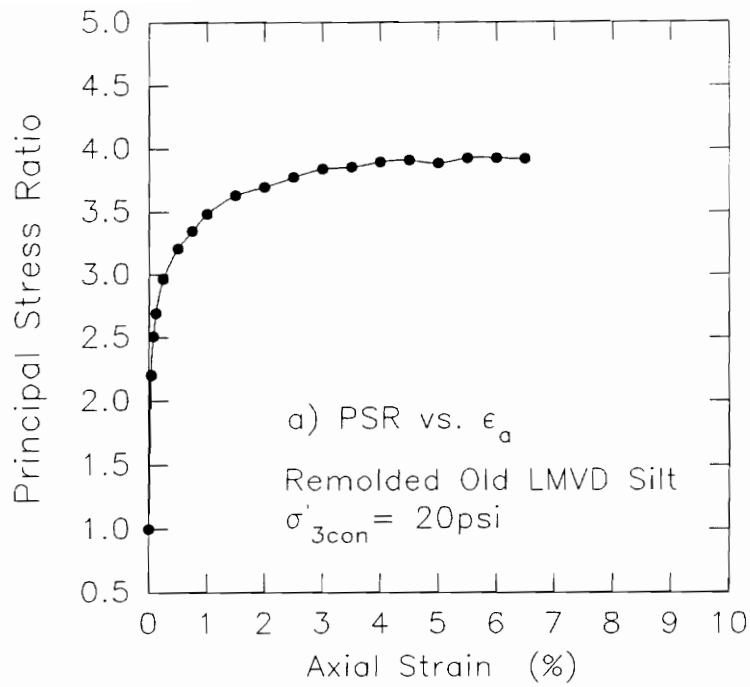


Figure 5.45. Principal stress ratio-strain relationship and effective stress path measured in the CU test on the unloading test sample of remolded old LMVD silt

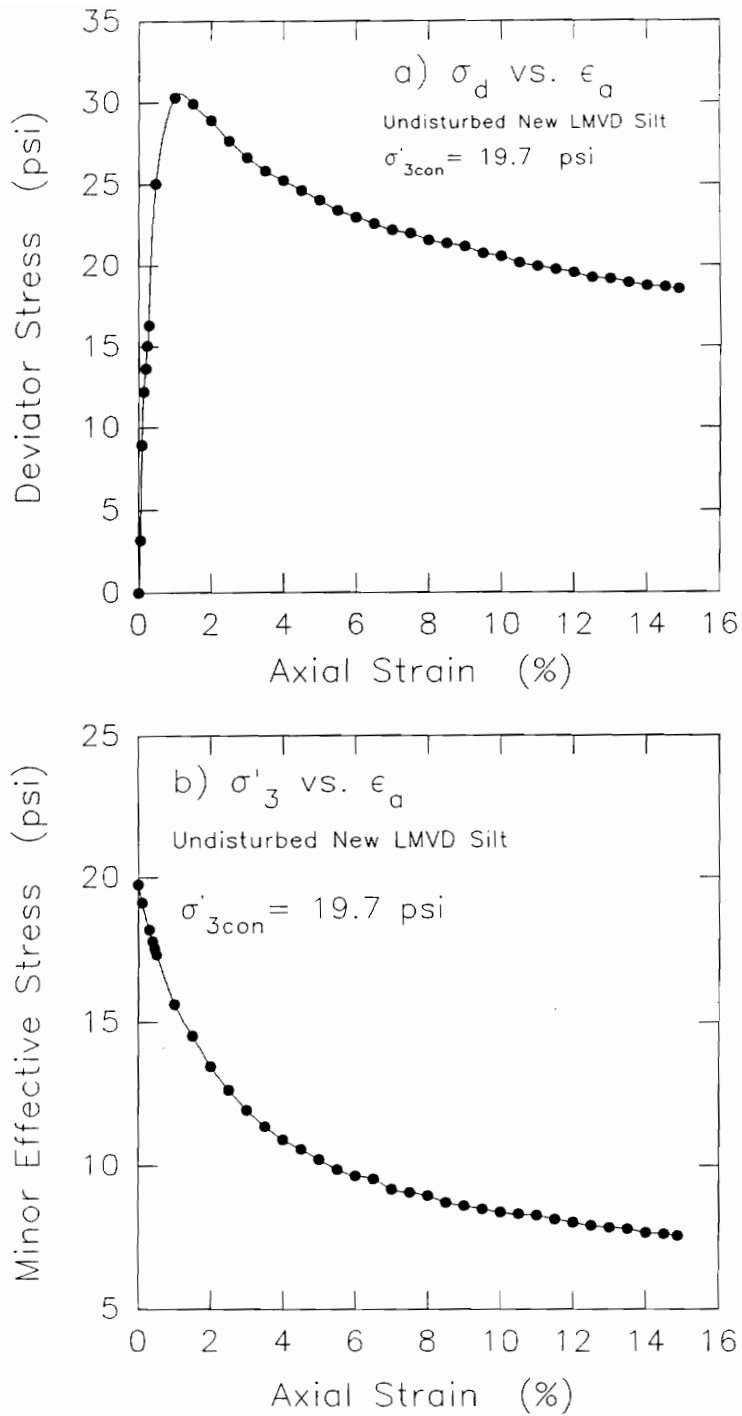


Figure 5.46. Deviator stress-strain behavior and minor principal effective stress-strain behavior for the consolidated-undrained test conducted on undisturbed LMVD silt

undisturbed silt specimen. Unlike the remolded sample, the undisturbed sample reached a peak deviator stress at about 1% axial strain, and exhibited strain softening behavior with increasing strain. The sample also exhibited compressive tendencies. The pore pressure continuously increased during the test. For tests conducted on remolded LMVD silt, and undisturbed and remolded Yazoo silt, Brandon, Duncan, and Huffman (1990), never observed compressive tendencies.

Plots of principal stress ratio versus axial strain along with the effective stress path for the CU test specimen are given in Figure 5.47. The stress path for the test, shown in Figure 5.47b, defines the K_f line for the silt. In this case, the K_f line gives an angle α of 27° and a q -intercept, d , of 1.02 psi. These correspond to an effective stress friction angle, ϕ' , equal to 31° , and a value of cohesion, c' , equal to 1.21 psi.

Similar to the undisturbed UU test specimen, the undisturbed CU test specimen had a very low dry density and was highly fissured. These characteristics may have been the cause of the strain softening behavior and compressive tendencies observed in this test.

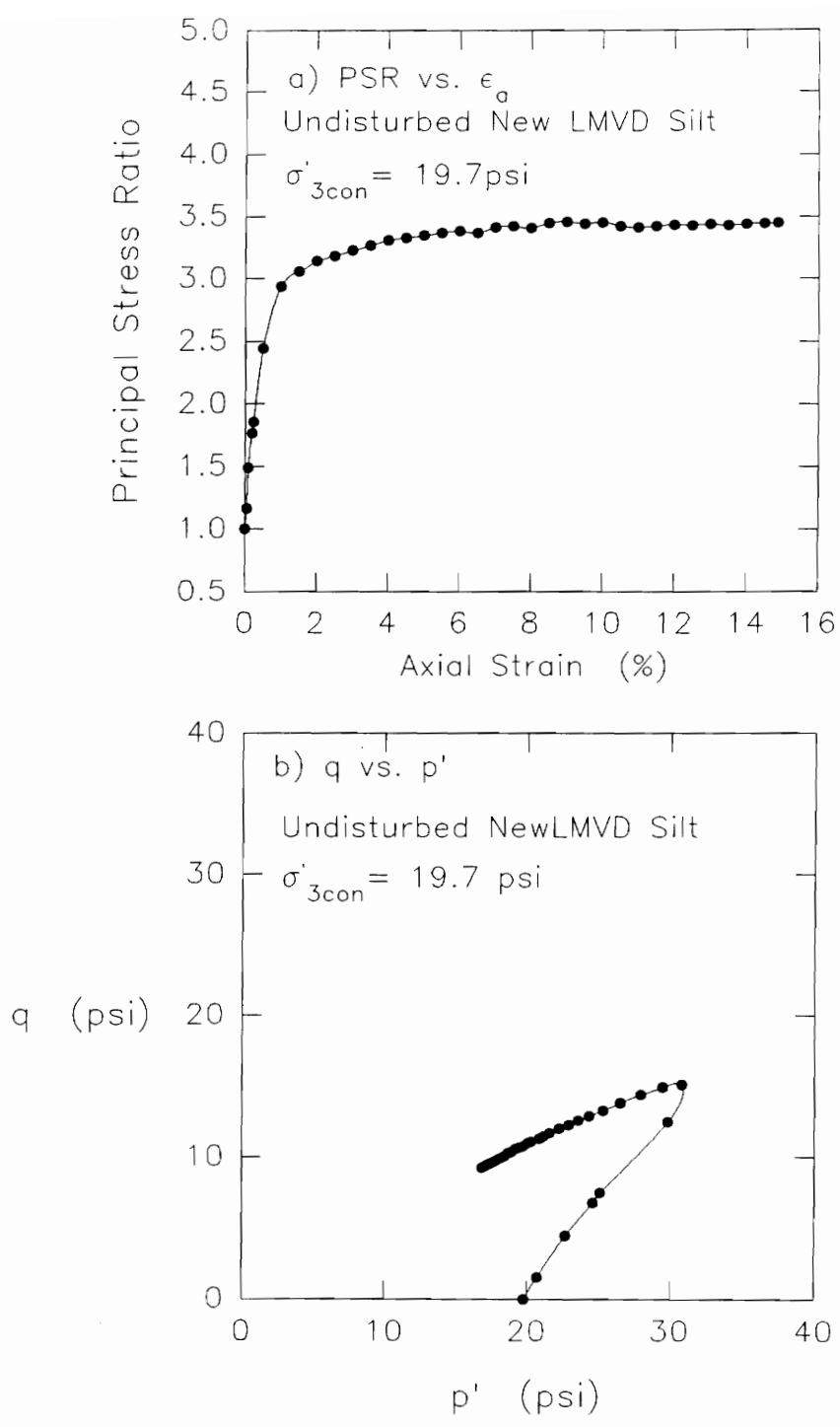


Figure 5.47. Principal stress ratio-strain relationship and effective stress path measured in the CU test on the sample of undisturbed new LMVD silt tested in an unloading test

One of the quarters of the 4-inch diameter consolidated-undrained unloading test specimen of old LMVD silt was trimmed to a 1.4-inch diameter by 3-inch high triaxial specimen and tested in a CU test. This CU test was used to define the K_f line for the silt for use in evaluating the pore pressure response of the three Q tests performed on the other three quarters. The CU test specimen was consolidated to 10.5 psi and its initial properties are given in Table 5.10.

Table 5.10: Initial properties of the remolded old LMVD silt CU test specimen trimmed from the 4-inch diameter unloading test specimen ($\sigma_3'_{con} = 10.5$ psi)

Property	Initial Value
w (%)	20.9
γ_d (pcf)	107.6
Initial S (%)	100
e	0.559

Figure 5.48 shows plots of deviator stress vs. axial strain and effective stress vs. axial strain. Plots of principal stress ratio vs. axial strain along with the effective stress path for the CU test specimen are given in Figure 5.49. The stress path for the test, shown in Figure 5.49b, defines the K_f line for the silt, and yields an angle α of 30° . This corresponds to an effective stress friction angle, ϕ' , equal to 35° .

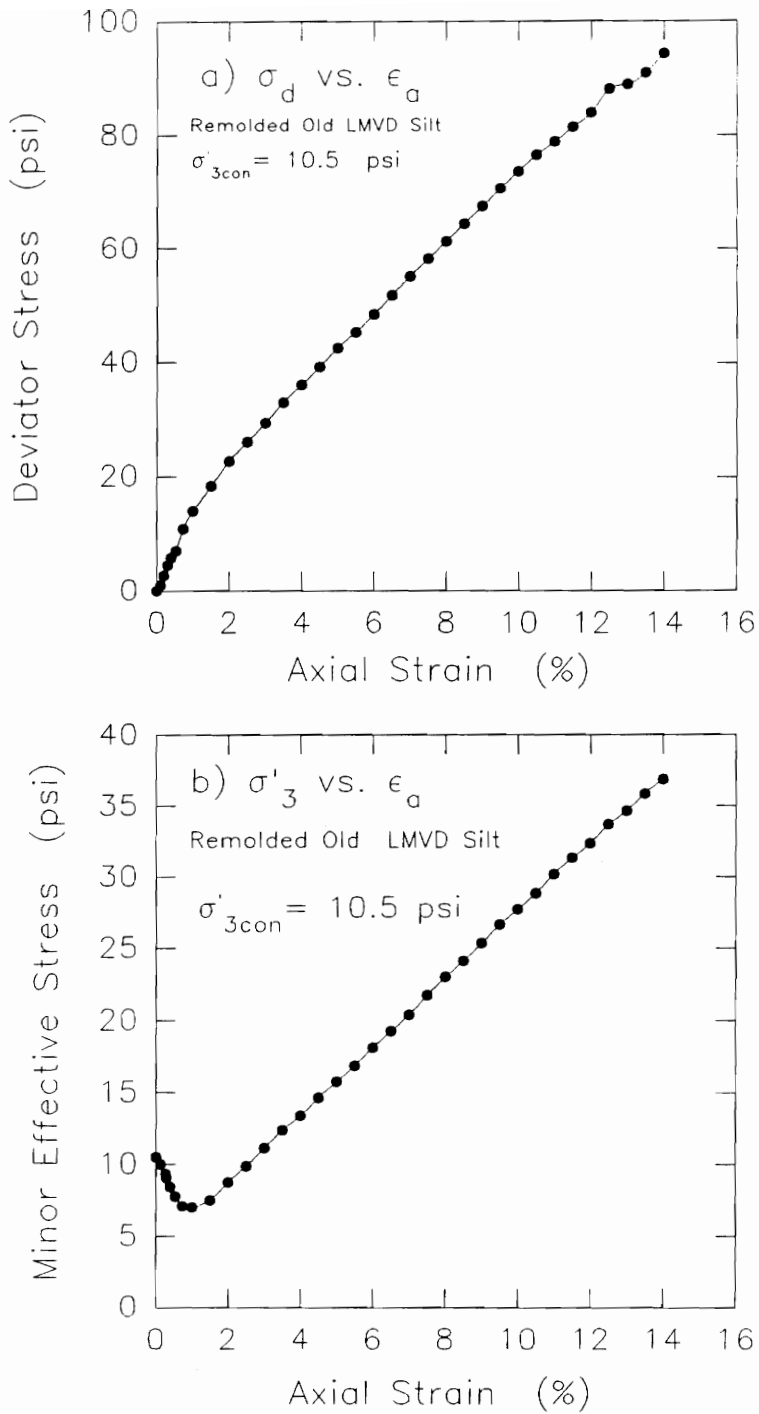


Figure 5.48. Deviator stress-strain and effective stress-strain relationships measured in the CU test on the sample of remolded old LMVD silt obtained from the 4-inch diameter unloading test specimen

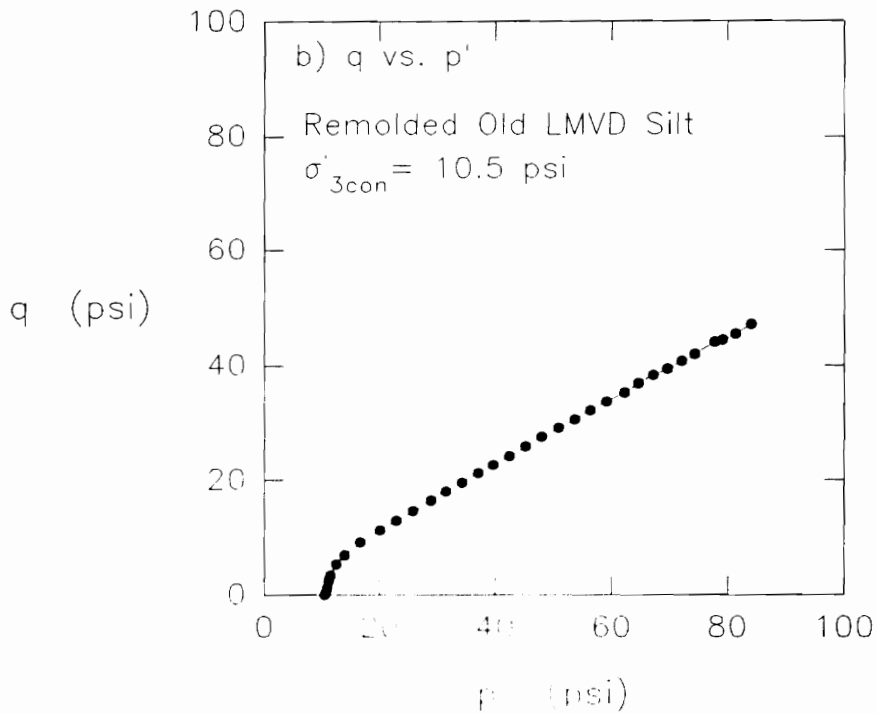
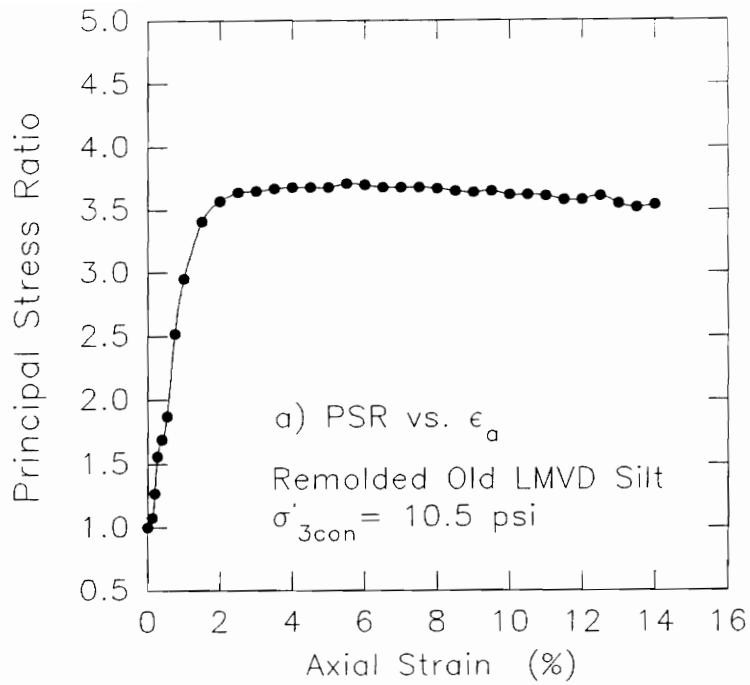


Figure 5.49. Principal stress ratio-strain relationship and effective stress path measured in the CU test on the sample of remolded old LMVD silt obtained from the 4-inch diameter unloading test specimen

5.5.2 Q Tests from Unloading Test Specimens

Three of the quarters obtained from each of the two 4-inch diameter consolidated-undrained unloading test specimens were trimmed to 1.4-inch diameter by 3-inch high triaxial specimens and tested in Q tests within 24 hours after completing the unloading tests. For one set of three Q tests, pore pressures were monitored at the midheight of the specimens. For the other set of three Q tests, pore pressures were not measured during the tests. The initial properties of the Q test specimens are given in Table 5.11.

Table 5.11: Initial properties of the remolded LMVD silt Q test specimens obtained from the quarters of the 4-inch diameter unloading test specimens

Sample No.	σ_3 (psi)	w (%)	γ_d (pcf)	S (%)	e
UU-22	0	20.2	107.0	95.4	0.569
UU-23	10	20.4	107.7	98.4	0.558
UU-24	20	20.9	106.4	97.3	0.578
UU-25*	0	25.5	98.5	96.7	0.705
UU-26*	10	25.4	99.6	99.8	0.686
UU-27*	20	25.6	98.8	97.2	0.699

* New LMVD silt - no pore pressure measurements

As can be seen from Table 5.11, all of the Q test specimens had degrees of saturation less than 100 percent. This may be the result of dissolved air having come out of solution from the pore water during the unloading tests. Most of the Q tests performed on specimens obtained from batch consolidometer samples and discussed in Section 5.4, had degrees of saturation of 100 percent. The samples

tested here were also obtained from batch consolidometer samples which had been prepared in the same manner as for the other Q test specimens discussed in Section 5.4.

The only difference between these Q test samples and the Q tests described in Section 5.4, was that these samples underwent undrained unloading to simulate sampling of the soil, whereas the other specimens were not subjected to undrained unloading conditions. The undrained unloading may have resulted in air coming out of solution from soil pore water making these Q test specimens less than 100 percent saturated.

Figure 5.50a shows plots of deviator stress vs. axial strain for Q test specimens UU-22, UU-23, and UU-24. As can be seen from this figure, for all three Q tests, the deviator stress underwent a similar increase with increasing axial strain up to about 5.5 or 6 percent axial strain. The deviator stress then decreased slightly with increasing axial strain and then began increasing again. The erratic stress-strain behavior observed for these Q test specimens at strains above 5.5 or 6 percent, may possibly be due to disturbance caused by the midheight pore pressure monitoring system.

The stress-strain curves in Figure 5.50a show that up to an axial strain of about 5.5 or 6 percent, the stress-

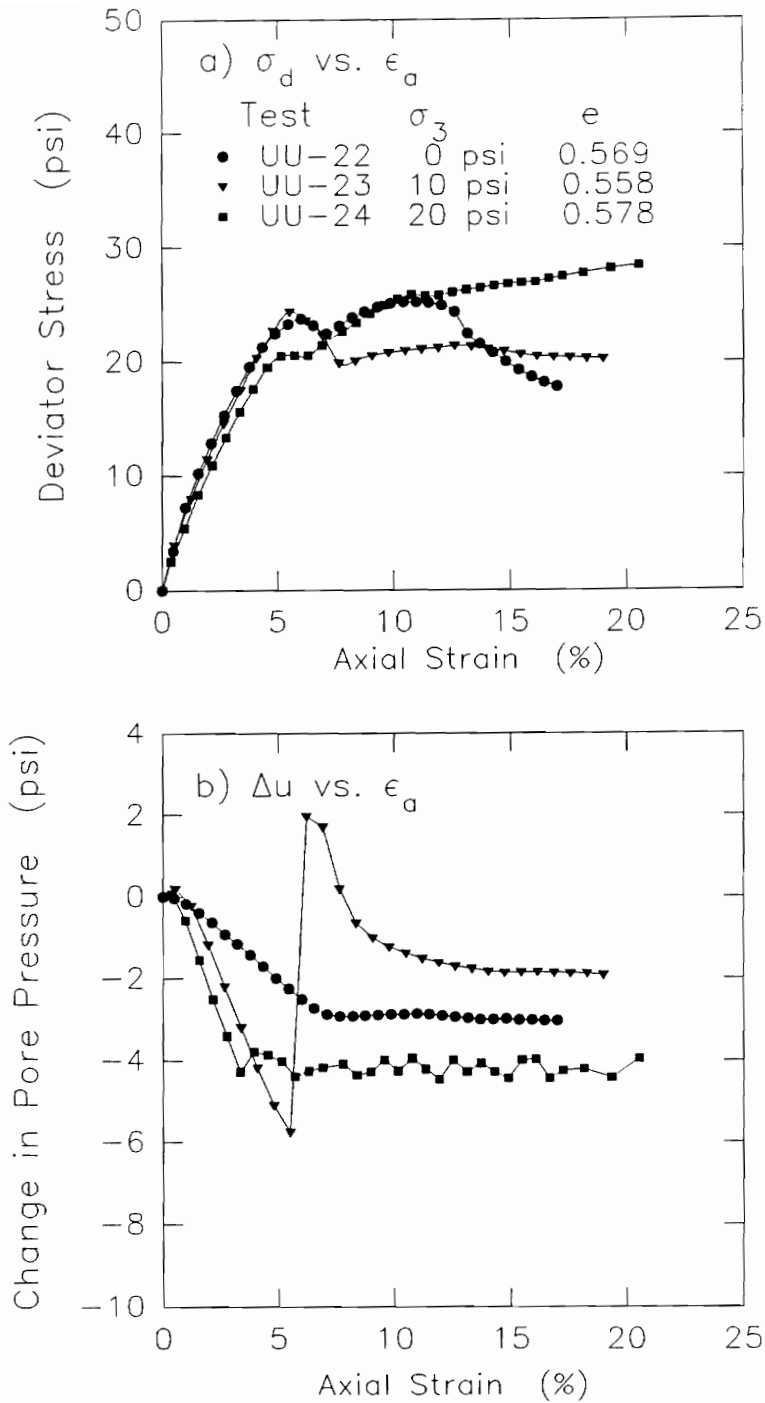


Figure 5.50. Deviator stress-strain and change in pore pressure-strain relationships measured in UU tests 22, 23, and 24 performed on samples trimmed from the quarters of the 4-inch diameter undrained unloading test specimen of remolded old LMVD silt

strain behavior of the three Q tests performed at confining pressures of 0, 10, and 20 psi are very nearly the same. With failure defined as an axial strain of 5 percent, Mohr's circles for the three tests have been plotted in Figure 5.51. This plot shows an undrained strength envelope for the silt which approaches a $\phi_u = 0$, $S_u = c = 12$ psi condition.

Although the deviator stress-strain curves were somewhat erratic at higher axial strains, the occurrence of a $\phi_u = 0$, $S_u = c$ envelope at an axial strain of 5 percent suggests that the time between sampling saturated silt specimens and performing Q tests on them may have some effect on the Q test results. These Q tests were performed relatively quickly (within 24 hours) after performing the unloading test on the 4-inch diameter specimen. If a longer time had elapsed between the undrained unloading test and performing the Q tests, perhaps a more erratic Mohr-Coulomb strength envelope would have been obtained. The occurrence of a $\phi_u = 0$, $S_u = c$ envelope is also somewhat surprising since the specimens were less than fully saturated. Perhaps this did not influence the behavior until strains greater than 5 percent had been reached.

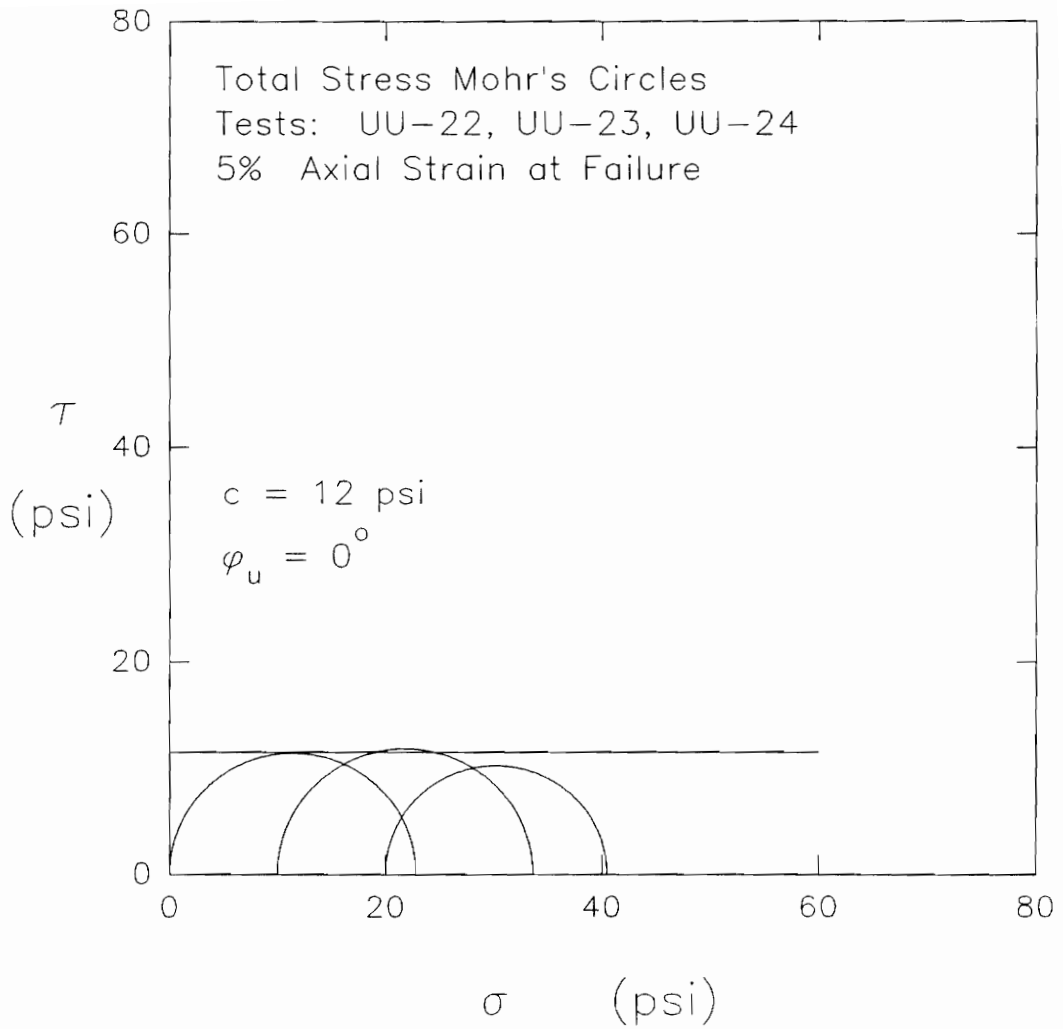


Figure 5.51. Total stress Mohr's circles for the three Q tests performed on samples of remolded old LMVD silt obtained from the 4-inch diameter unloading test specimen

Figure 5.50b shows plots of the change in pore pressure measured in these three Q test specimens. As can be seen from this figure, two of the tests showed erratic pore pressure responses beginning at axial strains of 3 and 3.5 percent. These erratic pore pressure responses can possibly be attributed to problems with the midheight pore pressure monitoring system. Test specimen UU-23, performed at a cell pressure of 10 psi, showed an abrupt increase in pore pressure that indicated a positive net change in pore pressure within the specimen. This type of pore pressure response had not been encountered in any of the previous tests in which erratic pore pressure measurements occurred.

As noted in Section 5.4.4, for the Q test specimens where erratic pore pressure measurements occurred, the pore pressure at failure that theoretically would occur, can be estimated based on the maximum total stresses, using Eq. 5-1. For a given test, the pore pressure throughout the test can be estimated assuming that the effective stress path follows the K_f line. The effective stress friction angle used in Eq. 5-1 could be varied to adjust the values of pore pressure calculated, so that these estimated pore pressures would closely correspond to the pore pressures actually measured during the early stages of the test.

Figure 5.52 shows the variations between the estimated and measured changes in pore pressure for the two Q tests where erratic pore pressure responses were observed. Effective stress friction angles of 43.5 and 40.5 degrees were used in Eq. 5-1 for Q tests UU-23 and UU-24, respectively. These high values were necessary so that the pore pressures calculated by Eq. 5-1 corresponded with the pore pressures measured in these two tests at axial strains of 5 and 3.5 percent, respectively. As pointed out in Section 5.4.4, however, in tests in which the pore pressure monitoring system may have failed and allowed the sample to experience drainage, the applicability of Eq. 5-1 is questionable.

Based on the measured or calculated change in pore pressure for the three Q tests, the maximum change in pore pressure and the minimum absolute pore pressure in each sample during testing have been determined and are presented in Table 5.12.

Table 5.12: Maximum change in pore pressure and minimum absolute pore pressure measured or calculated in the three Q tests on remolded LMVD silt

Test No.	σ_{cell} (psi)	Δu_{max} (psi)	u_{min} (psi abs)	Method
UU-22	0	-3.0	10.3	Measured
UU-23	10	-5.5	15.9	Calculated
UU-24	20	-7.7	24.4	Calculated

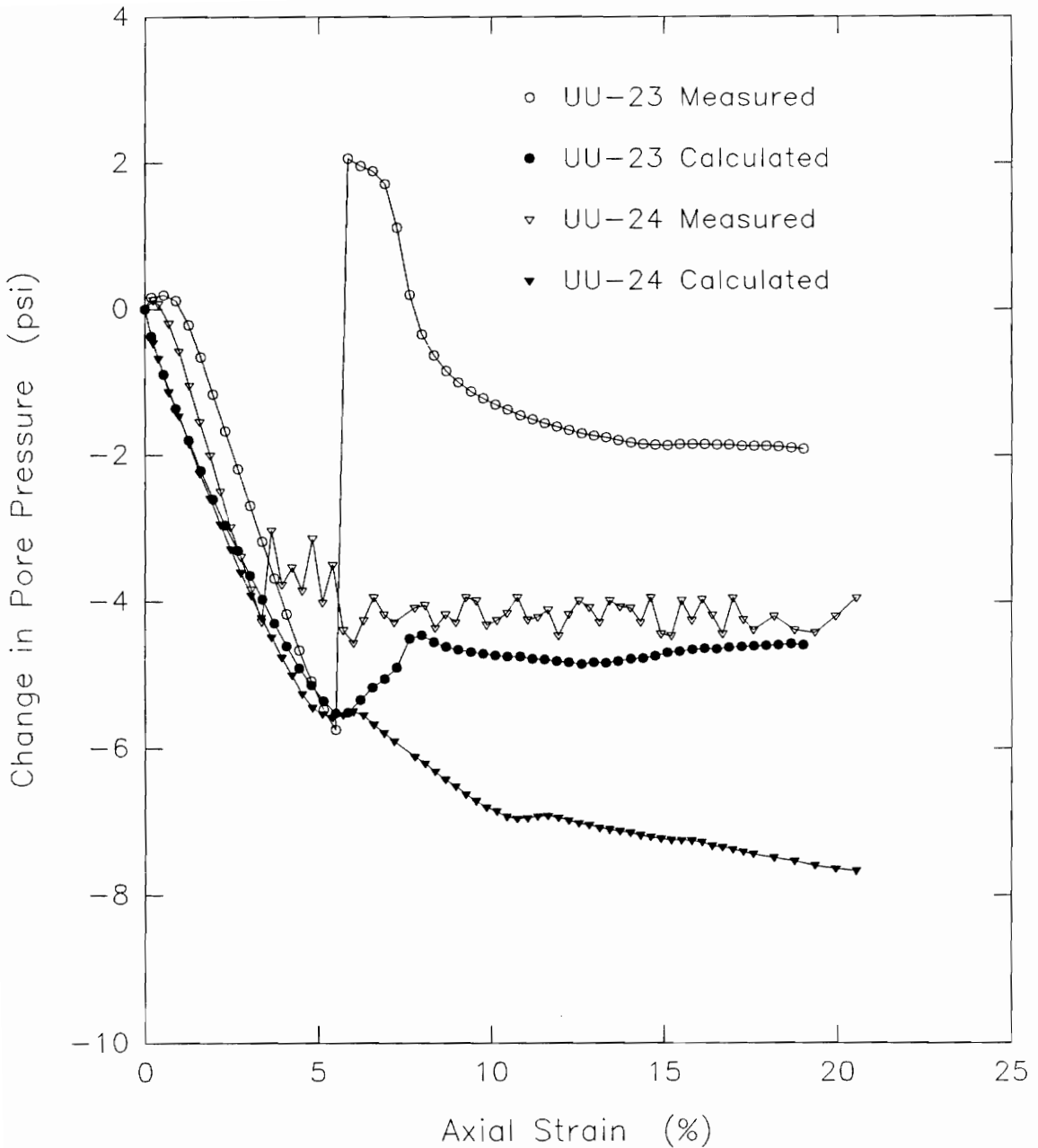


Figure 5.52. Calculated and measured change in pore pressure-strain relationships for UU tests 23 and 24 performed on samples trimmed from quarters of the 4-inch diameter undrained unloading test specimen of remolded LMVD silt

For the three Q tests, the maximum change in pore pressure was negative in all cases, as expected for a material with dilatant tendencies. The maximum change in pore pressure increased with increasing cell pressure. The change in pore pressure varied from -3 psi for the unconfined compression test to -7.7 psi for the Q test performed at a cell pressure of 20 psi. For all three Q tests, the minimum absolute pore pressure was greater than -1 atmosphere (0 psia) or the pressure at which vaporous cavitation would be expected to occur. The unconfined compression test was the only test in which the minimum absolute pore pressure was less than atmospheric pressure (13.7 psia at Virginia Tech, EL 2080 feet above sea level). The minimum absolute pore pressure varied from 10.3 psia for the unconfined compression test to 24.4 psia for the Q test performed at a cell pressure of 20 psi (33.7 psia).

This would tend to indicate that vaporous cavitation did not occur during these three Q tests on samples of close to fully saturated remolded LMVD silt. Gaseous cavitation could possibly have occurred due to such pressure reductions, depending on the dissolved air content of the pore water, and the duration of the pressure reduction. In addition, since the specimens were somewhat less than fully saturated, air bubbles were present within the specimens initially. These air bubbles could have

grown larger within the pores of the soil as pore pressures decreased during undrained shear, in accordance with Boyle's law. The formation and growth of gas bubbles within the pores of the soil could have affected the undrained behavior of the soil. However, at an axial strain of 5 percent, the occurrence of an approximate $\phi_u = 0$, $S_u = c$ strength envelope may indicate that gaseous cavitation had not occurred or existing bubbles had not expanded to the extent that they influenced the undrained stress-strain behavior of the soil. At axial strains above 5 percent, gas exiting solution and gas bubbles growing larger may have affected the undrained behavior of the soil, leading to the erratic behavior observed.

Figure 5.53 shows plots of deviator stress vs. axial strain for Q test specimens UU-25, UU-26, and UU-27, trimmed from the 4-inch diameter unloading test specimen of remolded new LMVD silt. These Q tests were performed without midheight pore pressure measurements.

As can be seen from this figure, for all three Q tests, the deviator stress increased with increasing axial strain until 5.5 or 6 percent strain. For the unconfined compression test, UU-25, and test UU-26 performed at a confining pressure of 10 psi, at strains above 5.5 or 6 percent, the deviator stress decreased until 7.5 to 8

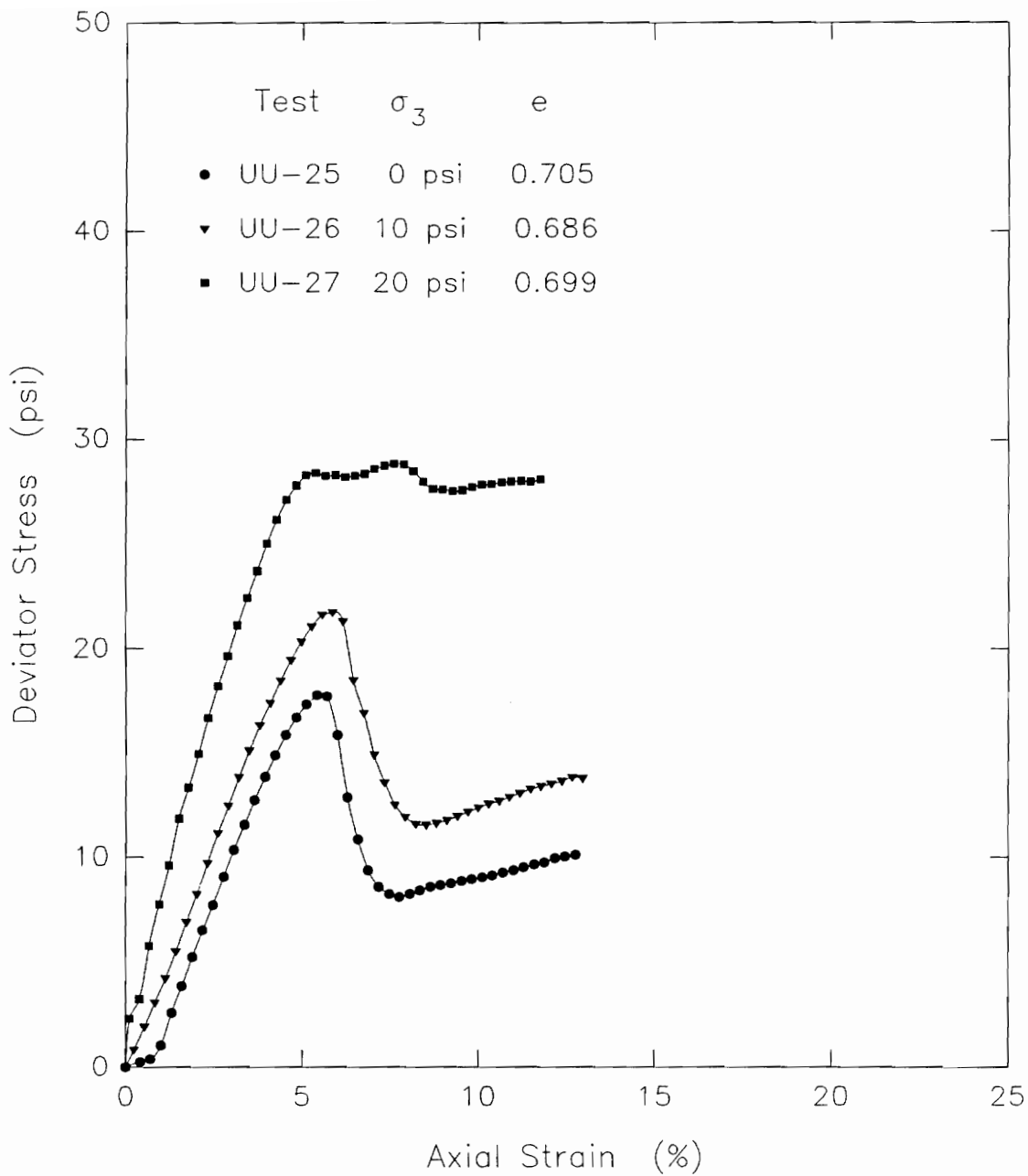


Figure 5.53. Deviator stress-strain relationships measured in UU tests 25, 26, and 27 performed on samples trimmed from quarters of the 4-inch diameter undrained unloading test specimen of remolded new LMVD silt

percent axial strain and then underwent a gradual increase with further increase in strain. For Q test UU-27 performed at 20 psi confining pressure, once the deviator stress peaked at an axial strain of about 5.5 percent it underwent little variation with increasing strain.

For the three confining pressures used, the deviator stress-strain curves given in Figure 5.53 show considerable variation in the magnitude of the deviator stress, at any given strain. The deviator stress and therefore the undrained strength of the soil increased with increasing cell pressure. Based on the peak deviator stress for each of the three tests at axial strains of about 5.5 or 6 percent, total stress Mohr's circles have been plotted in Figure 5.54. This plot shows that the undrained strength of the soil is characterized by a cohesion intercept of 7 psi and an undrained friction angle, ϕ_u , equal to 12°.

5.6 Q Tests Performed in Prepressurization Study

Based on the review of the cavitation literature, there appears to be considerable support for the concept that subjecting a liquid to high pressures for a short period of time can make the liquid less likely to cavitate during a pressure decrease. As discussed in Chapter 3, cavitation of a liquid is believed to be influenced by the presence of nuclei within the liquid. These nuclei are

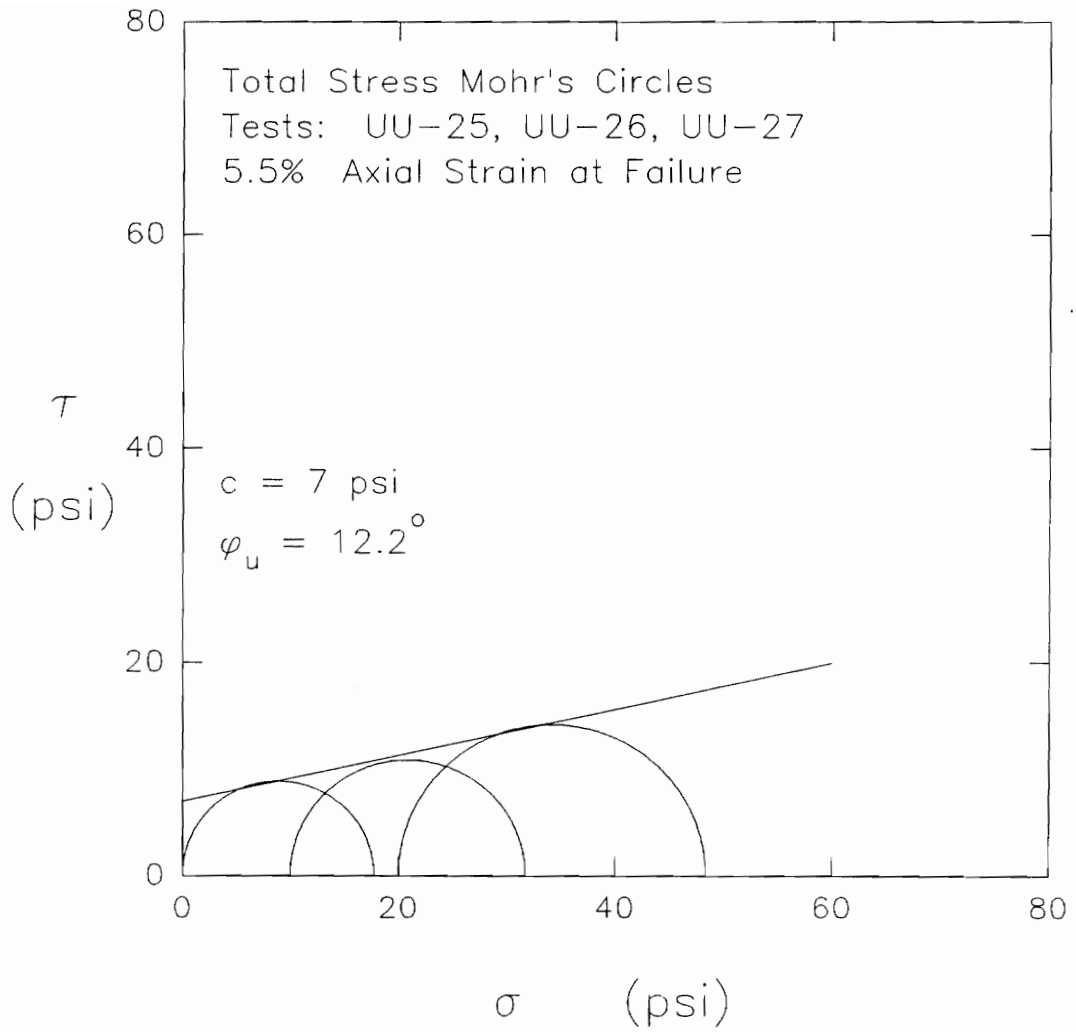


Figure 5.54. Total stress Mohr's circles for the three Q tests performed on samples of remolded new LMVD silt obtained from the 4-inch diameter unloading test specimen

felt to exist as pockets of undissolved gas trapped in cracks and crevices on solid surfaces in contact with the liquid. When a decrease in pressure occurs, these gas-filled nuclei can grow into visible bubbles. The application of high pressure to a liquid forces the liquid up into the unwetted cracks and crevices which may be present on solid surfaces in contact with the liquid. The high pressure dissolves the gas pockets in the cracks and crevices and eliminates the cavitation nuclei from the liquid.

Prepressurization of the liquid essentially eliminates the gas-liquid interfaces present in the liquid by dissolving the gas pockets trapped in the cracks and crevices on the surfaces of solid particles and more fully wetting the solid. When the pressure is released, the recently dissolved gas remains in solution since there are no longer any gas-liquid interfaces in the liquid which the gas can diffuse across to form a bubble.

Prepressurization pressures as high as 16,000 psi have been used to prevent cavitation of liquids (Harvey et al., 1944b, 1945; Pease and Blinks, 1947; Plesset, 1949). Other researchers have found that lower pressures, on the order of 100 to 500 psi, have had some effect in delaying the

onset of cavitation in liquids until higher tensions have been reached (Knapp, 1958; Hayward, 1970).

A preliminary investigation of this concept has been made on saturated silt specimens. High cell pressures were applied to saturated silt Q test specimens for a short time under undrained conditions in order to remove cavitation nuclei from soil pore water. This was followed by removing the high cell pressure and performing Q tests at normal cell pressures, in order to see what effect the application of high pressure had on the undrained behavior of saturated silts.

When a saturated silt specimen is placed in a triaxial cell with no drainage allowed and a high cell pressure is applied, the applied cell pressure will be carried by the pore water and not the soil structure. This is because the specimen is saturated and water is essentially incompressible. The high cell pressure, therefore, should not affect the void ratio of the specimen or its strength. The high pressure in the pore water would cause the water to move into the unwetted cracks and crevices on the surfaces of the silt particles. After a period of time, the high cell pressure could be reduced to the cell pressure at which the Q test is to be conducted. A series of Q tests performed at different cell pressures, after the

specimens had been prepressurized, may show some noticeable effect of the prepressurization on the measured strength values and the Mohr-Coulomb strength envelope of the silt, when compared to a series of tests on similar samples not subjected to a high cell pressure prior to testing.

Several uncertainties are involved in this approach. First and foremost is whether or not the specimen is 100 percent saturated. If the specimen is less than 100 percent saturated, the application of the prepressurization will alter the void ratio and the strength characteristics of the specimen, making this procedure unacceptable. This may be the case for the silt specimens tested, due to the difficulty with which silts become fully saturated (Smith and Browning, 1942). Triaxial specimens of silts may also contain small bubbles of gas as a result of sampling stress release and temperature increase.

An analysis can be performed to consider what effect the prepressurization pressure might have on the void ratio of Q test specimens. Based on a number of the Q test specimens tested in this research, a typical initial void ratio, e_i , of 0.530 can be assumed. For a saturated sample of this soil, the volume of water, V_w , and voids, V_v , will be equal. The degree of saturation, S , will therefore be:

$$S = \frac{V_w}{V_v} \times 100\% = 100\% \quad (5-3)$$

For the saturated specimen, the volume of soil solids, V_s , can be related to the volumes of voids and water and the void ratio using the equation:

$$V_s = \frac{V_v}{e_i} = \frac{V_w}{e_i} \quad (5-4)$$

If another soil sample is assumed to have the same volumes of water and solids as above, but is not fully saturated, the volume of voids can be related to the degree of saturation and volume of water by the equation:

$$V_v = \frac{V_w}{S} \quad (5-5)$$

The initial void ratio that the specimen would have for degrees of saturation less than 100% can then be calculated as follows:

$$e = \frac{V_v}{V_s} = \frac{V_w/S}{V_w/e_i} = \frac{e_i}{S} = \frac{0.530}{S} \quad (5-6)$$

Table 5.13 gives the calculated initial values of void ratio, e , for various initial degrees of saturation, S .

Table 5.13: Initial void ratio for various initial degrees of saturation

S (%)	e
100	0.530
99	0.535
98	0.541
97	0.546
96	0.552
95	0.557

Review of Table 5.13 shows that for a specimen with an initial degree of saturation of 95%, if prepressurization of the specimen increased the degree of saturation to 100%, the void ratio would have only changed from 0.557 to 0.530. It is uncertain what effect this change in void ratio would have on the undrained strength measured in Q tests.

Results of the Q tests presented in Section 5.4 did not show consistent differences in undrained strength for specimens with different void ratios. Unconfined compression test specimens UU-10 and UU-12 had void ratios of 0.541 and 0.531. Specimen UU-10 had a higher undrained strength, even though it had a higher void ratio. Specimens UU-14 and UU-15 were tested at a cell pressure of 10 psi and had void ratios of 0.539 and 0.509. They had similar undrained strengths up through 10% axial strain. At higher strains the specimen with a higher void ratio, UU-14, gave slightly higher values of undrained strength. Specimens UU-18 and UU-19 were tested at a cell pressure of

20 psi and had void ratios of 0.541 and 0.524. They tended to have similar undrained strengths up to 12% axial strain. At higher strains, the specimen with the smaller void ratio, UU-19, gave higher values of undrained strength. The inconsistencies noted here make it difficult to assess the change in undrained strength that might occur if the prepressurization of the Q test specimens lead to decreases in the void ratios of the specimens, to values similar to those given in Table 5.13.

The small reduction in void ratio may result in some increase in shear strength. The change from a partially saturated condition to a fully saturated condition may lead to a much more significant change in undrained behavior than the slight change in void ratio would suggest.

This may be especially true for the undrained behavior of a material with a tendency to dilate. During undrained shear, the decrease in pore pressure in the partly saturated specimen could result in volume increase and corresponding decreases in the void ratio and degree of saturation of the soil. This volume increase could occur and have an influence on the behavior of the soil throughout the entire Q test. For the fully saturated specimen, the volume and void ratio of the specimen may remain constant for a significant portion of the test,

until some limiting negative pore water pressure is reached and cavitation occurs.

Review of the initial specimen data, to be presented subsequently, indicates that the Q test specimens used in this portion of the research had measured degrees of saturation of 100%. Even if the specimens were actually slightly less than fully saturated, their high degree of saturation would have resulted in the changes in void ratio being even smaller than indicated in Table 5.13. The void ratios measured for some of these Q test specimens obtained from the same batch consolidometer samples in this research, in fact, showed considerable variation as a result of limitations in measuring the specimen dimensions. In some cases, the measured void ratios of similar specimens actually varied more than the void ratio values presented in Table 5.13. Finally, it is emphasized that the volume of gases that might be trapped in cracks and crevices on the surfaces of the solid silt particles would be extremely small, probably only a fraction of a percent of the total volume of voids. This small volume is essentially undetectable by normal specimen measurement techniques and probably would not have a significant effect on the void ratio and strength of the soil.

Another uncertainty in this procedure was whether the magnitude of the prepressurization pressures available was adequate to prevent cavitation of soil pore water. The cavitation literature described the use of a wide variety of prepressurization pressures, many with success and some without. The triaxial cell used in this research had a maximum allowable cell pressure of 300 psi, thus limiting the pressure which could be used in this study.

An additional uncertainty involved the surface of the membrane surrounding the soil. This membrane was initially dry and when placed around the soil specimen, its desire to be wetted could possibly have absorbed water out of the specimen, thereby decreasing the degree of saturation of the soil. The surface of the membrane could also have contained cracks and crevices in which air pockets could have remained or it could very well have trapped small pockets of air between the sample and membrane. Regardless of the source, pockets of undissolved air could have served as nuclei for cavitation of pore water as attempted dilation of the specimen and decreasing pore pressures occurred during the shearing of the sample.

Although these limitations existed, a preliminary application of this theory has been performed on saturated silt Q test specimens. Five sets of Q tests have been

performed on specimens of remolded LMVD silt. The specimens were consolidated from a slurry in a batch consolidometer. Each batch provided four Q test specimens. The four specimens from each batch were tested at the same cell pressure. The cell pressures used for the first three batches were 0, 10, and 20 psi. Two additional sets of Q tests were performed at a cell pressure of 10 psi to further investigate the behavior at this cell pressure.

For each batch tested at a given cell pressure, two of the specimens were tested in a conventional Q test without prepressurization or midheight pore pressure monitoring. The other two specimens from the same batch were placed in the triaxial cell with no drainage allowed. Once in the triaxial cell, these specimens were subjected to a high cell pressure for a short period of time. The high cell pressure was then removed and the specimen was tested in a Q test at the same cell pressure as the two other specimens which had not been subjected to the high cell pressure prior to testing. In these tests as well, midheight pore pressure measurements were not performed.

The prepressurization was applied to the triaxial cell using a tank of compressed air. The triaxial cell used was rated for a maximum pressure of 300 psi. The prepressurization pressure applied to the samples ranged

from 200 to 260 psi and was applied for 15 to 20 minutes. Because of the limitations of the equipment used, after prepressurization, the cell pressure was reduced to atmospheric pressure before the specified Q test cell pressure could be applied.

Based on specimen dimensions measured prior to testing and water contents determined at the completion of the tests, the silt samples tested were essentially fully saturated and no drainage was allowed into or out of the samples. The application of the prepressurization pressure should therefore not have altered the void ratio of the samples significantly. Attempts were made to measure the specimen dimensions in the triaxial cell before and after the prepressurization pressure was applied to confirm that the specimen volumes did not change, but difficulties and uncertainties in making the sensitive measurements were encountered, and the results were inconclusive. Other techniques would be required to assess whether these samples were truly 100 percent saturated and whether or not the high pressure applied to the specimens lead to changes in sample void ratio, thereby influencing the strengths measured in the Q tests. As noted previously, however, the slight changes in void ratio which may have resulted from the application of the high pressure would have been small

and their influence on specimen strength may not have been very significant.

The results of the Q tests on prepressurized samples and those on similar samples not subject to prepressurization will now be presented.

Four Q tests were performed as unconfined compression tests ($\sigma_{cell} = 0$ psi). Two tests were performed on prepressurized samples and two were performed on non-prepressurized samples. The initial specimen data for these four tests are given in Table 5.14.

Table 5.14: Initial properties of the remolded LMVD silt unconfined compression test specimens used in the prepressurization study (Based on specimen dimensions measured prior to prepressurization)

Sample No.	Pre-pressurized	w (%)	γ_d (pcf)	S (%)	e
HP-5	Yes	22.3	109.3	100	0.536
HP-6	Yes	22.5	110.8	100	0.515
NHP-5	No	22.3	108.7	100	0.545
NHP-6	No	21.9	108.9	100	0.542

Figure 5.55 shows plots of deviator stress vs. axial strain for the four unconfined compression tests. It can be seen from this figure that the two prepressurized samples have very similar stress-strain curves while the two non-prepressurized samples have stress-strain curves

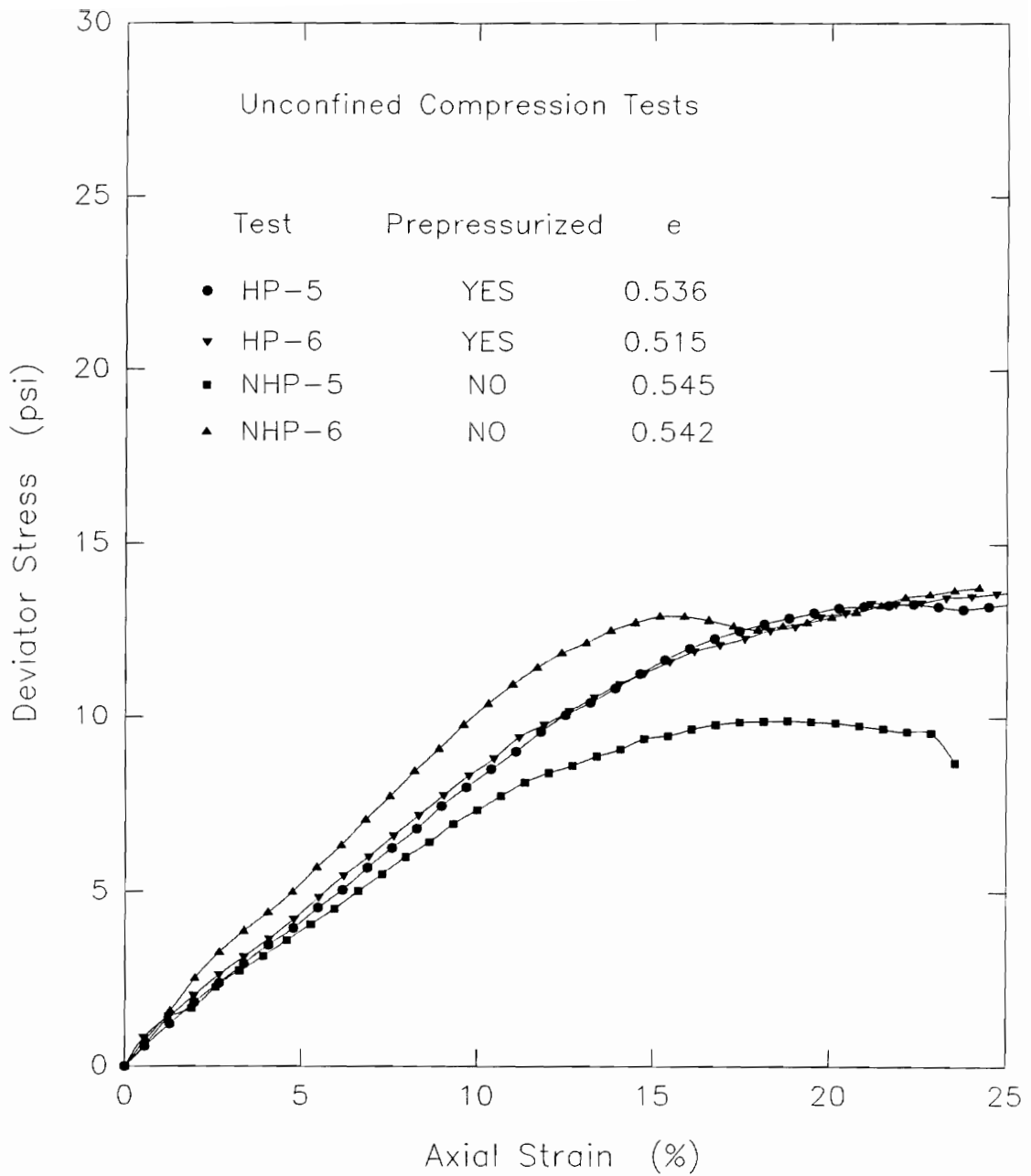


Figure 5.55. Deviator stress-strain relationships measured in the four unconfined compression tests performed on samples of remolded LMVD silt as part of the prepressurization study

which differ from those of the prepressurized samples as well as from each other.

Three batches of specimens were tested at a cell pressure of 10 psi. Four Q tests were performed from each batch and of the four tests, two tests were performed on prepressurized samples and two were performed on non-prepressurized samples. The initial specimen data for these twelve tests are given in Table 5.15.

Table 5.15: Initial properties of the remolded LMVD silt Q test specimens tested at a cell pressure of 10 psi in the prepressurization study (Based on specimen dimensions measured prior to prepressurization)

Sample No.	Pre-pressurized	w (%)	γ_d (pcf)	S (%)	e
HP-1	Yes	21.8	107.6	100	0.560
HP-2	Yes	22.1	106.7	100	0.573
NHP-1	No	21.9	107.4	100	0.563
NHP-2	No	21.8	108.2	100	0.551
HP-7	Yes	20.3	112.0	100	0.499
HP-8	Yes	20.1	112.4	100	0.493
NHP-7	No	20.5	111.6	100	0.504
NHP-8	No	20.1	112.1	100	0.497
HP-9	Yes	20.5	110.2	100	0.523
HP-10	Yes	20.5	110.4	100	0.520
NHP-9	No	20.6	112.0	100	0.498
NHP-10	No	20.5	111.4	100	0.507

Figures 5.56, 5.57, and 5.58 show plots of deviator stress vs. axial strain for the three sets of Q tests performed at a cell pressure of 10 psi. It can be seen from Figure 5.56 that there is no similarity between the stress-strain curves for any of the four samples in this

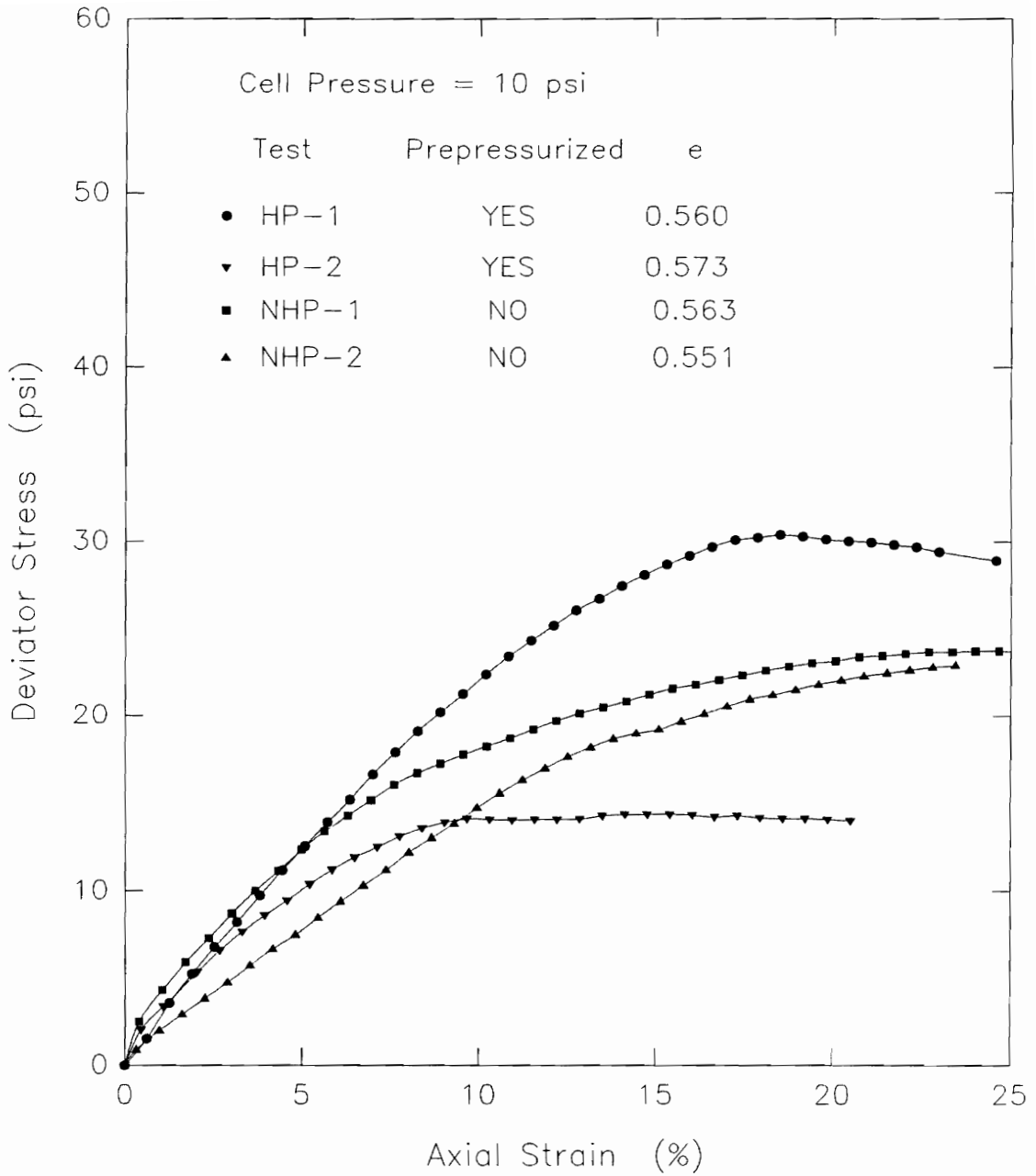


Figure 5.56. Deviator stress-strain relationships measured in the four Q tests performed at 10 psi cell pressure on samples of remolded LMVD silt as part of the prepressurization study

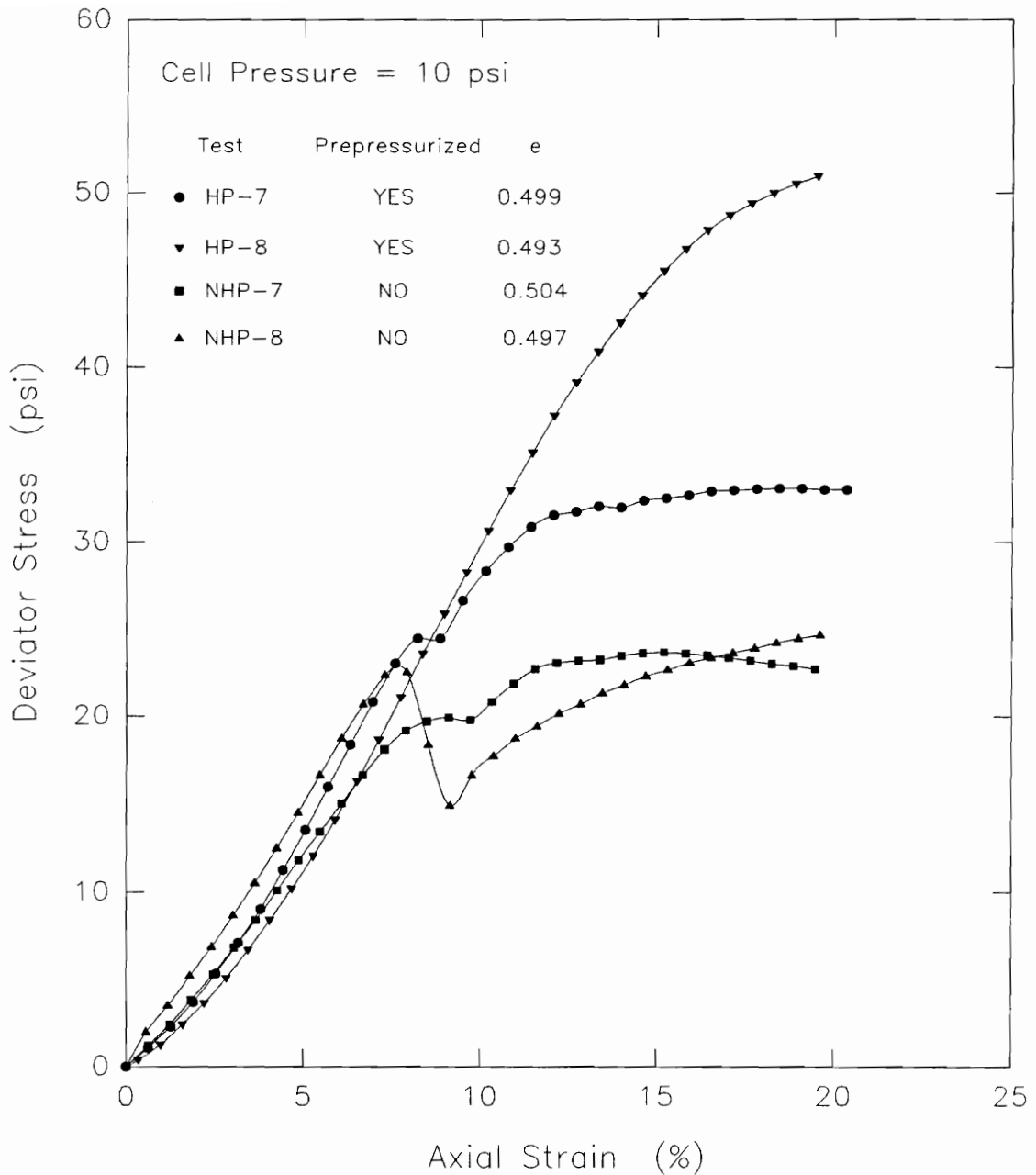


Figure 5.57. Deviator stress-strain relationships measured in the four Q tests performed at 10 psi cell pressure on samples of remolded LMVD silt as part of the prepressurization study

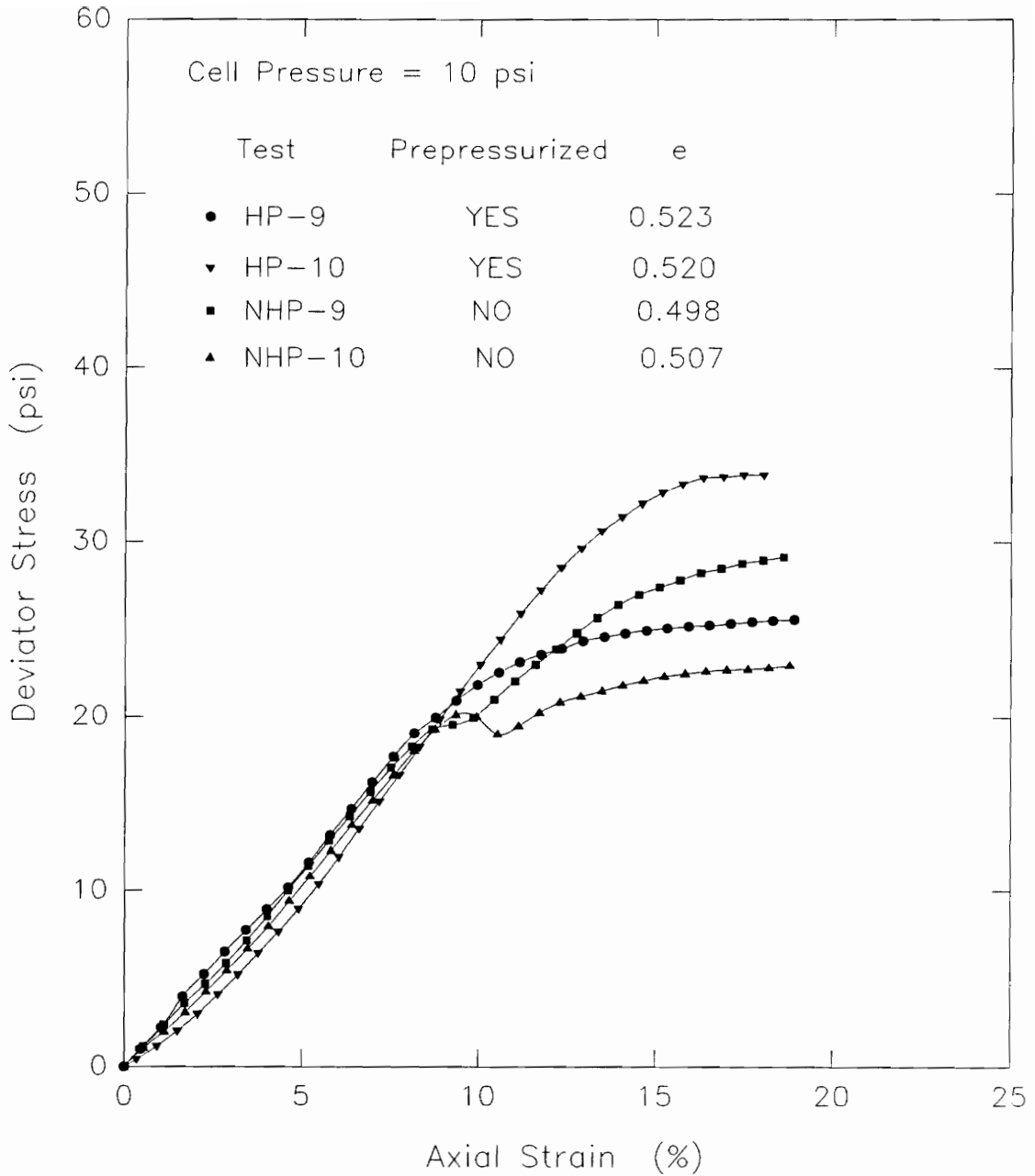


Figure 5.58. Deviator stress-strain relationships measured in the four Q tests performed at 10 psi cell pressure on samples of remolded LMVD silt as part of the prepressurization study

batch. The behavior of the two prepressurized samples differs considerably from each other and the two curves for the non-prepressurized samples are somewhat similar in shape but still show differences in magnitude.

For the four Q tests shown in Figure 5.57, the stress-strain curves are similar initially, up to an axial strain of about 7 or 8 percent. At higher strains, the behavior became more erratic in the two specimens not subjected to the prepressurization. One of the prepressurized specimens showed somewhat erratic behavior at higher strains, as well.

The stress-strain curves for the Q tests shown in Figure 5.58 were similar for all four tests, up to an axial strain of about 9 percent. At higher axial strains, the stress-strain behavior for the tests became more erratic. This erratic behavior was most noticeable in the two tests in which a high cell pressure was not applied to the specimens prior to performing the Q test.

Figure 5.59 shows the combined stress-strain curves for the twelve Q tests performed at a cell pressure of 10 psi in the prepressurization study. Figure 5.59a shows the curves for the six samples not subjected to prepressurization. The stress-strain curves for the six specimens subjected to a prepressurization pressure prior to performing the Q tests are shown in Figure 5.59b. As

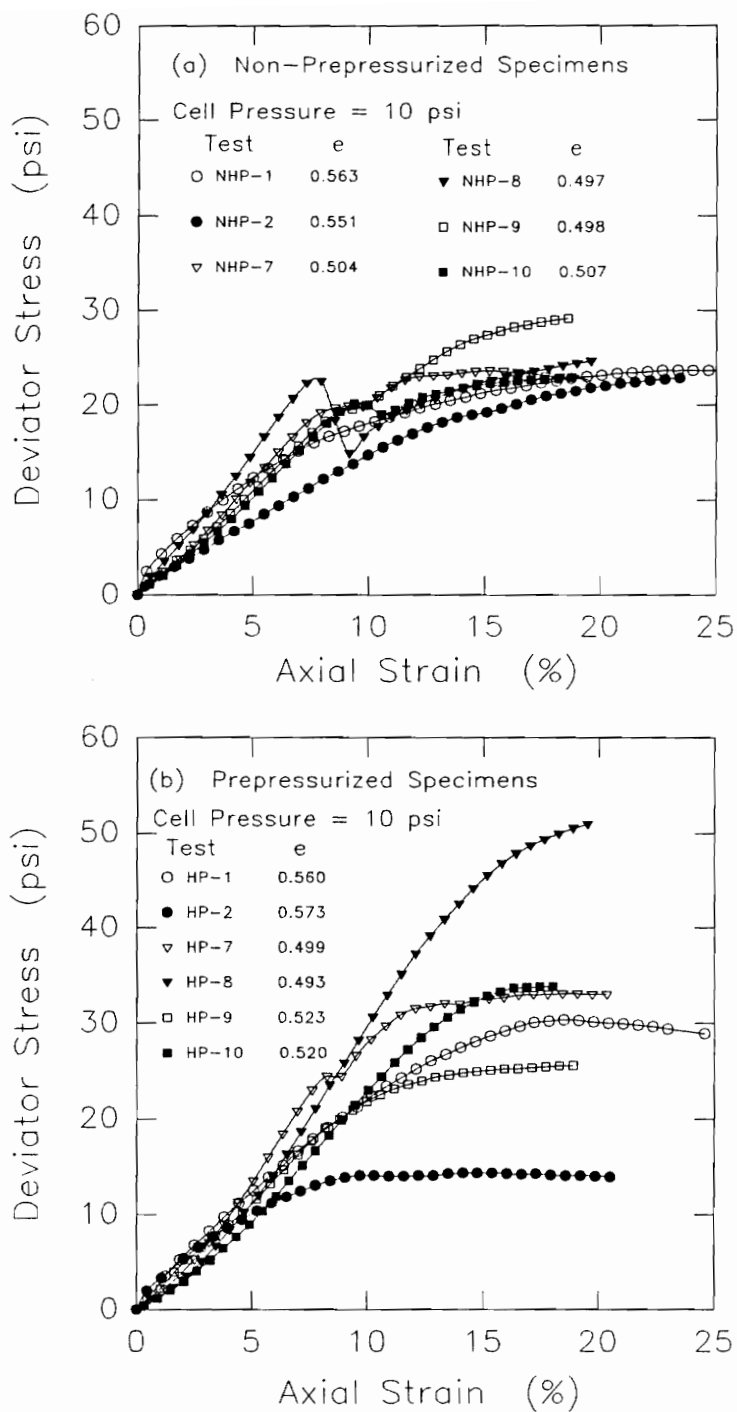


Figure 5.59. Deviator stress-strain relationships measured in the Q tests performed at 10 psi cell pressure on samples of remolded LMVD silt as part of the prepressurization study

can be seen from these two figures, there is a lot of scatter in the stress-strain behavior for these tests. It appears though, that the tests performed on prepressurized specimens gave smoother stress-strain behavior for the soil than the specimens not subjected to the prepressurization pressure. In the Q tests performed on specimens which were not prepressurized prior to testing, the stress-strain behavior tended to be more erratic in nature, showing occasional strain-softening during the tests.

Four Q tests were performed at a cell pressure of 20 psi. Two tests were performed on prepressurized samples and two were performed on non-prepressurized samples. The initial specimen data for these four tests are given in Table 5.16.

Table 5.16: Initial properties of the remolded LMVD silt Q test specimens tested at a cell pressure of 20 psi in the prepressurization study (Based on specimen dimensions measured prior to prepressurization)

Sample No.	Pre-pressurized	w (%)	γ_d (pcf)	S (%)	e
HP-3	Yes	21.2	108.9	100	0.541
HP-4	Yes	21.4	109.0	100	0.541
NHP-3	No	21.8	108.2	100	0.551
NHP-4	No	22.2	109.0	100	0.540

Figure 5.60 shows plots of deviator stress vs. axial strain for the four Q tests performed at a cell pressure of 20 psi. It can be seen from this figure that the two

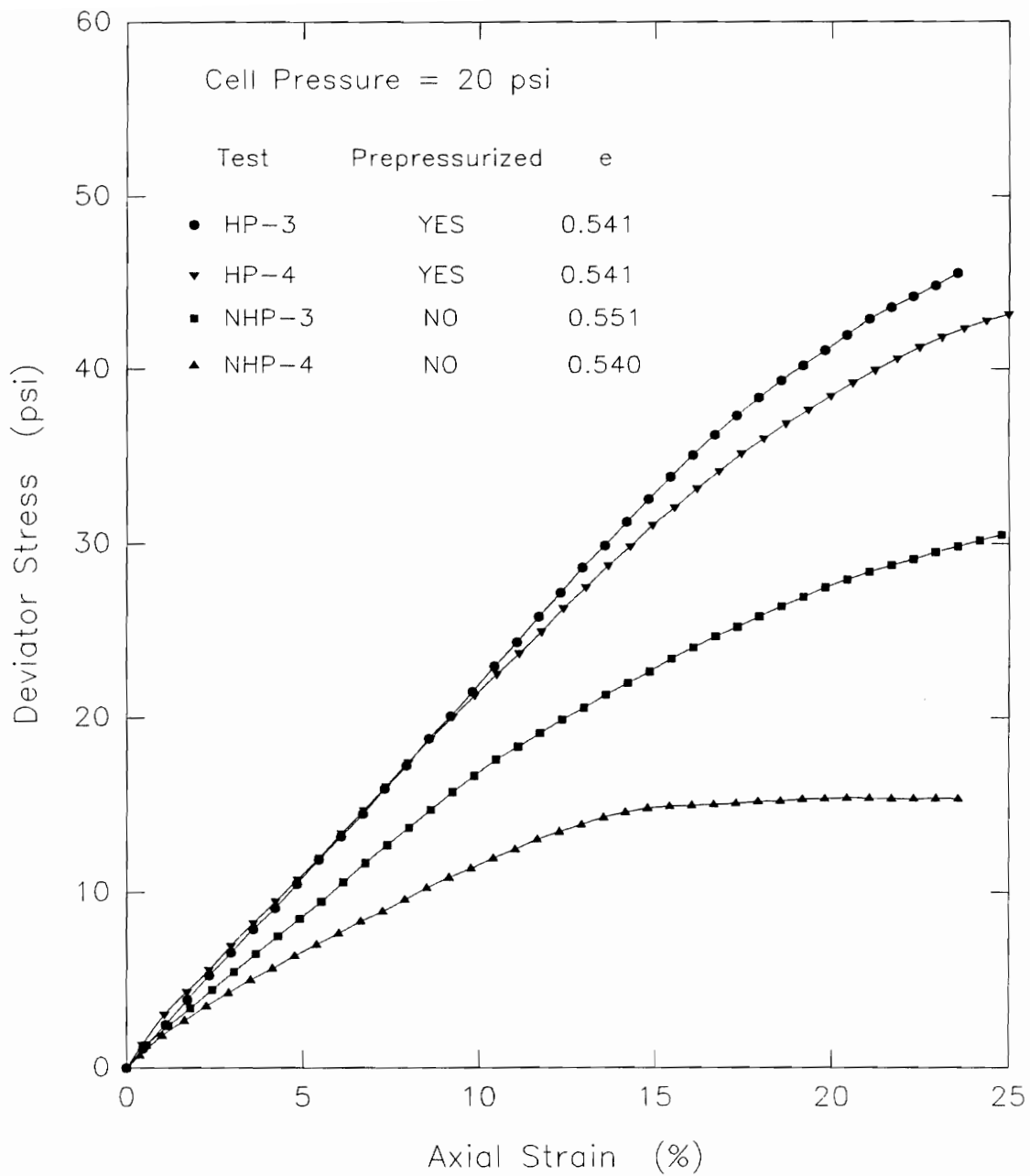


Figure 5.60. Deviator stress-strain relationships measured in the four Q tests performed at 20 psi cell pressure on samples of remolded LMVD silt as part of the prepressurization study

prepressurized samples have very similar stress-strain curves while the two non-prepressurized samples have stress-strain curves which differ from those of the prepressurized samples as well as from each other.

One interesting effect of the prepressurization which was observed in the unconfined compression tests and the Q tests performed at 20 psi cell pressure was that the two prepressurized samples in each group had very similar deviator stress-strain curves. This was initially felt to imply that the prepressurization of Q test specimens may lead to more consistent strength results for Q tests on saturated silts. This behavior was not observed for the first group of Q tests performed at 10 psi cell pressure. Subsequent groups of Q tests performed at a cell pressure of 10 psi did not provide any further support for the idea that prepressurization of Q test specimens leads to more consistent stress-strain behavior.

The differences observed in the stress-strain behavior of the prepressurized Q test specimens tested at a cell pressure of 10 psi may be due to the silt specimens being less than fully saturated or having slightly different initial degrees of saturation. If the silt specimens were less than fully saturated or had varying initial degrees of saturation, the prepressurization could have lead to

variations in specimen void ratio which then resulted in different stress-strain behavior for the two specimens. Accurate measurement of the degree of saturation of the silt specimens would be necessary, along with many more tests of this type, in order to more fully explore this behavior.

The stress-strain curves for all of the Q tests performed at 0, 10 and 20 psi on specimens not subjected to a prepressurization pressure prior to testing are shown in Figure 5.61a. Figure 5.61b shows the stress-strain curves for all of the Q tests performed on prepressurized specimens at the different cell pressures used in the tests.

As can be seen from these figures, considerable scatter exists between the stress-strain behavior of the different specimens. The prepressurized specimens do tend to show somewhat more consistent stress-strain behavior at small axial strains. It also appears that the prepressurized specimens generally had higher strengths than the non-prepressurized specimens. This may be a result of the prepressurized specimens being able to withstand larger decreases in pore water pressure without cavitation occurring, thus giving higher strengths than the non-prepressurized specimens. It could also indicate that

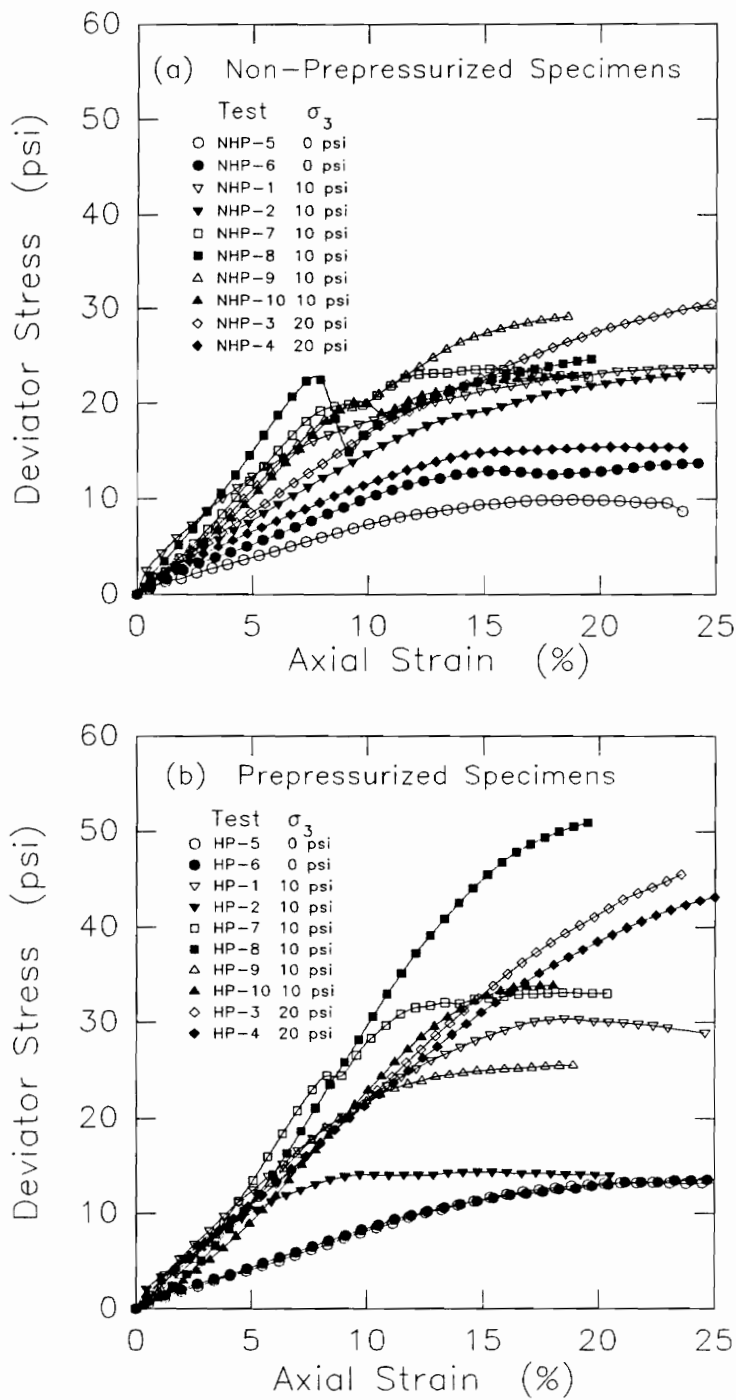


Figure 5.61. Deviator stress-strain relationships measured in the Q tests performed at 0, 10 and 20 psi cell pressure on samples of remolded LMVD silt as part of the prepressurization study

the prepressurized specimens had their void ratios reduced by the high pressure and therefore had higher strengths than the non-prepressurized specimens. Since it is not known for certain whether or not the specimens were fully saturated prior to prepressurization, it is difficult to interpret the effect of the prepressurization on the undrained behavior of the soil.

Based on a failure criterion of 10 percent axial strain at failure or a peak in the deviator stress-strain curve prior to 10% axial strain, Figure 5.62 shows the total stress Mohr's circles for the ten Q tests performed on non-prepressurized samples. Similarly, Figure 5.63 shows the total stress Mohr's circles at 10 percent axial strain for the ten Q tests performed on prepressurized samples. As with the stress-strain behavior of the soil, these two plots of Mohr's circles appear to be inconclusive as to the effect of the use of prepressurization on the strength values measured in Q tests on saturated silt specimens.

Although pore water pressures were not measured during these tests, the pore pressure at failure in each specimen can be estimated using Eq. 5-1:

$$u_f = \frac{\sigma_1 - \sigma_3 (\tan^2(45 + \phi'/2))}{1 - \tan^2(45 + \phi'/2)} \quad (5-1)$$

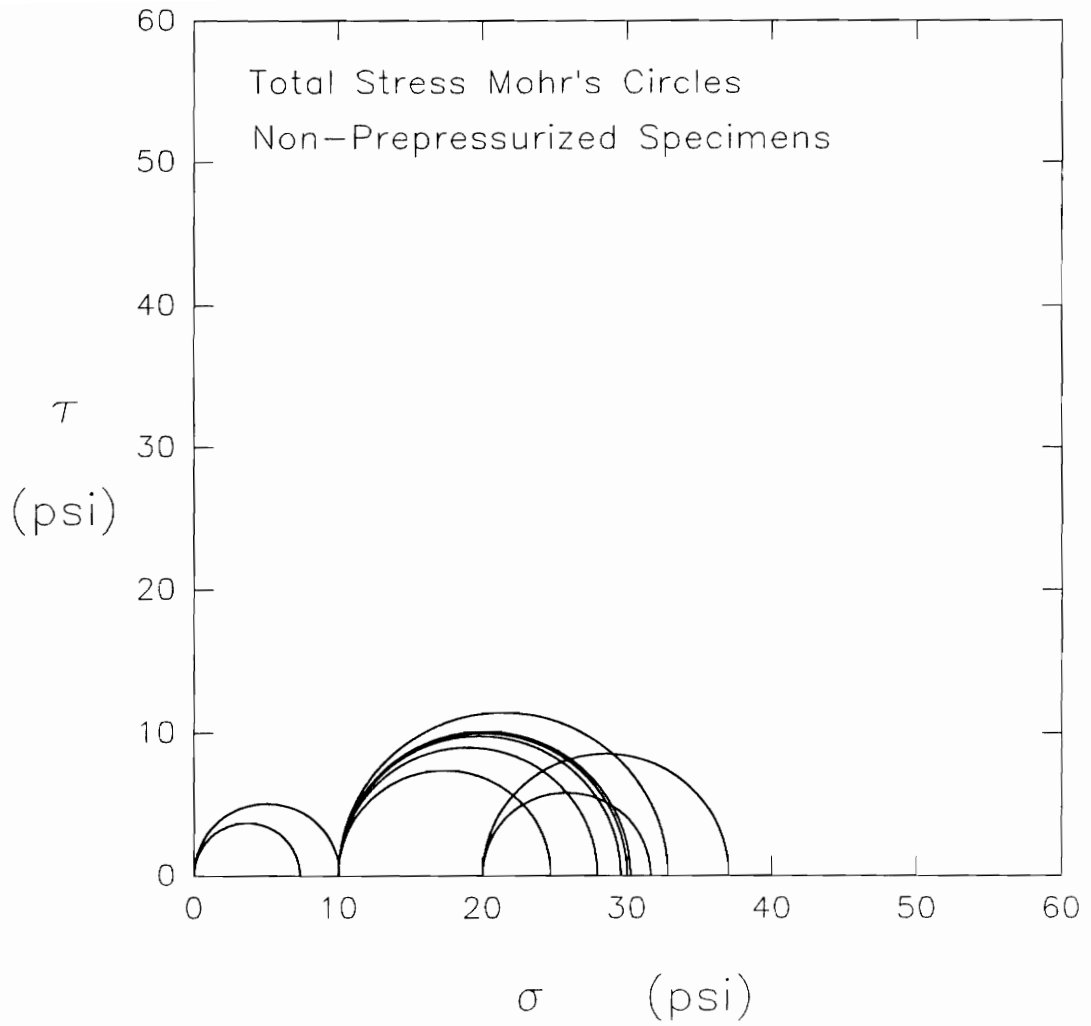


Figure 5.62. Total stress Mohr's circles at 10% axial strain for the six Q tests performed on non-prepressurized samples of remolded LMVD silt

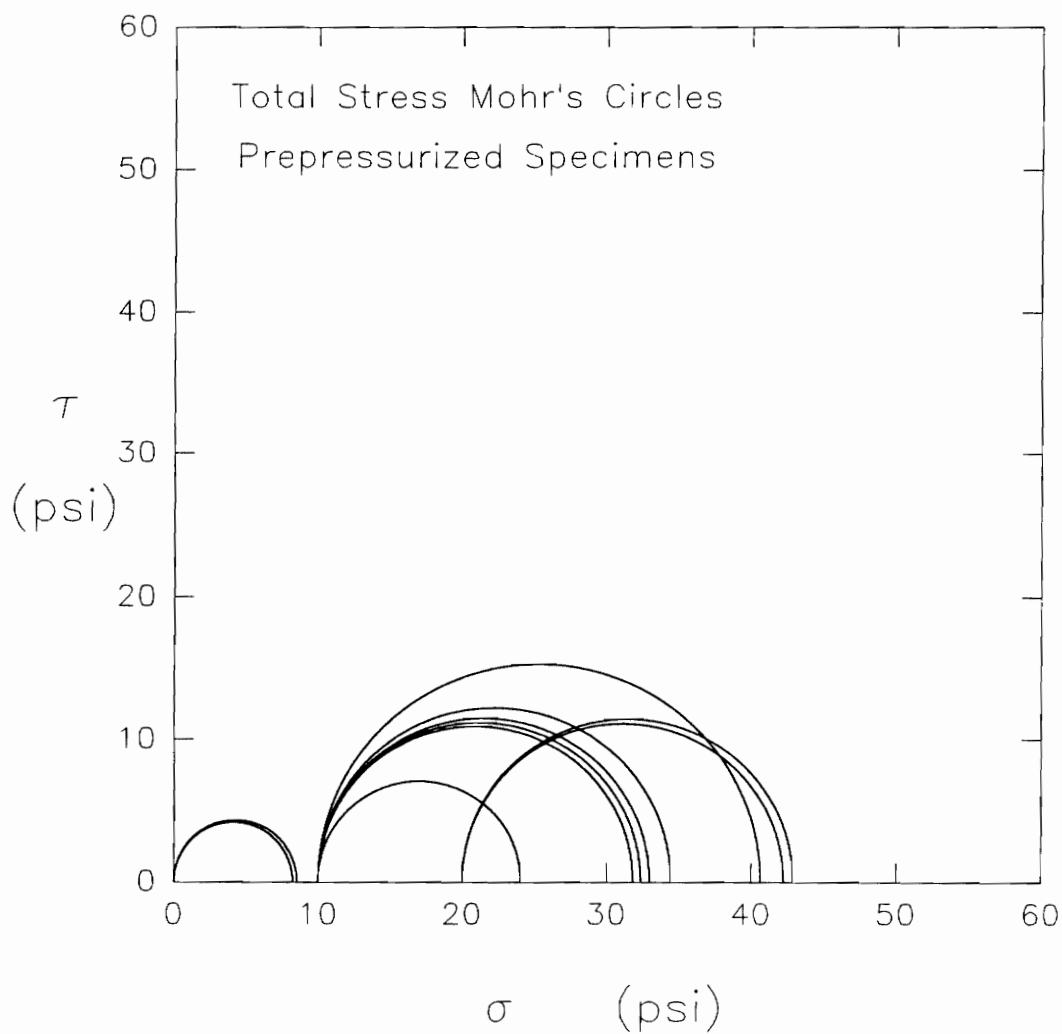


Figure 5.63. Total stress Mohr's circles at 10% axial strain for the six Q tests performed on prepressurized samples of remolded LMVD silt

where u_f = pore water pressure at failure,
 σ_1 and σ_3 = major and minor principal total stresses at failure, and
 ϕ' = effective stress friction angle of the soil.

This equation, given by Brandon, Duncan and Huffman (1990), estimates the pore pressure at failure, based on the maximum total stresses, σ_1 and σ_3 , measured during the tests. In order to apply Eq. 5-1 to these tests, the effective stress path of the Q test specimens has been assumed to follow the K_f line of the soil. Using this equation, the values of pore water pressure at failure in each specimen have been estimated assuming an effective stress friction angle, ϕ' , of 37° for the soil. Table 5.17 presents the calculated values of pore water pressure at failure based on the total stresses measured at 10% axial strain in each of the Q tests.

A plot of the pore water pressure at failure versus cell pressure for the values estimated by Eq. 5-1 for 10% axial strain and given in Table 5.17, is presented in Figure 5.64. At 10% axial strain, the prepressurized specimens tested at cell pressures of 10 and 20 psi tended to have larger estimated decreases in pore water pressure than the nonprepressurized specimens. A clear trend was not apparent at 10% axial strain for the tests performed at a cell pressure of 0 psi.

Table 5.17: Values of pore water pressure estimated by Eq. 5-1 for total stresses measured at 10% axial strain in the Q tests performed in the prepressurization study ($\phi' = 37^\circ$)

Test	σ_3 (psi)	u_i (psi)	σ_1 (psi)	u_f (psig)
NHP-1	10	10	28.23	3.97
HP-1	10	10	32.36	2.60
NHP-2	10	10	25.13	4.99
HP-2	10	10	24.05	5.35
NHP-3	20	20	37.04	14.36
HP-3	20	20	42.23	12.65
NHP-4	20	20	31.62	16.16
HP-4	20	20	41.89	12.76
NHP-5	0	0	7.34	-2.43
HP-5	0	0	8.24	-2.73
NHP-6	0	0	10.09	-3.34
HP-6	0	0	8.54	-2.83
NHP-7	10	10	30.27	3.29
HP-7	10	10	38.33	0.63
NHP-8	10	10	27.18	4.31
HP-8	10	10	39.44	0.26
NHP-9	10	10	30.48	3.22
HP-9	10	10	31.82	2.78
NHP-10	10	10	29.99	3.39
HP-10	10	10	32.97	2.40

Table 5.18 presents the estimated values of pore water pressure at failure based on the total stresses measured at the maximum deviator stress in each of the Q tests.

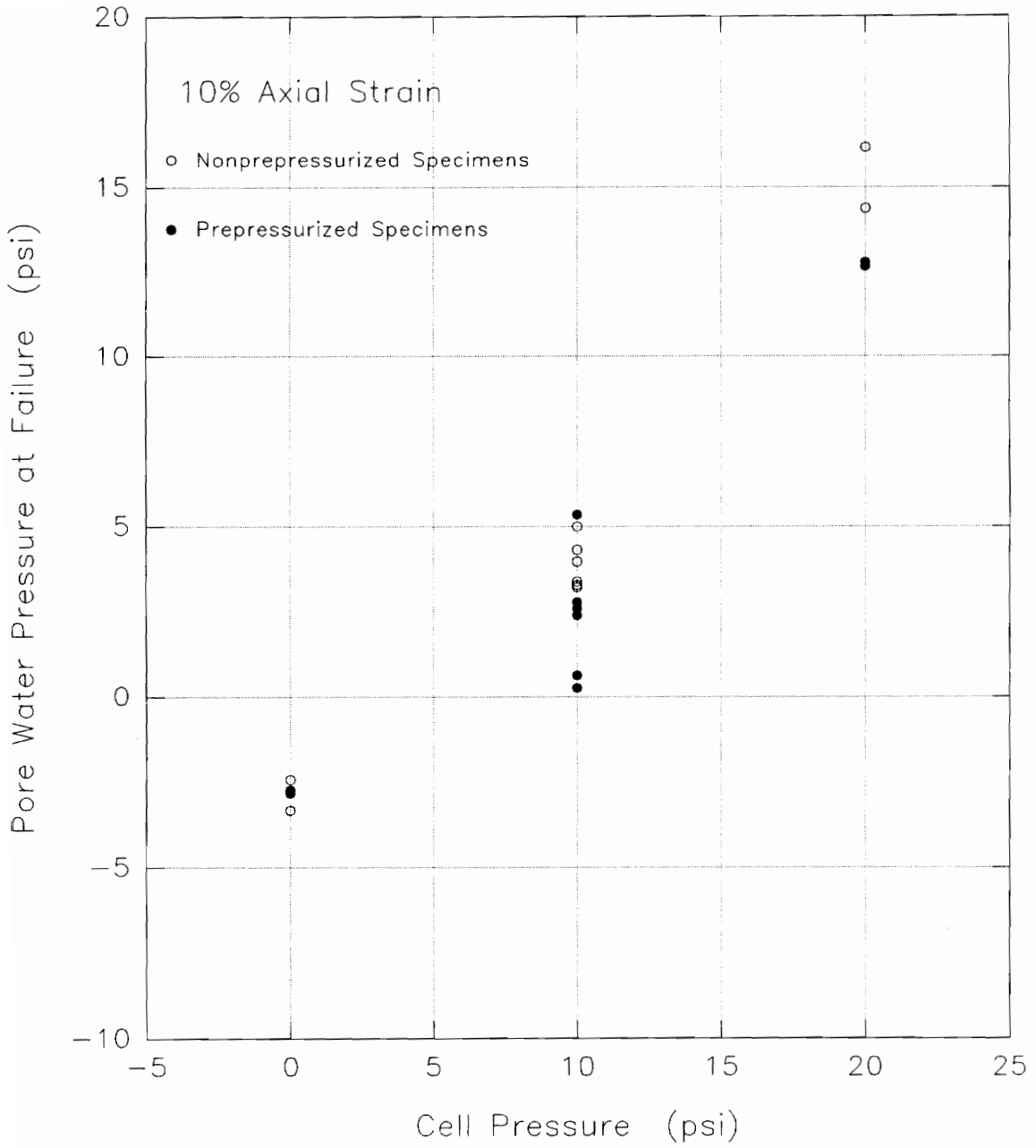


Figure 5.64. Pore water pressure at failure estimated by Eq. 5-1 for the Q tests performed at cell pressures of 0, 10, and 20 psi in the prepressurization study, based on 10% axial strain at failure

Table 5.18: Values of pore water pressure estimated by Eq. 5-1 for total stresses measured at maximum deviator stress in the Q tests performed in the prepressurization study ($\phi' = 37^\circ$)

Test	σ_3 (psi)	u_i (psi)	σ_{1max} (psi)	u_f (psi)	ϵ_a (%)
NHP-1	10	10	33.75	2.14	25.7
HP-1	10	10	40.38	-0.05	18.5
NHP-2	10	10	32.90	2.42	23.7
HP-2	10	10	24.10	5.34	9.7
NHP-3	20	20	50.37	9.95	24.5
HP-3	20	20	64.84	5.17	22.9
NHP-4	20	20	35.40	14.91	20.1
HP-4	20	20	61.82	6.17	23.1
NHP-5	0	0	9.91	-3.28	18.8
HP-5	0	0	13.27	-4.39	22.4
NHP-6	0	0	12.97	-4.29	15.5
HP-6	0	0	13.64	-4.51	25.8
NHP-7	10	10	33.66	2.17	14.9
HP-7	10	10	43.10	-0.95	18.8
NHP-8	10	10	34.78	1.80	19.9
HP-8	10	10	61.10	-6.90	19.8
NHP-9	10	10	39.20	0.34	18.9
HP-9	10	10	35.57	1.54	18.6
NHP-10	10	10	33.05	2.38	19.1
HP-10	10	10	43.83	-1.19	17.5

A plot of the estimated pore water pressure at failure versus cell pressure for maximum deviator stress conditions, is presented in Figure 5.65a. For maximum deviator stress conditions, the prepressurized specimens tested at cell pressures of 0, 10 and 20 psi tended to have larger estimated decreases in pore water pressure than the nonprepressurized specimens.

The larger decreases in pore water pressure estimated for the prepressurized specimens and the corresponding

higher strengths measured in the tests could have two possible causes. One possibility is that the application of the prepressurization pressure could have decreased the void ratios of the specimens if they were not fully saturated. With lower void ratios, these specimens would have had increased dilatant tendencies. As a result, they may have experienced larger decreases in pore water pressure and higher measured strengths than the nonprepressurized specimens.

The other possibility is that the application of the prepressurization pressure may have made the soil pore water less likely to cavitate. As a result, larger negative changes in pore water pressure were possible during undrained shear before cavitation took place. This could have resulted in the higher strengths which were measured in many of the prepressurized specimens.

Figure 5.65b shows a plot of the pore water pressure at failure estimated by Eq. 5-1 for maximum deviator stress conditions versus the axial strain at which the maximum deviator stress occurred. From this plot it appears that there is no definite trend between whether or not the specimens had been subjected to a prepressurization pressure and the axial strain at which the maximum deviator stress occurred.

Since the preliminary testing and comparison of prepressurized versus non-prepressurized specimens had limitations due to the equipment available and the results did not appear to suggest a definite trend in its effect on undrained behavior, no further testing has been performed comparing prepressurized Q test specimens to non-prepressurized specimens. The performance and interpretation of these tests was further complicated by the uncertainty of whether or not the specimens being tested were 100 percent saturated. If additional testing of this type is to be performed in future research studies on silt behavior, pore pressure measurements during the high pressure application will be necessary, in order to measure the pore pressure parameter B. This will enable a more reasonable assessment of whether or not the samples are in fact fully saturated prior to pressurization.

5.7 Q Tests with Pore Air and Pore Water Pressure Measurements

It was originally proposed to perform Q tests on saturated silts while measuring pore air and pore water pressures within the specimens during shear. For a fully saturated specimen, the pore air and pore water pressures should be equal (Sowers, 1979). As attempted dilation occurs during undrained shear, the pore water pressure will

decrease. If the reduction in pore pressure results in dissolved gases coming out of solution from the pore water, the specimen will no longer be fully saturated and there should be a measurable difference between the pore air and pore water pressures due to surface tension effects.

It was hoped that the pore air and pore water pressures within saturated silt Q test specimens could be measured during undrained shear. The point at which the measured pore air and pore water pressures began to differ would then indicate that gaseous cavitation had occurred. After further review of the literature, it became apparent that what had been proposed was not possible. Measurements of pore air pressures in soil are noted to be quite difficult (Bishop and Henkel, 1962). Such measurements are felt to only be accurate when the air is in a continuous phase throughout the soil (Bishop, 1960; Barden and Sides, 1967; Sides and Barden, 1967).

Fredlund and Rahardjo (1993) noted that at degrees of saturation below about 80 percent, the air present in soil pores is typically continuous throughout the soil. When the degree of saturation of the soil is greater than about 90 percent, the air typically exists within the soil pores in the form of occluded bubbles. They stated that for degrees of saturation between 80 and 90 percent, a

transition occurs from a continuous air phase to an occluded air phase.

In the occluded phase, the air bubbles are surrounded by a film of water and are not connected to each other. It is therefore not possible to measure the air pressure unless a probe is inserted directly into an air bubble. For an initially saturated sample, if an air bubble forms during undrained shear, its pressure could not be accurately measured unless the pressure measurement device was at the exact location of the newly formed bubble. Thus, measuring the pore air pressure at the end of the specimen will not give accurate pore air pressure measurements for samples with high initial degrees of saturation. The measurement of pore air pressures in soil specimens is only felt to be accurate when the degree of saturation of the soil is low enough so that the air is continuous throughout the specimen (Barden and Sides, 1967).

Even though it was not possible to measure pore air and pore water pressures in saturated silt specimens as originally planned, pore air and pore water pressures were measured in several compacted silt specimens which were less than fully saturated. This was done to give a general idea of the relationship between the changes in pore air

pressure and pore water pressure which occur during undrained shear.

A total of eight Q tests were performed on 1.4-inch diameter by 2.8-inch high compacted specimens of new LMVD silt. Two of the tests were performed as unconfined compression tests while six were performed at a cell pressure of 10 psi. These Q test specimens were sheared at a strain rate of about 1%/min. During these tests, pore water pressures were measured at the base of each specimen while pore air pressures were measured at the top of the specimen.

The pore water pressure monitoring system consisted of a fine porous stone connected by pore pressure lines to a pore pressure transducer. The fine porous stone had an air entry value of one bar or 14.5 psi. This means that when the negative pore water pressure decreased to 14.5 psi below atmospheric pressure, air would begin to enter the pores of the stone, thus influencing the measured pore water pressures. As long as the pore water pressure was greater than a gage pressure of -14.5 psi, the pores of the stone and the pore pressure monitoring system would remain saturated and should give accurate pore water pressure readings. The fine porous stone was saturated and deaired water was used in the pore pressure line to the transducer.

The pore air pressures were measured at the tops of the specimens with a conventional coarse porous stone which was connected by pore pressure lines to another pressure transducer. The coarse porous stone and pore pressure lines to this transducer were filled with air. The initial properties of the specimens tested are given in Table 5.19.

Table 5.19: Initial properties of Q test specimens of compacted new LMVD silt in which pore air and pore water pressures were measured during shear

Test	σ_3 (psi)	e	γ_d (pcf)	S (%)
Q1	10	0.689	99.4	60.7
Q2	0	0.694	99.1	46.8
Q3	0	0.637	102.5	75.1
Q4	10	0.678	100.0	88.5
Q5	10	0.626	103.3	88.2
Q7	10	0.676	100.2	57.8
Q8	10	0.638	102.5	75.7
Q9	10	0.629	103.1	82.8

As can be seen from Table 5.19, all of the specimens were less than fully saturated. The degree of saturation of the specimens varied from 46.8 percent to 88.5 percent. The void ratios of the specimens varied from 0.626 to 0.694.

Three of the tests were performed at degrees of saturation above 80 percent (Q4, Q5, and Q9). The results of these three tests showed a variety of pore pressure responses. The pore pressure behavior measured in two of

these tests tends to indicate that the degree of saturation may have been too high in these specimens to give accurate pore air pressure measurements. Figures 5.66, 5.67, and 5.68 show the deviator stress vs. axial strain and pore pressures vs. axial strain plots for these three tests. The pore pressure vs. axial strain plots show that for tests Q5 and Q9, the measured pore water pressure was greater than the measured pore air pressure during these tests. This, however, is not as expected. By surface tension, the pore air pressure should be greater than the pore water pressure, as given by Eq. 4-30:

$$u_a - u_w = P_a - P_w = \frac{2 T_s}{r} \cos\theta \quad (4-30)$$

where $u_a = P_a$ = the pore air pressure,
 $u_w = P_w$ = the pore water pressure,
 T_s = the surface tension of the water,
 r = the radius of curvature of the air-water interface, and
 θ = the angle of intersection between the water surface and the soil grains (for $\theta = 0$, $\cos \theta = 1$).

For test Q4, the measured pore air pressure at the start of the test was measured to be about 30 psi. This was considerably greater than the 10 psi cell pressure applied to the specimen. This suggests that the pore air pressures measured in this test may be inaccurate. Perhaps

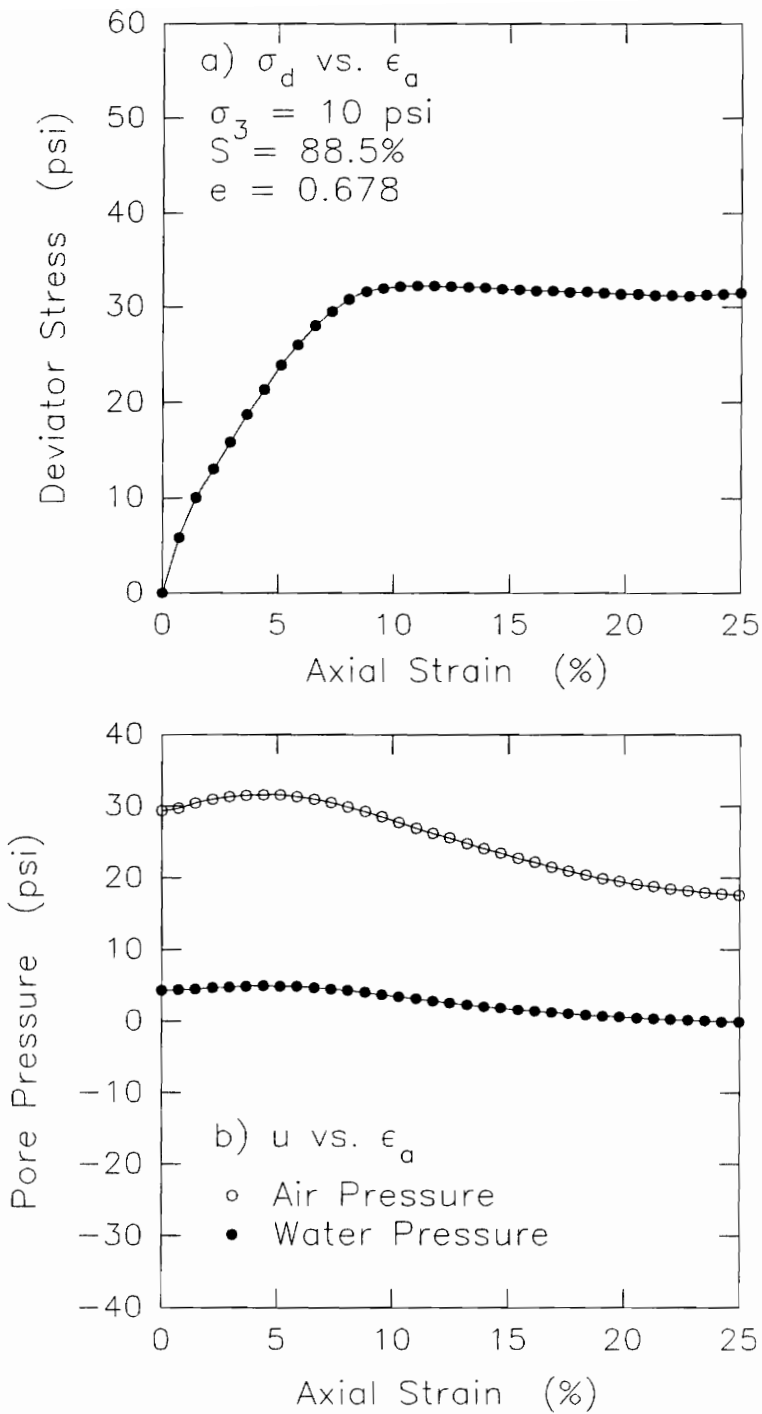


Figure 5.66. Deviator stress-strain and pore air and pore water pressure-strain relationships measured in test Q4 performed on compacted new LMVD silt

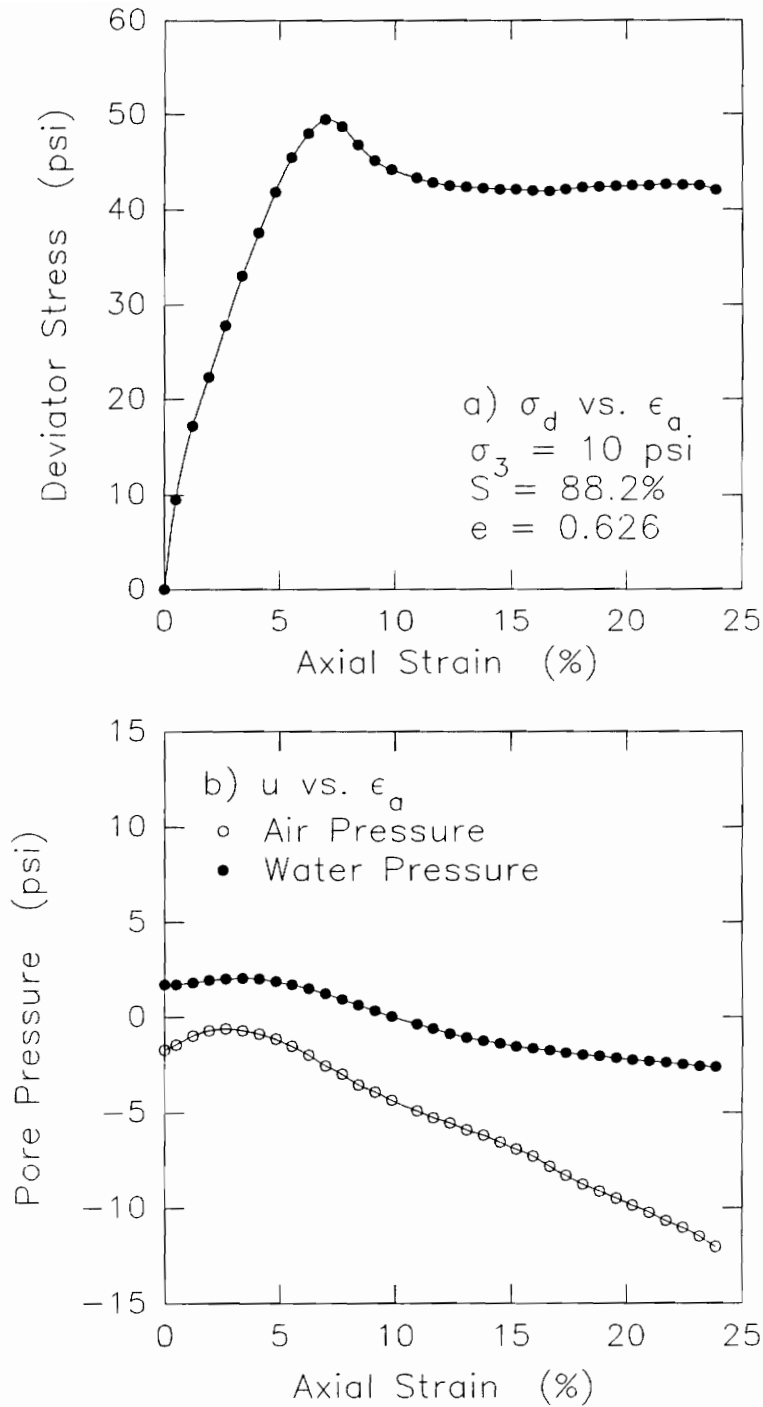


Figure 5.67. Deviator stress-strain and pore air and pore water pressure-strain relationships measured in test Q5 performed on compacted new LMVD silt

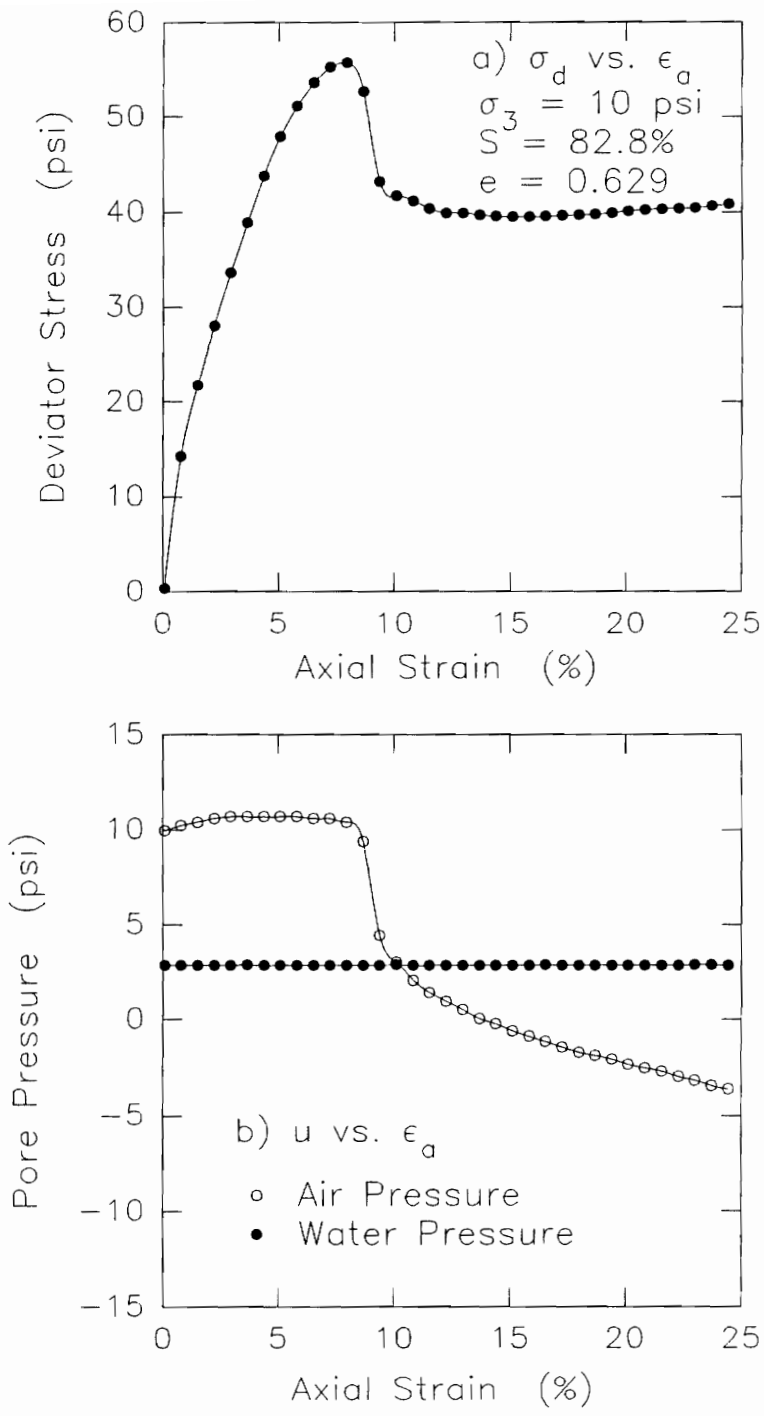


Figure 5.68. Deviator stress-strain and pore air and pore water pressure-strain relationships measured in test Q9 performed on compacted new LMVD silt

full pore pressure equalization due to the applied cell pressure had not been reached by the time the specimen was sheared. This may have resulted in pore air pressures higher than the applied cell pressure being observed in this test.

For these reasons, it is felt that in these three tests, where the degree of saturation was greater than 80 percent, the air may have been present in the form of occluded bubbles within the pores of the soil, rather than in a continuous phase. The pore air pressures which were measured at the tops of the specimens, therefore, are not felt to be accurate measurements of the actual pore air pressures within the air bubbles in the soil.

The two tests performed as unconfined compression tests, Q2 and Q3, also showed erratic behavior in their measured pore pressures. Figures 5.69 and 5.70 show the deviator stress vs. axial strain and pore pressures vs. axial strain plots for these two tests. As can be seen from the plots of pore water pressure vs. axial strain, erratic step-like decreases in pore water pressure were measured. In addition, the measured pore air pressure decreased below the measured pore water pressure during these two tests, which again is not in agreement with Eq. 4-30. The stress-strain curves for these tests are also

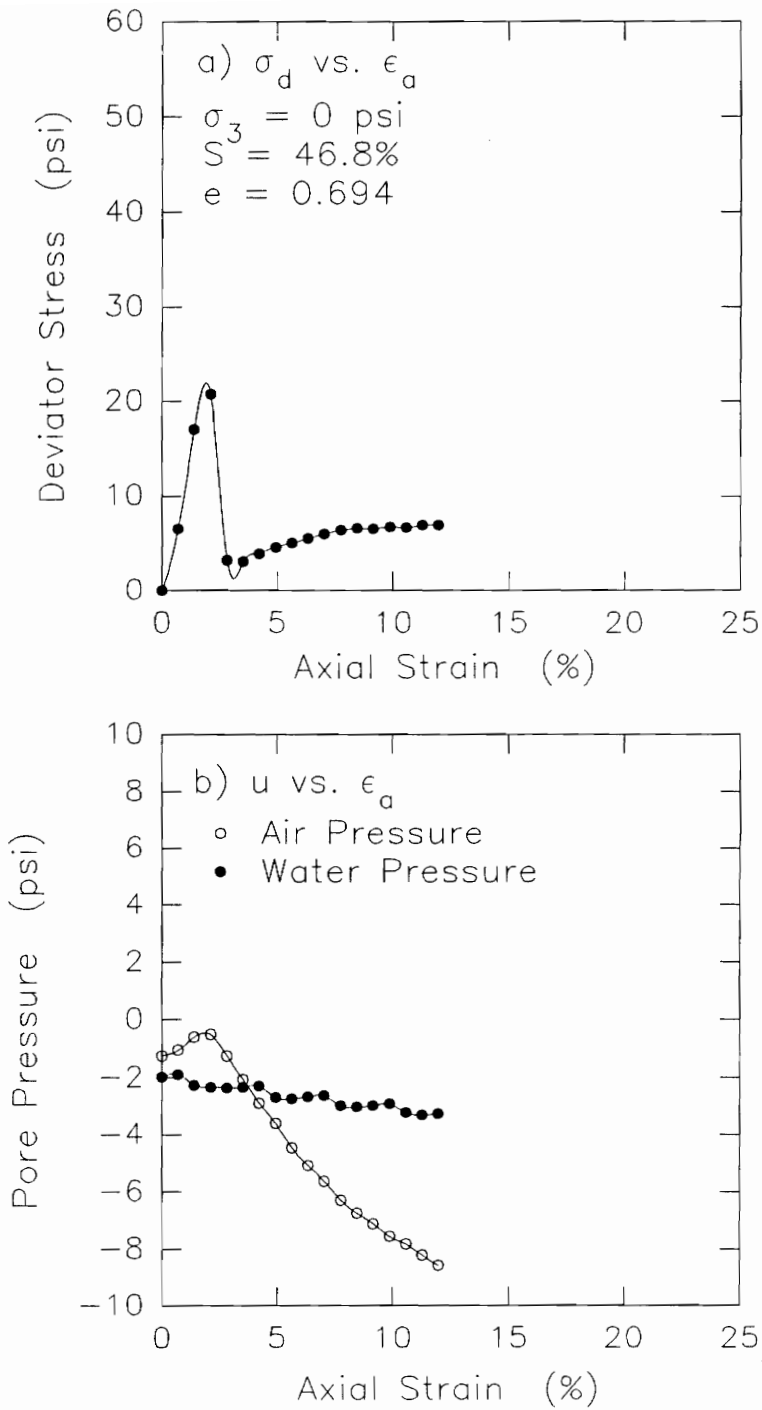


Figure 5.69. Deviator stress-strain and pore air and pore water pressure-strain relationships measured in test Q2 performed on compacted new LMVD silt

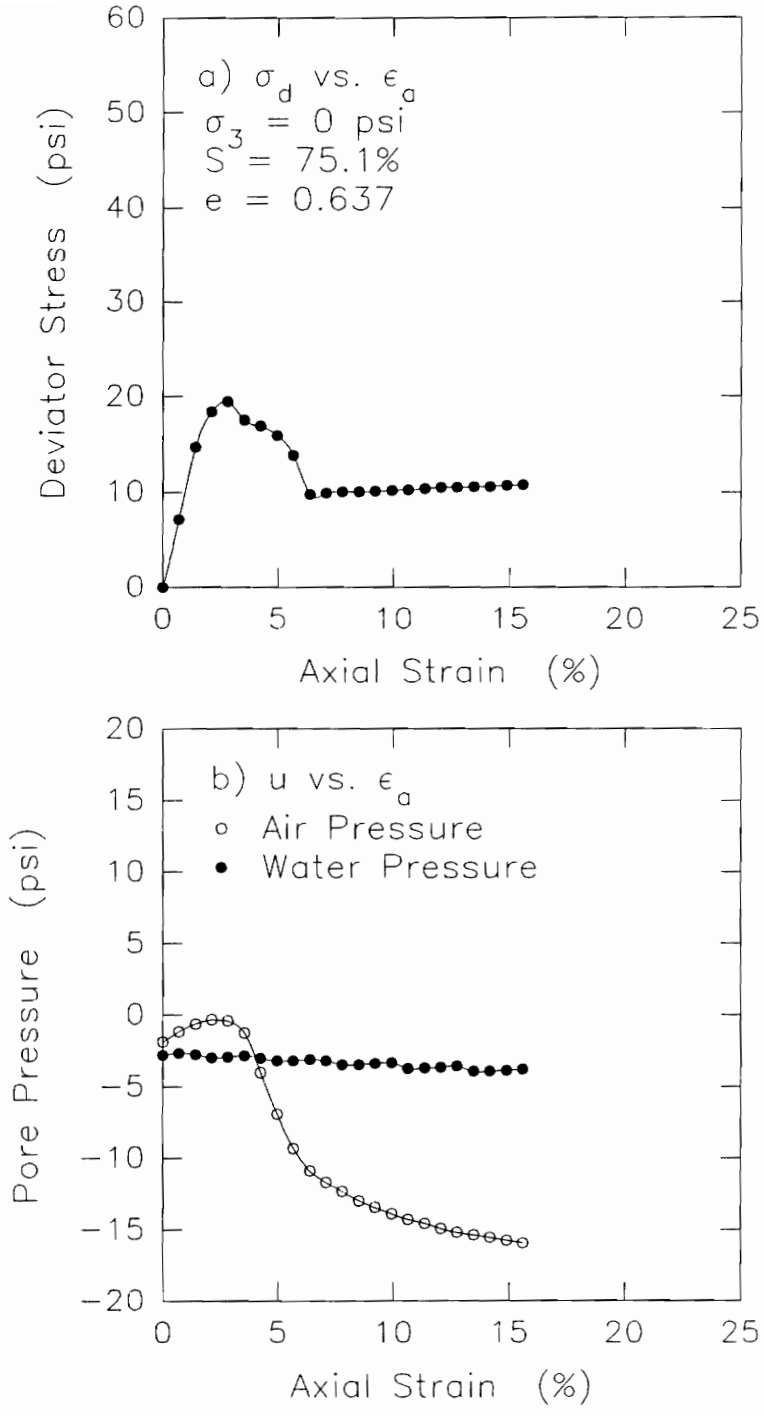


Figure 5.70. Deviator stress-strain and pore air and pore water pressure-strain relationships measured in test Q3 performed on compacted new LMVD silt

somewhat erratic. It may be that the decreases in pore water pressure which occurred in these tests were unable to be measured accurately by the pore pressure measurement equipment used.

These tests were performed as unconfined compression tests so that as pore water pressures decreased during shear, the absolute pressure was less than atmospheric pressure. This may have allowed dissolved gases to come out of solution within the water present in the pore pressure monitoring system. The cyclic nature of the erratic pore water pressure measurements further suggests that perhaps the pore pressure transducer was unable to measure these negative pore water pressures, even though a fine porous stone was used in the measuring system at the base of the specimens. In any case, the erratic pore water pressures measured are felt to be inaccurate representations of the actual pore water pressures within the soil during undrained shear.

The other three Q test specimens, Q1, Q7, and Q8, were all tested at a cell pressure of 10 psi and had degrees of saturation between 58 and 76 percent. The deviator stress vs. axial strain and pore pressure vs. axial strain relationships measured in these three tests are presented in Figures 5.71, 5.72, and 5.73.

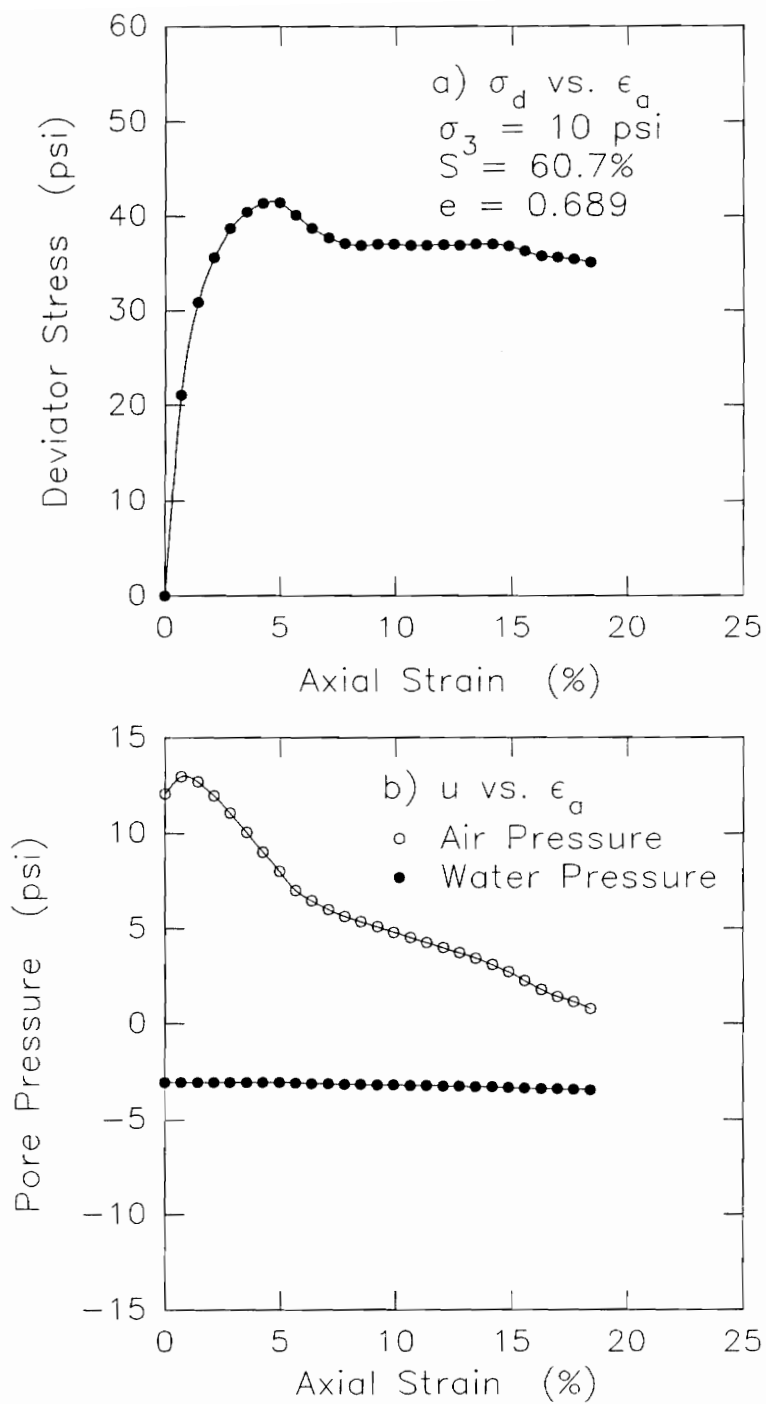


Figure 5.71. Deviator stress-strain and pore air and pore water pressure-strain relationships measured in test Q1 performed on compacted new LMVD silt

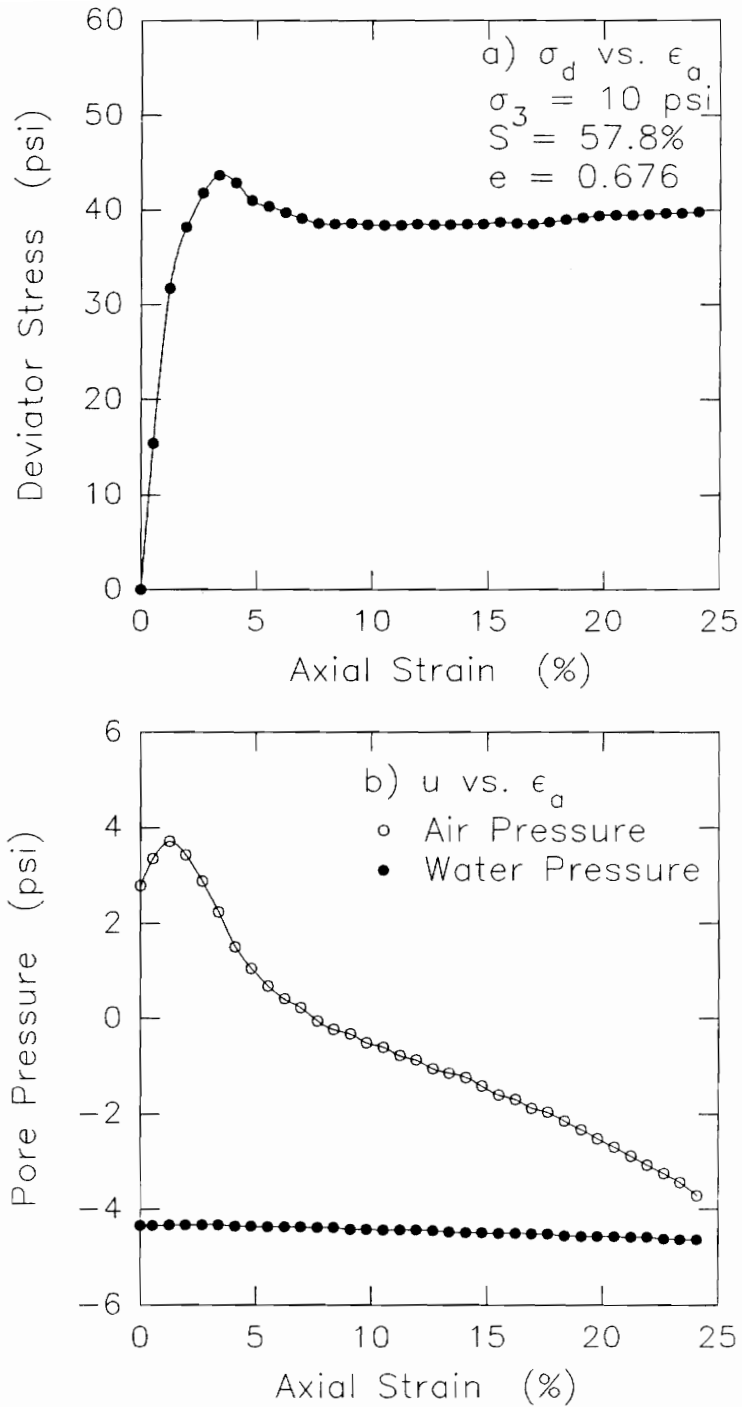


Figure 5.72. Deviator stress-strain and pore air and pore water pressure-strain relationships measured in test Q7 performed on compacted new LMVD silt

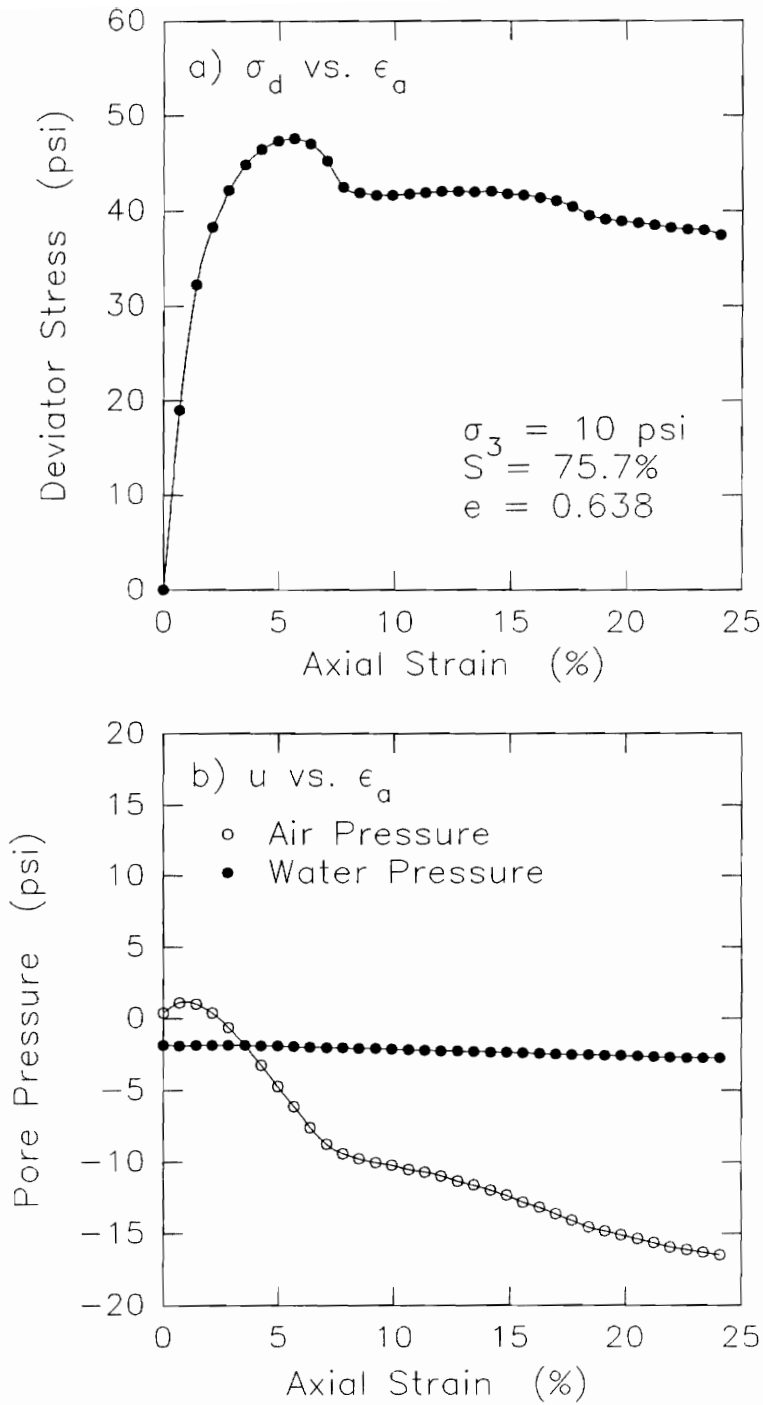


Figure 5.73. Deviator stress-strain and pore air and pore water pressure-strain relationships measured in test Q8 performed on compacted new LMVD silt

It can be seen that for tests Q1 and Q7, the pore air pressures were greater than the pore water pressures throughout the tests. Specimen Q8, however, showed a pore air pressure that decreased below the pore water pressure during the test. In all three tests the pore air pressures tended to exhibit a slight increase initially at the start of the tests, followed by a continuous decrease with increasing axial strain. The pore water pressures also increased slightly at the start of the tests, but not as much as the pore air pressures did. The pore air pressures tended to show larger decreases than the pore water pressures. These test specimens showed very little change in measured pore water pressure, as compared to the measured pore air pressures.

The pore water pressures in these Q tests were negative throughout the tests. These tests were performed at a cell pressure of 10 psi. It was expected that the pore water pressure would have been greater than 0 psi but less than 10 psi in a partially saturated specimen. It may very well be that the pore water pressures measured in these three tests are not accurate.

The actual magnitude of the pore air and pore water pressures at the start of the tests varied from one test to another, probably due to the variations in the initial

degrees of saturation of the specimens as well as variations in their void ratios. The initial degrees of saturation and the void ratios of these Q test specimens, prior to application of the 10 psi cell pressure, are presented in Table 5.20. The pore air and pore water pressures measured after the 10 psi cell pressure had been applied, but prior to shear, are also presented.

Table 5.20: Initial degree of saturation and void ratio of compacted Q test specimens of new LMVD silt prior to application of 10 psi cell pressure; and pore air and pore water pressures measured after application of 10 psi cell pressure

Test	σ_3 (psi)	e_i	S_i (%)	u_a (psi)	u_w (psi)	$u_a - u_w$ (psi)
Q1	10	0.689	60.7	12.1	-3.1	15.2
Q7	10	0.676	57.8	2.8	-4.3	7.1
Q8	10	0.638	75.7	0.4	-1.9	2.3

The measured initial pore air pressures of these three specimens varied from 0.4 to 12.1 psi. This range of values can not be totally justified by variations in the initial void ratios and degrees of saturation of the specimens, and may indicate inaccuracies in some or all of the pore air pressure measurements. However, it does appear that as the initial degree of saturation of the specimens increased, the measured pore water pressure became less negative, as expected. The differences between the measured pore air and pore water pressures did not show

a consistent decrease in magnitude as the initial degree of saturation of the specimens increased, as had been observed by Bishop and Henkel (1962). This further suggests that the pore pressures measured in these tests may not be correct.

The measurement of pore air and pore water pressures in these tests indicates the difficulties involved in measuring such pressures in Q test specimens. The uncertainties encountered in making these pore pressure measurements tend to make the accuracy of these test results questionable. Because of this, no useful applications or conclusions can be made from these tests.

5.8 Q Tests at Different Strain Rates

In order to investigate the effects of the rate of shear on the behavior of saturated, dilatant silts in Q tests, several sets of tests have been performed in which the specimens have been sheared at different strain rates.

By shearing saturated silt Q test specimens at different strain rates, it was expected that the magnitude of the decrease in pore water pressure within the specimens would vary. Specimens sheared at a rapid strain rate would be expected to develop larger negative pore water pressures along the shear plane. Pore water pressures throughout the

specimen, however, would be nonuniform. A specimen sheared at a slow rate of strain would be expected to develop a smaller decrease in pore water pressure along the shear plane. The decrease in pore water pressure would be more uniform throughout the specimen.

Specimens which were sheared rapidly and experienced larger decreases in pore water pressure along the shear plane might exhibit increased levels of strain-hardening or steeper stress-strain curves during shear. Specimens which were sheared slowly would experience smaller decreases in pore water pressure. As a result, they might show less strain-hardening, giving stress-strain curves which were not as steep as the rapidly sheared specimens.

The specimens which were sheared rapidly and had decreases in pore water pressure that were largest, might be expected to have pore water which would more readily cavitate than specimens sheared slowly and having smaller decreases in pore water pressure. More air would be expected to come out of solution from pore water which experienced larger decreases in pressure.

On the other hand, the pore water in the rapidly sheared specimens had less time for dissolved air to come out of solution than the specimens sheared at a slower rate. In addition, in the slowly sheared specimens, a

larger volume of pore water was subjected to a given decrease in pore water pressure, whereas in the rapidly sheared specimens, different volumes of pore water were subjected to different magnitudes of decreased pore water pressure.

It thus seems that a number of factors are involved which may influence the results of Q tests performed on saturated, dilatant silts at different strain rates. Isolation of the many variables involved would be difficult if not impossible. Preliminary tests were performed to see if the strain-rate at which the specimens were sheared had any noticeable effects on the stress-strain behavior of the specimens.

A total of four sets of Q tests have been performed on specimens of saturated, remolded old LMVD silt. All of the tests were performed at a cell pressure of 10 psi. Each set of tests consisted of four Q test specimens obtained from the same batch consolidometer sample of remolded silt. In most cases, the four Q tests were performed at four different strain rates. For one set of tests, two of the specimens were tested at the same strain rate while the other two specimens were performed at different strain rates.

Table 5.21 summarizes the initial specimen data for the Q tests performed in this research as part of the strain rate study.

Table 5.21: Initial specimen data for Q tests performed at different strain rates

Test	σ_3 (psi)	w (%)	γ_d (pcf)	S (%)	e	$\dot{\epsilon}$ (%/min)
B1-1	10	20.6	110.7	100	0.516	1.2
B1-2	10	20.8	111.0	100	0.513	5.1
B1-3	10	21.2	110.8	100	0.515	0.2
B1-4	10	21.0	110.1	100	0.524	0.01
B10-1	10	20.1	111.8	100	0.501	1.0
B10-2	10	20.0	113.0	100	0.485	9.9
B10-3	10	19.9	113.0	100	0.485	0.1
B10-4	10	19.6	113.3	100	0.481	0.01
B14-1	10	19.1	113.1	100	0.484	0.9
B14-2	10	19.0	112.9	100	0.487	9.7
B14-3	10	19.2	111.0	100	0.512	0.1
B14-4	10	19.1	112.1	100	0.498	0.01
B15-1	10	19.7	112.4	100	0.493	1.1
B15-2	10	19.3	113.6	100	0.477	9.9
B15-3	10	19.3	110.7	100	0.516	9.3
B15-4	10	19.4	113.2	100	0.484	0.01

Figures 5.74 through 5.77 show plots of deviator stress vs. axial strain for the Q tests performed at different strain rates. Each of these figures shows the stress-strain curves for Q test specimens obtained from the same remolded batch of silt and tested at different strain rates.

Figure 5.74 shows the stress-strain curves for Q tests performed at a cell pressure of 10 psi on specimens obtained from the same batch consolidometer sample of

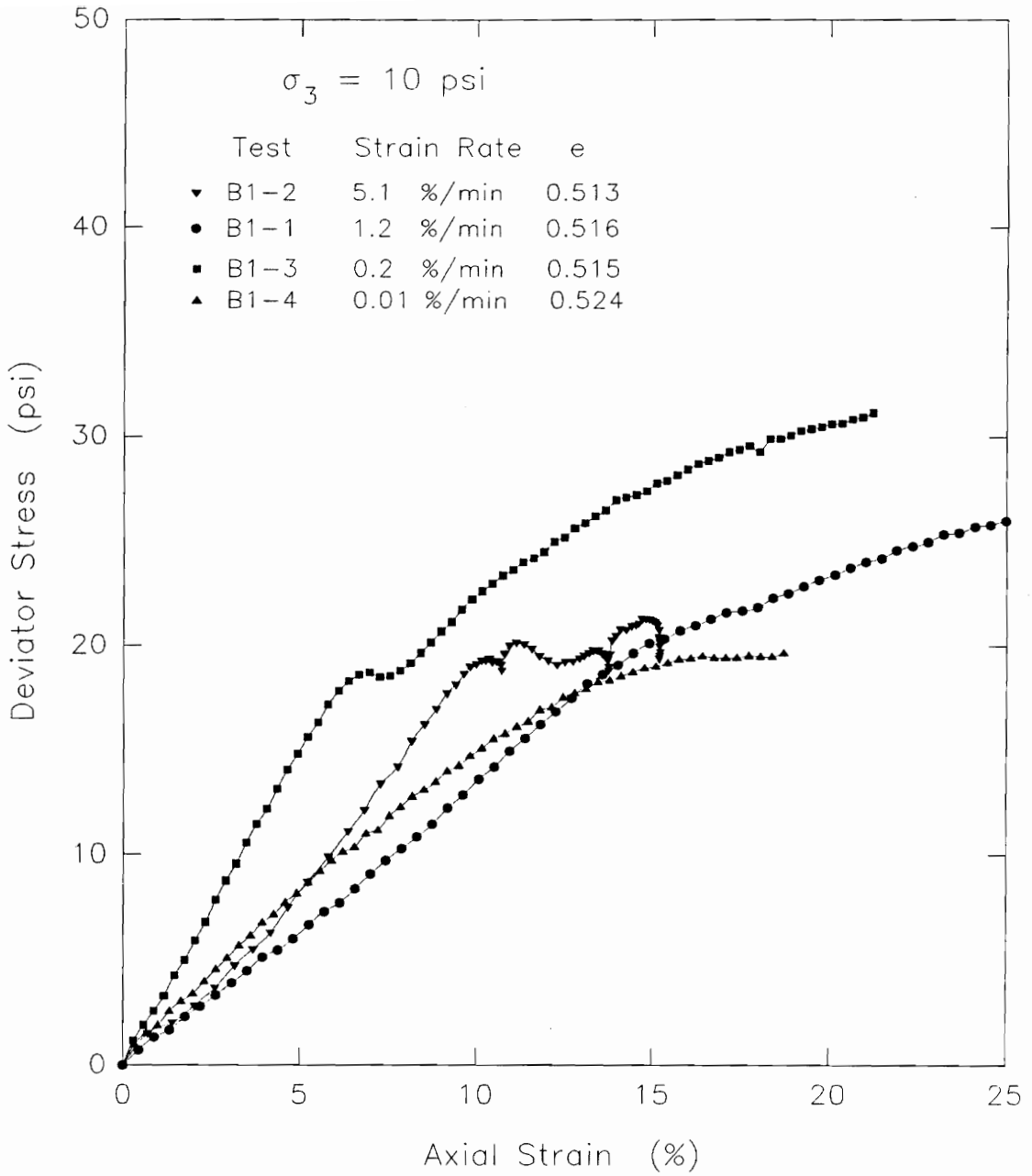


Figure 5.74. Deviator stress vs. axial strain behavior measured in Q tests performed at different strain rates on remolded old LMVD silt

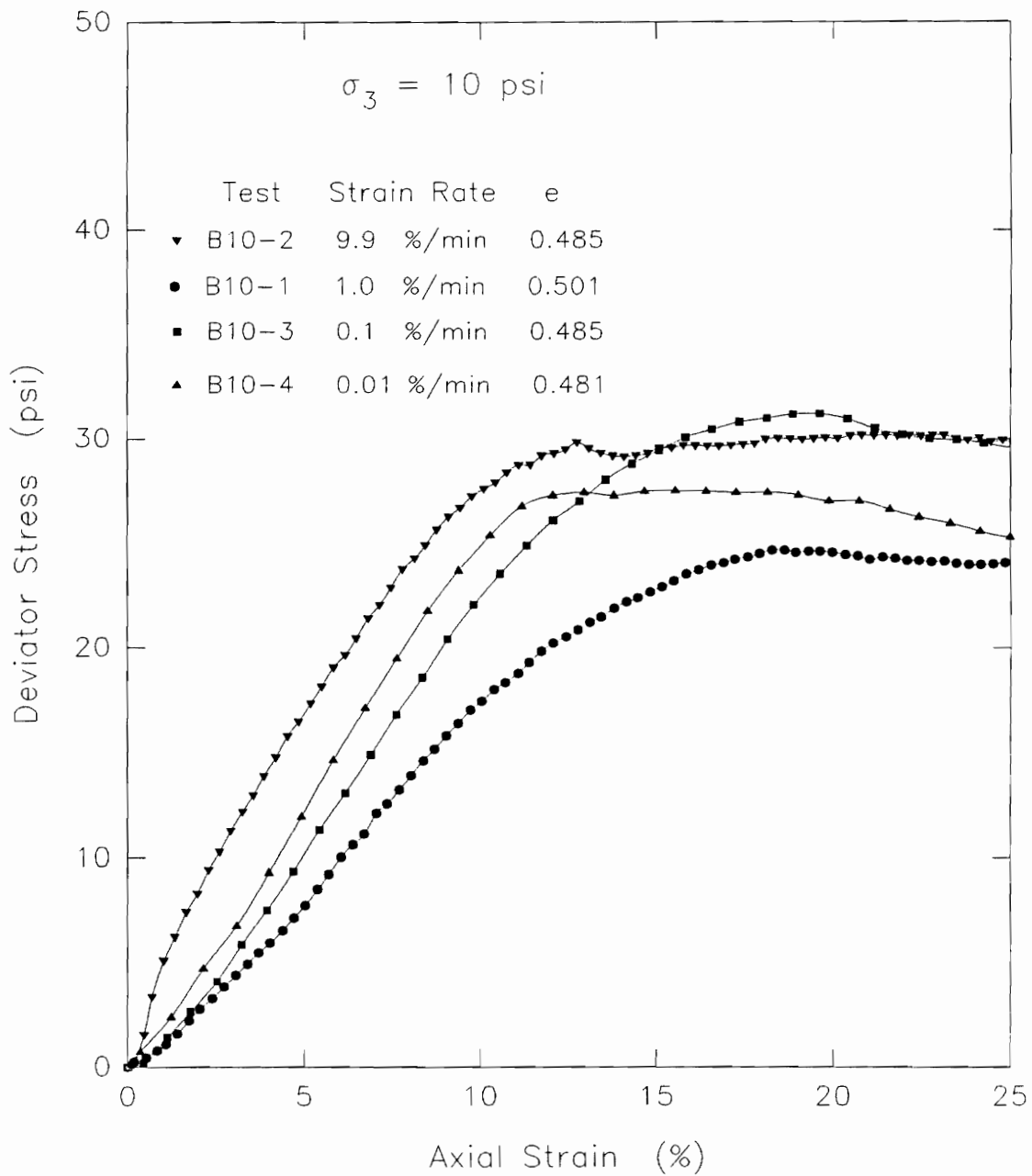


Figure 5.75. Deviator stress vs. axial strain behavior measured in Q tests performed at different strain rates on remolded old LMVD silt

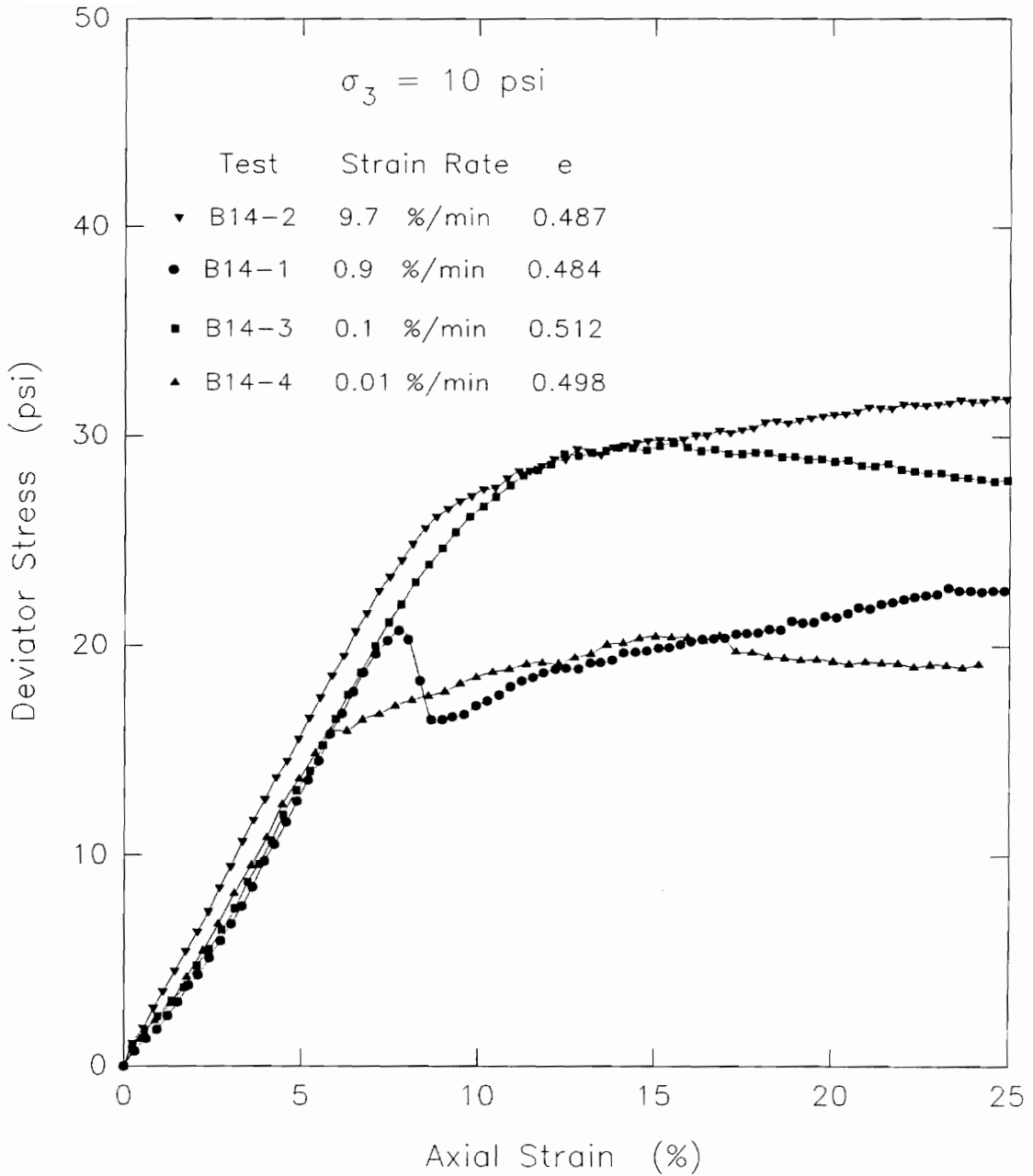


Figure 5.76. Deviator stress vs. axial strain behavior measured in Q tests performed at different strain rates on remolded old LMVD silt

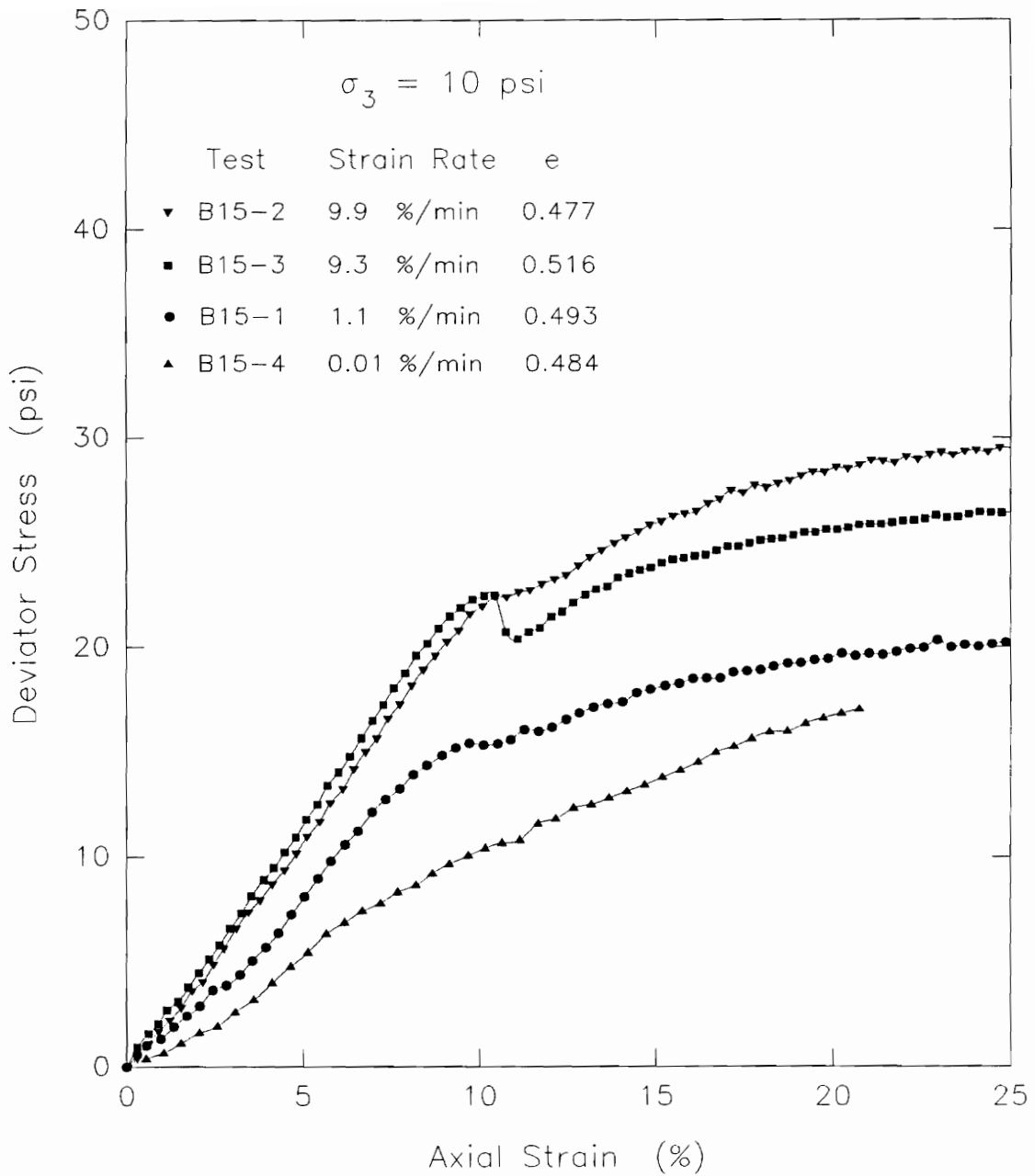


Figure 5.77. Deviator stress vs. axial strain behavior measured in Q tests performed at different strain rates on remolded old LMVD silt

remolded LMVD silt. The specimens were sheared at strain rates ranging from 0.01%/min to 5%/min. This figure shows that the stress-strain behavior and the slope of the stress-strain curves varied. The specimen sheared at the fastest rate did not, however, have the steepest stress-strain curve. The least steep stress-strain curve likewise was not obtained for the specimen sheared at the slowest rate. This was inconsistent with what was expected. The variation in the slopes of these stress-strain curves does not suggest a definite relationship between the rate of shear and the observed stress-strain behavior.

The four stress-strain curves shown in Figure 5.74 all show a peak value of deviator stress at some point during each test. Some of these peaks were slight in nature, and are followed by a subsequent increase in deviator stress with increasing strain. These peak deviator stresses ranged from about 18 to 22 psi in magnitude, and occurred at axial strains ranging from about 5% to 18%. The specimens sheared at rates of 0.2%/min and 1.2%/min both showed slight peaks in their stress-strain behavior. These slight peaks were followed by increasing deviator stress with increasing axial strain. The deviator stress for the specimen sheared at a rate of 0.01%/min increased to a peak value at about 15% axial strain and experienced little change in deviator stress throughout the rest of the test.

For the specimen sheared at the fastest rate, 5.1%/min, the deviator stress increased to a peak value and then underwent a series of slight increases and decreases until the test was terminated.

The erratic stress-strain behavior observed in the four Q tests shown in Figure 5.74 may possibly be the result of cavitation of the soil pore water during undrained shear. The occurrence of the slight peaks in the stress-strain curves and their relation to cavitation of soil pore water will be discussed in more detail in Section 6.12.

Figure 5.75 shows the stress-strain curves for Q tests performed at a cell pressure of 10 psi and tested at strain rates varying from 0.01%/min to 10%/min. This figure shows that the slope of the stress-strain curve of the specimen sheared at the fastest rate, 10%/min, was the steepest of the four tests. The stress-strain curve of the specimen sheared at a rate of 1%/min had the smallest slope of the four tests, even though it was not sheared at the slowest rate. The variation in the slopes of these four stress-strain curves does not suggest a consistent effect of the rate of shear on the stress-strain behavior. These four stress-strain curves also appear to be relatively smooth and do not exhibit any unusual strain-softening behavior.

Figure 5.76 shows the deviator stress vs. axial strain plots for Q tests performed on specimens obtained from the same batch consolidometer sample. All four of these Q tests were performed at a cell pressure of 10 psi and were sheared at strain rates which varied from 0.01%/min to 9.7%/min. The stress-strain curves for these tests all show very similar behavior at small axial strains. At about 6 percent axial strain the sample sheared at a rate of 0.01%/min shows a noticeable decrease in the slope of its stress-strain curve. The stress-strain curve for the Q test sheared at a rate of 1%/min shows a peak at about 8 percent axial strain followed by noticeable strain-softening.

The other two Q tests performed at strain rates of 0.1%/min and 9.7%/min showed similar stress-strain behavior up to about 15 percent axial strain. At higher strains, the specimen sheared at 0.1%/min showed slight strain-softening behavior. The specimen sheared at a rate of 9.7%/min continued to exhibit strain-hardening behavior.

Figure 5.77 shows the deviator stress vs. axial strain curves for Q tests performed at a cell pressure of 10 psi. Two of these specimens were sheared at a rate of about 10%/min. The other two specimens were sheared at rates of 0.01%/min and 1%/min.

As can be seen from this figure, as the rate of shear increased, the steepness of the initial portions of the stress-strain curves increased. The two specimens sheared at a rate of about 10%/min showed very similar stress-strain behavior up to about 10 percent axial strain. One of these tests then exhibited noticeable strain-softening followed by strain-hardening with increased axial strain. Although the other specimen sheared at a similar rate did not show very noticeable strain-softening as the first specimen had, it did show a slight change in slope at about the same axial strain. After this slight change in slope, the specimen continued to exhibit strain-hardening behavior.

The results of the Q tests from different batch consolidometer samples but performed at similar strain rates can also be compared. All of these Q tests were performed at a cell pressure of 10 psi.

Figure 5.78 shows the deviator stress vs. axial strain curves for the Q tests sheared at a strain rate of about 0.01%/min. These tests show considerable variation in their stress-strain behavior. It should be noted that none of these tests showed noticeable strain-softening behavior of an abrupt nature.

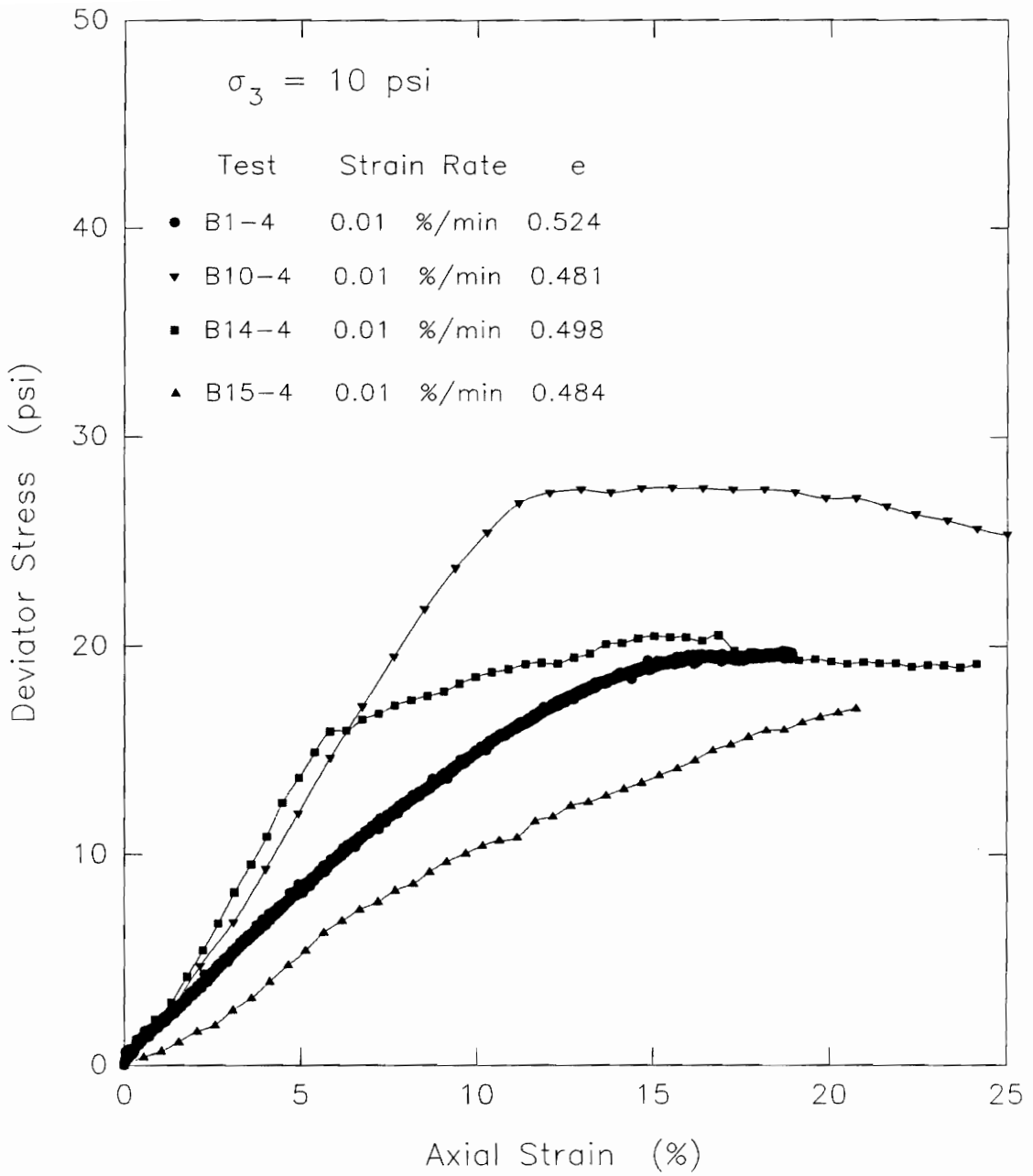


Figure 5.78. Deviator stress vs. axial strain behavior measured in Q tests performed at a strain rate of 0.01%/min on remolded old LMVD silt

Figure 5.79 shows the deviator stress vs. axial strain curves for three Q tests performed at 10 psi cell pressure and sheared at strain rates between 0.1%/min and 0.2%/min. These tests tended to show more consistent stress-strain behavior, reaching relatively the same ultimate strength for the soil. Of these three tests, only one showed a slight peak followed by abrupt strain-softening. This occurred at an axial strain of about 7% in test B1-3, sheared at a strain rate of about 0.2%/min.

The deviator stress vs. axial strain curves for the four Q tests sheared at a strain rate of about 1%/min are shown in Figure 5.80. These tests were all performed at a cell pressure of 10 psi. The strain rate varied slightly from about 0.9%/min to 1.2%/min. The stress-strain curves for these four tests show considerable variation. Test B14-1 shows very noticeable strain-softening at about 7% axial strain. A noticeable change in the slope of the stress-strain curve of test B15-1 occurred at about 8% axial strain. Both test B10-1 and B15-1 showed very similar stress-strain behavior up to axial strains of about 8%. At higher axial strains, the two tests showed more variation in their stress-strain behavior. Test B1-1 also shows some slight strain-softening or a change in slope at about 18% axial strain.

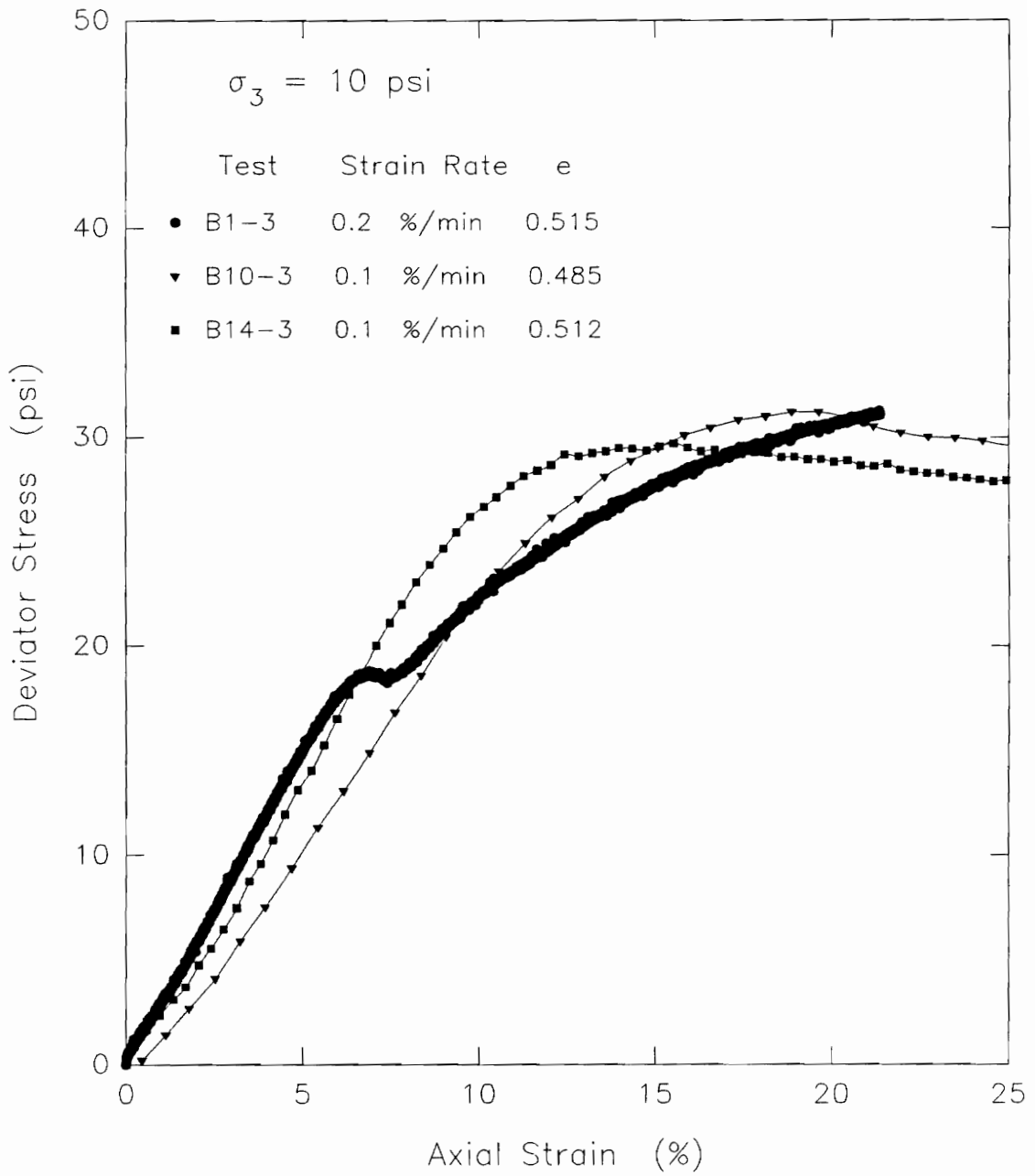


Figure 5.79. Deviator stress vs. axial strain behavior measured in Q tests performed at strain rates ranging from 0.1%/min to 0.2%/min on remolded old LMVD silt

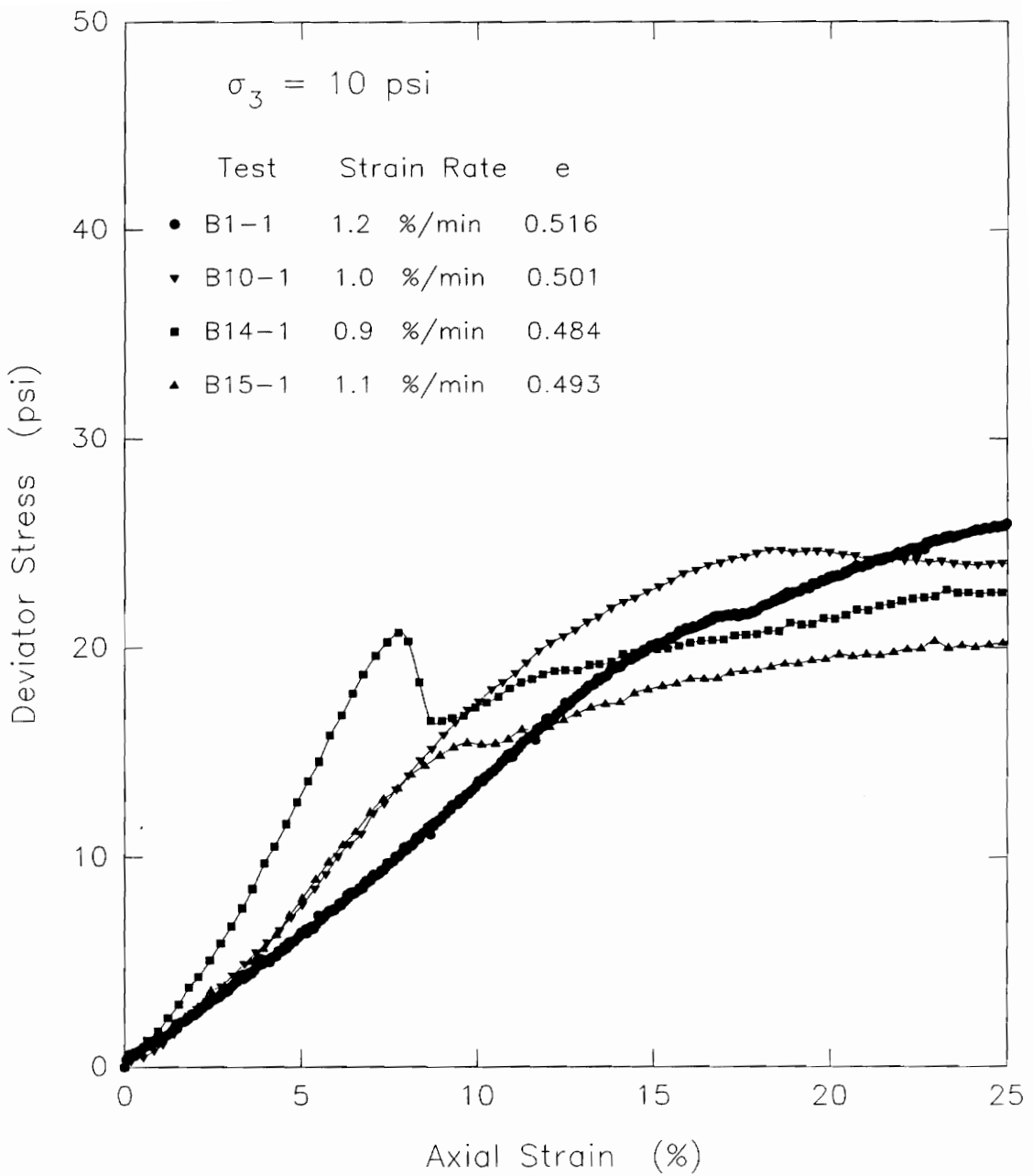


Figure 5.80. Deviator stress vs. axial strain behavior measured in Q tests performed at a strain rate ranging from 0.9 to 1.2%/min on remolded old LMVD silt

The stress-strain curves for the five Q tests performed at strain rates between 5%/min and 10%/min are shown in Figure 5.81. These tests showed some variation as well as some similarity in their stress-strain behavior. Two of the tests, B10-2 and B14-2, exhibited very similar stress-strain behavior throughout the tests. Two other tests, B15-2 and B15-3, showed stress-strain behavior which was similar up to 10% axial strain. At higher axial strains, their behavior varied. Test specimen B15-3 showed strain-softening at 10% axial strain whereas specimen B15-2 did not, but it did have a noticeable change in slope at a similar axial strain. Test specimen B1-2 was sheared at a strain rate of about 5%/min, whereas the other four tests were sheared at a strain rate of 10%/min. This test showed stress-strain behavior which was different from the other four tests. It did tend to show periods of strain-softening above 10% axial strain.

The Q tests performed at different strain rates in this research did not appear to show any behavior which was felt to be consistent enough to warrant further study in this research. As stated previously, it was expected that the faster a specimen was sheared, the larger the decrease in pore water pressure would be along the shear plane. This was expected to influence these tests by causing increased strain-hardening with increasing rate of shear.

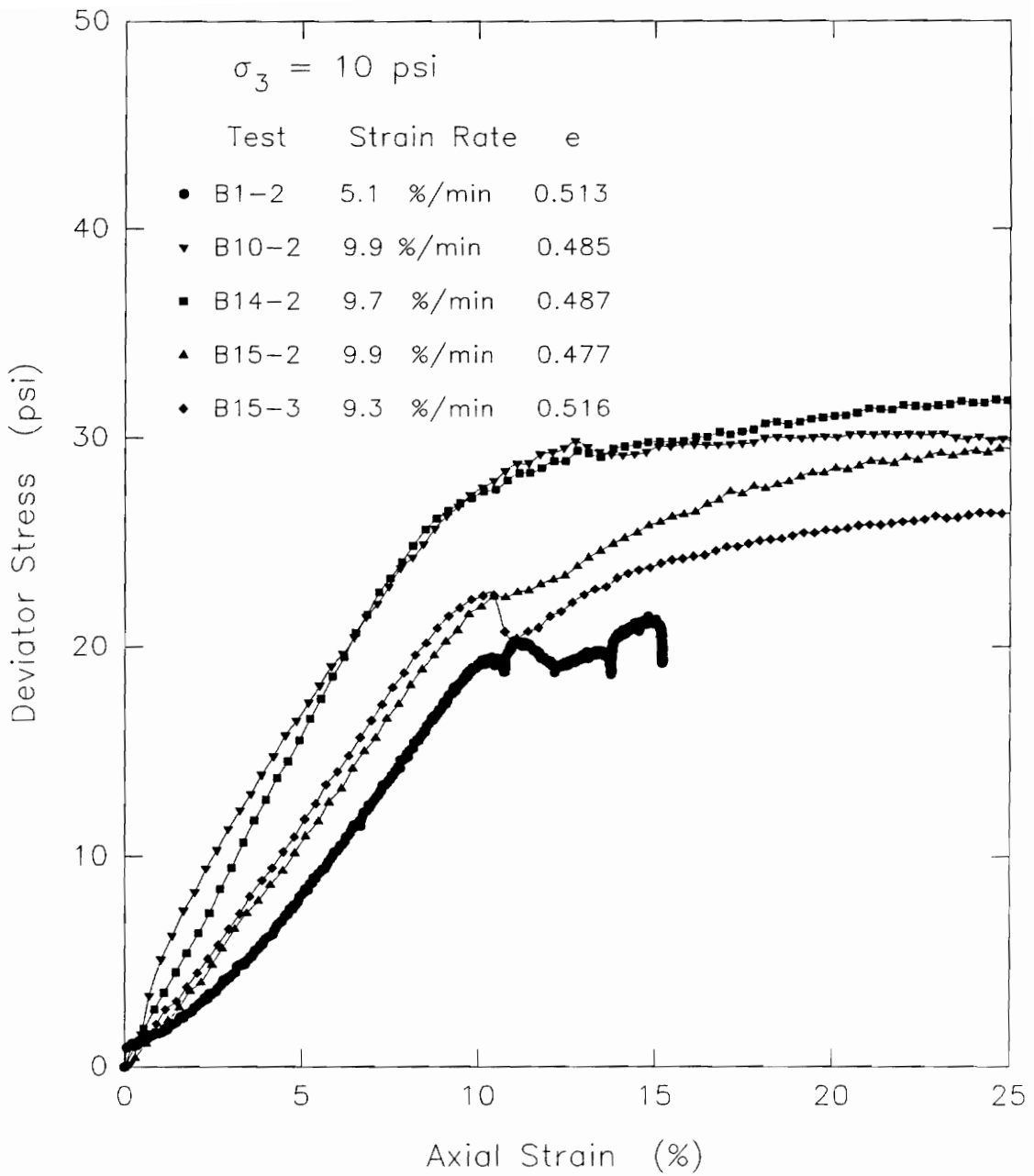


Figure 5.81. Deviator stress vs. axial strain behavior measured in Q tests performed at a strain rate ranging from 5 to 10%/min on remolded old LMVD silt

This was observed in the set of tests shown in Figure 5.78. This behavior, however, was not observed consistently in the other sets of tests. It may be that the samples in the other sets of tests experienced different levels of disturbance which affected their stress-strain behavior and distorted the influence of shearing the specimens at different strain rates.

The larger decreases in pore water pressure in the rapidly sheared specimens were also expected to lead to cavitation of the pore water more readily than in specimens sheared at a slower rate where smaller decreases in pore water pressure would have occurred. The time over which the decrease in pore water pressure took place may have influenced the extent to which gases were able to come out of solution from the pore water and affect the stress-strain behavior.

Some of the stress-strain curves exhibited abrupt peaks followed by strain-softening. As will be discussed in Section 6.12, the occurrence of abrupt strain-softening in the stress-strain curves, may possibly be related to cavitation of the soil pore water. For tests performed at the same strain rate, it appears that the tests sheared at the slowest rate tended not to exhibit strain-softening in their stress-strain behavior. At faster strain rates, the

silt specimens showed strain-softening behavior more frequently, but not always. Strain-softening or changes in the slope of the stress-strain curves were most often observed in the tests sheared at the fastest strain rates. Based on this, it appears that the more rapidly sheared specimens may have experienced cavitation of soil pore water resulting in the erratic stress-strain behavior observed. It is uncertain as to why strain-softening was observed for some of these rapidly sheared test specimens, but not in others. Again, it may be that the samples experienced different levels of disturbance which had variable influences on the stress-strain behavior observed.

5.9 Conventional Q Tests

A total of 26 conventional Q tests have been performed on remolded specimens of old and new LMVD silt. These tests have been performed without midheight pore pressure monitoring. The specimens were all sheared at a strain rate of 1%/min. These tests were performed in order to study in more detail the undrained stress-strain behavior of saturated, dilatant silts, at various cell pressures.

These Q tests were performed on samples obtained from 5-inch diameter specimens of saturated silt remolded from a slurry in a batch consolidometer. The slurry specimens were all consolidated to K_0 conditions under an effective

vertical consolidation pressure of 65 psi. The 5-inch diameter batch consolidometer specimens could be split into four quarters from which four 1.4-inch diameter triaxial specimens could be trimmed. In several cases, all four triaxial specimens were not testable or gave poor test results. Some of the specimens experienced excessive disturbance during trimming and placement in the triaxial cell and were discarded. Other specimens were observed to have leakage at the end platens during shear. The results from these Q tests have also been omitted from the discussions which follow. A few test specimens were slightly misaligned, relative to the end platens in the triaxial cell, so that they tended to experience a buckling failure. These test results have also been omitted.

Tests were performed on remolded specimens of both old and new LMVD silt. The initial properties of these Q test specimens are presented in Table 5.22.

The results of the Q tests on old and new LMVD silt will be presented and discussed separately. In presenting the results for a given silt, the Q tests performed on specimens obtained from the same batch consolidometer sample will be discussed first. Comparisons between Q tests on samples from different batches will be presented subsequently.

Table 5.22: Initial properties of triaxial specimens tested in conventional Q tests

Test	σ_3 (psi)	w (%)	e	γ_d (pcf)	S (%)
B4-4	0	20.55	0.531	109.6	100
B7-1	20	20.28	0.533	109.5	100
B7-2	40	19.96	0.512	111.0	100
B8-1	0	19.52	0.500	111.9	100
B8-2	10	19.44	0.466	114.5	100
B8-3	20	20.29	0.489	112.8	100
B8-4	30	19.64	0.456	115.3	100
B9-1	20	20.44	0.525	110.0	100
B9-2	50	20.44	0.521	110.4	100
B9-4	100	20.42	0.489	112.7	100
B11-1	0	19.55	0.483	113.2	100
B11-2	5	19.57	0.460	114.9	100
B11-3	10	19.66	0.468	114.3	100
B11-4	15	19.75	0.503	111.7	100
B12-1	20	18.53	0.493	112.4	100
B12-3	80	18.99	0.486	112.9	100
B13-1	10	19.04	0.490	112.7	100
B13-2	40	19.10	0.459	115.1	100
B17-1*	0	22.79	0.634	102.7	96.6
B17-2*	10	22.95	0.622	103.5	99.2
B17-3*	20	22.39	0.620	103.6	97.2
B17-4*	30	22.78	0.628	103.1	97.6
B18-1*	20	23.92	0.616	103.9	100
B18-2*	40	24.51	0.607	104.5	100
B18-3*	60	24.24	0.620	103.6	100
B18-4*	80	23.94	0.608	104.4	100

* New LMVD Silt

5.9.1 Old LMVD silt

The first group of specimens tested only provided one Q test which gave good results. Figure 5.82 shows the stress-strain curve for Q test B4-4, performed as an unconfined compression test. As can be seen from this stress-strain curve, the deviator stress reached an initial peak value of about 20 psi at about 10 percent axial

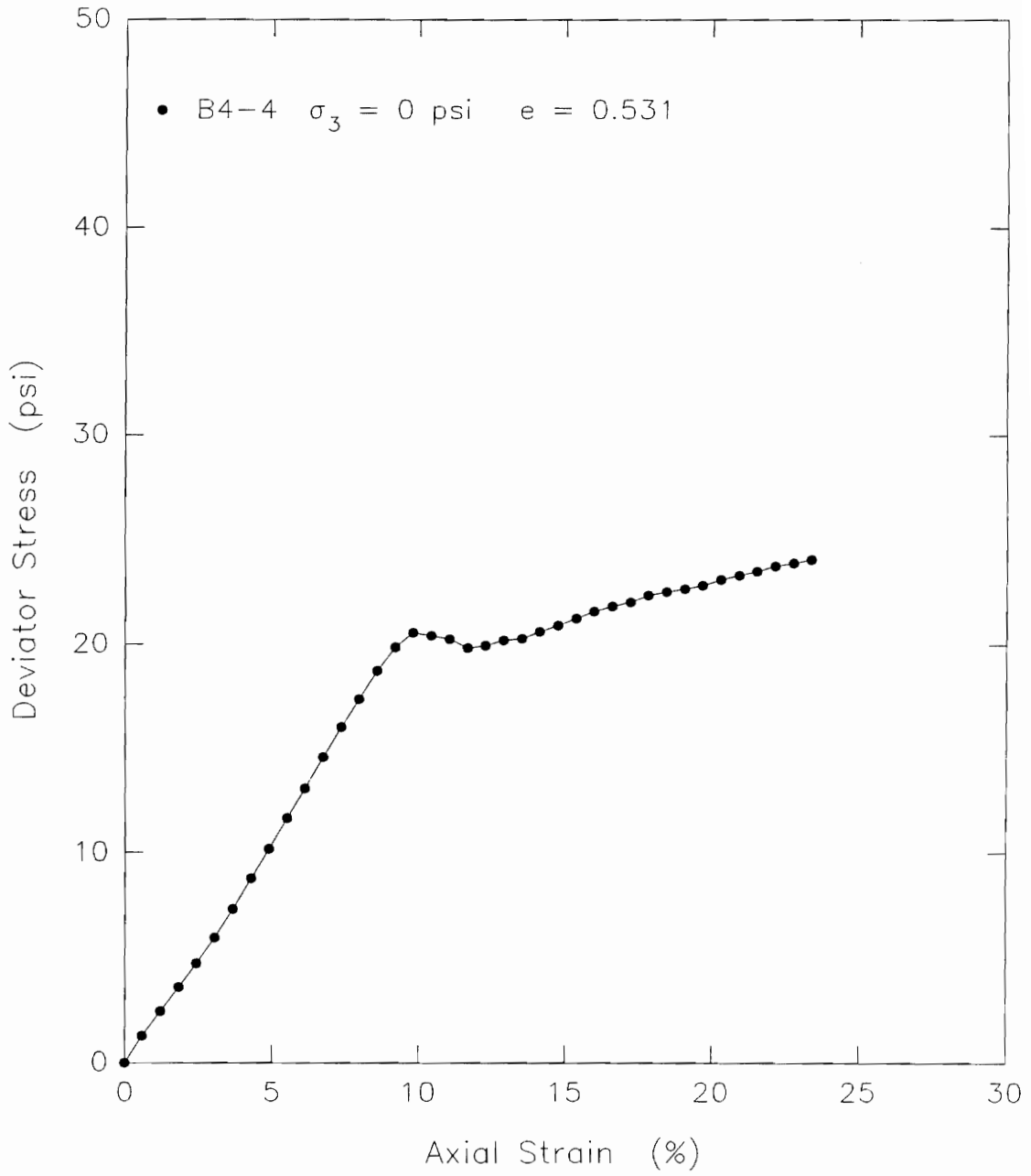


Figure 5.82. Deviator stress-strain relationship measured in Q test B4-4 on remolded old LMVD silt

strain. The deviator stress then decreased slightly until about 12 percent axial strain. With further increase in strain, the deviator stress again began to increase.

Figure 5.83 shows the deviator stress-strain curves for Q tests B7-1 and B7-2. These tests were performed at cell pressures of 20 and 40 psi, respectively. As can be seen in this figure, the deviator stress for these two tests did not reach peak values until about 15 percent axial strain. It is also worth noting that the peak deviator stress was higher for the test performed at a cell pressure of 20 psi than for the test performed at 40 psi. This was not as expected. Perhaps these two test specimens had experienced different levels of disturbance, leading to different stress-strain behavior and measured undrained strengths.

The stress-strain curves for Q tests B8-1, B8-2, B8-3 and B8-4 are presented in Figure 5.84. Tests B8-1 and B8-3, performed at cell pressures of 0 and 20 psi, showed slight peaks in deviator stress, or noticeable changes in slope at an axial strain of about 8 percent. The deviator stress in these two tests then increased with further increase in axial strain.

The stress-strain curves for the other two Q tests, B8-2 and B8-4 performed at cell pressures of 10 and 30 psi,

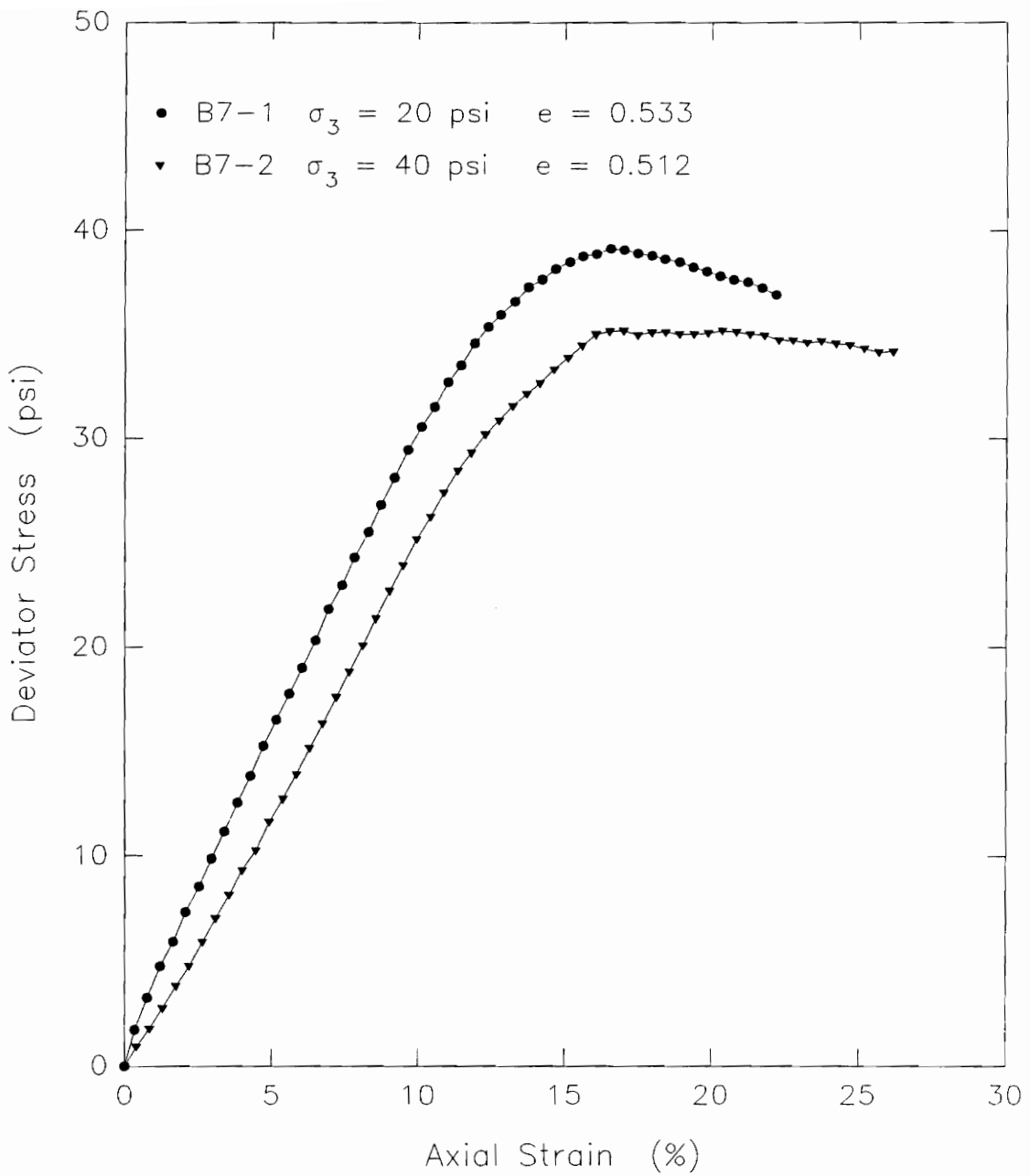


Figure 5.83. Deviator stress-strain relationships measured in Q tests B7-1 and B7-2 on remolded old LMVD silt

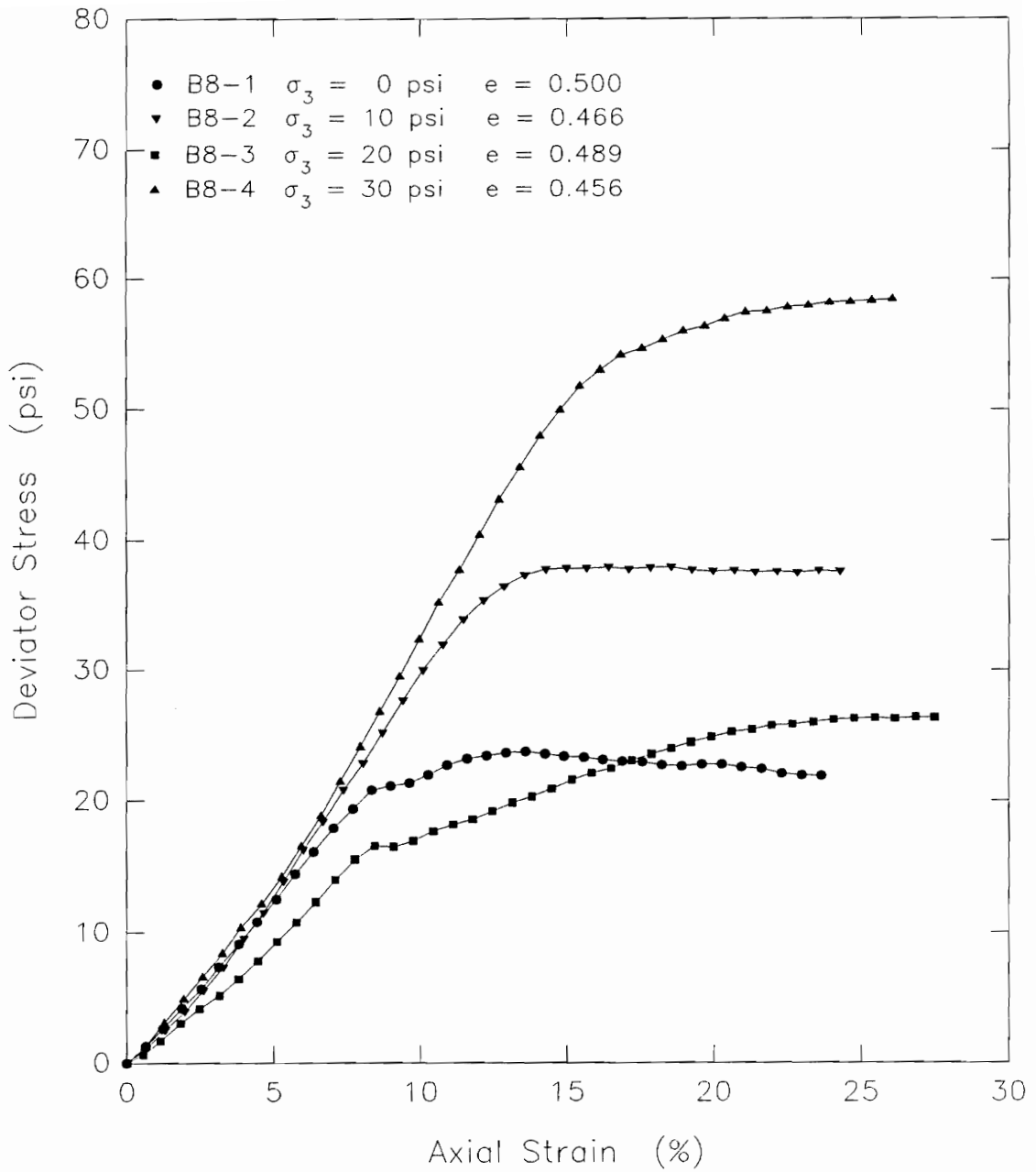


Figure 5.84. Deviator stress-strain relationships measured in Q tests B8-1, B8-2, B8-3, and B8-4 on remolded old LMVD silt

did not show peaks in their deviator stress-strain curves at strains less than 10 percent. Peak values were not reached until axial strains of 13 percent or greater.

Using a failure criterion of 8.5 percent axial strain, the total stress Mohr's circles have been plotted in Figure 5.85. Except for test B8-3, performed at a cell pressure of 20 psi, the Mohr's circles for this set of tests tended to yield a Mohr-Coulomb strength envelope characterized by a $\phi_u = 0$, $S_u = c$ condition. If the results of test B8-3 are neglected, the undrained strength envelope at 8.5% axial strain for this group of tests gives the undrained strength parameters, $c = 10.2$ psi and $\phi_u = 4^\circ$.

Considering peak deviator stress as the failure criterion, the Mohr's circles for this set of tests have been plotted in Figure 5.86. If the circle for test B8-3, is again neglected, the Mohr-Coulomb failure envelope for the other three tests gives the undrained shear strength parameters $c = 7.7$ psi and $\phi_u = 22.2^\circ$.

The test performed at 20 psi cell pressure in this set of tests illustrates the erratic behavior often observed in Q tests on saturated silt specimens. This test gave stress-strain behavior which was inconsistent with the other tests in this group. The erratic behavior makes the results of the group of Q tests difficult to interpret.

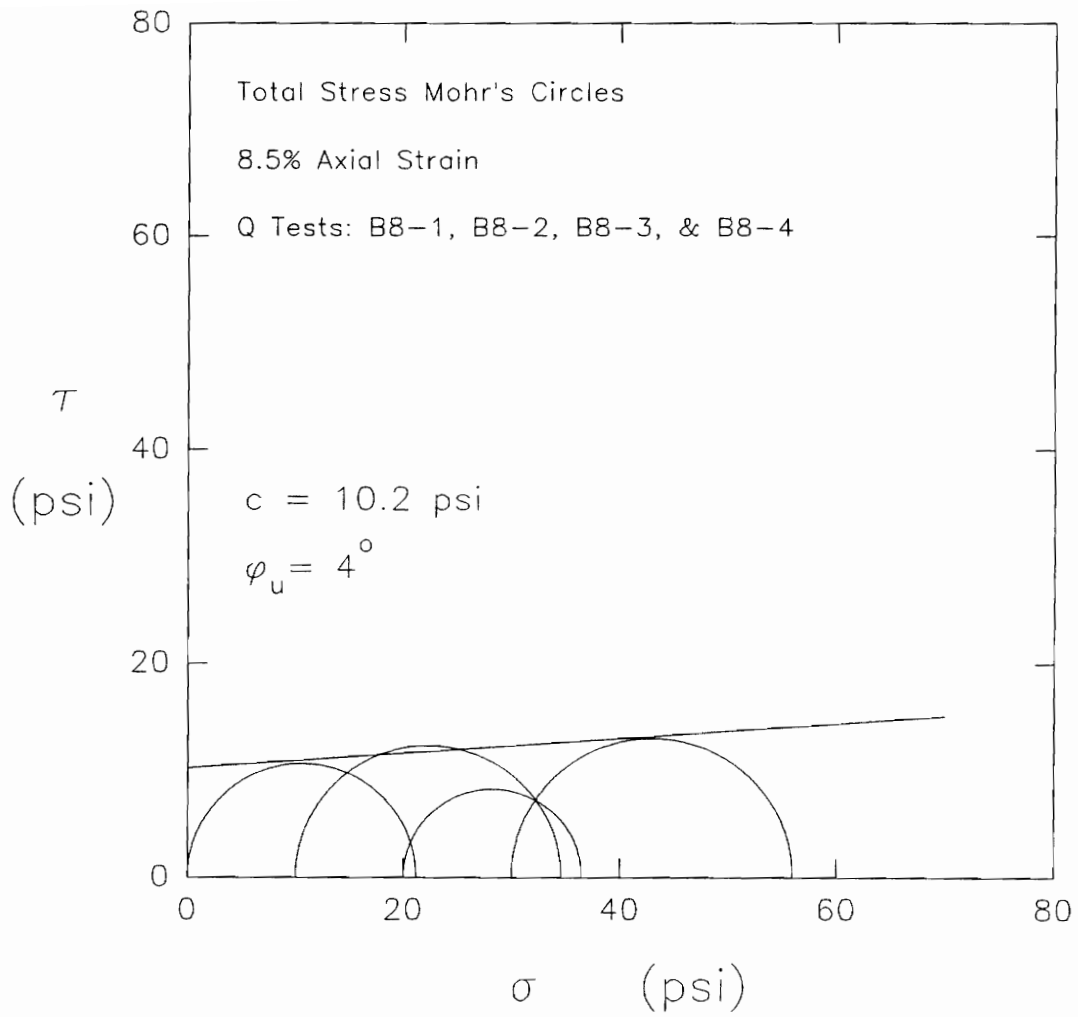


Figure 5.85. Total stress Mohr's circles at 8.5% axial strain for Q tests B8-1, B8-2, B8-3, and B8-4 on remolded old LMVD silt

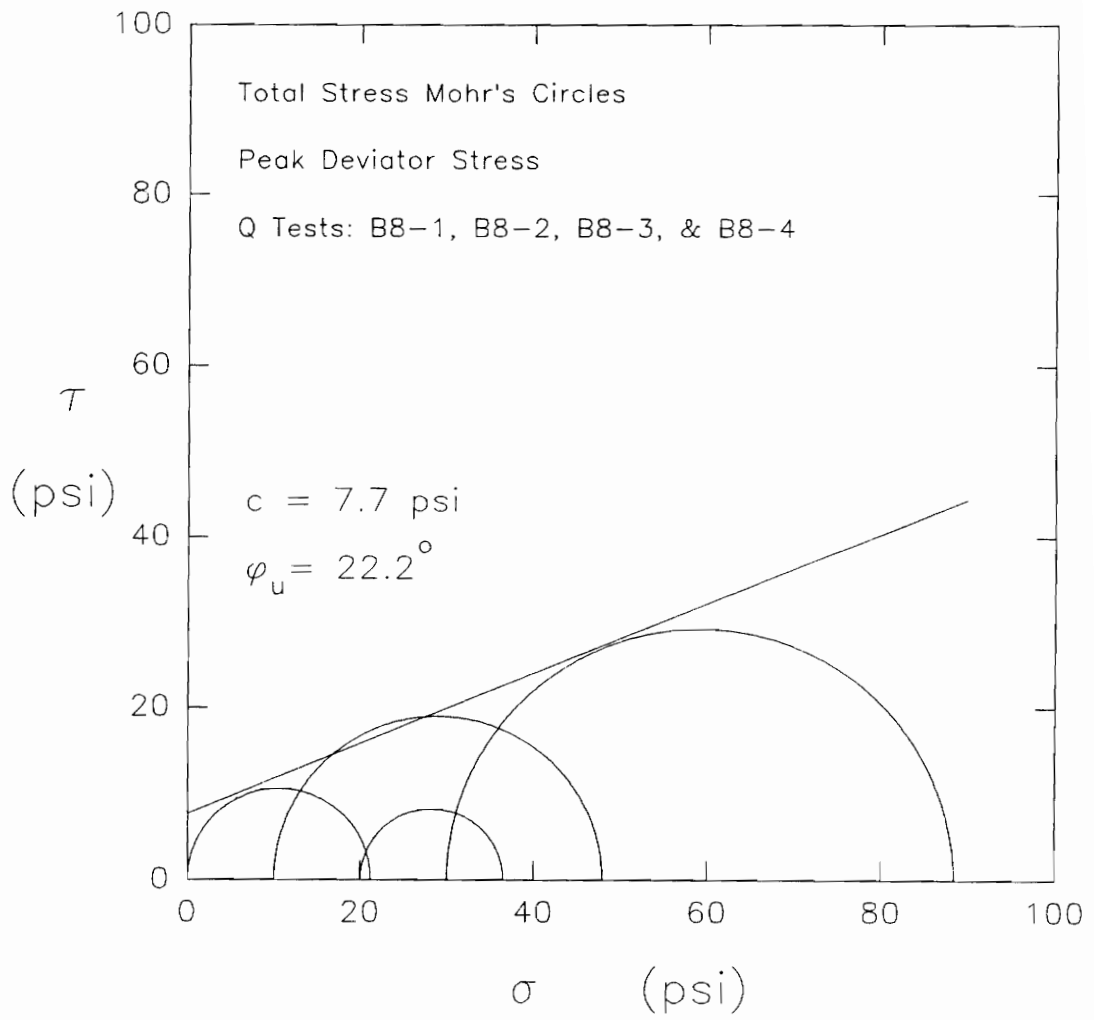


Figure 5.86. Total stress Mohr's circles at peak deviator stress for Q tests B8-1, B8-2, B8-3, and B8-4 on remolded old LMVD silt

The behavior of the other three tests tended to be more consistent with each other. This helps to make the interpretation of these test results more feasible. Other sets of Q tests often show much more erratic and inconsistent behavior. As a result, undrained strength interpretations can be much more difficult, if not impossible. Because silt specimens are very easily disturbed, it may be that specimen B8-3 experienced a different level of disturbance than the other three specimens, resulting in inconsistent stress-strain behavior for this specimen.

Figure 5.87 shows the stress-strain behavior of Q test specimens B9-1, B9-2, and B9-4. These Q tests were performed at cell pressures of 20, 50, and 100 psi, respectively. As can be seen from this figure, these three Q test specimens showed very similar stress-strain behavior at axial strains below about 10%. At higher axial strains, tests B9-2 and B9-4 performed at 50 and 100 psi, still showed very similar stress-strain behavior throughout the tests. Test B9-1, performed at a cell pressure of 20 psi, showed stress-strain behavior which differed from the other two tests at axial strains above about 10 percent. The difference between the deviator stress of this test and the other two increased with increasing axial strain.

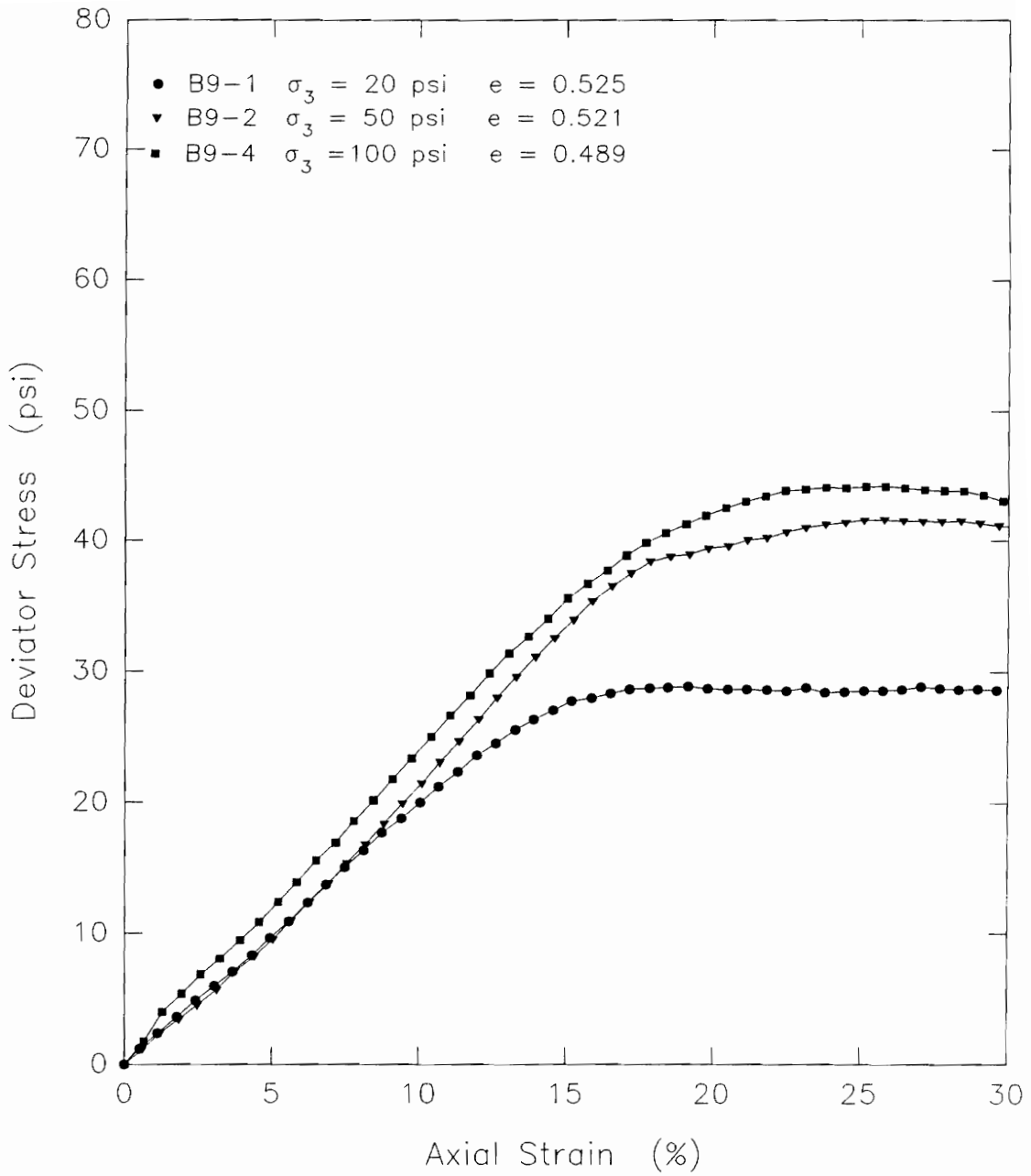


Figure 5.87. Deviator stress-strain relationships measured in Q tests B9-1, B9-2, and B9-4 on remolded old LMVD silt

Figure 5.88 shows the total stress Mohr's circles for these three Q tests at 10 percent axial strain at failure. From this figure, it can be seen that the Mohr-Coulomb strength envelope for the soil approaches a $\phi_u = 0$, $S_u = c$ condition. The actual undrained strength parameters for the given envelope are $c = 9.1$ psi and $\phi_u = 1.5^\circ$.

Figure 5.89 shows the Mohr-Coulomb failure envelope for the soil when peak deviator stresses are taken as the failure criterion. Here it can be seen that the Mohr-Coulomb envelope is bilinear. At low cell pressures the soil has a $\phi_u > 0$ envelope. Up to a normal stress of about 65 psi, the undrained strength parameters are $c = 8.6$ psi and $\phi_u = 10.1^\circ$. At higher cell pressures, a $\phi_u = 0$, $S_u = c = 23.7$ psi envelope is approached. The occurrence of a bilinear undrained strength envelope for saturated dilatant silts is similar to the observations of Penman (1953), as discussed in Section 2.2.

Figure 5.90 shows the stress-strain behavior measured for Q test specimens B11-1, B11-2, B11-3, and B11-4. These four Q tests were performed at cell pressures of 0, 5, 10, and 15 psi, respectively. As can be seen from this figure, the three Q tests performed at the lowest cell pressures all showed peaks in their deviator stress-strain curves between 9 and 11 percent axial strain. These peaks in

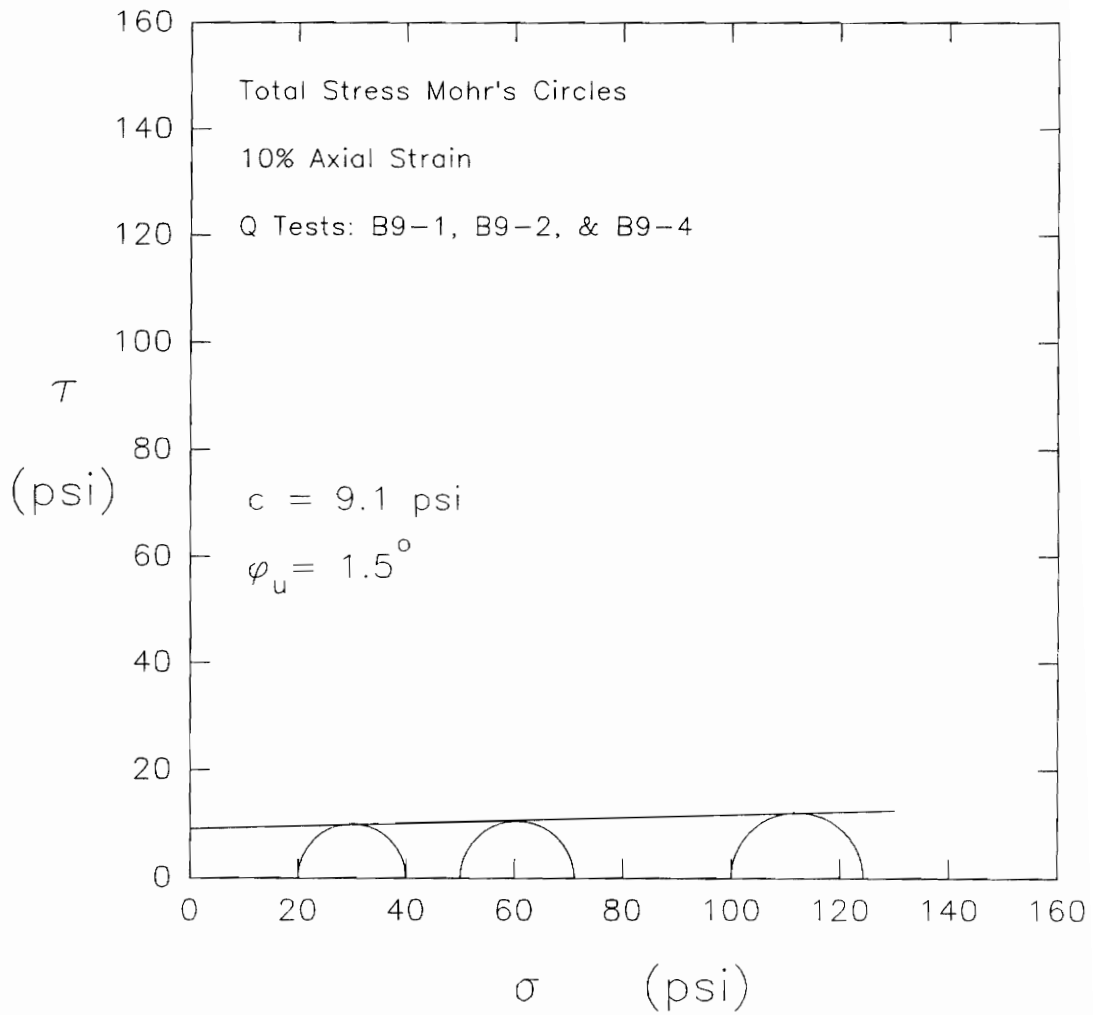


Figure 5.88. Total stress Mohr's circles at 10% axial strain for Q tests B9-1, B9-2, and B9-4 on remolded old LMVD silt

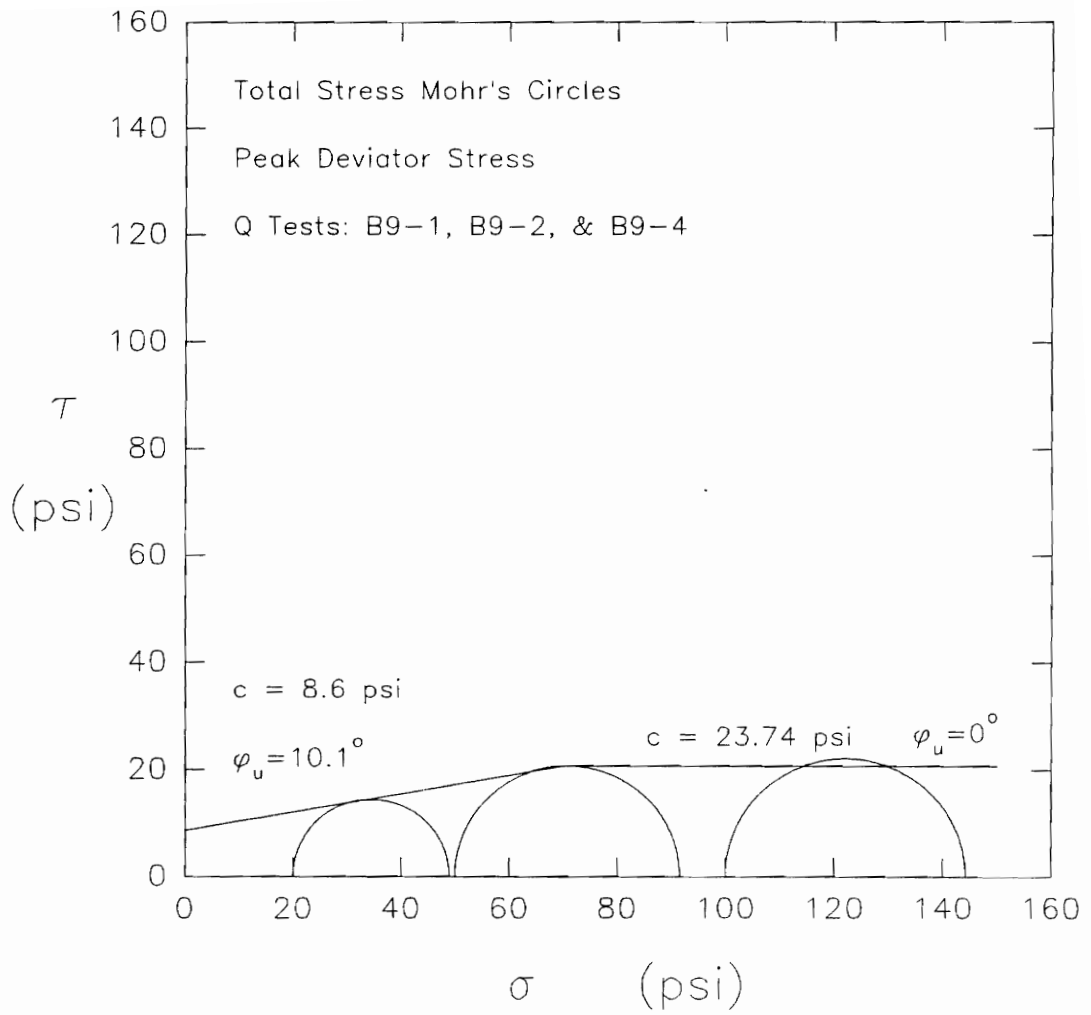


Figure 5.89. Total stress Mohr's circles at peak deviator stress for Q tests B9-1, B9-2, and B9-4 on remolded old LMVD silt

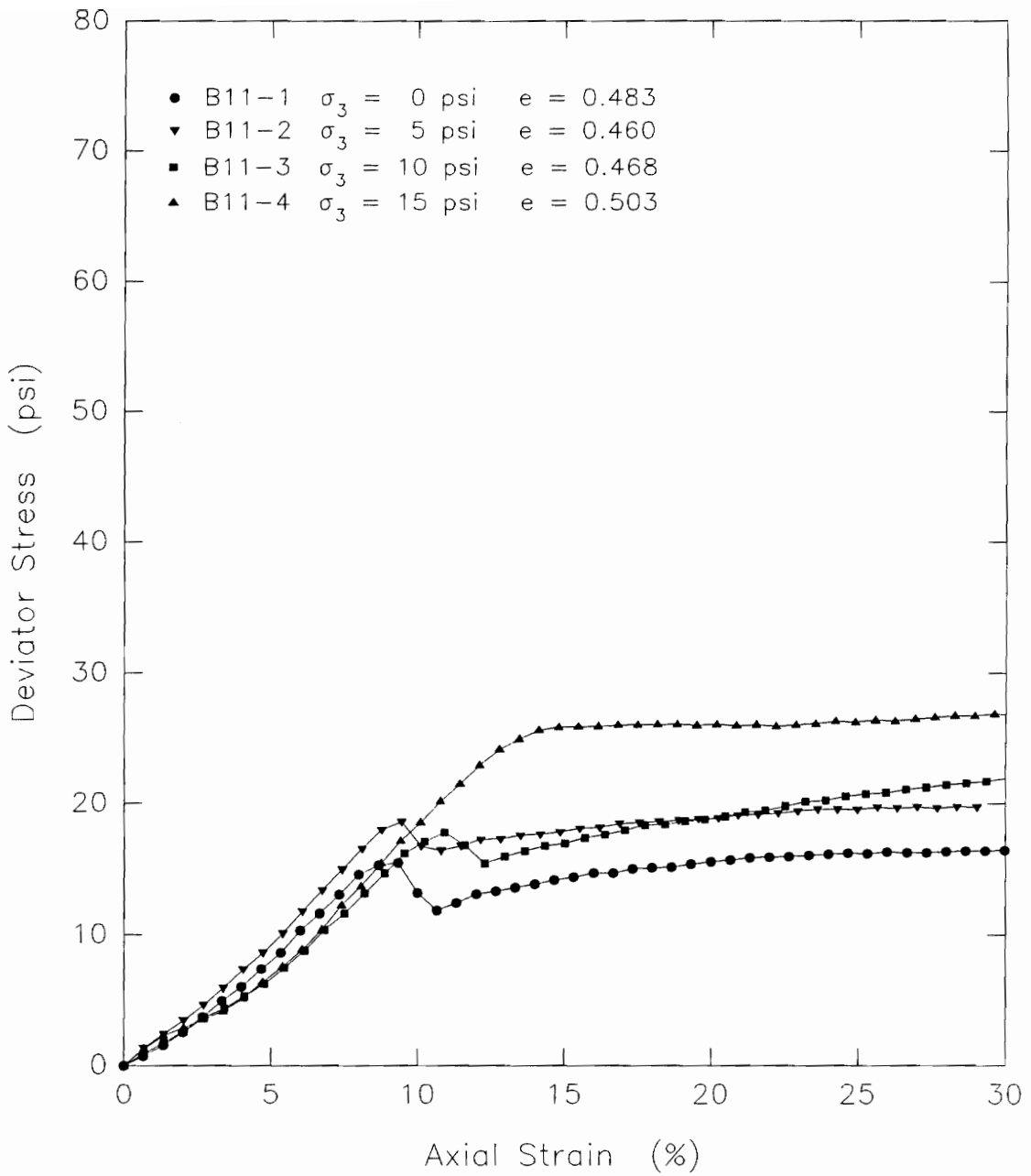


Figure 5.90. Deviator stress-strain relationships measured in Q tests B11-1, B11-2, B11-3, and B11-4 on remolded old LMVD silt

deviator stress were followed by slight strain-softening behavior. The tests then showed very slight strain-hardening with increasing axial strains. The Q test performed at 15 psi cell pressure did not have a peak in its deviator stress-strain curve at axial strains similar to the other three tests. The deviator stress continued to increase for this specimen until about 14 percent axial strain, at which point the deviator stress reached and maintained a constant value.

For a failure criterion of about 9 percent axial strain, the Mohr's circles for these tests have been plotted in Figure 5.91. At this value of axial strain, the undrained shear strength of the soil approaches a $\phi_u = 0$, $S_u = c = 8.1$ psi condition.

The Mohr's circles for these four tests, based on peak deviator stress as a failure criterion, are presented in Figure 5.92. In this case, the Mohr-Coulomb strength envelope for these four Q tests, gives the undrained shear strength parameters $c = 5.6$ psi and $\phi_u = 14.3^\circ$.

The deviator stress vs. axial strain curves for Q tests B12-1 and B12-3 are shown in Figure 5.93. These two tests were performed at cell pressures of 20 and 80 psi. As can be seen from this figure, the two Q tests showed similar stress-strain behavior up to about 7 percent axial

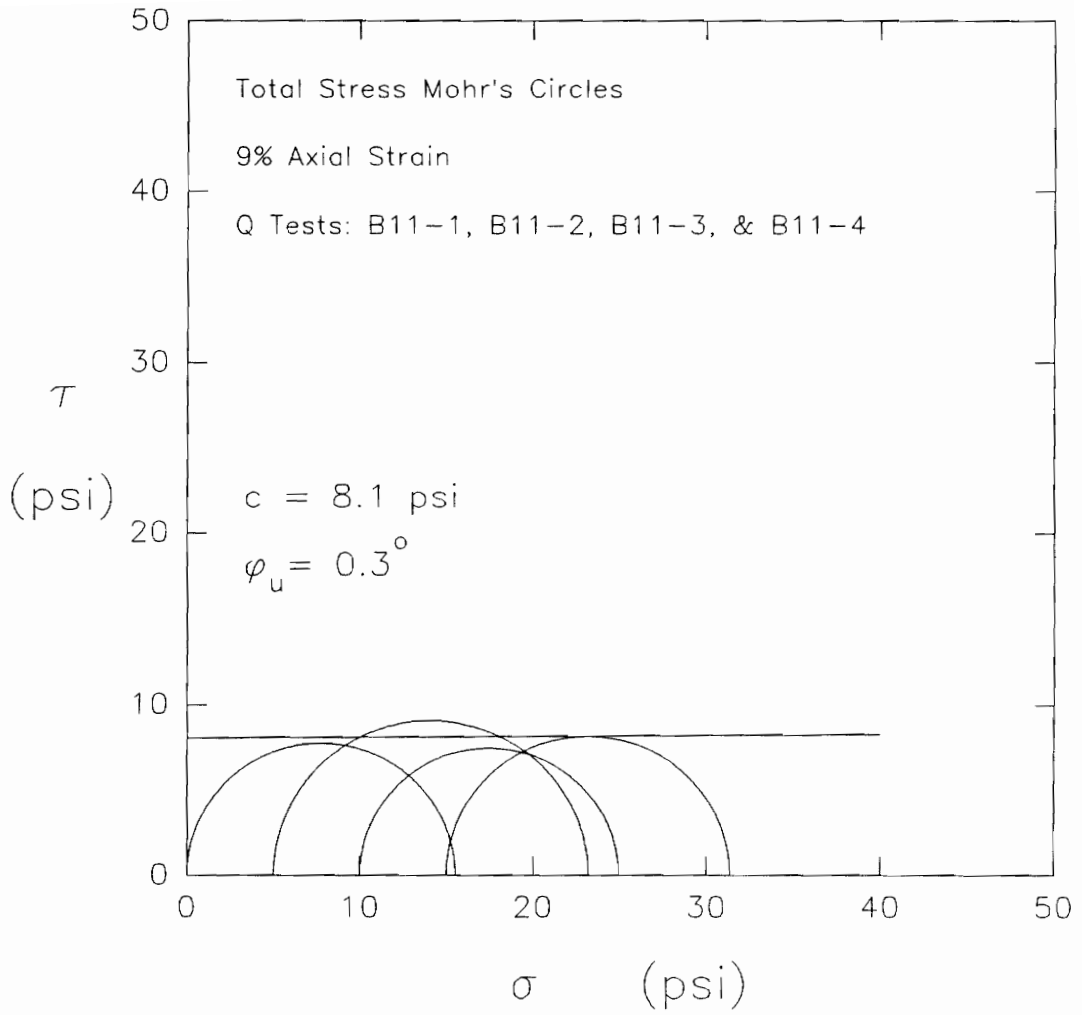


Figure 5.91. Total stress Mohr's circles at 9% axial strain for Q tests B11-1, B11-2, B11-3, and B11-4 on remolded old LMVD silt

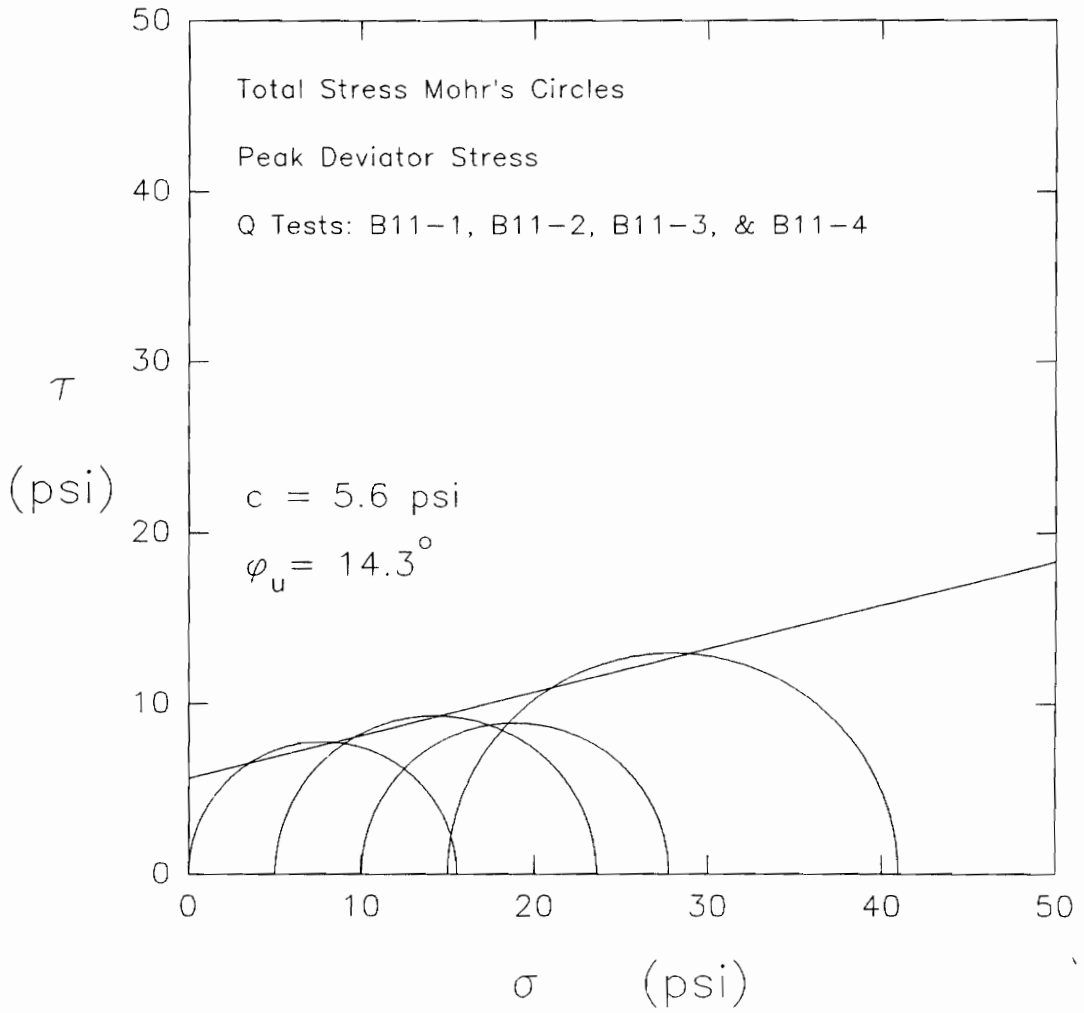


Figure 5.92. Total stress Mohr's circles at peak deviator stress for Q tests B11-1, B11-2, B11-3, and B11-4 on remolded old LMVD silt

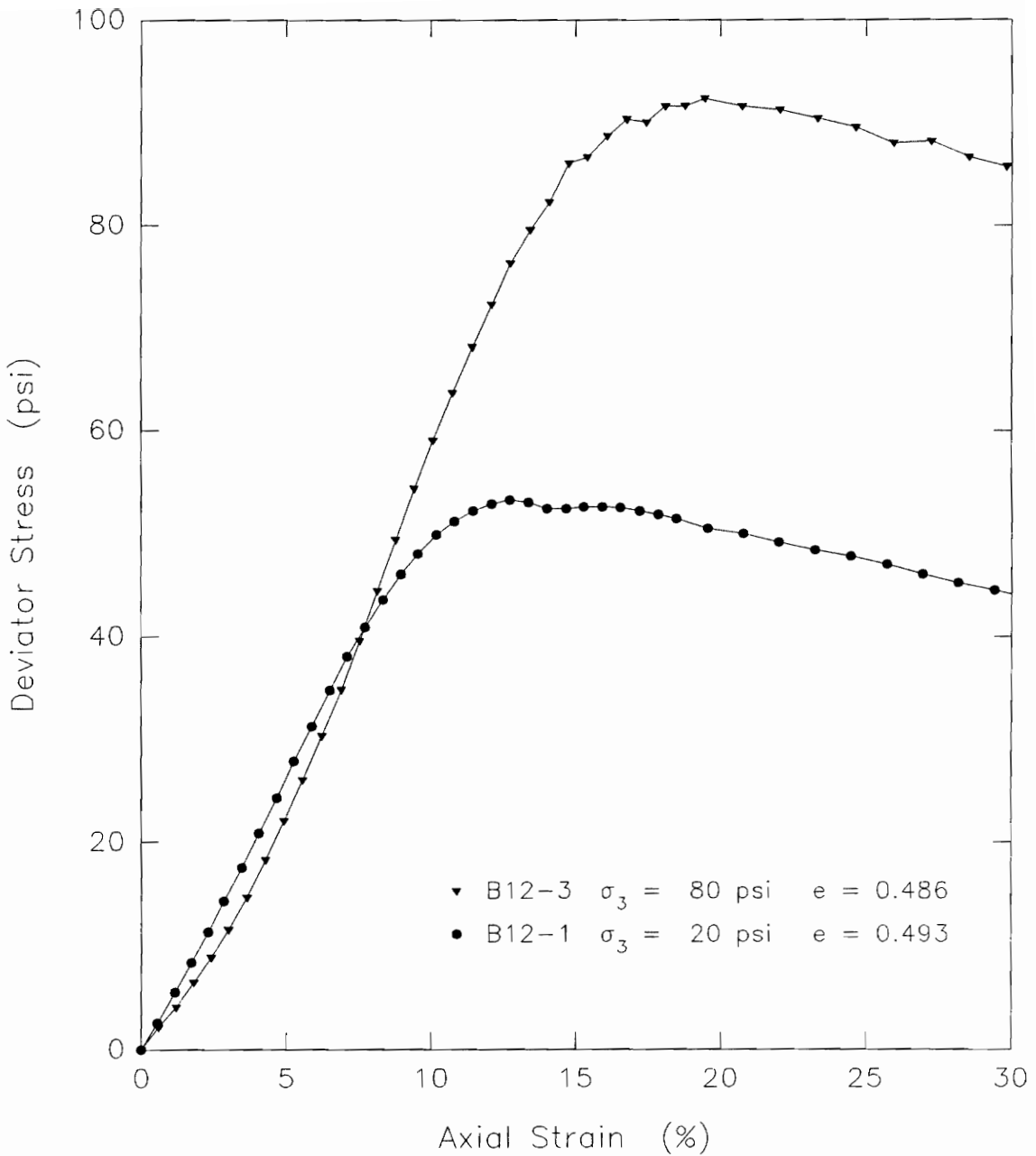


Figure 5.93. Deviator stress-strain relationships measured in Q tests B12-1 and B12-3 on remolded old LMVD silt

strain. At higher axial strains, the deviator stress of the two specimens began to show increased variation. A peak deviator stress was not reached until an axial strain of about 12 percent for the specimen tested at 20 psi. The specimen tested at 80 psi did not reach a peak deviator stress until about 18 percent axial strain.

At about 8 percent axial strain, these two Q tests give a $\phi_u = 0$, $S_u = c = 20.5$ psi Mohr-Coulomb strength envelope for the soil, as shown in Figure 5.94. Taking peak deviator stress as the failure criterion, these two tests give the Mohr-Coulomb envelope shown in Figure 5.95. In this case, the undrained shear strength parameters of the soil are $c = 15.5$ psi and $\phi_u = 14.4^\circ$.

The deviator stress-strain behavior measured in Q tests B13-1 and B13-2 are presented in Figure 5.96. It can be seen from this figure that the two specimens showed very similar stress-strain behavior up to about 7 percent axial strain. At higher axial strains, test B13-1, performed at a cell pressure of 10 psi, reached a relatively constant deviator stress of about 21 psi. The deviator stress of Q test B13-2, performed at a cell pressure of 40 psi, continued to increase with increasing axial strain. A peak deviator stress of about 62 psi was reached at about 20 percent axial strain in this test.

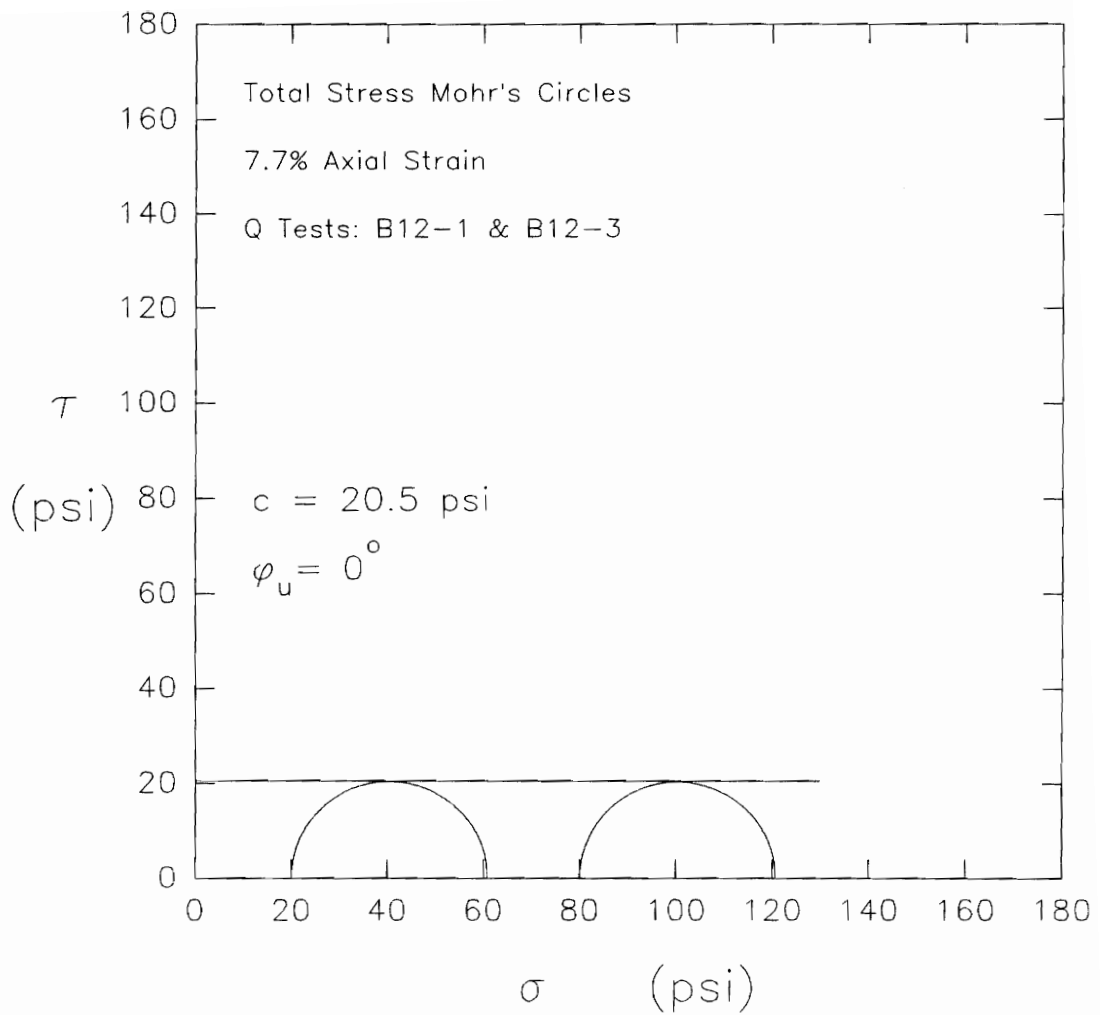


Figure 5.94. Total stress Mohr's circles at 7.7% axial strain for Q tests B12-1 and B12-3 on remolded old LMVD silt

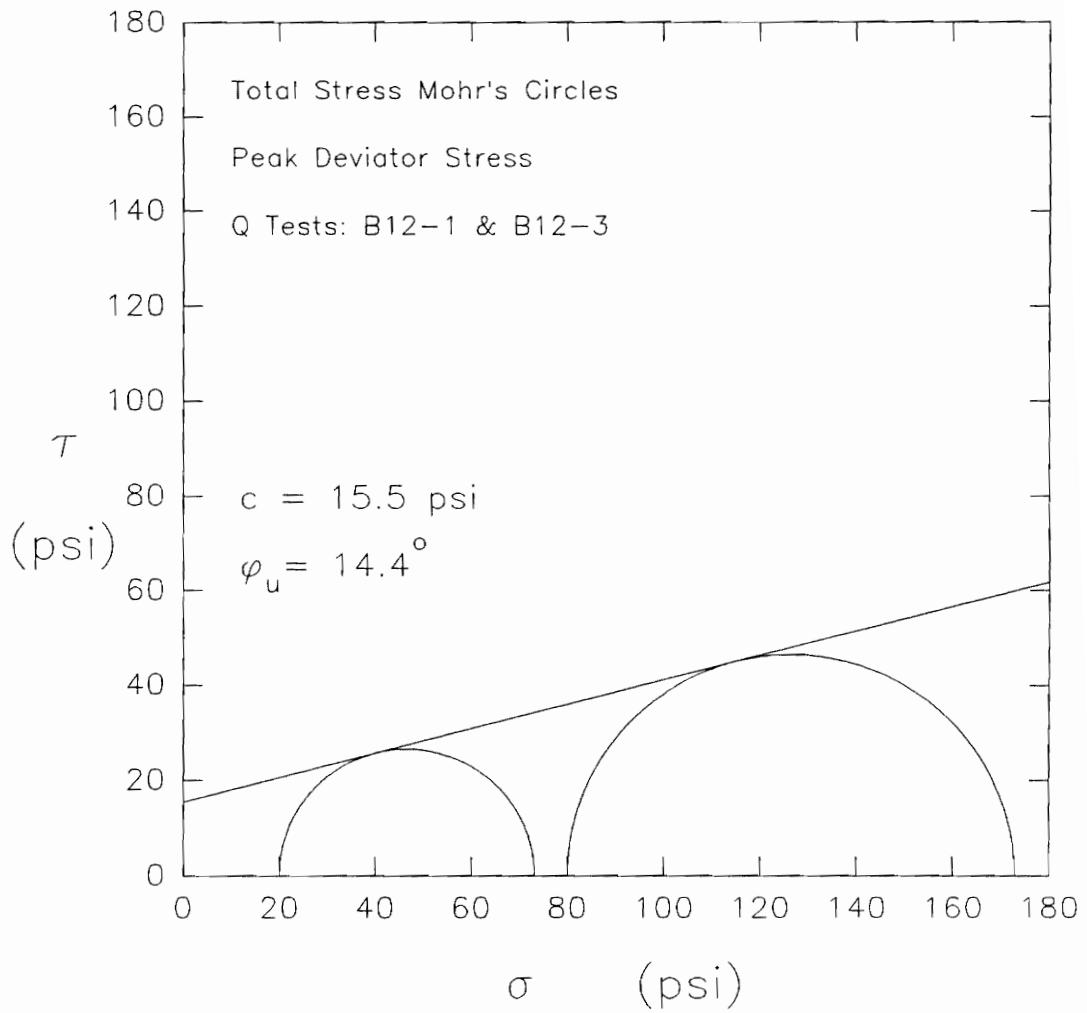


Figure 5.95. Total stress Mohr's circles at peak deviator stress for Q tests B12-1 and B12-3 on remolded old LMVD silt

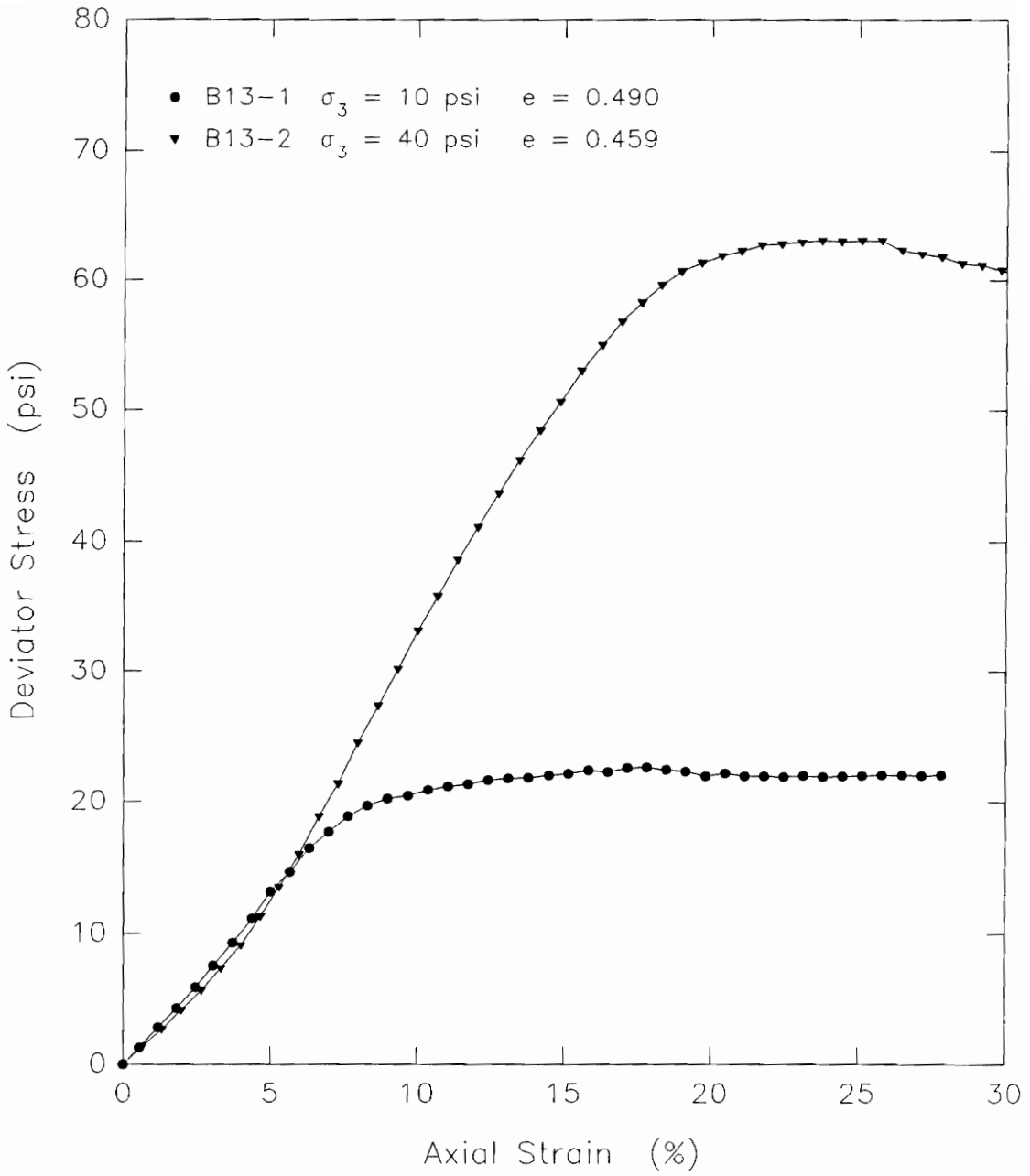


Figure 5.96. Deviator stress-strain relationships measured in Q tests B13-1 and B13-2 on remolded old LMVD silt

Figure 5.97 shows the Mohr's circles for these two Q tests for 7 percent axial strain at failure. For this condition, the undrained shear strength of the soil approaches a $\phi_u = 0$, $S_u = c$ condition. The actual undrained strength parameters for these two tests at 7% axial strain are $c = 8.1$ psi and $\phi_u = 2.2^\circ$. For peak deviator stress conditions, the Mohr-Coulomb envelope shown in Figure 5.98 gives an undrained shear strength which increases with increasing cell pressure. The undrained shear strength parameters of the soil in this case are $c = 3.0$ psi and $\phi_u = 23.7^\circ$.

The results of Q tests performed on specimens obtained from different batch consolidometer samples of old LMVD silt can also be compared. Figure 5.99 shows the stress-strain curves for Q tests B4-4, B9-1, B9-2, and B9-4, performed at cell pressures of 0, 20, 50, and 100 psi. As can be seen from this plot, up until about 9% axial strain, the four Q test specimens exhibited very similar stress-strain behavior. At higher axial strains the measured strength of the specimens began to vary. For test B4-4 performed as an unconfined compression test ($\sigma_3 = 0$ psi), a peak in the deviator stress-strain curve occurred at 9% axial strain. This was followed by some decrease in strength followed by a gradual increase in strength. The specimens tested at cell pressures of 50 and 100 psi had

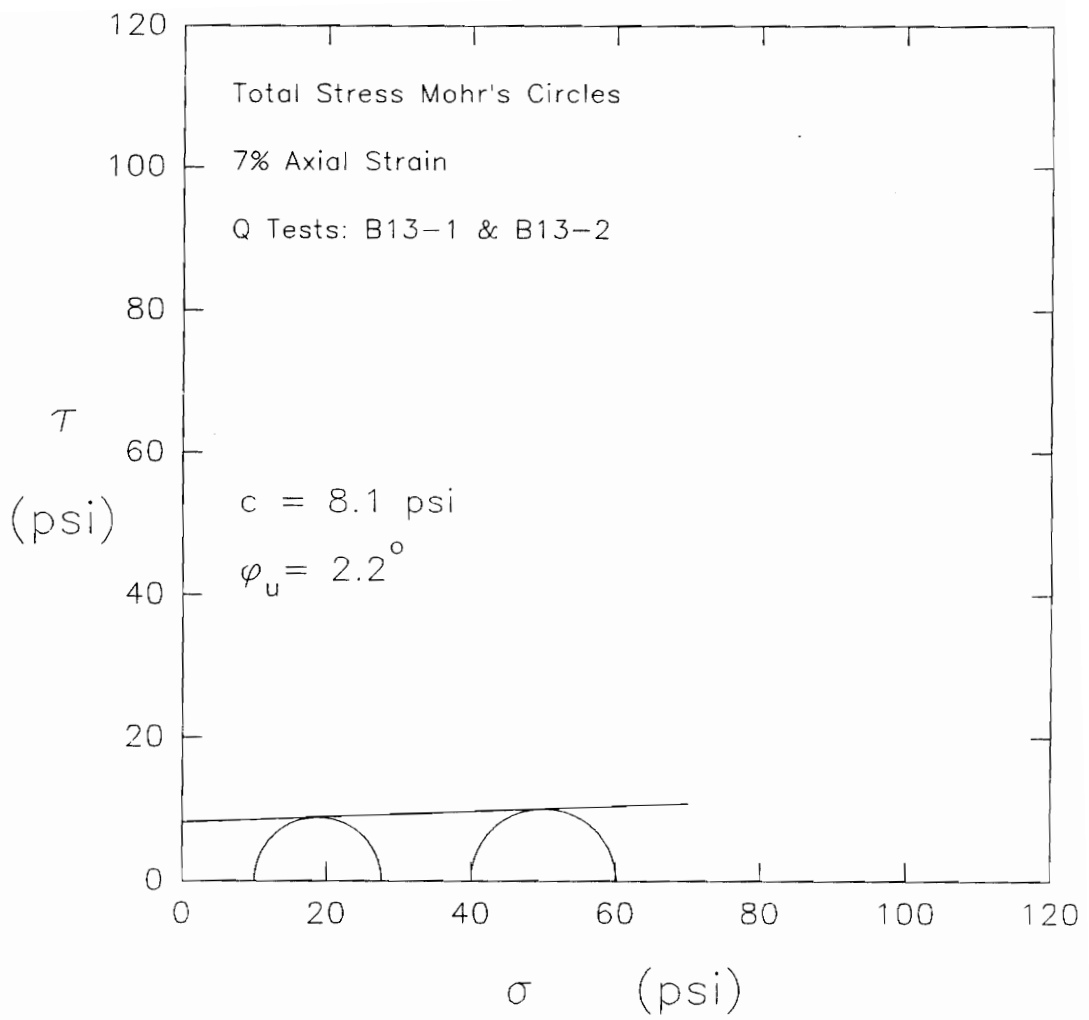


Figure 5.97. Total stress Mohr's circles at 7% axial strain for Q tests B13-1 and B13-2 on remolded old LMVD silt

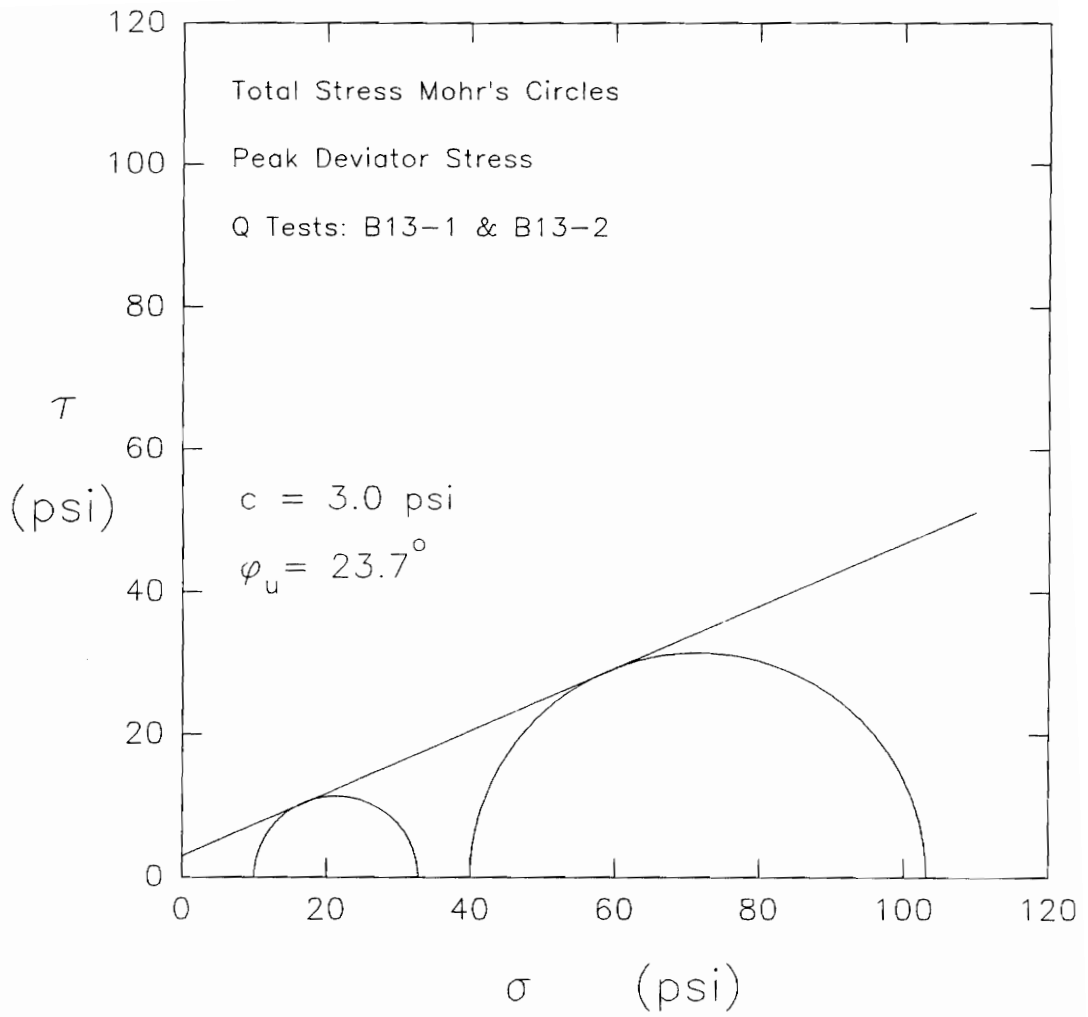


Figure 5.98. Total stress Mohr's circles at peak deviator stress for Q tests B13-1 and B13-2 on remolded old LMVD silt

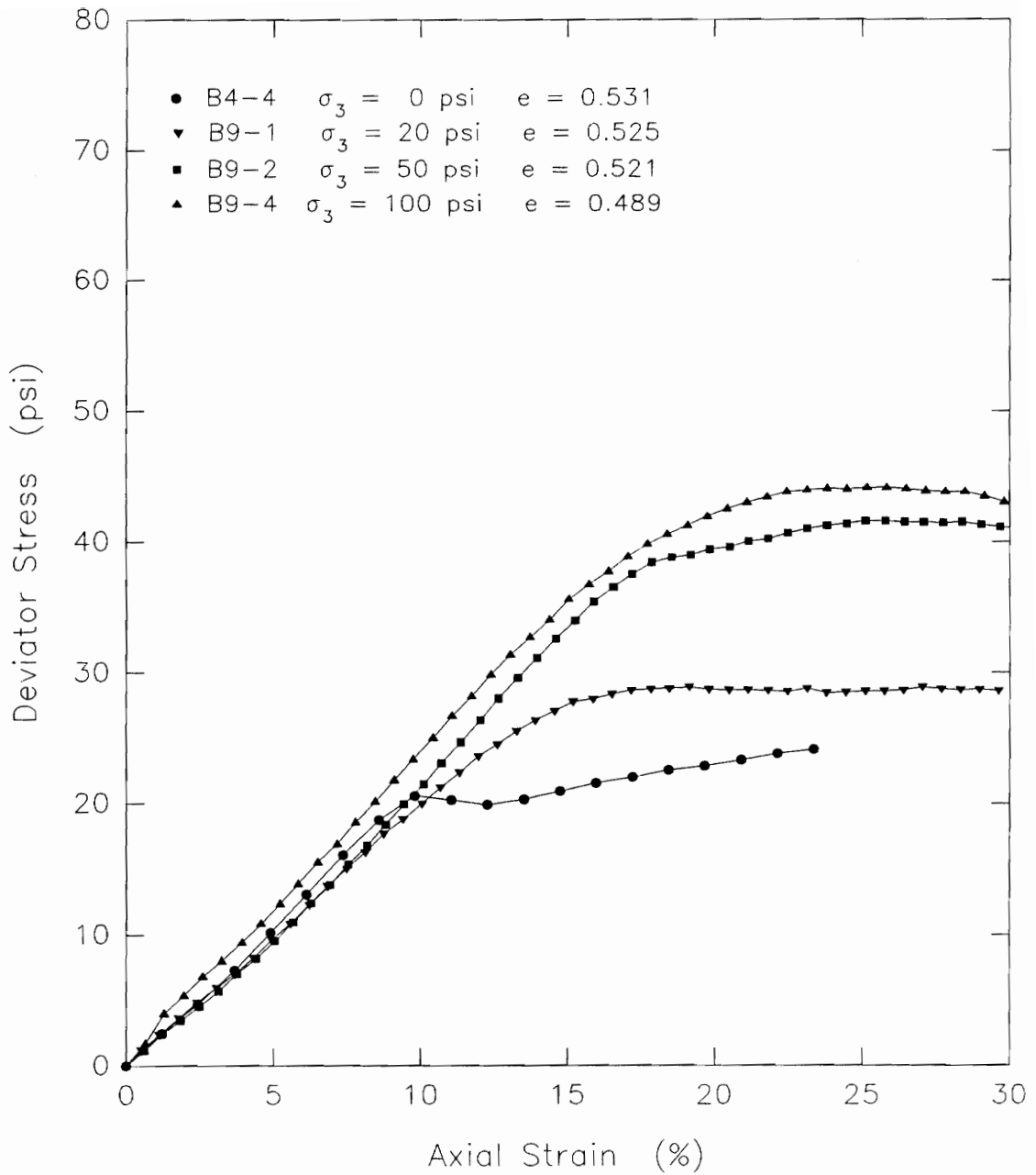


Figure 5.99. Deviator stress-strain relationships measured in Q tests B4-4, B9-1, B9-2, and B9-4 on remolded old LMVD silt

the highest strengths of these four specimens and showed somewhat similar stress-strain behavior throughout the tests. The strength of the specimen tested at a cell pressure of 20 psi was between that of the specimen tested at 0 psi and the two tested at 50 and 100 psi, at strains above 10%.

For 10% axial strain at failure, these four Q tests give the Mohr's circles shown in Figure 5.100. It can be seen from this figure that the Mohr-Coulomb envelope for the soil approaches a $\phi_u = 0$, $S_u = c$ condition. The actual undrained strength parameters are $c = 9.7$ psi and $\phi_u = 1.1^\circ$.

At higher axial strains, the peak deviator stress measured in each test can be used as the failure criterion to give the Mohr-Coulomb failure envelope shown in Figure 5.101. For this condition, the undrained strength of the soil is defined by a bilinear envelope. At normal stresses below about 70 psi, the undrained strength parameters are $c = 8.6$ psi and $\phi_u = 10^\circ$. At higher normal stresses, a $\phi_u = 0$, $S_u = c$ envelope is approached. The actual undrained shear strength parameters for the second linear portion are $c = 19$ psi and $\phi_u = 1.5^\circ$.

Figure 5.102 shows the stress-strain curves for Q tests B8-1, B8-2, B8-4, B7-1, and B7-2. These tests were

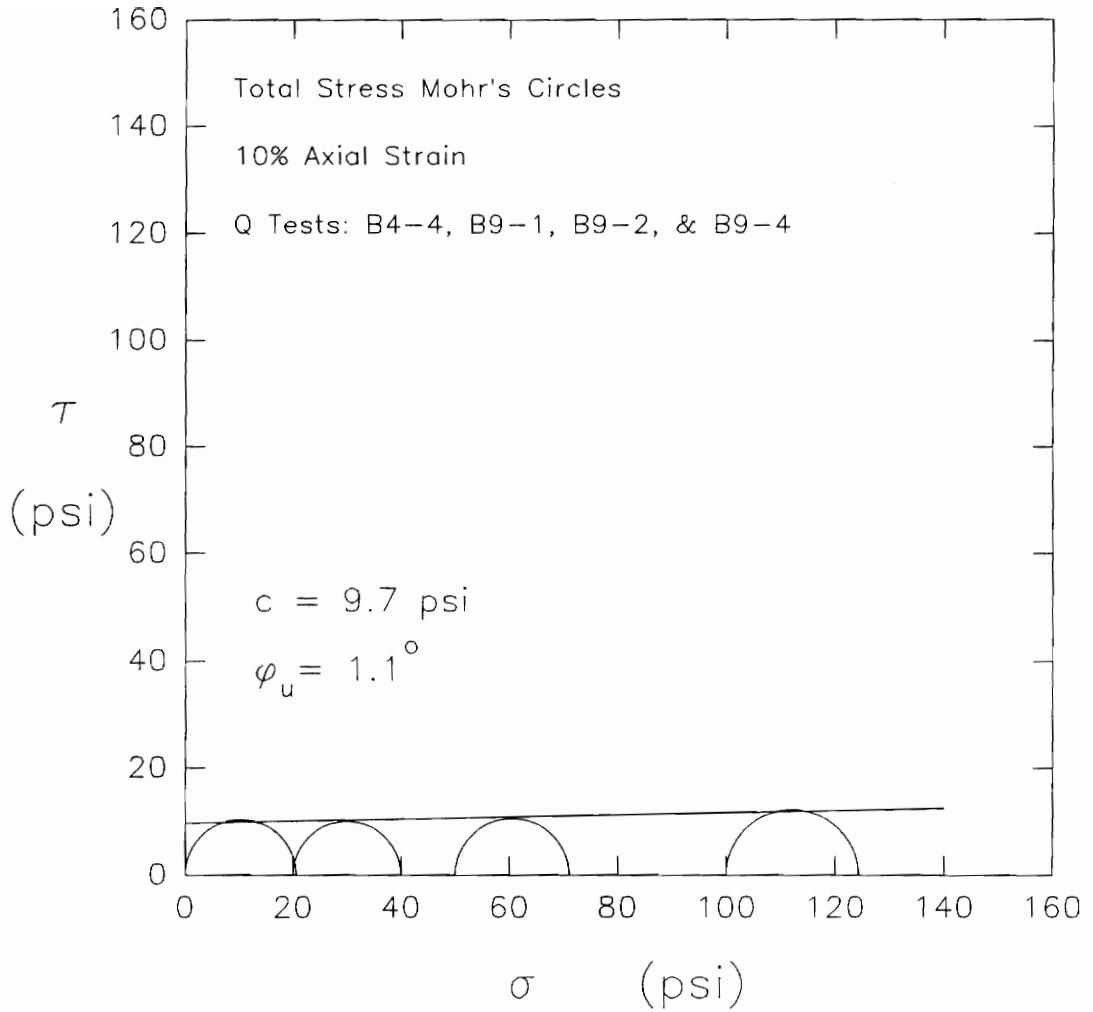


Figure 5.100. Total stress Mohr's circles at 10% axial strain for Q tests B4-4, B9-1, B9-2, and B9-4 on remolded old LMVD silt

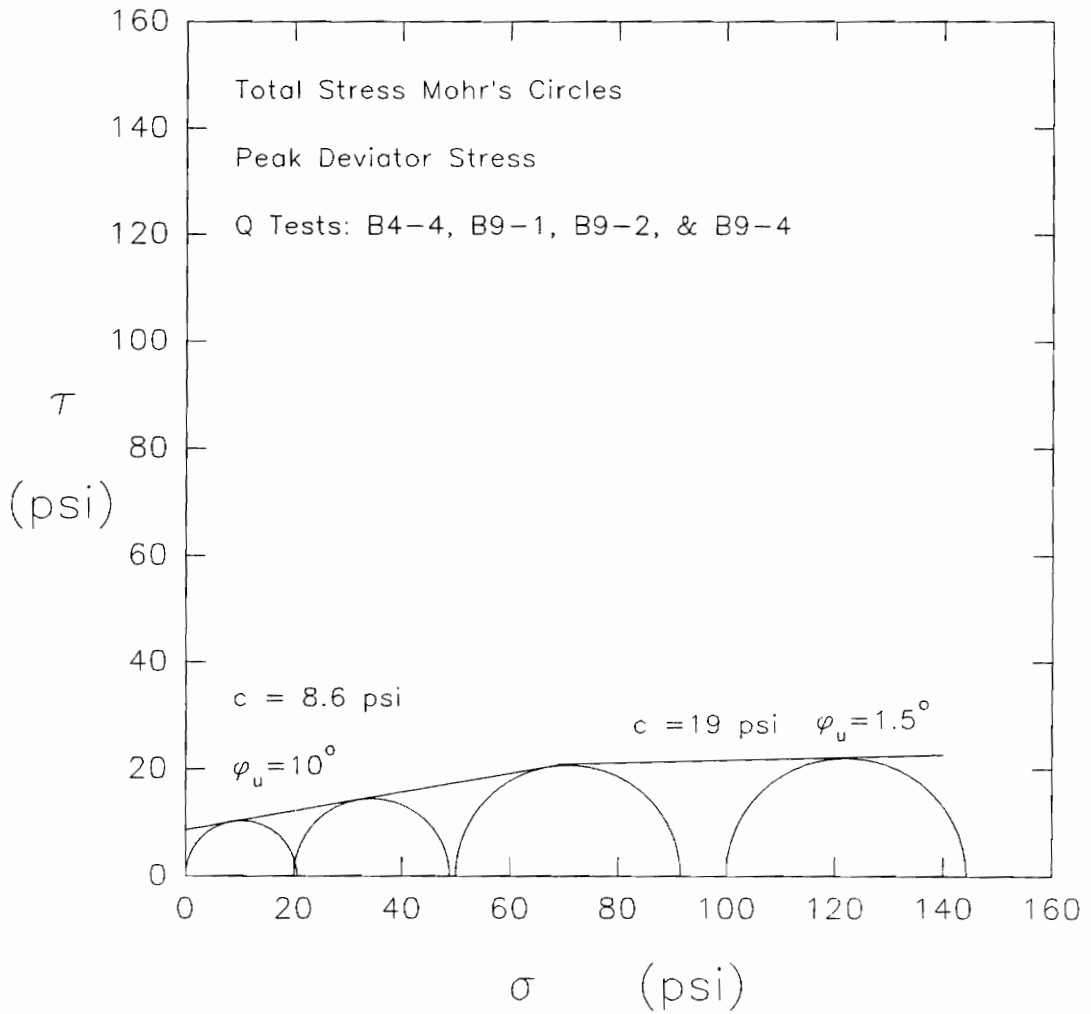


Figure 5.101. Total stress Mohr's circles at peak deviator stress for Q tests B4-4, B9-1, B9-2, and B9-4 on remolded old LMVD silt

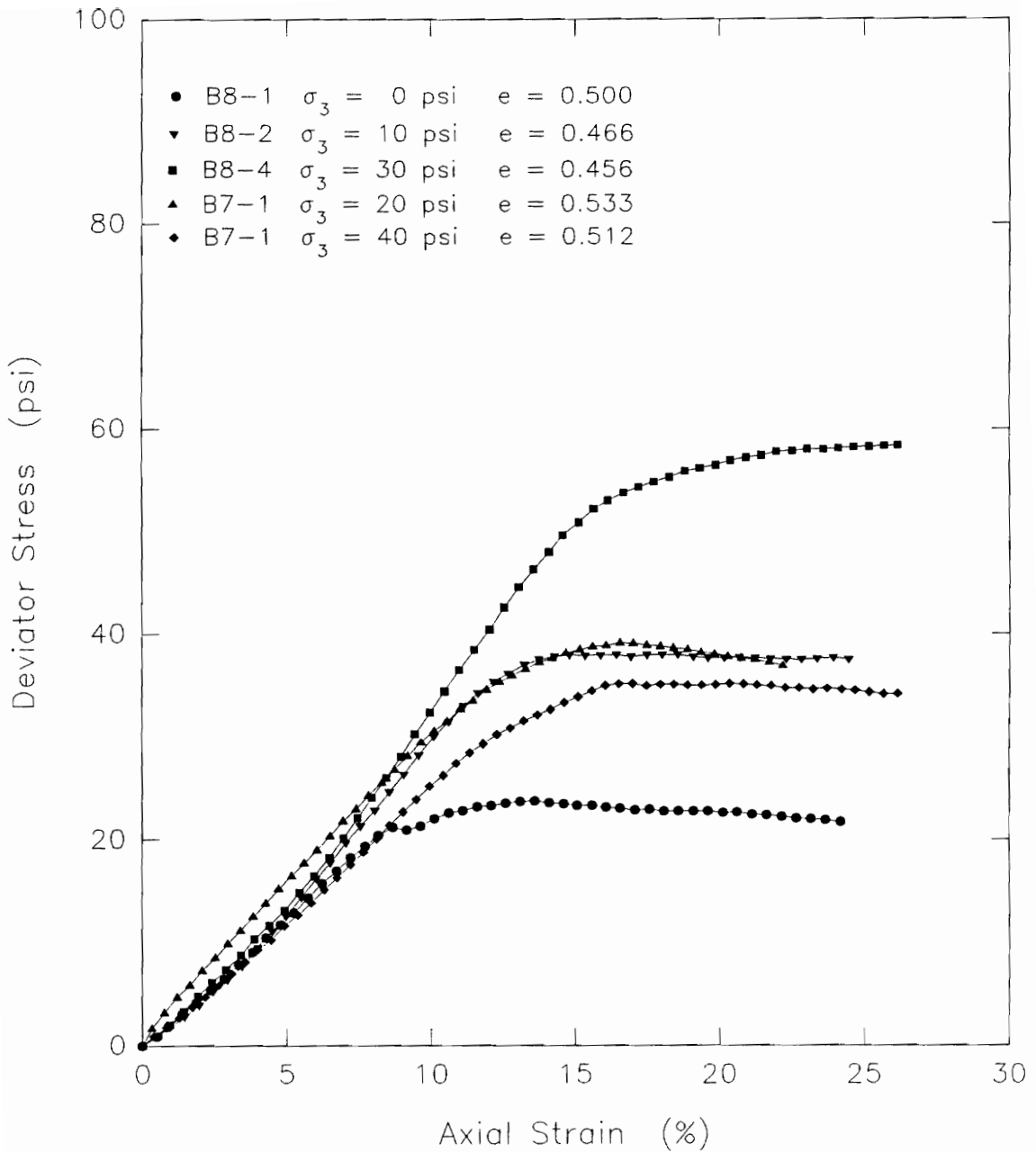


Figure 5.102. Deviator stress-strain relationships measured in Q tests B8-1, B8-2, B8-4, B7-1, and B7-2 on remolded old LMVD silt

performed at cell pressures of 0, 10, 30, 20, and 40 psi, respectively. The void ratios of the specimens varied from 0.456 to 0.533. As can be seen from this figure, the stress-strain behavior of these specimens was fairly similar up to about 9% axial strain. With further increase in strain, the measured strengths of these specimens began to show more variation. Only the test performed at a cell pressure of 0 psi, B8-1, exhibited noticeable strain-softening during shear. The other Q tests which were performed at higher cell pressures did not exhibit noticeable strain-softening in their stress-strain behavior.

The Mohr-Coulomb envelope for these five Q tests has been plotted in Figure 5.103, based on the measured strengths at 9% axial strain. It can be seen from this plot that if 9% axial strain is used as a failure criterion, the undrained strength of the soil approaches a $\phi_u = 0$, $S_u = c$ condition. The undrained shear strength parameters obtained for these Q test specimens at 9% axial strain are $c = 11.5$ psi and $\phi_u = 1.9^\circ$.

For the values of peak deviator stress, which were measured at higher axial strains in these tests, the Mohr-Coulomb failure envelope for the soil has been plotted in Figure 5.104. Here it can be seen that the undrained shear

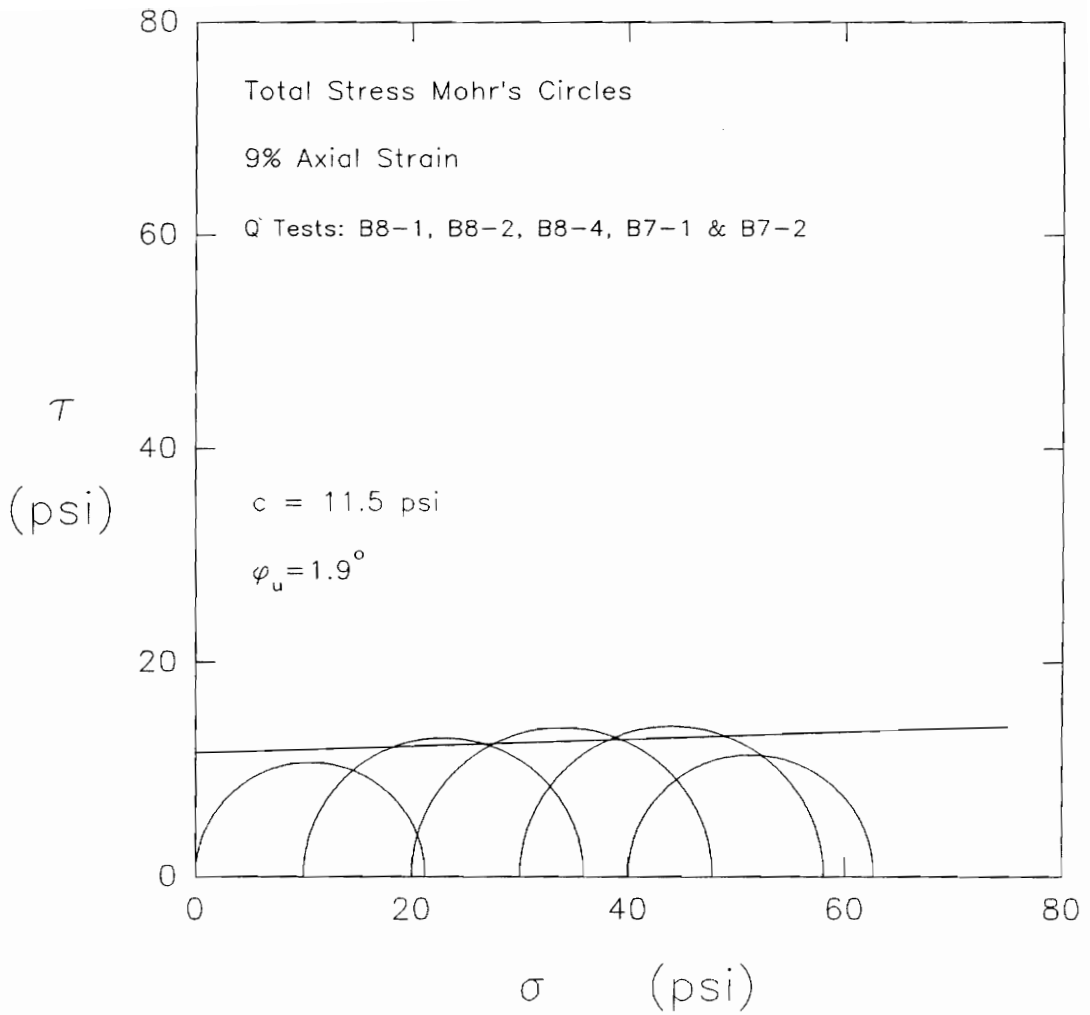


Figure 5.103. Total stress Mohr's circles at 9% axial strain for Q tests B8-1, B8-2, B8-4, B7-1, and B7-2 on remolded old LMVD silt

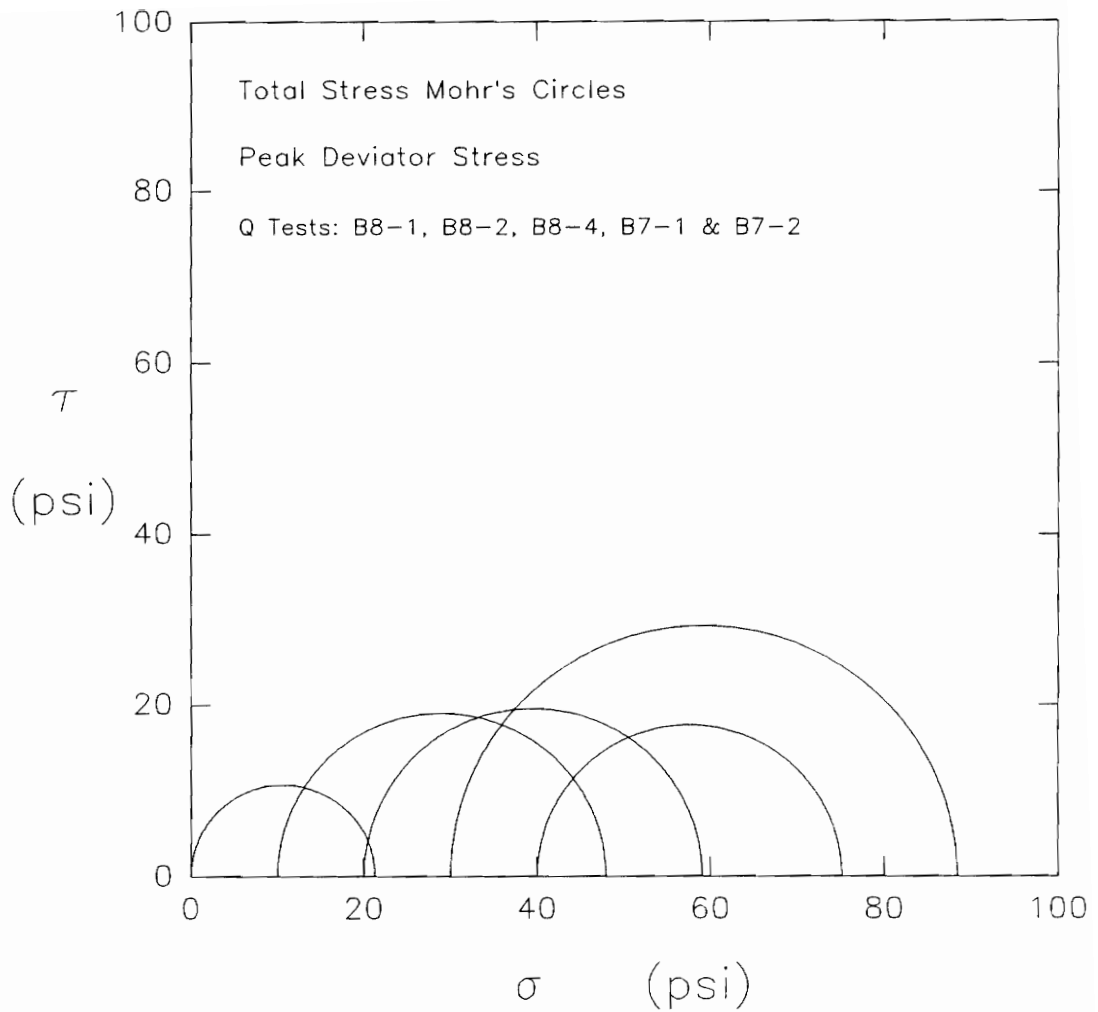


Figure 5.104. Total stress Mohr's circles at peak deviator stress for Q tests B8-1, B8-2, B8-4, B7-1, and B7-2 on remolded old LMVD silt

strength of the soil is much more erratic but tends to be characterized by a $\phi_u > 0$ condition.

The stress-strain curves for Q tests B10-1, B9-1, B9-2, and B9-3 are shown in Figure 5.105. These Q tests were performed at cell pressures of 10, 20, 50, and 100 psi. The specimens had void ratios between 0.489 and 0.525. The stress-strain behavior observed in these tests indicates an increase in strength with increasing cell pressure. The variation in measured strength is small at axial strains below about 8%. At higher axial strains, these tests began to show more variation in the magnitude of the undrained strength of the soil.

The Mohr-Coulomb envelope for these four Q tests is presented in Figure 5.106 for 10% axial strain at failure. As can be seen from this plot, a slight $\phi_u > 0$ strength envelope is obtained, giving the strength parameters $c = 8.5$ psi and $\phi_u = 1.9^\circ$.

When the values of peak deviator stress are used as the failure criterion to develop the strength envelope for the soil, a bilinear envelope is obtained, as can be seen in Figure 5.107. At normal stresses below about 70 psi, an undrained friction angle, ϕ_u , considerably greater than zero is obtained. At low normal stresses, the undrained strength of the soil is characterized by the strength

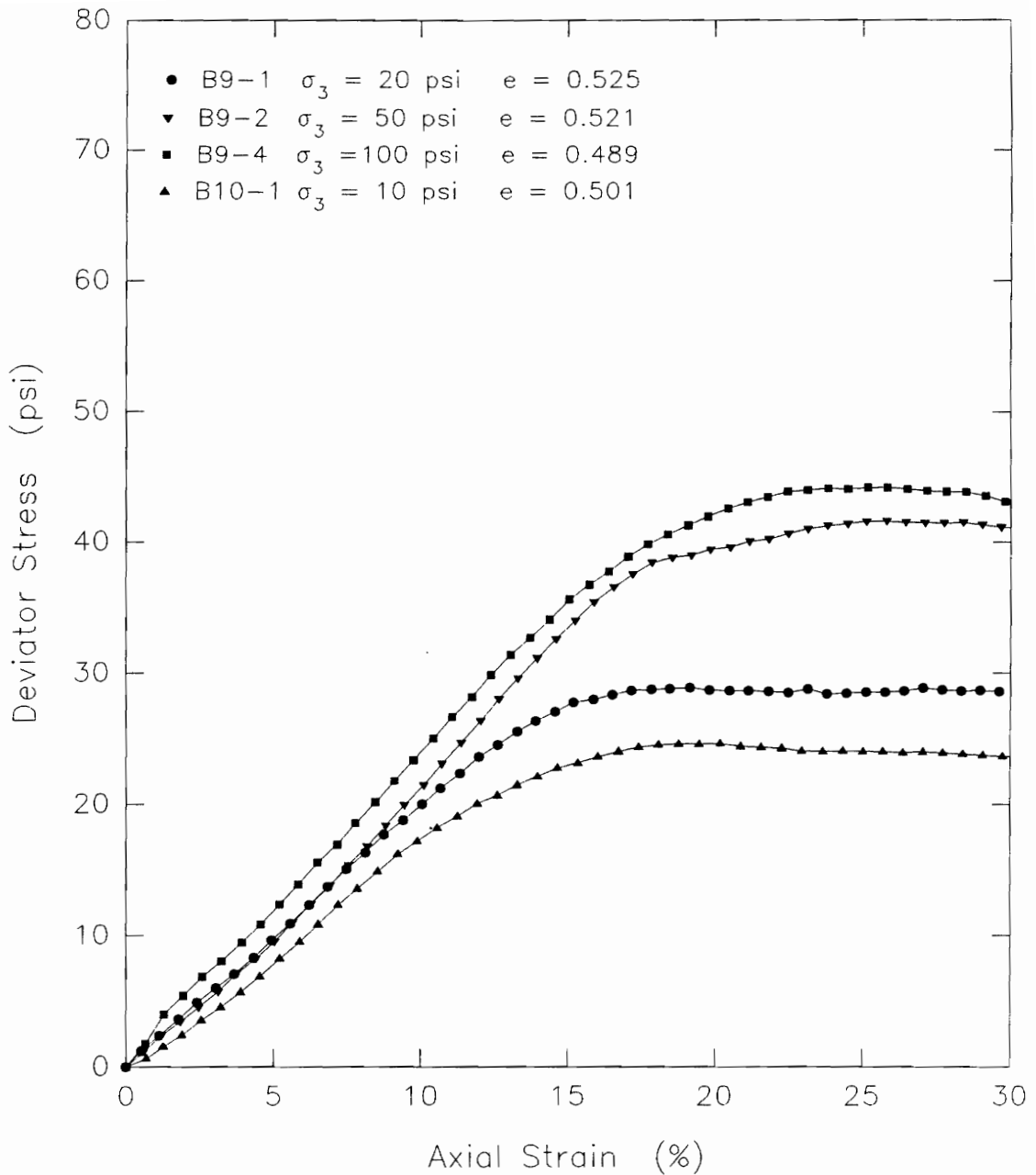


Figure 5.105. Deviator stress-strain relationships measured in Q tests B9-1, B9-2, B9-4, and B10-1 on remolded old LMVD silt

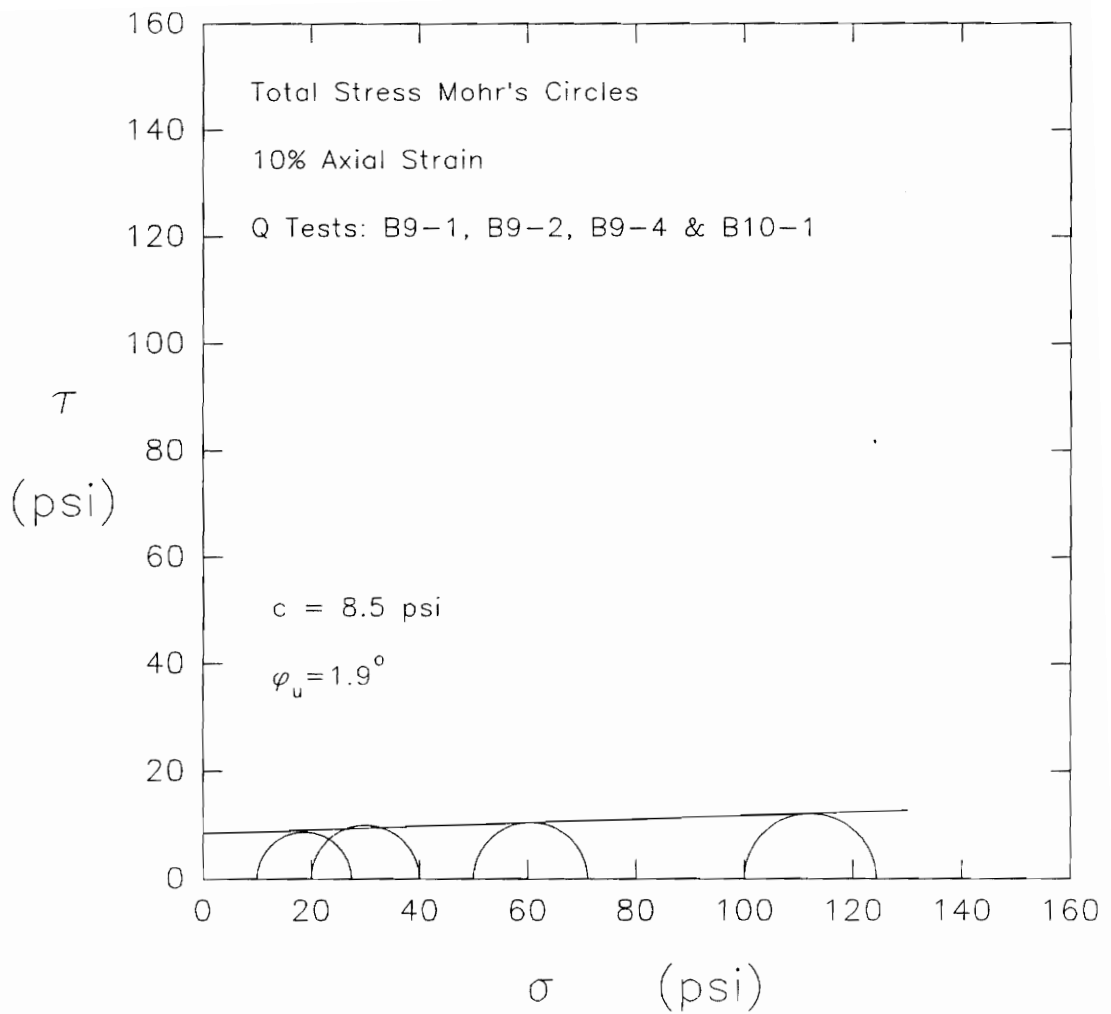


Figure 5.106. Total stress Mohr's circles at 10% axial strain for Q tests B9-1, B9-2, B9-4, and B10-1 on remolded old LMVD silt

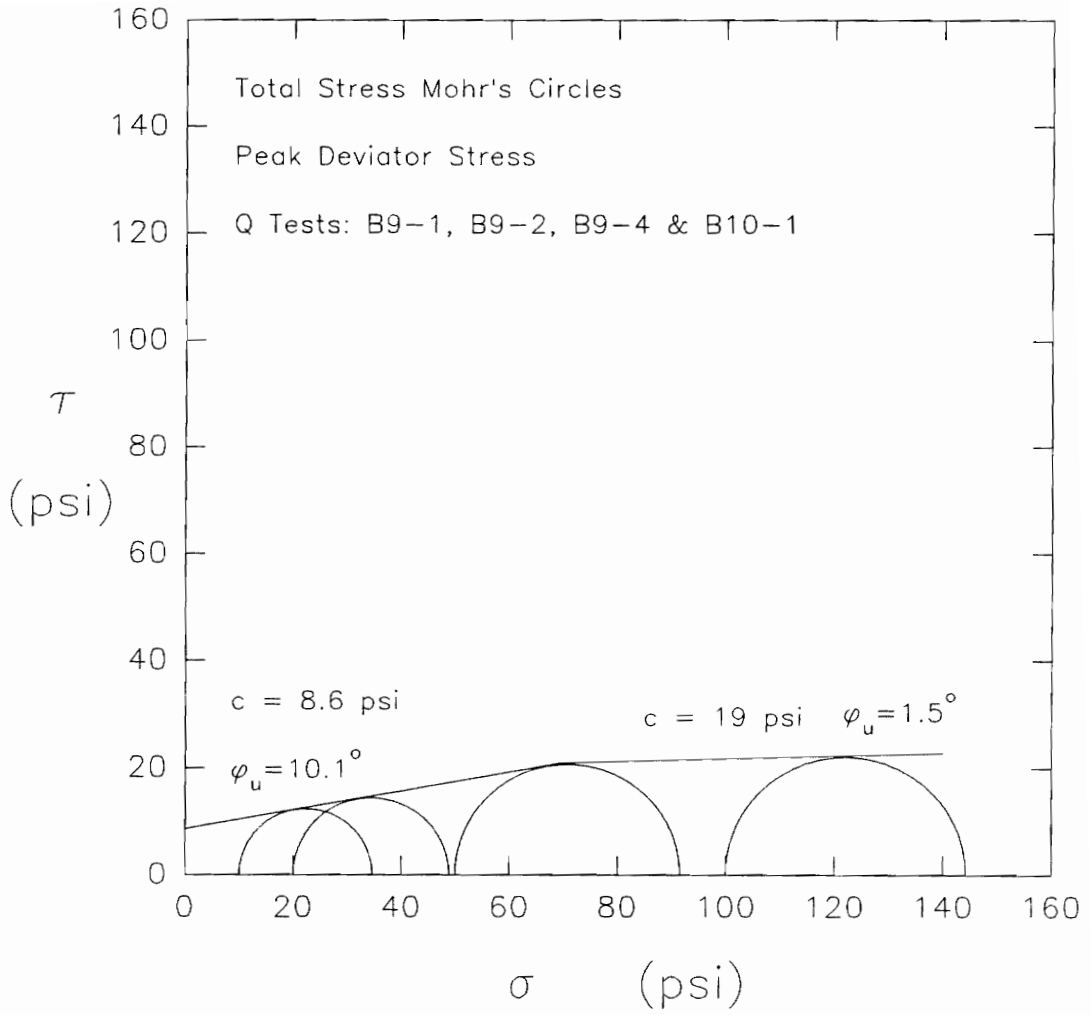


Figure 5.107. Total stress Mohr's circles at peak deviator stress for Q tests B9-1, B9-2, B9-4, and B10-1 on remolded old LMVD silt

parameters $c = 8.6$ psi and $\phi_U = 10.1^\circ$. At normal stresses above 70 psi, the undrained strength of the soil is characterized by the parameters $c = 19$ psi and $\phi_U = 1.5^\circ$.

Figure 5.108 presents the deviator stress vs. axial strain curves measured in Q tests B8-1, B8-2, B8-4, B11-1, B11-2, and B11-3. These Q tests were performed at cell pressures ranging from 0 to 30 psi. The void ratios of these specimens varied from 0.456 to 0.500. As can be seen from this plot, the stress-strain curves of these six Q tests showed considerable variation. The tests performed at the lowest cell pressures had the lowest strengths and tended to exhibit strain-softening behavior between 8 and 12 percent axial strain. One of the tests performed at 10 psi and the test performed at 30 psi had higher strengths and did not exhibit strain-softening during shear.

Taking the peak values of deviator stress measured in these tests as the failure criterion, the Mohr-Coulomb strength envelope for the soil is plotted in Figure 5.109. For this condition, the undrained shear strength of the soil is defined by the parameters, $c = 4.6$ psi and $\phi_U = 25.3^\circ$.

Figure 5.110 shows the stress-strain curves for Q tests B11-1, B11-2, B11-3, B9-1, B9-2, and B9-4. These Q tests were performed at cell pressures ranging from 0 to

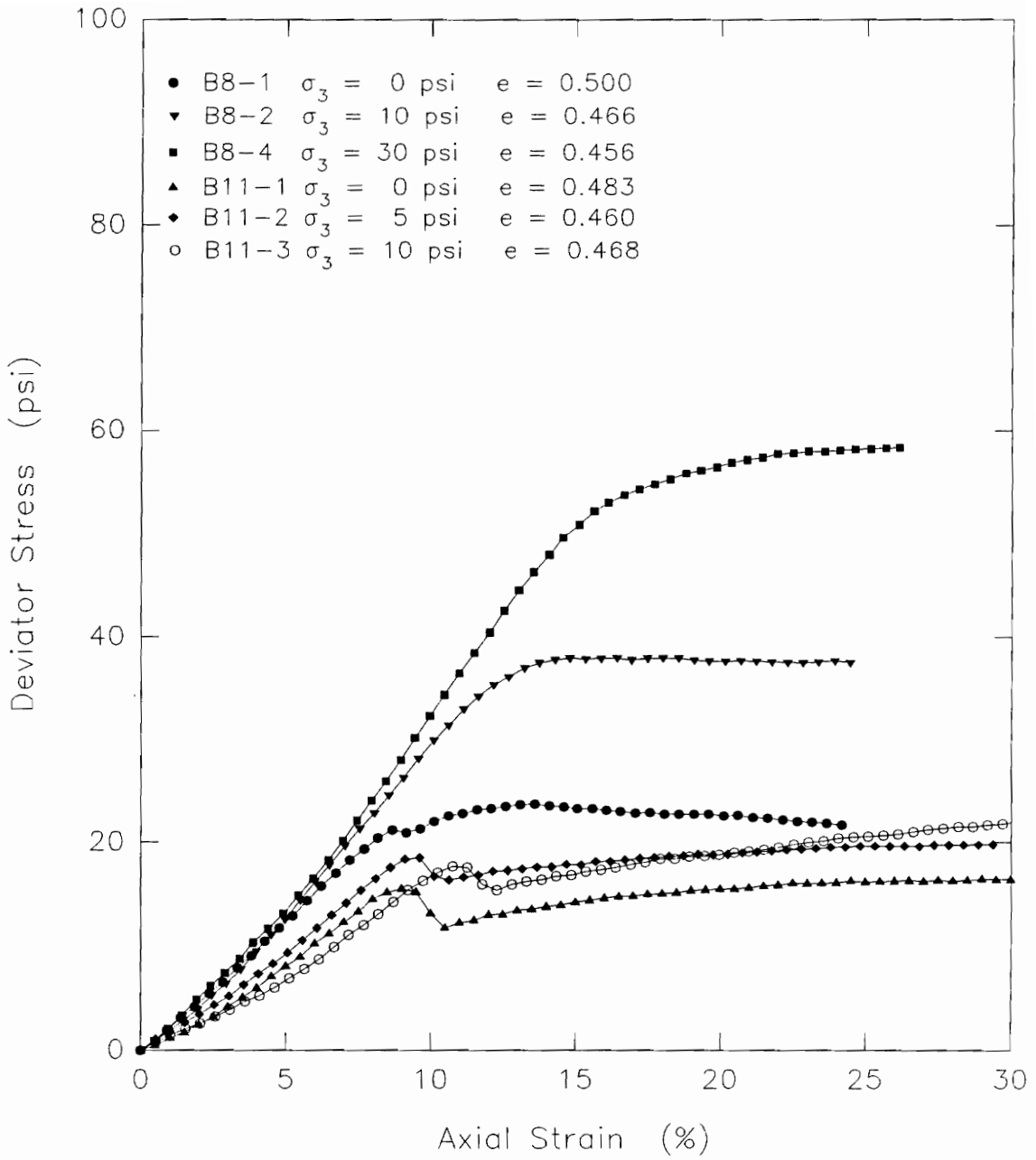


Figure 5.108. Deviator stress-strain relationships measured in Q tests B8-1, B8-2, B8-4, B11-1, B11-2 and B11-3 on remolded old LMVD silt

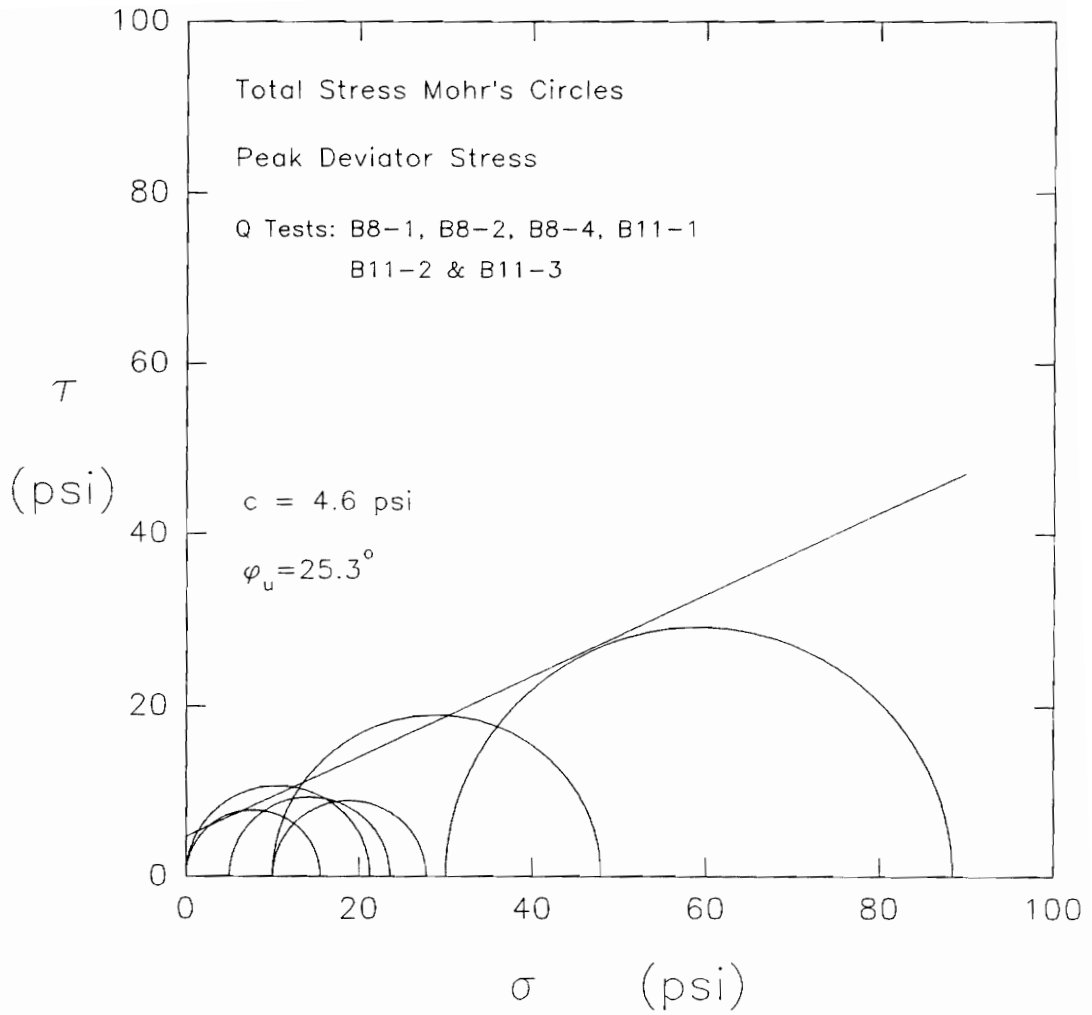


Figure 5.109. Total stress Mohr's circles at peak deviator stress for Q tests B8-1, B8-2, B8-4, B11-1, B11-2, and B11-3 on remolded old LMVD silt

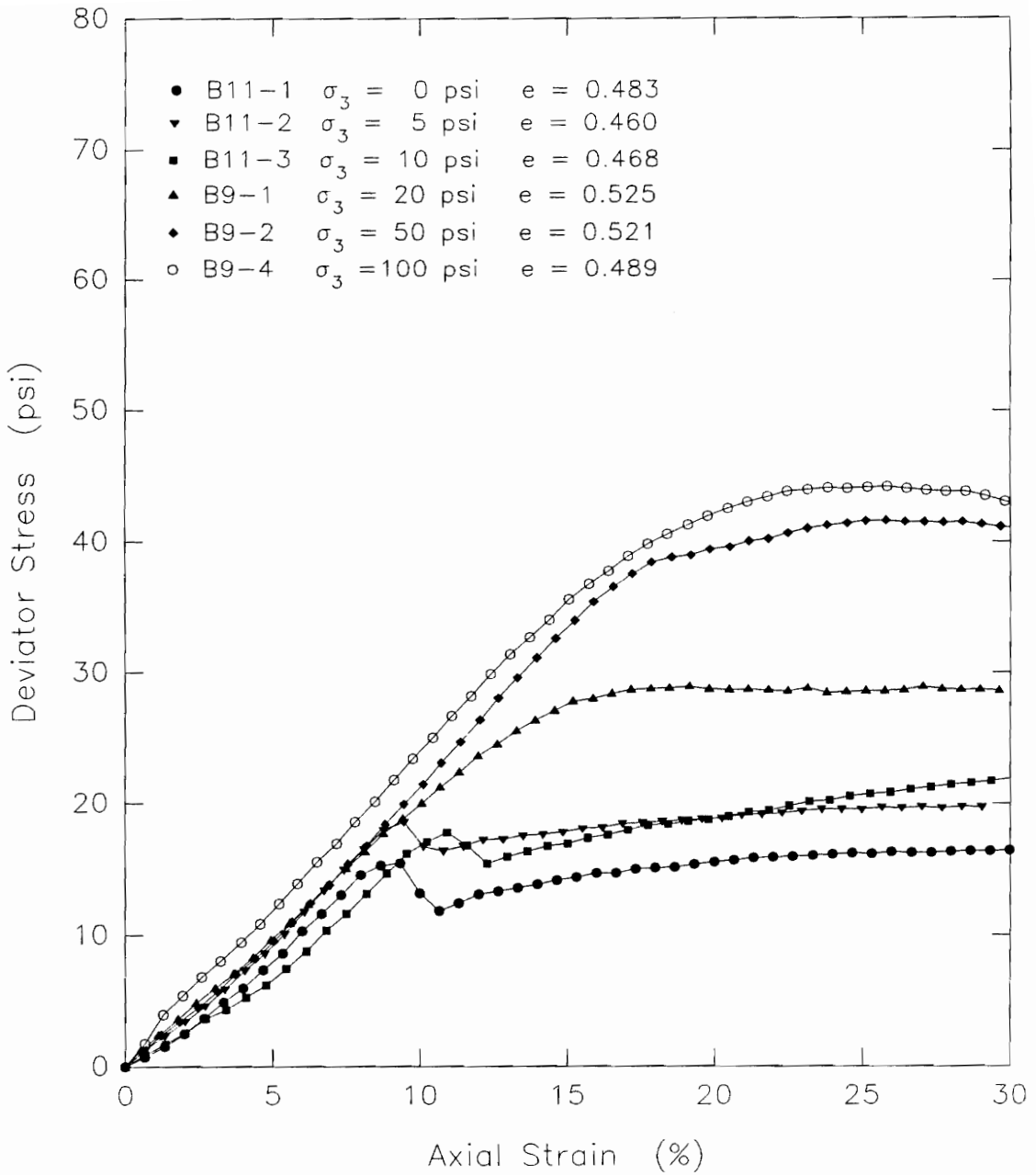


Figure 5.110. Deviator stress-strain relationships measured in Q tests B11-1, B11-2, B11-3, B9-1, B9-2, and B9-4 on remolded old LMVD silt

100 psi. These specimens had void ratios between 0.460 and 0.525. These six Q tests gave somewhat similar stress-strain behavior up until about 9% axial strain. Some variation between the undrained strengths of these specimens is still present in this range of strains. This is especially true for the tests performed at the lowest cell pressures compared to those performed at the highest cell pressures. At axial strains above 9%, the stress-strain curves of these test specimens show considerably more variation, giving an undrained shear strength which tends to increase with increasing cell pressure. The three specimens tested at cell pressures of 0, 5, and 10 psi all showed very noticeable strain-softening between 9 and 12 percent axial strain. The tests performed at higher cell pressures did not show noticeable strain-softening. The test performed at a cell pressure of 20 psi did show a noticeable change in slope at about the same axial strain that the specimen tested at 5 psi reached a peak and began to exhibit strain-softening.

Figure 5.111 shows the Mohr's circles for these six Q tests for 9% axial strain at failure. For this case, the undrained shear strength of the soil does not quite give a $\phi_u = 0$ condition. The undrained shear strength parameters for the soil are $c = 7.9$ psi and $\phi_u = 1.5^\circ$.

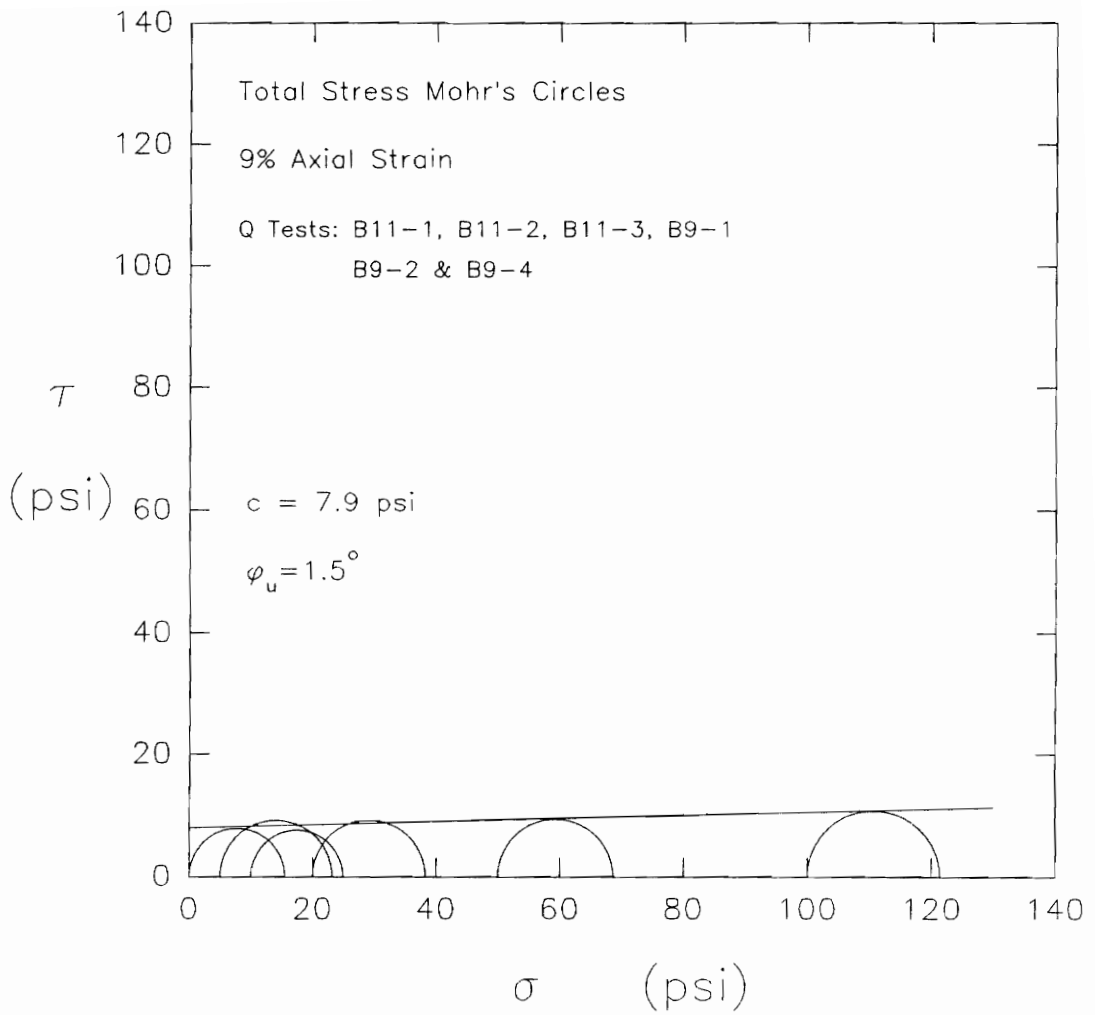


Figure 5.111. Total stress Mohr's circles at 9% axial strain for Q tests B11-1, B11-2, B11-3, B9-1, B9-2, and B9-4 on remolded old LMVD silt

For the values of peak deviator stress measured in these six tests, the Mohr-Coulomb failure envelope of the soil is plotted in Figure 5.112. Here it can be seen that an approximate bilinear envelope results. At low cell pressures a $\phi_u > 0$ condition predominates, whereas at high cell pressures, a $\phi_u = 0$ condition exists. Below a normal stress of about 57 psi, the undrained shear strength parameters are $c = 5.5$ psi and $\phi_u = 14.6^\circ$. At higher normal stresses, the undrained strength envelope is characterized by the parameters $c = 19$ psi and $\phi_u = 1.5^\circ$.

5.9.2 New LMVD Silt

Figure 5.113 shows the deviator stress vs. axial strain curves for Q tests B17-1, B17-2, B17-3, and B17-4, performed on specimens of remolded new LMVD silt. These four Q tests were performed at cell pressures of 0, 10, 20, and 30 psi. As can be seen from this figure, these four Q tests showed very similar deviator stress-strain behavior up to about 5 percent axial strain. At higher axial strains, the deviator stress tends to increase with increasing cell pressure used in the tests. All four Q test specimens reached peak deviator stresses at axial strains below 10 percent. The two tests performed at 20 and 30 psi cell pressure each showed similar stress-strain behavior up to the peak deviator stress, giving essentially

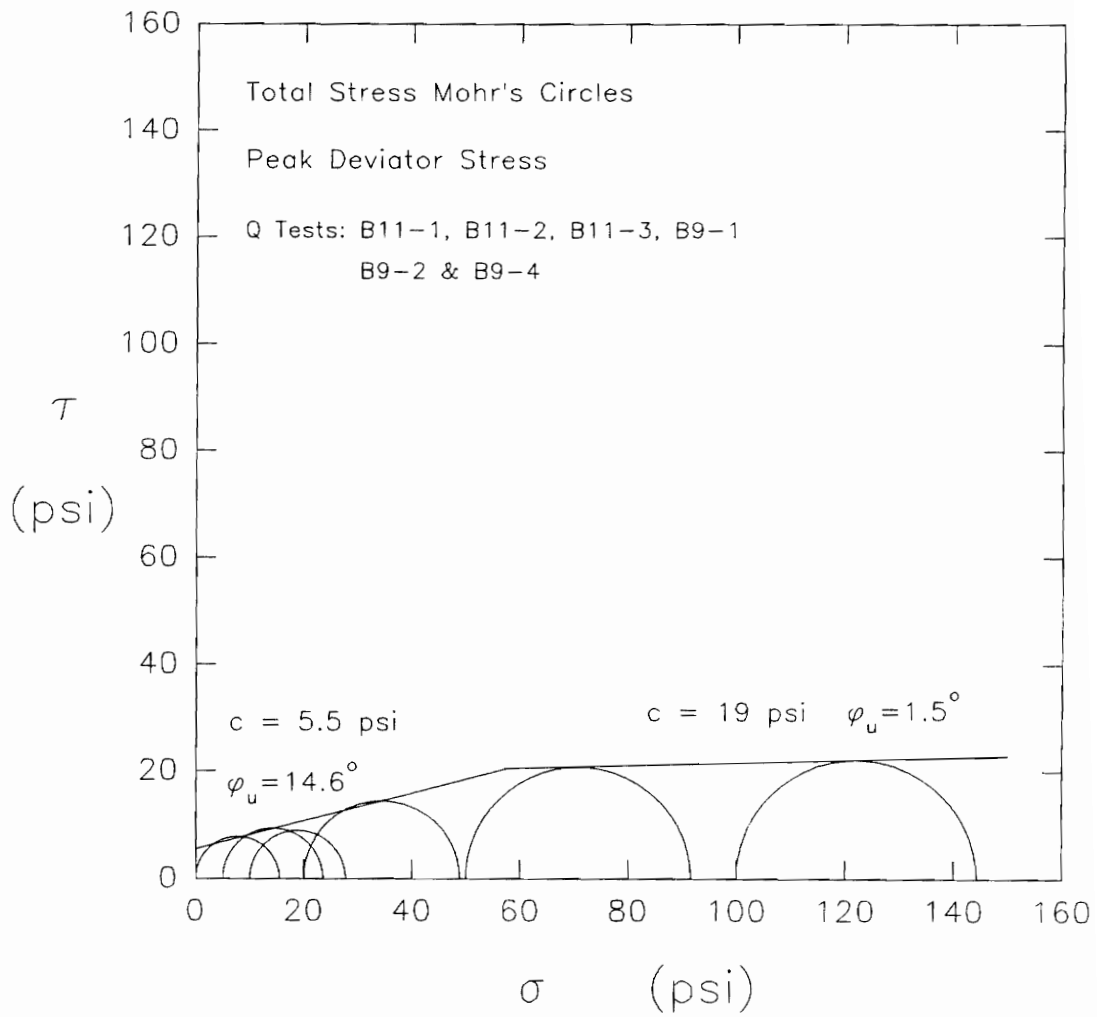


Figure 5.112. Total stress Mohr's circles at peak deviator stress for Q tests B11-1, B11-2, B11-3, B9-1, B9-2, and B9-4 on remolded old LMVD silt

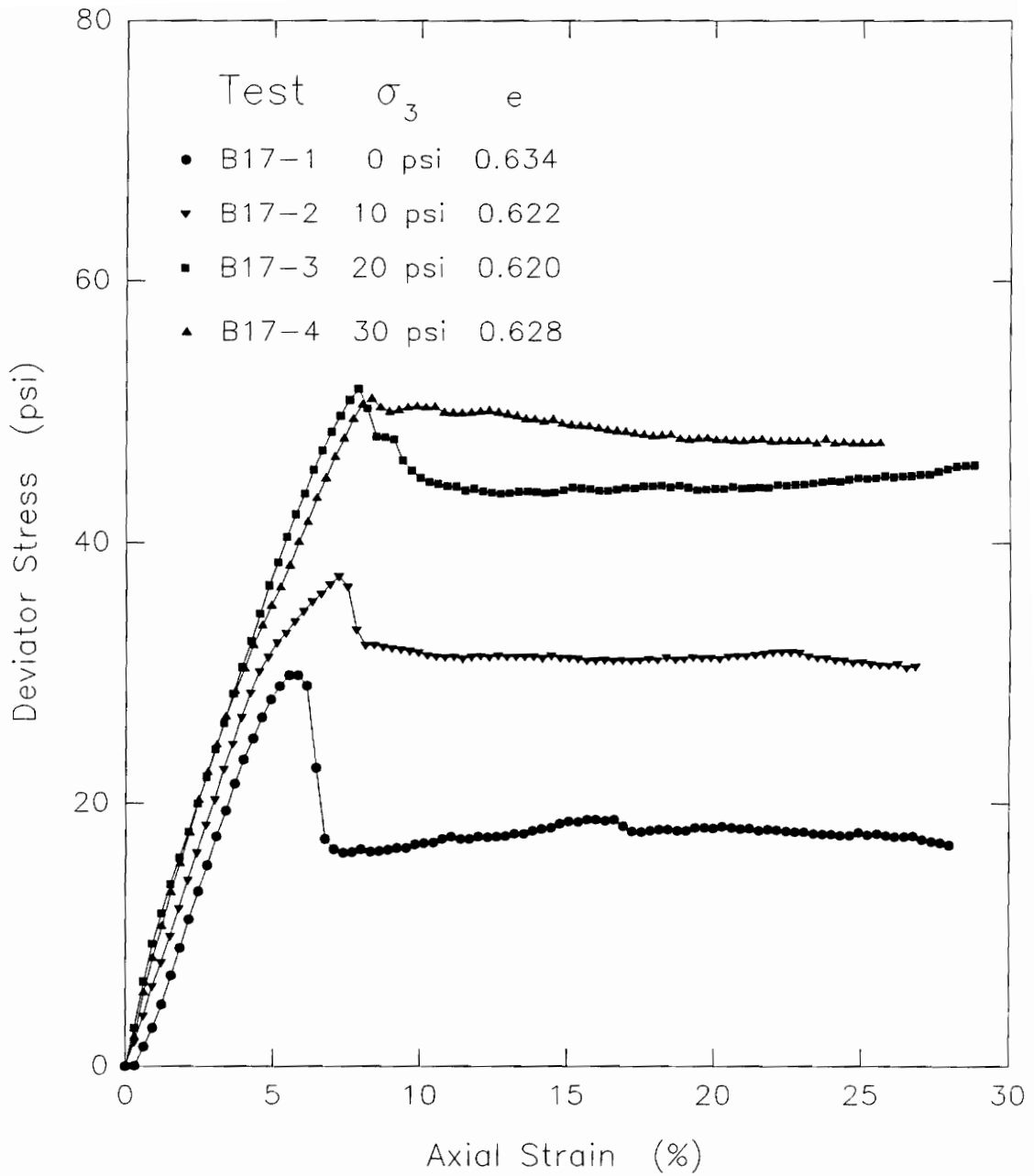


Figure 5.113. Deviator stress-strain relationships measured in Q tests B17-1, B17-2, B17-3, and B17-4 on remolded new LMVD silt

the same undrained shear strength for the soil. The stress-strain behavior after the peak deviator stress varied somewhat for these two Q test specimens.

Review of Table 5.22 shows that these four Q tests were all performed on remolded specimens of new LMVD silt. The Q test specimens were all found to have degrees of saturation less than 100 percent. The degrees of saturation of these specimens varied from 96.6 to 99.2 percent.

Figure 5.114 shows the Mohr-Coulomb strength envelope for these four Q tests for 4.5% axial strain at failure. At this value of axial strain, the undrained strength of the soil does not quite give a $\phi_u = 0$, $S_u = c$ condition. The undrained strength parameters at 4.5% axial strain are $c = 11.9$ psi and $\phi_u = 6.8^\circ$.

Figure 5.115 shows the Mohr-Coulomb strength envelope for these four Q tests, based on the peak deviator stress measured in each test. As can be seen from this figure, the Mohr-Coulomb envelope is bilinear. At low cell pressures, a $\phi_u > 0$ condition exists. This portion of the envelope is characterized by the undrained strength parameters $c = 9.9$ psi and $\phi_u = 20.8^\circ$. Above a normal stress of about 40 psi, the soil behaves as a $\phi_u = 0$, $S_u = c = 25.6$ psi material.

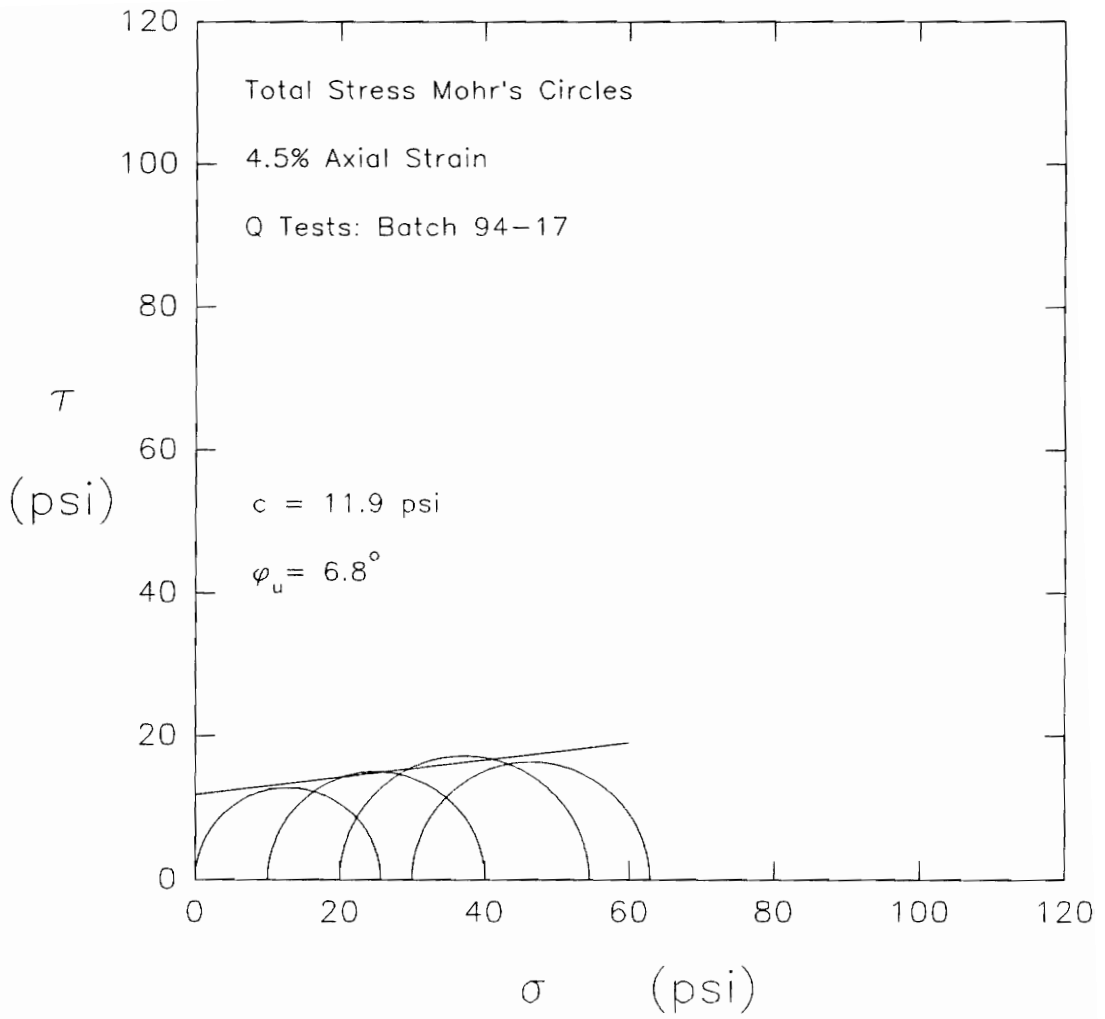


Figure 5.114. Total stress Mohr's circles at 4.5% axial strain for Q tests B17-1, B17-2, B17-3, and B17-4 on remolded new LMVD silt

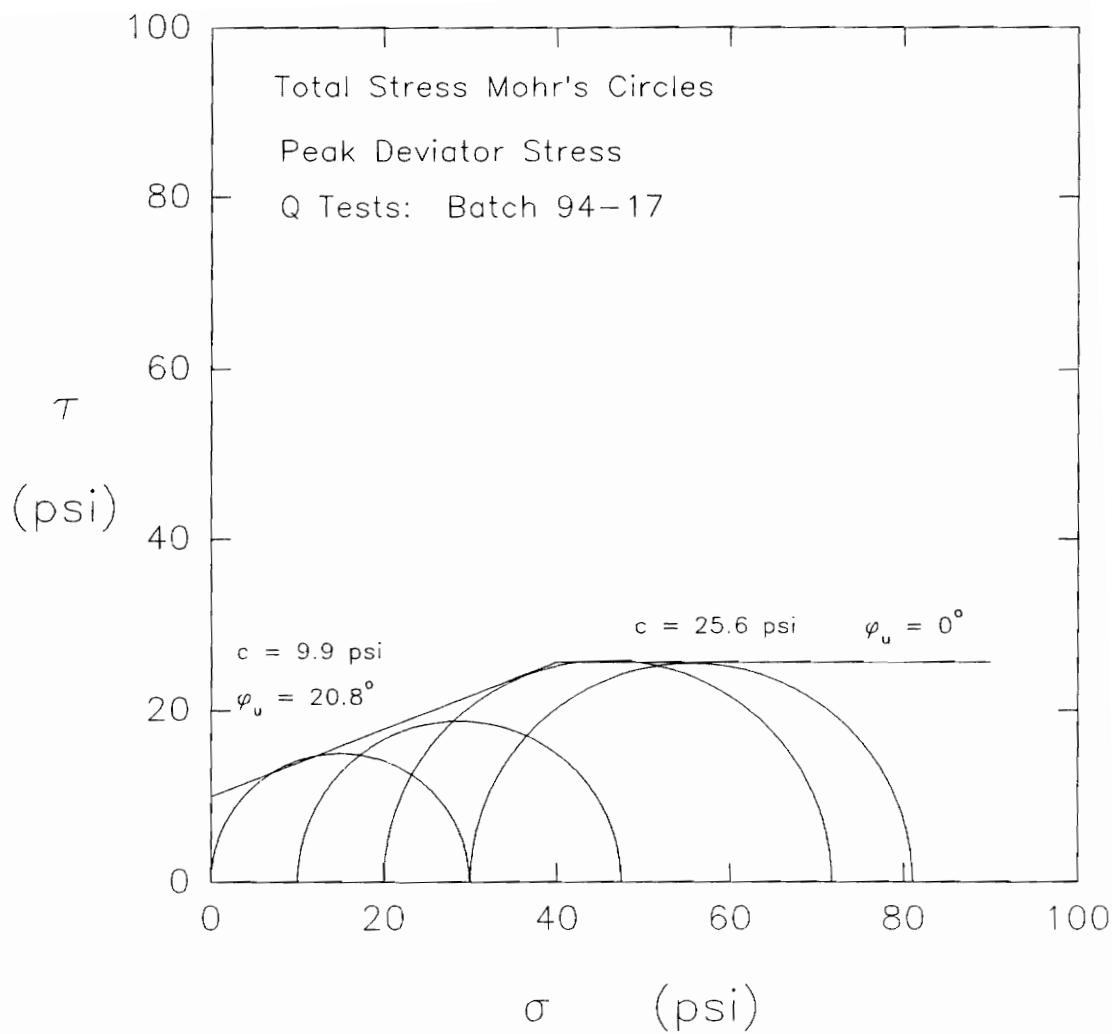


Figure 5.115. Total stress Mohr's circles at peak deviator stress for Q tests B17-1, B17-2, B17-3, and B17-4 on remolded new LMVD silt

The deviator stress vs. axial strain curves measured in Q tests B18-1, B18-2, B18-3, and B18-4 are shown in Figure 5.116. These four Q tests were performed on remolded specimens of new LMVD silt at cell pressures of 20, 40, 60, and 80 psi. These four Q tests showed very similar stress-strain behavior up to about 10% axial strain. At higher strains, the test performed at 60 psi cell pressure, gave a higher strength than the other three tests. The Q tests performed at 20, 40 and 80 psi cell pressure all showed fairly similar stress-strain behavior throughout the tests.

Taking 10% axial strain as the failure criterion, the four Q tests gave the Mohr-Coulomb strength envelope shown in Figure 5.117. This strength envelope approaches a $\phi_u = 0$, $S_u = c$ condition. The undrained shear strength parameters at this value of axial strain are $c = 18.1$ psi, $\phi_u = 1.4^\circ$.

The values of peak deviator stress which were measured in these four Q tests all occurred at 14 to 16% axial strain. Based on the values of peak deviator stress, the Mohr-Coulomb strength envelope for the soil is plotted in Figure 5.118. As can be seen from this figure, if the results from the test performed at 60 psi cell pressure are

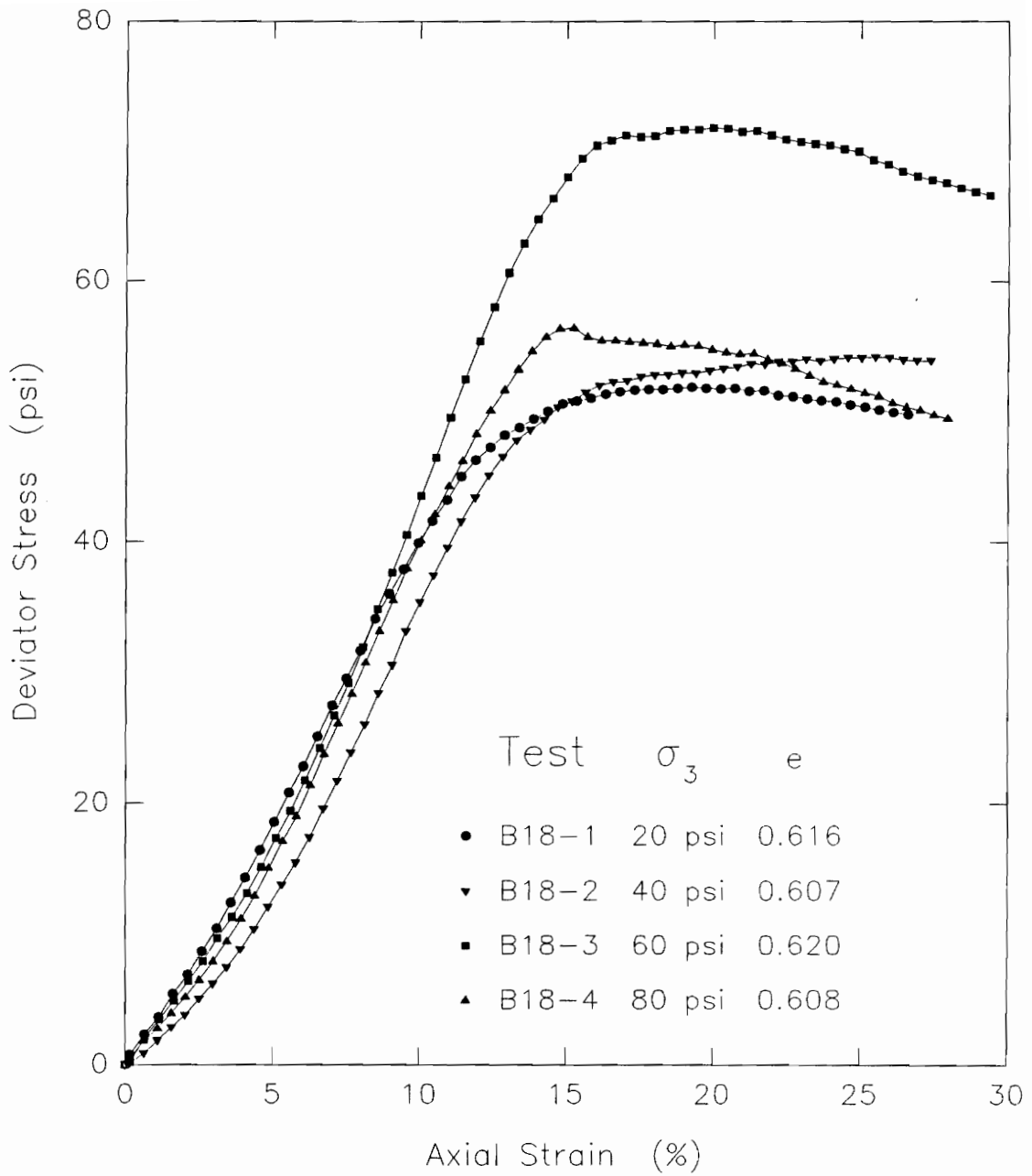


Figure 5.116. Deviator stress-strain relationships measured in Q tests B18-1, B18-2, B18-3, and B18-4 on remolded new LMVD silt

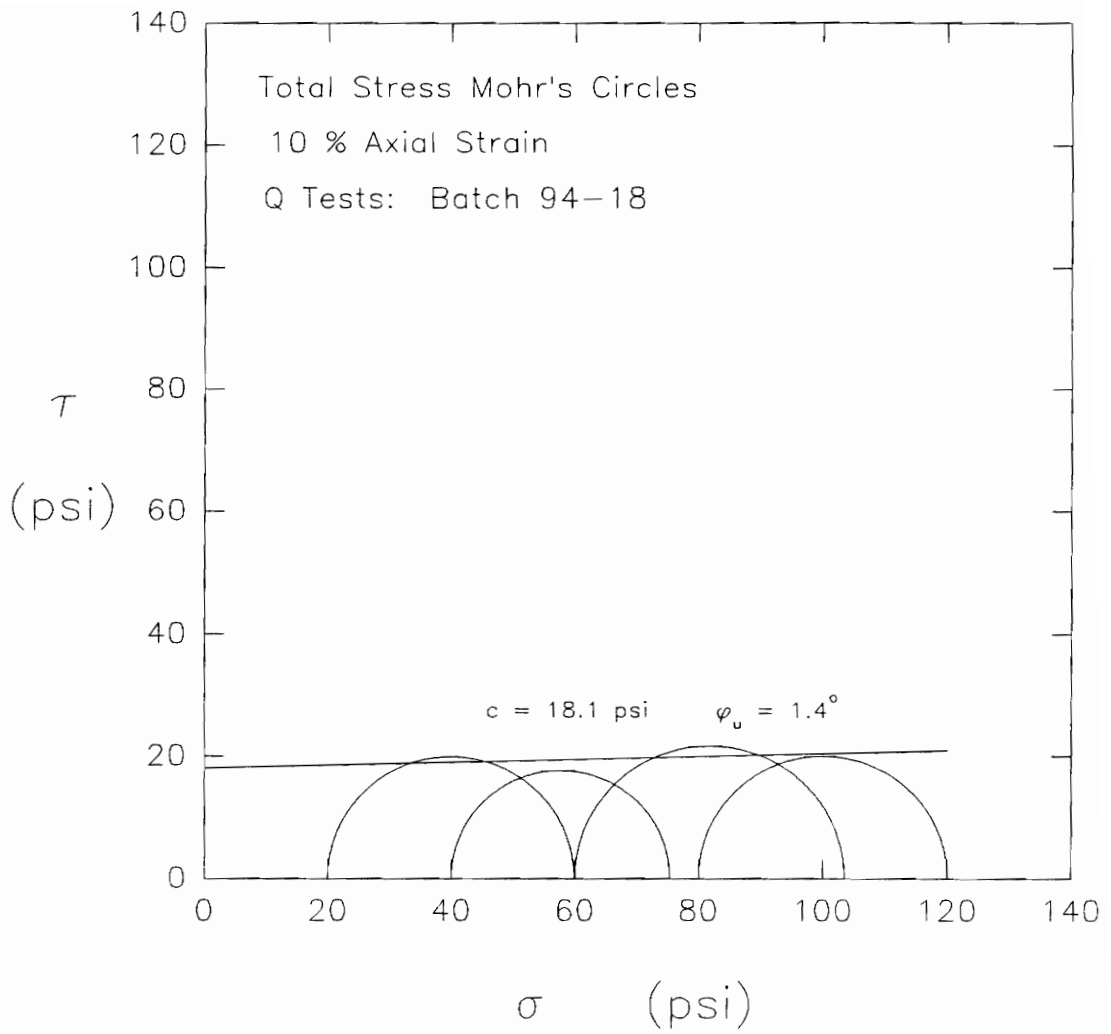


Figure 5.117. Total stress Mohr's circles at 10% axial strain for Q tests B18-1, B18-2, B18-3, and B18-4 on remolded new LMVD silt

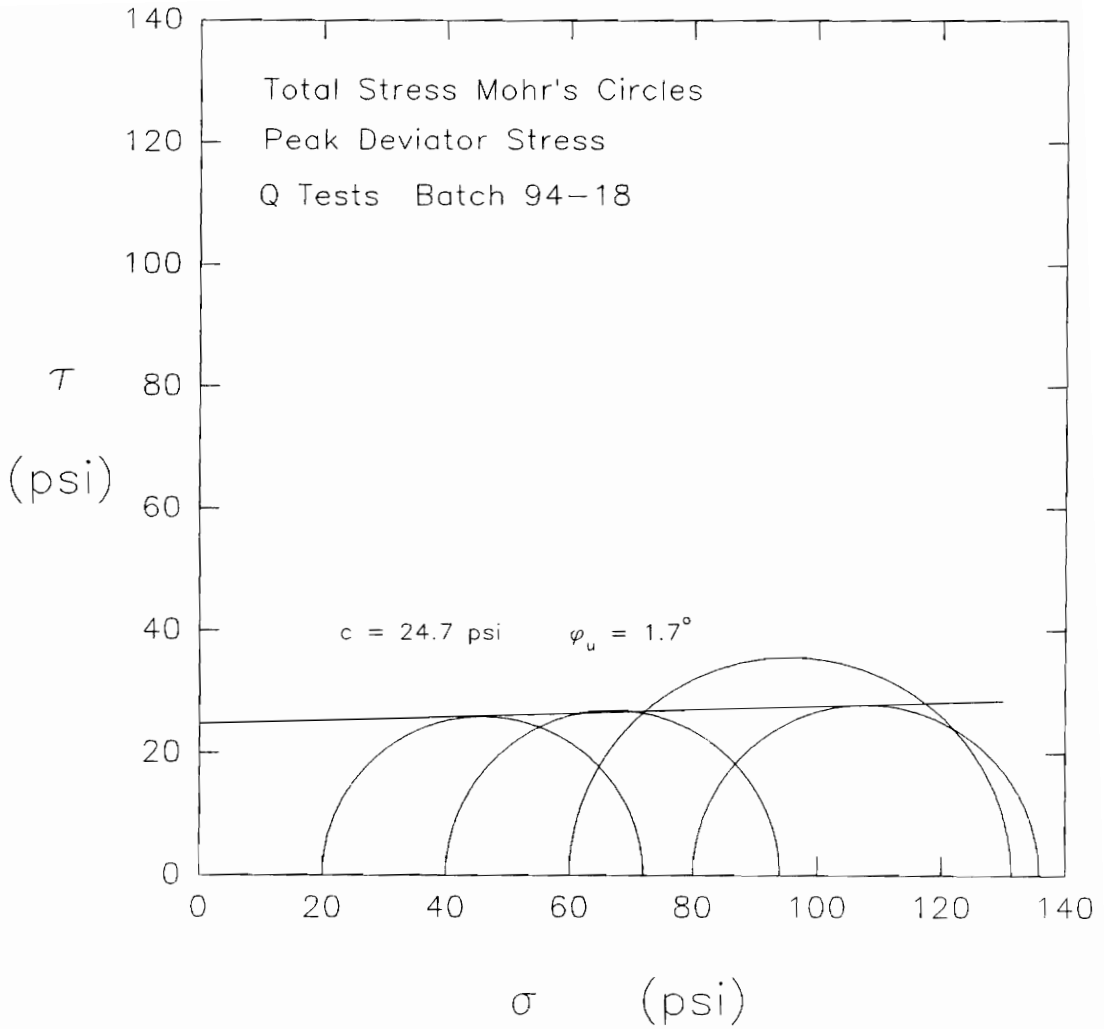


Figure 5.118. Total stress Mohr's circles at peak deviator stress for Q tests B18-1, B18-2, B18-3, and B18-4 on remolded new LMVD silt

omitted, the undrained strength of the soil is characterized by the parameters $c = 24.7$ psi and $\phi_u = 1.7^\circ$.

The stress-strain curves from the two sets of tests performed on remolded specimens of new LMVD silt are plotted together in Figure 5.119. It can be seen from this figure, that the stress-strain curves from these two different groups of specimens are noticeably different from each other.

One group of tests were performed at low cell pressures, whereas the other group of tests were performed at high cell pressures. The void ratios of the specimens tested at high cell pressures tended to be lower than those tested at low cell pressures, even though the specimens were remolded using the same procedure. The group of specimens tested at high cell pressures also were determined to be fully saturated. The specimens tested at low cell pressures were found to be less than fully saturated.

The group of specimens tested at high cell pressures tended to show stress-strain behavior which indicated dilatant tendencies. Their stress-strain curves showed considerable strain-hardening, as indicated by their concave-up shape. The stress-strain curves for the group

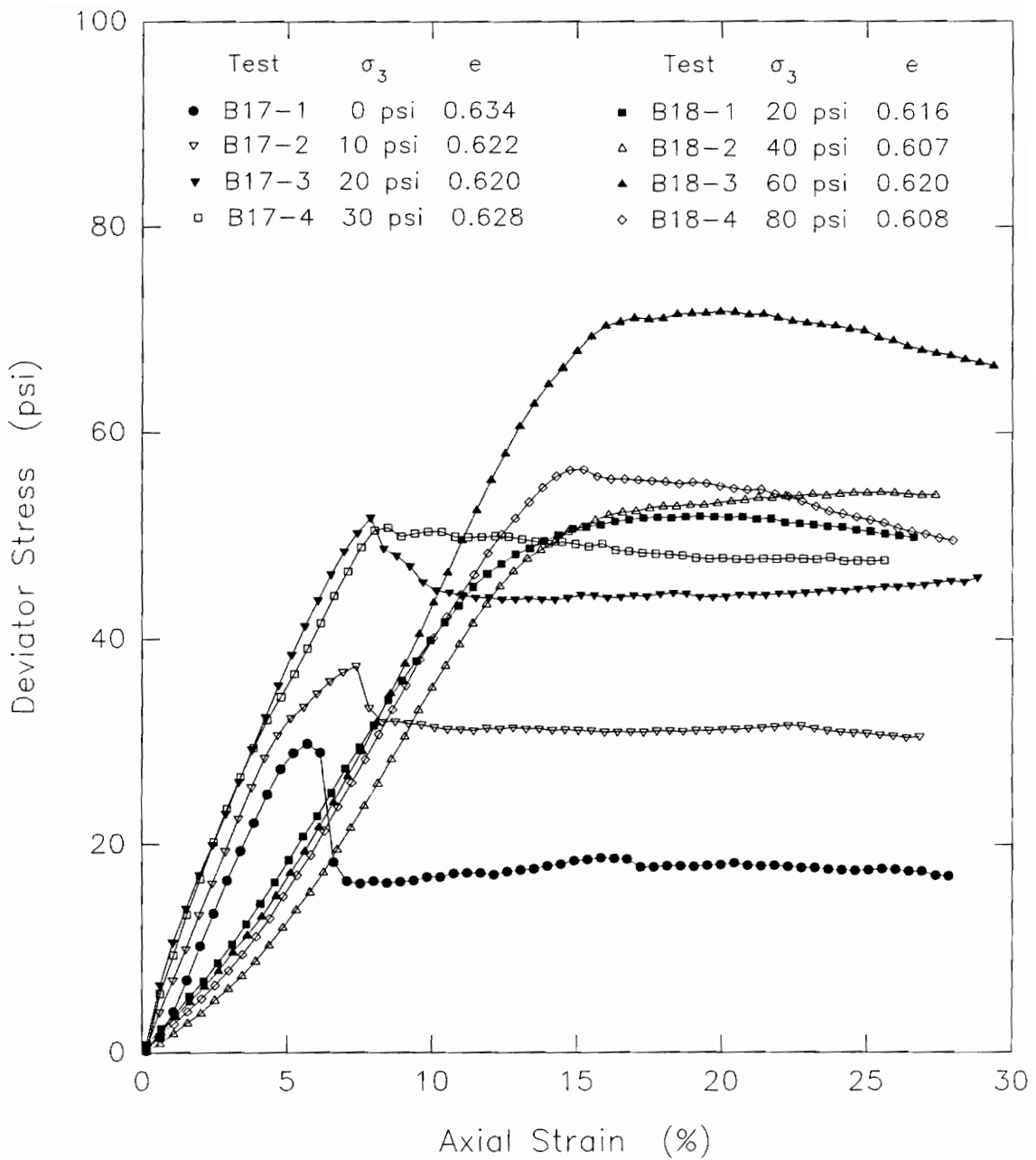


Figure 5.119. Deviator stress-strain relationships measured in Q tests B17-1, B17-2, B17-3, B17-4, B18-1, B18-2, B18-3, and B18-4 on remolded new LMVD silt

of specimens tested at low cell pressures did not exhibit this concave-up shape.

The differences in the observed stress-strain behaviors may be related to differences in the degree of saturation of the two groups of specimens. The specimens tested at low cell pressures were not fully saturated. As undrained shear occurred, preexisting air bubbles within these specimens may have begun to expand immediately. These expanding air bubbles may have influenced the stress-strain behavior of the specimens from the start of the tests.

In the group of specimens tested at high cell pressures, the fully saturated conditions may have resulted in different stress-strain behavior. In this case, air bubbles were not present or were extremely small initially. As undrained shear began, the pore water pressure would have decreased but larger negative pressures would have been necessary for air bubbles to form and expand and influence the stress-strain behavior. The development of negative pore water pressure with minimal air bubble expansion could have resulted in the observed strain-hardening and concave-up shape of the stress-strain curves. Eventually, if the pore water pressure decreased low enough during undrained shear, air bubbles may have formed and

expanded considerably within the soil pores and influenced the stress-strain behavior.

Even though these two groups of Q tests gave stress-strain behavior which appeared to be different, the Mohr-Coulomb strength envelope can be plotted, based on the values of maximum deviator stress measured in the different tests. Figure 5.120 shows the Mohr-Coulomb strength envelope for all eight Q tests performed on remolded specimens of new LMVD silt, based on the peak value of deviator stress measured in each test. As can be seen from this figure, a bilinear undrained shear strength envelope results. At values of normal stress below about 40 psi, the undrained shear strength of the soil is characterized by the parameters $c = 9.9$ psi and $\phi_u = 20.8^\circ$. At values of normal stress above about 40 psi, the undrained strength of the soil is characterized by a $\phi_u = 0$, $S_u = c = 26.5$ psi, condition.

It should be noted that the values of peak deviator stress used in plotting the Mohr-Coulomb envelope shown in Figure 5.120 occurred at a variety of axial strains. For the group of Q tests performed at low cell pressures, the peaks in the deviator stress-strain curves occurred at axial strains ranging from about 6% to 8%. The group of Q tests performed at high cell pressures did not reach peaks

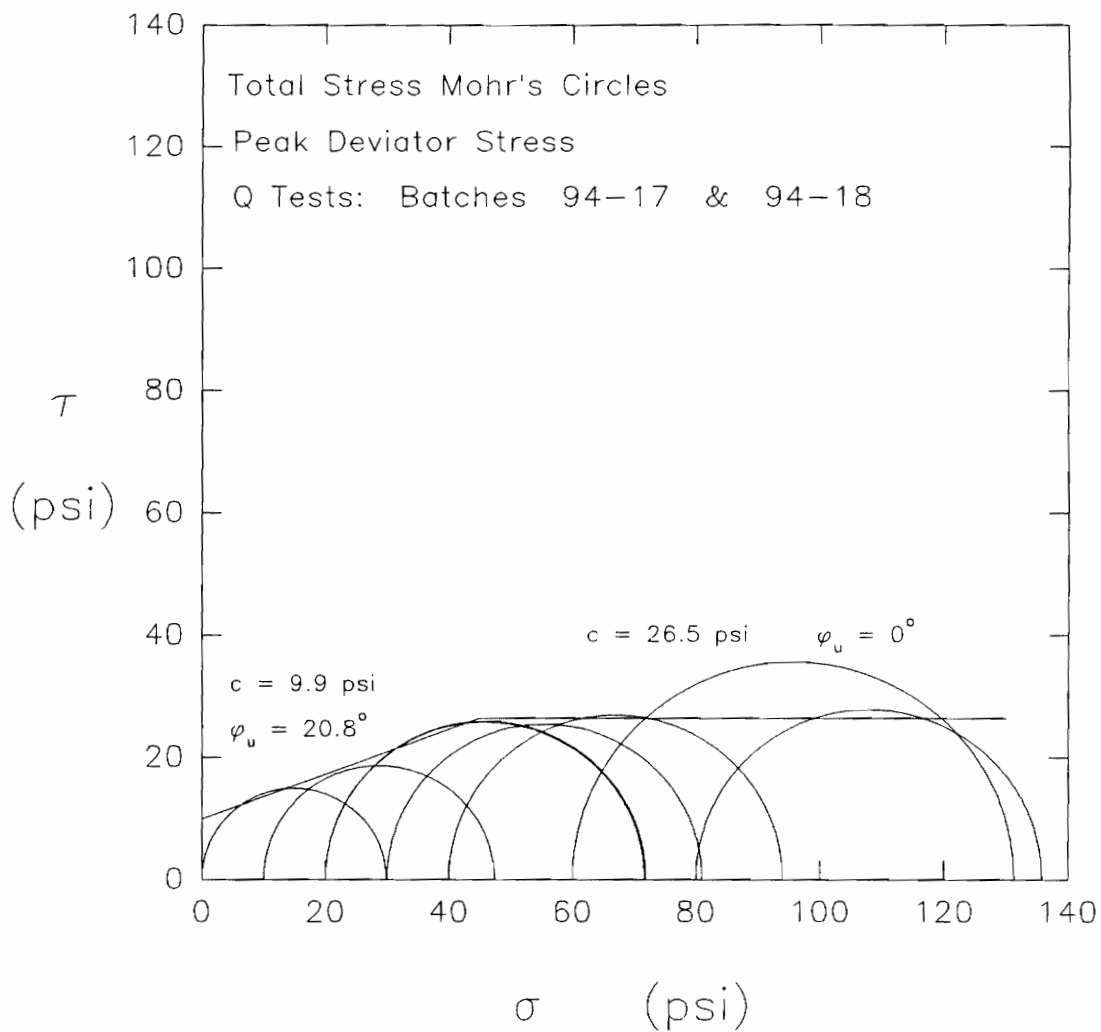


Figure 5.120. Total stress Mohr's circles at peak deviator stress for Q tests B17-1, B17-2, B17-3, B17-4, B18-1, B18-2, B18-3, and B18-4 on remolded new LMVD silt

in their stress-strain curves until about 14% to 16% axial strain and showed different stress-strain behavior than the other group of Q tests.

The values of void ratio for these specimens given in Table 5.22 suggest that the specimens should have had similar dilatant tendencies. The decreases in pore water pressure in the specimens should have been similar at the same axial strain. At different levels of axial strain, the pore pressure decreases should have been different. The effective stress in the specimens, therefore, might not have been the same for all of the Q test specimens when the peak deviator stress occurred. Obtaining undrained strengths from specimens having different values of effective stress is felt to be questionable (Torrey, 1982). The variation in the axial strain at which the peak deviator stress occurred and the differences in the stress-strain behavior may have resulted from the different initial degrees of saturation of the specimens.

5.10 CU Tests with Different Back Pressures

One batch consolidometer sample of old LMVD silt was used to provide 4 specimens for performing CU triaxial tests. All four remolded, saturated, silt specimens were consolidated isotropically to $\sigma'_{3con} = 10$ psi. The back pressures, u_b , used in these tests were varied from 0 to 90

psi. The initial specimen data for the CU test specimens are presented in Table 5.23.

Table 5.23: Initial specimen data for CU test specimens with different values of back pressure

Test	σ'_{3con} (psi)	u_b (psi)	e	w (%)	γ_d (pcf)	S (%)
B5-1	10	0	0.517	19.97	108.9	99.3
B5-2	10	0	0.528	20.05	108.1	97.5
B5-3	10	90	0.531	19.91	109.1	99.5
B5-4	10	10	0.526	20.16	109.2	98.9

By using different values of back pressure in these CU tests, the magnitude of the decrease in pore water pressure possible in each specimen would vary. During undrained shear, if the pore water pressure decreased low enough to eliminate the back pressure initially in the specimen, the specimen would experience desaturation (Head, 1986; Brandon, Duncan, and Huffman, 1990). The influence of specimen desaturation on the undrained stress-strain behavior could then be evaluated and possibly related to the stress-strain behavior observed in Q tests on saturated silts.

Figure 5.121a shows the deviator stress vs. axial strain behavior measured in these four CU tests. As can be seen from this plot, the deviator stress-strain behavior for the four tests varied. The variation in stress-strain behavior is a result of different back pressures being used

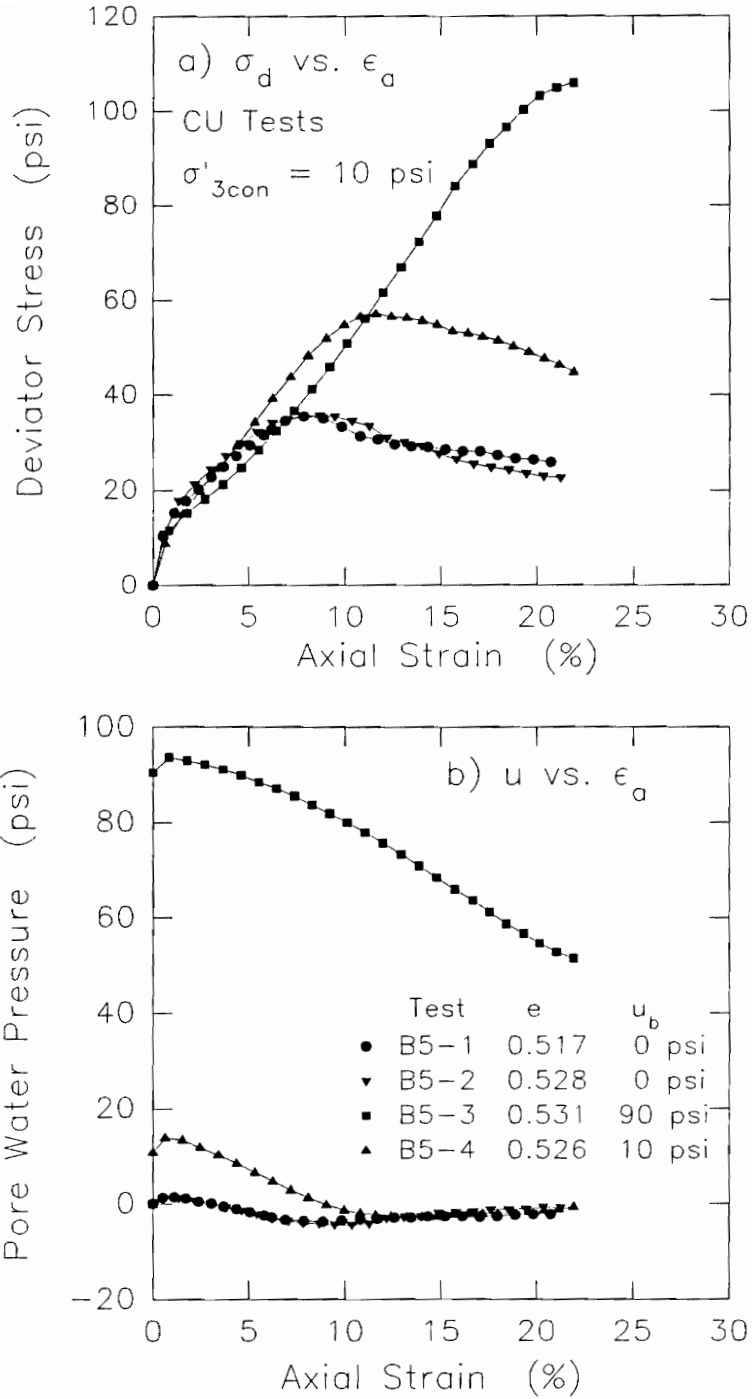


Figure 5.121. Deviator stress vs. axial strain and pore pressure vs. axial strain relationships measured in CU tests on remolded old LMVD silt

in the tests. In these tests, the higher the back pressure used, the higher the maximum deviator stress measured during undrained shear.

Figure 5.121b shows the pore pressures measured in these CU tests. For all four CU tests, the initial pore water pressure was equal to the back pressure used in the particular test specimen. As undrained shear began, each specimen experienced a slight increase in pore water pressure. With increasing axial strain, the tendency of the silt specimens to dilate lead to decreases in pore water pressure within the specimens. The decreasing pore water pressure resulted in the strengthening of the silt specimens. The magnitude of the decrease in pore water pressure that was possible in these four CU test specimens depended on the back pressure used in each test.

Figures 5.122 and 5.123 show the deviator stress-strain and pore pressure-strain relationships measured in the two CU test specimens consolidated isotropically to $\sigma'_{3con} = 10$ psi with a back pressure equal to zero psi or atmospheric pressure. For these two CU tests, the maximum deviator stress measured was about 36 psi and occurred at axial strains of about 8.4%, as shown in Figures 5.122a and 5.123a. The pore water pressure in these two CU tests initially increased above atmospheric pressure. Figures

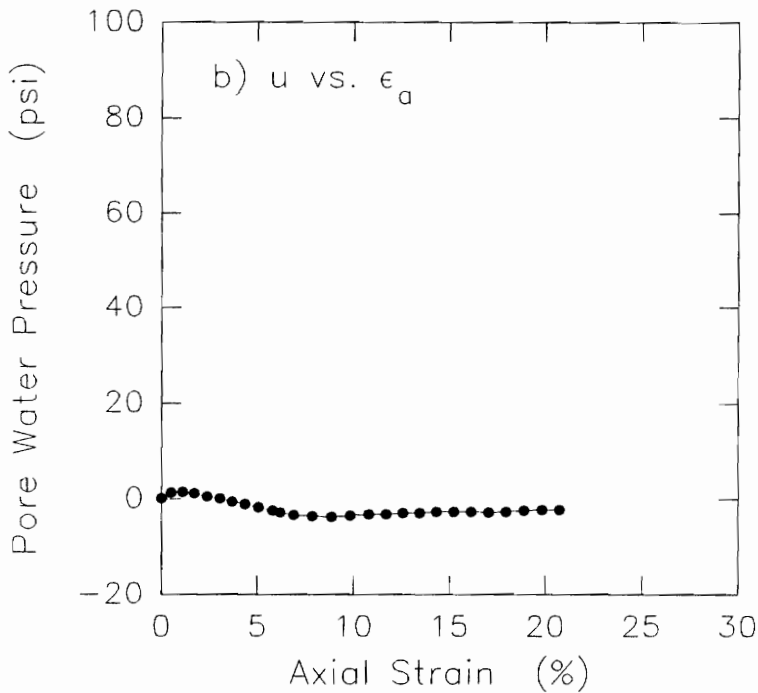
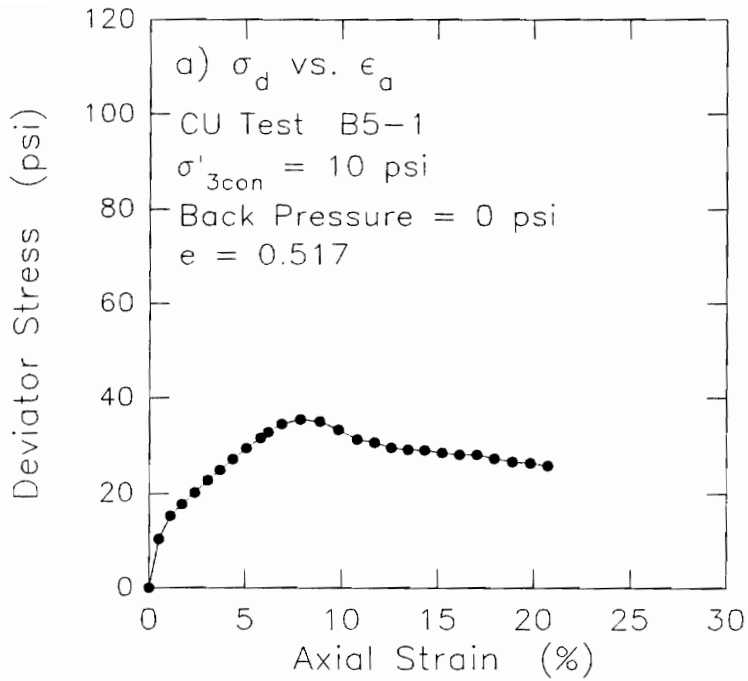


Figure 5.122. Deviator stress vs. axial strain and pore pressure vs. axial strain relationships measured in CU test B5-1 on remolded old LMVD silt

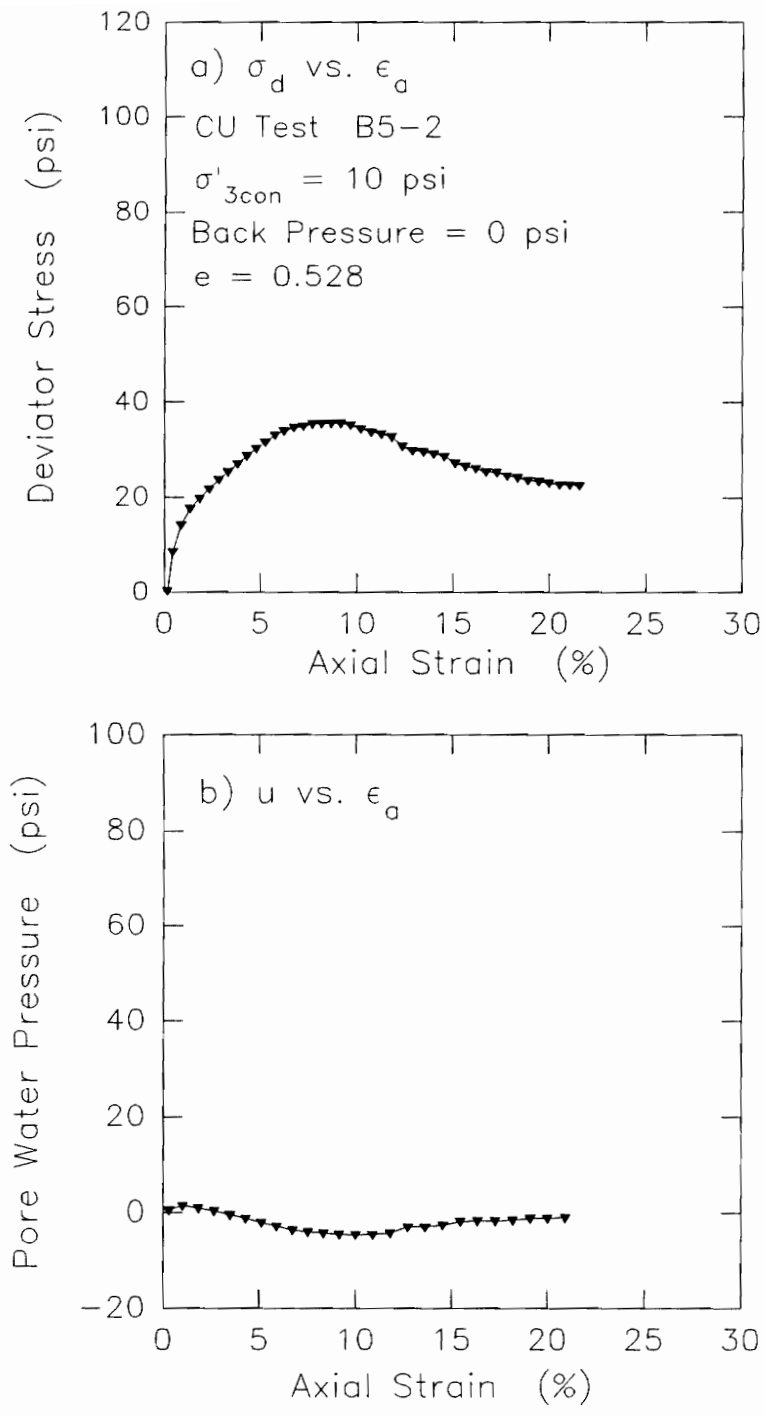


Figure 5.123. Deviator stress vs. axial strain and pore pressure vs. axial strain relationships measured in CU test B5-2 on remolded old LMVD silt

5.122b and 5.123b show that with continued shear, the pore water pressure decreased and went below atmospheric pressure. When the pore water pressure went below atmospheric pressure, desaturation of the specimens began to occur.

Desaturation of the specimens would have resulted in an increase in the volume of the samples, leading to drained rather than undrained conditions in the specimen. The occurrence of a minimum pore water pressure in these two tests tended to correspond with the stress-strain curve of the specimens reaching maximum values, followed by decreasing strength with increasing axial strain. At about the same axial strain that the deviator stress reached maximum values in these two tests, the pore water pressure had decreased to minimum values of about 4.5 psi below atmospheric pressure.

One CU test specimen was consolidated isotropically to $\sigma'_{3con} = 10$ psi with a back pressure of 10 psi. The deviator stress vs. axial strain and pore pressure vs. axial strain relationships measured in this CU test are shown in Figure 5.124. The higher back pressure in this test allowed the specimen to experience a larger decrease in pore water pressure during undrained shear before desaturation of the specimen would occur. As a result,

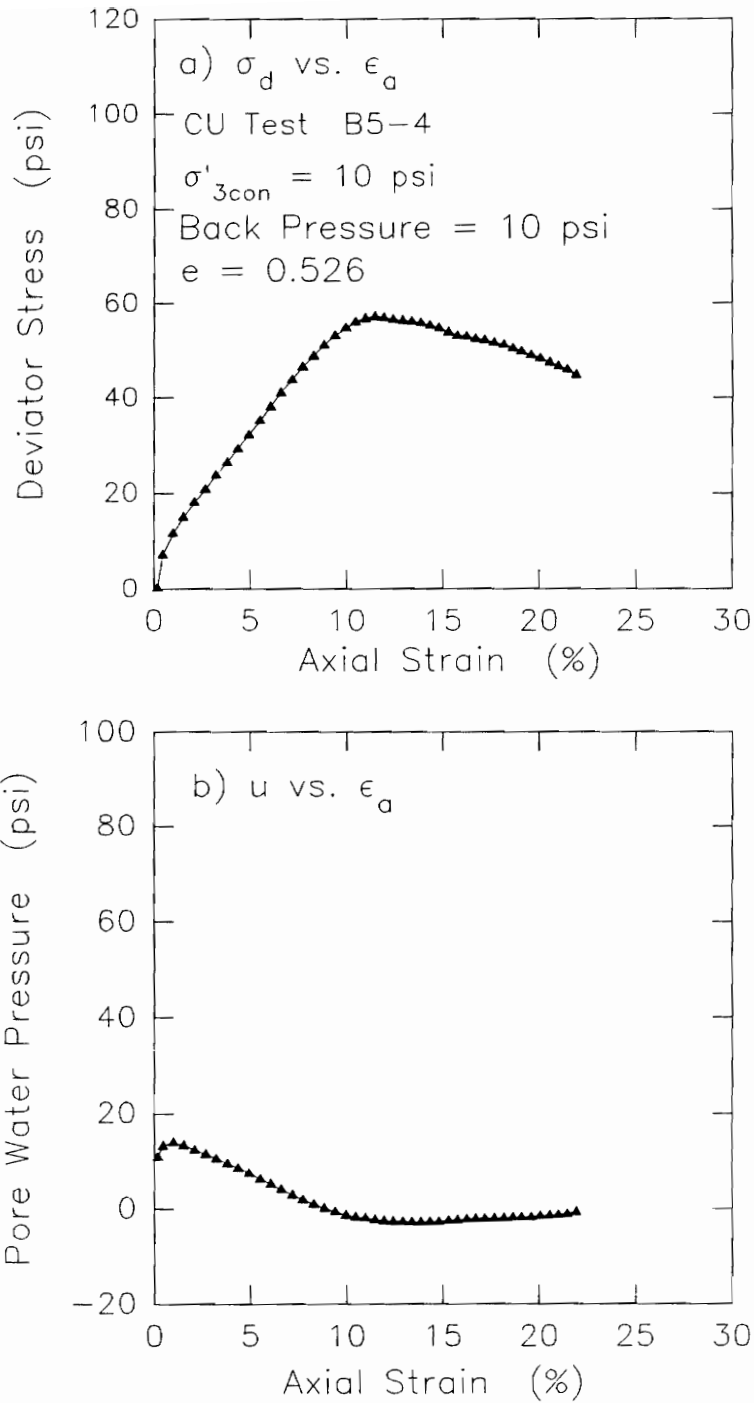


Figure 5.124. Deviator stress vs. axial strain and pore pressure vs. axial strain relationships measured in CU test B5-4 on remolded old LMVD silt

this specimen reached a higher peak deviator stress than the two specimens in which the back pressure had been equal to atmospheric pressure. As shown in Figure 5.124a, the maximum deviator stress measured in this test was 57 psi and occurred at an axial strain of about 11.5%.

As indicated by Figure 5.124b, the pore water pressure measured in this test was initially equal to 10 psi. As shear began, the pore water pressure increased slightly and then decreased as shear progressed. When the pore water pressure decreased below atmospheric pressure, desaturation of the specimen took place and the specimen no longer maintained a constant volume. Desaturation of the specimen corresponded with the maximum deviator stress being reached for the specimen. In this test, the pore water pressure decreased to a minimum value of about 2.5 psi below atmospheric pressure.

The fourth CU test specimen had been consolidated to $\sigma'_{3con} = 10$ psi with a back pressure of 90 psi. The deviator stress vs. axial strain and pore pressure vs. axial strain relationships measured in this CU test are shown in Figure 5.125. The magnitude of the back pressure used in this test allowed for a significant decrease in pore water pressure to occur during undrained shear without desaturation of the specimen taking place. As a result,

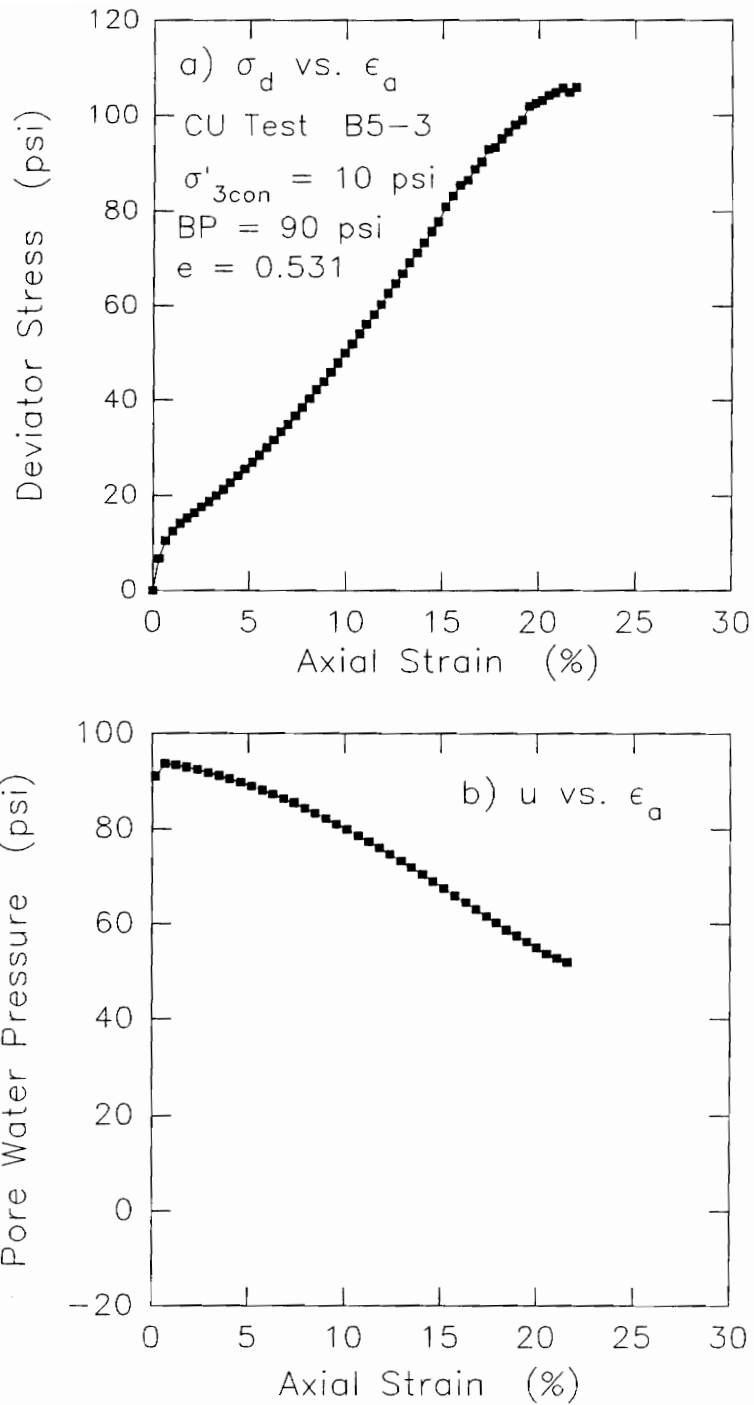


Figure 5.125. Deviator stress vs. axial strain and pore pressure vs. axial strain relationships measured in CU test B5-3 on remolded old LMVD silt

the deviator stress measured for this specimen continued to increase throughout the test, with no peak value occurring within the range of strains tested, as shown in Figure 5.125a. The deviator stress measured in this test was at its maximum value of 106 psi when the test was terminated at about 22% axial strain.

The pore water pressure in this test was initially 90 psi greater than atmospheric pressure. After a small increase in pore water pressure at the start of the test, the pore water pressure began to decrease and continued to decrease throughout the entire test. The pore water pressure ultimately decreased by about 40 psi during this test, as shown in Figure 5.125b. Because the pore water pressure in this specimen initially was 90 psi greater than atmospheric pressure, the final pore water pressure in the specimen was still about 50 psi greater than atmospheric pressure. As a result, the pore water pressure never went below atmospheric pressure, desaturation of the specimen did not occur and the specimen remained saturated and had a constant volume throughout the test. Because of this, the specimen did not reach a peak value of deviator stress during the test.

Figure 5.126 shows the effective stress paths for these four CU tests. All four specimens were consolidated

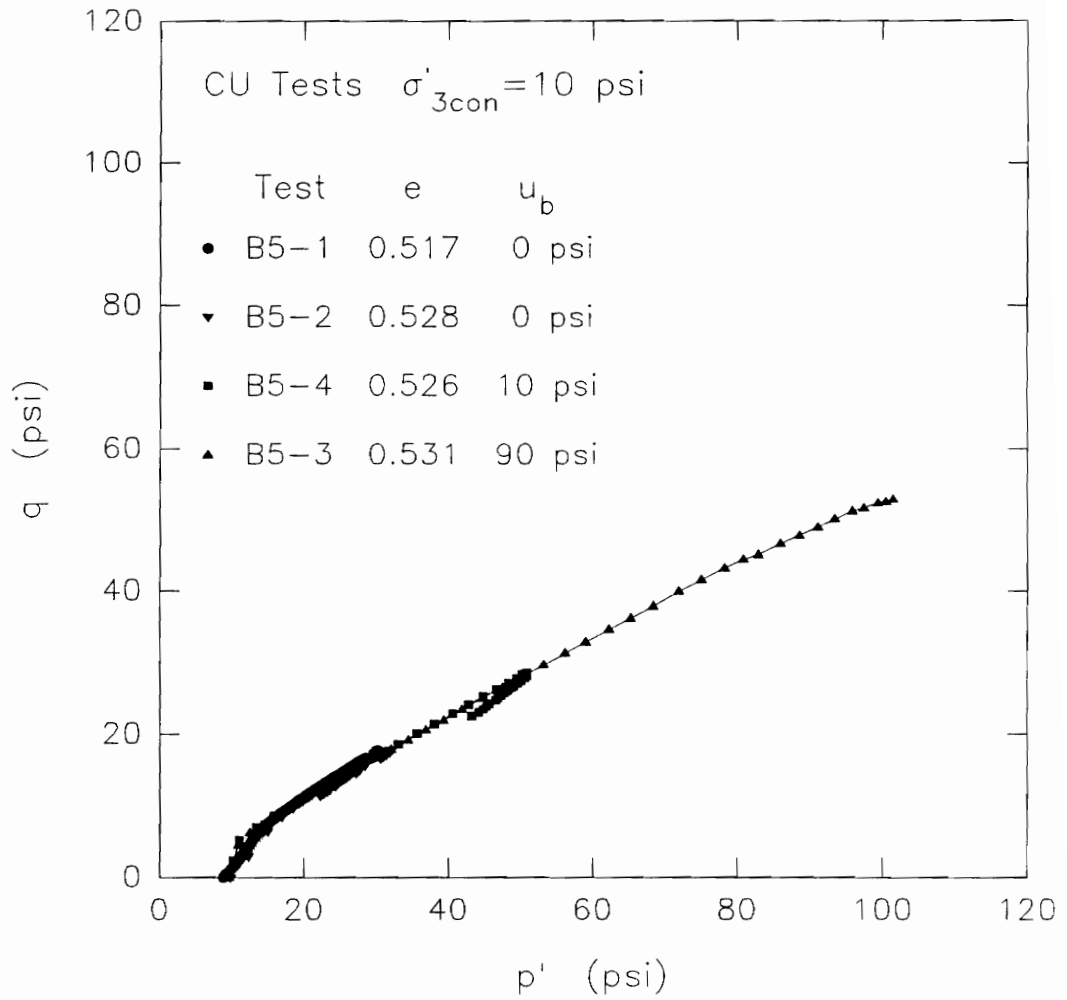


Figure 5.126. Effective stress paths measured in CU tests on remolded old LMVD silt

to an initial isotropic consolidation pressure, σ'_{3con} , of 10 psi. The stress paths for the four CU tests are all very similar. The tests with higher values of back pressure gave longer stress paths, but all four stress paths clearly define the K_f line for the soil. From these effective stress paths, the orientation of the K_f line for the soil is defined by $\alpha = 29^\circ$. This corresponds to an effective stress friction angle for the soil of $\phi' = 34^\circ$.

Plots of σ'_3 vs. axial strain and \bar{A} vs. axial strain for these four CU tests are presented in Figures 5.127 through 5.130.

The results of these CU tests on saturated silt specimens consolidated to $\sigma'_{3con} = 10$ psi with different values of back pressure can be compared to the results of CD tests on saturated silt specimens consolidated to different values of σ'_{3con} . Three CD tests were performed on remolded specimens of old LMVD silt. These three specimens were back pressure saturated and consolidated isotropically to 10, 20, and 30 psi. The specimens were then sheared under drained conditions. The initial specimen data prior to consolidation for these three CD test specimens are given in Table 5.24.

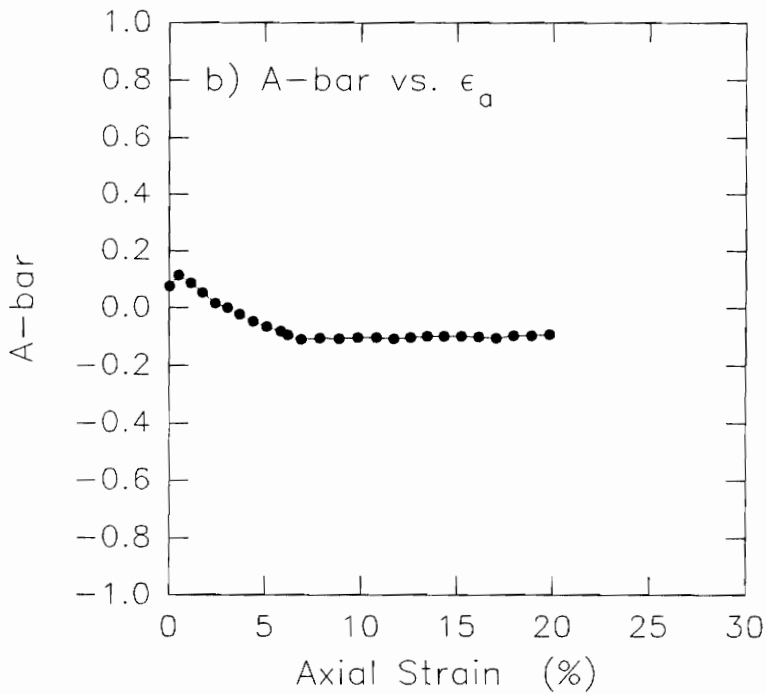
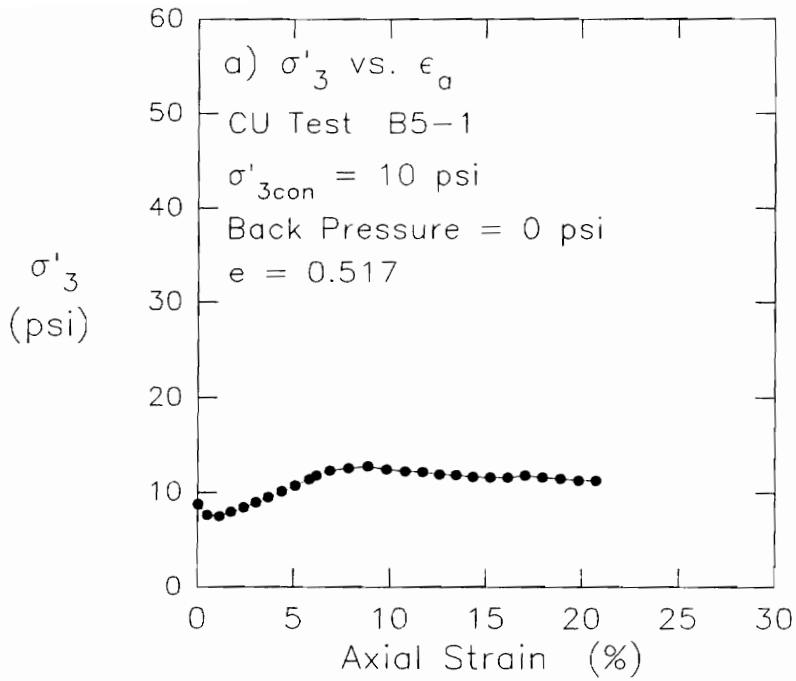


Figure 5.127. Minor principal effective stress vs. axial strain and \bar{A} vs. axial strain for CU test B5-1 on remolded old LMVD silt

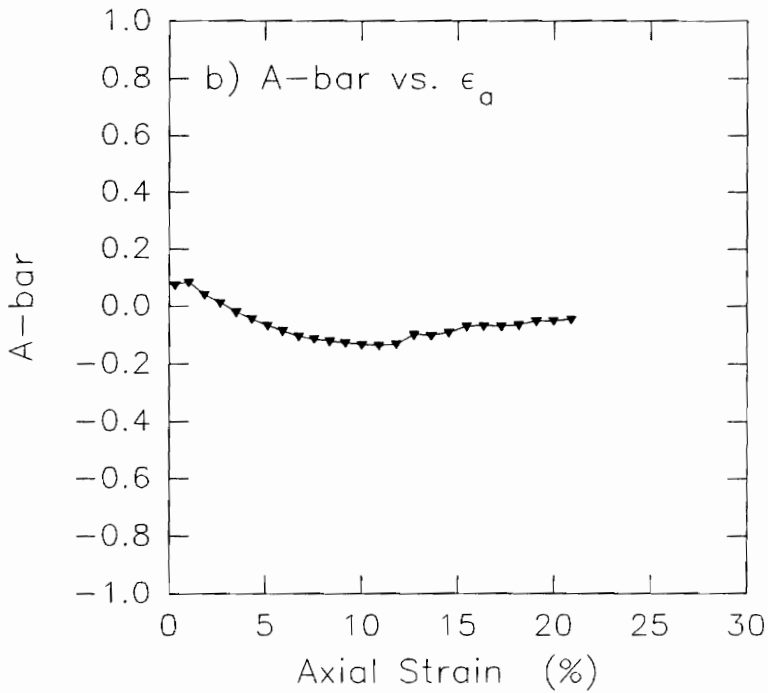
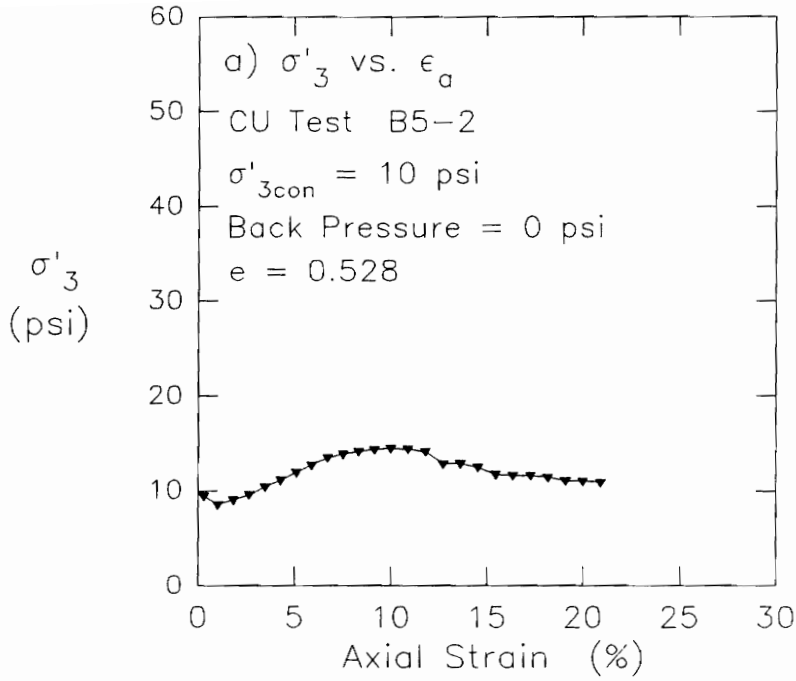


Figure 5.128. Minor principal effective stress vs. axial strain and \bar{A} vs. axial strain for CU test B5-2 on remolded old LMVD silt

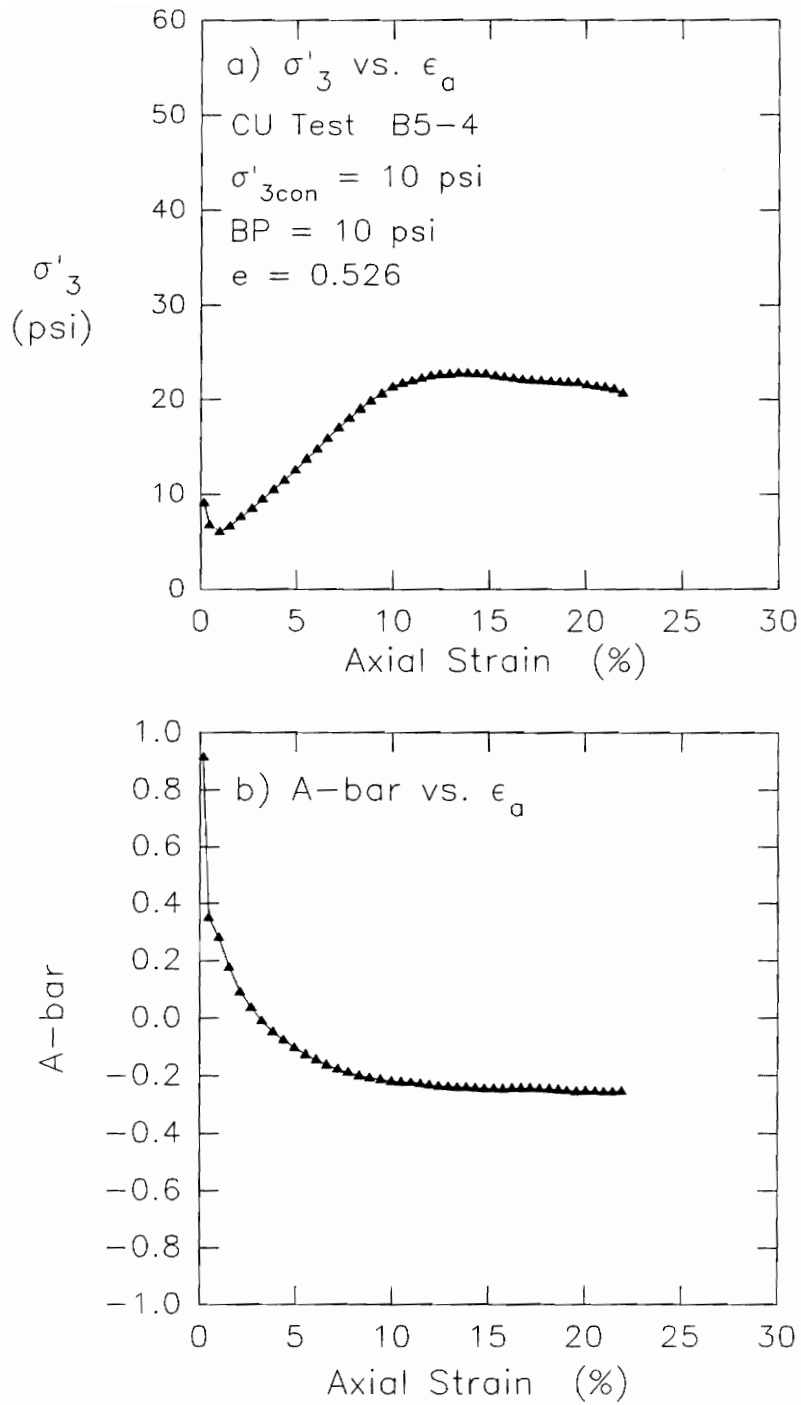


Figure 5.129. Minor principal effective stress vs. axial strain and \bar{A} vs. axial strain for CU test B5-4 on remolded old LMVD silt

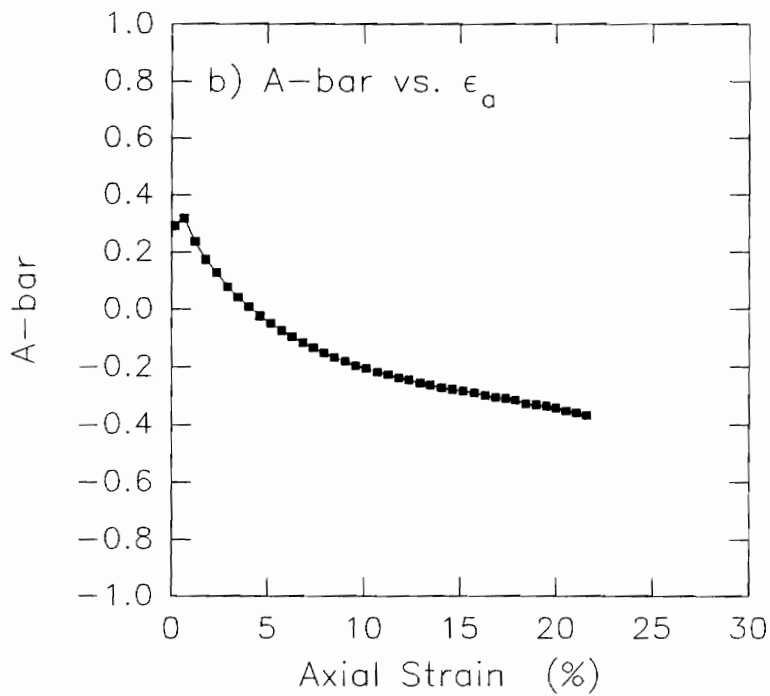
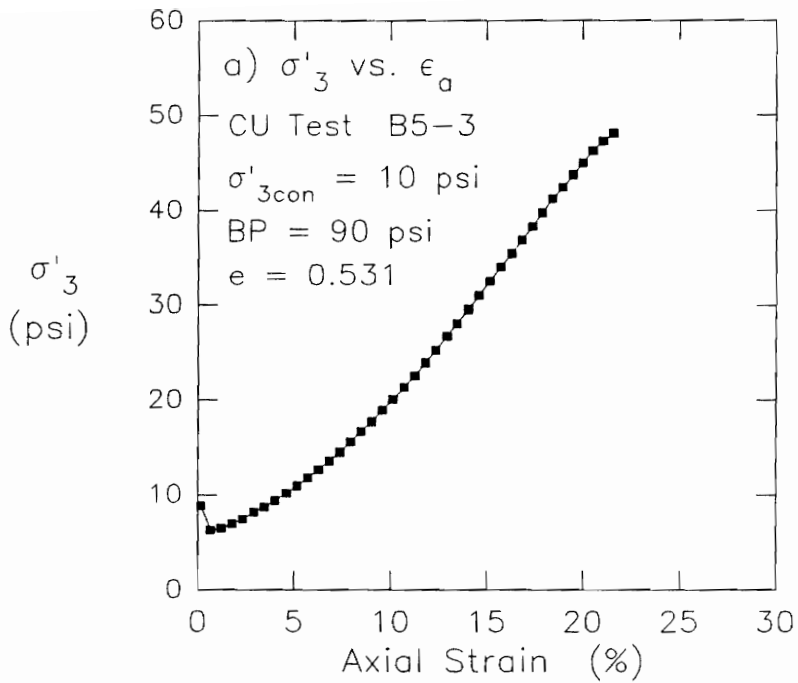


Figure 5.130. Minor principal effective stress vs. axial strain and \bar{A} vs. axial strain for CU test B5-3 on remolded old LMVD silt

Table 5.24: Initial specimen data prior to consolidation for CD test specimens of remolded old LMVD silt

Test	σ'_{3con} (psi)	e	w (%)	γ_d (pcf)	S (%)
CD-1	10	0.667	21.2	99.4	84.9
CD-2	20	0.570	20.8	106.1	97.4
CD-3	30	0.603	22.5	104	99.6

Figure 5.131 shows the deviator stress vs. axial strain and volumetric strain vs. axial strain relationships measured in the three CD tests performed on remolded specimens of old LMVD silt.

As can be seen from the plots of deviator stress vs. axial strain presented in Figure 5.131a, the strength of the soil increased with increasing consolidation pressure. The peak deviator stress measured in each of these CD tests occurred at axial strains between 6 and 7 percent. The peak values of deviator stress were followed by distinct strain-softening behavior.

The plots of volumetric strain vs. axial strain for these three tests shown in Figure 5.131b indicate that as drained shear began, the specimens contracted somewhat and experienced a decrease in volume until axial strains of about 2.5 percent. With increasing axial strain, the specimens began to experience dilation. The specimens continued to experience increases in volume from about 2.5% axial strain until termination of the tests.

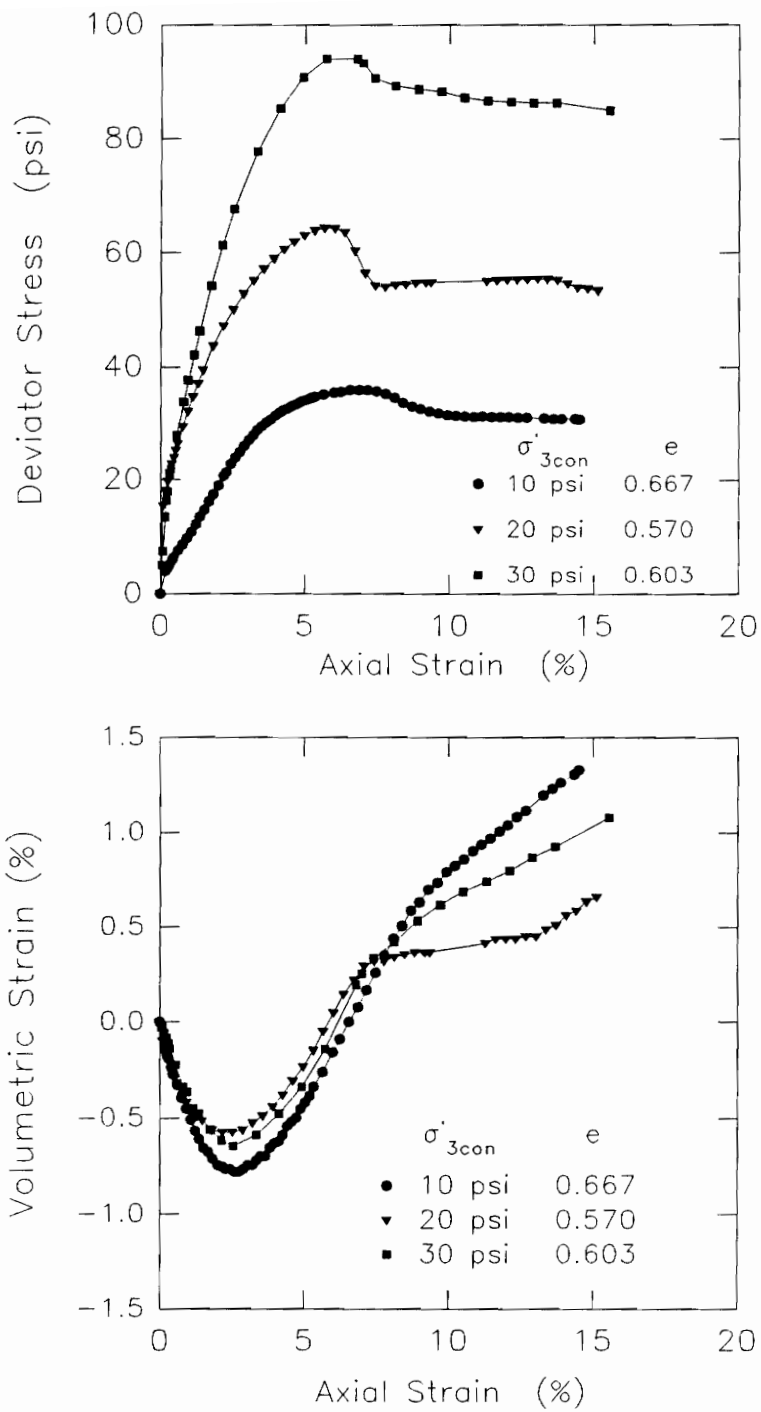


Figure 5.131. Deviator stress vs. axial strain and volumetric strain vs. axial strain relationships measured in CD tests on old LMVD silt

For these three CD tests, the peak in the deviator stress-strain curves occurred at about the same axial strain that the volumetric strain in the specimens went from negative to positive. The specimens initially decreased slightly in volume and then began to increase in volume with further strain and returned to approximately the initial specimen volume at the start of the test. As the volume of the specimens increased above the initial specimen volume, the peak in the deviator stress-strain curve occurred and the specimens experienced strain softening as the volume of the specimens continued to increase with increasing axial strain.

The results of these CD tests indicate that when the specimen volume increases above its initial volume, the strength of the soil decreases and strain softening behavior occurs. Taking the peak deviator stress as a failure criterion, the effective stress Mohr's circles have been plotted in Figure 5.132. From these CD tests, the effective stress friction angle for the soil, ϕ' , is found to be 38° .

The results of the CD test performed at an isotropic consolidation pressure, σ'_{3con} , of 10 psi can be compared to the results of the two CU tests consolidated isotropically to $\sigma'_{3con} = 10$ psi with a back pressure, u_b ,

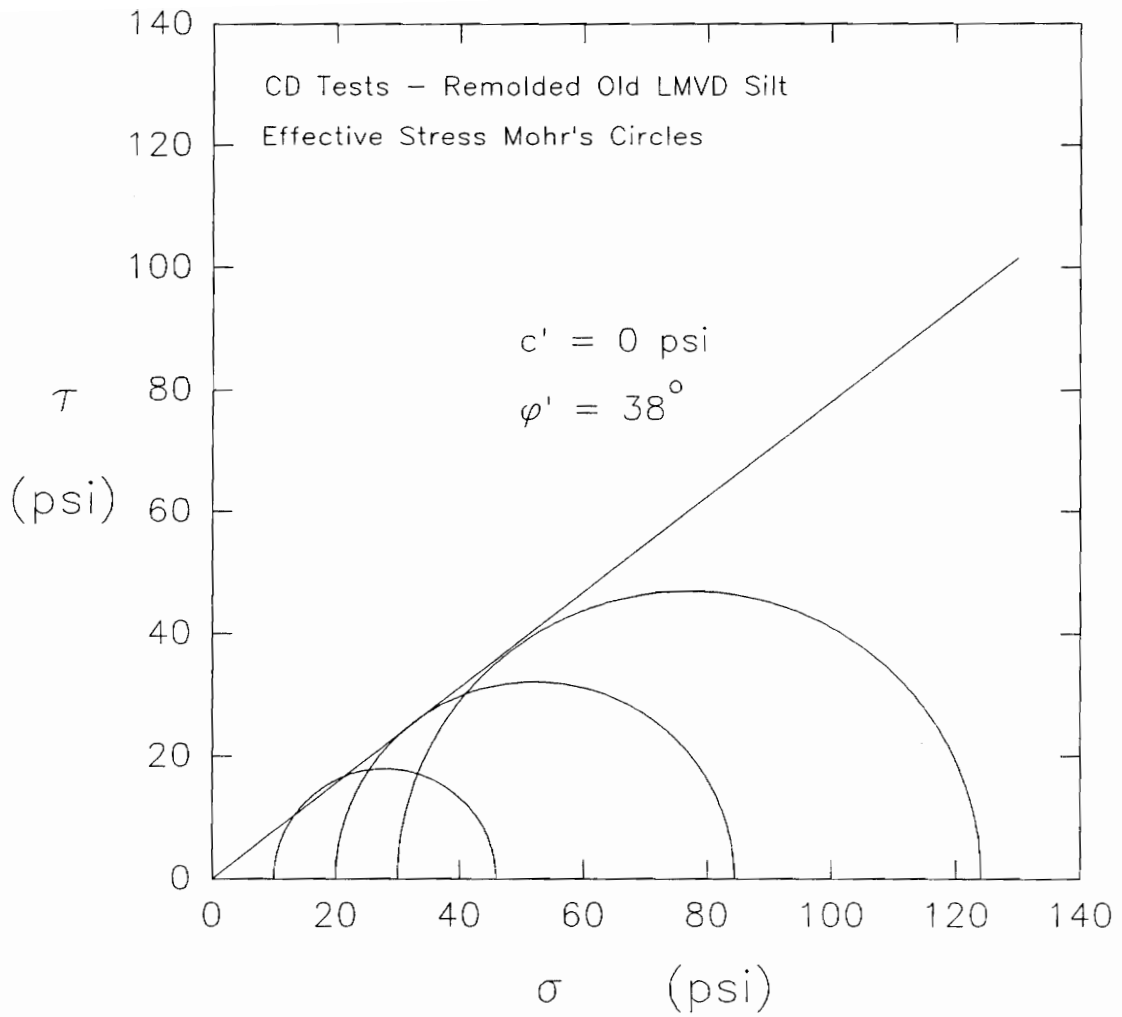


Figure 5.132. Effective stress Mohr's circles for CD tests on remolded old LMVD silt, based on maximum deviator stress failure criterion

of 0 psi or atmospheric pressure. The values of peak deviator stress measured in these two CU tests shown in Figure 5.122 and 5.123 are about 36 psi. This is the same as the peak deviator stress measured in test CD-1, 36 psi, as shown in Figure 5.131.

In the CD test with $\sigma'_{3con} = 10$ psi, the specimen underwent drained shear and volume change was able to occur. In the two CU tests, σ'_{3con} also was equal to 10 psi while the back pressure was equal to 0 psi or atmospheric pressure. As undrained shear proceeded and the pore water pressure went below atmospheric pressure, desaturation of the CU specimens occurred and volume expansion took place. The CU test specimens went from being undrained to having behavior characteristic of drained specimens. As a result, they gave a strength for the soil similar to that determined by the CD test. In the CD test and the two CU tests, the peak deviator stress was reached at similar values of axial strain.

The results of the CD test performed at an isotropic consolidation pressure, σ'_{3con} , equal to 20 psi, can be compared to the results of the CU test performed on the CU specimen consolidated isotropically to $\sigma'_{3con} = 10$ psi with a back pressure, u_p , of 10 psi. In this case, the CD specimen experienced drained shear and gave a peak deviator

stress of about 65 psi for the soil at a minor principal effective stress, σ'_3 , equal to the isotropic consolidation pressure σ'_{3con} of 20 psi. The CU test specimen was consolidated to $\sigma'_{3con} = 10$ psi. During undrained shear, the pore water pressure decreased. Due to the back pressure in the specimen being equal to 10 psi initially, the pore water pressure was able to decrease by 10 psi before desaturation of the specimens would begin.

In the CU test specimen, when the pore water pressure had decreased by 10 psi, the minor principal effective stress, σ'_3 , would have been equal to 20 psi, or the same effective stress as the isotropic consolidation pressure, σ'_{3con} , of the CD test specimen. With further decrease in pore water pressure, the CU test specimen would have begun to experience desaturation, because the initial back pressure in the specimen had been eliminated. In this situation, the CU test specimen would begin to exhibit drained behavior rather than undrained behavior. Since the CU test specimen would begin to experience drained behavior when $\sigma'_3 = 20$ psi, the strength measured should be similar to the strength of the CD test specimen consolidated to $\sigma'_{3con} = 20$ psi. Figure 5.124 shows that the CU test specimen consolidated initially to 10 psi with a back pressure equal to 10 psi, gave a peak deviator stress of about 57 psi. This is of a similar magnitude as the value

of 65 psi measured in the CD test specimen consolidated to 20 psi.

The CD test specimen reached its peak value at a lower axial strain than the CU test specimen. This is because the CD specimen had a minor principal effective stress of 20 psi from the start of the test and it experienced drained conditions throughout the test. The CU test specimen had a minor principal effective stress of 10 psi at the start of the test. The minor principal effective stress did not reach 20 psi until the pore water pressure had decreased sufficiently during undrained shear. This decrease in pore water pressure was dependent on the level of axial strain in the specimen. As a result, the CU test specimen did not reach a strength similar to the strength of the CD specimen until a sufficient amount of axial strain had occurred and the pore water pressure had decreased enough so that σ'_3 for the CU test specimen had reached 20 psi.

5.11 Q Tests on Back Pressure Saturated Specimens

Two batches of remolded new LMVD silt were used to perform eight Q tests on specimens which were back pressure saturated. Four triaxial specimens were trimmed from each batch consolidometer sample and were essentially fully saturated. These specimens were placed in the triaxial

cell between bottom and top platens. A saturated porous stone was placed on top of the bottom platen which was connected by pore pressure lines to the back pressure system. The pore pressure lines and back pressure system were filled with deaired water. The top platen had no pore pressure or drainage connections. Drainage lines were only connected to the bottom of the specimen in order to eliminate the possibility of trapping air in the top platen and its porous stone and pore pressure lines.

After placement in the triaxial cell, the silt specimens were subjected to an increase in back pressure and cell pressure. The cell pressure used during the back pressure saturation process was slightly greater than the back pressure so that the specimen was subjected to an effective consolidation pressure, σ'_{3con} , of 2 psi. In one set of four tests, the back pressure was equal to 10 psi, while the cell pressure was 12 psi. In the other set of tests, the back pressure was equal to 20 psi and the cell pressure was 22 psi.

The back pressure and cell pressure used in the back pressure saturation process were applied to the specimen for one hour. At the end of one hour, the drainage valve at the base of the triaxial cell was closed and the cell pressure was increased to the value for the particular

test. The specimen was then sheared undrained at a strain rate of about 1%/min. Pore water pressures were not measured in the specimens during undrained shear. The increases in cell pressure applied to the specimens after the back pressure saturation process was complete and the drainage valve had been closed, were 0, 10, 20, and 30 psi.

The initial specimen data for these eight back pressure saturated Q test specimens are given in Table 5.25.

Table 5.25: Initial specimen data for back pressure saturated Q test specimens of new LMVD silt ($\sigma'_{3con} = 2$ psi)

Test	Back Pressure (psi)	Undrained Increase in σ_3 (psi)	w (%)	γ_d (pcf)	S (%)	e
B19-1	10	0	24.13	102.3	100	0.640
B19-2	10	10	23.43	103.0	100	0.629
B19-3	10	20	23.54	104.7	100	0.604
B19-4	10	30	23.52	103.5	100	0.622
B20-1	20	0	24.71	102.5	100	0.638
B20-2	20	10	24.40	102.5	100	0.638
B20-3	20	20	24.44	103.0	100	0.630
B20-4	20	30	24.36	103.5	100	0.621

Figure 5.133 shows the deviator stress vs. axial strain curves for tests B19-1, B19-2, B19-3, and B19-4. These test specimens had a back pressure of 10 psi and were consolidated to an isotropic consolidation pressure of 2 psi. The cell pressure in these tests was increased under undrained conditions to 0, 10, 20, and 30 psi.

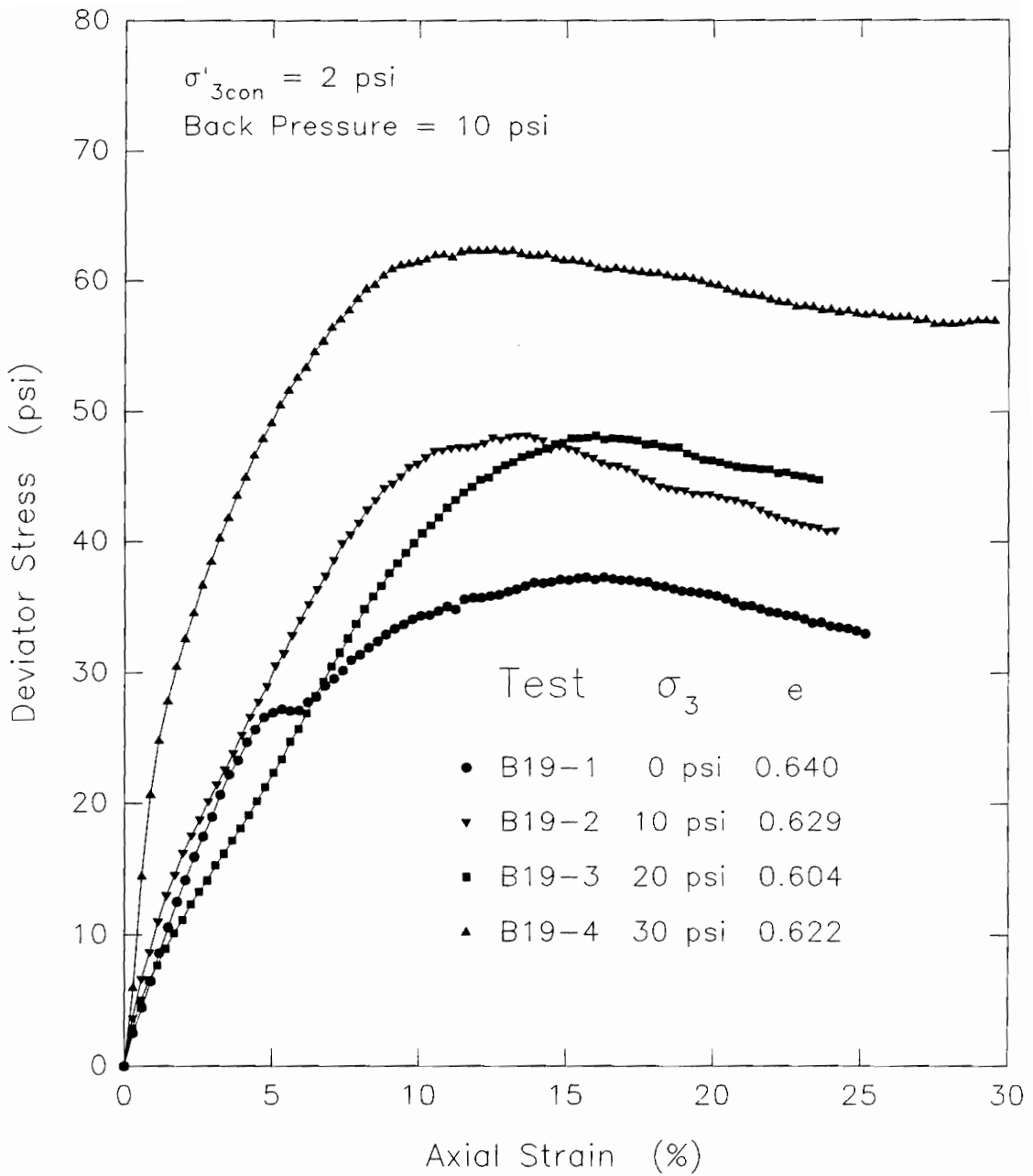


Figure 5.133. Deviator stress vs. axial strain behavior measured in Q tests B19-1, B19-2, B19-3, and B19-4 on back pressure saturated specimens of remolded new LMVD silt

The stress-strain behavior of these four tests shows some variation. The two specimens which had undrained increases in cell pressure of 0 and 10 psi had similar stress-strain behavior up to about 5% axial strain. The test with 0 psi increase in cell pressure, B19-1, then exhibited a slight peak followed by strain-softening. It then showed a further increase in strength with additional strain. For the test with an undrained increase in cell pressure of 10 psi, B19-2, the stress-strain curve continued to increase until a peak value of deviator stress was reached at about 13% axial strain.

The silt specimens which had an undrained increase in cell pressure of 20 psi, B19-3, showed somewhat similar behavior to the previous two tests. It gave a value of peak deviator stress similar to test B19-2, but the peak did not occur until about 16% axial strain.

The fourth test in this group, B19-4, was subjected to an undrained increase in cell pressure of 30 psi. The stress-strain behavior measured in this test varied considerably from the other three tests performed in this group. It had a steeper stress-strain curve during the initial stages of shear than the other three specimens. It also reached a higher value of peak deviator stress than

the other tests. This peak value occurred at an axial strain of about 10%.

Except for specimen B19-1, which exhibited somewhat abrupt strain-softening, after reaching the maximum value of deviator stress in these tests, the specimens generally showed gradual strain-softening or decreases in deviator stress with further increase in axial strain.

Figure 5.134 shows the Mohr's circles for these four tests, based on 5% axial strain at failure. The undrained strength envelope for the soil does not give a $\phi_u = 0$, $S_u = c$ condition. Instead, the undrained strength of the soil even at this low value of axial strain, is defined by the undrained shear strength parameters $c = 7.6$ psi and $\phi_u = 16.3^\circ$.

Using the values of peak deviator stress as the failure criterion, the Mohr's circles for these four tests have been plotted in Figure 5.135. For this failure criterion, the undrained strength parameters of the soil are $c = 10.3$ psi and $\phi_u = 20.8^\circ$.

Figure 5.136 shows the deviator stress vs. axial strain curves for tests B20-1, B20-2, B20-3, and B20-4. These test specimens had a back pressure of 20 psi and were consolidated to an isotropic consolidation pressure of 2

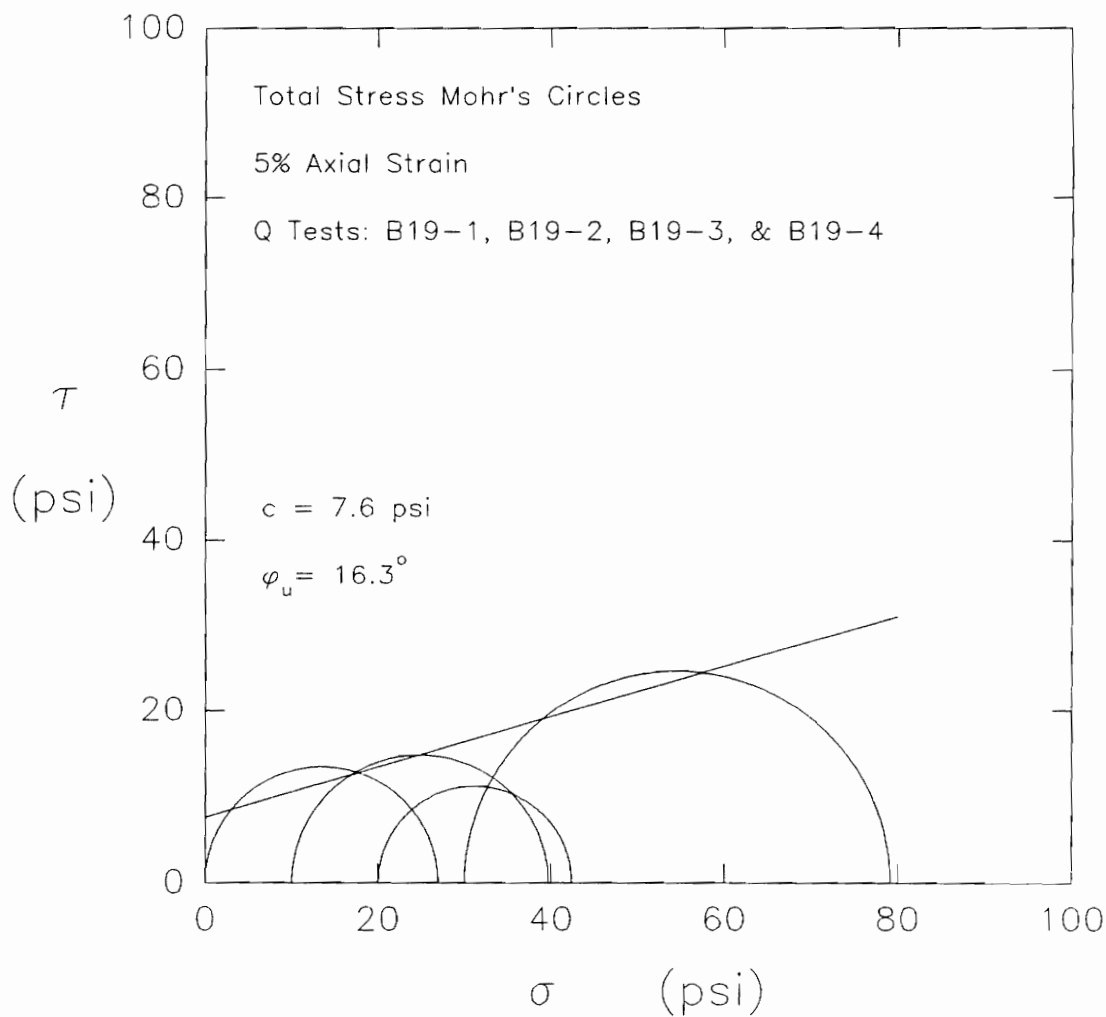


Figure 5.134. Total stress Mohr's circles at 5% axial strain for Q tests B19-1, B19-2, B19-3, and B19-4 on back pressure saturated specimens of remolded new LMVD silt

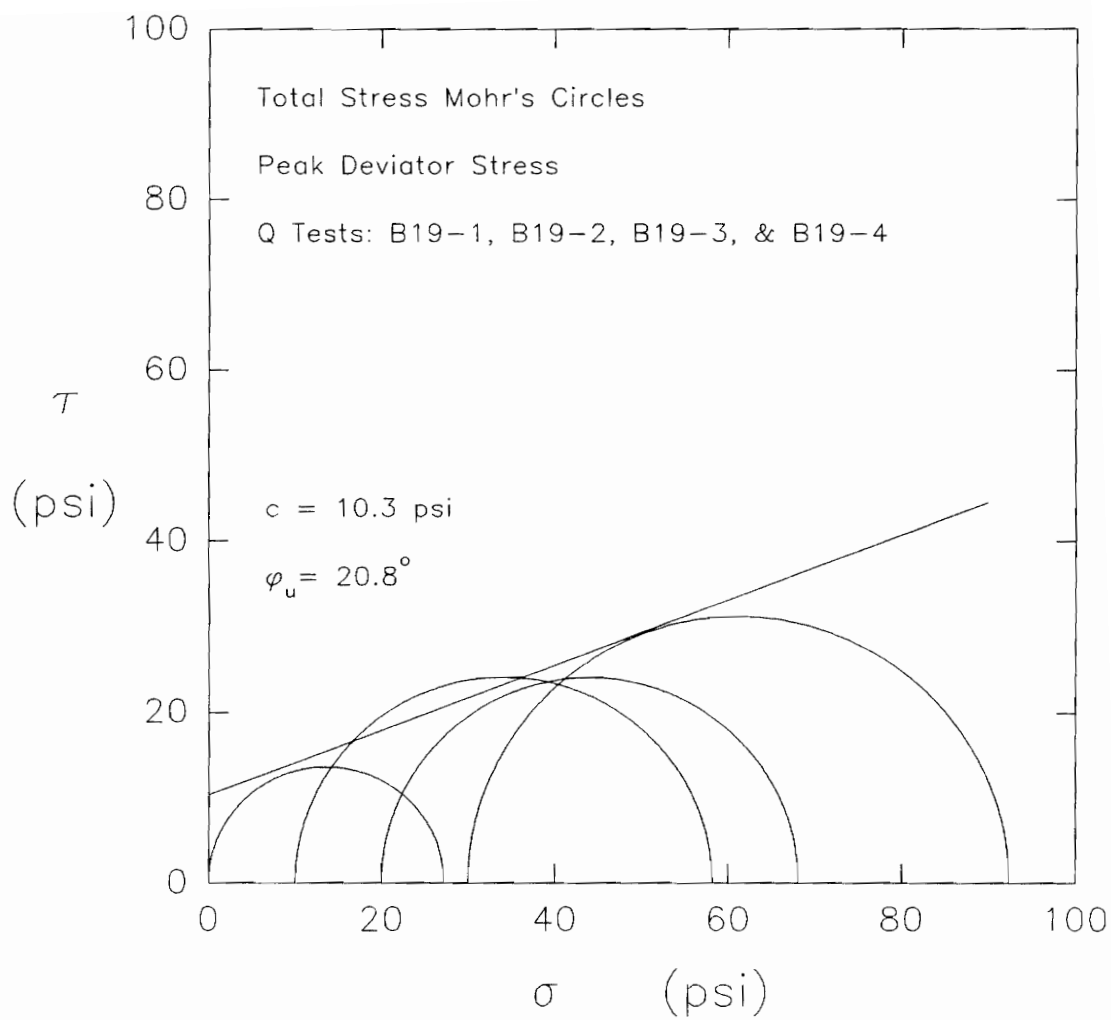


Figure 5.135. Total stress Mohr's circles at peak deviator stress for Q tests B19-1, B19-2, B19-3, and B19-4 on back pressure saturated specimens of remolded new LMVD silt

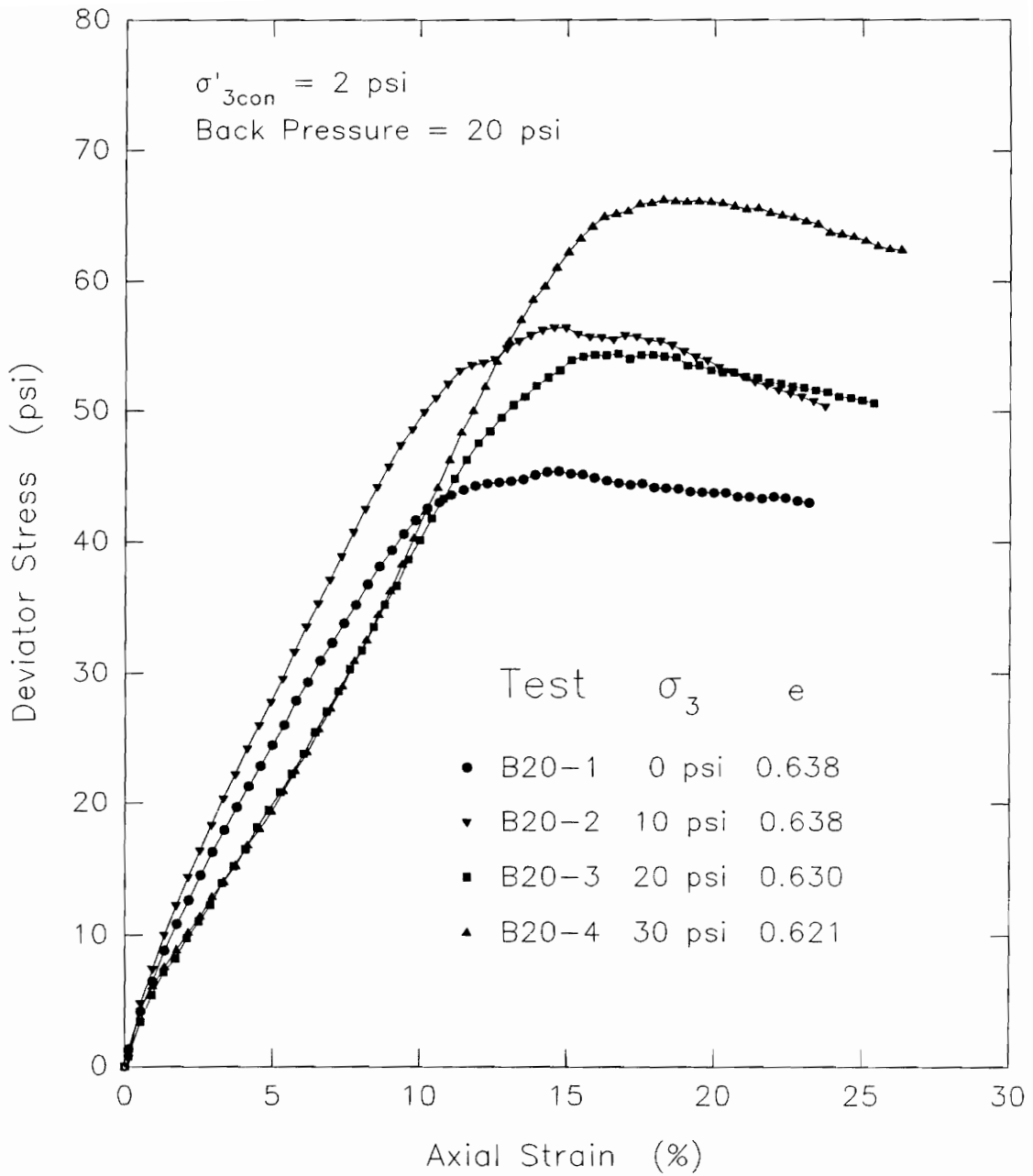


Figure 5.136. Deviator stress vs. axial strain behavior measured in Q tests B20-1, B20-2, B20-3, and B20-4 on back pressure saturated specimens of remolded new LMVD silt

psi. These specimens were subjected to undrained increases in cell pressure of 0, 10, 20, and 30 psi.

The stress-strain curves for these four tests showed more similar behavior than observed in the tests shown in Figure 5.133. These four tests tended to have similar stress-strain behavior up to about 10% axial strain, although the actual magnitude of the deviator stress still showed some variation for the different tests. Specimen B20-1, tested with the lowest undrained increase in cell pressure, 0 psi, gave the lowest value of peak deviator stress among these specimens. Specimen B20-4 had the largest undrained increase in cell pressure, 30 psi, and as a result, it gave the highest value of peak deviator stress of the group.

Test specimens B20-2 and B20-3 had intermediate undrained increases in cell pressure of 10 and 20 psi. These two tests gave peak values of deviator stress which were similar. The peaks, however, occurred at different axial strains. The axial strain at which the peak deviator stress occurred in these four Q tests tended to increase with increasing cell pressure.

Test specimens B20-3 and B20-4 had almost identical stress-strain curves up to 10% axial strain. These two specimens had undrained increases in cell pressure of 20

and 30 psi, respectively. At axial strains above 10%, more variation between the stress-strain curves occurred. The test specimen with $\sigma_3 = 30$ psi reached a higher peak deviator stress than the specimen with $\sigma_3 = 20$ psi.

Taking 10% axial strain as the failure criterion, the Mohr's circles for these four Q tests have been plotted in Figure 5.137. For this condition, an approximate $\phi_u = 0$ undrained strength envelope was obtained for the soil. The strength envelope shown is defined by the undrained strength parameters $\phi_u = 0^\circ$ and $S_u = c = 22.8$ psi.

If the peak values of deviator stress measured in each test are used to define failure, the Mohr's circles for these tests give the undrained strength envelope shown in Figure 5.138. For this condition, a $\phi_u > 0$ envelope results. The undrained shear strength parameters for the soil in this case are $c = 18.1$ psi and $\phi_u = 13.9^\circ$.

The stress-strain curves for all eight back pressure saturated Q test specimens are plotted together in Figure 5.139. The B19 specimens all had an initial back pressure of 10 psi and the B20 specimens had an initial back pressure of 20 psi. All eight specimens were consolidated to $\sigma'_{3con} = 2$ psi. This plot shows considerable scatter in the stress-strain behavior measured in these eight tests. A more useful approach will be to consider tests where

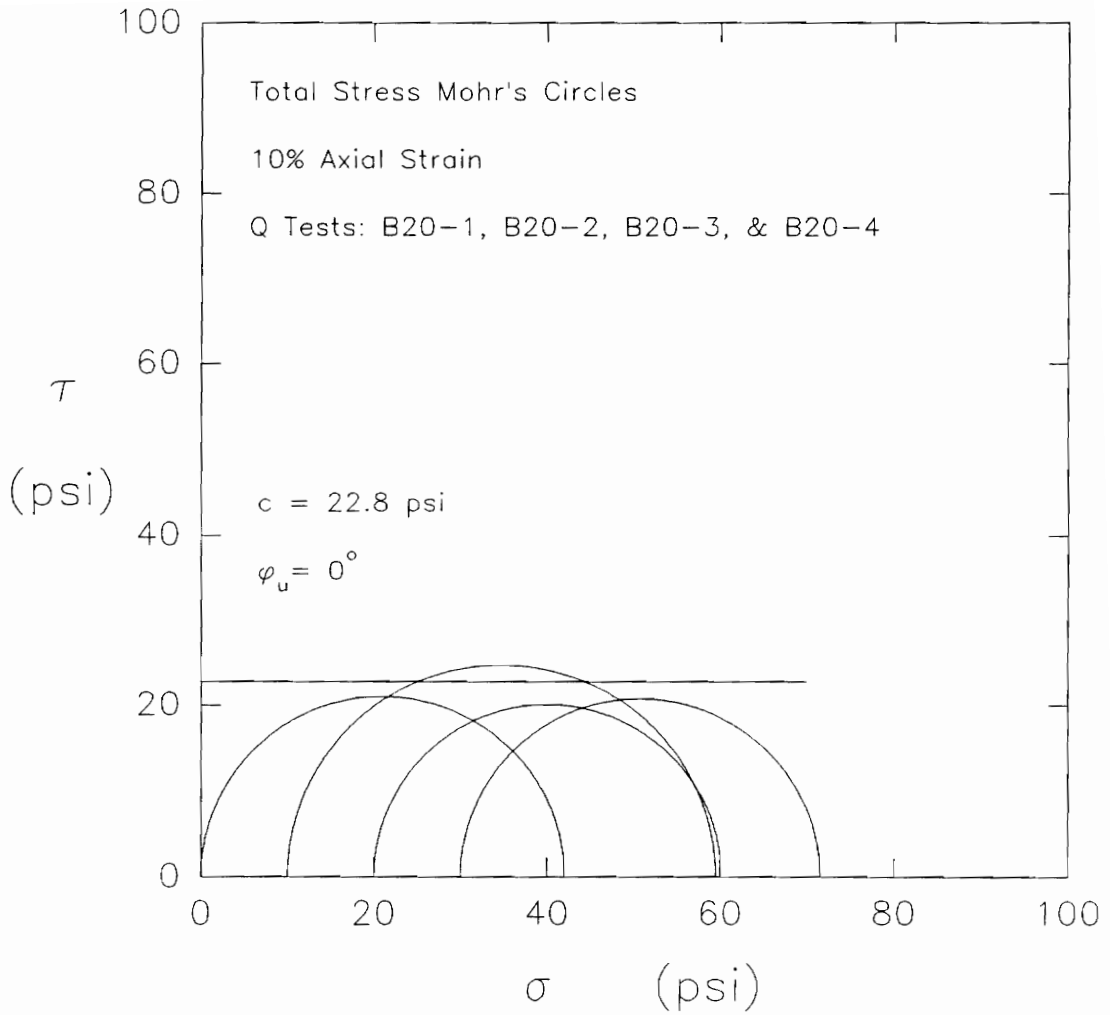


Figure 5.137. Total stress Mohr's circles at 10% axial strain for Q tests B20-1, B20-2, B20-3, and B20-4 on back pressure saturated specimens of remolded new LMVD silt

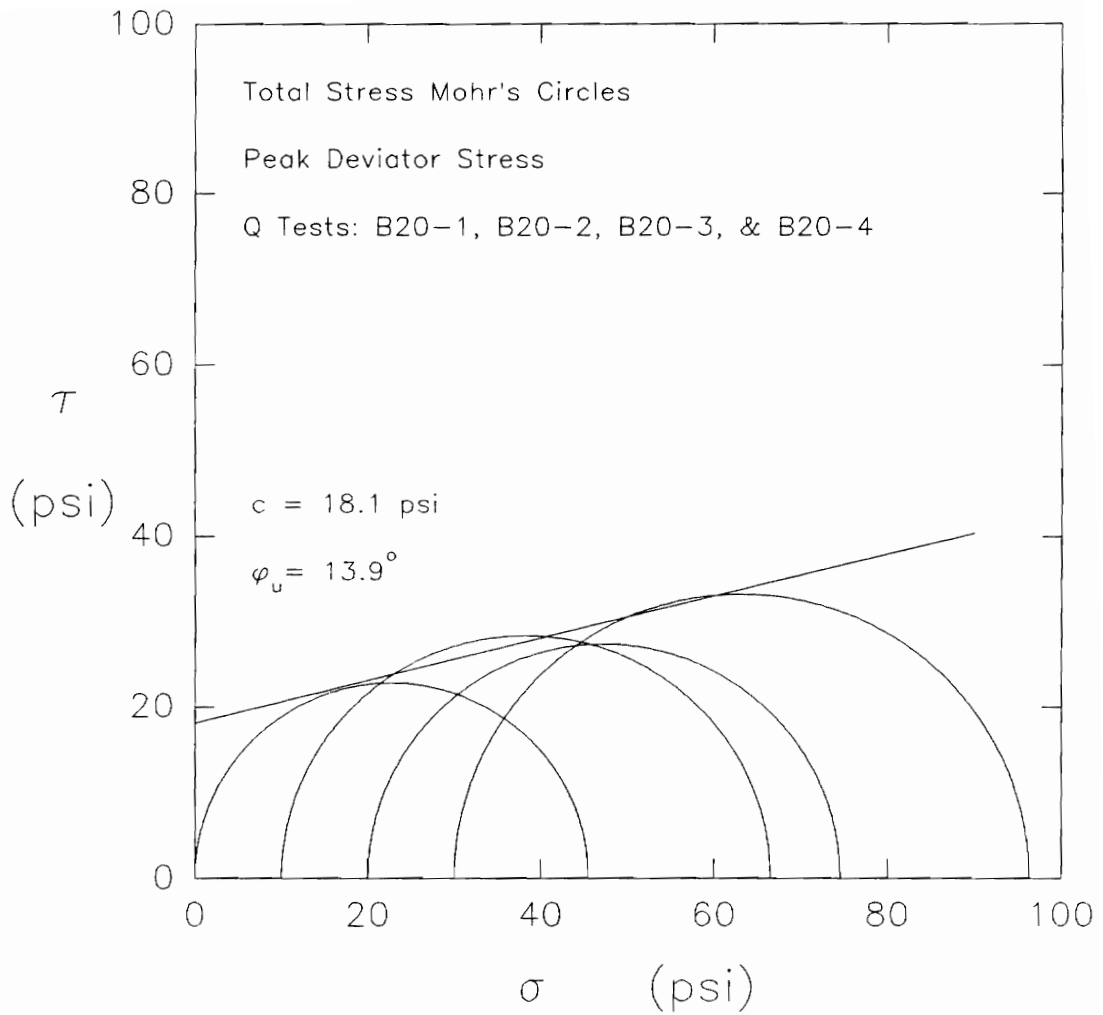


Figure 5.138. Total stress Mohr's circles at peak deviator stress for Q tests B20-1, B20-2, B20-3, and B20-4 on back pressure saturated specimens of remolded new LMVD silt

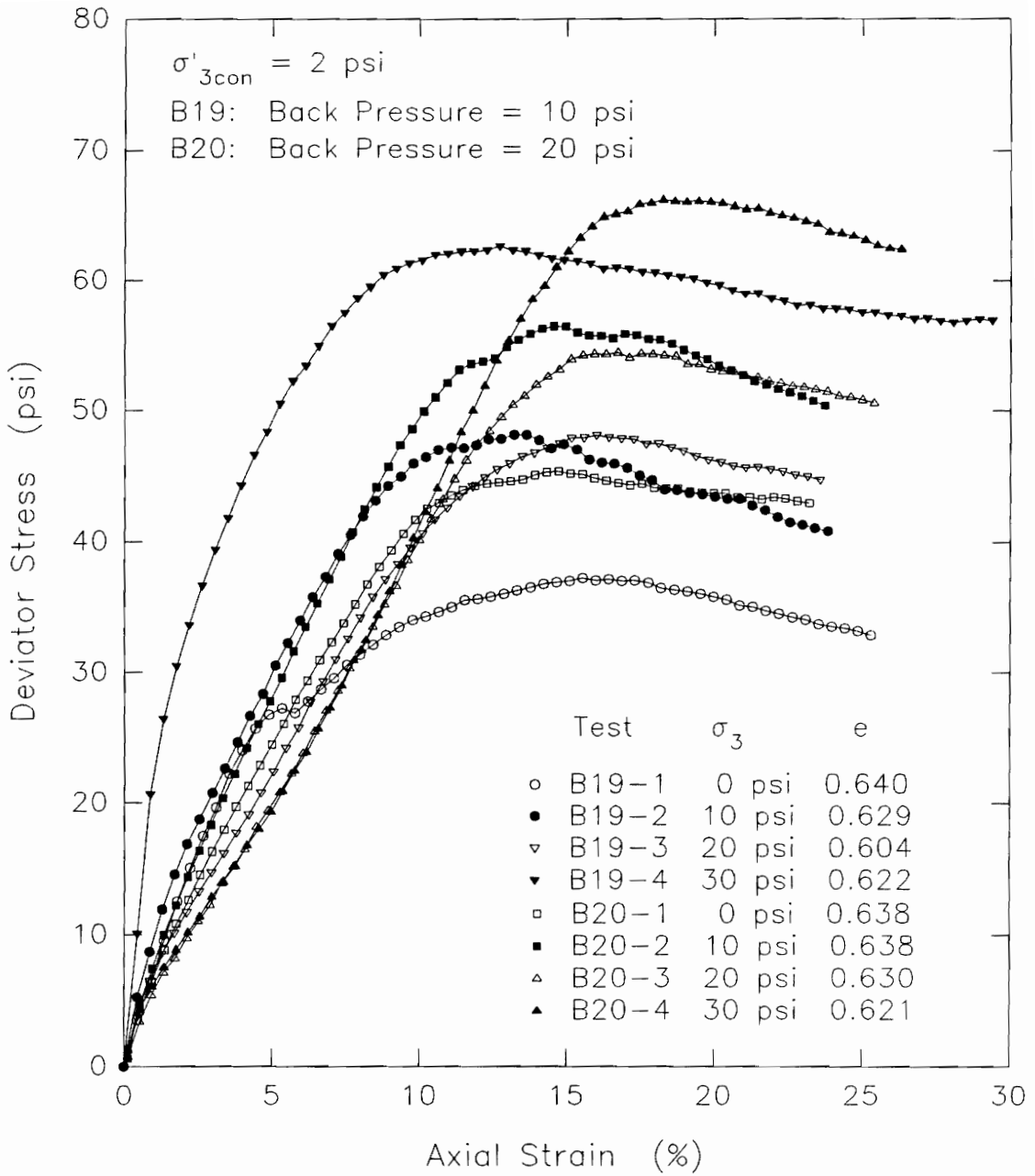


Figure 5.139. Deviator stress vs. axial strain behavior measured in Q tests on back pressure saturated specimens of remolded new LMVD silt

meaningful comparisons are possible. Some of the conventional Q tests performed on new LMVD silt without back pressure saturation and discussed in Section 5.9.2, can also be compared to the back pressure saturated Q tests.

Figure 5.140 shows the stress-strain curves for tests B17-1, B19-1 and B20-1. Test specimen B17-1 was tested in a conventional Q test. This specimen was not back pressure saturated or consolidated prior to shear. Both specimens B19-1 and B20-1 were isotropically consolidated to $\sigma'_{3con} = 2$ psi. Test specimen B19-1 had a back pressure of 10 psi while the back pressure in specimen B20-1 was 20 psi. These three test specimens were tested with no undrained increase in cell pressure applied to the specimens prior to shear. For the two back pressure saturated specimens, the initial pore water pressure at the start of shear would have been equal to the back pressure used in each specimen. For the specimen with no back pressure, the specimen would have had a negative pore water pressure at the start of shear.

As shown in Figure 5.140, the stress-strain curves for these three tests were similar up to about 5% axial strain. At higher strains, more variation between the stress-strain

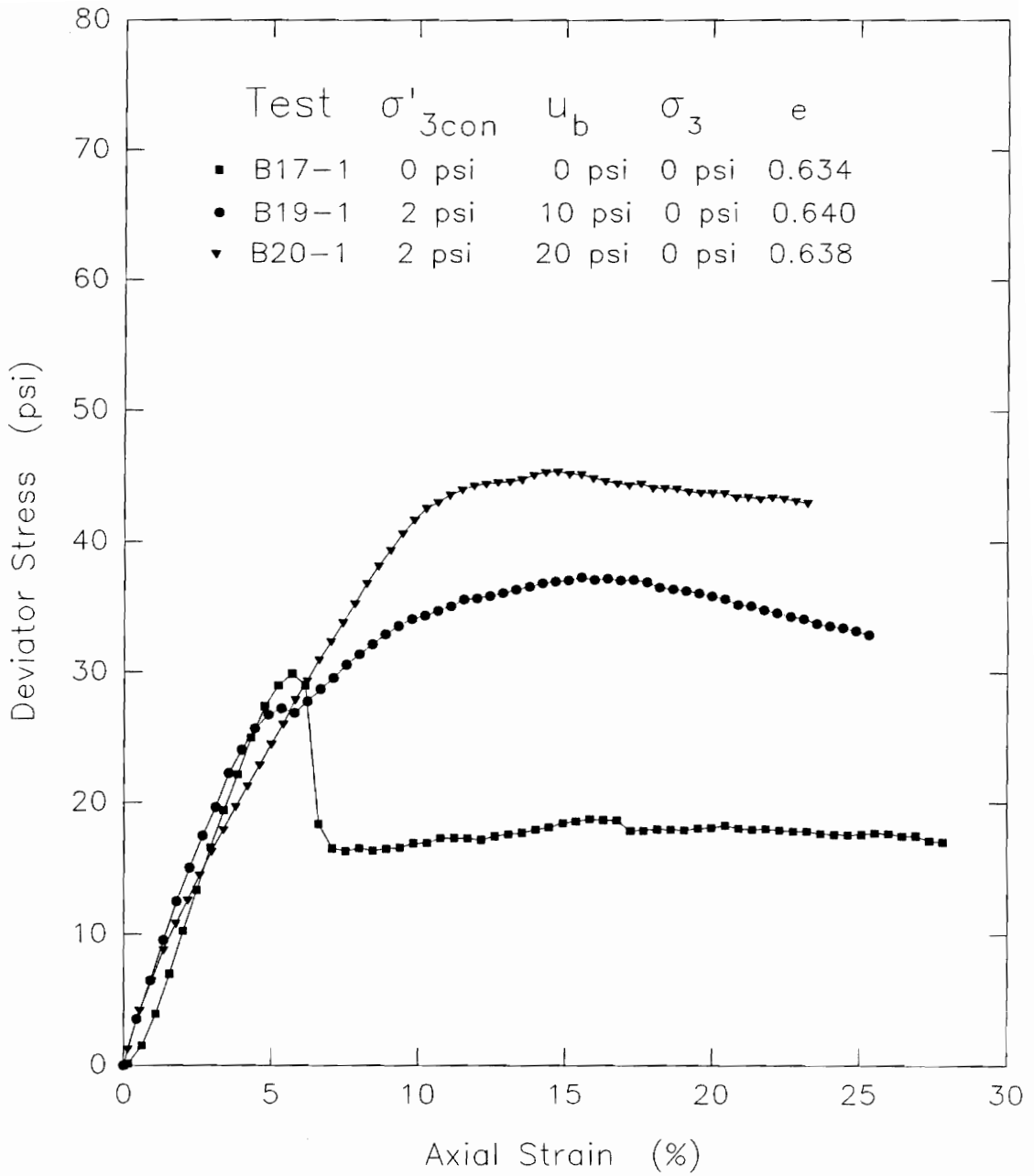


Figure 5.140. Deviator stress vs. axial strain behavior measured in Q tests B17-1, B19-1, and B20-1 on specimens of remolded new LMVD silt

behavior of the three specimens is apparent. Test specimen B17-1 reached a peak deviator stress at about 5.5% axial strain. This was followed by distinct strain-softening behavior. The specimen had no back pressure and therefore, the initial pore water pressure in the specimen was negative or slightly less than 0 psi. Decreasing pore water pressures during undrained shear would have resulted in the pore water pressure decreasing further below atmospheric pressure in this test.

Test specimen B19-1 reached a slight peak at about 5% axial strain. This specimen had a back pressure of 10 psi. This was greater than the back pressure in specimen B17-1 but less than that in specimen B20-1. As undrained shear proceeded, the pore water pressure in the specimens would have decreased due to the dilatant tendencies of the soil. With a lower back pressure in specimen B19-1, the decrease in pore water pressure during undrained shear could have resulted in dissolved gases coming out of solution from the pore water sooner than in specimen B20-1, if the decrease in pore water pressure was sufficient.

Test specimen B20-1 had a higher initial pore water pressure due to the higher back pressure used in the test. It therefore could have experienced a larger decrease in pore water pressure before gases dissolved in the pore

water would have been able to come out of solution. As a result, specimen B20-1 reached a higher value of deviator stress than specimens B17-1 and B19-1.

Figure 5.141 shows the stress-strain behavior measured for test specimens B17-2, B19-2, and B20-2. Specimen B17-2 was tested in a conventional Q test and had no back pressure applied to it. It was therefore not consolidated prior to shear. Both specimens B19-2 and B20-2 were isotropically consolidated to $\sigma'_{3con} = 2$ psi. Test specimen B19-2 had a back pressure equal to 10 psi and specimen B20-2 had a back pressure of 20 psi. All three of these test specimens were sheared undrained after applying a cell pressure of 10 psi to the specimens.

The stress-strain curves for these three test specimens were very similar up to about 7% axial strain. At higher strains, the tests began to show more variation in their stress-strain behavior. Specimen B17-2 had no back pressure applied to it and gave the lowest value of peak deviator stress of the three tests. It also gave a definite peak in the stress-strain curve followed by abrupt strain-softening behavior. In the other two tests, the peak deviator stress was followed by gradual strain softening.

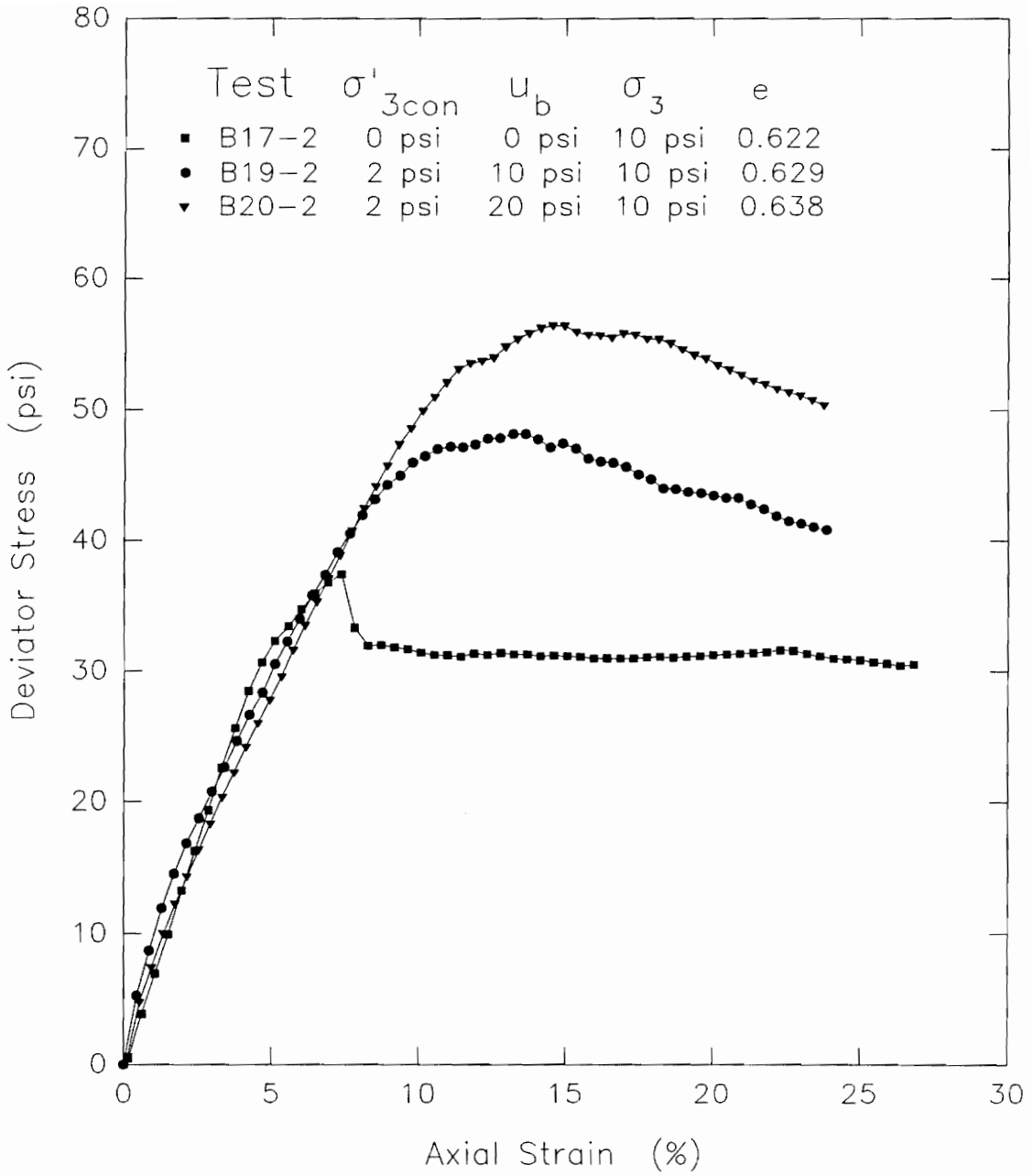


Figure 5.141. Deviator stress vs. axial strain behavior measured in Q tests B17-2, B19-2, and B20-2 on specimens of remolded new LMVD silt

The stress-strain curves for tests B19-2 and B20-2 continued to be similar up to about 8% axial strain. With further increase in axial strain, these two tests gave stress-strain curves which were similar in shape but had different magnitudes of deviator stress. Specimen B20-2 had a higher back pressure than specimen B19-2. As a result, specimen B20-2 could experience a larger decrease in pore water pressure than specimen B19-2. This led to a higher undrained strength being measured for the specimen with the higher back pressure.

Figure 5.142 shows the stress-strain behavior measured for test specimens B17-3, B18-1, B19-3, and B20-3. Specimens B17-3 and B18-1 were tested in conventional Q tests with no back pressure applied to the specimens. These specimens were not consolidated prior to shear. Both specimens B19-3 and B20-3 were isotropically consolidated to $\sigma'_{3con} = 2$ psi. Test specimen B19-3 had a back pressure equal to 10 psi and specimen B20-3 had a back pressure of 20 psi. A cell pressure of 20 psi was applied to all four of these specimens under undrained conditions, prior to shear.

The stress-strain curves for three of these four test specimens were very similar up to about 11% axial strain. At higher strains, the stress-strain curves were similar in

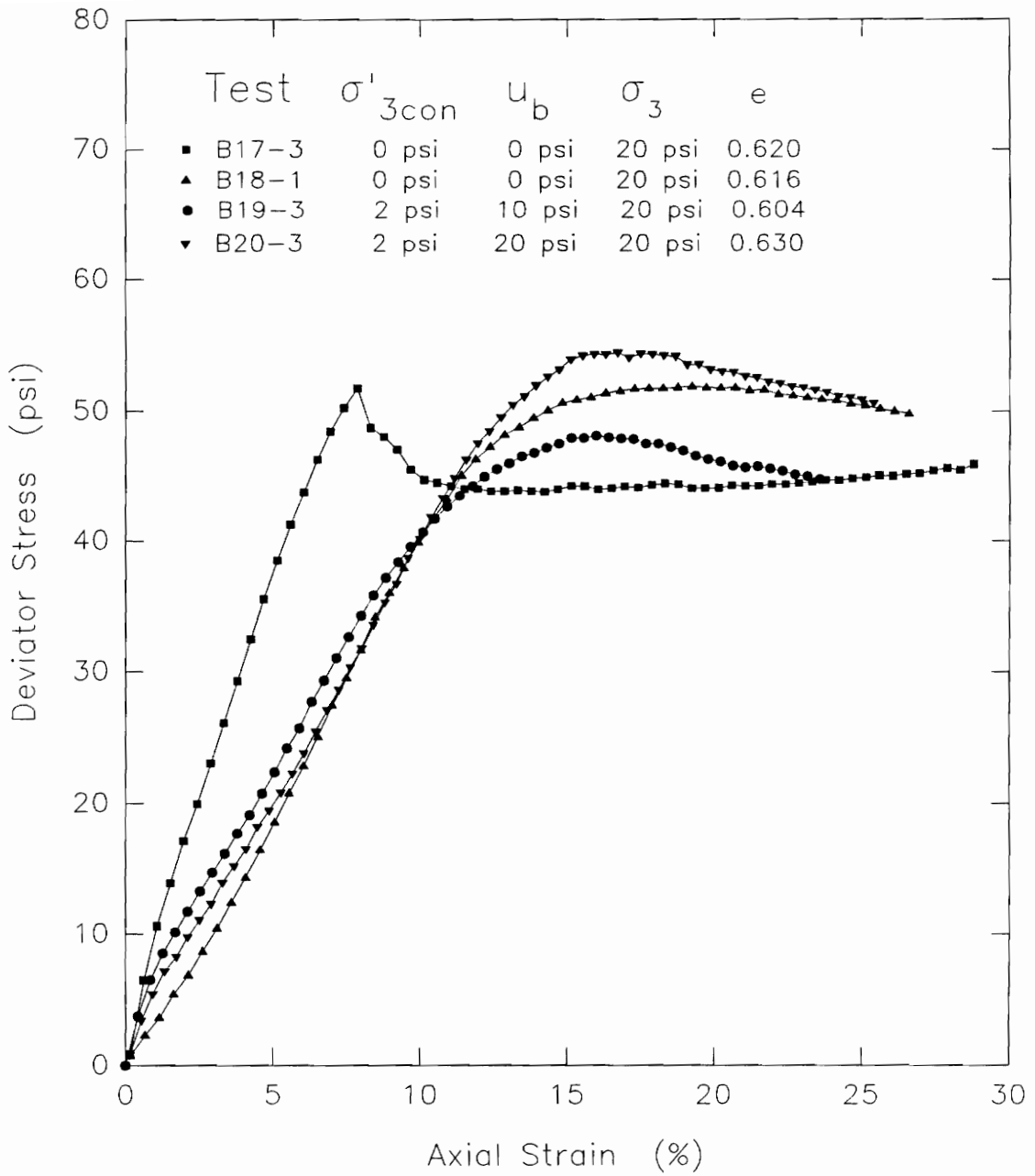


Figure 5.142. Deviator stress vs. axial strain behavior measured in Q tests B17-3, B18-1, B19-3, and B20-3 on specimens of remolded new LMVD silt

shape for the three tests but gave different magnitudes of deviator stress. Specimen B18-1 had no back pressure applied to it. It gave a value of peak deviator stress between the peak values obtained for the two specimens to which back pressures of 10 and 20 psi were applied. Specimen B20-3 had a higher back pressure than specimen B19-3. This allowed specimen B20-3 to experience a larger decrease in pore water pressure during undrained shear than specimen B19-3 before dissolved gases would come out of solution from the pore water and desaturate the specimen. Since a larger decrease in pore water pressure was possible, specimen B20-3 gave a higher undrained strength for the soil than specimen B19-3.

Specimen B17-3 gave stress-strain behavior which was considerably different than that of the other three specimens. This test gave a steeper stress-strain curve than the other tests and yielded a peak deviator stress at a lower axial strain than the other tests. The value of peak deviator stress, however, was similar to the values measured in the other test specimens. Test specimen B17-3 also showed distinct strain-softening in its stress-strain behavior after the peak deviator stress had been reached. The other three tests showed much more gradual strain-softening.

Figure 5.143 shows the stress-strain behavior measured for test specimens B17-4, B19-4, and B20-4. Specimen B17-4 was tested in a conventional Q test and had no back pressure applied to it. This specimen was not consolidated prior to shear. Both specimens B19-4 and B20-4 were isotropically consolidated to $\sigma'_{3con} = 2$ psi. Test specimen B19-4 had a back pressure equal to 10 psi and specimen B20-4 had a back pressure equal to 20 psi. All three of these specimens were subjected to an increase in cell pressure of 30 psi, prior to undrained shear.

The stress-strain curves for these three tests are quite different from each other. The curve for specimen B19-4 is much steeper in the initial stages of shear, than the curves for specimens B17-4 and B20-4. The stress-strain curve for specimen B17-4 was steeper than that for specimen B20-4. The stress-strain curve for specimen B20-4 shows a concave-up shape, characteristic of strain-hardening resulting from pore water pressure reduction.

Specimen B20-4 also reached a peak deviator stress which was slightly higher than that of specimen B19-4. The higher strength may be related to the higher back pressure in specimen B20-4, allowing for a larger decrease in pore water pressure than in specimen B19-4. Specimen B17-4, which had no back pressure applied, gave the lowest value

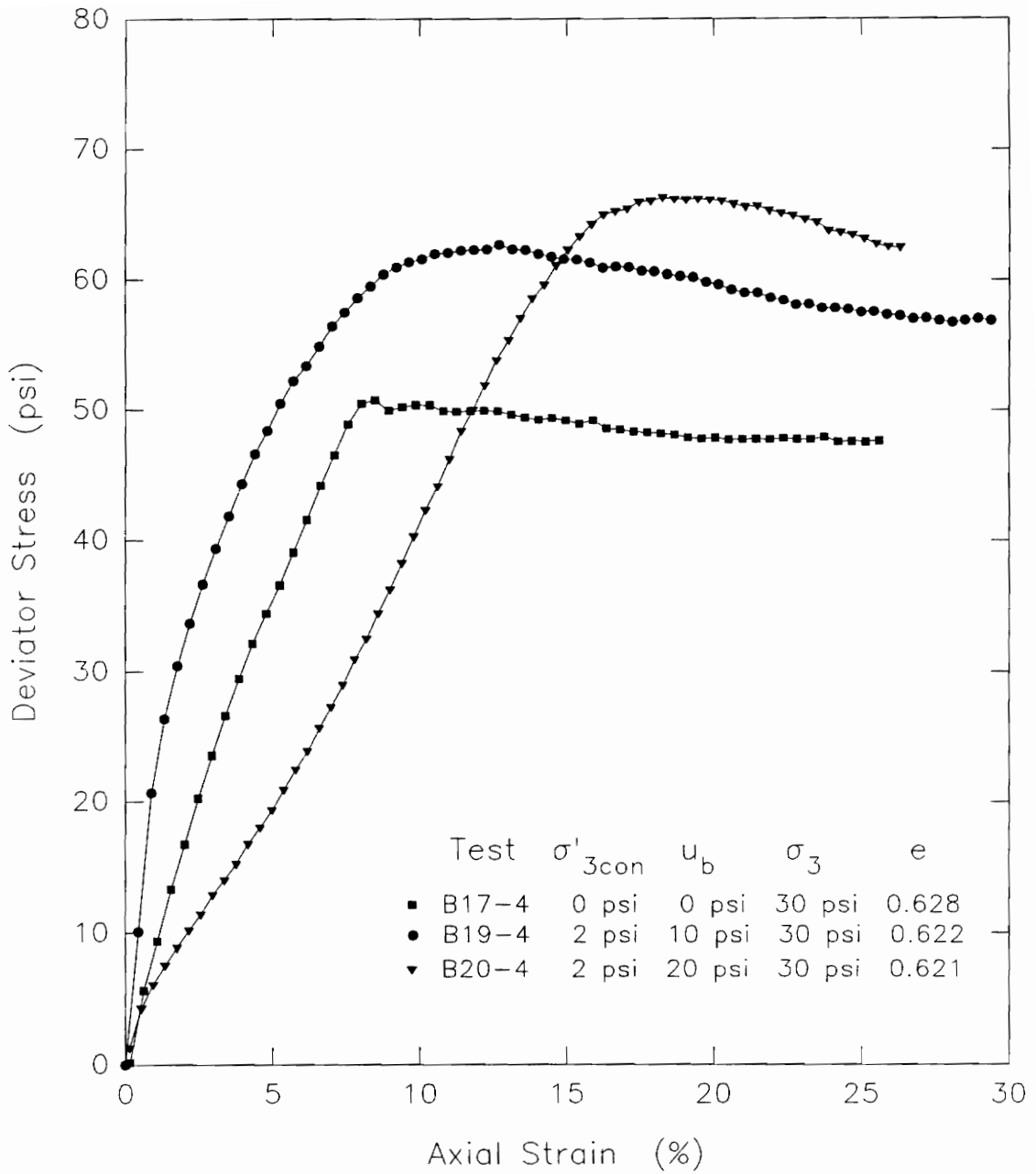


Figure 5.143. Deviator stress vs. axial strain behavior measured in Q tests B17-4, B19-4, and B20-4 on specimens of remolded new LMVD silt

of peak deviator stress of the three tests. This may be the result of there being no back pressure in this specimen. This would limit the magnitude of the pore pressure decrease possible in this specimen to a value less than that possible in the other two specimens in which back pressures of 10 and 20 psi were used.

Based on the results of the other seven tests performed on back pressure saturated Q test specimens, it appears that the stress-strain behavior of specimen B19-4 is inconsistent with the other tests. It may be that this specimen experienced a different level of disturbance than the other tests or had some leakage during undrained shear, such that the stress-strain behavior for this test was different than for the other specimens.

Figure 5.144 shows the stress-strain behavior measured in tests B17-2 and B19-1. The initial pore water pressure in these two specimens was on the order of 10 psi. Specimen B17-2 was tested in a conventional Q test. This specimen had no back pressure applied to it and was not consolidated prior to shear. The specimen would have had a negative pore water pressure initially. Because the specimen was essentially fully saturated, the application of a cell pressure of 10 psi to the specimen would have increased the pore water pressure within the specimen by

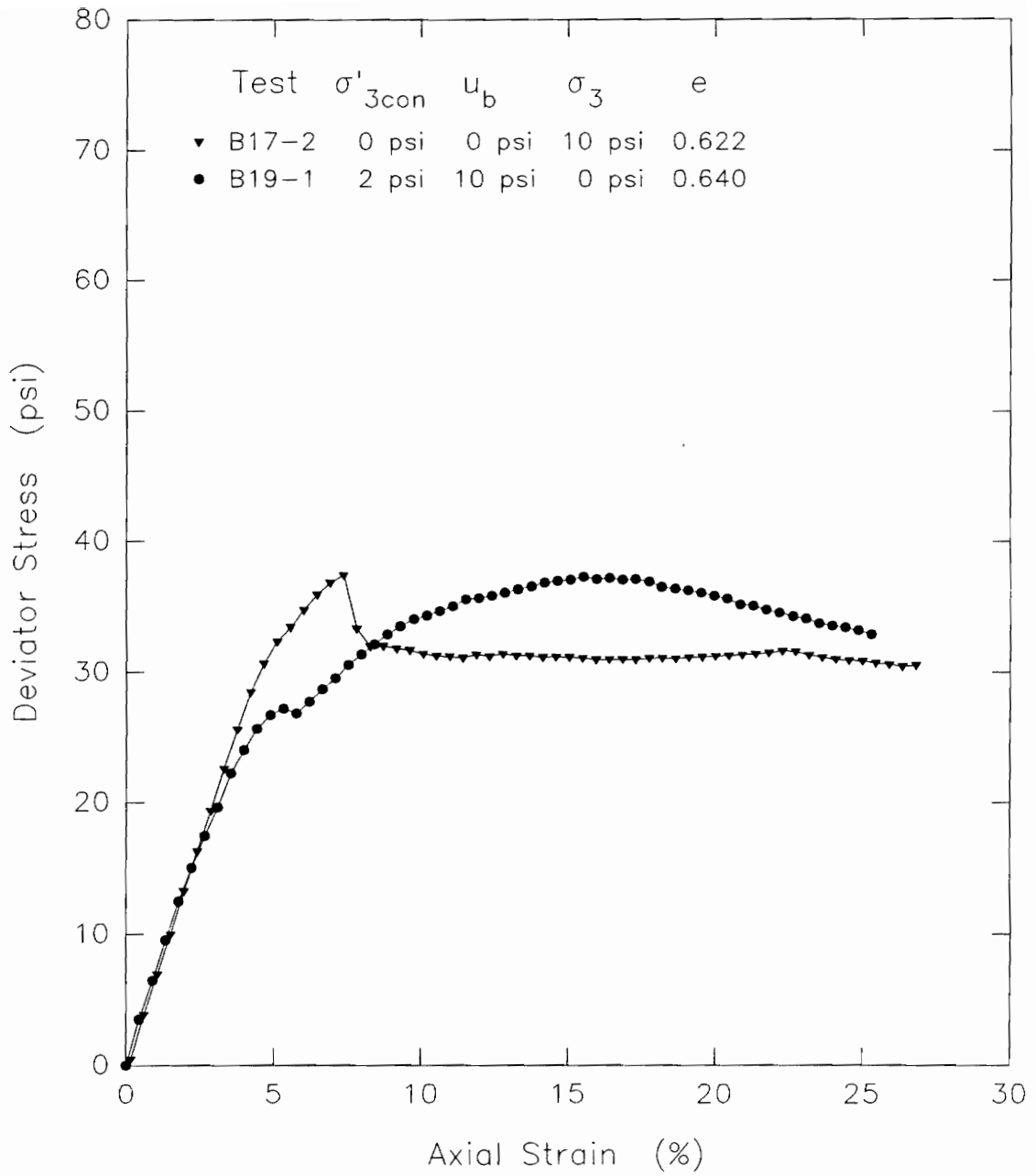


Figure 5.144. Deviator stress vs. axial strain behavior measured in Q tests B17-2 and B19-1 on specimens of remolded new LMVD silt

close to an equal amount. The initial pore water pressure in the specimen prior to shear would have been somewhat less than 10 psi.

Specimen B19-1 was isotropically consolidated to $\sigma'_{3con} = 2$ psi. The specimen had a back pressure of 10 psi. The cell pressure applied to this test specimen was 0 psi. The initial pore water pressure in this specimen, prior to shear, would therefore have been 10 psi, or about the same magnitude as in specimen B17-2.

As can be seen in Figure 5.144, these two tests with similar initial values of pore water pressure, gave similar stress-strain behavior at values of axial strain below about 4%. At higher axial strains, the stress-strain curves for these two specimens began to show more variation. Both specimens showed peaks in their stress-strain curves which were followed by strain-softening. The strain-softening in test B19-1 was followed by increasing strength with further strain, whereas the stress-strain curve of specimen B17-2 had a more significant decrease in strength after the peak deviator stress was reached and did not experience a further increase in strength. Specimen B17-2 reached a peak deviator stress of about 37 psi at an axial strain of 7%. The slight peak in deviator stress observed for specimen B19-1 was on the order of about 27

psi at 5.5% axial strain. The ultimate value of deviator stress measured in test B19-1, however, was about the same as in test B17-2. This ultimate value did not occur until about 15% axial strain in test B19-1.

Figure 5.145 shows the stress-strain behavior measured in tests B17-3, B18-1, B19-2, and B20-1. These four specimens all had an initial pore water pressure on the order of 20 psi. Specimens B17-3 and B18-1 were tested in conventional Q tests. These two specimens had no back pressure applied and were not consolidated prior to testing. These specimens would have had negative pore water pressures initially. Because the specimens were essentially fully saturated, the application of 20 psi cell pressure under undrained conditions would have resulted in an increase in pore water pressure of about 20 psi. The pore water pressure within the specimens prior to shear would therefore have been somewhat less than 20 psi.

Both specimens B19-2 and B20-1 were isotropically consolidated to $\sigma'_{3con} = 2$ psi. Test specimen B19-2 had a back pressure equal to 10 psi. The cell pressure in this test was increased under undrained conditions by 10 psi. The pore water pressure in the specimen prior to undrained shear should therefore have been about 20 psi. Test specimen B20-1 had a back pressure equal to 20 psi. No

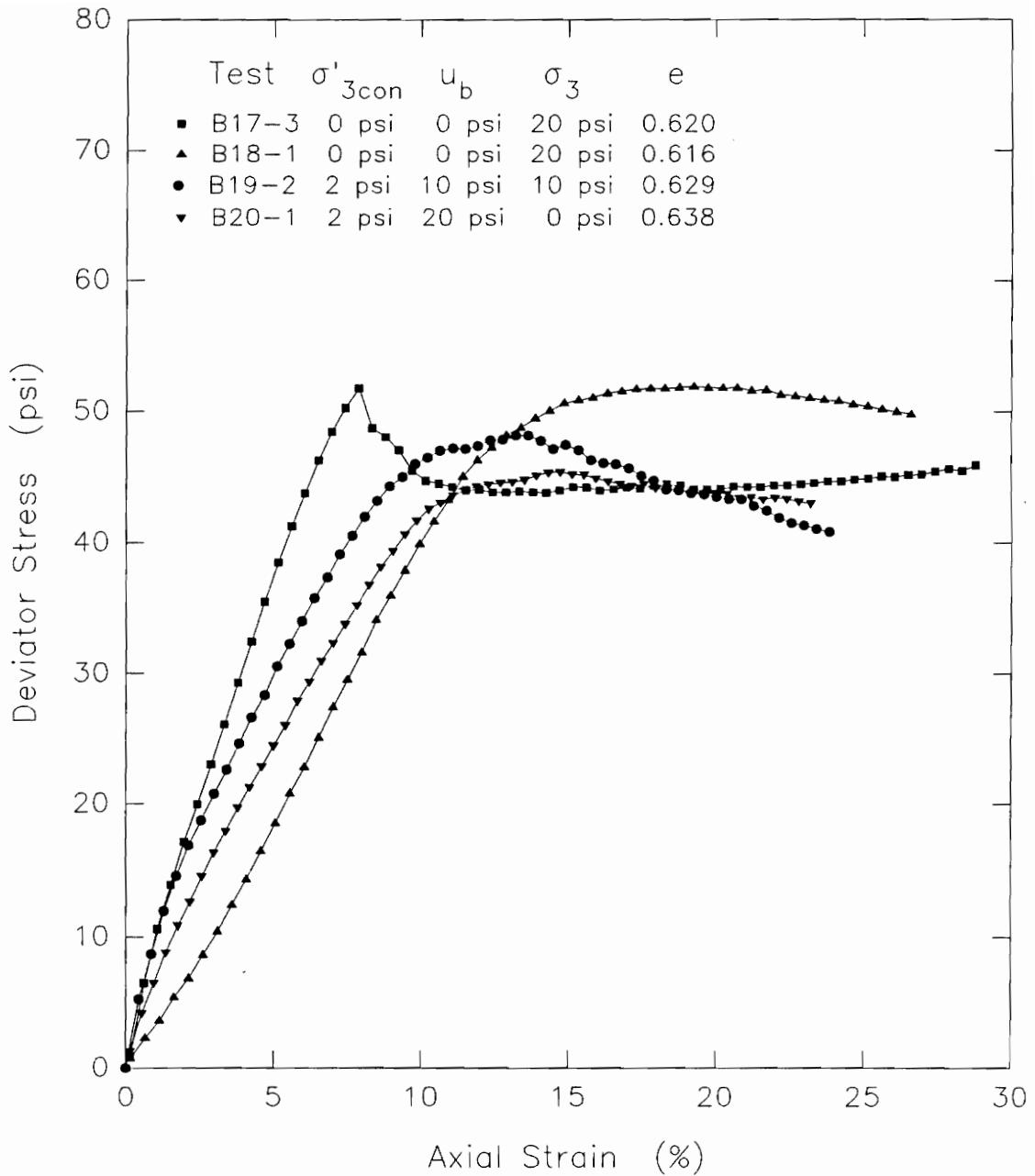


Figure 5.145. Deviator stress vs. axial strain behavior measured in Q tests B17-3, B18-1, B19-2, and B20-1 on specimens of remolded new LMVD silt

increase in cell pressure was applied to this specimen under undrained conditions. The initial pore water pressure in this specimen prior to undrained shear would therefore have been 20 psi, or about the same magnitude as in specimens B17-3, B18-1, and B19-2.

As can be seen in Figure 5.145, these four tests with similar initial values of pore water pressure, gave somewhat different stress-strain behavior. Test specimens B18-1, B19-2, and B20-1 gave stress-strain curves which were similar in shape. The stress-strain curve for specimen B17-3 was different from those of the other tests. It was steeper and gave a definite peak value followed by abrupt strain-softening. The other three tests exhibited gradual peaks in their stress-strain curves followed by much more gradual strain-softening. Even though the stress-strain curves for these tests are different, the tests tended to give similar values of peak deviator stress. These peak deviator stresses occurred at axial strains between 7 and 18%.

The similar values of peak deviator stress in these four tests may be the result of the specimens having similar initial values of pore water pressure prior to shear. With similar initial pore water pressures in the specimens, the decrease in pore water pressure which could

occur in the specimens before dissolved gases would exit solution, should be similar for the four specimens as well.

The differences in the shapes of the stress-strain curves up to the peak values of deviator stress may be due to the different ways in which the initial pore water pressure was developed within the different specimens, as well as the slight consolidation of two of the specimens. The initial pore water pressure due to an applied back pressure may have a different effect on the shape of the stress-strain curve than an initial pore water pressure which results from an applied cell pressure. This may be especially true for the conventional Q test where no back pressure was used. The ultimate strength of a dilatant specimen, however, may not be significantly influenced by the way in which the initial pore water pressure is developed within the specimen. The magnitude of the initial pore water pressure may be the important factor in determining the undrained strength of dilatant specimens.

Figure 5.146 shows the stress-strain behavior measured in tests B17-4, B19-3, and B20-2. The initial pore water pressure in these three specimens was on the order of 30 psi. Specimen B17-4 was tested in a conventional Q test. This specimen had no back pressure applied to it and was not consolidated prior to shear. The specimen would have

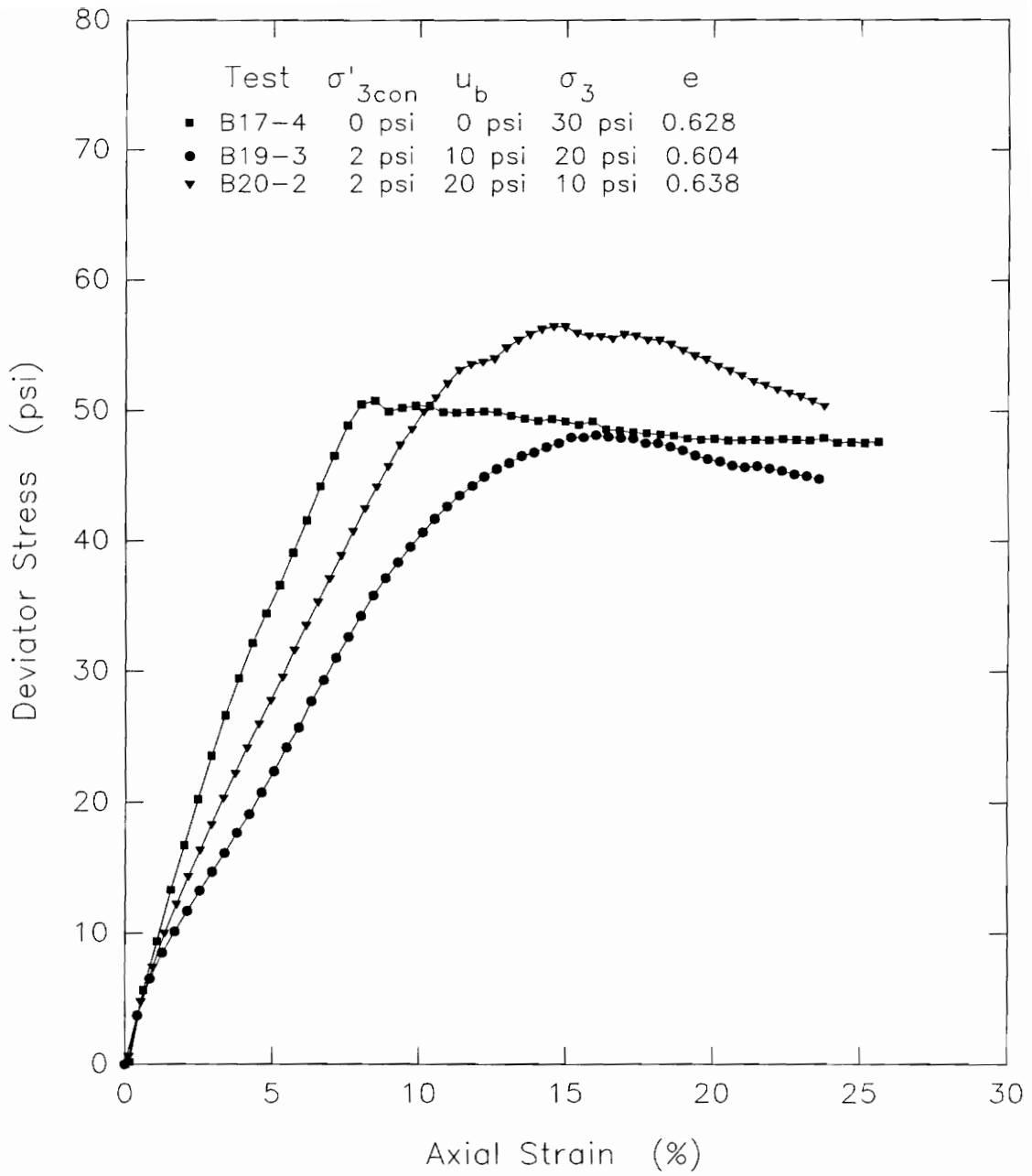


Figure 5.146. Deviator stress vs. axial strain behavior measured in Q tests B17-4, B19-3, and B20-2 on specimens of remolded new LMVD silt

had a negative pore water pressure initially. Because the specimen was essentially fully saturated, the application of a cell pressure of 30 psi to the specimen under undrained conditions should have resulted in an increase in pore water pressure of about 30 psi. The initial pore water pressure within the specimen would have been somewhat less than 30 psi.

Both specimens B19-3 and B20-2 were isotropically consolidated to $\sigma'_{3con} = 2$ psi. Test specimen B19-3 had a back pressure equal to 10 psi. The cell pressure applied to this test specimen was 20 psi. As a result, the initial pore water pressure in this specimen prior to undrained shear should have been about 30 psi. Test specimen B20-2 had a back pressure equal to 20 psi. The cell pressure in this test was increased by 10 psi under undrained conditions. The initial pore water pressure in this specimen, prior to undrained shear, should therefore have been about 30 psi, or close to the same value as in specimens B17-4 and B19-3.

These three tests with similar initial values of pore water pressure, gave stress-strain behavior which was somewhat different for the three test specimens. The shape of the stress-strain curves of specimens B19-3 and B20-2 were somewhat similar, but the magnitude of the deviator

stress was different for the two tests at any given value of axial strain. Test B20-2 reached a peak deviator stress of about 56.5 psi whereas the peak deviator stress measured in test B19-3 was about 48 psi. Both specimens reached their peak values of deviator stress at about the same axial strain. Specimen B17-4 had a steeper stress-strain curve than the other two tests. It reached a value of peak deviator stress of about 50 psi. The strength of this specimen was between that of test specimens B19-3 and B20-2. The peak value of deviator stress observed in test B17-4 occurred at an axial strain of about 8%, which was lower than in the other two tests.

Figure 5.147 shows the stress-strain behavior measured in tests B18-2, B19-4 and B20-3. The initial pore water pressure in these three specimens was on the order of 40 psi. Specimen B18-2 was tested in a conventional Q test. This specimen had no back pressure applied to it and was not consolidated prior to shear. The specimen would have had a negative pore water pressure initially. Because the specimen was essentially fully saturated, the application of a cell pressure of 40 psi to the specimen under undrained conditions would have resulted in an increase in pore water pressure of about 40 psi. The pore water pressure within the specimen prior to shear would have been somewhat less than 40 psi.

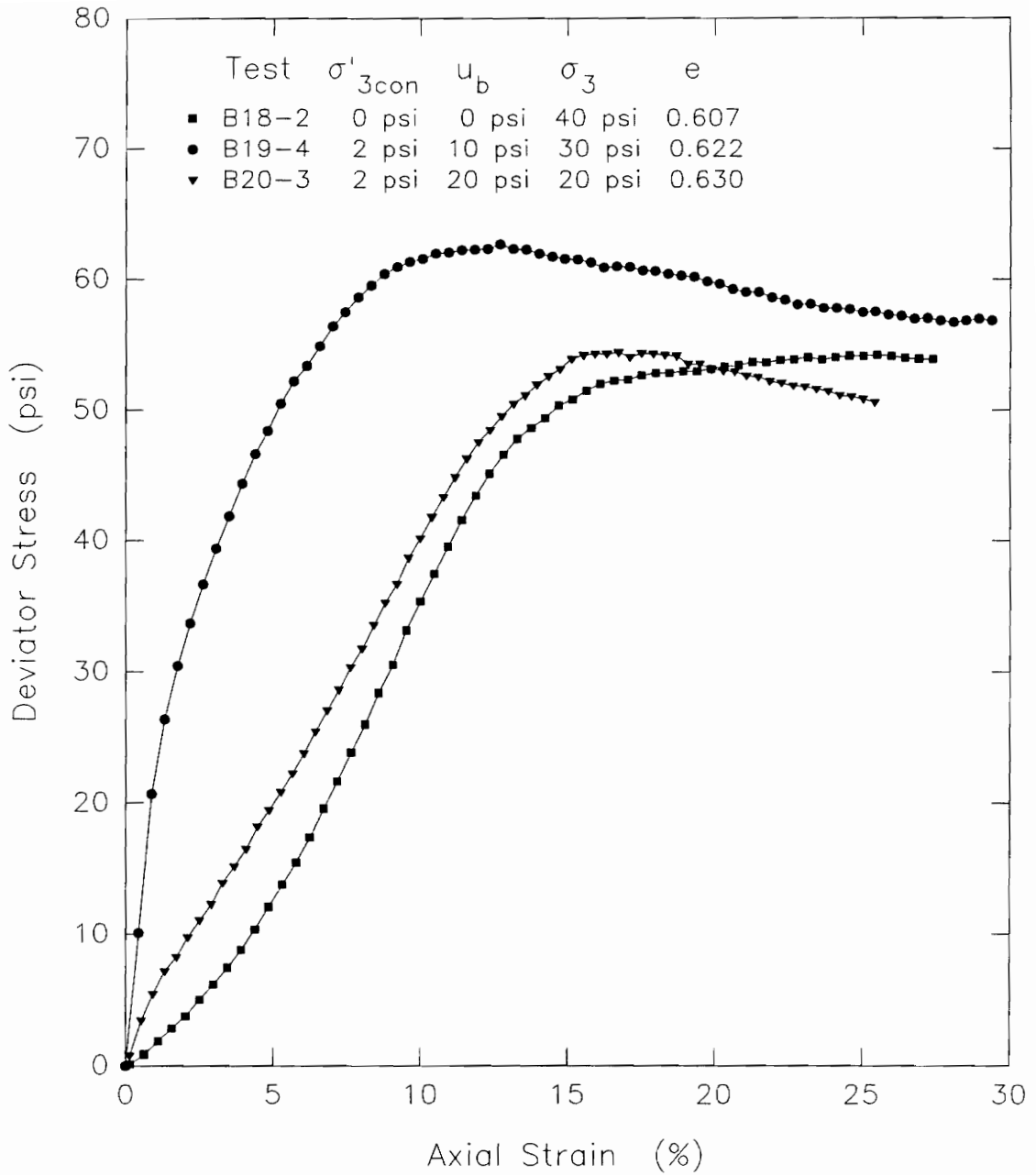


Figure 5.147. Deviator stress vs. axial strain behavior measured in Q tests B18-2, B19-4, and B20-3 on specimens of remolded new LMVD silt

Both specimens B19-4 and B20-3 were isotropically consolidated to $\sigma'_{3con} = 2$ psi. Test specimen B19-4 had a back pressure of 10 psi. The cell pressure applied to this test specimen was 30 psi. The initial pore water pressure in this specimen, prior to shear, should therefore have been about 40 psi. Test specimen B20-3 had a back pressure equal to 20 psi. The cell pressure in this test was increased under undrained conditions by 20 psi. As a result, the initial pore water pressure in this specimen, prior to shear, should have been about 40 psi, or a value similar to that in specimens B18-2 and B19-4.

As can be seen in Figure 5.147, these three tests with the same initial values of pore water pressure, gave very different stress-strain behavior. The stress-strain behavior of specimens B18-2 and B20-3 were somewhat similar. The behavior observed in test B19-4, however, was quite different from the other two specimens. This difference in behavior may again have resulted from the strength measured for specimen B19-4 being incorrect. The shape and characteristics of this stress-strain curve are unlike any of the other stress-strain curves for the back pressure saturated Q test specimens. This suggests that the strength of the soil measured in test B19-4 is in error and should be neglected in undrained strength interpretations for this soil.

Considering that the results of test B19-4 may be incorrect, the Mohr-Coulomb failure envelopes presented in Figures 5.133 and 5.135 can be redrawn neglecting test B19-4. Figure 5.148 shows the Mohr's circles for tests B19-1, B19-2, and B19-3, based on 5% axial strain at failure. The undrained shear strength of the soil for this condition is defined by the parameters, $c = 11$ psi and $\phi_u = 7.6^\circ$. These strength parameters are different than those for the strength envelope shown in Figure 5.133, where $c = 7.6$ psi and $\phi_u = 16.3^\circ$.

Figure 5.149 shows the Mohr's circles for tests B19-1, B19-2, and B19-3, based on the peak deviator stress failure criterion. In this case, the undrained shear strength of the soil is defined by a bilinear envelope. At normal stresses below about 27 psi, the undrained strength of the soil is defined by the parameters $c = 7.7$ psi and $\phi_u = 30.8^\circ$. At higher values of normal stress, the undrained shear strength of the soil is characterized by a $\phi_u = 0$, $S_u = c = 24$ psi condition. This strength envelope of the soil is quite different than the envelope presented in Figure 5.135, where $c = 10.3$ psi and $\phi_u = 20.8^\circ$ for the range of normal stresses tested.

The results of these tests on back pressure saturated Q test specimens tend to indicate that the undrained

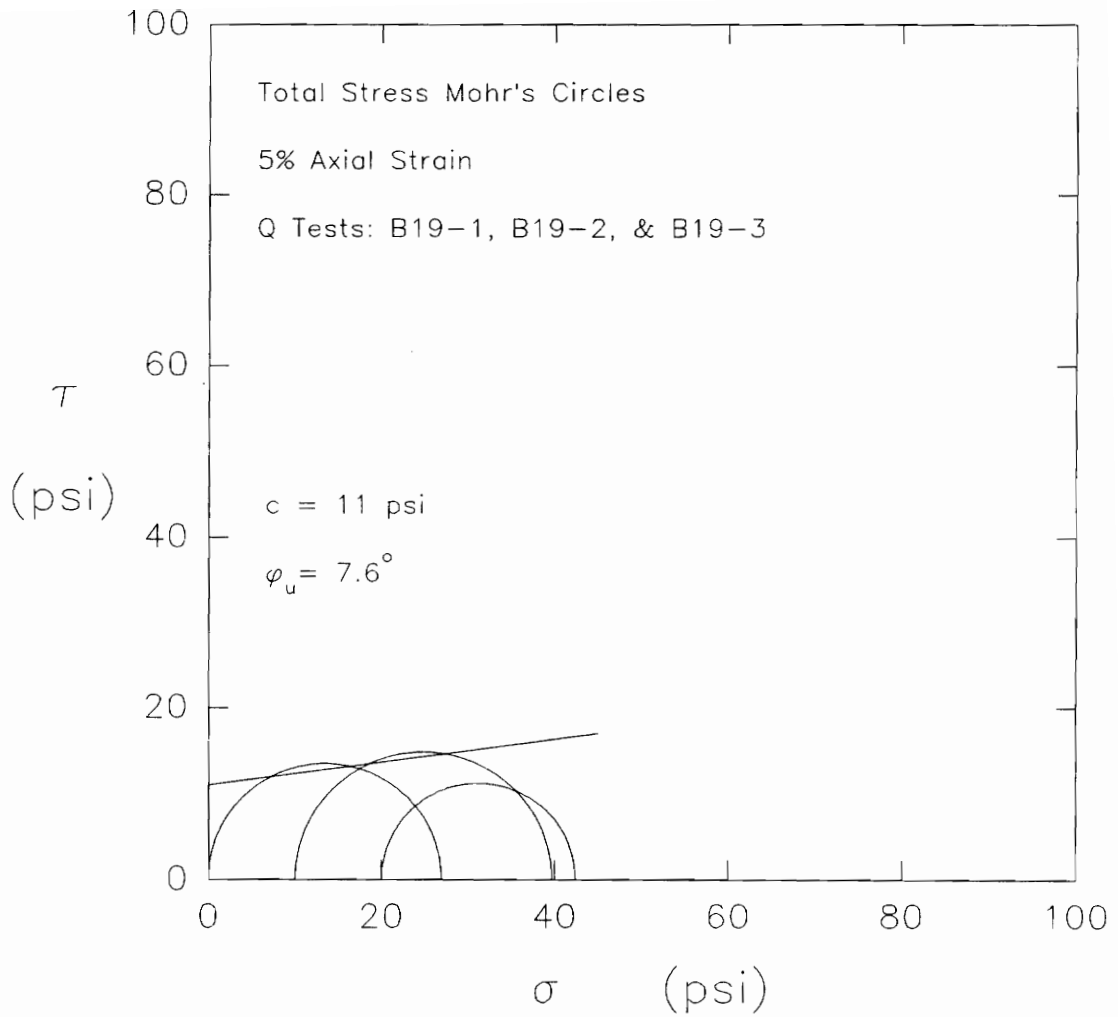


Figure 5.148. Total stress Mohr's circles at 5% axial strain for Q tests B19-1, B19-2, and B19-3 on back pressure saturated specimens of remolded new LMVD silt

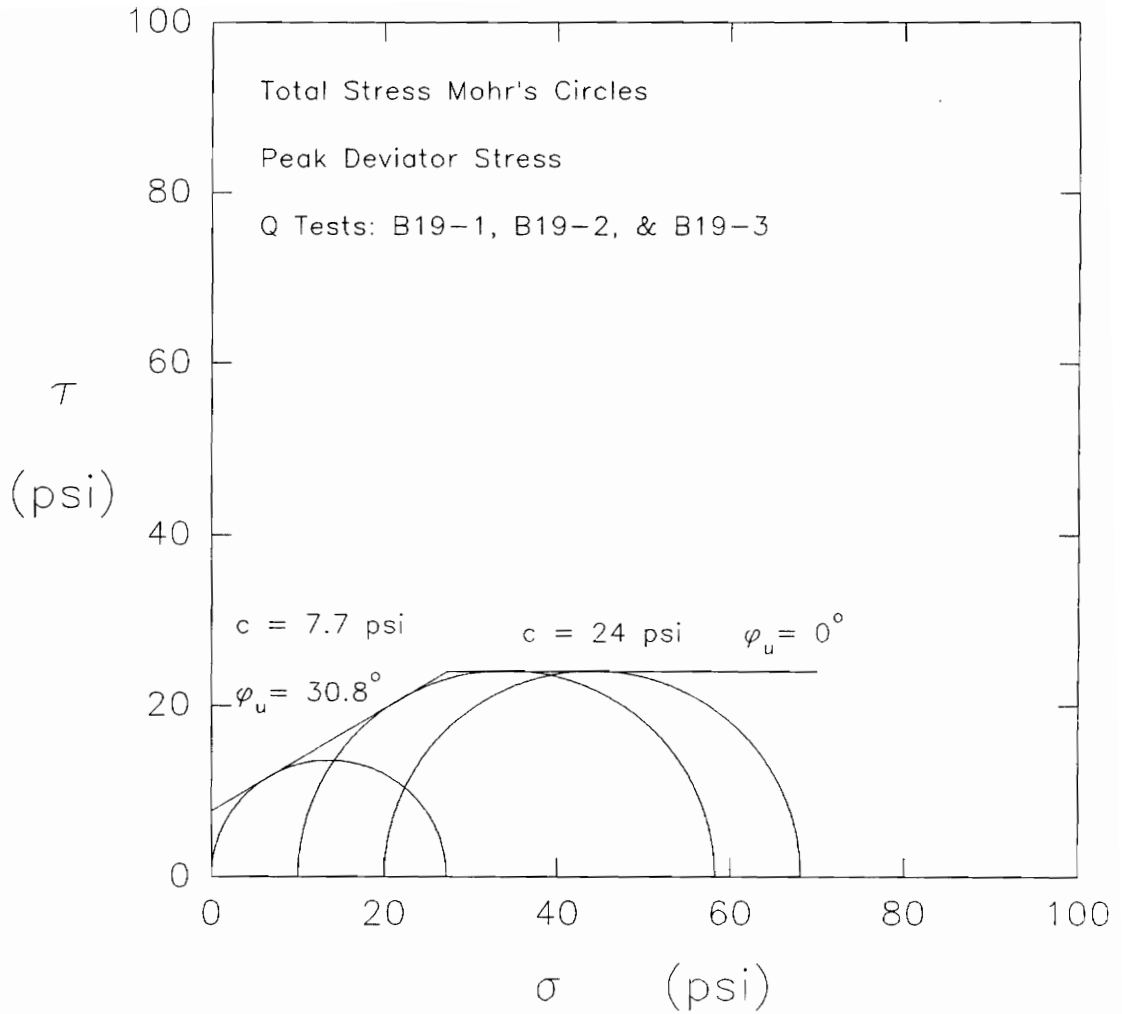


Figure 5.149. Total stress Mohr's circles at peak deviator stress for Q tests B19-1, B19-2, and B19-3 on back pressure saturated specimens of remolded new LMVD silt

strength of the soil increases as the initial pore water pressure within the specimen increases. The dilatant tendencies of the soil result in pore water pressure reductions during undrained shear. Decreasing pore water pressures during shear lead to strengthening of the soil specimen. The larger the initial pore water pressure in the specimen, the greater the decrease in pore water pressure possible, and therefore, the higher the measured strength of the soil. This could be especially important in field conditions where initial pore water pressures are often greater than 0 psi. When an additional loading is applied under undrained conditions, increases in pore water pressure will occur, giving the soil an initial pore water pressure which is larger than the newly applied confining pressure. The undrained strength of the soil in the field will be higher than that determined by performing a conventional Q test at a cell pressure equal to the applied field loading.

5.12 Summary and Conclusions

The experimental portion of this research involved the performance of a variety of tests on specimens of a dilatant silt. The tests performed were designed to investigate the possible occurrence of cavitation of soil pore water in saturated, dilatant silts during undrained

triaxial tests. The soil used in these tests was classified as an ML and is referred to as LMVD silt. It was provided by the U.S. Army Corps of Engineers, Lower Mississippi Valley Division.

A few tests were performed on undisturbed specimens and several tests were performed on compacted specimens of LMVD silt. The majority of the triaxial tests performed in this research were on specimens remolded from a slurry in a batch consolidometer. Each batch consolidometer sample ideally provided four 1.4-inch diameter specimens for testing. The remolding process provided specimens which were essentially fully saturated and had similar void ratios. A summary of the results of the experimental portion of this research follows.

The methods available for the measurement of pore pressures at the midheight of triaxial specimens have been reviewed. Such pore pressure measurements have been accomplished using several different devices. All appear, however, to have some disadvantages associated with them due to disturbance effects, installation difficulties, and the influence of the measuring device on the location of the failure plane.

Pore water pressures were measured at the midheight of Q test specimens in this study using a hypodermic needle

inserted into the specimen and connected to a pore pressure transducer. This method was used because the system would have a small volume, it would be easy to install, and it would cause a smaller amount of disturbance to the specimen than other devices. An adequate seal was found to be essential at the needle-membrane interface and the needle-transducer support system must be flexible if pore pressure measurements are to be made successfully throughout the test as axial strain increases. Failure of the needle-membrane seal during Q tests in this research lead to inaccurate pore pressure readings in some tests.

Pore pressure measurements in these Q tests indicated the existence of negative pore water pressures in the specimens initially. The measurement of negative pore water pressure suggests that somewhere in the triaxial specimen, air-water interfaces existed prior to performing the Q test (Lambe and Whitman, 1969; Sowers, 1979). This means that the specimens had a degree of saturation somewhat less than the measured value of 100%. This agrees with the observations of Bishop and Eldin (1950) and Bishop and Henkel (1962).

It is also apparent from the Q test on the undisturbed specimen that samples with a high degree of saturation are necessary to perform meaningful tests with midheight pore

pressure measurements. The undisturbed Q test specimen was about 50 percent saturated, had a low dry density, was highly fissured, and exhibited brittle behavior during testing. Meaningful pore pressure measurements were not possible in this specimen.

The decreases in pore water pressure measured at the midheight of the Q test specimens tested at cell pressures of 0, 10, and 20 psi, should have been close to the largest decreases in pore water pressure within the specimens. The magnitude of the decrease in pore water pressure tended to increase with increasing cell pressure in the Q tests. Specimens with higher values of pore water pressure at the start of undrained shear were able to experience larger decreases in pore water pressure. In all of the Q tests with midheight pore pressure monitoring, the absolute value of the pore water pressure never decreased to -13.7 psig, where vaporous cavitation would have been expected to occur. The minimum values of pore water pressure measured ranged from 10.10 psig for a Q test performed at a cell pressure of 20 psi to -8.7 psig for a specimen tested as an unconfined compression test. This suggests that some other limitation existed on the magnitude of the decrease in pore water pressure possible within the specimens.

The perfect sampling approach was used to evaluate the effect of sampling saturated silts on the pore pressure response and strength behavior of these soils. Undrained unloading tests conducted on anisotropically consolidated samples of remolded and undisturbed LMVD silt gave values of the pore pressure parameter for unloading, \bar{A}_u , similar to the values reported for clayey-silt by Ladd and Lambe (1963).

Q tests performed on samples trimmed from the quarters of two 4-inch diameter unloading test specimens were observed to show different behavior. The stress-strain behavior observed in the first group of tests was very similar at small strains and then became somewhat erratic at axial strains above 5.5 to 6 percent. For a failure criterion of 5 percent axial strain, an approximate $\phi_u = 0$, $S_u = c$ undrained strength envelope was obtained. The other set of Q tests showed stress-strain behavior in which the undrained strength of the soil increased with increasing confining pressure. This resulted in an undrained friction angle, ϕ_u , greater than zero at all values of axial strain.

The differences in the behavior of these two sets of Q tests may signify that more air came out of solution from the soil pore water during the second unloading test than the first. The LMVD silt used in the two unloading tests

was from two separate batches obtained from the Corps of Engineers so that further comparison seems questionable.

Prepressurization has been used on samples of saturated remolded LMVD silt in an attempt to reduce the possible occurrence of cavitation during Q tests on silt. Although too few tests have been performed to reach firm conclusions, several Q tests performed on specimens of remolded LMVD silt subjected to cell pressures on the order of 200 to 260 psi for 15 to 20 minutes, showed better consistency in their stress-strain behavior when compared to Q tests on similar specimens not subjected to prepressurization. This was especially true at small axial strains. The improved consistency in the stress-strain behavior of some sets of prepressurized samples may be the result of similar amounts of free air being initially present in the samples. The prepressurization would have eliminated this free air giving the samples similar void ratios for the Q tests, and thus, similar stress-strain behavior.

If additional tests are performed to further investigate the effect of prepressurization on the undrained strengths and stress-strain behavior of silts tested in Q tests, pore water pressures should be measured. This will allow for measurement of the pore pressure

parameter, B , and assessment of whether or not the samples are truly 100 percent saturated and whether or not the prepressurization is leading to changes in sample void ratio and thereby altering the corresponding strengths measured in the Q tests. Measuring the pore pressure reductions during undrained shear may show that larger decreases in pore water pressure are possible in the prepressurized specimens, as compared to the non-prepressurized specimens. This would imply that the prepressurization made the pore water more resistant to cavitation, so that dissolved gases would not come out of solution until larger negative pore water pressures had been reached.

The measurement of pore air and pore water pressures were attempted in Q tests on compacted specimens of partially saturated LMVD silt. These types of measurements have been noted to be quite difficult (Bishop, 1960; Bishop and Henkel, 1962). This was found to be true in this research as well. The results of these tests are felt to be questionable due to the inconsistencies and unusual pore pressure measurements observed. The results of these tests therefore were not useful in assessing the undrained behavior of dilatant silts in this research.

Saturated silt Q test specimens sheared at different strain rates showed somewhat inconsistent stress-strain behavior in this research. The stress-strain behavior or dilatant hardening in these Q tests was not observed to vary with strain rate in a consistent manner, as was expected. Strain rate effects on dilatant soils appear to be a very complex issue. Other variables, such as levels of specimen disturbance, may have influenced the stress-strain behavior in a way that could not be quantified.

It was observed in these tests that the specimens sheared at the fastest strain rates tended to exhibit abrupt strain-softening more frequently than specimens sheared at the slowest strain rates. This is believed to suggest that in the rapidly sheared specimens, the larger decreases in pore water pressure may have lead to cavitation of the soil pore water near the shear plane, resulting in abrupt yielding and failure.

The results of the undrained strength tests performed in this research illustrated the erratic undrained behavior characteristic of saturated, dilatant silts. In some groups of tests, $\phi_u = 0$, $S_u = c$ strength envelopes were obtained. In other groups of tests, under certain conditions, the undrained strength of the soil was defined by a $\phi_u > 0$ envelope. The undrained strength envelope

obtained for a group of Q tests tended to vary depending on the value of axial strain chosen as the failure criterion. In some cases, the undrained behavior of a group of tests was so erratic that an undrained strength envelope could not be developed from the results. The combination of dissolved gases exiting solution from the soil pore water and variable levels of specimen disturbance may have resulted in the very erratic behavior observed. The magnitude and effect of specimen disturbance could not be quantified in this research.

Several CU triaxial tests were performed on saturated silts in this study. An undisturbed specimen tested exhibited compressive tendencies throughout the test, unlike those reported on by Brandon, Duncan, and Huffman (1990). This undisturbed specimen had a very low dry density and was highly fissured, which may have lead to the strain softening behavior exhibited during the test. Remolded specimens of old LMVD silt tested in CU tests yielded effective stress friction angles, ϕ' , between 34° and 37° . A series of CD tests on old LMVD silt yielded an effective stress friction angle, ϕ' , of 38° .

A series of four CU tests were performed on saturated silt specimens consolidated to $\sigma'_{3con} = 10$ psi with different values of back pressure. These undrained tests

showed that once the pore water pressure went below atmospheric pressure or zero gage pressure, the pore water pressure only experienced a slight further decrease before becoming relatively constant. The pore water pressure never decreased to a value of -13.7 psig or 0 psia, where vaporous cavitation would have been expected. The limiting value of negative pore water pressure in these tests appeared to be only -2 to -4 psig.

The decrease in pore water pressure to a minimum limiting value in these CU tests was observed to correspond with peak values of deviator stress being reached in the tests. The peak values of deviator stress were followed by gradual strain-softening. As the pore water pressure went below atmospheric pressure in these tests, desaturation of the CU test specimens occurred, resulting in volume expansion and stress-strain behavior characteristic of drained conditions in the soil.

Two series of Q tests were performed on back pressure saturated silt specimens. In these tests, back pressures of 10 and 20 psi were applied, while the specimens were consolidated to $\sigma'_{3con} = 2$ psi. After the back pressure was applied, the cell pressure was increased under undrained conditions and the specimens were sheared at a strain rate of 1%/min.

Pore pressures were not measured during shear. The Q tests performed on these two sets of specimens were then compared to the results of conventional Q tests performed at the same cell pressures on specimens that were not consolidated in the triaxial cell and did not have a back pressure applied.

For the sets of Q tests performed with a given value of back pressure, the stress-strain behavior of the group was not always consistently similar, but it did tend to be less erratic than the behavior of the Q tests performed on specimens without back pressure. When comparing tests at a given value of cell pressure, the stress-strain behavior of the specimens tended to be similar at low values of axial strain, regardless of whether or not a back pressure was used in the specimens.

At a given cell pressure, the peak value of undrained shear strength of the soil measured in Q tests, increased with increasing back pressure. The higher the back pressure, the higher the axial strain at which the peak occurred in the deviator stress-strain curves for tests at a given cell pressure.

When no back pressure was used, the specimens tested at low cell pressures tended to exhibit abrupt strain-softening. The strain-softening observed in the back

pressure saturated Q tests tended to be more gradual than that observed in the Q tests performed without back pressure.

The use of a back pressure in Q test specimens of saturated silt is believed to have delayed desaturation of the specimens until higher axial strains had been reached. This could be especially important in field conditions where initial pore water pressures are often greater than 0 psi. The initial hydrostatic pore water pressure in the field is comparable to the back pressure used in these laboratory tests. When an additional loading is applied under undrained conditions, increases in pore water pressure will occur, giving the soil an initial pore water pressure which is larger than the newly applied loading. If all other conditions are equal, the undrained strength of the soil in the field should be higher than that determined by performing conventional Q tests at cell pressures equal to the newly applied field loading. This is because the higher initial pore water pressure in the field plus the increase in pore water pressure due to the newly applied loading will allow for more dilatant hardening of the soil in-situ, resulting in a higher undrained strength than the measured in the Q test specimens.

The laboratory testing program completed as part of this research revealed important aspects of the undrained behavior of saturated, dilatant silts. It also raised more questions regarding their behavior. The results of the laboratory tests are believed to strongly suggest that the exit of dissolved gases from solution in pore water of saturated, dilatant silts may very well contribute significantly to the occurrence of erratic behavior in Q tests. Although its influence could not be quantified or eliminated, specimen disturbance is also felt to be significant when performing Q tests on saturated, dilatant silts. Specimen disturbance may be a significant cause of the erratic undrained behavior observed for these soils.